Synthesis and Physical Evaluation of Urea- and Thiourea-based Receptors and Sensors for Anions

by

Haslin Dato Paduka Haji Ali, B.A. (Mod.)

April 2007
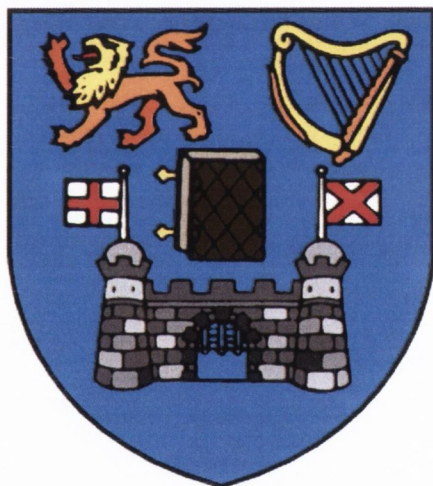
University of Dublin
Trinity College

Based on research carried out under the direction of
Prof. Thorfinnur Gunnlaugsson and Dr Paul E. Kruger
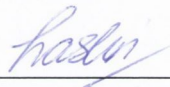
A thesis submitted to the School of Chemistry, University of Dublin, Trinity College for the degree of Doctor of Philosophy
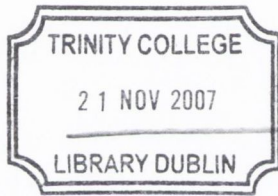
Declaration

This thesis is submitted for the degree of Doctor of Philosophy to the University of Dublin, Trinity College and has not been submitted for any degree or examination to this or any other University. Other than where acknowledged, all work described herein is original and is carried out by the author. The author gives permission such that the Library may lend or copy this thesis upon request. This permission covers only single copies made for study purposes, subject to normal conditions of acknowledgement.

Haslin Dato Paduka Haji Ali

Abstract

This thesis, entitled "Synthesis and Physical Evaluation of Urea- and Thiourea-based Receptors and Sensors for Anions", consists of five chapters.

Chapter 1 briefly introduces the field of molecular sensing, followed by a general description of anion sensing, which includes the design principles of anion receptors and sensors as well as the advantages of their practical use. A review of various recent examples of urea- and thiourea-based fluorescent and colorimetric anion sensors is also presented, which is then followed by a summary of the anion sensing work carried out within the Gunnlaugsson research group. Finally, an outline of the project objectives is described.

Chapter 2 discusses the synthesis of *bis*-phenyl urea and thiourea receptors, substituted at the 2- and 4-position of the aromatic rings by electron-donating (*i.e.* CH_3) and electron-withdrawing (*i.e.* F, CF_3) groups. These compounds were purified and fully characterised, and their binding abilities towards putative anions (such as acetate, dihydrogenphosphate, fluoride, chloride and bromide) were studied in DMSO-d_6 using ^1H NMR spectroscopy. The stability constants for the complex formation of these receptors with each anionic guest were calculated from the data collected. These values were then analysed in terms of the electronic nature of the substituent and its location on the phenyl ring, as well as the type of binding site (either urea or thiourea) present. The analysis reinforced the characteristic anion-binding behaviour of the urea and thiourea moieties. However, it also gave rise to some unexpected and sometimes counter-intuitive trends in the electronic influence towards the anion binding abilities.

In Chapter 3, the synthesis of polyaromatic thiourea-based fluorescent anion sensors is described and the physical evaluation of their anion binding abilities in DMSO or DMSO-d_6 using various techniques (such as ^1H NMR, fluorescence and CD spectroscopies) is discussed. The two types of fluorophore incorporated into these sensors are anthracene and naphthalene. These sensors were titrated with the selected anions (as in Chapter 2). The data obtained from the binding studies was analysed and stability constants were calculated in order to compare the anion binding abilities of such sensors.

Chapter 4 concentrates on the synthesis and anion binding studies of hydrazine-based naphthalimide colorimetric sensors, consisting of either a urea or thiourea moiety. Binding experiments with anions (as in Chapter 2) were carried out in DMSO or

DMSO-d_6 on the urea-based compounds using ^{1}H NMR, UV-vis and fluorescence spectroscopies. In the case of the thiourea derivative, binding studies were performed in a more competitive solvent (*i.e.* EtOH/H$_2$O (50:50)). The chromogenic response of such sensors to the selected anions was significant and the thiourea-based sensor also showed selectivity in terms of visual discrimination towards acetate in the highly competitive solvent.

Finally, Chapter 5 outlines the experimental procedures used in Chapter 2 - 4, and presents the characterisation of the compounds prepared.

Acknowledgements

I would like to sincerely thank my supervisors, **Prof. Thorfinnur Gunnlaugsson** and **Dr Paul E. Kruger**, for all their advice, encouragement and support throughout my Ph.D. career.

I would also like to take this opportunity to thank the TG Research Group, old and new – **Andrew, Ann-Marie, Aoife, Célia, Céline, Cidália, Christophe, Danni, Debbie, Doireann, Emma, Eoin, Floriana, Fred, Gary, Jennifer, Jilly, Joe, Julie, Julien, Katell, Lisa, Niamh, Raman, Rebecca, Sally, Sinéad** and **Susan** – many thanks for all their support and friendship and for making working in the lab (and out of it!) really fun and most definitely interesting! Also, many thanks to the Kruger Research Group – **Claire, Jen, Murray, Niamh, Sandrine** and **Sylvie** – for taking me in and making me feel really welcome! A special thank-you must go to **Célia, Céline, Joe** and **Julien** for all the advice, support and proofreading expertise, and **Julie** and **Susan** for the help they have given me regarding various aspects of my work.

Many thanks to **Dr John O'Brien** and **Dr Manuel Ruether** for their help with my ^{1}H NMR titrations, especially for giving lots of NMR time! And thanks to **Dr Paul Jensen, Dr Sandrine Goetz** and **Dr Tom McCabe** for all the X-ray diffraction studies. Also, a big thank-you to the School of Chemistry, especially the Head of School (**Prof. John Corish**), administrative staff (**Corinne, Helen, Maria** and **Teresa**) and technical staff (**Brendan B., Brendan M., Colm, Dorothy, Ed, Fred, John, Kieron, Marcus, Mark, Martin, Patsy, Peggy, Seamus** and **Teresa**) for all their help along the way.

I would also like to offer my sincerest gratitude to the organisations which funded my research – **Enterprise Ireland, IRCSET** and **Trinity College Dublin**.

Thanks very much as well to the many people I have met and befriended within the diplomatic community, especially from the Bruneian embassies (in Berlin, Hanoi and Cairo) where my parents were posted during my academic years. Vielen Dank zu meinen Freunden in inLingua – Ich kann jetzt ein bisschen Deutsch sprechen, haha!

<div align="center">

THANK YOU

TERIMA KASIH

謝 **ARIGATOU** 謝

GO RAIBH MAITH AGAIBH

GRACIAS

MERCI

GRAZIE

OBRIGADO

DANKE

TAKK FYRIR

</div>

物事の始まりは易しいが、続くのが難しい。

"Beginning is easy, continuing is hard."
− Japanese proverb −

Dedicated to my beloved parents,
Dato Paduka Haji Ali & Pengiran Datin Hajah Noriah,
as well as my dearest aniki, Haslan

Abbreviations

[x]	Concentration of substance x (in M or mol.L^{-1})
A$^-$	Anion
AcO$^-$	Acetate ion
app	Apparent (for chemical shifts)
Ar	Aromatic ring
An	Anthracene ring
β (or K)	Stability or binding constant (in M^{-1})
Bu	Butyl group
Br$^-$	Bromide ion
br s	Broad singlet
CD	Circular dichroism
CDCl$_3$	Deuterated chloroform
(CD$_3$)$_2$SO	Deuterated dimethylsulfoxide
CH$_3$	Methyl group
CHN	Elemental analysis
CF$_3$	Trifluoromethyl group
Cl$^-$	Chloride ion
Cyclohex	Cyclohexane ring
δ	Chemical shift (in ppm)
d	Doublet
d_6	Deuterated
DCM	Dichloromethane
Δδ	Cumulative change in chemical shift (in ppm)

dd	Double doublet
DMF	Dimethylformamide
DMSO	Dimethylsulfoxide
DMSO-d_6	Deuterated dimethylsulfoxide
E	Energy (in J)
equiv.	Equivalents
ES$^+$	Electron spray (positive mode)
ESIPT	Excited-state intramolecular proton transfer
ET	Electronic energy transfer
EtOH	Ethanol
F	fluoro group
F$^-$	Fluoride ion
G	Guest
h	Planck's constant (in J.s^{-1})
H	Host
H$_2$PO$_4^-$	Dihydrogenphosphate ion
Hex	Hexane
HOMO	Highest occupied molecular orbital
HRMS	High resolution mass spectrometry
ICT	Internal charge transfer
IR	Infrared
ISC	Intersystem crossing
J	Coupling constant (in Hz)
λ	Wavelength (in nm)
lit.	Literature

LUMO	Lowest unoccupied molecular orbital
m	Multiplet
MeCN	Acetonitrile
MeOH	Methanol
MLCT	Metal-to-ligand charge transfer
m.p.	Melting point (in °C)
MS	Mass spectroscopy
Nap	Naphthalene ring
Naph	Naphthalimide ring
NMR	Nuclear magnetic resonance
PET	Photo-induced electron transfer
ppm	Parts per million
q	Quartet
RD	Radiationless decay
RT	Room temperature (in °C)
s	Singlet
S_0	Ground state
S_1	Singlet excited state
SOMO	Semi-occupied molecular orbital
t	Triplet
T_1	Triplet excited state
TBA	Tetrabutylammonium
UV-vis	Ultraviolet-visible
υ	Frequency (in Hz or s^{-1})
v/v	Volume per volume

TOWARDS THE DEVELOPMENT OF POLY-AROMATIC FLUORESCENT ANION SENSORS

REFERENCES

APPENDICES

PUBLICATIONS

Colorimetric "naked eye" sensing of anions in aqueous solution.
J. Org. Chem. **2005**, 10875.

Fluorescent photoinduced electron transfer (PET) sensors for anions;
From design to potential application.
J. Fluoresc. **2005**, 287.

1.1 Sensing

The term "sensing" refers to the detection of a particular entity (*e.g.* matter, energy) by a specialised device (*i.e.* sensor). Sensors are used in everyday life, and have been applied to various areas such as medicine (*e.g.* blood content monitors, drugs) and industry (*e.g.* automobiles, electronics, waste management). Hence, the development of sensors holds great importance, and many endeavours have been made to further research in this area.

1.2 Sensing in Supramolecular Chemistry

As a result of the growing recognition of scientific fields such as nanotechnology, the idea of molecular detection by suitably engineered individual molecules has become of increasing importance over the last few decades.[1,2] Molecular recognition is a fundamental feature of various natural systems and plays a key role in biosynthesis and protein folding. Hence, research in the area of developing chemosensors to detect biological analytes is of current significance to the biochemical and pharmaceutical industries, especially in the synthesis and development of real-time sensitive analytical techniques.[2,3]

In supramolecular chemistry, sensing is achieved by designing synthetic molecular devices (*i.e.* sensors) having the ability to detect matter or energy that yields a measurable signal in response.[2] There are three characteristic groups of analyte for which these sensors are designed to detect: cationic (*e.g.* metal ions such as Na^+ and K^+),[4,5] anionic (*e.g.* carboxylates, halide ions)[6,7] and charge neutral (*e.g.* amino acids, saccharides) species.[8,9]

1.2.1 Chemosensors

Until a few decades ago, the classical term used for a sensor referred to a macromolecular device (*e.g.* pH sensor). Supramolecular chemists are now eager to develop such synthetic devices on a molecular scale. The various kinds of molecular devices are categorised according to two main factors:

1. **Target of detection**
2. **Signal transduction mechanism**

1

We have briefly mentioned the different targets of detection. The latter factor therefore depends mainly on the method of detection (*e.g.* electrochemical techniques, luminescence techniques, *etc.*). Our project focuses mainly on developing sensors for anions that employ luminescence or colour as the signal reporter.

1.3   Methods of Detection

Sensors must be able to give a measurable signal in response to analyte recognition. The mechanism by which the interaction of a sensor with its analyte yields a measurable form of energy is known as signal transduction.[2] The energy measured may reside in wavelength regimes characterised by various types of spectroscopy (*e.g.* fluorescence, UV, visible, ^{1}H nuclear magnetic resonance) or may yield electrochemical responses.[2] Fluorescence is believed to be one of the optimal signal transduction mechanisms in potential sensing applications as it provides an enormously sensitive technique, mainly because the emission wavelength is always longer than that of the excitation wavelength and only low concentrations of analyte (10^{-6} M) are required for signalling purposes.[4,10] Another popular mode of detecting a binding event is the so-called "naked-eye" effect, whereby visual discrimination *via* a colour change is achieved. This is advantageous in that such sensors can be used in "one-off" testing without the need for expensive instrumentation.

1.3.1 ^{1}H Nuclear Magnetic Resonance

Nuclear magnetic resonance (NMR) spectroscopy is one of the most widely used techniques in molecular recognition.[11] Although it is not as sensitive as other spectroscopic methods such as luminescence techniques, it is still useful in indicating the presence of host-guest complexation and monitoring of the binding process. ^{1}H NMR is very important when dealing with hydrogen-bonding receptors due to the fact that hydrogen atoms lie at the periphery of most compounds and are therefore the first nuclei to experience any 'disturbance' from an approaching guest. Hence, it provides extra information such as direct interactions of receptors with guest molecules, which is not observed when using the other techniques as they only show the overall effect of the recognition event.

Both slow and fast exchange can occur in NMR spectroscopy. Protons of polar functionalities such as NH, OH and SH groups can exchange intermolecularly in solution. A slow exchange is such that the protons are exchanging with a rate that is

slower than the coupling constant (J), resulting in chemical shifts which illustrate clearly the mutliplity of any direct coupling to the protons. When the rate of exchange is appreciably faster than J (*i.e.* a fast exchange), then an average signal of the possible microenvironments (due to the coupling) is observed. Therefore, when considering a proton that forms a hydrogen bond with an anion guest, two signals would be present in the spectrum during a slow exchange – one peak would indicate the host-guest complex and the other would indicate the free host. On a fast exchange, only one peak would be observed for the binding proton and this is due to an average of the chemical shifts of the free host and the complex. A binding event would be indicated by the shift (upfield or downfield) of this peak.

1.3.1.1 Calculation of Stability Constants from ^{1}H NMR Titrations

Stability (or binding) constants for 1:1 host:guest (H:G) complex formation can be determined using a non-linear least-squares regression equation (Equation 1.1). This equation is used to estimate the value of δ_{HG} (the chemical shift of the host-guest complex). Stability constants for other stoichiometries are difficult to obtain, as they require more complicated calculations.

$$\delta_{HG} = \frac{[H]_i(\delta_{obs} - \delta_H)}{\left(\dfrac{([H]_i+[G]_i+1/K) - \sqrt{\{([H]_i+[G]_i-1/K)^2 - 4[H]_i[G]_i\}}}{2} \right)} + \delta_H \quad \textbf{(Equation 1.1)}$$

$\boldsymbol{\delta_{HG}}$ – chemical shift of the host-guest complex **HG** (in ppm)

$\boldsymbol{\delta_H}$ – chemical shift of the free host **H** (in ppm)

$\boldsymbol{\delta_{obs}}$ – observed chemical shift of the host guest complex **HG** at any stage (in ppm)

$\boldsymbol{[H]_i}$ – initial concentration of the host **H** (in M)

$\boldsymbol{[G]_i}$ – initial concentration of the guest **G** (in M)

$\boldsymbol{K}$ (or $\boldsymbol{\beta}$) – stability (or binding) constant (in M^{-1})

Computer programs such as WinEQNMR[12] base their calculation of the stability constants for 1:1 complexation process on the above equation. The derivation of this

equation from first principles can be obtained by considering the rate constant equation (Equation 1.2) of the following 1:1 host:guest complex formation equilibrium:

$$H + G \rightleftharpoons HG$$

$$K = \frac{[HG]}{[H][G]} \qquad \textbf{(Equation 1.2)}$$

The initial concentrations of the host, guest and complex are denoted by $[H]_i$, $[G]_i$ and $[HG]_i$ respectively. Since there is no complex formed initially, $[HG]_i$ is therefore equal to 0. By assigning $[HG]$ at equilibrium as x, it follows that the concentrations of the host and guest at equilibrium are $([H]_i - x)$ and $([G]_i - x)$ respectively. Hence, the substitution of Equation 1.2 with the above notation of the relevant equilibrium concentrations gives the following equation (Equation 1.3), where K is the stability constant for the host-guest association:

$$K = \frac{x}{([H]_i - x)([G]_i - x)} \qquad \textbf{(Equation 1.3)}$$

Equation 1.3 can be expanded and rearranged *via* multiplication of the denominator and algebraic solution (using the equation used to solve quadratic equations) such that an equation to determine $[HG]$ may be obtained (Equation 1.4):

$$x = [HG] = \frac{([H]_i+[G]_i+1/K) - \sqrt{\{([H]_i+[G]_i-1/K)^2 - 4[H]_i[G]_i\}}}{2} \qquad \textbf{(Equation 1.4)}$$

The actual $[HG]$ at any stage is indicated by the observed chemical shift (δ_{obs}) on the ^1H NMR spectrum, which varies depending on the fraction of free host present and the fraction of host:guest complex formed.

Given that the chemical shifts of the concentration of the free host when no guest has been added, and that of the complex when all the host molecules are completely bound are denoted as δ_H and δ_{HG} respectively (and δ_{obs} depends on the amount of each of these two species present), an equation (Equation 1.5) can be written relating δ_{obs} to $[H]$ and $[HG]$:

$$\delta_{obs} = \frac{[H]}{[H]_i} \delta_H + \frac{[HG]}{[H]_i} \delta_{HG} \qquad \textbf{(Equation 1.5)}$$

The concentration of free host [H] can be estimated as ([H]$_i$ – [HG]) and by substituting this expression into Equation 1.5, it can be expanded and rearranged to give the following equation (Equation 1.6):

$$\delta_{HG} = \frac{[H]_i(\delta_{obs} - \delta_H)}{[HG]} + \delta_H \qquad \textbf{(Equation 1.6)}$$

Substituting Equation 1.4 into Equation 1.6 will therefore give the non-linear least-squares regression equation used to calculate the stability constant K (Equation 1.1). δ_{HG} is dependent on [HG], and since [HG] is dependent on K, δ_{HG} is then also dependent on this stability constant.

1.3.2 Fluorescence[13]

When a beam of light passes through a compound, the molecules absorb energy at discrete wavelengths and produce electronically excited species that usually have a short-lived lifetime (*i.e.* the excited state). This excited species will return to its ground state *via* several possible mechanisms, releasing its energy either in the form of light or heat. These processes are shown in Figure 1.1 in terms of a Jablonski diagram demonstrating the many possible pathways taken by the excited species to return to its ground state.

The absorption of light by an atom or molecule is a process whereby an electron in the ground state (S_0) or highest occupied molecular orbital (HOMO), is promoted to the excited state or lowest unoccupied molecular orbital (LUMO), giving rise to the formation of two semi-occupied molecular orbitals (SOMO). Each electronic state consists of a set of vibrational states, which are of discrete energies. In solution, the excited state typically relaxes to the S_1 level (*i.e.* the lowest vibrational state of the lowest electronic state, thus releasing vibrational energy into its surroundings *via* radiationless decay (RD)). When the excited electron returns to its ground state, the energy released may be in the form of heat (*i.e.* radiationless relaxation).

However, an alternative mechanism may come into play, where the energy is released *via* the emission of light. This phenomenon is known as fluorescence, which is a form of luminescence (*i.e.* radiative decay). This occurs when the excited electron returns directly from the S_1 state to the S_0 state, within a nanosecond (ns) time range. If intersystem crossing (ISC) occurs (*i.e.* the excited electron moves from the singlet excited state S_1 to the triplet excited state T_1), the energy released by the electron from

T_1 to the ground state is also in the form of light, but this process (called phosphorescence) is more long-lived compared to fluorescence.
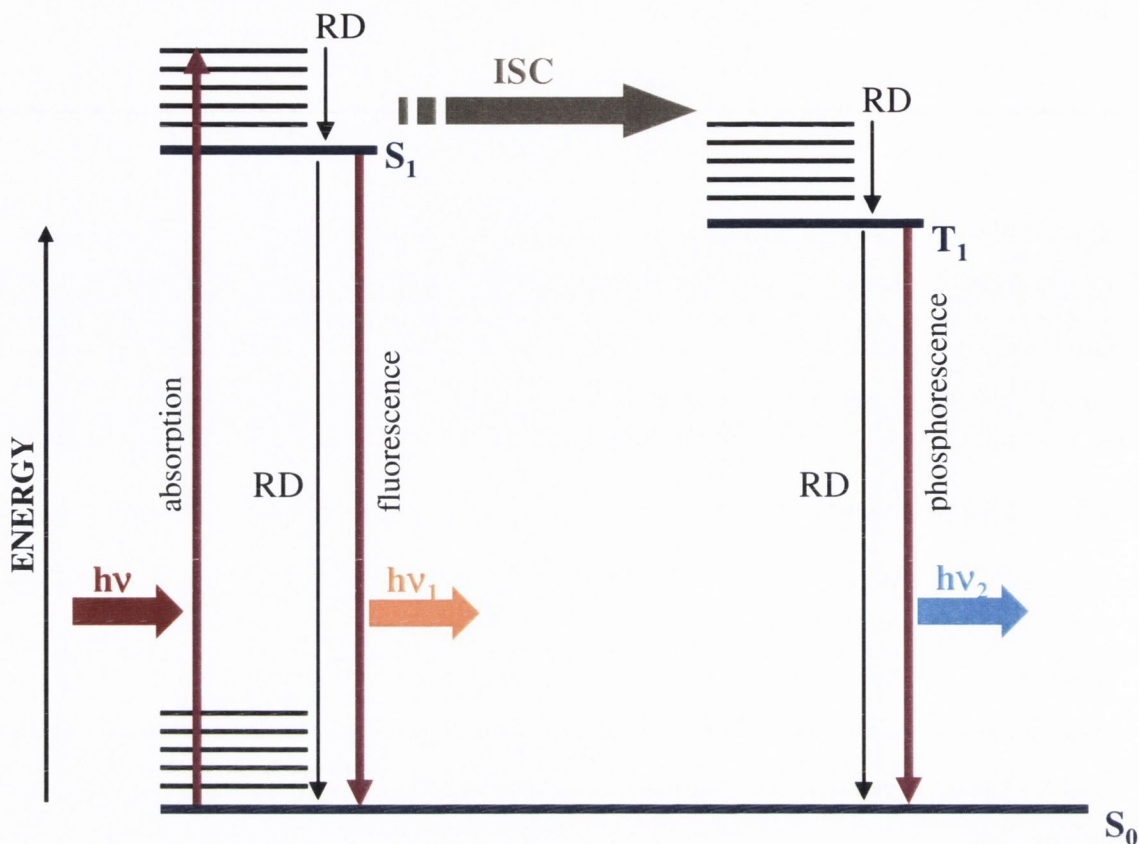
Figure 1.1 A Jablonski diagram illustrating the mechanisms that a molecule can employ to release the energy it absorbed. (**ISC** = intersystem crossing; **RD** = radiationless decay; **hν** = energy)

1.3.2.1 Photo-induced Electron Transfer (PET) in Fluorescent Sensors[3]

Luminescence is an extremely useful property that can be exploited in ion and molecular sensing. It is a sensitive and non-destructive technique, and luminophores incorporated in the sensors can be designed to emit at much longer wavelengths, which can assist in overcoming problems such as signal interference from autofluorescing biological samples. Luminescence can be stimulated by several different mechanisms, including metal-to-ligand charge transfer (MLCT), electronic energy transfer (ET) and photo-induced electron transfer (PET). The latter mechanism is of most relevance to this project, and hence, will be described in detail.
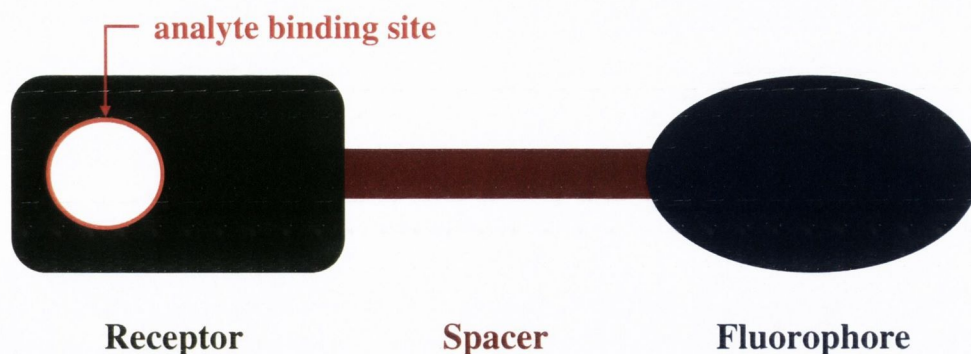
Figure 1.2 Classical model of a fluorescent sensor as developed by de Silva.[10]

Figure 1.2 is the typical blueprint used when designing PET fluorescent sensors. It basically consists of a receptor (which binds to the analyte) connected to a fluorophore (which transmits energy in the form of light) *via* a spacer (which provides a suitable distance between the receptor and fluorophore to prevent any ground state orbital interactions). There are two types of fluorescent sensors: "switch-on" and "switch-off" sensors. The former is where the reporter initially does not fluoresce and upon complexation of the receptor with its target guest (which modulates its photophysical properties), the fluorescence is then "switched on" (as PET is prevented). A "switch-off" sensor works in the opposite way, where the fluorescence is present initially and is then quenched upon guest complexation. The mechanisms governing these two types of sensors are clearly illustrated in the following diagram (Figure 1.3).

The amount of change in the fluorescence intensity of the sensor corresponds to the strength of binding interaction between the receptor and analyte. The sensor is said to be showing ideal PET behaviour, when changes are observed only in the fluorescence (due to the changes in the free energy of electron transfer between the excited state of the fluorophore and that of the receptor) while the absorption spectrum remains the same (since the spacer prevents any π-π^* or n-π interactions between the two parts).
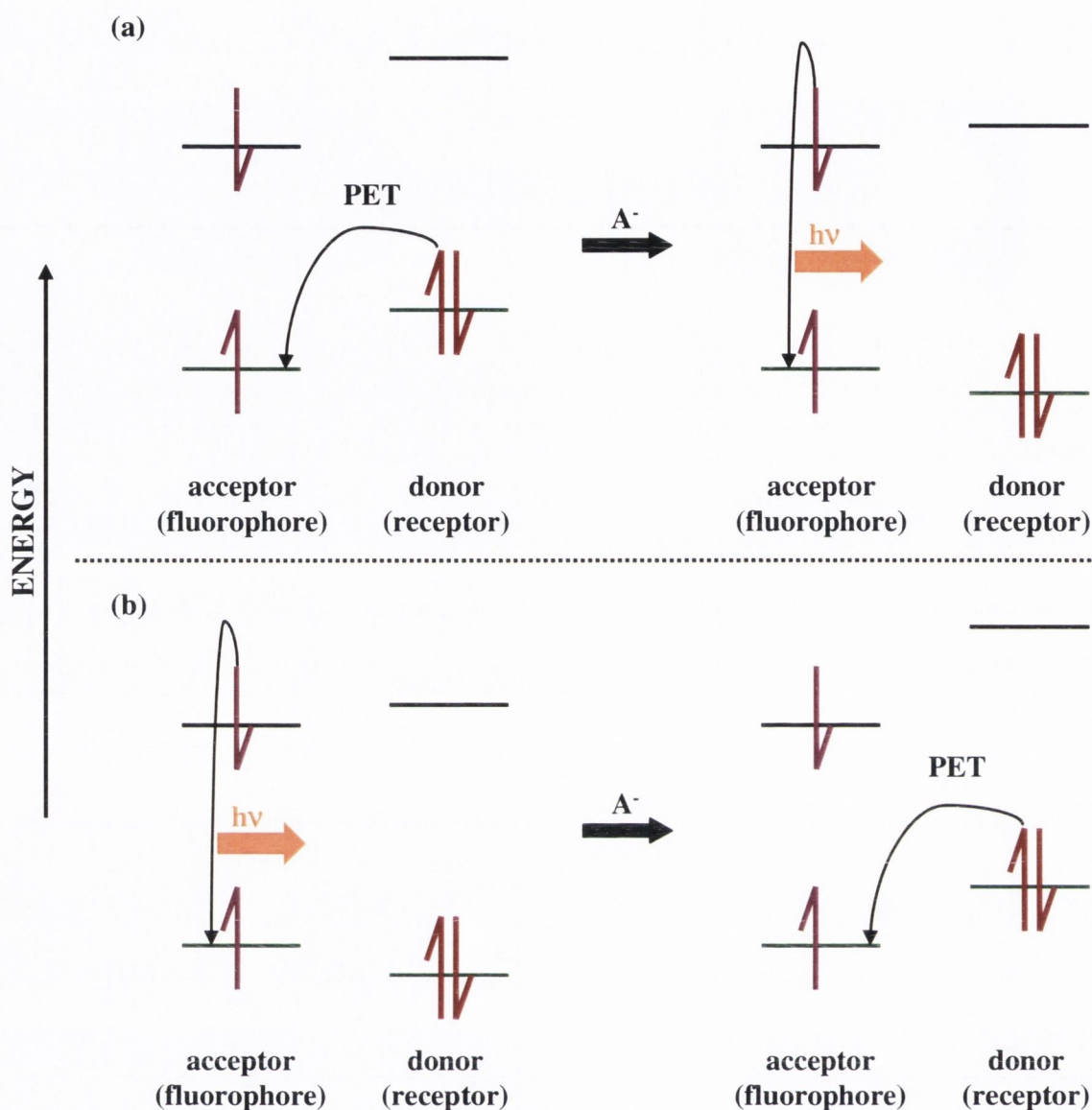
Figure 1.3 Energy level diagram illustrating the mechanism of the two types of fluorescent sensor: (a) "switch-on" fluorescent sensor, (b) "switch-off" fluorescent sensor (**black energy level** = LUMO; **green energy level** = HOMO; **hv** = energy released in the form of fluorescence)

1.3.3   Light Absorption[13]

The process by which a molecule can be promoted from the ground electronic state to an electronically excited state *via* the absorption of a quantum of light is known as absorption. This absorption of radiation is only possible if the amount of energy of that quantum of light is equivalent to the difference in energy between the ground state and the excited state. The energy difference corresponds to light in the visible (vis) and ultra-violet (UV) regions. Techniques using UV-vis spectroscopy are also frequently employed in binding experiments, especially in colorimetric chemosensors.

1.3.3.1 Internal Charge Transfer (ICT) in Colorimetric Sensors[3]

A sensor that provides a chromogenic response (*i.e.* a colour change) upon the recognition of its target analyte is extremely useful for selective visual discrimination, despite its qualitative nature. Hence, there have been many colorimetric chemosensors developed to date.[14,15] The design of a colorimetric sensor basically employs the same design principles as a fluorescent sensor. In fact, there are examples of fluorescent sensors giving chromogenic responses upon host:guest complexation.[16-20] The colour change observed is generally ascribed to the internal charge transfer (ICT) between the guest-bound receptor and the chromophore.[15] This ICT process is achieved due to the presence of partial electronic charges within the system, and this will be discussed further in Section 4.2.
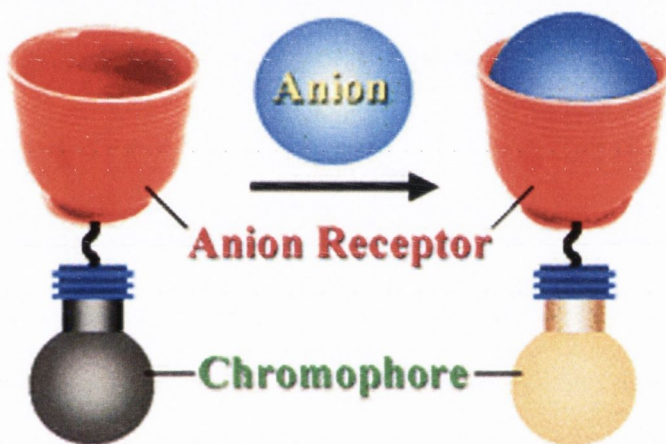
Figure 1.4 Operating principle of colorimetic anion sensors, where the colour change goes from grey (left) to yellow (right) upon anion binding.[15]

The diagram (designed by Suksai and Tuntulani) shown in Figure 1.4 illustrates the functioning of a colorimetric anion sensor.[15] The chromophore of the sensor is represented by a light bulb, while the cup (connected to the light bulb by a spacer-like wire) acts like a receptor. When the anionic guest is captured by the receptor, the grey colour of the chromophore is changed to yellow, as a result of the perturbation of the electronic properties of the receptor.

All the above methods of detections provide much information with regards to the processes involved in anion sensing. The next several sections will look briefly at the history of anion sensing, and discuss the factors which may affect the development of anion receptors and sensors.

1.4 Anion Sensing

Research into the development of synthetic anion-coordinating molecules[21] is a relatively recent pursuit, compared to the intensive study of molecules developed for the detection of cations and charge neutral molecules.[6] Interestingly, the phenomena of cation and anion complexation using synthetic molecules were discovered around the same time.[6] In April 1967, Pedersen submitted an article, presenting crown ethers capable of binding cations (*e.g.* **1**),[22] while in 1968, Park and Simmons reported the first bicyclic diammonium-derived synthetic organic ligands (**2** - **5**), capable of halide complexation.[23] For a historical overview of anion receptor chemistry, there are a number of excellent books and reviews available for reference.[6,7,24-27]
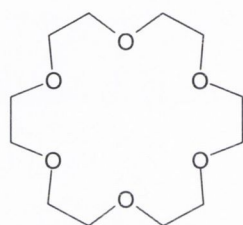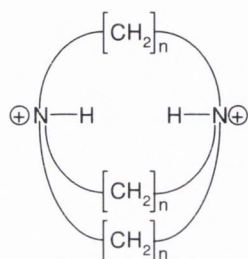
1   **2 - 5** n = 7 - 10

Various factors influenced the huge interest in the development of molecules for anion sensing. Many anions are found to be of physiological importance and play a key role in many biological processes, such as gene replication, energy transduction and transport in ion-channels.[28] In industry, waste management and pollution are extremely important issues as they include anionic species that are environmentally and biologically hazardous. Fluoride is one of the most common anionic culprits affecting the environment. In many regions, it is added to drinking water as a preventative measure towards dental cavities. However, high concentrations of this anion can cause dental fluorosis, especially in children.[29-31] The presence of fluoride is also found in industries utilising fluoride-rich resources and nerve gases used in military combat (which release highly toxic hydrogen fluoride gas). In biology, fluoride is an essential nutrient involved in certain enzymatic systems.[32] Choride and iodide are also biologically important halides. The inability to produce chloride-containing channel proteins leads to a genetic disorder known as cystic fibrosis,[33] while iodide is required for proper thyroid gland functions.[34] Other anions that are hazardous to the well being of the population as well as the environment are nitrates and phosphates, released from

the use of agricultural products and detergents. Nitrates can promote the growth of plant life in aquatic areas. This can be viewed as an advantage, but if left unchecked, may lead to an overgrowth in rivers and lakes, causing a phenomenon known as eutrophication (*i.e.* lack of oxygen available for animal life in these aquatic areas).[35] Therefore, developing sensors for the purpose of detecting and monitoring the quantities of these potentially hazardous anionic species is of great importance.

1.4.1 Factors Affecting the Development of Anion Sensors

The design of an anion sensor is not an easy or straightforward feat, since a number of inherent traits may hinder the development of anion sensor,[7] such as:

- **Anions have lower charge-to-radius ratio than the corresponding isoelectric cations.**
- **They may compete with the surrounding solvent molecules.**
- **They may be pH sensitive.**
- **They may form significant ion-pairs with their counter ions.**
- **They have a wide range of geometries.**

1.4.1.1 Charge-to-Radius Ratio of Anions[7]

The charge-to-radius ratio of anions are lower than that of the equivalent cations, as a result of their larger size. Table 1.1 illustrates how the anions are more diffuse in nature compared to the corresponding isoelectric cations by comparing their difference in radii. This in turn causes them to have less effective electrostatic binding interactions.

Table 1.1 Difference in the radii of typical isoelectric anions and cations (in octahedral environments).[36]

Group 1 (cations)	radius r (Å)	Group 17 (anions)	radius r (Å)	Δr (Å)
Na^+	1.16	F^-	1.19	0.03
K^+	1.52	Cl^-	1.67	0.15
Rb^+	1.66	Br^-	1.82	0.16
Cs^+	1.81	I^-	2.06	0.25

1.4.1.2 Competition between Anions and Solvent Molecules[7]

The solvent used determines the nature and strength of the host:guest interaction, and hence, it depends on the type of receptor that is incorporated in the sensor. For example, if the receptor is positively charged, then it is possible to use protic solvents, such as water and methanol. The ionic interaction between the anion and the receptor would be sufficiently strong enough to reduce the potential competition from the solvent molecules, since electrostatic interactions are generally stronger than other recognition interactions. However, if the receptor is charge neutral and the interaction is of an ion-dipole nature, then aprotic solvents would be the more ideal media.

1.4.1.3 pH Sensitivity of Anions[7]

The sensitivity of anions towards pH limits the function of a particular anion receptor such that it must be able to work in the pH window of its target anion. This is especially challenging when designing positively-charged receptors since the pH at which they remain protonated (acidic pH) may also protonate the anion. Hence, this poses less of a problem for charge-neutral receptors as they are able to work in aprotic media.

1.4.1.4 Significance of Ion-pairing[7]

The presence of ion-pairing between the anion and the counter ion also dictates the solvent in which anion binding experiments are performed. In polar solvents, the strength of ion-pairs is greatly reduced, which is advantageous for successful anion binding. Non-polar solvents, on the other hand, provide little solvation effects to the anion and hence, the ion-pairing interaction is much stronger. Therefore, the existence of ion-pairing make it more challenging to decide on the "right" receptor to use as well as the optimal conditions, especially since solvent effects are also an issue.

1.4.1.5 Geometries of Anions[7]

The geometry of the anion must also be taken into account when designing an anion sensor. These geometries provide a directional nature in the anion-receptor interaction.

Figure 1.5 shows the various geometries that can be adopted by anions. With the exception of the halides (which are spherical in shape, and hence provide no directional interaction), the directionality in the anion-receptor interaction observed in the rest of geometries offer a useful property that can be used to control the selectivity of the receptor. In addition, the incorporation of multiple receptors will enhance the selectivity of the anion-binding interaction, even in the case of the spherical halides. Preorganisation of these multiple receptors is also very important. One way to preorganise receptors for successful anion binding is by using scaffolds such as steroids,[37,38] calixpyrroles[39,40] and calixarenes.[41]

spherical	linear	trigonal planar
F^-, Cl^-, Br^-, I^-	OH^-, CN^-	CO_3^{2-}, NO_3^-, $CH_3CO_2^-$

tetrahedral	octahedral
PO_4^{3-}, SO_4^{2-}, $H_2PO_4^-$	$Fe(CN)_6^{4-}$, $Co(CN)_6^{3-}$, SiF_6^{2-}
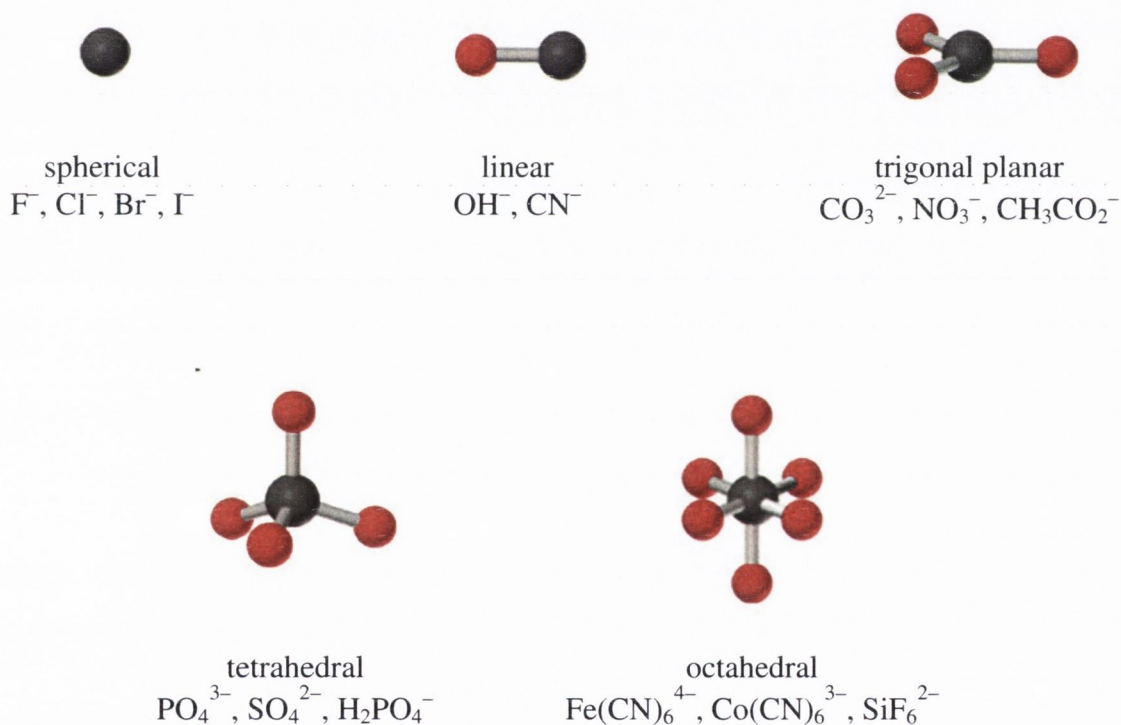
Figure 1.5 Examples of the various geometries that can be adopted by anions.

1.4.2 Types of Anion Receptors

There are two main types of anion receptors; positively-charged anion receptors and charge-neutral anion receptors.[24-27] The focus of our project is on charge-neutral ureas and thioureas as receptors for anions, and therefore, we will only briefly mention the other types of receptors (and sensors).

1.4.2.1 Positively-charged Anion Receptors

These positively-charged receptors can be either metal-coordinated receptors[42-44] or metal-free receptors. The latter includes ammonium-based,[45] guanidinium-based,[46] amidinium-based,[47] sapphyrins[48-50] and pyridinium-based[51-53] receptors.

1.4.2.2 Charge-neutral Anion Receptors

Ureas (and thioureas),[54,20] amides (and thioamides),[54-57] pyrroles,[58] calix[4]pyrroles,[39,59,60] and boranes[17,61,62] are some examples of charge-neutral anion receptors. The anion receptors which are of interest to our project are ureas and thioureas, and as such, all examples of anion receptors and sensors mentioned henceforth will only be of these types.

1.5   Ureas and Thioureas

Ureas and thioureas, also known as carbamides and thiocarbamides respectively, are a class of chemical compounds sharing the same functional group RHN-CX-NHR (where X = O and S respectively) based on a carbonyl or thiocarbonyl group located between two organic amine residues (Figure 1.6).

Figure 1.6 Molecular structures of urea (left) and thiourea (right) moieties.

The main characteristic of these derivatives, which makes them rather multipurpose compounds, is the acidity of the NH protons. Ureas and thioureas have shown potential as prodrugs,[63] anti-tumour binding agents,[64] switches,[65] supramolecular polymers,[66] peptidomimetics,[67] membrane transporters,[68-70] organocatalysts,[71-77] organogelators[78-86] and last but not least, anion receptors.[87-93] The following subsections will touch briefly on the development of ureas and thioureas as organocatalysts and organogelators, followed by a more detailed overview of urea- and thiourea-based anion receptors and sensors.

1.5.1 Ureas and Thioureas as Anion Receptors

Ureas and thioureas are known to have an extremely good binding ability towards certain anions due to the acidic nature of their amino protons. The anions form hydrogen bonds with these protons and since the hydrogen bond has a directional character, it allows the urea and thiourea to be more selective in its binding. Generally, thiourea derivatives have generally stronger anion-binding ability than that of the corresponding ureas due to the higher acidity of the thiourea derivatives. Hence, the ability to accurately adjust the acidity of the urea or thiourea NH protons would be extremely useful, as it allows for higher specificity towards one particular anion over another. The following sections will summarise several examples of urea- and thiourea-based fluorescent and colorimetric anion sensors (as these are the two main types of signal reporting mechanisms used in our sensors) reported over the last decade and thus, explain our interest in employing such functionalities as receptors for anion sensing.

1.6 Fluorescent Anion Sensors

There has been a variety of metal-free fluorescent anion sensors developed to date, as fluorescence spectroscopy is one of the more sensitive methods of detection used in chemosensors. Several reviews have been published, bringing together the many aspects of these types of chemosensors.[20,94-97]

Using the classical model of a fluorescent sensor as developed by de Silva illustrated previously in Figure 1.2 (*i.e. fluorophore-spacer-receptor*), there is a plethora of fluorophores that can be incorporated into an anion sensor for successful fluorescent sensing. These include many fused aromatic hydrocarbon rings such as naphthalene,[98-102] anthracene[60,89,103] and pyrene,[92,104,105] as well as heterocyclic aromatic rings such as fluorescein,[106,107] naphthalimide[20,108] and coumarin.[109-111]

1.6.1 Urea- and Thiourea-based Fluorescent Anion Sensors

In this section, a short review exemplifying some non-metallated charge-neutral urea- and thiourea-based fluorescent anion sensors will be given.

The naphthalene moiety is one of the commonly used fluorophores in anion sensing. In 1999, Wu and co-workers synthesised three anion-binding derivatives **14** - **16**, which contained three, two and one naphthyl urea moieties, respectively.[112]
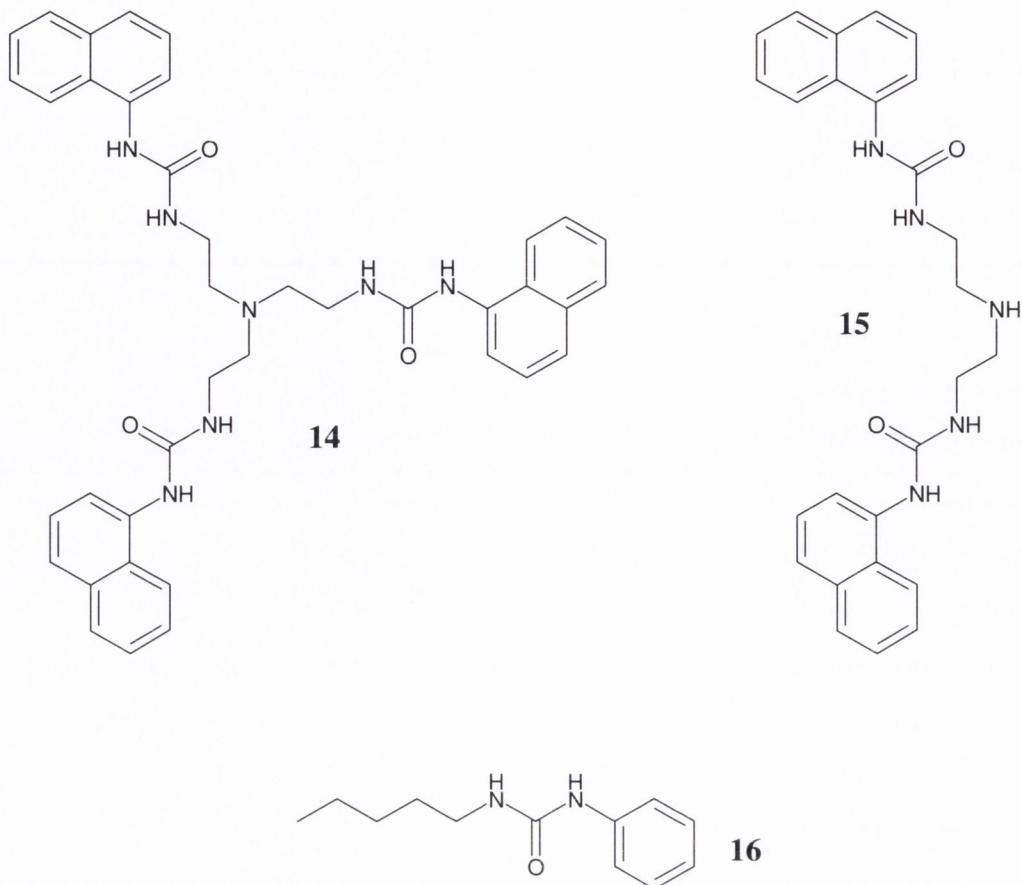
Compounds **14** - **16** exhibit strong fluorescence emission in DMF, with quantum yields (Φ_f) of 0.215, 0.493 and 0.333 respectively. It should be noted that the quantum yield of **14** is much less than the other two compounds, even though it has the most number of naphthyl rings. This is attributed to the strong intramolecular π-π* interaction between the fluorophores, resulting in an excimer emission, thus concomitantly reducing the monomer emission of **14**. Also, the tertiary amine group is a strong electron donor which may quench the emission *via* photo-induced electron transfer (PET).

Upon the addition of $H_2PO_4^-$ to a DMF solution of **14** (1×10^{-5} M), an enhancement in the fluorescent intensity was observed (Φ_f = 0.299). The same behaviour was seen for the binding of HSO_4^- but to a much smaller extent (Φ_f = 0.222), and there was no significant change in the presence of Br^- and I^- (Φ_f = 0.215 and 0.216 respectively). In the case of **15** and **16**, no significant change was observed for all the selected anions. The authors attributed the increase in fluorescence observed upon the binding of $H_2PO_4^-$ and HSO_4^- to the protonation of tertiary amine of **14** by the anions themselves, since $H_2PO_4^-$ and HSO_4^- show acidic properties. This resulted in the inhibition of the PET process, thus enhancing the fluorescence.

16

Wu *et al.* later developed further fluorescent sensors containing the napthylurea moiety, one of which was a *bis*-system (displaying PET) designed to bind *bis*-carboxylates, with a selectivity dependent on the chain length of these target anions.[98]

Another example of a fluorescent sensor (**17**) able to recognise carboxylates was designed by Valiyaveetil and co-workers.[113] In this study, they also performed aromatic carboxylate binding studies with the sensor developed by Wu *et al.* **14**.

17 n = 5
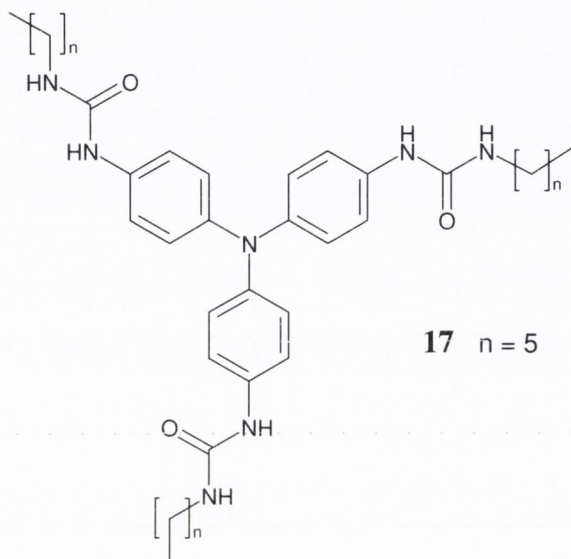
Both **14** and **17** showed significant fluorescence quenching in the presence of terephthalate and trimesylate in THF, but no changes were observed when titrated with small anions such as halides, acetate, nitrate and dihydrogenphosphate (which may be due to the large cavity and the rigidity of the receptor. Compound **17** bound to both aromatic carboxylates with a 1:1 host:guest stoichiometry.

More recently, Costero and co-workers synthesised the naphthylthiourea-based fluorescent sensor **18** for *bis*-carboxylate recognition.[114]

18
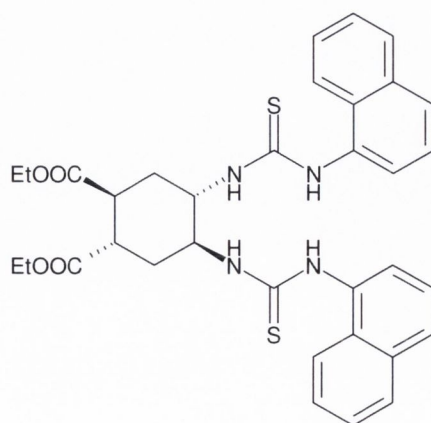
Sensor **18** displayed a selectivity for maleate over fumarate in both DMSO and DMSO/H_2O (9.5:0.5, v/v) media. However, the extent of the selectivity in the latter solvent media was considerably smaller than that in DMSO. Upon maleate recognition, an excimer emission band centred at *ca.* 500 nm was observed after one equivalent, while this new band was not seen in the presence of fumarate.
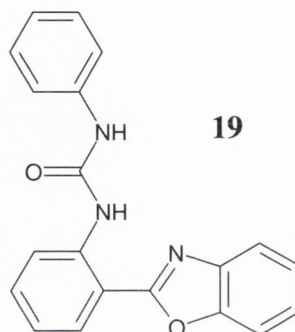
The final example in this section is that of the 2-phenyl benzoxazole-based urea derivative **19** synthesised by Peng and co-workers.[115] This sensor undergoes excited-state intramolecular proton transfer (ESIPT) as seen in Figure 1.6, resulting in the observed fluorescence character. Compound **19** showed good anion-binding affinity for F^- and AcO^- (pK_a in H_2O = 3 and 4.7 respectively), the former due to the deprotonation and the latter through hydrogen-bonding interactions between the anion and the receptor. These changes were due to the ESIPT being inhibited as a result of strong anion coordination. Hence, $H_2PO_4^-$ was not basic enough to cause this inhibition process.
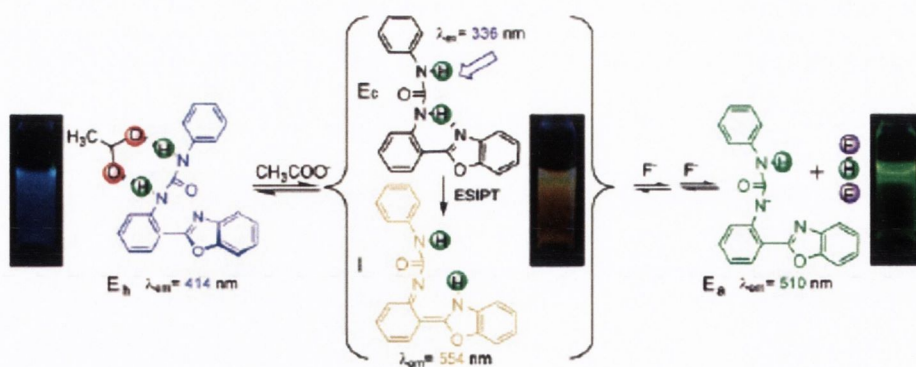
Figure 1.6 The changes in the fluorescence of **19** (1.0×10^{-5} M) observed for the recognition of AcO^- (left) and F^- (right). The fluorescence of **19** is due to the ESIPT upon excitation.[115]
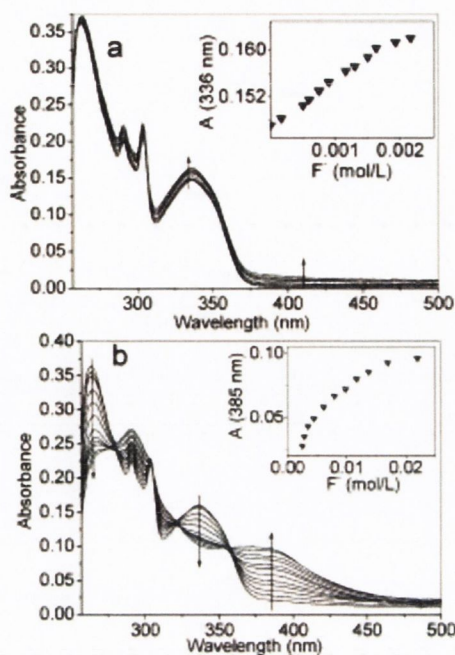
Figure 1.7 Changes in the absorption spectra for **19** (1.0×10^{-5} M) with the addition of TBA-fluoride: (a) from 0 to 0.002 M, (b) from 0.002 to 0.022 M.[115]

Figure 1.7 shows the two-step process for the recognition of fluoride by **19**, where Figure 1.7(a) shows the hydrogen-bonding interaction of fluoride with the urea moiety, producing minimal disturbance to the dipole associated with the charge-transfer transition of the sensor. Further additions of fluoride then led to the changes observed in Figure 1.7(b), with the decrease of the absorption bands at 336 nm and the growth of a new band at 385 nm. There was also an isosbestic point located at 322 nm. These observations were further supported by the analysis of the ^{1}H NMR binding experiments. The binding of AcO$^-$ only showed the presence of the 1:1 complexation process due to the lack of a new band, as in F$^-$. The new absorption is the cause of the yellow colour of the host solution with F$^-$ (Figure 1.8).
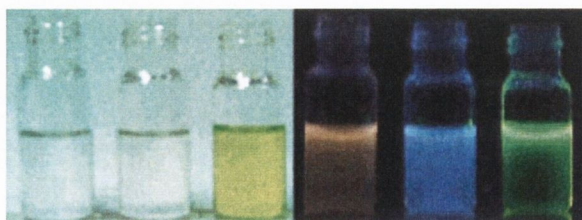
Figure 1.8 Colour and fluorescence changes of **19** in DMSO (2.0×10^{-4} M) after addition of 0.01 M solutions of anions. From left to right: **19**, **19** + AcO$^-$, **19** + F$^-$, **19** (emission), **19** + AcO$^-$ (emission), **19** + F$^-$ (emission). (Note: emission of last three solutions observed when irradiated at 365 nm using a UV lamp)[115]

This additional characteristic behaviour displayed by **19** in the presence of F⁻ shows the sensor's potential as a colorimetric sensor. Therefore, examples of such anion receptors will be presented in the following sections.

1.7 Colorimetric Anion Sensors

Visual discrimination is an attractive means of qualitative detection in anion sensors, and with the help of modern technology, it is also possible to quantitatively determine the extent of this detection. There are many examples of metal-free chromogenic anion-binding agents, and several publications regarding this type of sensor are available for reference.[14,15,20,97,94,116]

Many of the heterocyclic aromatic rings used in fluorescent anion sensing (*e.g.* napthalimide, coumarin) have been used as chromophores in colorimetric sensors.[110,117,118] Other chromophores used include nitro-substituted phenyl rings (especially *p*-nitrophenyl),[119,120] anthraquinone,[121] naphthoquinone,[122] oxazine[123] and azophenol.[124]

1.7.1 Urea- and Thiourea-based Colorimetric Anion Sensors

This particular section will present several examples of colorimetric anion sensors which utilise ureas and thioureas as the anion-binding motifs. However, some of the chromogenic sensors developed do not only perform anion recognition *via* hydrogen-bonding interactions between the receptor site and the target anion, but also, through the deprotonation of the urea (or thiourea) NH protons by the anion itself. Therefore, the examples of hydrogen-bonding-induced colorimetric anion sensors will be discussed first, followed by those of deprotonation-induced sensors.
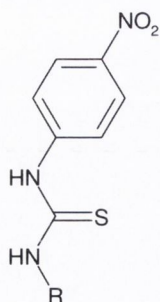
20 R = *p*-nitrophenyl
21 R = CH₃

In 2001, Kato *et al.* prepared a thiourea-based chromoionophore **20** that was conjugated with two *p*-nitrophenyl units.[125] Comparative studies performed between this compound and a previously prepared thiourea sensor (with only one *p*-nitrophenyl

moiety) **21**[119] showed that both complex stability and optical responses could be significantly improved by having two electron-withdrawing *p*-nitrophenyl units instead of one. Compound **20** was found to bind the anions exclusively *via* the formation of hydrogen bonds in H_2O/MeCN (0.1:9.9, v/v) with 1:1 host:guest stoichiometry, and it produced a colour change from colourless to yellow with a selectivity of $AcO^- > H_2PO_4^- > Cl^- \gg ClO_4^-$.

In the same year, Lee and co-workers developed colorimetric azophenolurea-based porphyrin anion sensors which showed selective colour changes for the complexation of F^-, $H_2PO_4^-$ and AcO^- in that order.[126] The azophenol group adds another effective hydrogen-bonding site for anions.

22 X = O
23 X = S
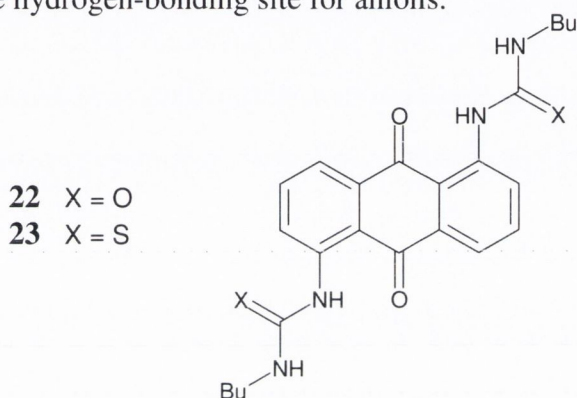
Martinez-Mànez *et al.* incorporated the anthraquinone chromophore into their urea- and thiourea-based anion sensors (**22** and **23** respectively) to act as the signalling unit.[121] Upon addition of fluoride, both sensors experienced a colour change from orange to brown in DMSO, while only **23** changes colour in MeCN. Fluoride is known to be the most basic of the selected anions (halides and oxoanions) and hence, has the strongest interaction, resulting in the significant colour change. There was no reported evidence of any deprotonation occurring upon fluoride recognition.

24 X = O
25 X = S
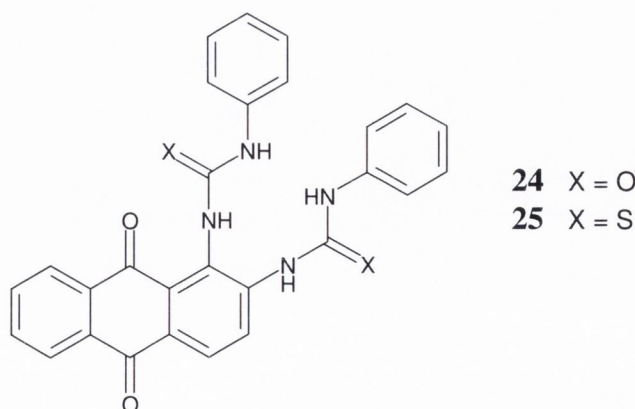
Later, Das and co-workers also developed colorimetric fluoride ion sensors, urea **24** and thiourea **25** using anthraquinone as the chromogenic signalling unit.[127]

However, in this case, the anthraquinone moiety was also acting as a kind of scaffold for preorganising the two urea (or thiourea) receptor arms. This preoganised structure as well as the multiple receptor sites may lead to an enhancement in the selectivity of the sensors towards the various halides. Conversely, neither sensor showed any affinity to chloride, bromide and iodide when titrated in DMSO/MeCN (1:9, v/v). Compound **24** also did not show any colour change upon addition of fluoride, even after being left standing in solution for 24 hours. Interestingly, when the solution was heated at 60 °C, its yellow colour turned red immediately. As for **25**, this colour change occurred at room temperature.

In order to understand this behaviour, *ab initio* quantum chemical calculations were performed, which provided a computational model of **24**, showing intramolecular hydrogen bonding of both urea moieties, hence preventing the complexation of fluoride at room temp. Thiourea **25** on the other hand was shown to have much weaker intramolecular interactions, and therefore, allowing the thiourea moieties to align themself with more ease for fluoride complexation.

In 2003, a naphthalene derivative **26** synthesised by Cho *et al.*, which contains urea groups at the 1- and 8-positions of naphthalene.[99] Binding studies showed that this sensor was 40 times more selective towards F^- than Cl^- and unique absorption and fluorescence peaks were observed in the presence of F^-. They later developed a further five analogues of this naphthalene-based anion sensor (*e.g.* **27** and **28**), of which four were reported to show interesting colour changes upon complexation with fluoride.[128] Compound **27** showed visual selectivity for fluoride as the colour of DMSO solution went from pale yellow to red. No colour change was observed for any of the other selected anions (chloride, dihydrogenphosphate, benzoate and acetate). The same colour change was observed for the fluoride binding of **28**, but also, in the presence of the other anions, the pale yellow colour deepened. The colour changes could be attributed to the charge-transfer interactions between the electron-rich donor units and the electron-deficient *p*-nitrophenyl and azophenyl moieties. Stable hydrogen-bonded complexes were formed upon anion binding, thus increasing the electron density within the system, which led to the enhancement of the charge-transfer interactions.
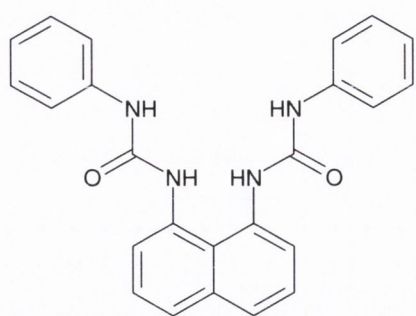
26
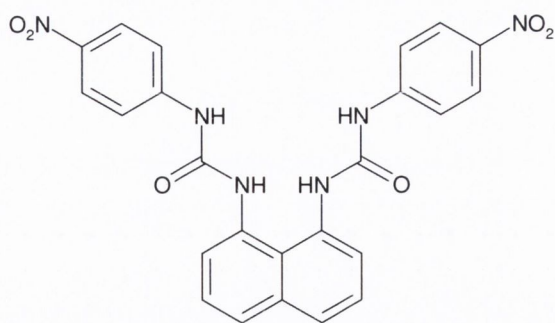
27
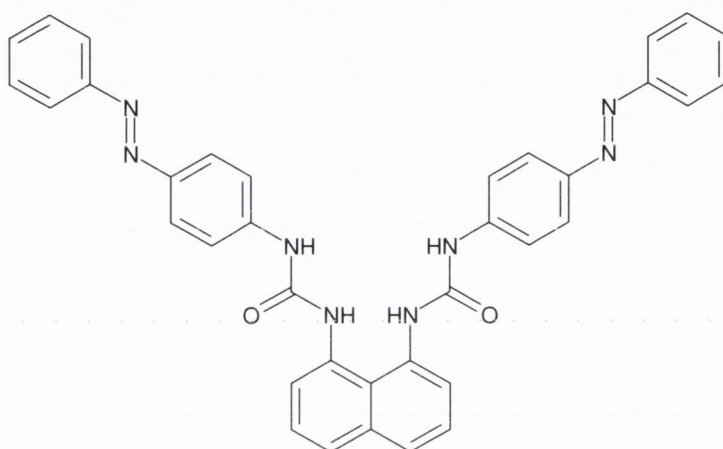
28

Wu *et al.* developed a charge-neutral phenanthroline-based *bis*-thiourea anion receptor **29**, which bound to fluoride with a 1:2 host:guest stoichiometry, while it forms a 1:1 complex with either AcO⁻ or $H_2PO_4^-$.[129]
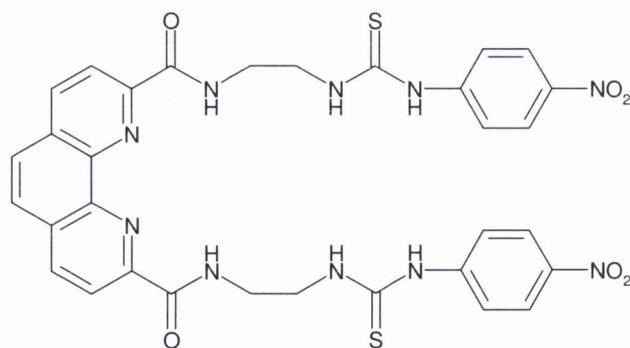
29

Upon fluoride complexation, the colour change went from light yellow to blood red. The original yellow colour may be due to charge-transfer interactions between the electron-deficient *p*-nitrophenyl ring and the electron-rich thiourea donor units. When

an anion was bound to the receptor, the interactions were enhanced leading to the red shift into the visible region, giving the red colour of the complex solution. The order of selectivity of **29** was such that $F^- \gg AcO^-$, $H_2PO_4^- \gg Cl^-$, Br^-, I^-. The smaller size and higher basicity of the fluoride ion may explain the high binding affinity of **29** to this particular halide ion. ^1H NMR spectroscopy gave evidence that this receptor experienced intramolecular interactions between the amide NH and the phenanthroline N atom, which upon anion binding, were broken and intermolecular hydrogen bonds form between the anion and the NH protons.

Fabbrizzi and co-workers incorporated the urea and thiourea moieties into the majority of their anion sensors, many of which showed chromogenic anion-binding behaviour due to the deprotonation process.[87,116,118,130,131] However, they have developed a *bis*-thiourea appended to a pyridine receptor (**30**), which illustrates "naked-eye" recognition of fluoride without the presence of a defined chromophore.[130]

30

(a)   (b)
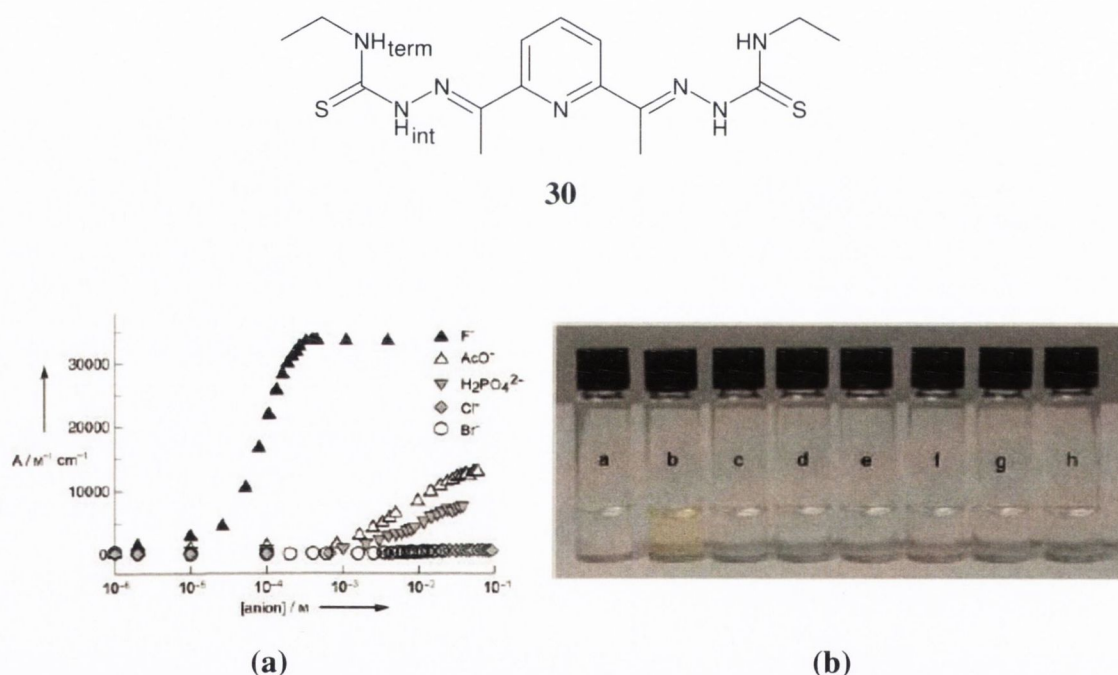
Figure 1.9 (a) Titrations of solutions of **30** in MeCN with standard solutions of selected anions (A = molar absorbance at 412 nm). Therefore, the bis-thiourea sensor is selective for fluoride. No evidence of deprotonation; (b) Visual features of the interactions of anions with **30** in MeCN (a: **30** (1×10^{-4} M); b: **30**.F^- (1 equiv.); c: **30**.Cl^- (10 equiv.); d: **30**.Br^- (10 equiv.); e: **30**.I^- (10 equiv.); f: **30**.AcO^- (10 equiv.); g: **30**.$H_2PO_4^-$ (10 equiv.); h: **30**.HSO_4^- (10 equiv.)).[130]

Spectroscopic titrations of 10^{-5} M solutions of **30** with TBA salts of various anions were performed in MeCN. It was observed that **30** was selective for fluoride (log β for fluoride = 4.14 ± 0.02) over the other anions tested, as illustrated in Figure

1.9(a). The absorption spectra showed the absorption band at 324 nm decreasing with the concomitant appearance of a new band at 412 nm. The presence of isosbestic points indicated that only two species (free host and 1:1 host:guest complex) were present at equilibrium. Upon fluoride binding, the colour of the MeCN solution of **30** went from colourless to yellow (Figure 1.9(b)), which was due to enhancement of π delocalisation and π–π* transition was shifted from the UV to the visible (*i.e.* energy of the transition is reduced). Interestingly, ^{1}H NMR titrations in CDCl$_3$ showed that only the internal NH protons (NH$_{int}$) were interacting with the fluoride ion, since the chemical shifts of the terminal NH protons (NH$_{term}$) only experienced a trivial perturbation in comparison to those of the NH$_{int}$ protons. Optimisation calculations by a semiempirical method (AM1) supported this observation (Figure 1.10). The *anti*-conformation observed in this calculated structure was also seen in the solid state analysis of the receptor.
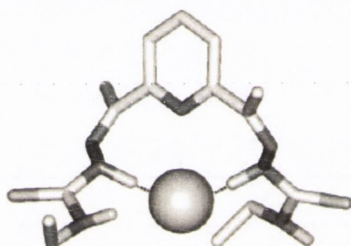
Figure 1.10 Optimised structure of the **30**.F⁻ adduct, as calculated by AM1, showing the interactions of the anion with the internal NH protons.[130]

In 2005, Tian and Liu synthesised the hydrazine-based naphthalimide thiourea **31** for anion-binding studies.[132]
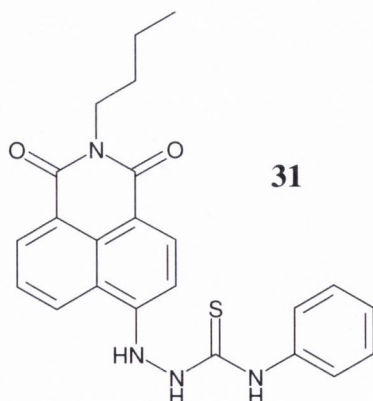
This colorimetric sensor **31** was similar to those developed by Gunnlaugsson and co-workers that same year,[117] in which an ethyl group is attached to the N atom within the naphthalimide ring instead of a butyl chain. However, unlike observed in

Gunnlaugsson's work, there was no report of a deprotonation process occurring in the presence of fluoride. The colour change attributed to fluoride complexation was said to be due to the enhancement of the ICT which was induced by the PET between the thiourea-bound fluoride and the NH proton at the 4-position of the ring (formation of the two new bands at 335 and 555 nm). The anion-binding studies done in both MeCN and DMSO, and in both solvent media, the colour changed from yellow to purple. This chromogenic response was almost reversible, as the addition of protic solvents such as methanol or water turned the colour back to yellow. The fluorescence emission of **31** occured in the region between 450 and 650 nm in MeCN. Fluoride binding caused the emission to be reduced in intensity, as the binding process triggered the PET between the thiourea and fluorophore, thus affecting the physical properties of the ICT fluorophore due to its effect on the efficiency of charge transfer.[133,134]

The examples of colorimetric anion sensors given thus far do not report any evidence of the deprotonation of the urea or thiourea NH protons, especially in the case of fluoride recognition. It only became apparent in the past few years that there may be another process other than host:guest complexation occurring in the presence of such basic anions. The next few examples will be of urea- and thiourea-based anion receptors and sensors which show visual discrimination due to the deprotonation process.

In 2003, Gunnlaugsson and co-workers synthesised naphthalimide-based colorimetric anion sensors **32 - 33**,[135] which later prompted Pfeffer *et al.* to synthesise **34**.[136]

32   R = H
33   R = CF$_3$

34
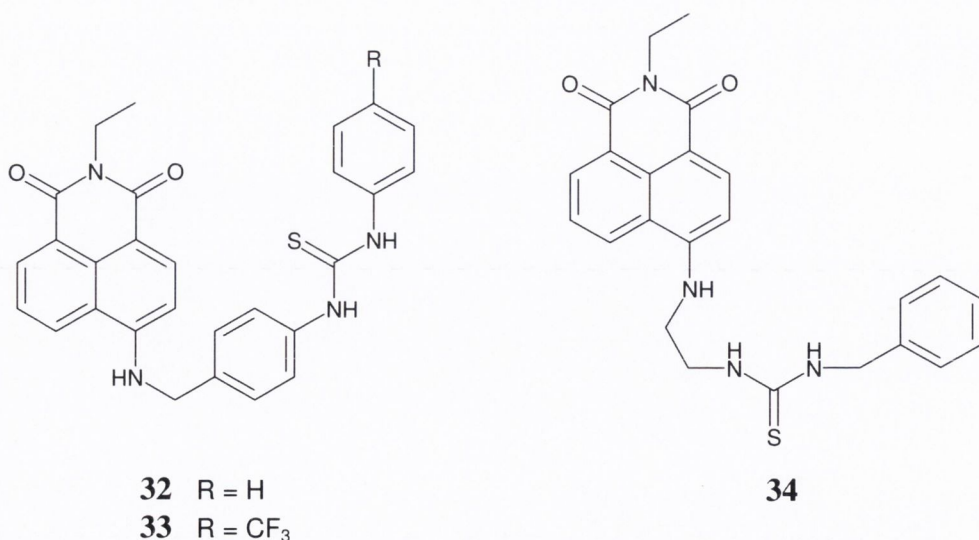
Compounds **32** - **33** were shown to give substantial spectroscopic changes when bound to anions, including a "naked-eye" effect (*i.e.* the colour changed from yellow/green to red/purple) in the presence of high concentrations of fluoride. Since the amino proton at the 4-position is significantly basic, it would provide another point of interaction to a suitable anionic guest (*e.g.* $H_2PO_4^-$), and hence, it would enhance the complexation process. However, this compound is quite rigid due to the aromatic rings on either side of the thiourea receptor. Therefore, **32** was modified by replacing the phenyl methylene spacer with an ethyl chain and placing a methylene group between the thiourea moiety and the aromatic ring at the very far end (*i.e.* compound **34**).

^1H NMR binding studies of **34** with a series of simple anions in DMSO were carried out. The binding of fluoride by **34** showed similar behaviour to that observed for **32** and **33**, including the formation of the triplet at *ca.* 16 ppm, accompanied by the same colour changes. The appearance of this new signal in the ^1H NMR spectrum was attributed to the formation of a bifluoride ion (HF_2^-) due to the deprotonation of one of the NH protons after the addition of *ca.* 2 equivalents of F^-. Although no colour changes were observed upon the recognition of AcO^- and $H_2PO_4^-$, there was significant perturbation in the chemical shifts of the thiourea NH protons, indicating successful binding. However, the involvement of the naphthalimidic amino proton in the complexation process was only observed in the presence of $H_2PO_4^-$. For **32**, the stability constant for AcO^- complexation was significantly higher than that for $H_2PO_4^-$, while the stability constants for the binding of these two anions by **34** were very similar to one another, further supporting the argument that the 4-amino naphthalimidic proton is cooperatively binding $H_2PO_4^-$. The lack of significant spectroscopic changes may be due to the fact that the longer spacer in **34** as well as the lack of an aromatic ring reduces the PET quenching efficiency. Later, luminescent anion-binding studies were performed on these sensors as well as other analogues of **32** and **33**,[108] and will be discussed later in Section 1.8.

Pfeffer and co-workers have also synthesised [3]polynorbornane-based *bis*-thiourea derivatives as cleft-like receptors for anions.[91] These receptors showed good affinity for dihydrogenphosphate and hydrogenpyrophosphate with host:guest stoichiometries of 1:1 and 2:1 respectively. The derivative which contained *p*-nitrophenyl groups showed striking colour changes from light yellow to red upon fluoride binding, again due to the deprotonation of the NH protons of the thiourea motifs in the presence of *ca.* 2 equivalents of the anion.

Coumarin-based thiourea receptors **35** and **36** were recently developed by Ghosh and Adhikari.[110] These receptors showed potential as colorimetric and fluorescent sensors upon anion recognition.

35 R = NO$_2$
36 R = H

a   b   c
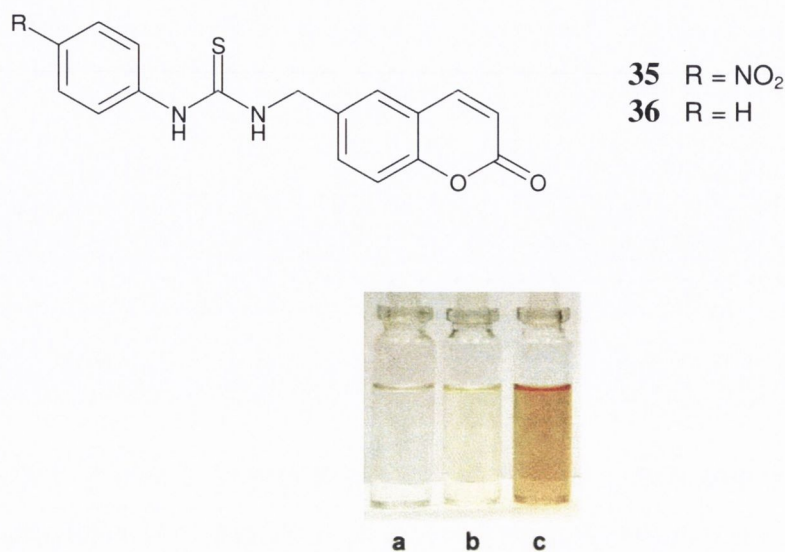
Figure 1.11 Colour changes observed: (a) receptor **35**; (b) **35** in the presence of benzoate; (c) **35** in presence of fluoride.[110]

Binding abilities of **35** and **36** were investigated by observing their behaviour towards fluoride, bromide, iodide, hydrogen sulphate and benzoate using fluorescence, UV-vis (in MeCN with 0.08%DMSO) and ^{1}H NMR (in CDCl$_3$) spectroscopies. **35** showed significant changes in the absorption and fluorescence spectra upon fluoride complexation with a visual change in colour from almost colourless to yellow brown as well as a quenching in its fluorescence (Figure 1.11). With benzoate, the changes were not as clear, and the colour change went from almost colourless to a light green colour. Both anions were bound in a 1:1 fashion. No significant changes were observed in the absorption, fluorescence and visual colour of the receptor solution with the other anions.

Receptor **36** also showed similar behaviour in its fluorescence upon the addition of either fluoride or benzoate but the changes were not as significant. There was also no colour change observed upon anion recognition. The stability constants β calculated for the binding of benzoate by both receptors were larger (β_{35} = 2.02 × 10^4 M^{-1} and β_{36} = 1.04 × 10^4 M^{-1}) than those for the binding of fluoride (β_{35} = 5.78 × 10^3 M^{-1} and β_{36} = 2.26 × 10^3 M^{-1}). This was due to the strong hydrogen bonding interactions of the benzoate to the thiourea receptor rather than the deprotonation process observed for fluoride recognition.

The non-covalent interactions in the complexation of benzoate increased the efficiency of the PET process due to the increase in the reduction potential of the thiourea moiety after anion recognition. As a result, the rate of electron transfer from the HOMO of the thiourea-anion complex to the excited state of the coumarin moiety was increased. Since the deprotonated species was more electron-rich compared to the hydrogen-bonded complex the PET process was activated more efficiently, thus showing a greater quenching.

Kim *et al.* synthesised *bis*-(*p*-nitrophenyl)-based **37** and **38** as colorimetric sensors for biologically important anions such as acetate, fluoride, chloride and bromide.[137] These sensors are analogous to a urea compound previously studied by Gale and co-workers, which showed excellent selectivity for carboxylates in solution.[138,139]

37 X = O
38 X = S
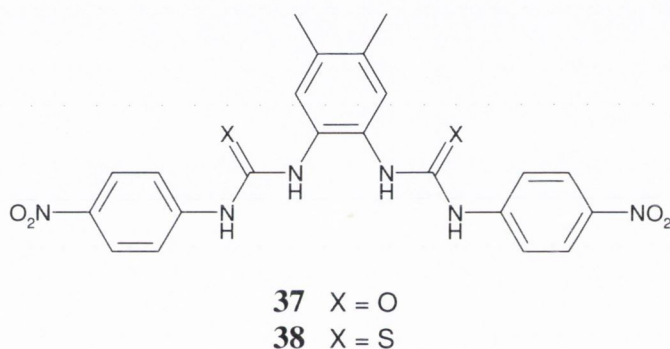
Sensors **37** and **38** were selective for fluoride among the halides tested and this was evident in the ^{1}H NMR titration experiments, where the NH signals disappeared in the presence of one equivalent amount of fluoride (due to broadening of the signals), whereas they were shifted a small amount downfield in the presence of chloride and bromide. They both showed a colour change in the presence of F⁻ at room temperature. UV-vis spectroscopy showed that the thiourea experienced much more drastic changes in the absorption spectrum compared to its urea analogue upon fluoride binding, indicating that the NH protons of the thiourea are more acidic in nature than those of the urea sensor. When titrated with acetate, **38** again showed more significant changes compared to **37** in the absorption spectra, and this was also observed visually from the colour change experienced by the thiourea and the lack of that change in the solution of the urea analogue (Figure 1.12).

The colour change observed was a gradual change from almost colourless to an orange-red colour. Thus, in terms of visual discrimination, it can be stated that urea **37** showed selectivity towards fluoride among the anions. This colour change was ascribed

to the deprotonation of the NH protons adjacent to the *p*-nitrophenyl rings. This deprotonation was observed in both sensors in the presence of fluoride, but only the NH protons of **38** were acidic enough to be deprotonated by acetate. Further supporting data was provided by *ab initio* calculations of the binding modes of these sensors with the different anions.
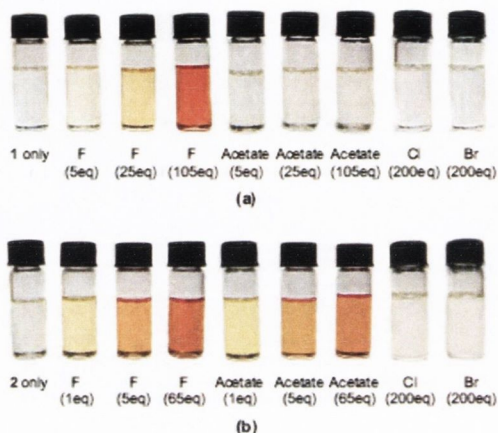
Figure 1.12 Colour changes observed for: (a) **37**, and (b) **38**, in DMSO upon the addition of anions as their TBA salts at room temperature. All solutions of both sensors are 2.5×10^{-5} M in concentration.[137]

Gale and co-workers had previously reported that the deprotonation of the urea and thiourea NH protons may occur in the presence of anions other than fluoride for a number of pyrrolylamidourea- and thiourea-based anion receptors they developed (**39 - 45**).[88,140] In the anion-binding experiments performed in DMSO, all but receptor **39** showed significant changes in the ^{1}H NMR and absorption spectra upon recognition of the anions (fluoride, acetate, benzoate, dihydrogenphosphate).
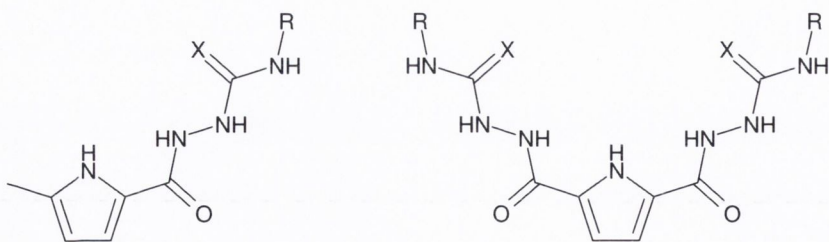
39 X = O, R = phenyl
40 X = O, R = 4-nitrophenyl
41 X = S, R = phenyl
42 X = S, R = 4-nitrophenyl

43 X = O, R = phenyl
44 X = O, R = 4-nitrophenyl
45 X = O, R = 3,5-dinitrophenyl

The presence of the 4-nitro substituent as in **40** resulted in the increase in acidity of the urea moiety (compared to that in **39**) and hence, changes were observed in the [1]H

NMR spectrum upon anion complexation. In the absorption spectrum, there was an increase in the absorbance centred at 450 nm with the formation of two isosbestic points at *ca.* 280 and 340 nm (Figure 1.13(a)), due to the 1:1 host:guest complexation. A colour change from almost colourless to dark yellow was also observed (Figure 1.14). Similar binding studies were performed on the thiourea analogues **41** and **42** which showed significant changes in the absorption spectra with new bands forming at 330 and 430 nm respectively (Figure 1.13(b)). However, the binding curves of these receptors were very steep which prevented the calculation of the stability constants. In **42**, there was a colour change from yellow to red (Figure 1.14).

(a) (b)
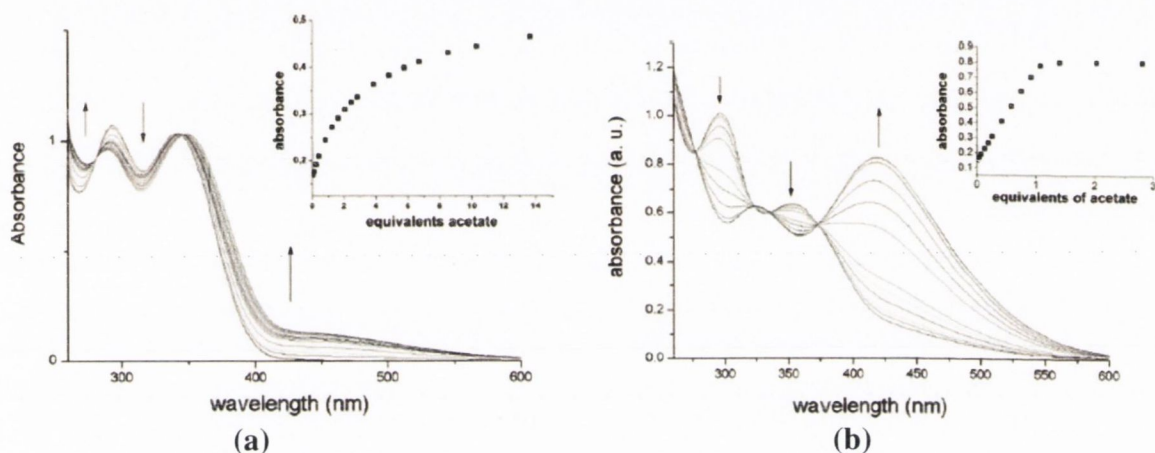
Figure 1.13 (a) UV-vis spectrophotometric titration of **40** with AcO⁻ in DMSO at 25 °C. Inset: increase in absorbance at 390 nm *vs* equivalents of AcO⁻; (b) UV-vis spectrophotometric titration of **42** with AcO⁻ in DMSO at 25 °C. Inset: increase in absorbance at 450 nm *vs* equivalents of AcO⁻.[88]

Figure 1.14 DMSO solutions (2×10^{-3} M) of **40** (left set) and **42** (right set). From left to right in each group: solution of receptor, followed by solutions with receptor in the presence of 1 equiv. of fluoride, acetate, benzoate and dihdyrogenphosphate.[88]

Figure 1.15 shows part of the solid state structure of the deprotonated species of **42**. The ¹H NMR spectrum of the crystals formed was the same as the spectrum of the receptor titrated with the other anions after one equivalent was added, which suggests that the red colour was the result of the deprotonation of the NH proton and not a

formation of a 1:1 complex. Other research groups have observed this deprotonation process with fluoride, as previously discussed.[87,111,135] However, it is usually due to the addition of two equivalents of fluoride, thus forming a bifluoride ion (HF_2^-). Therefore, this is one of the few cases where one equivalent of fluoride deprotonates an NH proton of the thiourea motif.
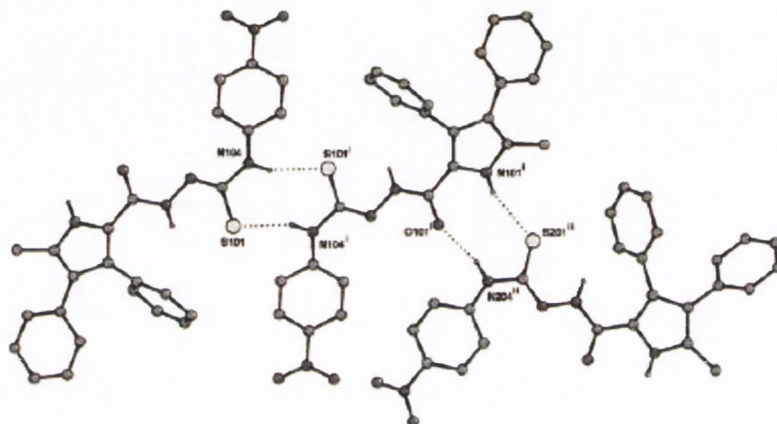
Figure 1.15 Part of the hydrogen-bonded chain defined by the deprotonated amidothiourea (**42** - H$^+$)$^-$ in the solid state.[88]

Anion binding studies performed on the disubstituted receptors **43** - **45** all showed an enhancement in their binding affinities compared to their monosubstituted analogues, but they were not selective in their binding of the selected anions. Other urea- and thiourea-based anion receptors and sensors developed by Gale *et al.* include macrocyclic amidoureas[141] and acridinone-based derivatives.[142]
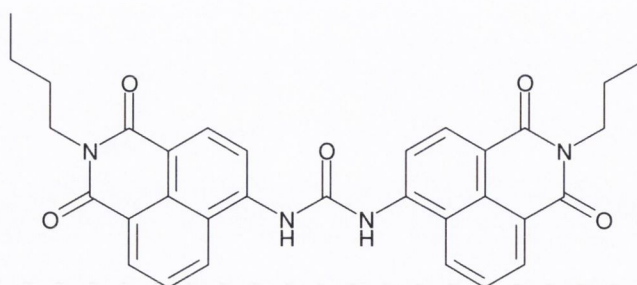
46

Another interesting phenomenon regarding the deprotonation process was reported by Fabbrizzi *et al.*, which was observed in the *bis*-naphthalimide-based urea derivative **46**.[118] This sensor was found to undergo the deprotonation of at least one NH proton in the presence of the selected anions. Previously, in their nitrophenyl-based compounds, the urea receptor only undergoes deprotonation in the presence of

fluoride.[143] However, when replaced by the naphthalimide chromophore, the acidity of the NH protons increased, thus enhancing the tendency for deprotonation. Furthermore, fluoride now deprotonates both NH protons, as does hydroxide.

In DMSO, the 1:2 host:guest complex formed in the presence of fluoride gives a yellow colour, but after the deprotonation of one NH proton (upon the addition of a few equivalents of excess fluoride), the colour changed to red. Further deprotonation of the second NH proton (upon the addition of up to 10 equivalents) leads to a blue colour. Further studies were performed on **46** to observe its binding abilities towards sodium salts of certain bile acids (*e.g.* sodium cholate),[144] in which a yellow-to-red colour change occurred due to the deprotonation of one of the NH protons.
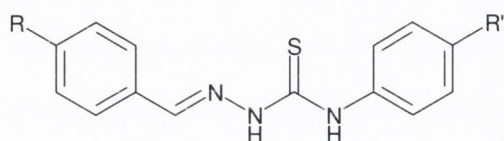
47

Fabbrizzi and co-workers also developed a family of analogues of the neutral (benzylideneamino)thiourea **47** (where R and R' can be either H, F, NO$_2$, CF$_3$, OCH$_3$) to act as anion receptors.[87] However, their interaction with oxoanions in MeCN (studied *via* spectroscopic methods) showed their potential as chromogenic binding agents, due to the deprotonation of the thiourea NH protons. Interestingly, it was observed that the deprotonation tended to occur at the NH proton nearer to the R' substituent, and the binding is scarely affected by the nature of the R substituent.

This review on the various urea- and thiourea-based fluorogenic and chromogenic anion receptors and sensors demonstrate the numerous possibilities for further research as well as in their practical applications. Thus, we will go on to present previous work carried out by the Gunnlaugsson research group on such anion receptors and sensors, followed by the objectives of this research project.

1.8 Urea- and Thiourea-based Fluorescent and Colorimetric Anion Sensors by Gunnlaugsson *et al.*

The development of charge-neutral anion receptors and sensors is one of the areas of interest within the Gunnlaugsson research group.[20,95] The others include the development of lanthanide-based luminescent sensors (for anion and cation sensing as well as RNA hydrolysis) and anti-cancer drug research.

The anthracene moiety is one of the two fluorophores utilised by Gunnlaugsson and co-workers, which was initially incorporated into their cation-binding molecules.[145,146] It was following the success of this fluorophore in such chemosensors that it was then incorporated into anion sensors to act as the signal reporter.[89,103,134,147,148] The other fluorophore, naphthalimide, was first used with the intention of fluorescent anion sensing, but it was also found to show potential for chromogenic anion recognition.[117,133,135,136] Gunnlaugsson *et al.* also incorporated the naphthalimide moiety into their cation sensors[149] and hydrogels.[150] Recently, the *p*-nitrophenyl moiety was used in the calix[4]arene-based colorimetric anion sensors developed by Gunnlaugsson and co-workers.[120]

48 X = S; R = H
49 X = S; R = CF$_3$
50 X = O; R = H
51 X = O; R = CF$_3$
52 X = O; R = F

53

54

55

56 X = S; R = H
57 X = S; R = CF$_3$
58 X = O; R = CF$_3$
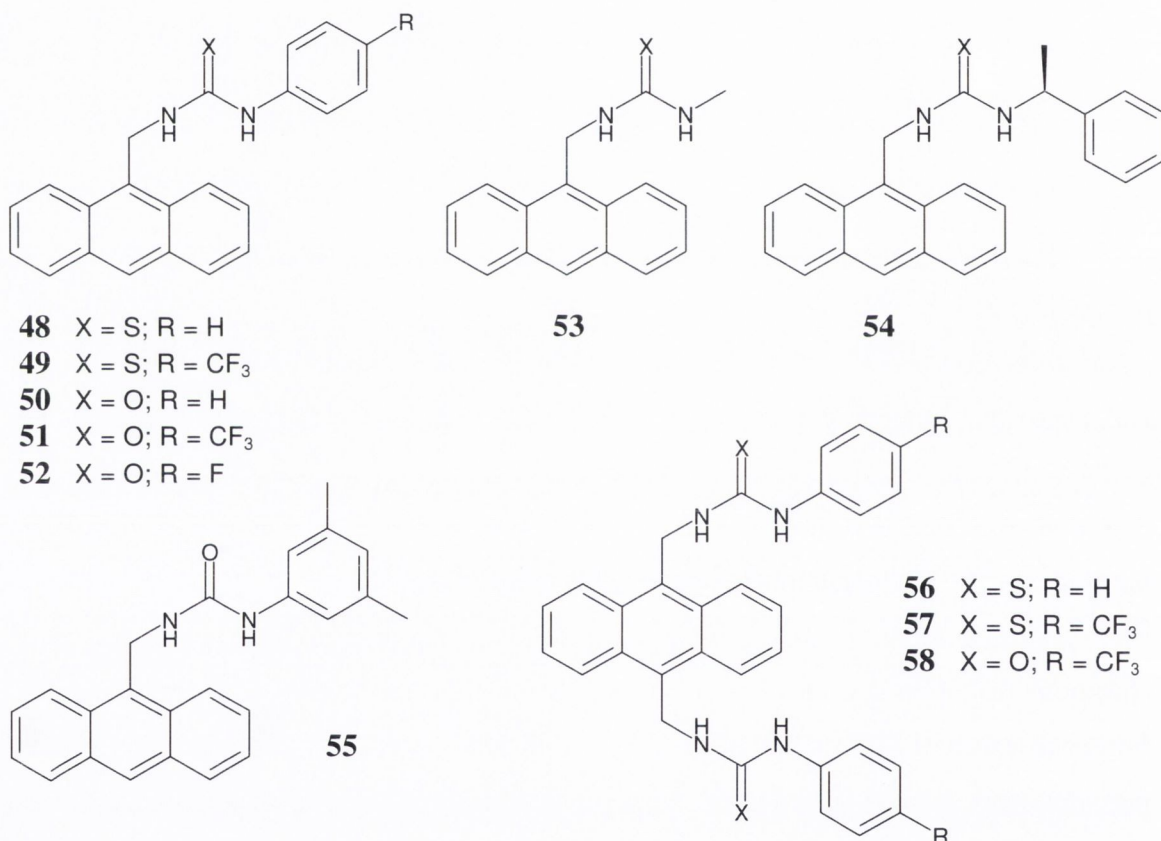
Compounds **48** - **58** are the urea- and thiourea-based fluorescent PET anion sensors developed by Gunnlaugsson and co-workers to date, all of which show fluorescent emission quenching upon anion recognition (*i.e.* "switch-off" sensors). Sensors **56** - **58** contain two receptor sites, while the rest are all mono-systems. The *bis*-systems were designed such that they would bind anionic guests such as *bis*-carboxylates and pyrophosphate. They were found to bind pyrophosphate and malonate

with 1:1 host:guest stoichiometries, while glutarate was bound in a ~1:2 stoichiometry, except in the case of the urea-based *bis*-system **58**. Compound **54** was incorporated with a chiral centre in order to enabled it to selectively bind to chiral guests such as *N*-protected amino acids. However, when titrated with tetrabutylammonium (TBA) salts of D- and L-alanine in DMSO, efficient selectivity was not successfully achieved, despite the significant quenching of the fluorescent emission of the sensor.

The most recent anion-binding study was performed on the urea-based mono-systems, **50** - **52** and **55**.[148] Again, these sensors showed enhanced quenching of fluorescence upon anion recognition. The binding of these compounds to fluoride resulted in the deprotonation of the urea NH protons after the initial hydrogen-binding interactions of the complex, forming the bifluoride ion (HF_2^-), a phenomenon observed initially in the anion sensing work by both the Gunnlaugsson and Gale research groups.

32	R = H
33	R = CF_3
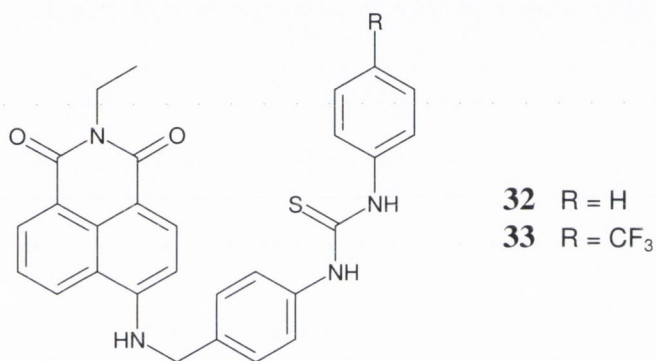
In 2003, Gunnlaugsson *et al.* reported the potential of compounds **32** and **33** as potential fluorescent and colorimetric sensors.[133] Both sensors showed significant PET quenching in their fluorescence spectra upon complexation with AcO^-, $H_2PO_4^-$ and F^-. The emission was fully quenched in the case of fluoride complexation, with concomitant change in colour from yellow/green to red/purple (visible to the naked eye), which might be a result of the deprotonation of the amino proton at the 4-position of the naphthalimide ring.

The following compounds **59** - **62** were synthesised in order to further study the colorimetric changes (yellow/green to red/purple) observed in the previously studied naphthalimido-thiourea anion sensor upon complexation of fluoride.[135] It was hypothesised that this colour change was due to the deprotonation of the acidic amino proton at the 4-position of the napthalimide ring.

59 n = 1, m = 3
60 n = m = 3

61

62 R = NH$_2$
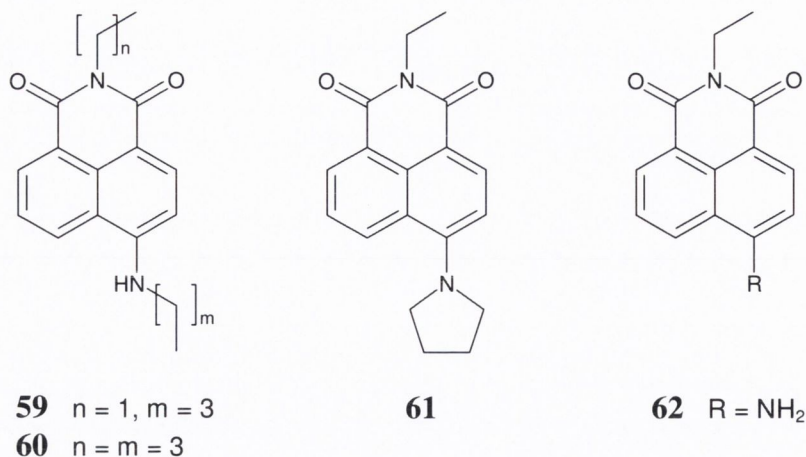
The absorption spectrum of **59** consisted of a strong absorption band at 446 nm and a second band at 287 nm (n→π* transition). The changes in the absorption spectrum of **59** in DMSO upon addition of TBA salts of AcO⁻, H$_2$PO$_4$⁻, F⁻, Cl⁻ and Br⁻ were investigated. Changes in the absorption bands were only observed in the presence of fluoride, where both bands were significantly reduced with concomitant formation of two new bands at *ca.* 535 and 341 nm and three isosbestic points at *ca.* 480, 380 and 300 nm. Compounds **60** and **62** showed similar behaviour in their complexation of fluoride. When fluoride was added to **61**, no changes were observed in the absorption spectrum. Since this compound lacks the acidic amino proton, the results indicate that the spectroscopic changes are due to the deprotonation of the amino proton, rather than hydrogen bonding.

¹H NMR titrations were also performed on **59** with the same anions. Again, only fluoride caused significant spectral changes. The changes only reached saturation at 2 equivalents of fluoride and a new triplet peak was observed at *ca.* 16 ppm. It was proposed that HF$_2$⁻ was being formed. Sensor **59** was also found to be able to fix atmospheric CO$_2$ in the presence of fluoride. Crystals of the 1:1 adduct formed between **59** and hydrogencarbonate (due to the fixation of CO$_2$) were obtained (Figure 1.16), which were suitable for a single crystal X-ray diffraction experiment.
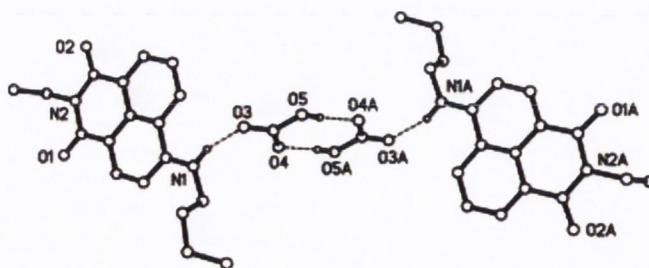
Figure 1.16 The structure of the 1:1 adduct formed between **59** and HCO$_3$⁻, showing the H-bonded pairs. TBA cations were omitted for clarity.[135]

Quinn *et al.* reported a process by which bifluoride and hydrogencarbonate was formed when melts of partially hydrated tetraalkylammonium salts of fluoride absorb CO_2.[151] The presence of water was required as it caused the fluoride to be more basic through hydrogen bonding, enhancing its reaction with CO_2. This report supports the deprotonation hypothesis. However, since **59** was also able to fix CO_2 in the presence TBA-hydroxide, there was a possibility that the CO_2 fixation process may be due to the deprotonated amine, rather than the fluoride.

63   R = CH_3
64   R = CF_3
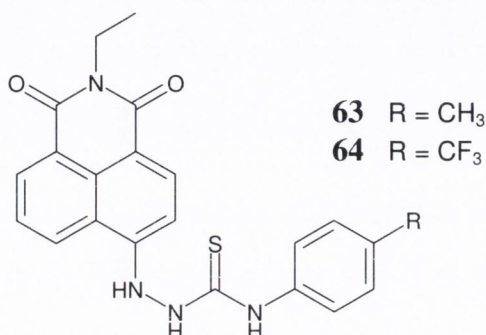
Hydrazine-based naphthalimide thiourea derivatives **63** and **64** were designed and synthesised for colorimetric anion sensing.[117] Binding studies were performed in polar solvents such as DMSO and EtOH. In DMSO, both sensors showed colour changes in the presence of AcO^-, $H_2PO_4^-$ and F^-, from bright yellow to purple. However, in the case of fluoride binding, an excess of the anion causes further colour changes and the formation of the bifluoride ion (due to deprotonation of the NH proton). The binding studies showed similar behaviour as in DMSO when performed in EtOH. They also showed very little affinity for Cl^- and Br^- in the solvent media used.

Gunnlaugsson and co-workers also developed the first example of an amidourea-based 1,3-disubstituted calix[4]arene-based colorimetic anion sensor **65** (containing *p*-nitrophenyl groups adjacent to the urea moieties at the lower rim).[120] The amidourea arm was previously utilised by Gale *et al.* in their pyrrole-based derivatives, as discussed in Section 1.7.[88] The calix[4]arene-based compound experienced a hypsochromic shift of the absorption band at 336 nm upon the recognition of AcO^-, $H_2PO_4^-$ and F^-, but only the latter showed concomitant colour changes from pale yellow to purple. The sensing of hydrogenpyrophosphate initially also show the red shift of the band at 336 nm. However, at higher concentrations, the red-shift band (now at 377 nm) gave way to two new bands at 346 and 384 nm. Also, the shoulder previously observed at 500 nm became a full transition.

65
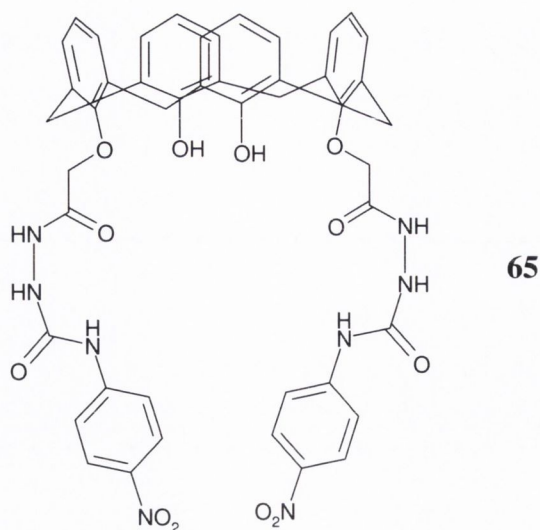
Recently, a urea-functionalised phenanthroline (*phen*) sensor **66** was synthesised, which gave rise to significant PET quenching of fluorescence in MeCN upon complexation with AcO⁻, $H_2PO_4^-$ and F⁻ with 1:1 host:guest stoichiometry.[152] In the presence of Cl⁻, the fluorescence was instead enhanced with stoichiometries of 1:1 and 1:2 being observed from the non-linear regression data analysis. It was proposed that fluorescence enhancement in Cl⁻ binding was due to the PET quenching effect from the trifluoro-*p*-tolyl group to the *phen* fluorophore being reduced, as a result of the bound spherical anion "blocking" the pathway of the electron transfer. Hence, **66** showed potential as a selective fluorescent sensor for Cl⁻.

66
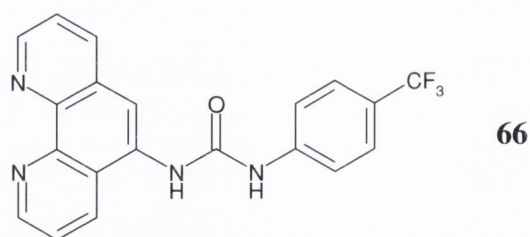
This section summarised some of the anion sensing work carried out in the Gunnlaugsson group thus far. The aims of this project will now be described in the following section.

1.9   Project Objectives

With the vast anthology of anion sensors in mind, we set out to develop more sensors incorporating the same basic ideas to hopefully lead to potential uses. Hence, this project concentrates mainly on developing the anion sensing work previously

carried out by Gunnlaugsson and co-workers, as well as designing new urea- and thiourea-based anion sensors, to be used as not only fluorescent and colorimetric sensors, but also as potential chiral anion sensors.

In order to understand the binding of ureas and thioureas to anions, the anion binding abilities of 36 *bis*-phenyl urea and thiourea receptors towards a selection of anions (AcO⁻, $H_2PO_4^-$, F⁻, Cl⁻, Br⁻) will be studied in DMSO-d_6 using ¹H NMR spectroscopy (as discussed later in Chapter 2). These *bis*-phenyl urea and thiourea receptors will contain various substitutents (*i.e.* H, CH_3, F, CF_3) at the 2- and 4-position of the aromatic rings by electron-donating groups. The data collected from the ¹H NMR titrations will then be treated using a non-linear least-squares regression program (WinEQNMR[12]) in order to calculate the stability constants (log β) for the complex formation of these receptors with each anionic guest. These log β values were then analysed in terms of the electronic nature of the substituent and its location on the phenyl ring, as well as the type of binding site (either urea or thiourea) present. Following on from this study, we would then proceed to further develop new urea- and thiourea-based compounds in order to achieve sensors ideal for use in pharmaceutical and industrial areas.

Chapter 3 discusses the synthesis of polyaromatic thiourea-based fluorescent anion sensors (some of which are ditopic in nature) for the physical evaluation of their anion binding abilities in DMSO or DMSO-d_6 using various techniques (such as ¹H NMR, fluorescence and circular dichroism (CD) spectroscopies). Two types of fluorophore utilised in these sensors are anthracene and naphthalene. These sensors will be titrated with the selected anions, but in the case of the ditopic anthracene-based sensors, *bis*-carboxylates will also be used. The data obtained from the ¹H NMR and fluorescence binding studies will then analysed using SPECFIT/32™ to obtain log β values for the binding processes in order to compare the anion binding abilities of such sensors. Data collected from the CD titrations, however, will only be interpreted *via* graphical analysis.

Finally, in Chapter 4, the synthesis and anion binding studies of hydrazine-based naphthalimide colorimetric sensors (consisting of either a urea or thiourea moiety) will be discussed. Binding experiments with putative anions will be carried out in DMSO or DMSO-d_6 out on the urea-based compounds using ¹H NMR, UV-vis and fluorescence spectroscopies, while in the case of the thiourea derivative, a more competitive solvent (*i.e.* EtOH/H_2O (50:50)) will be used. The stability constants for the anion binding

processes will calculated from the data collected from ^{1}H NMR titrations using WinEQNMR,[12] while the data obtained from the absorption and fluorescence titrations will be analysed using SPECFIT/32™.

The project objectives are outlined below in the flowchart illustrated in Figure 1.17.
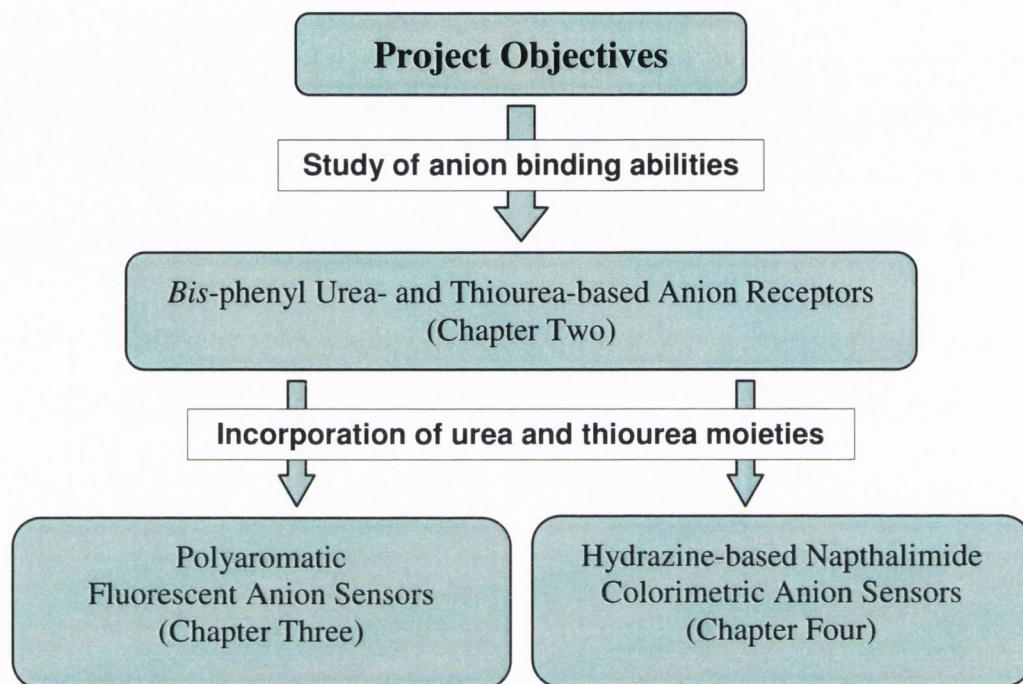
Figure 1.17 Flowchart outlining the project objectives.

2.1 Introduction

Ureas and thioureas are among the commonly used charge-neutral receptors in the field of anion sensing.[26,27,54,95,116,153-156] In particular, several anion binding studies performed on phenyl-based ureas and thioureas have been previously reported.[157-161] Wilcox and co-workers reported a systemic study done on the substituent effects towards zwitterion recognition by various arylurea and thiourea derivatives consisting of at least one phenyl group.[159] Their aim was to devise a method that could be used as a predictor based on the Hammett equation (Appendix 7.1.1 (a)) for the anion binding affinity of their receptors.

This was achieved by studying the electronic effects of electron-withdrawing and electron-donating groups (strategically substituted at either the *para* or *meta* positions of the phenyl rings) on the hydrogen bonding abilities of the anion binding moieties.

Several studies on ureas and thioureas have also been performed by Hamilton and collaborators, not only for purposes of anion recognition,[157,162] but also organogelation.[79-81]

67 X = O
68 X = S
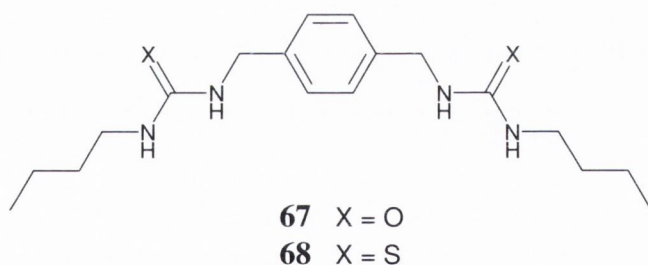
One report describes, through calorimetric studies, the thermodynamic effects of various solvents on the *bis*-carboxylate complexation of *bis*-receptors such as **67** and **68**.[162] The calorimetric analysis of the anion binding process of these receptors shows that it is exothermic in DMSO. However, upon addition of more polar solvents such as methanol and water, this binding becomes more endothermic. Therefore, binding of *bis*-carboxylate guests becomes weaker as the polarity and hydrogen bonding ability of the solvent increases. These studies have proved beneficial in the development of urea- and thiourea-based receptors for use in anion sensors, by furthering our understanding of the anion binding processes undergone by such receptors. Nevertheless, there still exist an opportunity to explore the nature of the anion recognition further, particularly from the point of investigating steric contributions from *o*- and *p*-substituted *bis*-aryl

derivatives as well as the effect of electron-donating and withdrawing groups have on the hydrogen bonding ability and structure of such receptors. The aim of this chapter is to attempt to explore both aspects.

2.2   Objectives

This project aims to study the mechanism of the binding process of *bis*-phenyl ureas and thioureas with various simple anions (such as oxoanions and halides), and thus establish a better understanding of the binding abilities of these charge-neutral *bis*-phenyl receptors as well as the host:guest stoichiometries of the anion recognition. Our study will look at the electronic and steric effects of three different substituents towards the anion binding affinities of these receptors.

With this in mind, 36 *bis*-phenyl urea and thiourea derivatives were designed, whereby each derivative differs from the other by the substituents located at the *ortho* and *para* positions of the phenyl rings. These substituents are either electron-donating (*e.g.* CH_3) or electron-withdrawing (*e.g.* F or CF_3) in nature.

We first synthesised, purified and fully characterised the above 36 compounds. This was then followed by binding studies of these receptors with various anions (acetate, dihydrogenphosphate, fluoride, choride and bromide) monitored by ^{1}H NMR spectroscopic titrations in deuterated DMSO (DMSO-d_6). The stability constants (log β) were calculated from the ^{1}H NMR titration data collected using the NMR data fitting program, WinEQNMR.[12] It was hoped that this exercise would result in the formulation of "rules" that could be applied with the aim of achieving both enhanced selectivity as well as sensitivity for the recognition of anions by such *bis*-aryl ureas and thioureas. This may be achieved by analysing the log β values obtained such that trends may be postulated about the effect that the different substituents and their positions on the phenyl rings have towards the anion binding abilities of such receptors, and hence, potentially providing the ability of "fine-tuning" the binding site for optimal anion recognition.

2.3   Synthesis of Urea- and Thiourea-based Anion Receptors 69 - 104

The synthesis of these receptors involves a nucleophilic addition between either an isocyanate or isothiocyanate and the corresponding aniline in anhydrous chloroform at room temperature under inert atmosphere (Scheme 2.1).
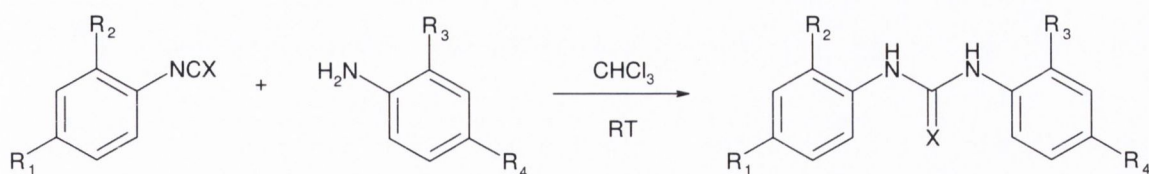
Scheme 2.1 General scheme for the formation of urea (X = O) or thiourea (X = S).

The resulting ureas or thioureas were obtained as white, off-white or pale purple solids in a reasonably pure form either *via* precipitation or extraction with chloroform with reasonably good yields. It is noteworthy that the yields for the ureas (80 - 90%) were generally much higher than those for the thioureas (20 - 40%), as ureas tend to precipitate out of the reaction with more ease. The mechanism of this reaction is a nucleophilic attack of the carbon atom on the carbonyl (or thiocarbonyl) group by the lone pair of the amino group.[163] Table 2.1 indicates the different substituents on the phenyl groups of the 36 receptors synthesised, which are based on the above parent structure (Figure 2.1).
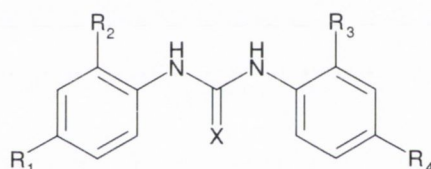
Figure 2.1 Parent structure of *bis*-phenyl urea and thiourea anion receptors.

Table 2.1 *Bis*-phenyl ureas and thioureas with varying substituents. (*unsuccessful syntheses)

Urea (X = O)	Thiourea (X = S)	R_1	R_2	R_3	R_4
69	70	H	H	H	H
71	72	H	H	H	CH_3
73	74	H	H	H	F
75	76	H	H	H	CF_3
77	78	H	H	F	F
79	80	F	H	H	F
81	82	F	H	H	CH_3
83	84	F	H	H	CF_3
85	86	F	H	F	F
87	88	CF_3	H	H	CH_3
89	90	CF_3	H	H	CF_3
91	92	CF_3	H	F	F

93	94	F	F	H	CH$_3$
95	96	F	F	F	F
97	98	CH$_3$	H	H	CH$_3$
99	100	H	F	F	H
101	102	H	CF$_3$	CF$_3$	H
*	103	H	CH$_3$	CH$_3$	H
104	*	CH$_3$	CH$_3$	CH$_3$	CH$_3$

2.3.1   Characterisation of 69 - 104

Several trends in the characterisation of the above ureas and thioureas were observed. For instance, in the ^{1}H NMR spectrum (400 MHz, DMSO-d_6), the chemical shifts of NH protons of the urea receptors were generally located between 8.0 - 9.0 ppm, whereas those of the thioureas were located between 9.5 - 11.0 ppm due to the thiourea NH protons being more deshielded (as shown for the most simplest *bis*-aryl derivatives, **69** and **70**, in Figure 2.2). This characteristic NMR property is due to the differences in the predominance of the two possible resonance forms of such functional groups. Further explanation of this phenomenon may be found in Appendix 7.1.1 (b).
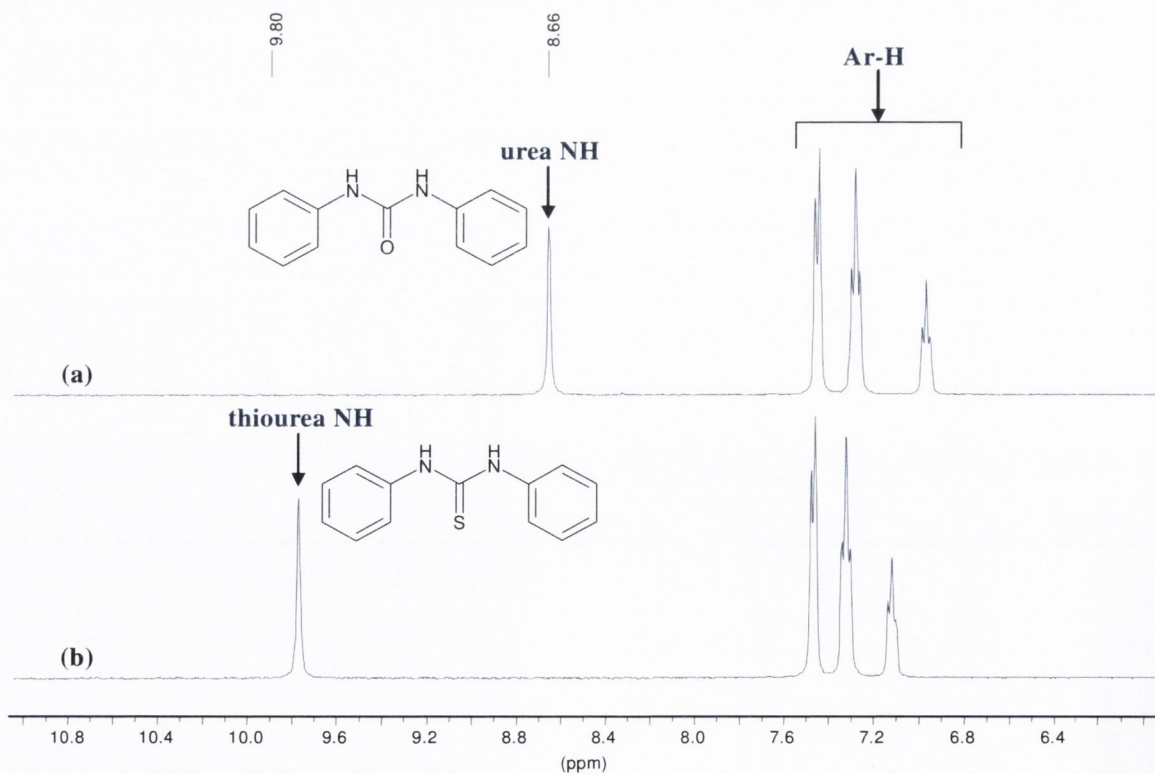
Figure 2.2 ^{1}H NMR (400 MHz, DMSO-d$_6$) spectra of (a) bis-phenyl urea **69**, and (b) bis-phenyl thiourea **70**.

The receptors containing fluorine atoms showed splitting of the chemical shifts observed in the ^{13}C NMR spectra, as ^{19}F has a spin of ½ and hence, the splitting pattern observed is similar to that in ^{1}H NMR spectroscopy (*e.g.* if a carbon atom is coupled to one fluorine, then a doublet is obtained). Figure 2.3 shows the ^{13}C NMR (100 MHz, DMSO-d_6) spectrum of 1,3-*bis*-(2-trifluoromethylphenyl)urea **101,** where the splitting due to the coupling effect of the fluorine atoms can be clearly observed. Due to the presence of three fluorine atoms in the trifluoromethyl substituent, the chemical shift of the quaternary carbon at 123.9 ppm is split into a quartet with a coupling constant $J_{C\text{-}F}$ of 271.1 Hz (denoted by ❶). Such large coupling constants are typically observed in short-range C-F coupling interactions.[164]
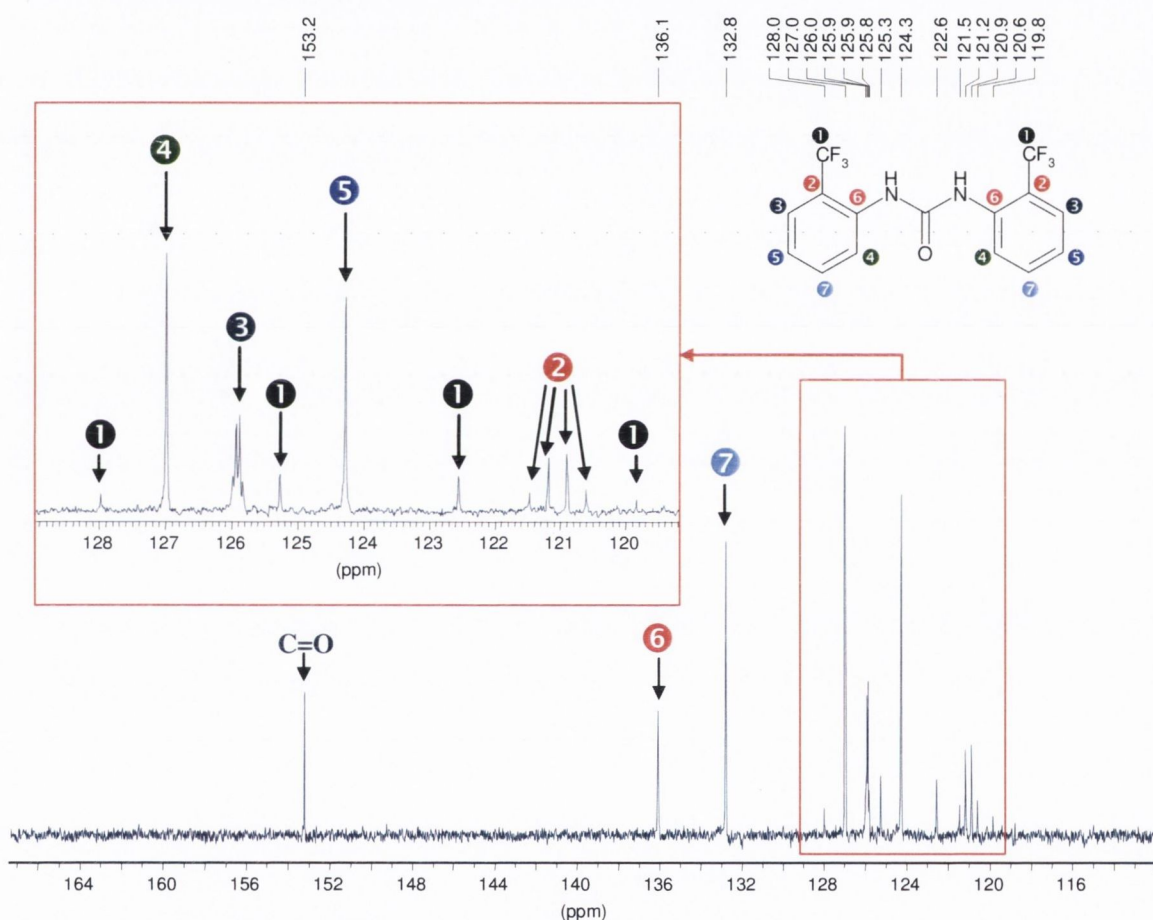
Figure 2.3 ^{13}C NMR (100 MHz, DMSO-d_6) spectrum of urea **101**.

Some of the carbons also experience long-range coupling from the fluorine atoms present in their vicinity, with a significant proportional decrease in the coupling constants with respect to distance. The quartet indicating the quaternary carbon that is immediately adjacent to the CF$_3$ group has a $J_{C\text{-}F}$ of 29.0 H (denoted by ❷), while the carbon of the aromatic CH group directly next to this carbon also experiences coupling from the fluorine atoms, but to a smaller extent with a $J_{C\text{-}F}$ of 5.2 Hz (denoted by ❸).

Singlet peaks denoted by ❹, ❺, ❻ and ❼ represent the rest of the aromatic CH and quarternary carbons, which does not experience any observable coupling with the CF_3 group.

Other characteristic physical properties such as the difference in their melting points were also apparent, where the melting points of the urea receptors were found to be between 230-270 °C, while those of the thioureas were between 120-200 °C.

2.3.2 Crystal Structure Analysis of 70, 80, 81, 84 and 89

Upon recrystallisation from $CHCl_3$, a mixture of $CHCl_3$:MeOH or a mixture of Hex:$CHCl_3$:MeOH solutions, several receptors were obtained as either needle-like or flat crystals. Receptors containing fluorophenyl groups were purple in colour while the rest formed either white or off-white crystals. The crystals obtained, which were deemed suitable for X-ray diffraction analysis, included those of ureas **81** and **89**, and thioureas **70**, **80** and **84**. The crystal structures of these receptors are shown in Figure 2.4. All hydrogen atoms (except for those of the methyl substituent, urea and thiourea) and solvent molecules have been omitted for clarity.
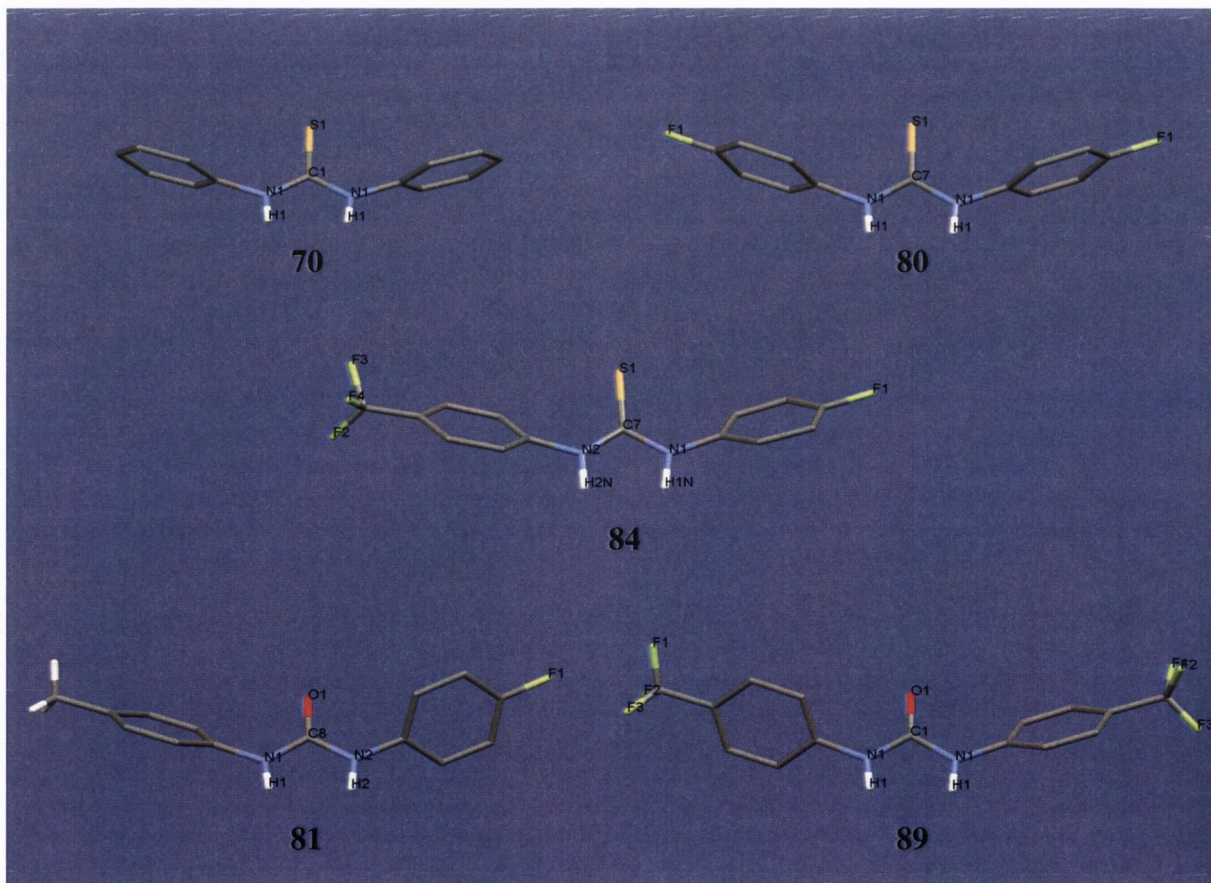
Figure 2.4 Crystal structures of **70**, **80**, **81**, **84** and **89** (see Appendices 7.1.2 - 7.1.6).

One interesting difference observed between the crystal structures of the ureas and those of the thioureas is that the phenyl groups on either side of the urea moieties are close to being orthogonal to each other, whereas those of the thiourea lie almost in the same plane. This may be the result in the difference in the electronic properties of the O and S atoms. Another possible reason for this phenomenon is the presence of the bulky methyl and trifluoromethyl substituents at the 4-position of the phenyl rings, as this orthogonal orientation is not observed in the crystal structure of **84**, which has a 4-trifluoromethylphenyl group adjacent to the thiourea moiety. Despite the structural difference observed, the NH protons of all five receptors were in the *syn* conformation (*i.e.* NH protons are facing in the same direction). Hay and co-workers carried out electronic structural calculations on urea complexes of Cl⁻, NO_3^- (nitrate) and ClO_4^- (perchlorate), which showed that the the *s-cis* form provides a more stable hydrogen bonding complex than the *s-trans* form.[165]

Table 2.2 shows the values for the N-C-X bond angles and the distances in space between the NH protons of the receptors, obtained from the X-ray diffraction analysis. The N–C–X bond angles of **70**, **80** and **89** are (122.5 ± 0.1) °, (122.7 ± 0.1) ° and (123.0 ± 0.2) ° respectively, and they are identical on either side of the urea or thiourea moiety for each compound, since **70**, **80** and **89** have symmetrical structures. The N1–C8–O1 and N2–C8–O1 bond angles of **81** are (122.9 ± 0.3) ° and (121.7 ± 0.3) ° respectively, whereas the N1–C7–S1 and N2–C7–S1 bond angles of **84** are (123.2 ± 0.5) ° and (123.4 ± 0.5) ° respectively. The N–C–O and N–C–S bond angles of these crystal structures obtained indicated that the expected approximate trigonal planar geometries of these compounds at the carbon atom between the NH protons.

Table 2.2 N-C-X bond angles and distances in space between the acidic NH protons.

Compound	R₁	X	R₄	N-C-X bond angle (°)	Distance in space between the NH protons (Å)
70	H	S	H	(122.5 ± 0.1)	2.114
80	F	S	F	(122.7 ± 0.1)	2.131
81	F	O	CH₃	$(122.9 \pm 0.3), (121.7 \pm 0.3)$	2.115
84	F	S	CF₃	$(123.2 \pm 0.5), (123.4 \pm 0.5)$	2.074
89	CF₃	O	CF₃	(123.0 ± 0.2)	2.116

The spatial distances measured between the NH protons of the urea and thiourea groups are approximately 2.115 Å. However, this distance was found to be 2.131 Å and 2.074 Å in **80** and **84** respectively. The increase in the spatial distance of **80** may be due to the presence of strongly electron-withdrawing fluorine substituents at the 4-position of the phenyl groups. This effect is, however, counteracted when at least one of the substituents is a bulky group, leading to a decrease in the NH···HN distance. The electronic structural calculations performed by Hay and co-workers on urea-anion complexes also provided further insight into the influence of geometrical factors (including NH···HN distance and linearity of NH···A bond) towards the anion binding arrangement.[165] In order to obtain optimal hydrogen bonding interactions between a urea or thiourea receptor and an anion, the NH···A bonds must be linear.[166] Therefore, the structural calculations showed that the complexation of an anion by the receptor may cause distortions in the urea geometry, as this would optimise the linearity of the NH···A bonds. Hay and co-workers also calculated that the optimal O···O distance for oxyanions in order to achieve linearity is 2.27 Å for the *syn* form of the urea.

Table 2.3 Dihedral angles (in °) of the aromatic rings with respect to the urea or thiourea moiety.

Compound	R_1	X	R_4	Dihedral angle (°) of phenyl ring containing R_1	Dihedral angle (°) of phenyl ring containing R_2
70	H	S	H	74.34	74.34
80	F	S	F	95.09	95.09
81	F	O	CH$_3$	128.26	56.35
84	F	S	CF$_3$	128.32	135.52
89	CF$_3$	O	CF$_3$	52.23	129.60

The dihedral angles obtained from the X-ray diffraction data are listed in Table 2.3. These angles were obtained from the angular difference between the plane formed by the C atom of the urea or thiourea moiety (C_X), the N atom (N_1) and the adjacent phenyl C atom (C_1), and the plane formed by N_1, C_1 and the next adjacent aromatic C atom (C_2), and will be denoted by C_X–N_1–C_1–C_2. The C_2 atom is chosen such that this aromatic carbon is facing out of the plane when the NH protons of the urea or thiourea moiety are directed downwards within the plane (Figure 2.4). The dihedral angle for

optimal conjugation of the aromatic electron density with that of the adjacent N atom is 90 °. Therefore, **80** should experience the most enhancement of the acidity of the NH protons of thiourea moiety as the $C_X–N_1–C_1–C_2$ angle is calculated to be 95.09 °. The other solid state structures have dihedral angles which are significantly different from 90 °, indicating the possibility of deconjugation of the electron density between the aromatic rings and the urea or thiourea moiety. This deconjugation, if also seen in solution, may have significant consequences towards the anion binding affinities of these receptors.

2.3.2.1 Crystal Structure Packing

The crystal structure packing of **70**, **80** and **84** are shown in Figures 2.5, 2.6 and 2.7, respectively. Due to the symmetrical structures of **70** and **80**, the packing is relatively simple with the *syn* thiourea NH protons hydrogen bonding to the S atom of the neighbouring molecule to form chains.[167] However, the crystal structure packing becomes more complex when asymmetry is introduced in the structure as well as the presence of bulky substituents on the aryl moieties, as seen in the packing of **84**. The view along the c crystallographic axis of the packed structure of **84** (Figure 2.7(b)) shows the hydrogen-bonded tapes formed as a result of a bridging effect between the partially negative fluorine atoms on the aryl moieties and the neighbouring aromatic protons, as well as the hydrogen bonding interactions of the thiourea NH protons with the S atom of the neighbouring receptor. Gale *et al.* observed the formation of hydrogen-bonded tapes in their *ortho*-phenylenediamine-based *bis*-urea cleft systems due to the bridging of such receptors by carboxylates such as terephthalate.[168]
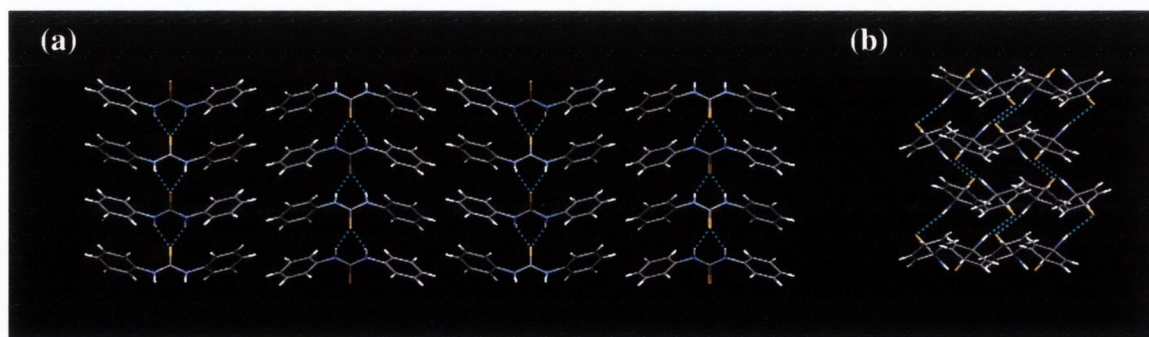
Figure 2.5 View along the (a) c crystallographic axis, and (b) b crystallographic axis of the packed structure of thiourea **70**.
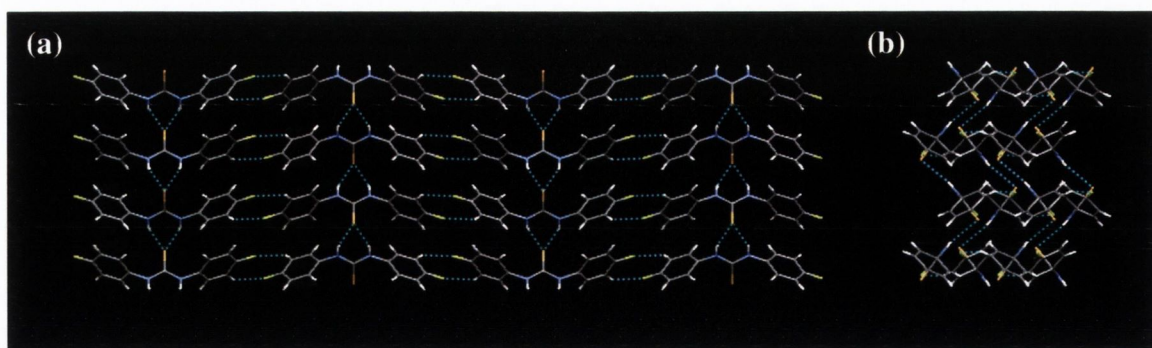
Figure 2.6 View along the (a) c crystallographic axis, and (b) b crystallographic axis of the packed structure of thiourea **80**.
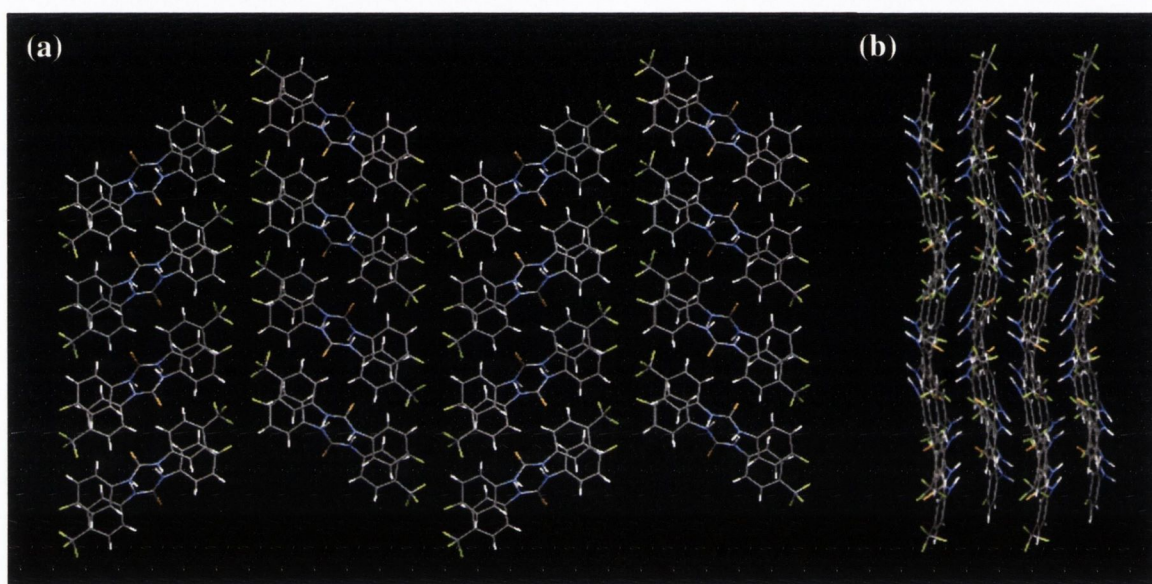
Figure 2.7 View along the (a) b crystallographic axis, and (b) c crystallographic axis of the packed structure of thiourea **84**.

In the case of ureas **81** and **89** (Figures 2.8 and 2.9 respectively), the 3-dimensional networks are further complicated by the orthogonal geometry of the phenyl groups with respect to each other. In both cases, zig-zag chains were formed, as seen in Figures 2.8(b) and 2.9(b).
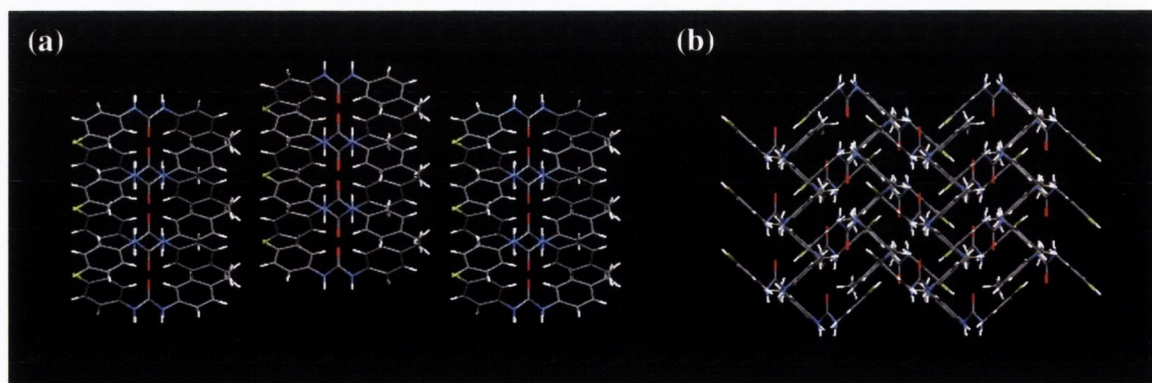
Figure 2.8 View along the (a) a crystallographic axis, and (b) c crystallographic axis of the packed structure of urea **81**.
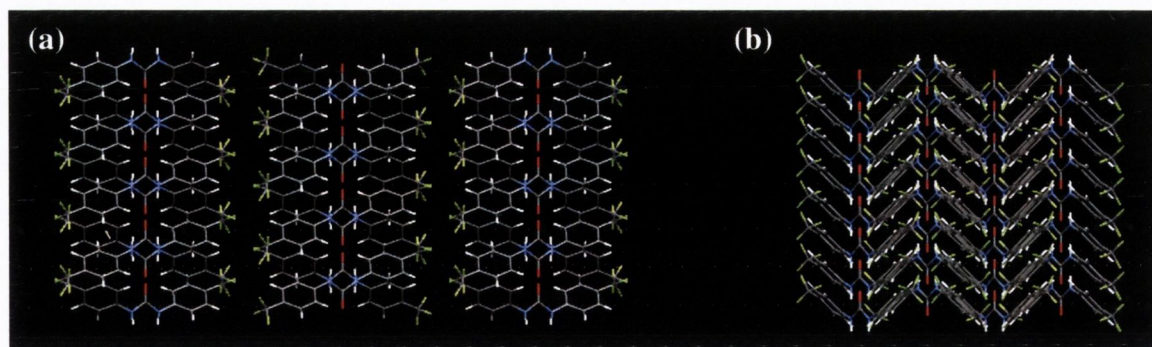
Figure 2.9 View along the (a) c crystallographic axis, and (b) a crystallographic axis of the packed structure of urea **89**.

In all the above crystal structures, the NH protons of the urea and thiourea moieties are in *s-cis* conformation. Hence, hydrogen bonds form between both the NH protons of one receptor with the O or S atom of its neighbour. *N,N'*-disubstituted ureas have the persistent nature of forming chains in this manner.[167] However, their thiourea analogues are conformationally more flexible, existing as two possible rotamers (*i.e. s-cis* and *s-trans*). Hence, two types of hydrogen-bonding arrays (*i.e.* zig-zag chains and dimers) may be formed. Custelcean and co-workers recently demonstrated that the presence of bulky organic moieties at the thiourea N atoms can result in the exclusive formation of zig-zag chains over dimers.[167] Therefore, the *ortho*-substituted aryl groups in **70**, **80** and **84** led to the *s-cis* conformation of the NH protons being favoured.

Even though these various structural differences are observed in the solid state, they may have possible effects on the anion binding affinities of the urea and thiourea active sites in solution.

2.4 ^{1}H NMR Titrations of 69 - 104 with Anions

The binding affinities of the above receptors towards various simple anions were studied using ^{1}H NMR spectroscopy. All titrations were performed at 20 °C in deuterated dimethylsulphoxide (d_6-DMSO) for each compound using the following anionic guests: acetate (AcO$^-$), dihydrogenphosphate (H$_2$PO$_4^-$), fluoride (F$^-$), chloride (Cl$^-$) and bromide (Br$^-$). Urea and thiourea receptors are best studied in DMSO, since the anion binding affinities of such receptors to anionic guests becomes weaker as the hydrogen bonding ability of the solvent increases.[162] Preliminary titrations using either CDCl$_3$ or DMSO-d_6 also showed that the chemical shifts for the NH protons are more clearly visible in the latter solvent.

The experiments were carried out by using a known amount of the host dissolved in 0.8 mL of solvent ([host] = 1.0×10^{-2} M). The anion guest solutions were prepared such that 5 μL of the solution would give 0.1 equivalents of anion ([anion] ≈ 1.5×10^{-1} M). After each addition of the anion guest to the NMR tubes, the ^{1}H NMR spectrum was recorded. The data obtained from these titrations was plotted as the cumulative changes in the chemical shifts against the equivalents of anion added and the resulting plots were analysed using WinEQNMR.[12]

2.4.1   Stack Plots and Binding Curves of ^{1}H NMR Titrations of 69 - 104

The stack plot of the ^{1}H NMR spectra of **70** upon addition of various equivalents of AcO$^-$ is shown in Figure 2.10. It illustrates the typical changes in the chemical shifts of the thiourea (NH) and aromatic (Ar-H) protons during the course of the ^{1}H NMR titration. As is clear from Figure 2.10, the chemical shifts for the NH protons tend to move gradually downfield on complexation. These changes were preferably monitored as they were significantly larger than those observed for the aromatic protons and hence, carry less error. However, these are often broad, which contributes to the high error in the determination of the stability constants. Nevertheless, as shown, the Ar-H protons were also perturbed upon anion recognition and the changes in these chemical shifts were also recorded. The binding constants log β calculated from these changes were identical within experimental errors to those determined from the NH protons, therefore these aromatic proton changes are useful when the chemical shifts of the NH protons become too broad to be located accurately. This method has also been employed by several research groups such as Pfeffer *et al.* and Gale *et al.*[91,136,108,88,141] In general, the changes observed for $H_2PO_4^-$ recognition were smaller than those observed for AcO$^-$, but the binding curves were, nevertheless, quite similar in appearance. Figures 2.11(a) and 2.11(b) illustrate the directional binding modes of AcO$^-$ and $H_2PO_4^-$ respectively, for the simplest of the thiourea receptors, **70**.
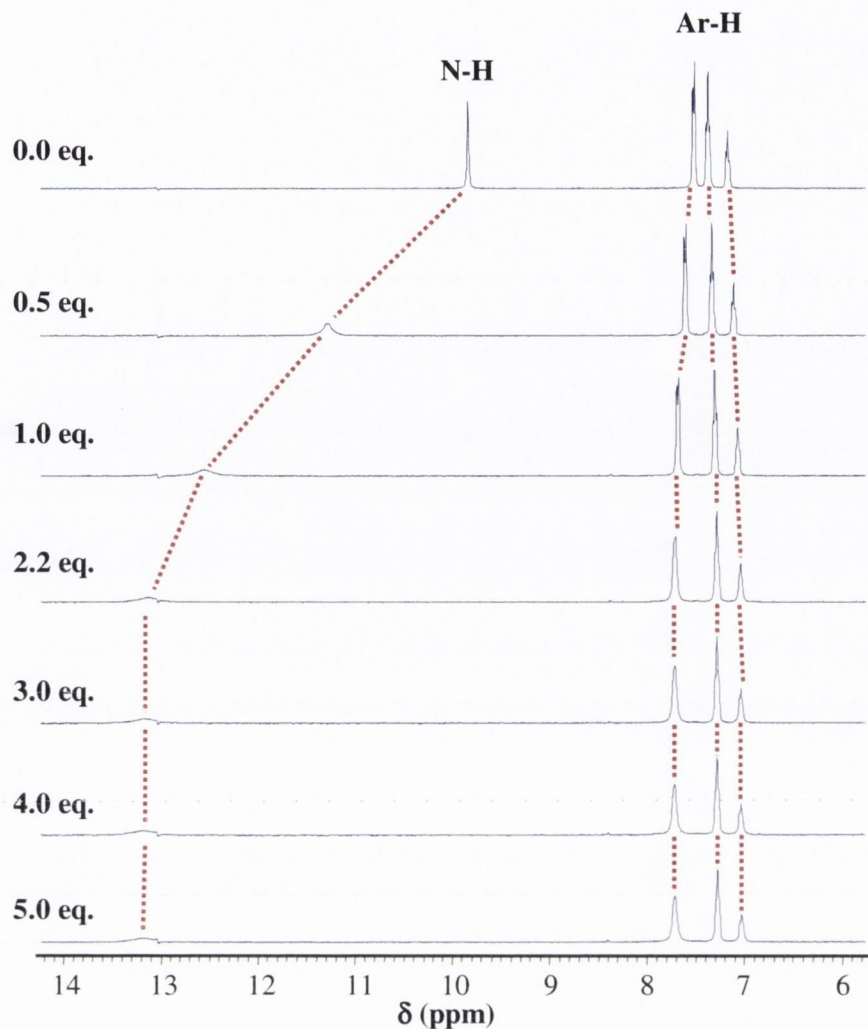
Figure 2.10 Stack plot of the ^{1}H NMR (400 MHz) spectra of **70** (1.0×10^{-2} M) titrated with AcO$^-$ in DMSO-d_6.
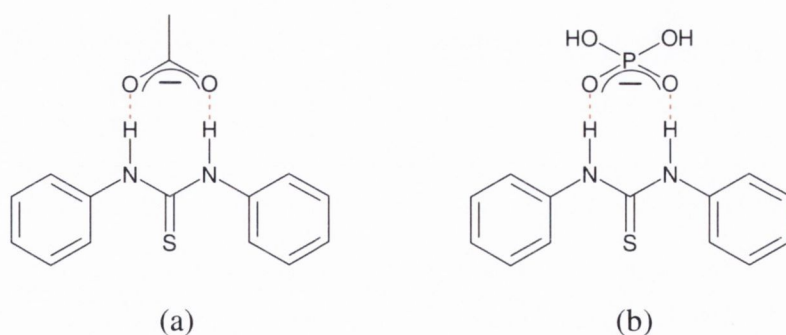
Figure 2.11 Directional hydrogen bonding complexation of **70** with: (a) AcO$^-$, and (b) H$_2$PO$_4^-$.

The process for the complexation of F$^-$ was more complex as there seemed to be more than one binding process occurring during the course of the titration. In all the titrations of F$^-$, a characteristic triplet peak appeared at approximately 16 ppm generally after the addition of 2 equivalents of fluoride. This is seen in Figure 2.12, and is, as

previously established in Chapter 1, due to the deprotonation of at least one of the NH protons by fluoride, resulting in the formation of a bifluoride ion pair, HF_2^- in solution.
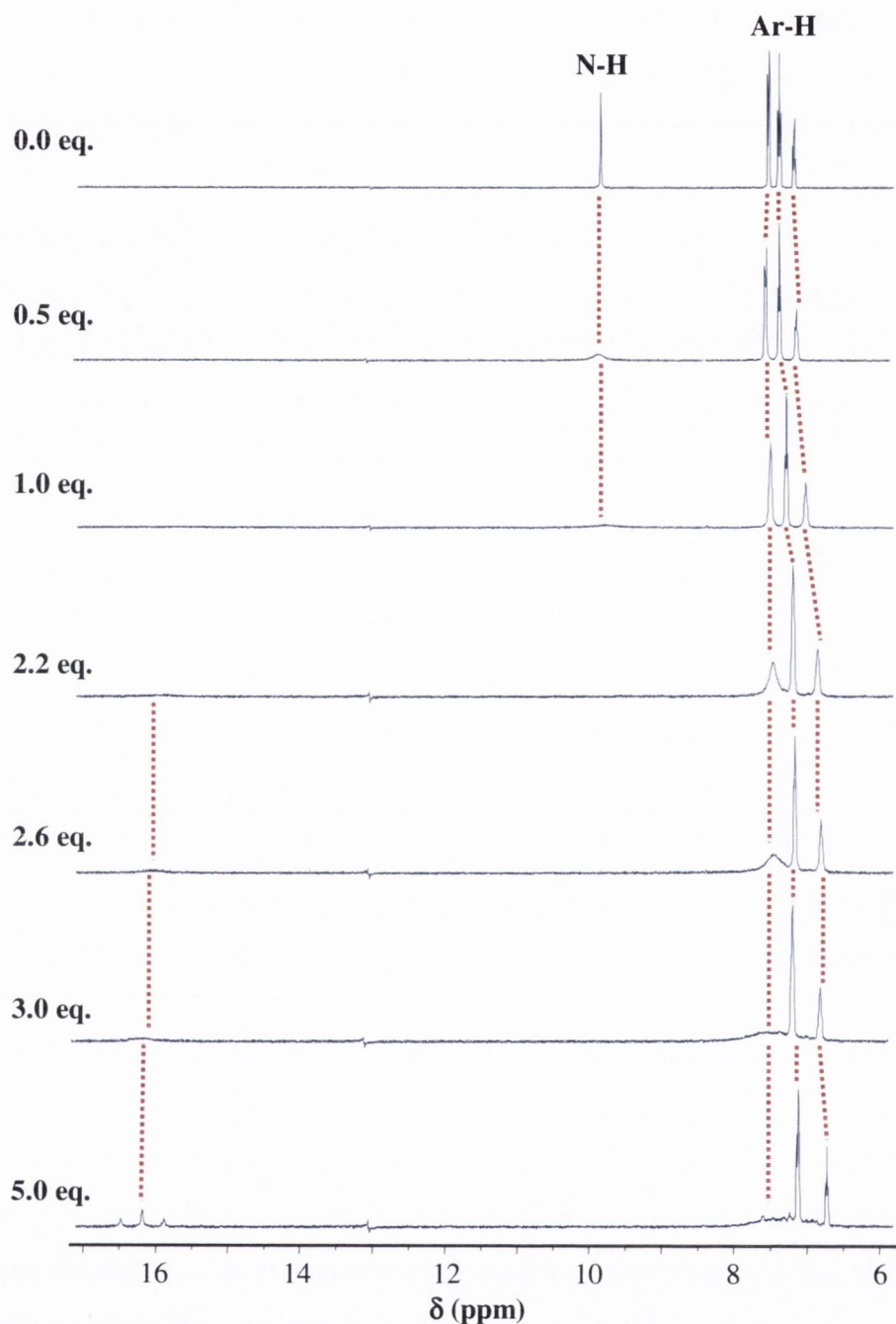
Figure 2.12 Stack plot of the ^{1}H NMR (400 MHz) spectra of **70** (*ca.* 1.0×10^{-2} M) titrated with F$^-$ in DMSO-d_6.

Another interesting observation from the titration of **70** with F$^-$ is the significant perturbation of the aromatic proton signal furthest downfield, after the addition of 2 equivalents of fluoride. This is believed to be due to the delocalisation of the excess electron density on the deprotonated nitrogen of the thiourea motif over its adjacent

phenyl group as a result of resonance (Figure 2.13). Therefore, it seems that the resonance form denoted by (i) may be the predominant species after the deprotonation of the NH proton. Fabrizzi and co-workers have also observed similar resonance behaviour in their thiourea-based sensor upon complexation with fluoride.[154]
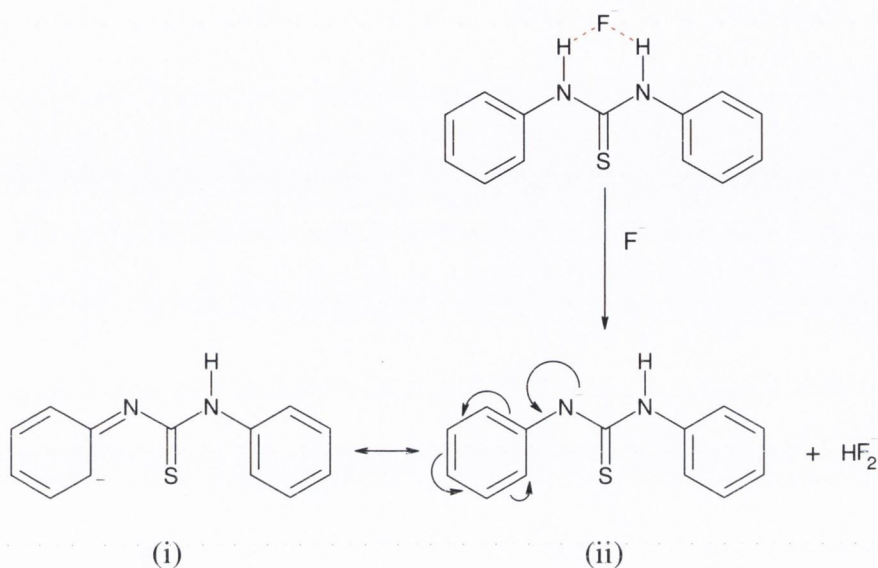
Figure 2.13 Proposed mechanism for the deprotonation of the thiourea proton in **70** by F⁻.

This deprotonation has been observed in the ¹H NMR spectrum by other research groups,[91,88,135,143,169,118,140] but Bowman-James and co-workers have successfully obtained a crystal structure of an encapsulated bifluoride within their macrocyclic amide-based anion receptor.[170] Further evidence may be obtained from the ¹H NMR titration of 1,3-*bis*-(2,4-dimethylphenyl)urea **104** with F⁻ (Figure 2.14), since the chemical shifts of the NH peaks are still clearly visible throughout the experiment. Receptor **104** is a symmetrical *bis*-phenyl urea derivative and therefore, there is initially only one broad singlet peak observed at 8.0 ppm in the ¹H NMR spectrum for the two NH protons of the urea. After the addition of approximately 2 equivalents of fluoride, a new broad peak begins to appear adjacent and downfield to the original singlet, with the concomitant appearance of the triplet peak at approximately 16 ppm. The appearance of this new peak may indicate the presence of two possible complexed species, one being the original fluoride-bound urea receptor and the other being the complex of the deprotonated ligand, which gave rise to the formation of HF_2^-. Another possible reason is that one of the NH protons may be bound to a second F⁻, an occurrence that has been observed in anion complexes of urea- and thiourea-based sensors.[171] However, if this was the case, there should not be any appearance of the triplet peak further downfield.

Figure 2.14 shows the stack plot of the ^{1}H NMR spectra of **104** on addition of F$^-$ illustrating the postulated deprotonation process.
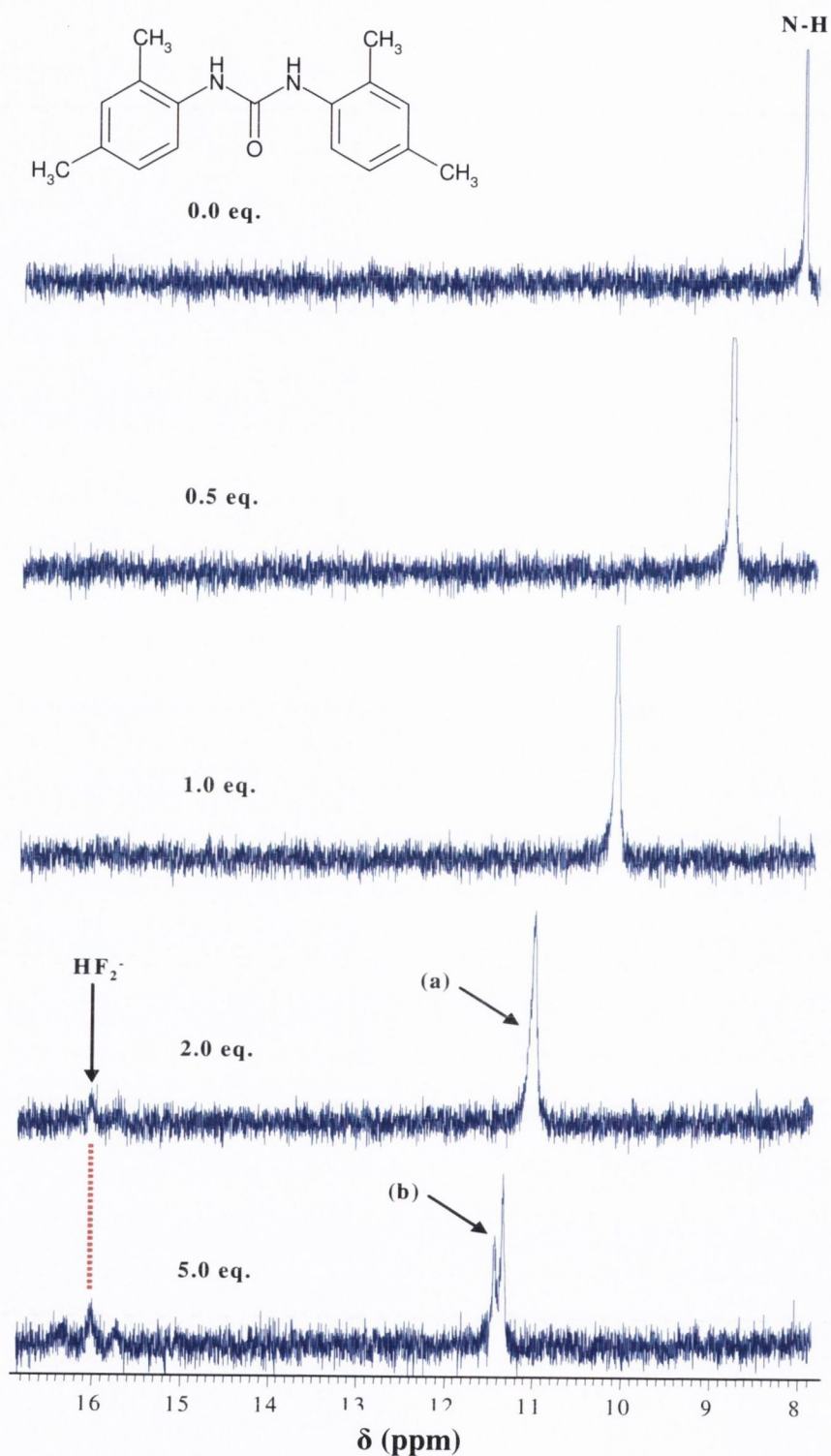
Figure 2.14 Stack plot of ^{1}H NMR (400 MHz) spectra of **104** (*ca.* 1.0×10^{-2} M) titrated with F$^-$ in DMSO-d_6: (a) initial appearance of new NH peak; (b) new peak clearly observable at the end of the titration. (Note: the triplet indicating HF$_2^-$ ion pair was not clearly visible due to the noisy baseline.)
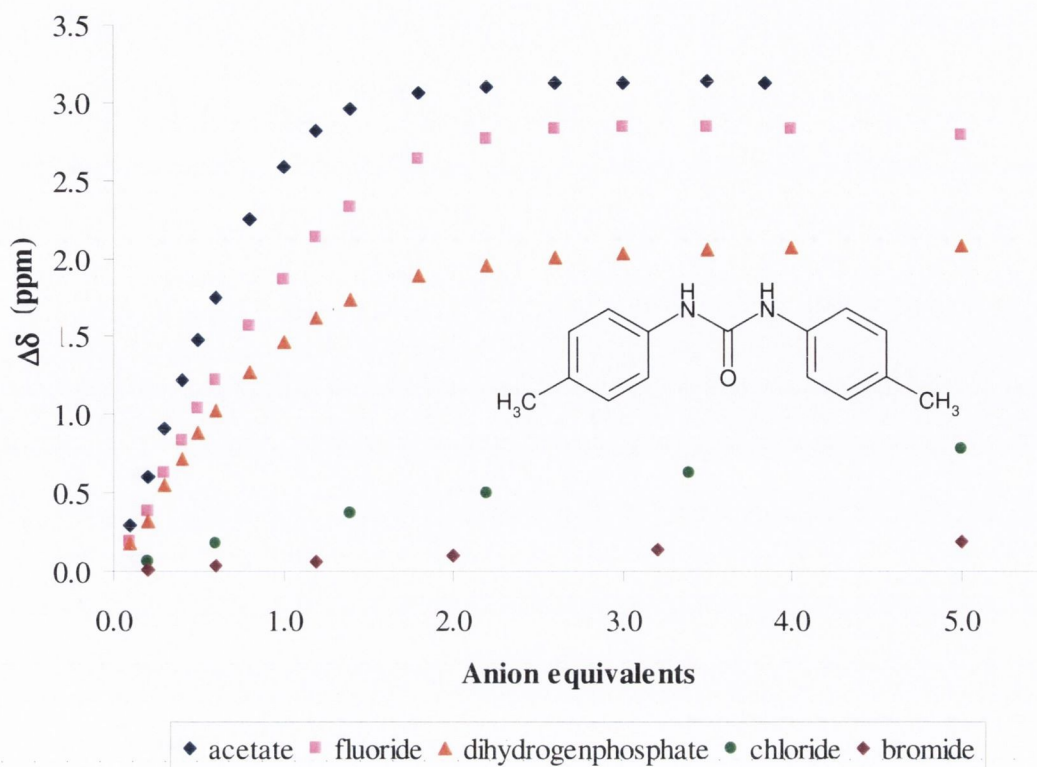
Figure 2.15 Changes in the chemical shifts ($\Delta\delta$) of the urea protons in **97** (*ca.* 1.0×10^{-2} M) with anions in DMSO-d_6.

Figure 2.15 shows the anion binding curves of urea **97** with various anionic guests as a function of guest equivalents added. These results demonstrated that there was very little change observed in the chemical shifts of the urea NH protons when the receptor was titrated with Cl$^-$ and Br$^-$. As can be clearly seen from these changes, the same chemical shifts of the NH protons of **97** are greatly perturbed by the addition of AcO$^-$, H$_2$PO$_4^-$ and F$^-$. Among these results, the binding of AcO$^-$ and F$^-$ show significantly larger changes compared to that of H$_2$PO$_4^-$. Similar overall changes were also generally seen in the binding studies of most of the *bis*-phenyl receptors.

These anion binding curves also provide some information on the host:guest (H:G) stoichiometry of the binding process. The H:G stoichiometries for AcO$^-$ and H$_2$PO$_4^-$ complexation were found to be 1:1, whereas that for F$^-$ was 1:2. The next few sections will deal the analysis of the anion binding processes of the various *bis*-phenyl urea and thiourea families (based on structural relations) designed, followed by a summary of the conclusions derived from these studies.

2.5 Stability Constants (log β) of 69 - 104 with Anions

As stated in the previous section, all the receptors showed significant changes in the ^{1}H NMR chemical shifts upon anion recognition. These changes were used to assess the anion binding affinity of such receptors. Tables 2.4 and 2.5 list the log β values calculated for the 1:1 complexation of AcO$^-$and H$_2$PO$_4$$^-$ with the *bis*-phenyl ureas and *bis*-phenyl thioureas respectively. These values were calculated from the ^{1}H NMR titration data collected using the Fortran-based WinEQNMR program.[12] The errors in all values were within 15%, which is consistent with those observed in the ^{1}H NMR anion binding experiments carried out by Gale and co-workers.[60] It was not possible to calculate the stability constants from the data obtained for the 1:2 complexation of F$^-$ with the receptors, since the binding process may be too complicated for WinEQNMR to process.

Table 2.4. Stability constants (log β) of the *bis*-phenyl urea receptors titrated with the various anions (with errors within 15%).

Compound	log β(AcO$^-$)	log β(H$_2$PO$_4$$^-$)
69	3.06	3.02
71	3.49	2.83
73	3.14	3.23
75	4.07	3.16
77	3.06	2.59
79	3.70	3.62
81	3.72	2.64
83	3.95	3.69
85	3.01	2.45
87	3.34	3.64
89	3.81	3.85
91	3.17	3.20
93	2.61	2.40
95	2.30	1.94
97	3.34	2.86
99	2.17	1.54
101	1.79	1.49
104	1.90	1.99

Table 2.5 Stability constants log β of the *bis*-phenyl thiourea receptors titrated with the various anions.

Compound	log β(AcO⁻)	log β(H₂PO₄⁻)
70	3.11	2.71
72	3.63	2.94
74	3.63	2.77
76	2.59	2.54
78	3.26	2.64
80	3.68	2.56
82	3.58	2.76
84	3.45	3.53
86	3.00	2.63
88	2.75	2.62
90	3.10	2.24
92	3.50	2.17
94	3.11	2.37
96	2.38	1.94
98	2.92	2.82
100	2.83	2.14
102	3.77	2.37
103	2.72	2.44

The errors in the stability constants are further supported by the graphs plotting the changes in chemical shift against anion concentration, which are generated by WinEQNMR. Figures 2.16, 2.17 and 2.18 illustrate the reasonably good fit between the observed and calculated data for AcO⁻ binding of *bis*-phenyl urea **69**, AcO⁻ binding of *bis*-phenyl thiourea **70** and H₂PO₄⁻ binding of *bis*-phenyl urea **69** respectively. To ensure the validity of the log β values calculated, many of the titrations were repeated, especially those giving rise to stability constants which were significantly different from the others (see Appendix 7.1.7).
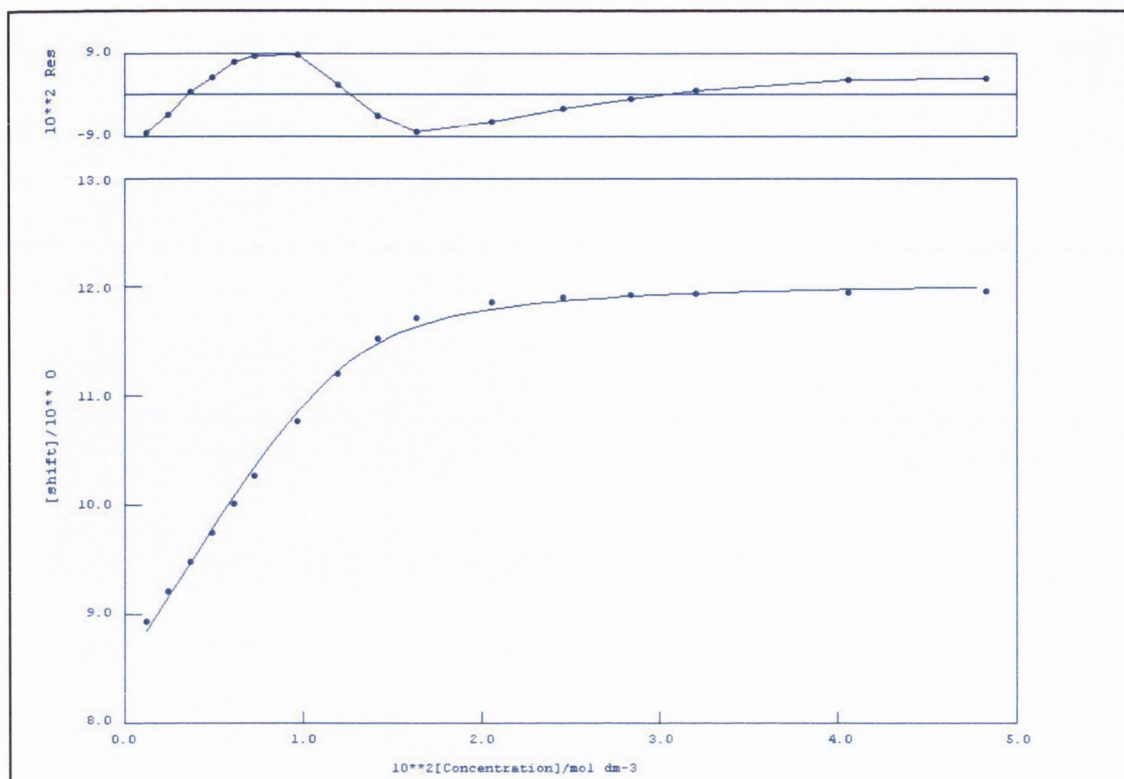
Figure 2.16 WinEQNMR-generated plot of the observed and calculated changes in chemical shift against [AcO⁻] of *bis*-phenyl urea **69**.
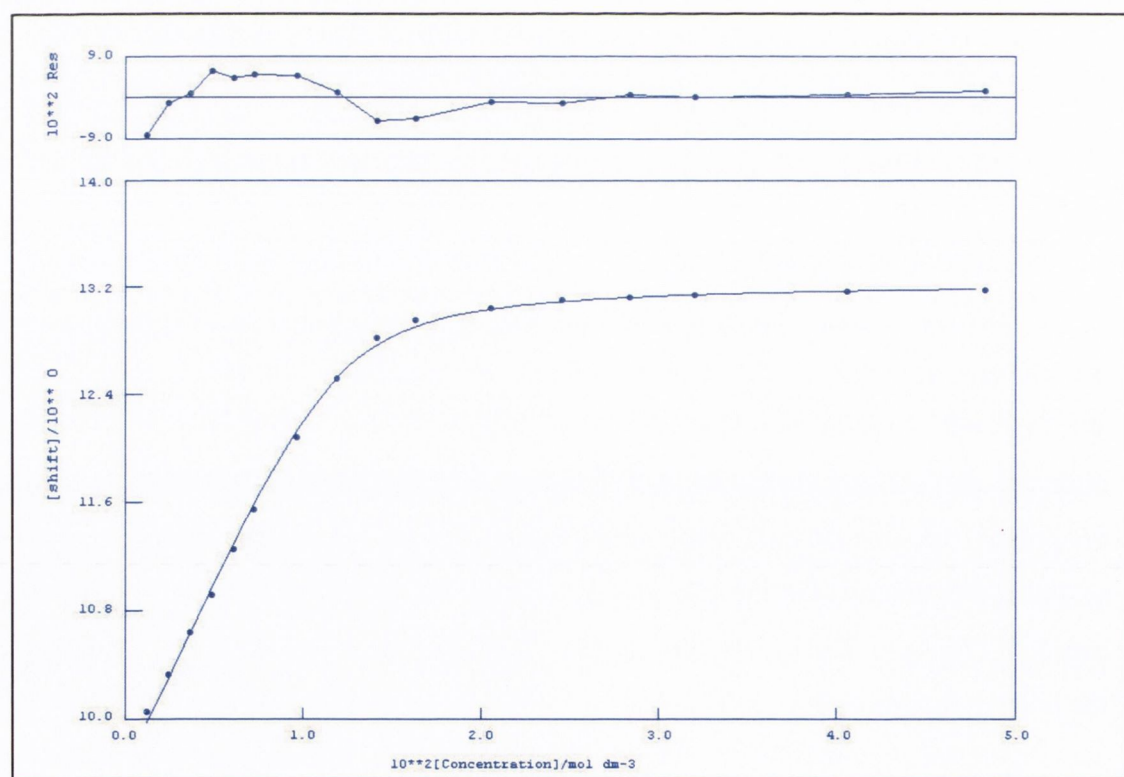
Figure 2.17 WinEQNMR-generated plot of the observed and calculated changes in chemical shift against [AcO⁻] of *bis*-phenyl thiourea **70**.
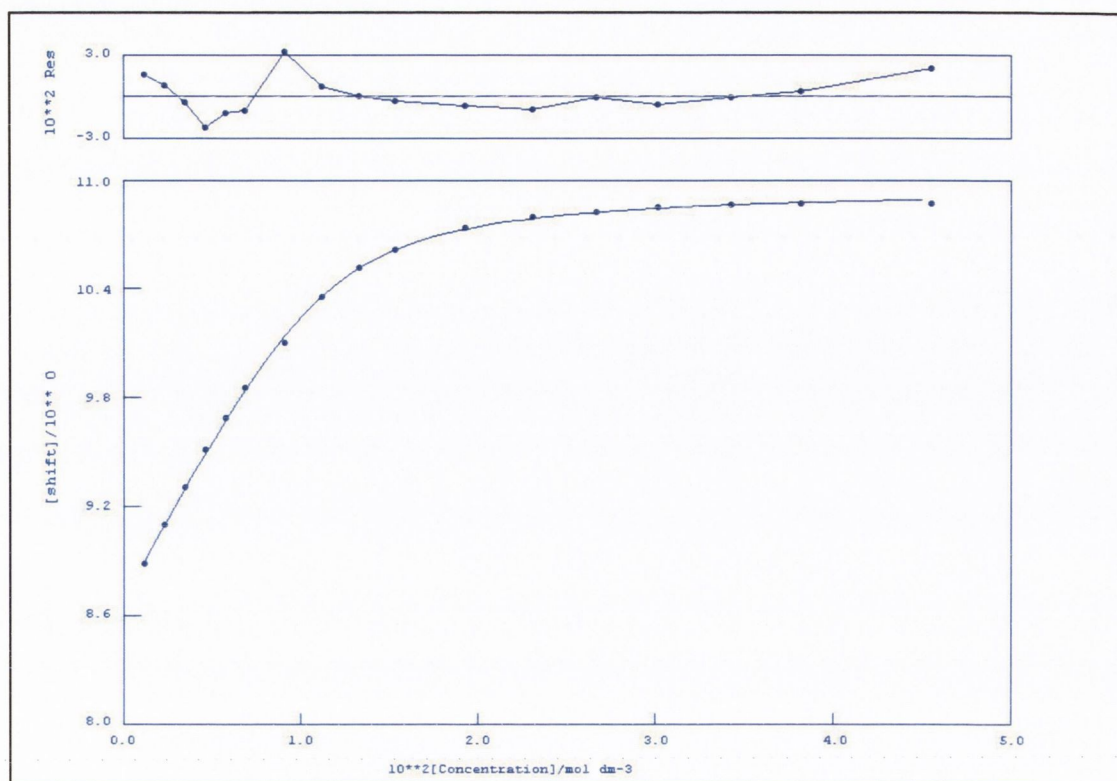
Figure 2.18 WinEQNMR-generated plot of the observed and calculated changes in chemical shift against [H$_2$PO$_4^-$] of *bis*-phenyl urea **69**.

2.5.1 General Observations from Stability Constants (log β)

From the log β values listed in Table 2.4, it can be observed that the urea-based receptors which bound most strongly to AcO$^-$ were **75**, **83** and **89** with log β values of 4.07, 3.95 and 3.81 respectively, while the weakest ureas were **99**, **101** and **104** with log β values of 2.17, 1.79 and 1.90 respectively. The same behaviour is seen the complexation of H$_2$PO$_4^-$, with the exception of **75**. In this case, **75** did not give rise to the highest stability constant (log β = 3.16), when compared to the simplest urea receptor, **69** (log β = 3.02). It is important to note that the three strongest urea receptors all contain electron-withdrawing groups at the *para* position of the phenyl rings, which leads to the conclusion that these substituents may enhance the anion binding ability of the urea motif. However, the weakest three receptors showed that the presence of substituents at the *ortho* position results in lowering the stability constants of the complexation process, possibly due to steric reasons.

Interestingly, in the case of the thiourea analogues (Table 2.5), the receptor which binds the strongest to AcO$^-$ is an *ortho*-substituted thiourea compound, **102**, which has a log β value of 3.77 (*cf.* **70** with log β = 3.11). Since the urea analogue **101**

61

does not show this unusual behaviour in the presence of AcO⁻, it is possible that it is the result of the difference in the properties of the O atom in ureas and the S atom in thioureas. Therefore, we will go on to further analyse the log β values calculated by looking for possible trends, which may assist in the understanding of the anion binding behaviour of these *bis*-phenyl receptors.

2.5.2   Trends from Stability Constants (log β)

Since there is a large number of log β values, we will attempt to analyse the trends in an structured manner. Therefore, this section will consists of the following categories:

- **Symmetrical *bis*-phenyl receptors**
- ***Bis*-phenyl receptors containing electron-withdrawing substituents (F and CF₃)**
- ***Bis*-phenyl receptors containing electron-donating substituents (CH₃)**
- **"Hybrid" *bis*-phenyl receptors**

For each category, the anion abilities of the receptors will be assessed by relating the stability constants to the following criteria:

- **the target anion guest**
- **the type of substituent on the phenyl rings (*i.e.* whether it is electron-donating or withdrawing)**
- **the position of such substituents on the phenyl rings (*i.e.* whether it is *ortho* or *para*)**
- **the possible structural consequences such as deconjugation of the electron density between the phenyl rings and the urea or thiourea moiety**

2.5.2.1 Symmetrical *Bis*-Phenyl Receptors

The stability constants of the symmetrical *bis*-phenyl receptors tabulated in Tables 2.6 and 2.7 for AcO⁻ and $H_2PO_4^-$ complexation respectively.
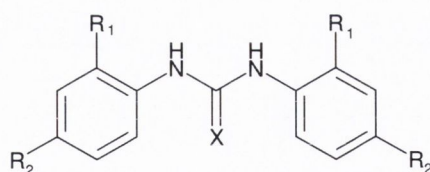
Figure 2.19 Parent structure of symmetrical *bis*-phenyl receptors.

Table 2.6 Stability constants log β of the complexation of symmetrical receptors with AcO⁻.

R₁	R₂	Urea		Thiourea	
		Compound	log β(AcO⁻)	Log β(AcO⁻)	Compound
H	H	69	3.06	3.11	70
H	F	79	3.70	3.68	80
H	CF₃	89	3.81	3.10	90
F	F	95	2.30	2.38	96
H	CH₃	97	3.34	2.92	98
F	H	99	2.17	2.83	100
CF₃	H	101	1.79	3.77	102
CH₃	H	–	–	2.72	103
CH₃	CH₃	104	1.90	–	–

In the complexation of AcO⁻, the stability constant of the unsubstituted *bis*-phenyl thiourea **70** was, within experimental errors, similar to that of **69**. However, with the presence of the different substituents, significant changes were observed in the log β values of the binding processes.

When the phenyl rings are substituted by electron-withdrawing groups such as fluorine groups at the 4-position, there was an increase in the stability constants in both the urea and thiourea derivatives. This was due to the electron-withdrawing nature of the substituents, which through an inductive effect, rendered the urea and thiourea NH protons more acidic. Hence, **79** bound to AcO⁻ with log β = 3.70, whereas **80** gave a log β = 3.68. Although there was no significant difference in log β between the urea and thiourea derivative, the anion binding affinity of these receptors were much enhanced with respect to the simplest of the receptors, **69** and **70**. However, when the *ortho* position of the phenyl rings were substituted with fluorine as in ureas **95** and **99**, there was an appreciable decrease in log β. Receptor **95** and **99** bound AcO⁻ with log β = 2.30 and 2.17, respectively. The presence of the *para* fluorine groups in **95** did not seem to significantly affect the observed decrease in log β. In the case of the thiourea

analogues **96** and **100**, there was again a decrease in log β for the binding of AcO⁻. However, the presence of the *para* fluorine group in **96** resulted in a much lower log β (*i.e.* 2.38), compared to that for **100** (log β = 2.83). Nevertheless, the observed decrease in the stability constant in such receptors may be due to steric hindrance experienced by the urea and thiourea receptor sites by the fluorine substituents at the 2-position. This effect can be further supported by the log β value obtained for the AcO⁻ complexation of 2-substituted *bis*-phenyl ureas, **101** (log β = 1.79) and **104** (log β = 1.90). Also, there is a partial negative charge in the fluorine substituents, which may lead to a repulsive effect towards anions approaching the binding site.

The electron-withdrawing nature of the trifluoromethyl substituent should also cause an increase in the binding affinity of the receptors. But this was only the case for the 4-substituted urea receptor **89** with a log β = 3.81, as no significant change was observed for thiourea **90**. When this substituent is at the 2-position, the receptor bound less strongly in the urea analogue **101** (log β = 1.79) and interestingly, the log β value increased in the case of the thiourea **102** (log β = 3.77). The fact that the bulky group is next to the receptor did not seem to have any major influence sterically, unlike that trend that was observed previously with the *ortho* fluorine substituents. As previously mentioned, *N,N'*-disubstituted thioureas are conformationally more flexible in solution, resulting in the presence of two rotamers (*i.e.* the thiourea NH protons are either *syn* or *anti* in conformation, and are also known as *trans-trans* or *trans-cis* rotamers, respectively).[167] Therefore, there is a possibility of structural rotation within the *ortho*-substituted thiourea receptors to adopt the next available low-energy alternative, potentially providing a more accessible and complementary acidic binding site.

When methyl groups are substituted at the 4-position of the phenyl moieties of the urea receptor **97**, it seemed that the AcO⁻ binding affinity was enhanced. This behaviour was counter-intuitive, as it has been shown that the presence of electron-donating groups may result in reducing the acidity of the NH protons of the urea or thiourea moiety, thus decreasing the binding strength.[159] In the case of the thiourea analogue **98**, the binding affinity was somewhat decreased (log β = 2.92), but not to a significant degree. The substitution of the 2-position of the phenyl rings led to a further decrease in the binding strength, as seen in **103**. This is most likely the result of steric hindrance from the bulky methyl substituent, a hypothesis which is further supported by the significant decrease in the stability constant for the AcO⁻ binding by the *bis*-(2,4-

dimethylphenyl) urea **104**, especially since the electron-donating methyl groups in the 4-substituted urea **97** appeared to enhance the binding ability of the receptor.

Table 2.7 Stability constants $\log \beta$ of the complexation of symmetrical receptors with $H_2PO_4^-$.

R_1	R_2	Urea		Thiourea	
		Compound	$\log \beta(H_2PO_4^-)$	$\text{Log } \beta(H_2PO_4^-)$	Compound
H	H	**69**	3.02	2.71	**70**
H	F	**79**	3.62	2.56	**80**
H	CF_3	**89**	3.85	2.24	**90**
F	F	**95**	1.94	1.94	**96**
H	CH_3	**97**	2.86	2.82	**98**
F	H	**99**	1.54	2.14	**100**
CF_3	H	**101**	1.49	2.37	**102**
CH_3	H	–	–	2.44	**103**
CH_3	CH_3	**104**	1.99	–	–

The behaviour of the different symmetrical receptors towards $H_2PO_4^-$ was also assessed. From the stability constants listed in Table 2.7, it was observed that the thiourea receptors tended to bind to $H_2PO_4^-$ less strongly compared to their urea analogues, which contradicted the general behaviour reported where thioureas usually have larger stability constants with anions than their urea counterparts.[89,137,154,162,172,173] This difference was clearly seen between the unsubstituted urea **69** and thiourea **70**, where $\log \beta$ = 3.02 and 2.71 respectively. Another unusual trend is the fact that electron-withdrawing substituents located at the 4-position of the rings caused a decrease in the stability constants of the thiourea receptors upon $H_2PO_4^-$ recognition (as seen for **80** and **90**), while electron-donating groups increased the binding affinities (as seen for **98**). Again, the opposite was observed in the urea analogues. The only property that was similarly experienced by both ureas and thioureas is the steric effect of substituents located at the 2-position of the phenyl rings, thus decreasing the stability constants of the complexation. However, this decrease was more significant for the urea receptors. As previously mentioned, the thiourea receptors may be able to change its conformation with more ease,[167] thus reducing the extent of the effective steric hindrance posed by the *ortho* substituents of the rings.

2.5.2.2 *Bis*-Phenyl Receptors containing Electron-withdrawing Substituents

Two types of electron-withdrawing substituents have been incorporated into the *bis*-phenyl receptors (*i.e.* F and CF₃). We will first compare the fluoro-substituted receptors followed by the trifluoromethyl-substituted ones. Tables 2.8 and 2.9 list the stability constants of the various *bis*-phenyl derivatives containing fluorine substituents with AcO⁻ and $H_2PO_4^-$ respectively.
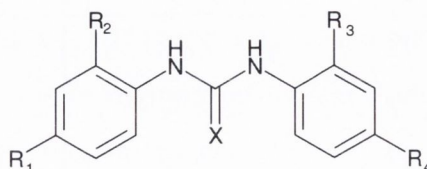
Figure 2.20 Parent structure of substituted *bis*-phenyl receptors.

Table 2.8 Stability constants log β of the complexation of fluoro-substituted *bis*-phenyl receptors with AcO⁻.

R₁	R₂	R₃	R₄	Urea		Thiourea	
				Compound	log β (AcO⁻)	log β (AcO⁻)	Compound
H	H	H	H	69	3.06	3.11	70
H	H	H	F	73	3.14	3.63	74
F	H	H	F	79	3.70	3.68	80
H	H	F	F	77	3.06	3.26	78
F	H	F	F	85	3.01	3.00	86
F	F	F	F	95	2.30	2.38	96
H	F	F	H	99	2.17	2.83	100

The presence of a fluorine group at the *para* position of one of the phenyl rings in **73** slightly increased the AcO⁻ binding affinity from 3.06 to 3.14, which was an expected result because of the electron-withdrawing nature of the fluorine group. The stability constant was further increased by the *para* subsitition of the second aromatic ring. When the *ortho* position of one ring was substituted, log β was decreased but this effect was more significant when both rings were substituted at this position. The thiourea analogues followed similar trends, except that in the case of **80**, which bound AcO⁻ with log β = 3.68, which was similar to **74** (log β = 3.63). It seems that the additive effect of both rings substituted at the 4-position was not experienced by the thiourea moiety. Solid-state results of **80** from the X-ray crystallography discussed in Section 2.3.2 showed that the spatial distance between the protons of the thiourea

binding site (NH···HN distance = 2.131 Å) was larger than its unsubstituted analogue **70** (NH···HN distance = 2.114 Å). If the same occurs in solution, then it may explain the behaviour of **80** since the complementarity of the site with AcO⁻ has somewhat changed.

Table 2.9 Stability constants log β of the complexation of fluoro-substituted *bis*-phenyl receptors with $H_2PO_4^-$.

R_1	R_2	R_3	R_4	Urea		Thiourea	
				Compound	Log β ($H_2PO_4^-$)	log β ($H_2PO_4^-$)	Compound
H	H	H	H	69	3.02	2.71	70
H	H	H	F	73	3.23	2.77	74
F	H	H	F	79	3.62	2.56	80
H	H	F	F	77	2.59	2.64	78
F	H	F	F	85	2.45	2.63	86
F	F	F	F	95	1.94	1.94	96
H	F	F	H	99	1.54	2.14	100

In the recognition of $H_2PO_4^-$, the substitution of both phenyl rings by fluorine at the 2-position decreases the anion binding affinities of the ureas. This is much more pronounced than in the case of AcO⁻, and may be due to the larger size of the tetrahedral $H_2PO_4^-$ anion. However, unlike in acetate binding, the thiourea analogues show a different behaviour to that of the ureas. The *para* substitution of both phenyl rings by fluorine as in **80** reduces the stability constant to log β = 2.56. This may explain why the substitution at the 2- and 4-positions of the phenyl rings by fluorine (**96**) resulted in a lower log β value than that when only the 2-positions are substituted (**100**). There may be an additive effect influencing the acidity of the NH groups in **96**.

From the observations made thus far in this section, it is clear the best binders for AcO⁻ and $H_2PO_4^-$ are the *bis*-phenyl ureas and thioureas consisting of electron-withdrawing fluorine substituents at the *para* positions. In addition, the fluorine substitution of the *para* position in both phenyl rings within the receptors tended to result in the highest stability constants among the other fluorine-substituted receptors.

Table 2.10 Stability constants log β of the complexation of trifluoromethyl-substituted *bis*-phenyl receptors with AcO⁻.

R_1	R_2	R_3	R_4	Urea		Thiourea	
				Compound	log β (AcO⁻)	log β (AcO⁻)	Compound
H	H	H	H	69	3.06	3.11	70
H	H	H	CF$_3$	75	4.07	2.59	76
CF$_3$	H	H	CF$_3$	89	3.81	3.10	90
H	CF$_3$	CF$_3$	H	101	1.79	3.77	102

The trifluoromethyl substituent was expected to have a stronger electron-withdrawing influence due to the presence of multiple fluorine atoms. This was observed in the stability constants for the binding of AcO⁻ by the substituted urea derivatives listed in Tables 2.10. Hence, **75** bound AcO⁻ with log β = 4.07 whereas the 4-fluoro-substituted **73** gave a log β of 3.23, which was a significant difference. However, the substitution of both rings at the *para* position by CF$_3$ did not show the same additive effect on the stability constant. In fact, the stability constant of **89** (log β = 3.81) was lower than the mono-substituted derivative **75**. The crystal structure of **89** (Figure 2.4) showed that the phenyl rings were almost orthogonal with respect to each other, which may result in the deconjugation of the urea moiety from the phenyl rings, and hence, lowering its binding affinity. Although this structural characteristic is of the solid state, it gives some insight as to the possible reasons for the unexpected decrease in the binding affinity. When the 2-position of both phenyl rings was substituted, the log β was reduced even further and was now almost half its original value. This decrease in stability constant may be the result of the steric hindrance of the bulky trifluoromethyl groups close to the urea moiety, and followed the same trend as observed previously.

The AcO⁻ binding behaviour of the thiourea analogues, on the other hand, was the opposite to that of the ureas. The CF$_3$ substituent at the *para* position of one phenyl ring (as in **76**) seemed to significantly reduce the binding affinity of the thiourea receptor (log β = 2.59), whereas the presence of the 4-substituent on both rings (as in **90**) appeared to counteract this effect, thus the log β = 3.10 was only slightly less than that of the unsubstituted analogue **70** (log β = 3.11). Interestingly, the bulky groups at the 2-position on both rings in **102** did not have the same expected influence of reducing

the binding affinity of the receptor. In fact, it gave a log β value of 3.77, which makes it the strongest AcO^- binder among the thiourea-based receptors.

Table 2.11 Stability constants log β of the complexation of trifluoromethyl-substituted *bis*-phenyl receptors with $H_2PO_4^-$.

R_1	R_2	R_3	R_4	Urea		Thiourea	
				Compound	log β $(H_2PO_4^-)$	log β $(H_2PO_4^-)$	Compound
H	H	H	H	69	3.02	2.71	70
H	H	H	CF_3	75	3.16	2.54	76
CF_3	H	H	CF_3	89	3.85	2.24	90
H	CF_3	CF_3	H	101	1.49	2.37	102

Table 2.11 show the stability constants of these receptors upon the binding of $H_2PO_4^-$. The ureas, once again, illustrated the expected behaviour of the presence of electron-withdrawing groups, where the stability constant was increased by the presence of at least one 4-substituted phenyl group. However, unlike previously observed for the acetate recognition, the receptor actually experienced an additive electron-withdrawing effect when both rings were substituted at the *para* position in **89**. Also, this receptor bound the anion with log β = 3.85, which was only slightly higher than that of the fluoro-substituted analogue **79** (log β = 3.62). This does not provide enough evidence to support the hypothesis that the CF_3 substituent has a stronger electron-withdrawing influence on the urea moiety than F. Again, the presence of the substituents at the 2-position of the phenyl rings caused the expected decrease in the binding affinity of the receptor.

The recognition of $H_2PO_4^-$ by the thiourea analogues showed a similar behaviour to that of AcO^-, where the CF_3 substituents at the *para* position of the rings caused a reduction in the binding affinities of the receptors. When the 2-substituted derivative **102** bound to $H_2PO_4^-$, the expected decrease in log β (due on steric hindrance) was observed, but not to a great extent. Even though the $H_2PO_4^-$ binding of **102** is not enhanced like that seen for AcO^- binding, the small degree of this sterically influenced decrease in log β demonstrates that **102** may have undergone a conformational change in order to provide a better access for the $H_2PO_4^-$ anion. However, due to the bulky nature of this tetrahedral anion, it may still be experiencing

steric hindrance from the *ortho* substituents, resulting in small decrease instead of an enhancement in the stability constant.

Overall, it was observed that the best urea-based binder for AcO⁻ and $H_2PO_4^-$ in this receptor category were those containing at least one 2-substituted electron-withdrawing group (either F or CF_3). In the case of the thiourea analogues, a similar trend was observed for the fluorine substituted receptors. However, for the CF_3 substituted thioureas, it appears that the best AcO⁻ binder was **102** which possesses substituents at the 2-position of both its phenyl rings. As previously mentioned, this unusual behaviour may be attributed to the fact that thioureas tend to be conformationally more flexible than ureas, and hence, have the potential to undergo rotational structural changes in solution.[167]

2.5.2.3 *Bis*-Phenyl Receptors containing Electron-donating Substituents

The methyl-substituted urea and thiourea receptors showed some interesting results in their binding of AcO⁻ and $H_2PO_4^-$, as seen from their stability constants listed in Tables 2.12 and 2.13 respectively. The methyl groups are electron-donating in nature and it is believed that this would result in reducing the acidity of the NH protons of the urea and thiourea moieties.

Table 2.12 Stability constants log β of the complexation of methyl-substituted *bis*-phenyl receptors with AcO⁻.

R_1	R_2	R_3	R_4	Urea		Thiourea	
				Compound	log β (AcO⁻)	log β (AcO⁻)	Compound
H	H	H	H	69	3.06	3.11	70
H	H	H	CH_3	71	3.49	3.63	72
CH_3	H	H	CH_3	97	3.34	2.92	98
H	CH_3	CH_3	H	–	–	2.72	103
CH_3	CH_3	CH_3	CH_3	104	1.90	–	–

Table 2.13 Stability constants log β of the complexation of methyl-substituted *bis*-phenyl receptors with $H_2PO_4^-$.

R_1	R_2	R_3	R_4	Urea		Thiourea	
				Compound	log β $(H_2PO_4^-)$	log β $(H_2PO_4^-)$	Compound
H	H	H	H	69	3.02	2.71	70
H	H	H	CH_3	71	2.83	2.94	72
CH_3	H	H	CH_3	97	2.86	2.82	98
H	CH_3	CH_3	H	–	–	2.44	103
CH_3	CH_3	CH_3	CH_3	104	1.99	–	–

However, the above log β values obtained from this study illustrate the opposite result. The *para* methyl substitution of the phenyl rings in fact increases the stability constants of these receptors in almost all the cases, except for those of the urea derivatives binding to $H_2PO_4^-$. In this case, the stability constants followed the expected trend of being lowered by the presence of electron-donating methyl groups. The presence of methyl groups at the 2-position of the phenyl rings of these receptors led to a decrease in their stability constants. Again, this is expected as the methyl groups may be sterically hindering the binding of the anion to the urea or thiourea moiety.

2.5.2.4 "Hybrid" *Bis*-Phenyl Receptors

We will now consider *bis*-phenyl anion receptors containing both electron-withdrawing and electron-donating substituents (*i.e.* "hybrid" receptors).

Table 2.14 Stability constants log β of the complexation of *bis*-phenyl receptors containing a trifluoromethyl or/and methyl substituents with AcO^-.

R_1	R_2	R_3	R_4	Urea		Thiourea	
				Compound	log β (AcO^-)	log β (AcO^-)	Compound
H	H	H	H	69	3.06	3.11	70
H	H	H	CF_3	75	4.07	2.59	76
H	H	H	CH_3	71	3.49	3.63	72
CH_3	H	H	CF_3	87	3.34	2.75	88

Table 2.15 Stability constants log β of the complexation of *bis*-phenyl receptors containing trifluoromethyl or/and methyl substituents with $H_2PO_4^-$.

R_1	R_2	R_3	R_4	Urea		Thiourea	
				Compound	log β $(H_2PO_4^-)$	log β $(H_2PO_4^-)$	Compound
H	H	H	H	69	3.02	2.71	70
H	H	H	CF_3	75	3.16	2.54	76
H	H	H	CH_3	71	2.83	2.94	72
CH_3	H	H	CF_3	87	3.64	2.62	88

From Table 2.14, the presence of both CF_3 and CH_3 in both the urea and the thiourea derivatives seemed to result in a kind of additive effect. Here, **87** still bound to AcO^- stronger than its unsubstituted analogue **69**, but the stability constant was affected such that the CH_3 substituent has a greater influence on the overall binding than CF_3. The opposite is observed in the thiourea analogue **88**, where $CF_3 > CH_3$ in influence. A similar trend was observed both urea and thiourea "hybrid" derivatives in the case of complexation with $H_2PO_4^-$ (Table 2.15).

Table 2.16 Stability constants log β of the complexation of *bis*-phenyl receptors containing fluorine or/and methyl substituents with AcO^-.

R_1	R_2	R_3	R_4	Urea		Thiourea	
				Compound	log β (AcO^-)	log β (AcO^-)	Compound
H	H	H	H	69	3.06	3.11	70
H	H	H	F	73	3.14	3.63	74
H	H	H	CH_3	71	3.49	3.63	72
CH_3	H	H	F	81	3.72	3.58	82
CH_3	H	F	F	93	2.61	3.11	94
H	H	F	F	77	3.06	3.26	78

Table 2.17 Stability constants log β of the complexation of *bis*-phenyl receptors containing fluorine or/and methyl substituents with $H_2PO_4^-$.

R_1	R_2	R_3	R_4	Urea		Thiourea	
				Compound	log β ($H_2PO_4^-$)	log β ($H_2PO_4^-$)	Compound
H	H	H	H	69	3.02	2.71	70
H	H	H	F	73	3.23	2.77	74
H	H	H	CH_3	71	2.83	2.94	72
CH_3	H	H	F	81	2.64	2.76	82
CH_3	H	F	F	93	2.40	2.37	94
H	H	F	F	77	2.59	2.64	78

In the AcO⁻ complexation of F-CH_3 "hybrid" *bis*-phenyl urea receptors, the presence of both F and CH_3 resulted in an enhancement in the stability constant (Table 2.16); this is most likely an additive effect. However, when the 2-position of one phenyl ring was also substituted by F as in **93**, the stability constant was significantly lowered. This may be the result of steric influences of the fluorine atom at the *ortho* position of the ring. As for the thiourea analogues, the combination of two types of substituents did not seem to cause an additive effect since **82** has a log β value very similar to those of the thioureas subsitituted by only one substituent type. However, the *ortho* substitution again influenced the binding affinity of **94**, possibly due to the steric influence of the 2-substituent. This was also observed in the recognition of $H_2PO_4^-$ for both urea and thiourea analogues (Table 2.17).

Table 2.18 Stability constants log β of the complexation of *bis*-phenyl receptors containing fluorine or/and trifluoromethyl substituents with AcO⁻.

R_1	R_2	R_3	R_4	Urea		Thiourea	
				Compound	log β (AcO⁻)	log β (AcO⁻)	Compound
H	H	H	H	69	3.06	3.11	70
H	H	H	F	73	3.14	3.63	74
H	H	H	CF_3	75	4.07	2.59	76
CF_3	H	H	F	83	3.95	3.45	84
CF_3	H	F	F	91	3.17	3.50	92
H	H	F	F	77	3.06	3.26	78

Table 2.19 Stability constants log β of the complexation of *bis*-phenyl receptors containing fluorine or/and trifluoromethyl substituents with $H_2PO_4^-$.

R_1	R_2	R_3	R_4	Urea		Thiourea	
				Compound	log β ($H_2PO_4^-$)	log β ($H_2PO_4^-$)	Compound
H	H	H	H	69	3.02	2.71	70
H	H	H	F	73	3.23	2.77	74
H	H	H	CF$_3$	75	3.16	2.54	76
CF$_3$	H	H	F	83	3.69	3.53	84
CF$_3$	H	F	F	91	3.20	2.17	92
H	H	F	F	77	2.59	2.64	78

Tables 2.18 and 2.19 list the stability constants of F-CF$_3$ "hybrid" urea and thiourea receptors for the recognition of AcO$^-$ and $H_2PO_4^-$, respectively. In the case of AcO$^-$ binding, the log β value of **83** (3.95) appeared to be influenced mainly by the *para* CF$_3$ substituent, whereas its thiourea analogue, **84**, experienced the electron-withdrawing nature of the *para* F substituent. When the 2-position of the 4-fluorophenyl ring was substituted by a fluorine group, a decrease in the log β was observed for the recognition of AcO$^-$ by **91**. However, this was not the case for the thiourea analogue **92**, whose log β remains almost unchanged. Again, this may be due to the flexibility of the thiourea moiety,[167] enabling the molecule to rotationally adjust its structure to provide a more accessible binding site despite the potential steric crowding.

When binding to $H_2PO_4^-$, the presence of both F and CF$_3$ resulted in an enhancement of log β in these urea and thiourea receptors, and this was significantly reduced by the steric influence of F group at the 2-position of the one phenyl ring.

2.6 Conclusions

This anion binding study was carried with the aim of establishing a better understanding of the binding abilities of charge-neutral *bis*-phenyl receptors by looking at the electronic and steric effects of three different substituents towards the anion binding affinities of these receptors.

We therefore designed and synthesised 36 *bis*-phenyl receptors (18 ureas and 18 thioureas) for the purpose of studying their binding abilities towards various simple

anions. Their binding affinities of these receptors mainly follow the trend: $AcO^- \approx F^- >$ $H_2PO_4^- > Cl^- > Br^-$, with a few exceptions. In general, the host:guest stoichiometries of AcO^- and $H_2PO_4^-$ complexation are 1:1, whereas that of F^- is 1:2. The binding of F^- is believed to involve two processes (*i.e.* complexation and deprotonation).[91,88,135,143,169,118,140,170] The latter processs leads to the formation of a bifluoride ion (HF_2^-) due to one of the NH protons of the urea or thiourea moiety being deprotonated. Figure 2.13 (in Section 2.4.1) illustrates the proposed mechanism for this deprotonation. One indicative observation for the deprotonation is the appearance of a triplet at *ca.* 16 ppm in the ^{1}H NMR spectrum, which is attributed to the bifluoride ion. These urea- and thiourea-based receptors all have very little affinity towards the halides, Cl^- and Br^-.

Thioureas are generally believed to bind stronger to anions then their urea analogues due to the S atom increasing the acidity of the NH protons.[89,137,154,162,172,173] However, this is not the trend that is observed in our simple *bis*-phenyl systems. In most cases, the stability constants of the thioureas were found to be almost equivalent or less than those of the ureas. The following lists the main observations made from the study:

o In the recognition of AcO^- by the *bis*-phenyl ureas, the three best receptors were **75**, **83** and **89**, while the three weakest binders were **99**, **101** and **104**. The best thiourea-based receptor for AcO^- is **102**, and the weakest is **96**. The four receptors with strong binding affinities all contained at least one CF_3 substituent, but interestingly, **102** is substituted at the 2-position of the phenyl rings, while the others are *para* substituted. Hence, when designing sensor based on these *bis*-phenyl receptors such that it would bind well to AcO^-, it is best to choose a compound which contains either F or CF_3 substituent at the 4-position on at least one of the phenyl rings, while in the case of thiourea, the best one to incorporate is that which has CF_3 groups at the 2-position on both rings.
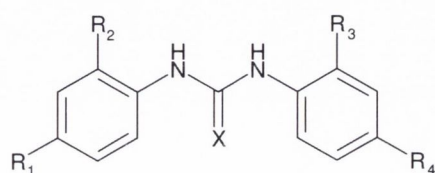
75	X = O; R_1 = R_2 = R_3 = H; R_4 = CF_3
83	X = O; R_1 = F; R_2 = R_3 = H; R_4 = CF_3
84	X = S; R_1 = F; R_2 = R_3 = H; R_4 = CF_3
89	X = O; R_1 = R_4 = CF_3; R_2 = R_3 = H
96	X = S; R_1 = R_2 = R_3 = R_4 = F
99	X = O; R_1 = R_4 = H; R_2 = R_3 = F
101	X = O; R_1 = R_4 = H; R_2 = R_3 = CF_3
102	X = S; R_1 = R_4 = H; R_2 = R_3 = CF_3

o The strongest urea-based receptor for $H_2PO_4^-$ is **89**, and the weakest one is **101**. The thiourea-based receptor which binds best to $H_2PO_4^-$ is **84**, while **96** has the weakest affinity to this anion. Again, like in the recognition of AcO^-, the strongest binders contain a CF_3 group, and the weakest ones were substituted at the 2-position of the phenyl rings.

o Receptors substituted at the 2-position of their phenyl rings experience a decrease in their anion binding abilities, and this is most likely due to the steric hinderance of the substituents towards any approaching anion. One exception is **102** (substituted by CF_3 at the 2-position of both rings), which binds AcO^- with a log β value of 3.77, making it the best receptor among the *bis*-phenyl thiourea receptors for AcO^- recognition.

o The thiourea-based receptors tend to bind less strongly to $H_2PO_4^-$ than their urea analogues. This is counter-intuitive since the NH protons of thioureas are generally believed to be more acidic than those of ureas, and thus, they should have stronger anion binding affinities.[89,173,154,162,172,137] Another anomalous behaviour observed in the recognition of $H_2PO_4^-$ by the thiourea receptors is that electron-withdrawing substituents seem to lower the binding affinities, whereas electron-donating ones causes an enhancement in these affinities. These atypical observations may be due to the fact that thioureas are conformationally more flexible than their urea analogues,[167] and therefore, there is a possibility that any conformational changes within the thiourea receptors may affect their anion binding properties to a certain extent.

o The electron-donating nature of the CH_3 substituent does not have as strong an influence on the urea or thiourea motif in comparison to the electron-withdrawing groups. Also, the electron-donating group tend to increase the stability constants of the anion recognition process, except in the case of the $H_2PO_4^-$ binding by the urea-based receptors, in which there is a reduction in the binding affinities. The crystal structure of the methyl-substituted *bis*-phenyl urea **81** (Figure 2.4) showed that the phenyl rings were almost orthogonal with respect to each other, which may cause the deconjugation of the urea moiety from the phenyl ring. Even though this structural characteristic is of the solid state, it gives some insight as to the possible causes for the unexpected increase in the binding affinity in the presence of an electron-donating group.

- o The CF$_3$ substituent does not always have a stronger electronic influence compared to the F group, which may be due to the fact that the F group is directly attached to the aromatic rings.
- o There is generally an additive effect observed in the electronic influence of the substituents in the *bis*-phenyl receptors containing both electron-withdrawing and electron-donating groups.

Therefore, the analysis of the possible trends from the stability constants calculated from the ^{1}H NMR titrations gave rise to several counter-intuitive behaviours in both urea/thiourea and electron-donating/electron-withdrawing principles. These observations made it quite challenging to form definite trends that would be useful in designing urea- and thiourea-based anion sensors. It is very possible that other factors, such as solvent and structural effects (even though attempts have been made to keep them constant), are also influencing the anion binding processes.

Finally, despite the difficulties faced in analysing the observations made from this study, we can safely conclude that the presence of a CF$_3$ group on the aromatic rings (generally at the *para* position) greatly enhances the anion binding affinities of these *bis*-phenyl receptors in DMSO, while substituents located at the *ortho* position tended to significantly lower the stability constants of the anion binding process. Figure 2.21 illustrates a flowchart outline a simple strategy for choosing the most suitable receptor for a particular target anion. The most selective receptor for AcO$^-$ over H$_2$PO$_4^-$ in this study was the thiourea receptor **102**, which was substituted by CF$_3$ groups at the 2-position on both phenyl rings.
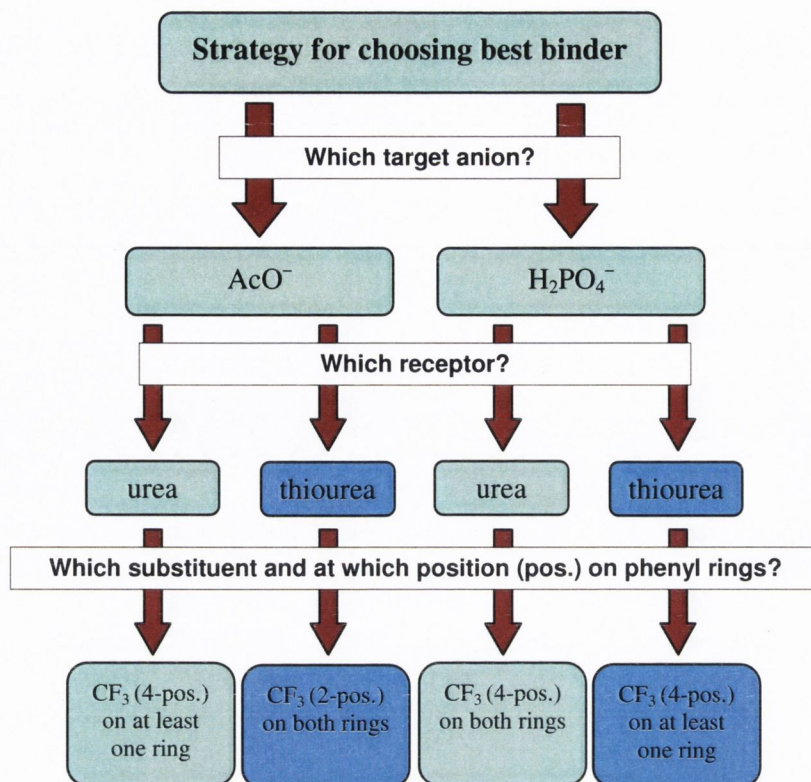
Figure 2.21 Flowchart outlining a simple strategy to choose the best urea- or thiourea-based binder for a particular target anion.

2.7 Future Work

Since the anion binding studies of these *bis*-phenyl ureas and thioureas gave rise to several interesting results, it may be worthwhile to design more receptors incorporating other substituents, such as Et, OH, NO$_2$, Cl, Br and I. Anion binding studies of the above suggested receptors may provide even more information regarding the counter-intuitive behaviour observed in some of the previously studied *bis*-phenyl receptors, and thus, provide further support towards the conclusions made from our study.

Another structural modification which may be useful is the substitution of the 3-position of the aromatic rings. The stability constants obtained from the anion binding studies of these receptors would not only provide information towards the influence of substituents on the binding affinity, they would also be useful in a study based on the Hammett equation, which states that a property may be directionally proportional to the electronic nature of the substituent at either the *meta* or *para* position of the phenyl ring.

It is hoped that the log β values obtained from all these anion binding studies would provide a substantial library for future reference.

3.1 Introduction

This chapter will deal with two kinds of anion sensors based on the use of molecular tweezers and chiral receptors. In both cases, it incorporates the principle of preorganisation to enhance the selectivity of receptor towards a particular guest.

Molecular tweezers utilising the urea and thiourea moieties as anion receptors have been designed based on a number of structural backbones such as [3]polynorbonanes,[91] chenodeoxycholic acid[174-176] and 2,2'-biphenol.[177] Kim and Kim synthesised the first example of an chenodeoxycholic acid-based molecular tweezer (**105**) containing urea moieties acting as the anion receptor.[174] Binding studies with selected anions showed that this molecular tweezer binds strongest to $H_2PO_4^-$ with a host:guest stoichiometry of 1:1, indicating a cooperative binding.

105

106
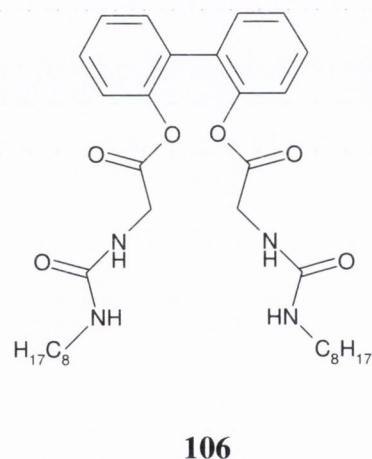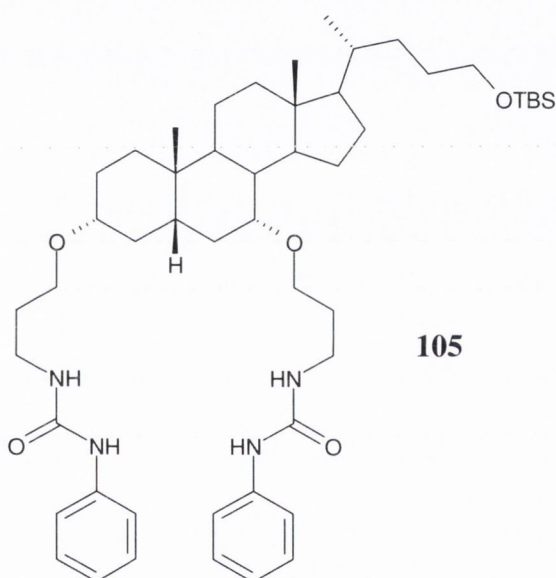
Another example of an anion-binding molecular tweezer used is one designed by Albrecht and co-workers.[177] This molecule (**106**) is based on a 2,2'-biphenol backbone, using urea moieties as the receptors. This receptor binds selectively to NO_3^-, forming a 1:1 host:guest complex *via* hydrogen bonding. This binding was achieved in an additive manner (*i.e.* the more hydrogen bond donors available, the higher the anion binding affinity).

Mu *et al.* designed and synthesised anion sensors which incorporates both principles discussed in this chapter (*i.e.* these sensors are chiral and behave as molecular tweezers).[176] Compound **107** is an example of this novel type of chiral molecular tweezer which shows significant binding towards halides, in particular, chloride ions.
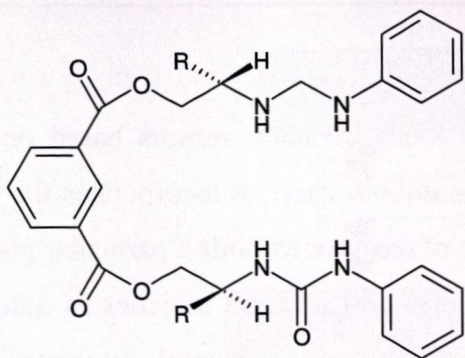
107 R = CH₂Ph
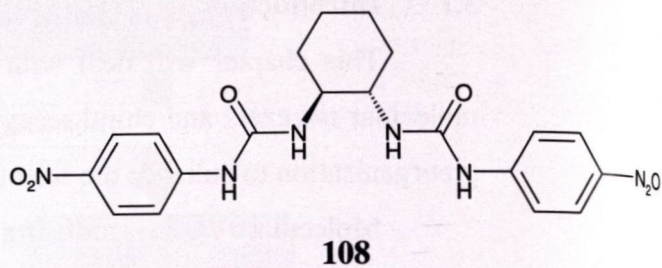
108

There have also been a number of reports in literature exemplifying anion sensing using chiral molecules.[101,178,179] Fabbrizzi *et al.* synthesised *bis*-(*p*-nitrophenyl)urea-based *trans*-1,2-cyclohexane *R,R* and *S,S* enantiomers (*e.g.* **108**) which are capable of enantioselective recognition of the biologically relevant D-2,3-diphosphoglycerate anion in DMSO with a host:guest stoichiometry of 1:1.[179]

The next section will now consider the fluorophores which will be utilised in the fluorescent anion sensors discussed in this chapter.

3.2   Fluorescence of Anthracenes and Naphthalenes

Most rigid aromatic hydrocarbons, such as benzene, naphthalene and anthracene, are in general measurably fluorescent ($1 \geq \Phi_f \geq 0.01$).[180] This fluorescence may be enhanced by molecular rigidity (due to structural and environmental constraints). In this chapter, the fluorophores incorporated into potential anion sensors are anthracenes and naphthalenes. Anthracene itself generally fluoresces with a quantum yield higher than that of naphthalene, although this property is dependent on the solvent they are measured in. This is due to the fact that the π-π $S_0 \rightarrow S_1$ transition in anthracene is "orbital symmetry allowed" (*i.e.* the molecule contains a long axis which is suitable for the electric vector to induce electron oscillation), while that in naphthalene is "orbital symmetry forbidden" (*i.e.* the molecule is so symmetrical that the electric vector of the light cannot easily find an axis along which to oscillate an electron).[180]

The emission of the anthracene moiety is in the wavelength region between 400 and 500 nm (absorption between 200 and 400 nm), and that for naphthalene, 300 and 450 nm (absorption between 250 and 300 nm).[180,181] The fine structure of the absorption and fluorescence spectra of such molecules is dependent on their solvent environment.[180] Substituents on these polyaromatic rings can also induce changes in their absorption and fluorescence, such as shifting to different wavelengths as well as changes in their fine structures (*e.g.* broadening).

3.3   Objectives

As aforementioned, this chapter deals with tweezer-type and chiral fluorescent anion sensors which utilises two types of polyaromatic fluorophores; anthracene and naphthalene. Hence, there will be two main sections in this chapter; the first will be on *bis*-anthracene systems and the second on *bis*-naphthalene systems.

The objective of the first part follows on from the photo-induced electron transfer (PET) anion sensing work carried out within the Gunnlaugsson research group.[147,103,134,89,20,148]   All the PET anion sensors previously studied were mono-anthracene systems, which showed significant fluorescence quenching upon anion recognition.   Therefore, it was hoped that the incorporation of another anthracene moiety to form a *bis*-system would enhance the anion binding properties. One possible means for this enhancement to occur may be through π-π interactions between the two anthracene moieties as the binding of a target anion may bring them closer together. Three *bis*-anthracene systems **109 - 111** were designed and synthesised. Compound **109** contains one thiourea receptor site, while the other two sensors **110** and **111** were *bis*-thiourea derivatives. The physical evaluation of the anion binding ability of these PET sensors was then carried out using techniques such as ^{1}H NMR and fluorescence spectroscopies.
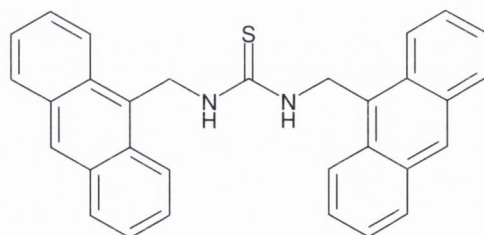
109
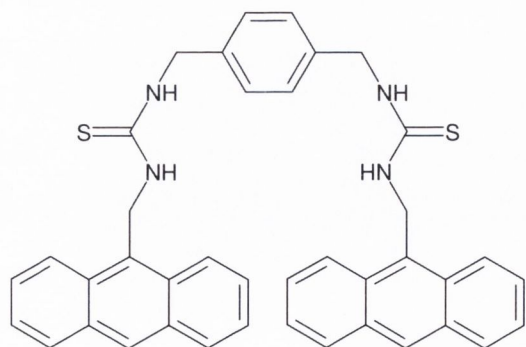
110
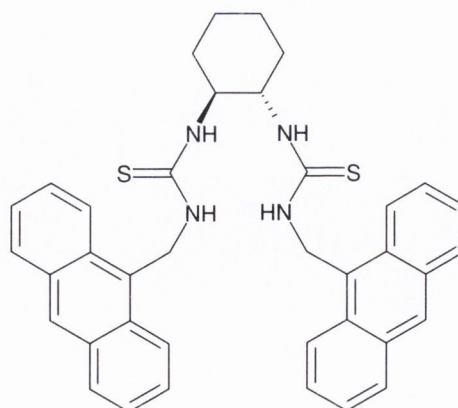
111

The second part of this chapter looks at the possibility of monitoring anion recognition *via* changes in the chiro-optical properties of the anion sensor. Hence, *bis*-napthalene derivatives **112 - 114** containing chiral centres were designed and synthesised. Anion binding of **112 - 114** were monitored using ^{1}H NMR, fluorescence and circular dichroism (CD) spectroscopies.

112   **113**

114
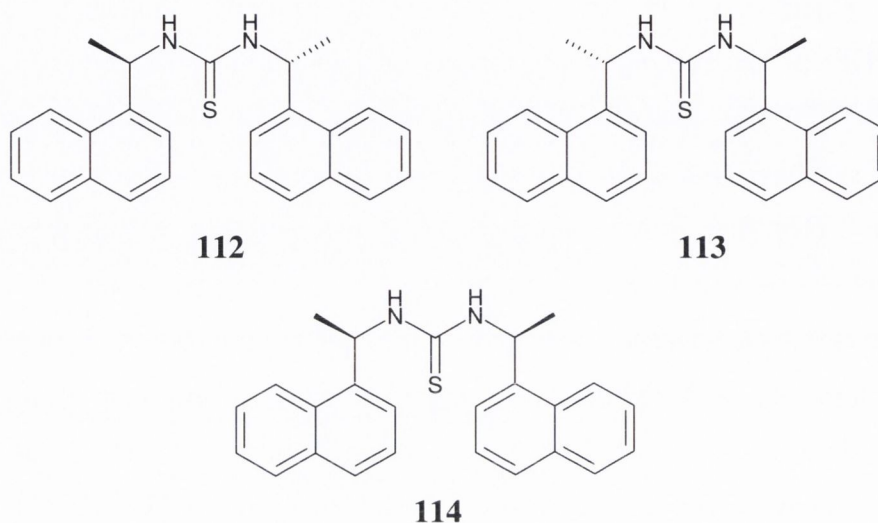
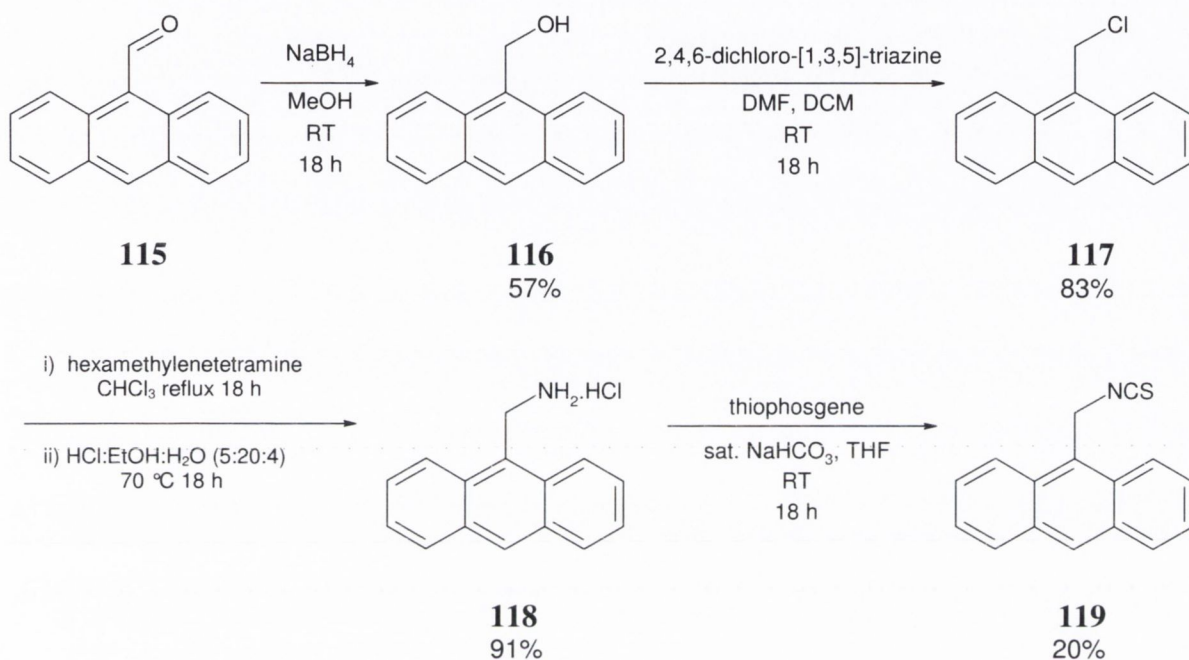## 3.4   *Bis*-Anthracene-based Fluorescent Anion Sensors 109 - 111

In this section of Chapter 3, the synthesis of fluorescent thiourea-based anion sensors containing two anthracene moieties (**109 – 111**) and the physical evaluation of their anion binding abilities will be discussed.

3.4.1   Synthesis of Sensors 109 - 111

Compounds **109 - 111** used in the anion binding experiments (discussed later in this chapter) were designed by Dr Tierney within the Gunnlaugsson research group. The synthesis of all three compounds began with the readily available starting material 9-anthraaldehyde **115**, which was converted to 9-(isothiocyanatomethyl)anthracene **119** in four steps following a previously published procedure (Scheme 3.1).[134] This isothiocyanate derivative is the main component required for the synthesis of the designed *bis*-anthracene systems **109 - 111**.

The aldehyde **115** was first reduced to its alcohol **116** using NaBH$_4$. Chloro-substitution of **116** was achieved using 2,4,6-trichloro-[1,3,5]-triazine (cyanuric chloride) to give **117**. This was then converted into the amine using hexamethylene tetraamine and isolated as the HCl salt **118**. Finally, **119** was formed from the reaction

of 9-(aminomethyl)anthracene hydrochloride **118** with thiophosgene in a biphasic mixture of saturated NaHCO$_3$ and THF. The crude product was isolated as an oil, which was purified using silica gel chromatography with ethyl acetate-hexane (9:1) as the eluent. The pure isothiocyanate **119** was obtained as an yellow solid with a yield of 20%. However, the precursors of this compound were all obtained with reasonably high yields (57 - 91%).


Scheme 3.1 Four-step conversion of 9-anthraaldehyde **115** into 9-(isothiocyanatomethyl) anthracene **119**.

The anthracene-based fluorescent sensor **109** was formed from the reaction of **118** and **119** in the presence of a catalytic amount of triethylamine in anhydrous DCM (Scheme 3.2). The reaction was left stirring at room temperature for 30 minutes after which a yellow precipitate had formed. The desired precipitate was isolated by filtration and was washed with DCM and diethyl ether to remove any impurities or starting material. The yield for the synthesis of **109** was 78%.
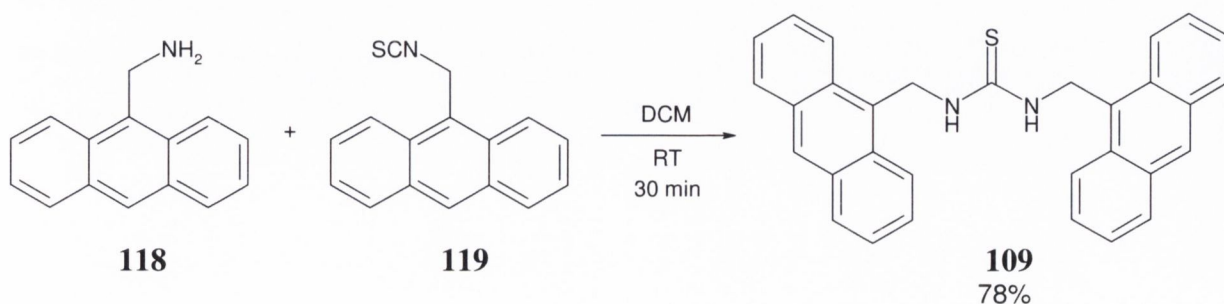
Scheme 3.2 Synthesis of fluorescent sensor **109**.

Compounds **110** and **111** were obtained by the reaction of two equivalents of the isothiocyanate α,α'-diamino-*p*-xylene **120** and (1S,2S)-(+)-1,2-diaminocyclohexane **121** respectively, using the same method as for the synthesis of **109** (Scheme 3.3). They were also obtained as yellow solids with yields of 78% and 43% for **110** and **111** respectively.
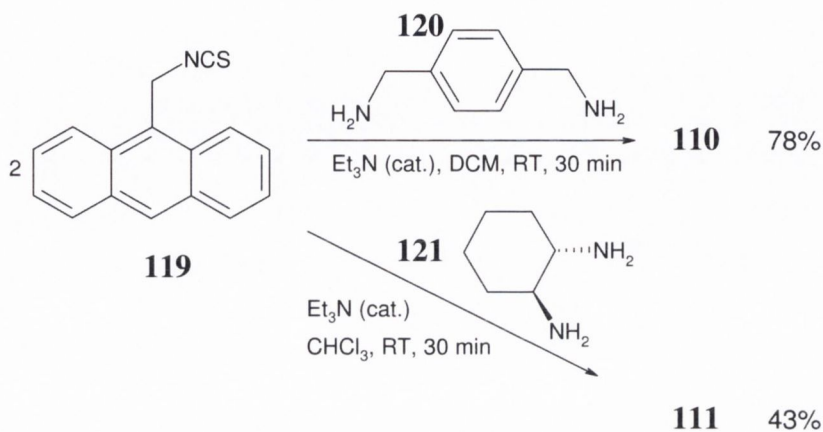

Scheme 3.3 Synthesis of fluorescent sensors **110** and **111**.

3.4.1.1 Characterisation of 109 - 111

The characterisation of **109** - **111** were achieved by ^{1}H and ^{13}C NMR spectroscopy, infrared (IR) spectroscopy (IR) and elemental analysis (CHN).

Figure 3.1 shows the ^{1}H NMR spectrum of **109** in DMSO-d_6. The characteristic anthracene aromatic shifts can be clearly observed, with a singlet at 8.52 ppm, doublets at 8.33 and 8.01 ppm, and a multiplet centred at 7.45 ppm. The signals for the NH protons of the thiourea moiety are masked under the anthracene multiplet, and their presence were verified using a D$_2$O shake. Compound **109** is clearly symmetrical as only one set of each type of proton can be observed in the spectrum.

The ^{1}H NMR spectra of the *bis*-anthracene systems **110** and **111** also showed the characteristic signals for anthracene. Two of the NH protons of the thiourea moieties in **110** are also masked under the anthracene multiplet at 7.50 ppm, as observed in compound **109**. However, the other two NH protons are not hidden and are located at 7.75 ppm. Only in compound **111** are all four NH protons unmasked by other peaks on the spectrum.
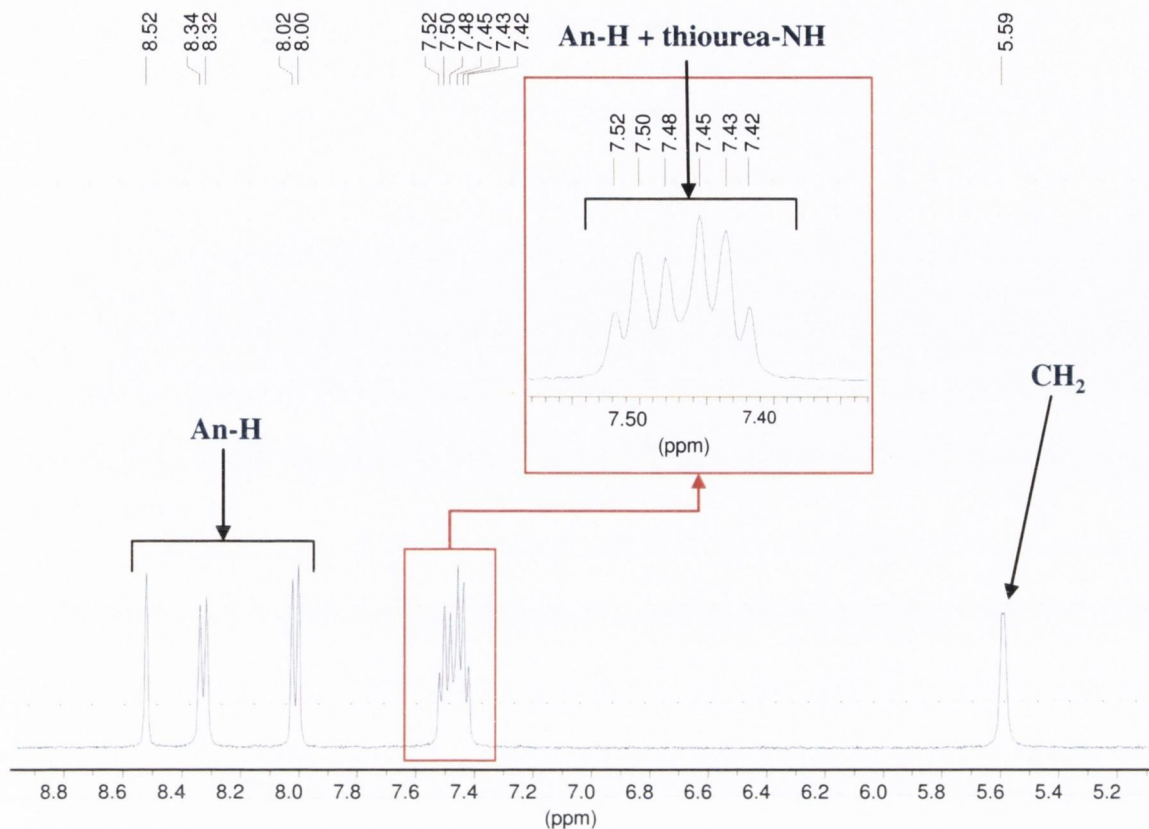
Figure 3.1 ^{1}H NMR spectrum (400 MHz, DMSO-d_6) of thiourea **109**.

Figure **3.2** illustrates the ^{1}H NMR spectrum of compound **111** in DMSO-d_6. The chemical shifts for the thiourea NH protons in **111** are located 7.16 and 7.68 ppm. Another characteristic set of chemical shifts observed in **111** are the CH$_2$ and chiral CH protons on the cyclohexane ring. Since cyclohexane is generally stable in the chair conformation, five broad singlet peaks observed in the ^{1}H NMR spectrum may be assigned to the protons of this ring. The methylene protons are in sets of two protons located at 0.98, 1.14, 1.50 and 2.06 ppm, while the CH protons at the chiral centres of the cyclohexane ring adjacent to the NH protons of the thioureas are found further downfield at 4.01 ppm.

The melting points of thioureas **109**, **110** and **111** were also obtained and found to be in the region between 240 and 260 °C.
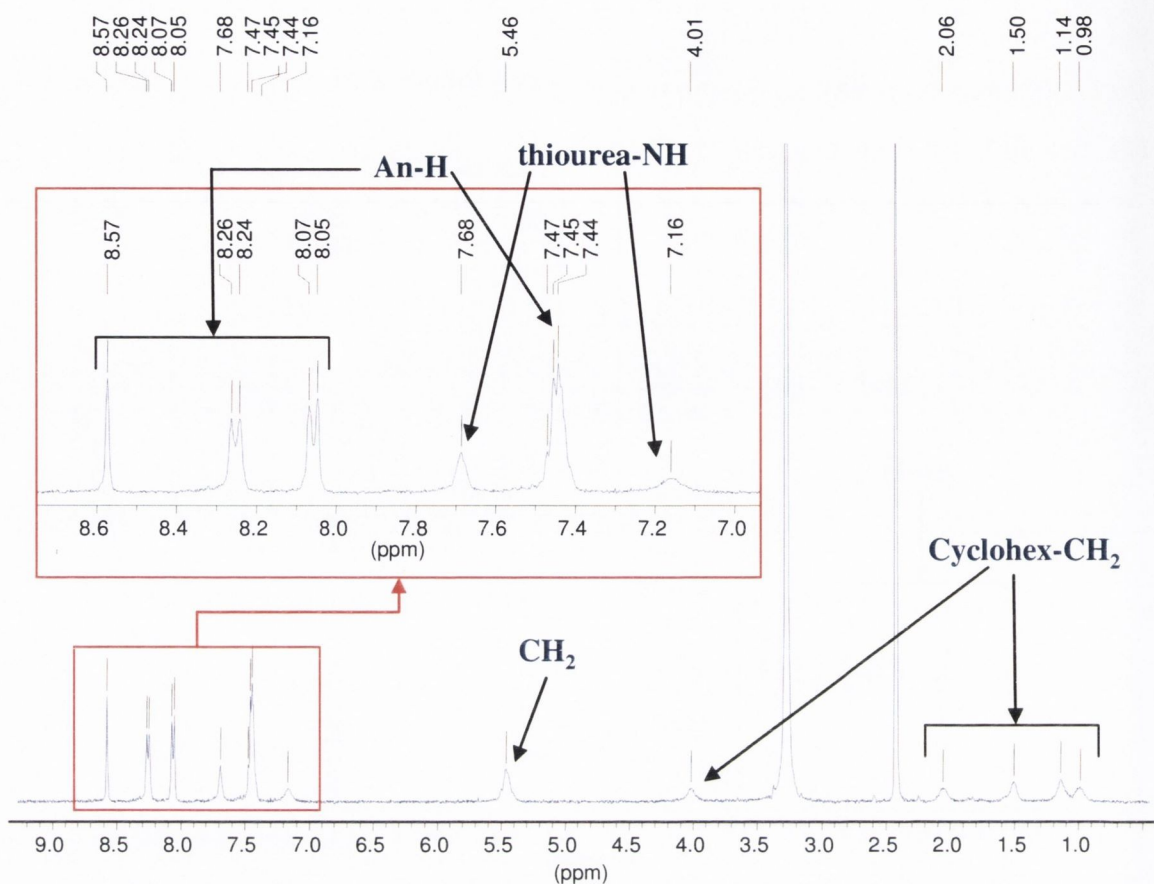
Figure 3.2 ^{1}H NMR spectrum (400 MHz, DMSO-d_6) of thiourea **111**.

### 3.4.2   Physical Evaluation of the Anion Recognition of 109 - 111

The ability of **109 - 111** to recognise anions in DMSO were initially studied by ^{1}H NMR spectroscopy, which is a useful technique to directly observe the effect of anion complexation on the NH protons of such sensors. Photophysical studies (using mainly fluorescence spectroscopy) were also conducted.

3.4.2.1 ^{1}H NMR Titrations of 109 - 111 with Anions

The ^{1}H NMR spectroscopic experiments were performed on host solutions of **109 - 111** in DMSO-d_6 (0.5×10^{-2} M - 1.0×10^{-2} M) at 25 °C. On all occasions, it was possible to monitor the thiourea NH protons in these experiments as their chemical shifts did not broaden significantly and were clearly distinct. In general, the signals for these NH protons were shifted downfield upon anion recognition. This recognition event was clearly observed for all the three sensors upon addition of AcO$^-$, H$_2$PO$_4^-$ and F$^-$. One exception was the lack of binding observed in the titration of **109** with H$_2$PO$_4^-$,

as none of the NH protons were significantly perturbed. This may be attributed to the bulky shape of $H_2PO_4^-$ compared to AcO^- and F^-, and hence, it is difficult for this guest to approach the sterically hindered thiourea receptor site.

Figures 3.3 and 3.4 illustrate, by means of stackplots, the changes observed in the ^1H NMR spectrum of **109** upon the addition of AcO^- and F^- respectively. When AcO^- or F^- was added to **109**, only the peaks indicating the NH protons were significantly perturbed. Although the chemical shifts of the anthracene moiety showed very little shift upon anion binding, the peaks broadened appreciably. In the case of F^- binding, there was also an appearance of a new triplet peak at *ca.* 16 ppm, which indicated the formation of HF_2^- upon the deprotonation of one of the thiourea NH protons. The appearance of this peak in presence of *ca.* two equivalents of fluoride has been reported in the literature.[91,118,135,143,169,170,182] Interestingly, the appearance of the HF_2^- in this case occurred after the addition of *ca.* one equivalent of fluoride. Gale and co-workers have reported a similar case where the deprotonation also takes place upon the addition of only one guest equivalent, possibly due to the high acidity of the urea or thiourea NH protons.[88,140]
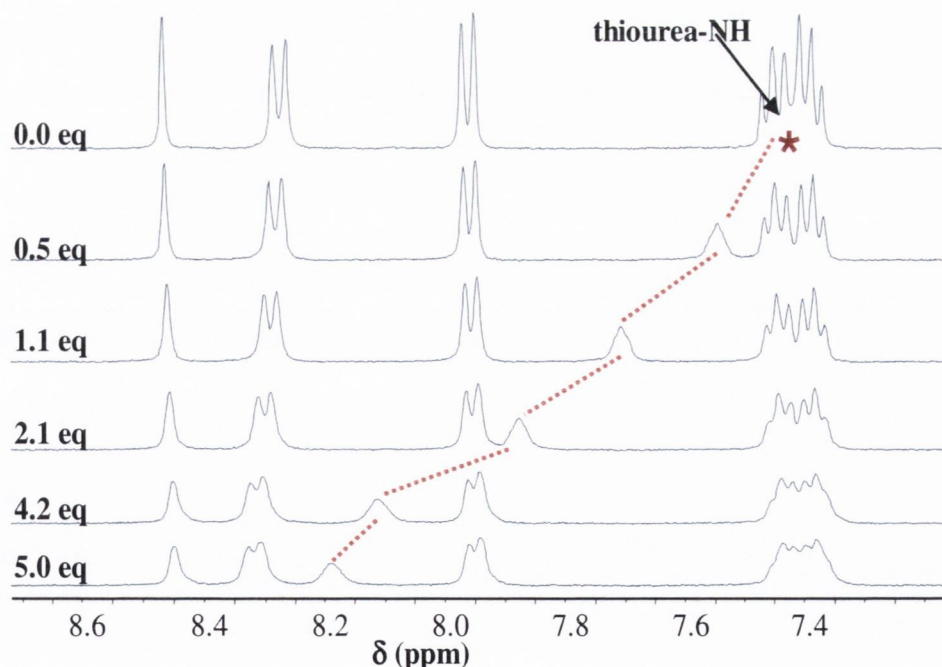
Figure 3.3 Stack plot of ^1H NMR spectra of **109** (1.0×10^{-2} M) upon addition of AcO^- in DMSO-d_6. (*the peak indicating thiourea NH protons are hidden underneath the anthracene multiplet in the free host of **109**.)
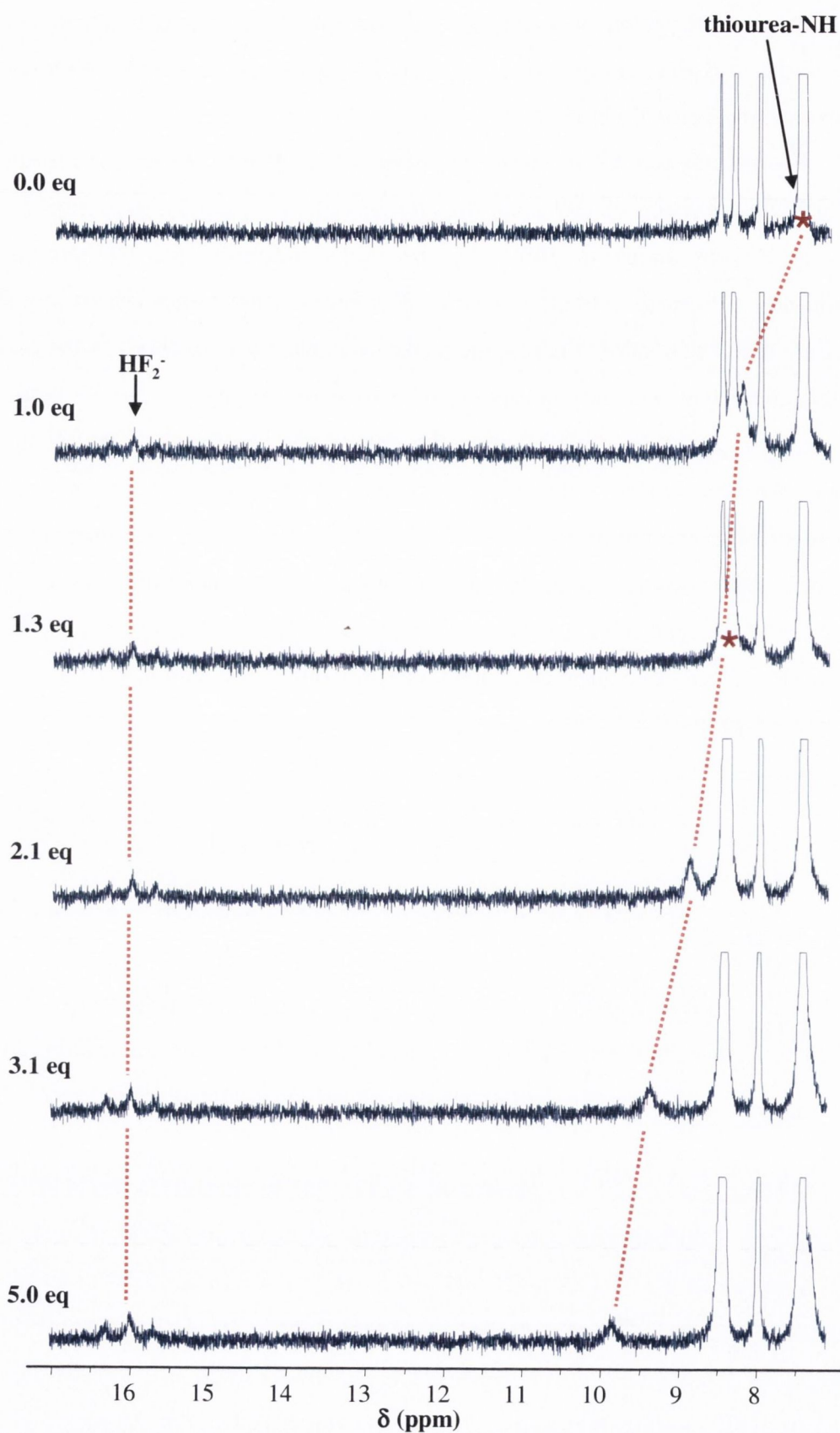
Figure 3.4 Stack plot of ^{1}H NMR spectra of **109** (1.0×10^{-2} M) upon addition of F$^-$ in DMSO-d_6. (*the peak indicating thiourea NH protons are hidden underneath the anthracene multiplet in the free host of **109**.)

**3.4.2.1.1 Analysis of the ^{1}H NMR Titration Data for 109 - 111**

The results obtained from these titrations was plotted as the cumulative changes in chemical shift ($\Delta\delta$) against the equivalents of anion added. Figures 3.5, 3.6 and 3.7 show the plots of $\Delta\delta$ against equivalents of various anions for thioureas **109**, **110** and **111**, respectively. Compound **109** bound to F$^-$ the strongest, followed by AcO$^-$. However, the binding curves did not fully achieve a plateau even after 5 equivalents of guest are added, indicating weak binding. There was very little binding observed for H$_2$PO$_4^-$ and Cl$^-$. The lack of binding to H$_2$PO$_4^-$ may be due to steric crowding of the thiourea receptor site by the two bulky anthracene moieties as previously discussed.
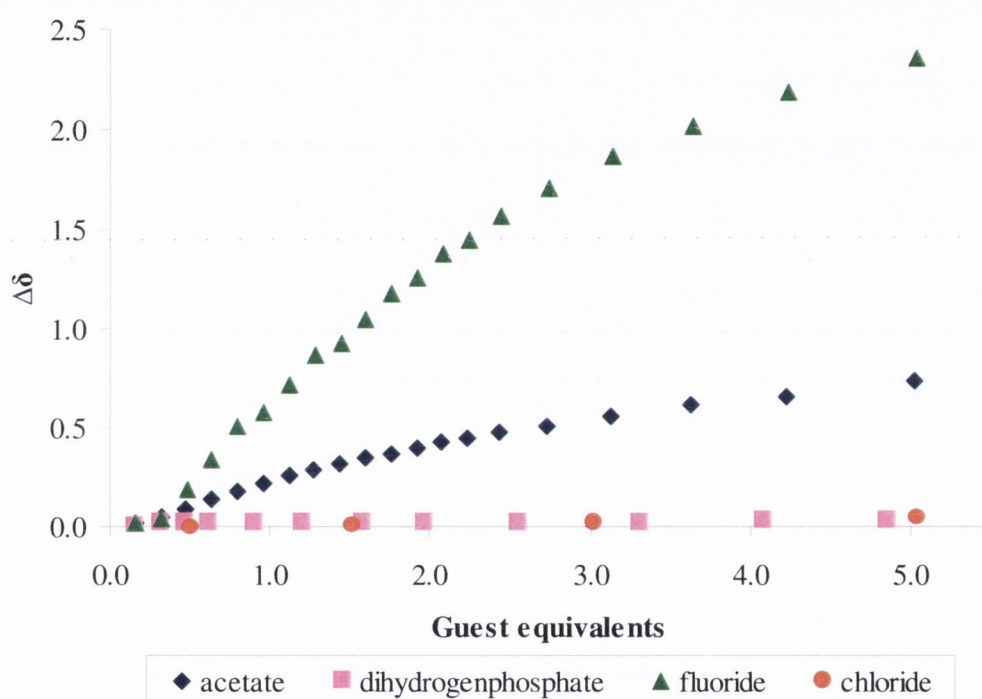
Figure 3.5 Relative cumulative changes in the chemical shift of NH proton at 7.5 ppm for sensor **109** (1.0 × 10^{-2} M) against equivalents of various anions in DMSO-d_6.

In the case of the *bis*-anthracene systems **110** and **111**, the magnitude of perturbation of the thiourea NH protons appeared to be similar for the AcO$^-$ and F$^-$ recognition. The apparent increase in the binding affinity of these compounds to AcO$^-$ may be the due to these hosts being more flexible as a result of the methylene spacers appending the thiourea receptors to the structural backbones (*i.e.* phenyl and cyclohexane rings). Hence, more bulky anions such as AcO$^-$ and H$_2$PO$_4^-$ may be able to approach the receptor sites with more ease. The lessening of the steric hindrance also led to more significant changes in the thiourea NH peaks upon H$_2$PO$_4^-$ complexation. However, there is still very little binding observed in the presence of chloride.
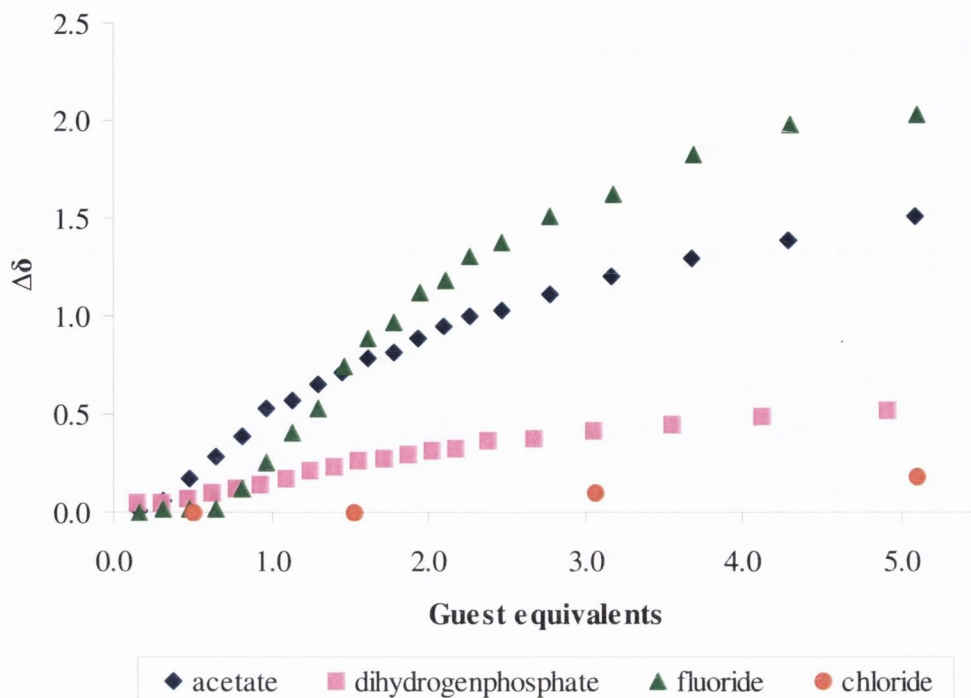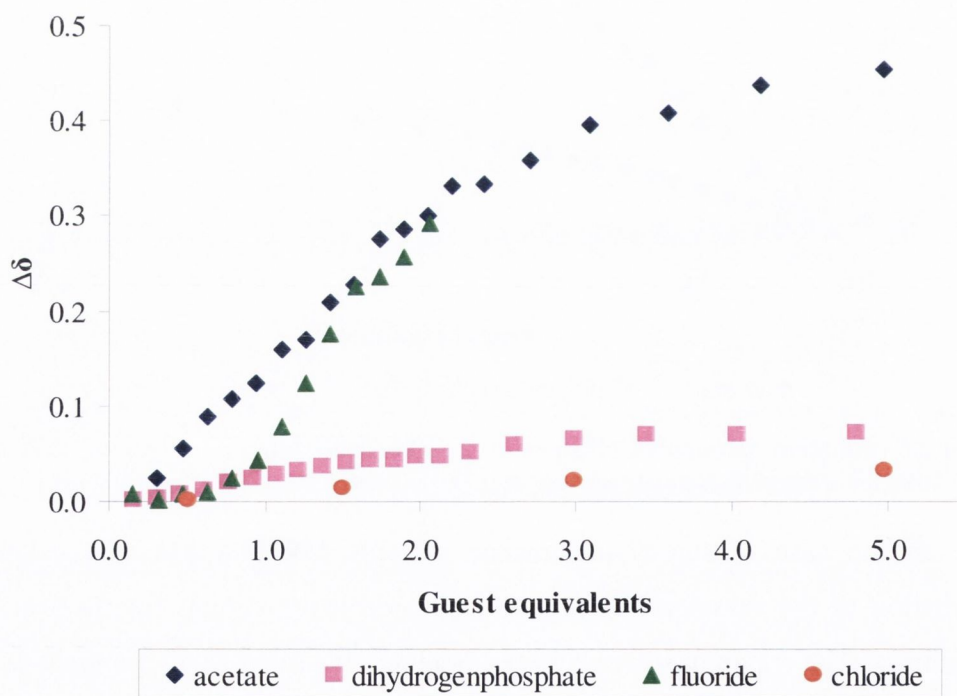
Figure 3.6 Relative cumulative changes in the chemical shift of proton at 7.5 ppm for sensor **110** (1.0×10^{-2} M) against equivalents of various anions in DMSO-d_6.

Figure 3.7 Relative cumulative changes in the chemical shift of proton at 7.2 ppm for sensor **111** (0.5×10^{-2} M) against equivalents of various anions in DMSO-d_6.

It is also notable that **111** seemed to bind F⁻ more strongly than **110**, since the NH peaks completely disappeared in **111** after the addition of *ca.* two equivalents of the guest, which is a characteristic point for the deprotonation of the thiourea NH protons to occur.

3.4.2.1.2 Stability Constants (log β) from ^{1}H NMR Titration Data of 109 - 111

The stability constants (log β) for the complexation of **109** - **111** with the selected anions (Table 3.1) were determined from the data collected using the Fortran-based WinEQNMR program.[12] It was not possible to obtain log β values obtained for the complexation of the monotopic thiourea sensor **109** with the selected anions. This may be due to the weak binding of **109** to AcO$^-$ and F$^-$, while there was no significant binding to $H_2PO_4^-$ and Cl$^-$.

Table 3.1 Binding constants (log β) of **109** - **111** upon complexation with putative anions in DMSO-d_6. All values were obtained from WinEQNMR,[12] and are within 15% error. ^{a} the binding process is too complicated for analysis by WinEQNMR; ^{b} the binding is too weak for analysis by WinEQNMR.

Sensor	log β (AcO$^-$)	log β ($H_2PO_4^-$)	log β (F$^-$)
109	^{b}	^{b}	$^{a, b}$
110	1.67	1.49	^{a}
111	1.99	1.96	^{a}

The presence of two thiourea moieties within these *bis*-anthracene molecules seemed to enhance the anion binding abilities. However, it is uncertain whether this is due to the multiple binding sites, or the possibility that the NH protons may be less sterically obstructed by the anthracene rings. From the stability constants obtained, it is observed that compound **111** bound the strongest to AcO$^-$ with a log β value of 1.99, while compound **110** bound the anion with a log β value of 1.67. In the case of $H_2PO_4^-$ binding, compound **111** achieved a higher stability constant (log β = 1.96) than compound **110** (log β = 1.49). The log β values for the F$^-$ complexation by **110** and **111** could not be obtained, as this may involve more than one process and may not have 1:1 host:guest (H:G) stoichiometries. The presence of the triplet peak at 16 ppm in the ^{1}H NMR titration also indicated the possibility of a second process (*i.e.* the deprotonation of one of the NH protons of the thiourea).

From these ^{1}H NMR binding studies, it was observed that all three *bis*-anthracene compounds generally bind anions in the following order: F$^-$ > AcO$^-$ > $H_2PO_4^-$ > Cl$^-$. However, the binding is still considerably weak in comparison to that of mono-anthracene thiourea sensors previously studied within the group.[20,89,103,134,147,148]

Compound **111** appears to bind anions the best of all three compounds, which may be the result of less steric hindrance present within this molecule.

Figures 3.8 (a) - (d) show the graphs generated by WinEQNMR illustrating the fit between the observed and calculated data for the binding of AcO$^-$ and H$_2$PO$_4^-$ by **110** and **111**. A good fit ensures that the log β value calculated by the program is reasonable, even though the value of the error may be quite big.
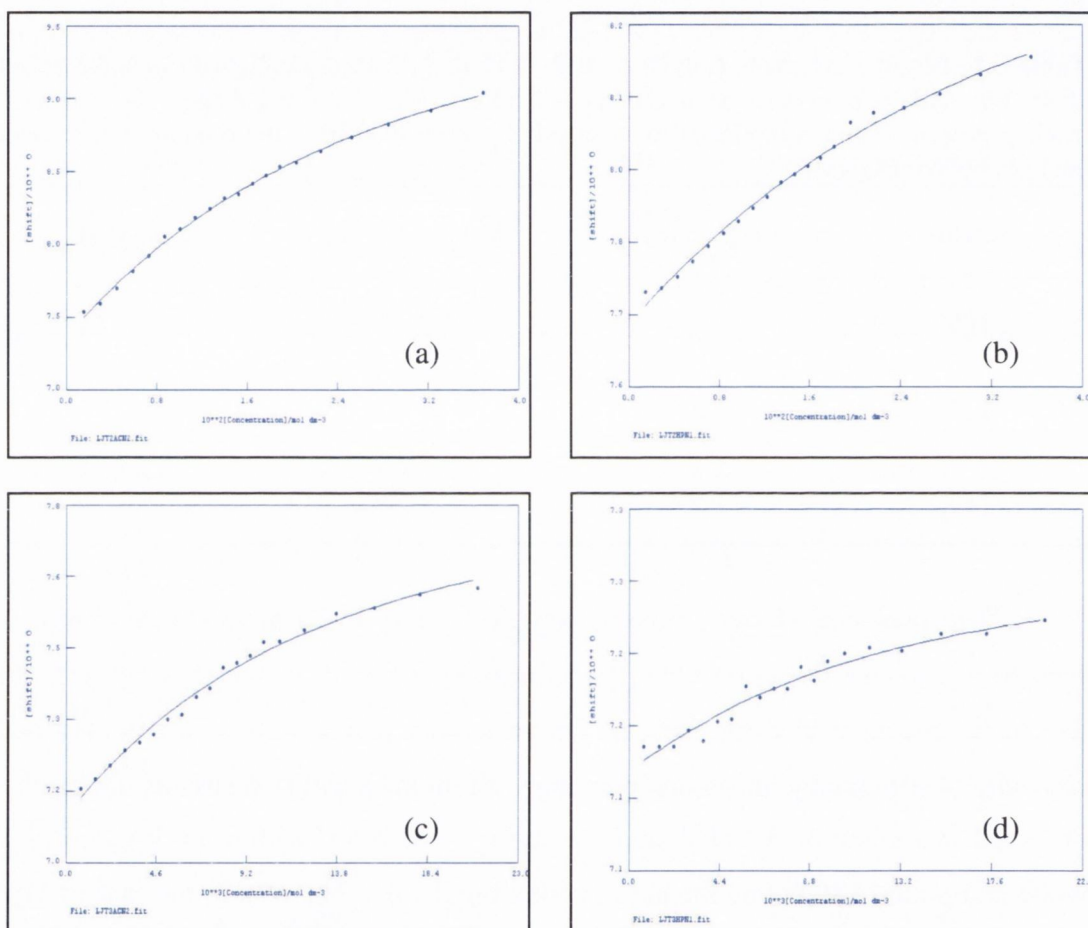
Figure 3.8 WinEQNMR-generated graphs of the fit between the observed (points) and calculated (line) data for the binding of: (a) AcO$^-$ with **110** (1.0×10^{-2} M); (b) H$_2$PO$_4^-$ with **110** (1.0×10^{-2} M); (c) AcO$^-$ with **111** (0.5×10^{-2} M); (d) H$_2$PO$_4^-$ with **111** (0.5×10^{-2} M), carried out in DMSO-d_6.

### 3.4.2.2 Fluorescence Titrations of 109 - 111 with Anions

The photophysical properties of **109** - **111** were initially measured in DMSO at 25 °C. The absorption spectra for these compounds exhibited the characteristic fine structure that is usually observed for anthracene, consisting of a central main band at 370 nm, and two other bands at 352 and 391 nm. The extinction coefficients of **109**, **110** and **111** in DMSO were calculated from the absorbances obtained at 370 nm and

were found to be 18131, 18773 and 18600 $M^{-1}cm^{-1}$ respectively. The fluorescence emission of all three compounds (excited at 370 nm) were also similar to each other, demonstrating the characteristic fine structure of anthacene. The band with maximum intensity occurred at 420 nm, followed by the bands at 398 and 444 nm and a shoulder located at 475 nm.

Anion binding studies monitoring fluorescence changes upon anion recognition were carried out on DMSO solution of **109** - **111** (6×10^{-6} M) at 25 °C. The absorption of the samples were monitored in parallel with these experiments. The host solution was excited at the wavelength at which the main absorption band occurs (*i.e.* 370 nm), and any changes to the fluorescence upon anion recognition were recorded. Upon anion complexation, the fluorescence of all the *bis*-anthracene systems were quenched, but only to a small extent. Figures 3.9 - 3.12 illustrate the changes in the fluorescence intensity of **109** in the presence of AcO^-, $H_2PO_4^-$, F^- and Cl^-, respectively. As previously observed in the ^1H NMR binding studies, compound **109** bound weakly to AcO^- and F^- and had little affinity for $H_2PO_4^-$ and Cl^-. This trend was reflected in the small quenching of the fluorescence spectra observed upon anion recognition. As for the absorption of **109**, there was little change in the absorbance upon the addition of anions except at shorter wavelengths ($\lambda < 355$ nm), where there was an increase in the magnitude of the absorbance (Figure 3.9 - inset). This increase was due to the hydrogen-bonding interactions of the thiourea moiety with the anion, and has been previously confirmed from the studies carried out by Gunnlaugsson *et al.* on the mono-anthracene thiourea systems.[134] Their findings also showed that there are no significant ground state interactions between the anthracene ring and the thiourea moiety, as any π-π or n-π interaction is prevented by the methylene spacer.

The changes observed (in the fluorescence and absorption) for the binding of the selected anions by **110** and **111** were similar to those observed for **109**, where they bound best to AcO^- and F^-. The graphs illustrating the changes in the fluorescence intensity of **110** and **111** in the presence of AcO^-, $H_2PO_4^-$, F^- and Cl^- may be viewed in Appendix 7.2.1.
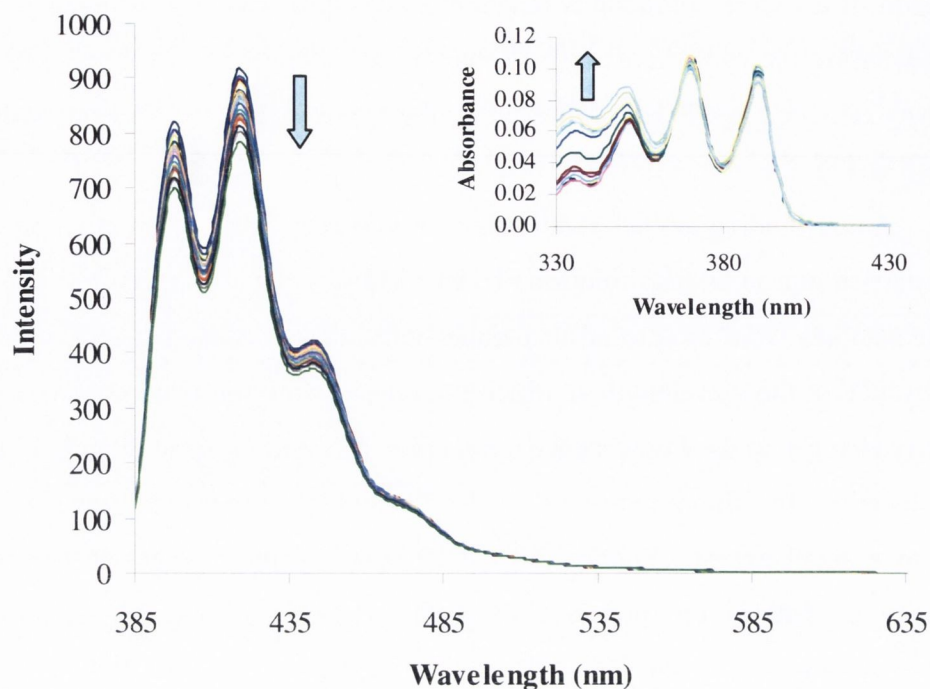
Figure 3.9 Changes in the fluorescence spectrum of **109** (6×10^{-6} M) in DMSO on addition of AcO⁻ (excited at 370 nm; 0 M → 6×10^{-3} M). Inset: Changes observed in the absorption spectrum of **109** in DMSO on addition of AcO⁻ (0 M → 6×10^{-3} M).
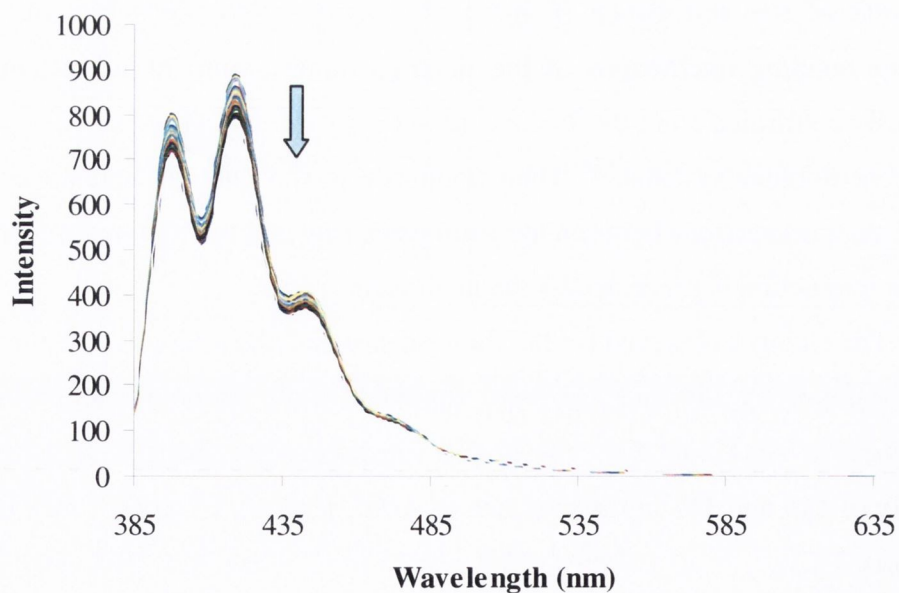
Figure 3.10 Changes in the fluorescence spectrum of **109** (6×10^{-6} M) in DMSO on addition of $H_2PO_4^-$ (excited at 370 nm; 0 M → 6×10^{-3} M).
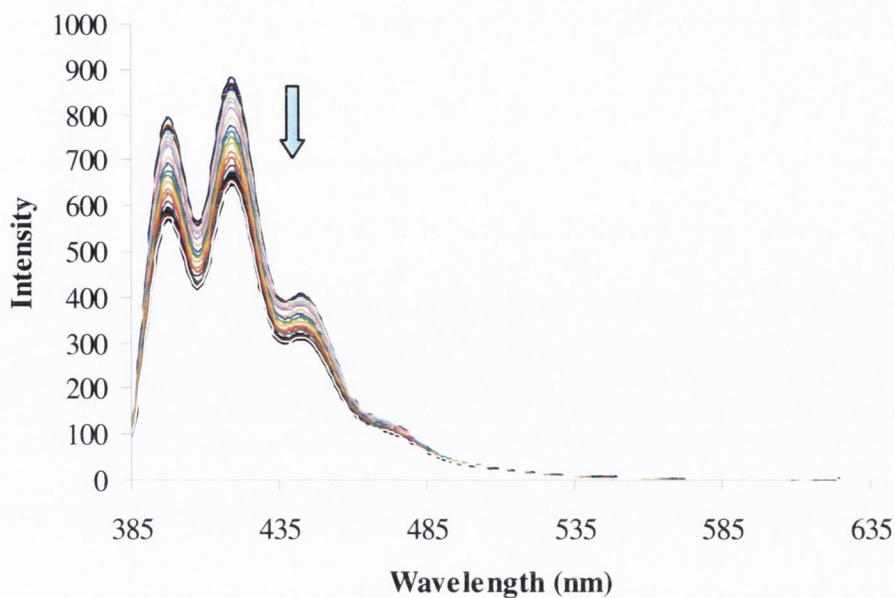
Figure 3.11 Changes in the fluorescence spectrum of **109** (6×10^{-6} M) in DMSO on addition of F⁻ (excited at 370 nm; 0 M → 6×10^{-3} M).
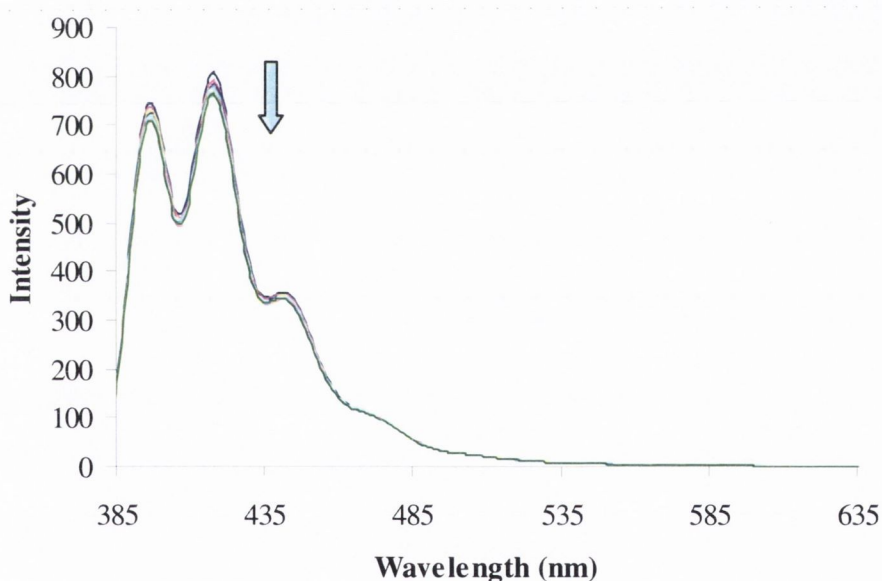

Figure 3.12 Changes in the fluorescence spectrum of **109** (6×10^{-6} M) in DMSO on addition of Cl⁻ (excited at 370 nm; 0 M → 6×10^{-3} M).

3.4.2.2.1 Analysis of the Fluorescence Titration Data for 109 - 111

The changes in the maximum emission band at 420 nm of these *bis*-anthracene fluorescent systems were plotted as a function of -log[anion] (Figures 3.13 - 3.15). It is clear from the graphs that the magnitude of the fluorescence quenching effect due to anion binding of **109 - 111** is relatively small, which reflects their low anion binding affinity observed in the previously discussed ¹H NMR binding experiments.

Figure 3.13 illustrates the relative changes observed at 420 nm in the fluorescence spectrum of **109** in the presence of the selected anions in DMSO. Compound **109** showed the most changes in the binding of F⁻, followed by that of AcO⁻. The presence of $H_2PO_4^-$ and Cl⁻ had very little effect on the fluorescence of **109**. As previously mentioned, the lack of binding in the case of $H_2PO_4^-$ may be the result of the thiourea receptor site being sterically obstructed by the bulky anthracene rings.
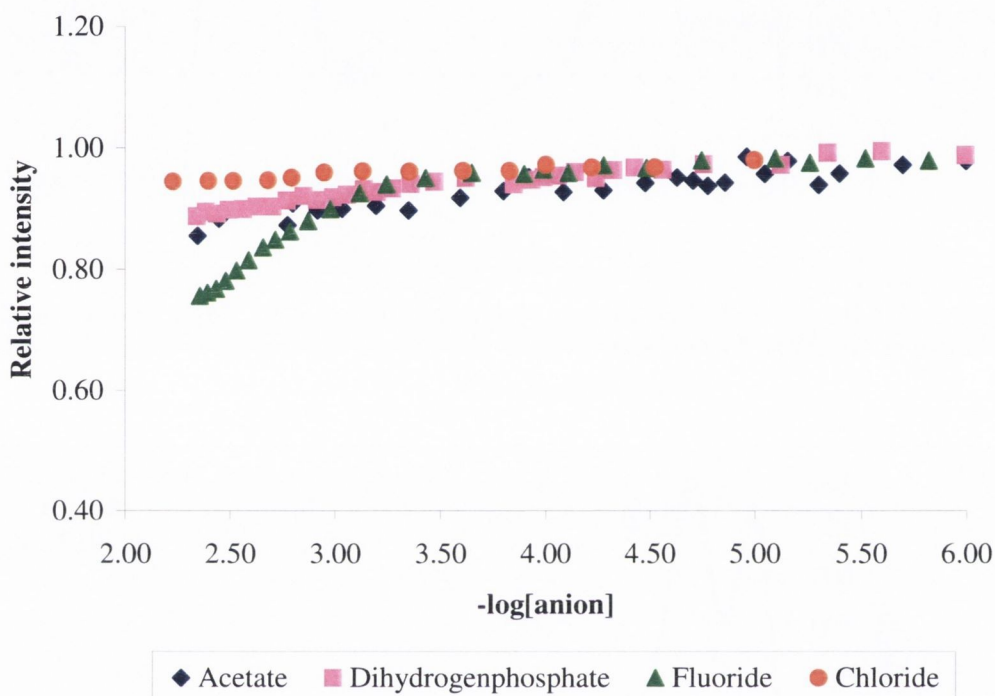
Figure 3.13 Relative fluorescence intensity of sensor **109** at 420 nm against -log[anion] in DMSO on addition of various anions (excited at 370 nm; 0 M → 6×10^{-3} M).

The changes at 420 nm in the fluorescence spectra of the *bis*-anthracene ditopic sensors **110** and **111** upon anion recognition are illustrated in Figures 3.14 and 3.15, respectively. Again, the emission quenching due to anion binding was not significant, and the most effect was observed for the complexation of F⁻, followed by AcO⁻. The $H_2PO_4^-$ molecule also appeared to be bound by these *bis*-anthracene systems, in contrast to the monotopic thiourea sensor **109**. This may be attributed to the decrease in steric hindrance in both **110** and **111**, as a result of wider spatial distances between tohe two receptor arms as well as the increase in flexibity of these systems.
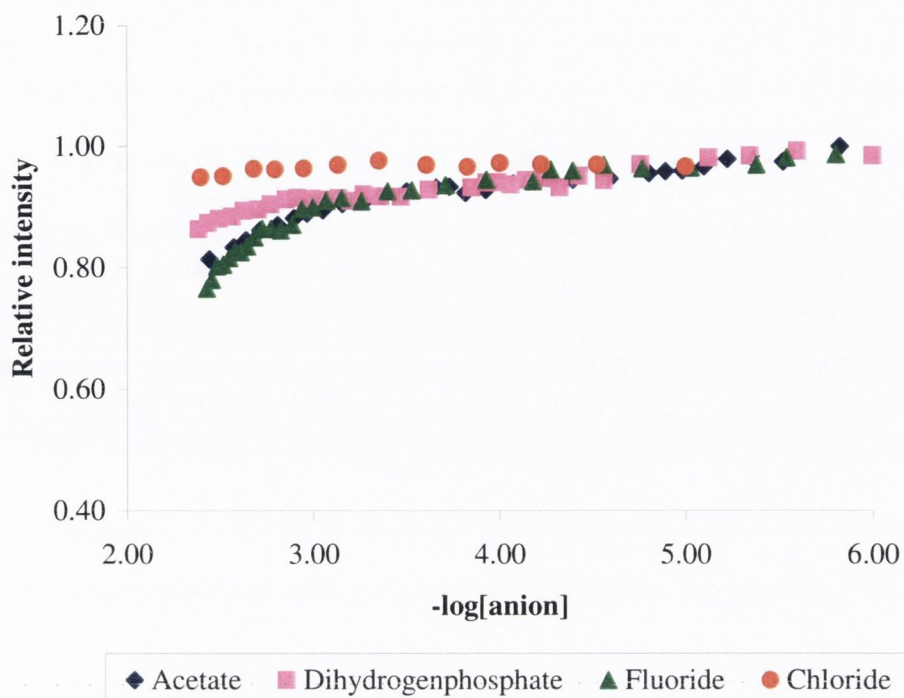
Figure 3.14 Relative fluorescence intensity of sensor **110** at 420 nm against -log[anion] in DMSO on addition of various anions (excited at 370 nm; 0 M → 6 × 10⁻³ M).
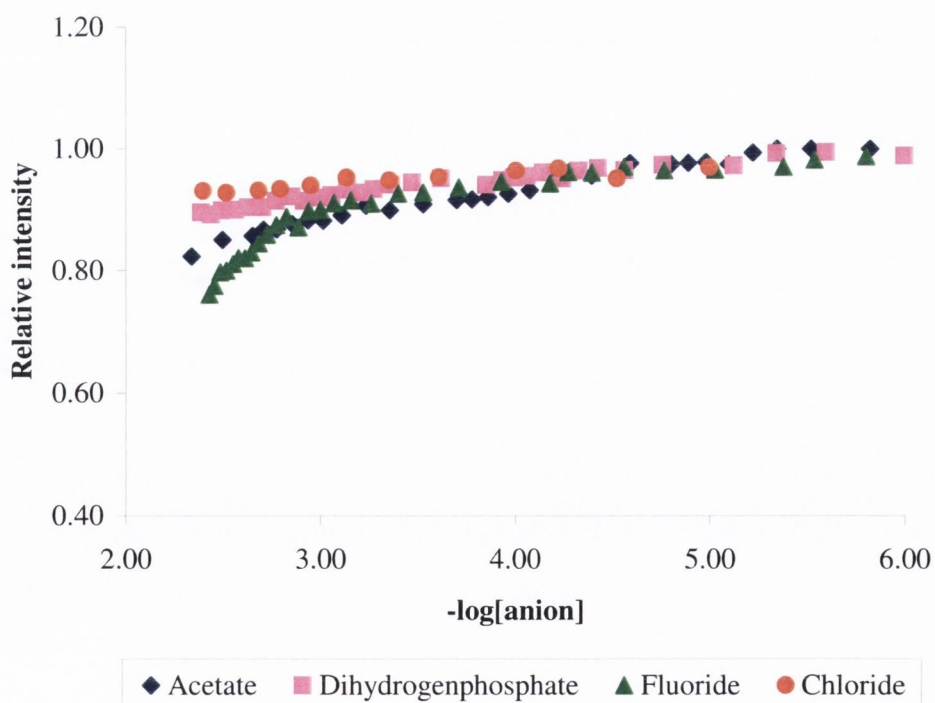

Figure 3.15 Relative fluorescence intensity of sensor **111** at 420 nm against -log[anion] in DMSO on addition of various anions (excited at 370 nm; 0 M → 6 × 10⁻³ M).

The previous graphs illustrate the weak response of these sensors towards the selected anions in DMSO (*i.e.* changes were observed only after [anion] $\approx 6 \times 10^{-3}$ M). Even at very high concentrations, the binding curves did not reach a plateau, clearly illustrated by the example in Figure 3.16, showing the changes in the intensity of **110** when [anion] $\approx 2 \times 10^{-1}$ M.
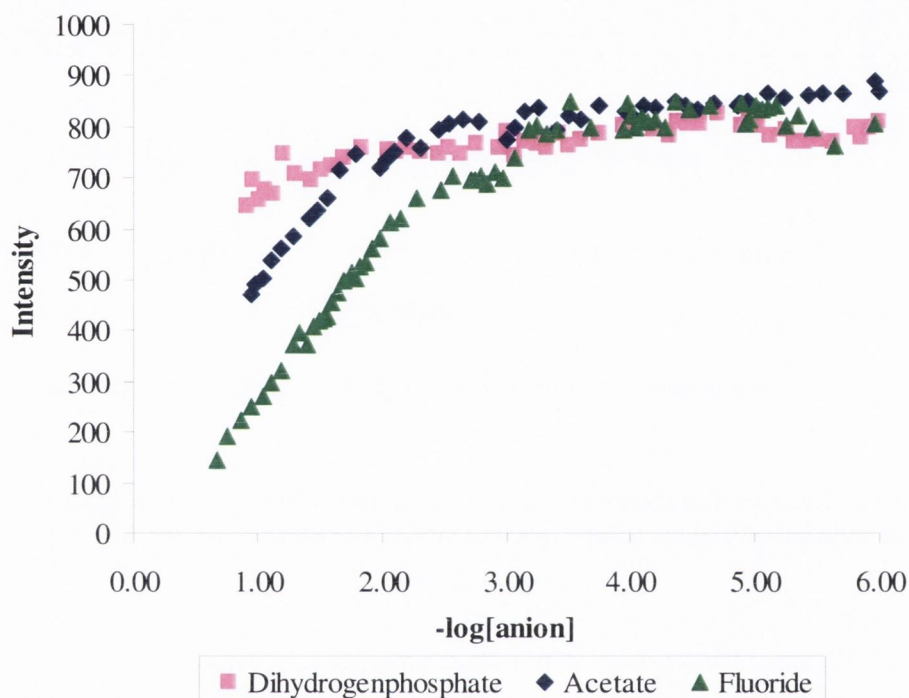

Figure 3.16 Relative fluorescence intensity of sensor **110** at 420 nm against -log[anion] in DMSO on addition of various anions (excited at 370 nm; 0 M $\rightarrow$ 2×10^{-1} M).

3.4.2.2.2 Stability Constants (log β) from Fluorescence Titration Data of 109 - 111

SPECFIT/32™ was used in order to obtain the stability constants (log β) for the anion binding processes undergone by compounds **109** - **111**. This program analyses data obtained from both fluorescence and absorption titrations using a non-linear least-squares regression method. However, in the case of these *bis*-anthracene systems, the quenching of their fluorescence intensities in the presence of anion was too small for successful evaluation by SPECFIT/32™. In fact, a large quantity of anion (> 1000 equivalents) was required to induce a large change in the fluorescence spectra of these sensors.

3.4.3   Conclusions

It can be concluded from the physical evaluation carried out on compounds **109** - **111** that such *bis*-anthracene systems are not suitable for successful fluorescent anion sensing. This is most probably due to the amount of steric hindrance present around the thiourea receptors (due to the anthracene rings as well as the phenyl ring in **110** and cyclohexane ring in **111**), preventing the anion to approach these binding sites with ease. All three sensors show the strongest binding to F⁻, as this anion is small enough to reach the thiourea NH protons for binding.
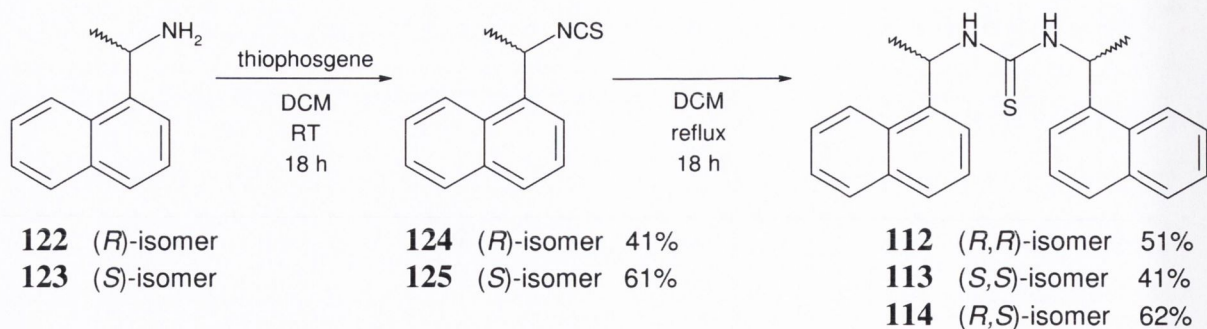
In response to these findings, it was then decided to incorporate naphthalene rings as the fluorophores in the chiral sensors **112** - **114** in an attempt to reduce the steric hindrance presented by such bulky polyaromatic fluorophores.

3.5   Chiral Naphthalene-based Fluorescent Anion Sensors 112 - 114

This section will discuss the synthesis of chiral *bis*-naphthalene-based thiourea derivatives (**112** - **114**) and the physical evaluation of their binding abilities towards putative anions employing techniques previously mentioned (such as ¹H NMR, UV-vis and fluorescence spectroscopies) as well as an additional method which monitors changes in the chira-optical properties of these sensors (*i.e.* circular dichroism).

3.5.1   Synthesis of Sensors 112 - 114

The synthesis of **109** - **111** were carried out in two steps (Scheme 3.4). Commercially available chiral naphthalene-based amines, (*R*)-(+)-1-(1-naphthyl) ethylamine **18** and (*S*)-(-)-1-(1-naphthyl)ethylamine **19,** were first converted using thiophosgene to their corresponding isothiocyanate **20** and **21**, respectively. It was found that these isocyanate precursors have very low boiling points, and therefore, they were isolated as reasonably pure gel-like solids (with yields of 41% and 61% for **20** and **21** respectively) *via* natural evaporation of the reaction solutions. Sensors **112** and **114** were then formed by reacting **18** with **20** and **21** respectively, whereas compound **113** was synthesised using **19** and **21**. The reaction was carried out under argon at room temperature for 18 hours in dry DCM. The desired products were obtained as off-white crystalline solids with reasonable yields (41 - 62%), which readily formed crystals in DMSO, which were suitable for single crystal X-ray diffraction studies.

122	(*R*)-isomer		**124**	(*R*)-isomer	41%	**112**	(*R,R*)-isomer	51%
123	(*S*)-isomer		**125**	(*S*)-isomer	61%	**113**	(*S,S*)-isomer	41%
						114	(*R,S*)-isomer	62%

Scheme 3.4 Two-step synthesis of *bis*-naphthalene-based sensors **112** - **114**.

3.5.1.1 Characterisation of 112 - 114

Compounds **112** - **114** were characterised by ^{1}H and ^{13}C NMR spectroscopy, infrared (IR) spectroscopy (IR), electrospray mass spectroscopy (ESMS) and elemental analysis (CHN). Figure 3.17 ahows the ^{1}H NMR spectrum of **112** in DMSO-d_6. A characteristic pattern for the chemical shifts of the naphthalene protons can be observed in this spectrum (*i.e.* three doublets at 8.18, 7.96 and 7.85 ppm, and a multiplet centred at 7.54 ppm). The thiourea NH resonances were located at 7.76 ppm, and they were verified bya D$_2$O shake. The proton at each chiral centre was located as a broad singlet at 6.21 ppm, while the protons of the methyl groups at the same chiral centres were a doublet at 1.53 ppm. Since compounds **112** and **113** are enantiomers, they gave identical ^{1}H NMR spectra, as observed in Figure 3.18 (a) and (b). The spectrum for the *meso* compound **114** (Figure 3.18 (c)) showed slight differences from the other two spectra, especially for the thiourea singlet, where it was located at 7.69 ppm.
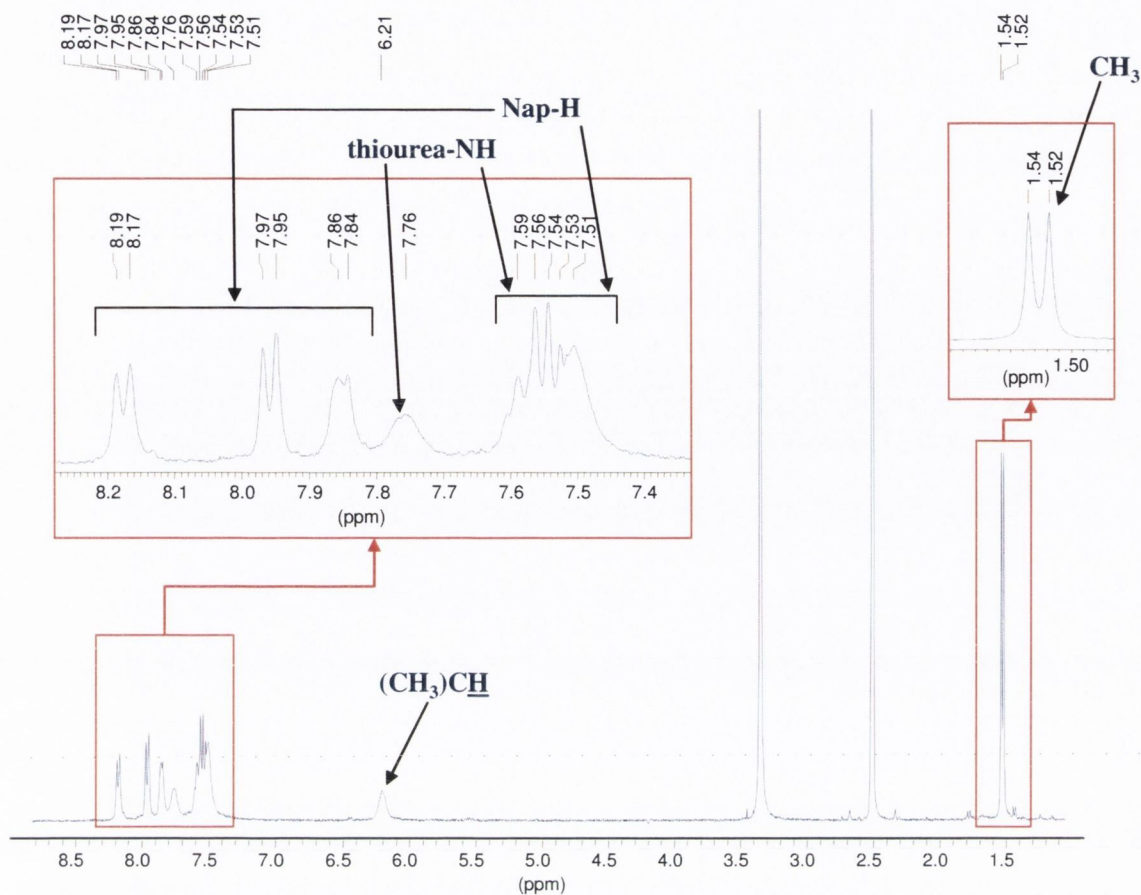
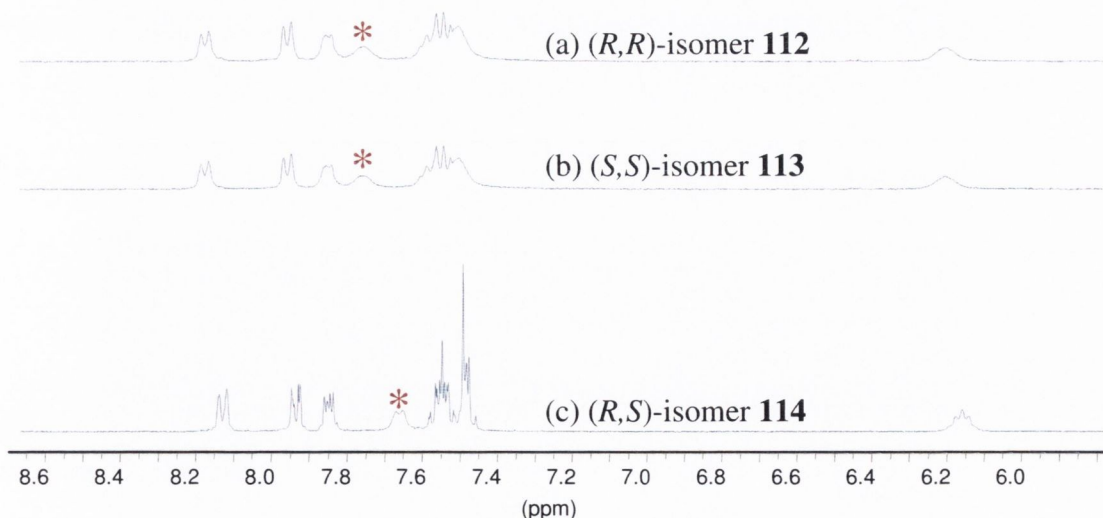**Figure 3.17** ^1H NMR spectrum (400 MHz, DMSO-d_6) of thiourea **112**.

Figure 3.18 Comparison of the ^1H NMR (400 MHz, DMSO-d_6)spectra of thioureas **112 - 114**. (* chemical shift of thiourea NH protons)

3.5.1.2 Crystal Structure Analysis of 112 - 114

Single off-white crystals of compounds **112 – 114** suitable for X-ray diffraction studies were successfully grown from DMSO solutions. Figures 3.19, 3.20 and 3.21 show the crystal structures of **112**, **113** and **114**, respectively. All the hydrogen atoms (except the methyl, thiourea and chiral centre protons) and solvent molecules (DMSO) have been omitted for clarity.
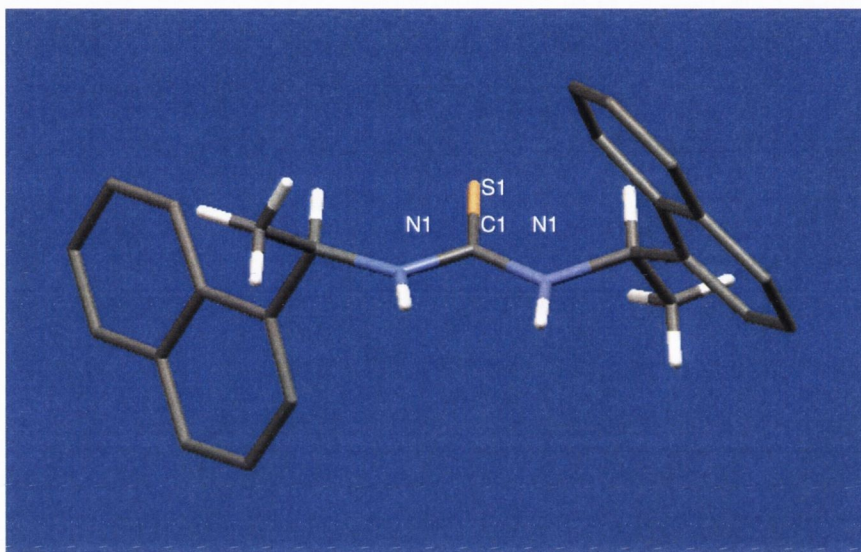
Figure 3.19 Crystal structure of the (*R,R*)-enantiomer **112** (Appendix 7.2.2).
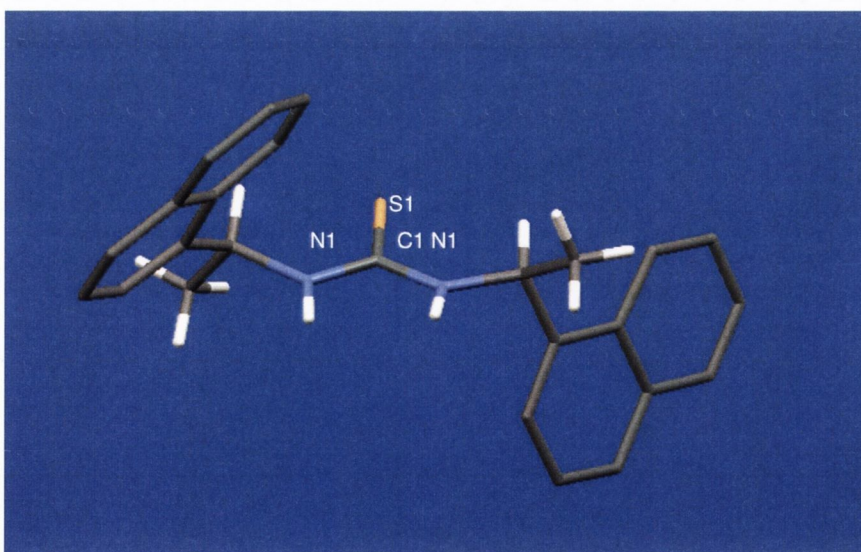
Figure 3.20 Crystal structure of the (*S,S*)-enantiomer **113** (Appendix 7.2.3).
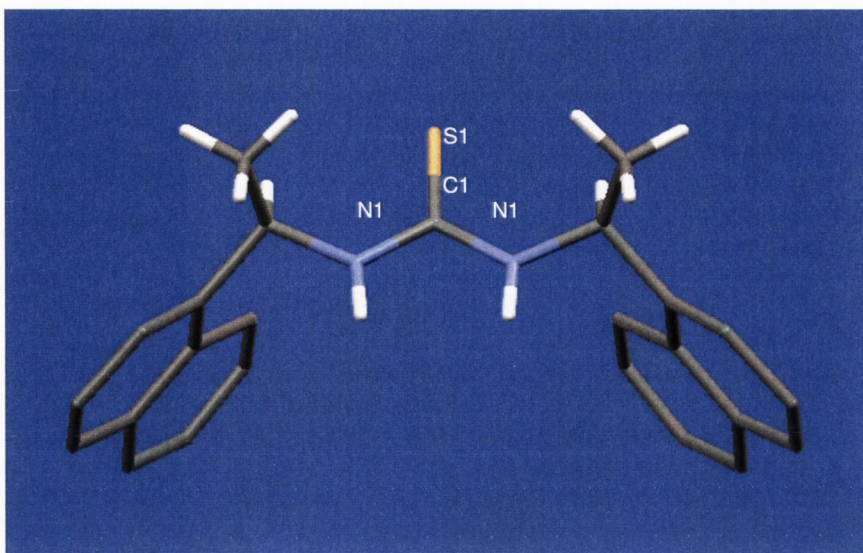
Figure 3.21 Crystal structure of the (*R,S*) *meso* compound **114** (Appendix 7.2.4).

The crystal structures for **112** and **113** are mirror images of each other, being enantiomers. Also, in all three compounds, the NH protons of the thiourea moiety are *syn* to each other, which makes the receptor suitable for directional hydrogen bonding with complementary anions such as AcO⁻. Figure 3.22 illustrates the hydrogen-bonding interaction between the thiourea NH protons of compound **112** with the O atom of the DMSO molecule.
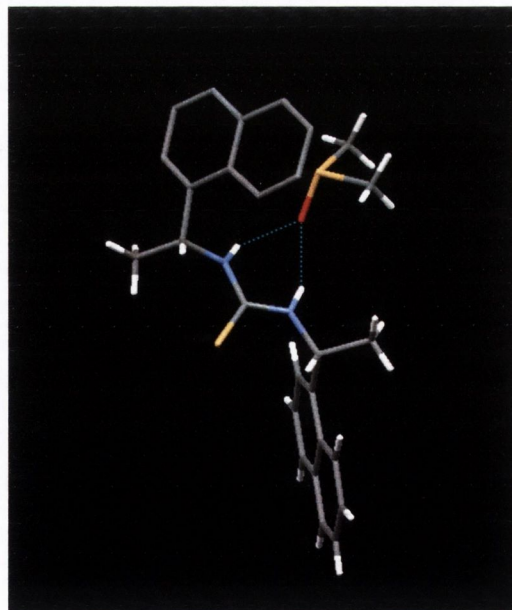
Figure 3.22 Hydrogen-bonding interaction between NH protons of the thiourea moiety within **112** and the O atom of a DMSO molecule.

3.5.1.2.1 Crystal Structure Packing

Figures 3.23, 3.24 and 3.25 illustrate the crystal structure packing of **114**, **112** and **113** respectively. Due to the symmetrical structure of **114**, the packing is relatively simple following an ABAB sequence. In the case of the two enantiomers **112** and **113**, the crystal structure packing appears more complex, which again are identical but opposite relative to each other. Some intermolecular π-π stacking interactions are also observed in these enantiomers between the naphthalene rings.
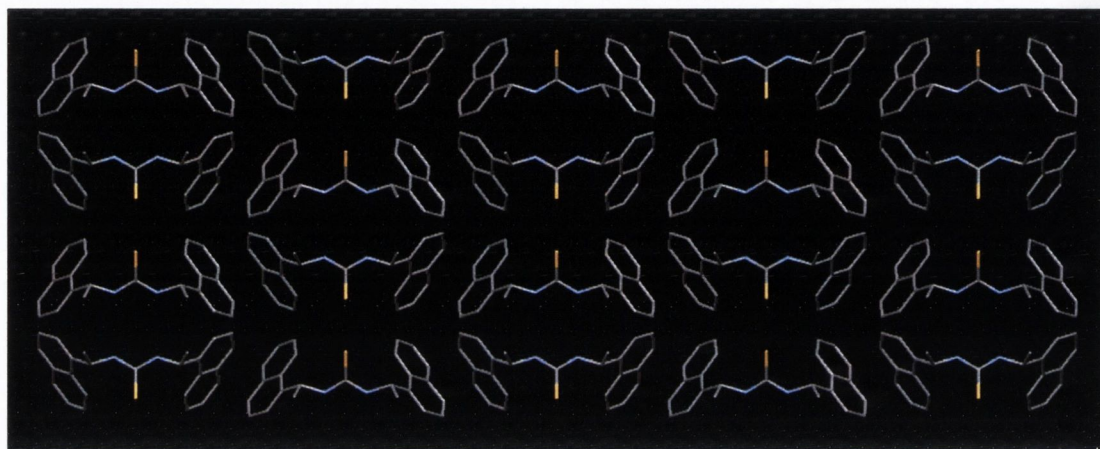
Figure 3.23 View along the c* crystallographic axis of structure of **114**.
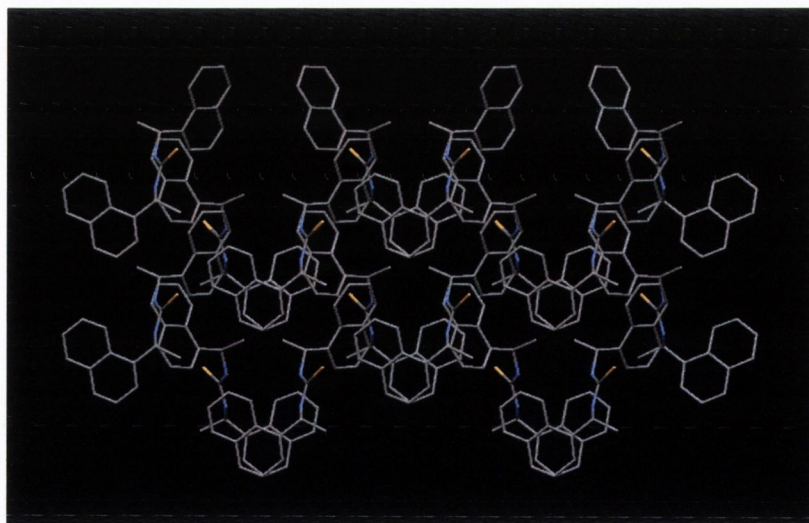
Figure 3.24 View along the c crystallographic axis of structure of **112**.
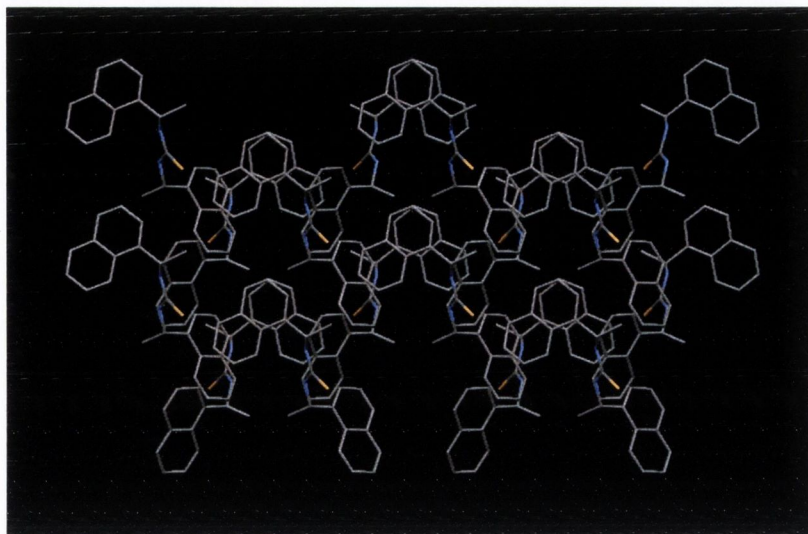
Figure 3.25 View along the c crystallographic axis of structure of **113**.

3.5.2   Physical Evaluation of the Anion Recognition of 112 - 114

The anion binding properties of sensors **112 - 114** in DMSO were first studied by ^{1}H NMR spectroscopy, followed by photophysical measurements using fluorescence spectroscopy.   Since the two enantiomers **112** and **113** are chiral, studies were also carried out using the circular dichroism spectroscopy to monitor any changes in the chiro-optical properties of these molecules upon anion recognition.

3.5.2.1 ^{1}H NMR Titrations of 112 - 114 with Anions

^{1}H NMR spectroscopic experiments were performed on DMSO-d_6 host solutions of **112 - 114** (6×10^{-3} M) at 25 °C.   Similar to those of the *bis*-anthracene compounds, the chemical shifts of the thiourea NH protons of **112 - 114**   did not broaden significantly upon anion recognition and hence, it was possible to monitor any changes to this peak upon anion recognition.   The binding of anions to these compounds generally resulted in a downfield shift in the thiourea NH peaks.   Figures 3.26 and 3.27 are stackplots illustrating the changes observed in the ^{1}H NMR spectrum of **112** upon the addition of AcO$^-$ and F$^-$ respectively.   In the presence of either AcO$^-$ or F$^-$, the peaks indicating the NH protons of **112** were appreciably shifted.   There was also the formation of a new peak at *ca.* 16 ppm, which is at a similar resonance observed for the triplet indicating the formation of HF$_2^-$ upon the deprotonation of an NH proton of the thiourea moiety.   The appearance of this new resonance occured upon the addition of

ca. one equivalent of fluoride, which again, is similar to the case reported by Gale and co-workers.[88,140]
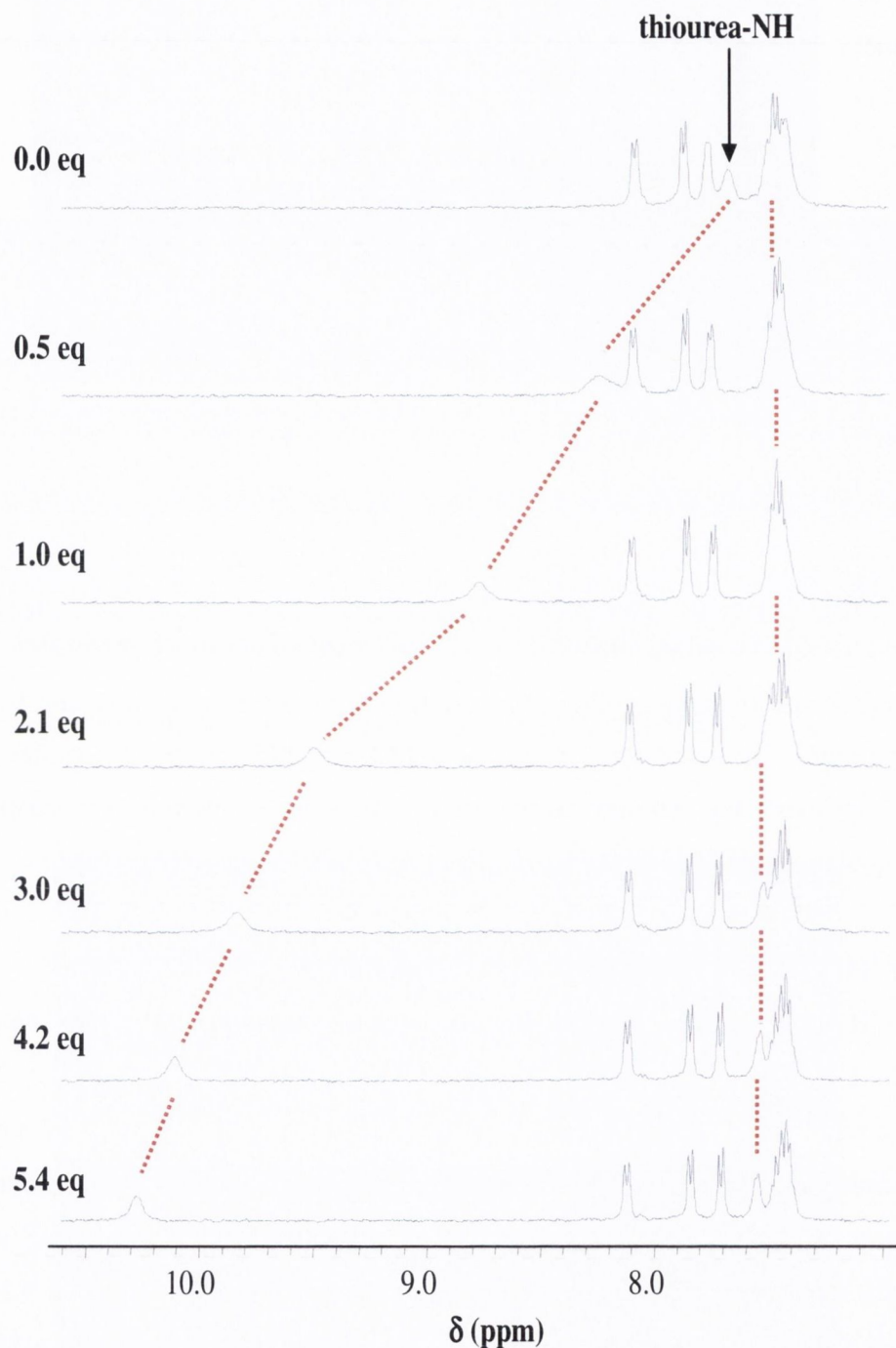
Figure 3.26 Stack plot of ^{1}H NMR spectra of **112** (6×10^{-3} M) upon addition of AcO$^-$ in DMSO-d_6.
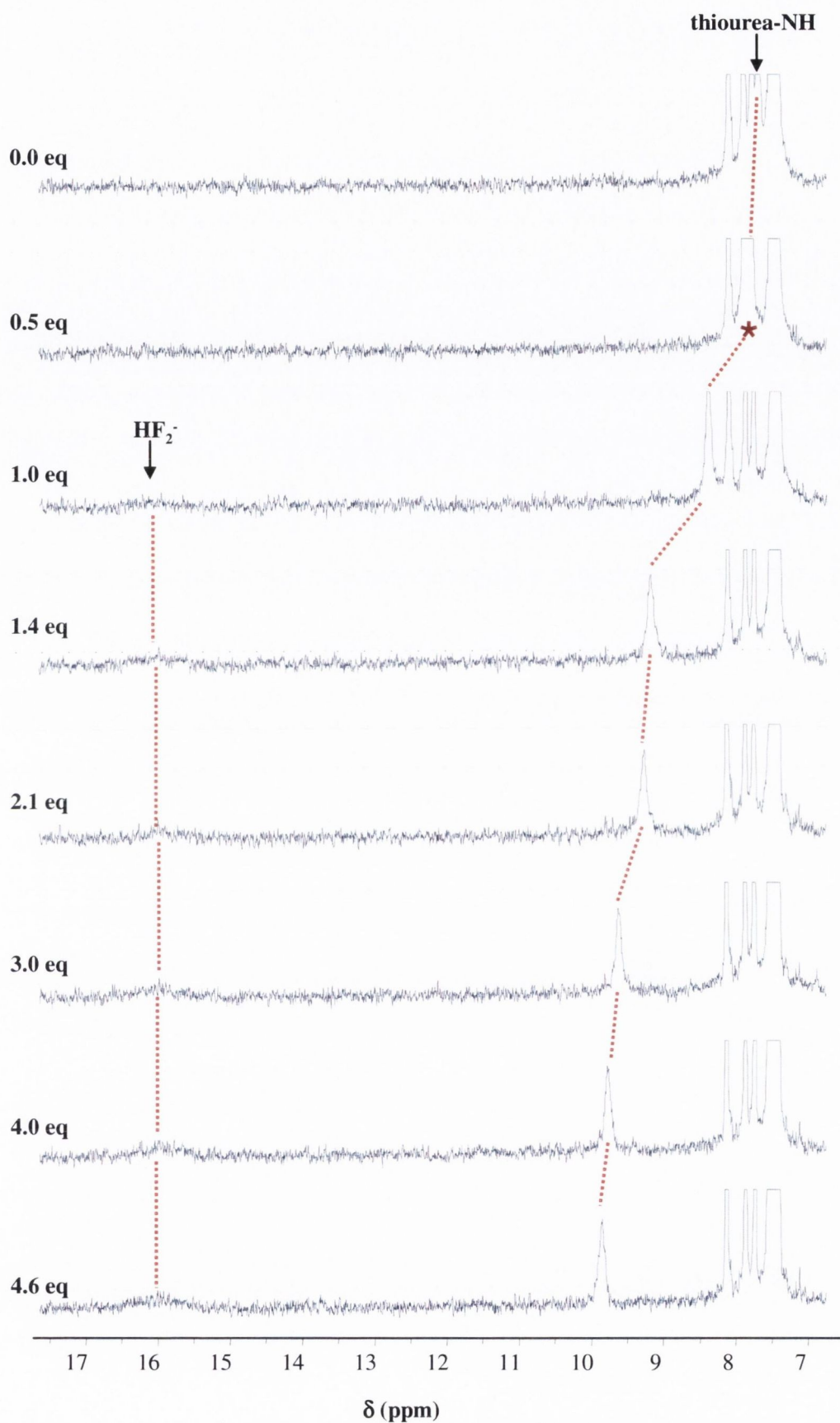
Figure 3.27 Stack plot of ^{1}H NMR spectra of **112** (6×10^{-3} M) upon addition of F$^-$ in DMSO-d_6. (*the peak indicating thiourea NH protons are hidden underneath the naphthalene chemical shifts.)

3.5.2.1.1 Analysis of the ^{1}H NMR Titration Data for 112 - 114

The data collected in these titrations was plotted as the cumulative changes in chemical shift ($\Delta\delta$) against the equivalents of anion added. Figures 3.28, 3.29 and 3.30 show the plots of $\Delta\delta$ against equivalents of the selected anions for thioureas **112**, **113** and **114** respectively. From the appearance of the binding curves, it may be observed that in all the three *bis*-naphthalene systems, the binding of AcO$^-$ appeared much stronger than that of H$_2$PO$_4^-$, while the complexation of F$^-$ seemed to be stronger than that of AcO$^-$ in the titration of compound **113**. Again, the binding curves did not fully achieve a plateau even after the addition of 5 equivalents of guest are added. There was very little binding observed for Cl$^-$ and Br$^-$, as the chemical shifts for the thiourea NH peaks were not perturbed.
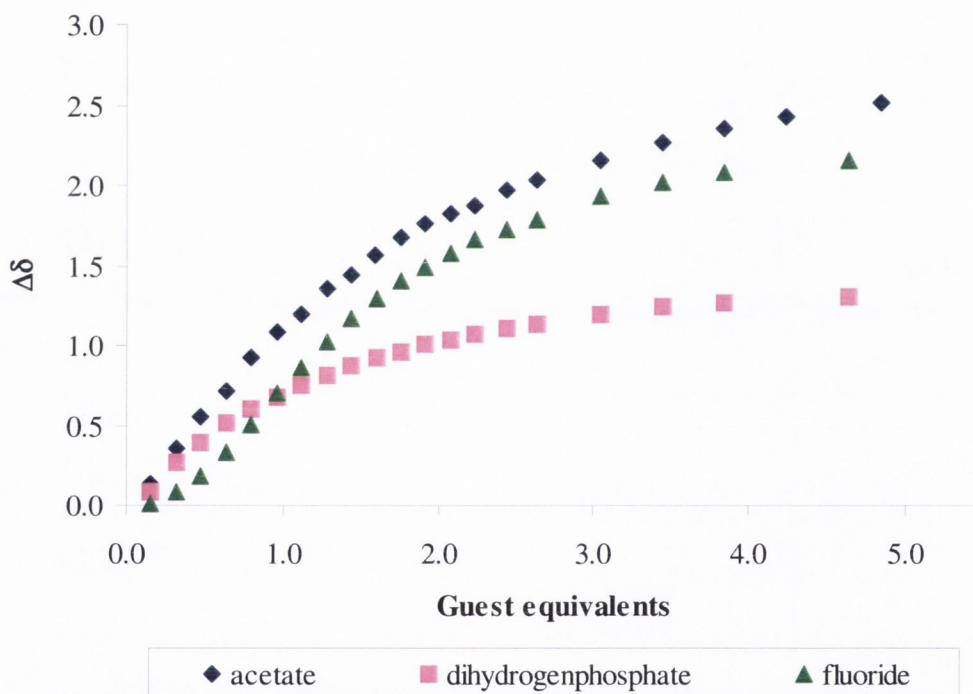
Figure 3.28 Relative cumulative changes in the chemical shift of NH proton at 7.7 ppm for sensor **112** (6×10^{-3} M) against equivalents of anions in DMSO-d_6.
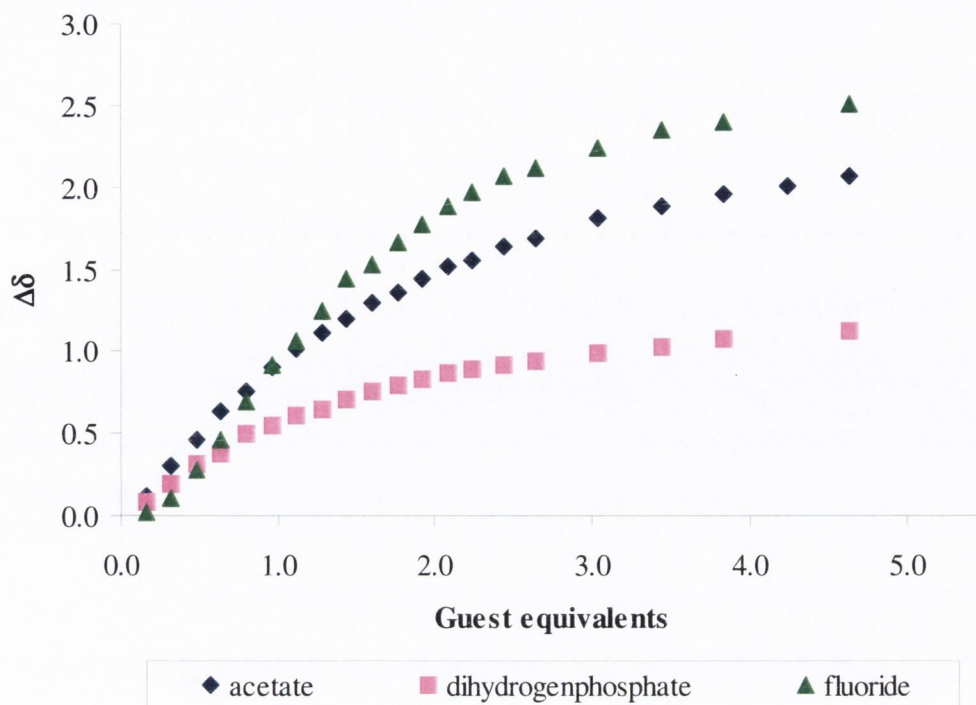
Figure 3.29 Relative cumulative changes in the chemical shift of NH proton at 7.7 ppm for sensor **113** (6×10^{-3} M) against equivalents of anions in DMSO-d_6.
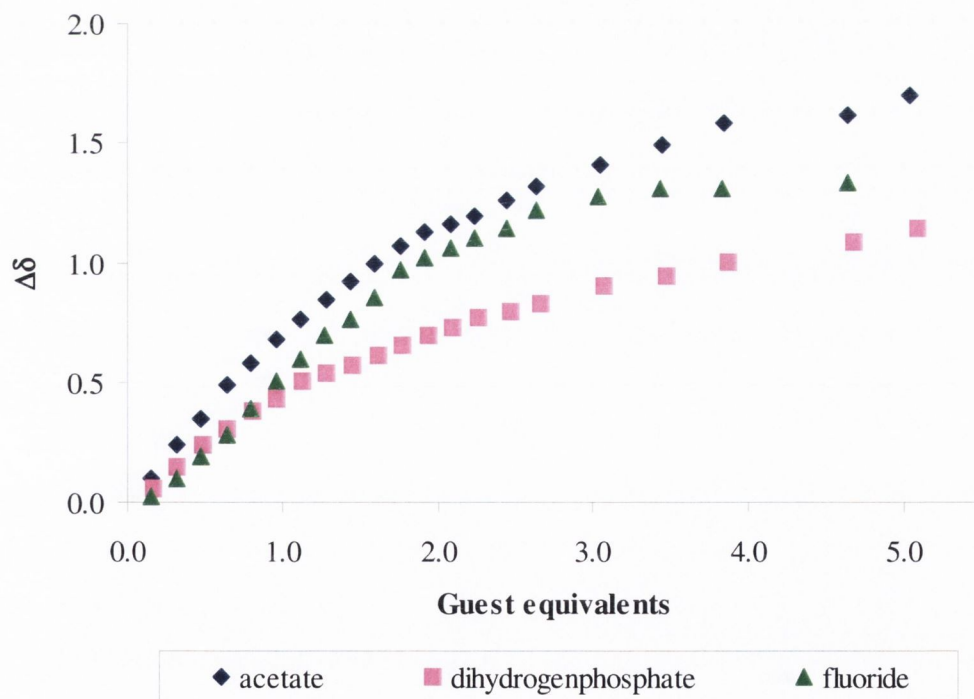
Figure 3.30 Relative cumulative changes in the chemical shift of NH proton at 7.7 ppm for sensor **114** (6×10^{-3} M) against equivalents of anions in DMSO-d_6.

3.5.2.1.2 Stability Constants (log β) from ^{1}H NMR Titration Data of 112 - 114

The stability constants (log β) for the anion binding processes of **112 - 114** with the selected anions (Table 3.2) were calculated from the data collected using the Fortran-based WinEQNMR program.[12] It was not possible to obtain log β values obtained for the complexation of F$^-$ as there may be the possibility of more than one process occurring (such as binding and deprotonation).

Table 3.2 Binding constants (log β) of **112 - 114** upon 1:1 complexation with putative anions in DMSO-d_6. All values were obtained from WinEQNMR,[12] and are within 15% error. ^{a} the binding process is too complicated for analysis by WinEQNMR.

Sensor	log β (AcO$^-$)	Log β (H$_2$PO$_4^-$)	log β (F$^-$)
112	2.13	2.39	a
113	2.13	2.28	a
114	2.86	1.83	a

In the complexation of either AcO$^-$ or H$_2$PO$_4^-$, the two enantiomers **112** and **113** gave similar log β values, where compound **112** bound to AcO$^-$ and H$_2$PO$_4^-$ with log β of 2.13 and 2.39 respectively, while **113** bound to AcO$^-$ and H$_2$PO$_4^-$ with log β of 2.13 and 2.28, respectively. This is to be expected as they are mirror images of each other. The *meso* compound **114**, on the other hand, showed distinctly different stability constants to the two enantiomers, where log β for AcO$^-$ and H$_2$PO$_4^-$ are found to be 2.86 and 1.83 respectively. The similarities observed in the stability constants of the enantiomers and the differences for those of the *meso* compound illustrate the effect of structural differences on the anion binding ability of a particular receptor or sensor.

Interestingly, **114** bound to AcO$^-$ more strongly than **112** and **113**, while the opposite was observed in the binding of H$_2$PO$_4^-$. In the case of AcO$^-$, the reason may be due to the fact that the naphthalene rings in **114** are in the same direction as seen in the solid-state structure in Figure 3.28. If this occurs in solution, then the AcO$^-$ molecule may be able to approach the thiourea binding site with more ease, than in the case of **112** and **113**. As for H$_2$PO$_4^-$ binding, a possible explanation for the enantiomers to bind to this anion better than the *meso* compound is that the *trans*-like structure of the enantiomers may provide a more complementary receptor towards this particular anion.

The log β values for the F⁻ complexation by all three compounds could not be obtained, as the binding processes may be complicated (*i.e.* not 1:1 host:guest complexation).

Figures 3.31 (a) - (f) show the graphs generated by WinEQNMR illustrating the fit between the observed and calculated data for the binding of AcO⁻ and $H_2PO_4^-$ by **112** - **114**. A good fit ensures that the log β value calculated by the program is reasonable.
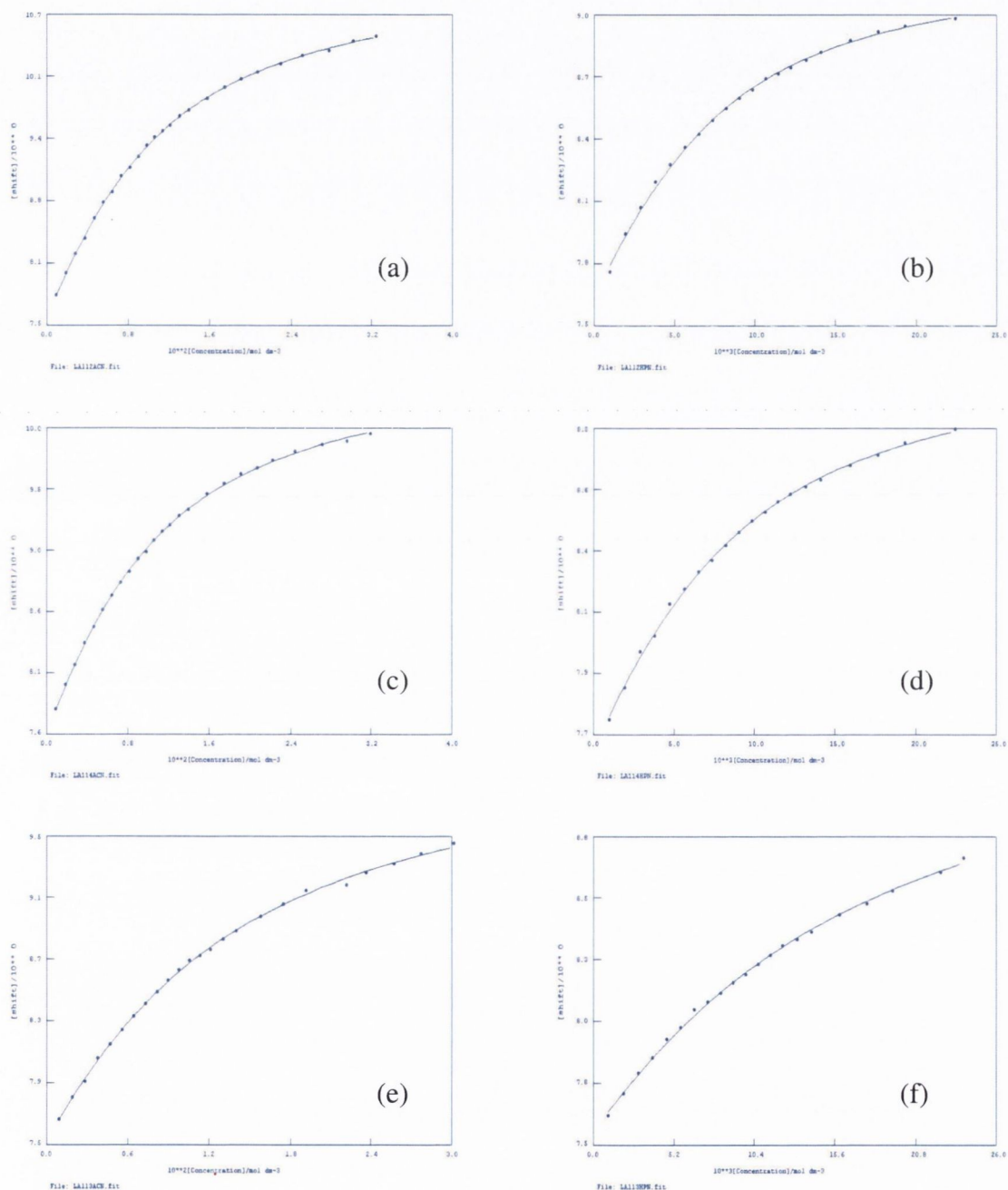
Figure 3.31 WinEQNMR-generated graphs of the fit between the observed (points) and calculated (line) data for the binding of: (a) AcO⁻ with **112** (6×10^{-3} M); (b) $H_2PO_4^-$ with **112** (6×10^{-3} M); (c) AcO⁻ with **113** (6×10^{-3} M); (d) $H_2PO_4^-$ with **113** (6×10^{-3} M); (e) AcO⁻ with **114** (6×10^{-3} M); (f) $H_2PO_4^-$ with **114** (6×10^{-3} M), carried out in DMSO-d_6.

3.5.2.2 Fluorescence Titrations of 112 - 114 with Anions

The photophysical properties of **112** - **114** were initially measured in DMSO at 25 °C. The absorption spectra for these compounds exhibit the characteristic naphthalene fine structure, consisting of a central main band at 284 nm, with two shoulders at 274 and 296 nm and a much smaller shoulder at 314 nm. The extinction coefficients of **112**, **113** and **114** at 284 nm in DMSO were found to be 15538, 14639 and 19051 $M^{-1}cm^{-1}$ respectively. The fluorescence emission of all three compounds (excited at 248 nm) are also similar to each other, demonstrating the characteristic fine structure of naphthalene. The smooth band with maximum intensity occurs at 338 nm. However, the fluorescence of compound **114** also consists of shoulders *ca.* 425 and 510 nm and a shoulder located at 475 nm. Figures 3.32 and 3.33 show the absorption and emission spectra respectively, for compounds **112** - **114**.

Binding studies with various anions using fluorescence spectroscopy were carried out on DMSO solution of **112** - **114** (1×10^{-5} M) at 25 °C. The absorption of the samples were monitored in parallel with these experiments. The host solution was excited at the wavelength at which the main absorption band occurs (*i.e.* 284 nm), and any changes to the fluorescence following anion addition were recorded.
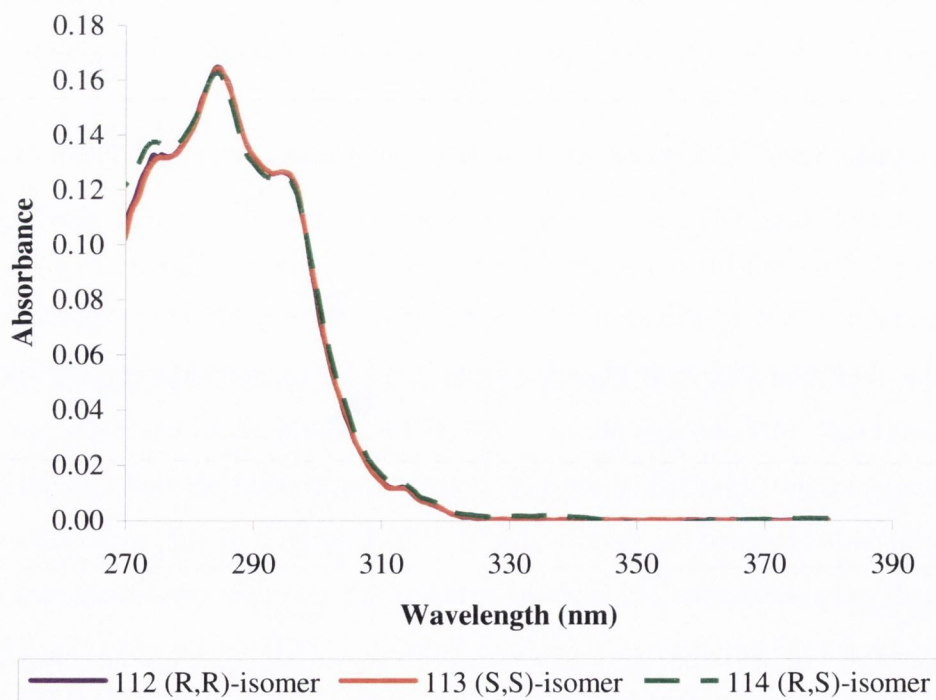
Figure 3.32 Absorption spectra of DMSO solutions of **112** - **114** (1×10^{-5} M).
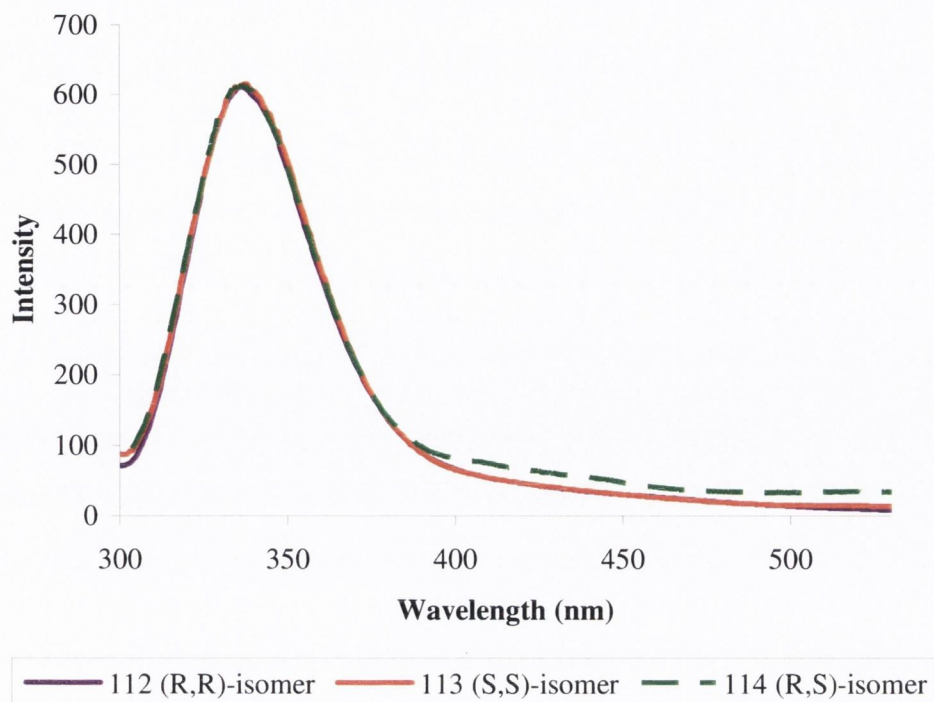
Figure 3.33 Fluorescence spectra of DMSO solutions of **112** - **114** (1×10^{-5} M; excited at 284 nm).

The fluorescence binding experiments of these sensors in DMSO were performed numerous times with all the selected anions. However, it was not possible to achieve reproducible results. There is a possibility of π-π stacking interactions between the naphthalene rings of the sensors. Hence, attempts were made using another solvent media, MeCN, which was less competitive and offers no solubility issues.
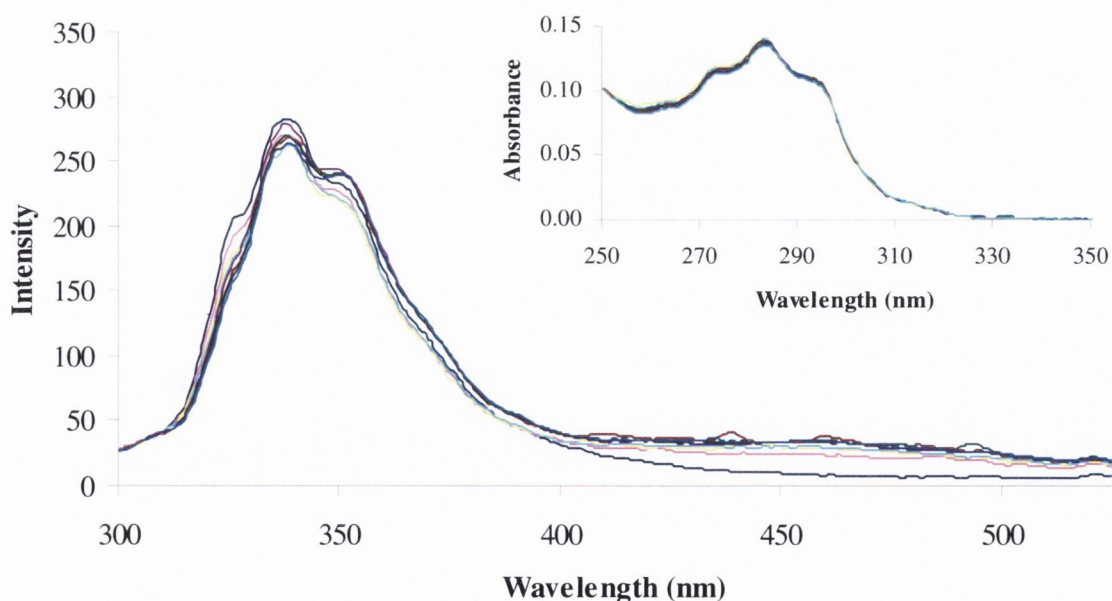
Figure 3.34 Changes in the fluorescence spectrum of **113** (1×10^{-5} M) in MeCN on addition of $H_2PO_4^-$ (excited at 284 nm; $0 \rightarrow 1000$ eq.). Inset: Changes in the absorbance spectrum of **113** (1×10^{-5} M) in MeCN upon the addition of $H_2PO_4^-$ ($0 \text{ M} \rightarrow 1 \times 10^{-2}$ M).

Figure 3.34 shows the changes in the fluorescence and absorption spectra of **113** in MeCN upon the addition of $H_2PO_4^-$. The absorption band of the free host has a maximum absorbance at 284 nm. There are three shoulders present at 274, 294 and 314 nm. Therefore, the sample was excited at the wavelength of maximum absorbance (*i.e.* 284 nm), which gave an emission spectrum which has a maximum intensity centred at 338 nm, with shoulders at 327 and 351 nm. Upon complexation with $H_2PO_4^-$, little change is observed in both the emission and absorption spectra. The only significant change was the appearance of a small band at longer wavelength (*ca.* 460 nm). This may be attributed to the formation of an excimer, which is often observed in naphthalene derivatives.[112,114]

As the changes were not very significant in the binding experiments using MeCN and there is the problem of reproducibility with those carried out in DMSO, we were unable to study in detail the binding properties of **112 - 114** using fluorescence and UV-vis spectroscopic techniques. Therefore, binding studies were then carried out using circular dichroism.

3.5.2.3 Circular Dichroism (CD) Titrations of 112 - 114 with Anions

Circular dichroism (CD) is defined as the difference in absorbance (A) of incident left and right circularly polarised light (Equation 3.1).

$$CD = A_{left} - A_{right}$$ **(Equation 3.1)**

The basis behind CD spectroscopy is such that the interaction between a chiral molecule and left- and right-handed photons will result in a signal consisting of a fine structure that is unique to that particular compound.[183] This is due to the chiral compound absorbing certain quantities of each circularly polarised light.

Therefore, techniques using CD can provide information regarding molecular structure of chiral compounds as well as interactions between molecules (both chiral and achiral). For example, Suzuki *et al.* reported a rectangular-shaped achiral host which, upon complexation with chiral guests, assumes an induced chirality detectable by CD.[184] Therefore, it is hoped that upon anion complexation, the CD signals of the chiral hosts **112 - 114** may change significantly.

To obtain a CD spectrum of a particular compound, a solution of the compound should be prepared such that its absorbance would be between 0.5 and 1.0. Figure 3.35 shows the CD signals of the *bis*-naphthalene thiourea-based sensors **112 - 114** as the

free hosts in DMSO (6.5×10^{-5} M). Since **112** and **113** are enantiomers of each other, their CD spectra were identical, in which the intensity of the CD signals for **112** (*i.e.* (*R,R*)-isomer) were found in the positive region and those for **113** (*i.e.* (*S,S*)-isomer) were in the negative region. The fine structure of the CD spectrum for **112** was such that there were two main peaks at 268.5 and 291.0 nm, with shoulder-like peaks at 279.5 and 305.5 nm. In the case of the CD spectrum of **113**, the two peaks were at 269.0 and 290.0 nm, while the shoulders were at 281.0 and 305.0 nm. Compound **114** did not show any CD signal since it is a *meso* compound.
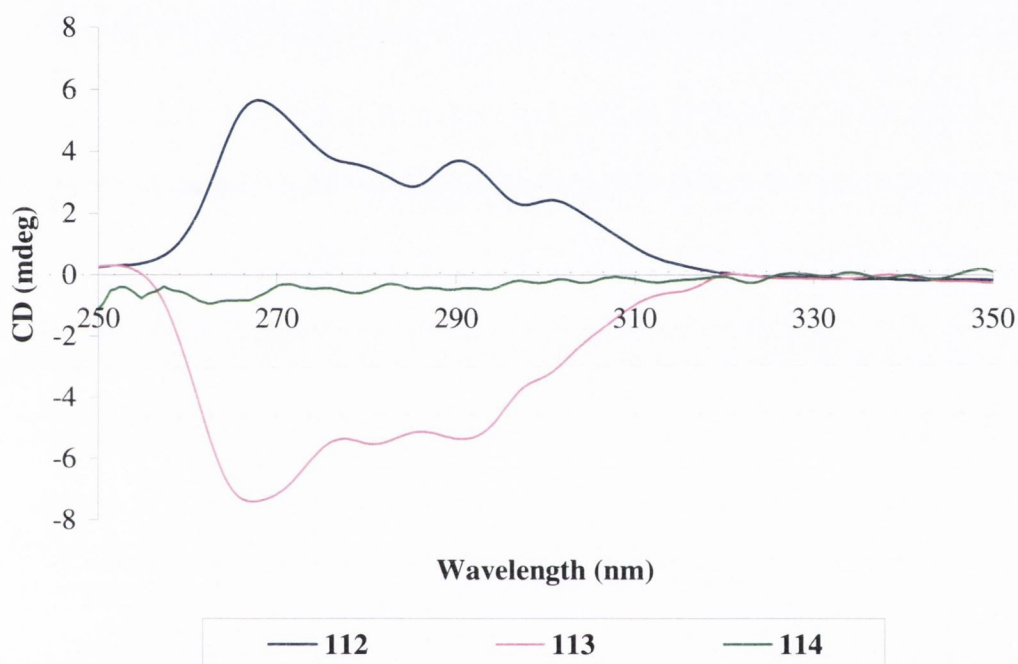
Figure 3.35 CD spectra of DMSO solutions of enantiomers **112** and **113**, and *meso* compound **114**.

Upon addition of anions to **112**, the CD signals decreased in magnitude with increasing anion equivalence. Figure 3.36 show the changes in CD signals of **112** in DMSO with increasing amounts of AcO⁻. However, in CD studies, it is preferable to observe the changes in terms of the quantitative changes (*i.e.* the free host CD spectrum is subtracted from the spectrum at each guest equivalent). This is illustrated in Figure 3.37, where the changes in CD for the AcO⁻ binding for **112** are now found in the negative region of the CD spectrum. Figures 3.38 and 3.39 show the changes in the CD signals and the quantitative changes for the binding of AcO⁻ by **113**. Hence, the

quantitative changes are now found in the positive region of the CD spectrum, which is the opposite to those for **112**.

The presence of $H_2PO_4^-$ and F^- resulted in significant changes in the CD signals of these sensors (see Appendix 7.2.5). However, it should be noted that at least 1000 equivalents of the anion is required to reach a plateau. No significant CD changes were observed upon the addition of Cl^-. As for the *meso* compound **114**, the presence of anions did not induce chirality in this non-chiral molecule, as expected.
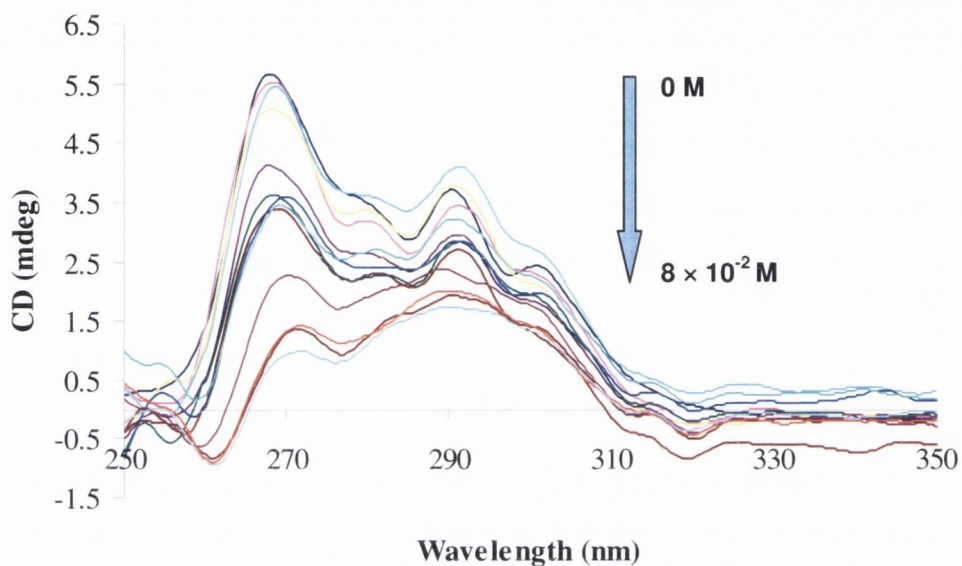
Figure 3.36 CD spectra of **112** in DMSO in the presence of various equivalents of AcO^-.
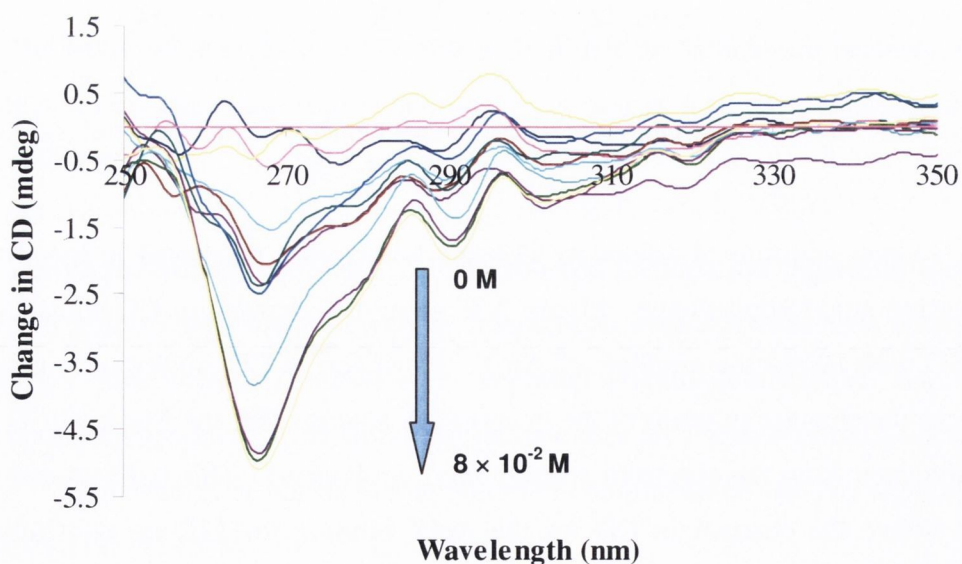
Figure 3.37 Quantitative changes observed in the CD spectrum of **112** in DMSO in the presence of AcO^-.
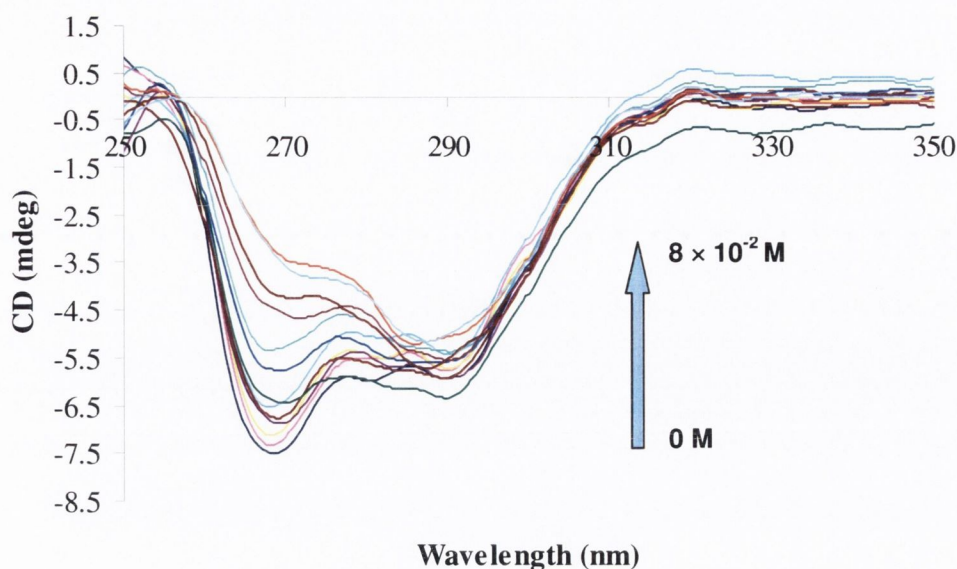
Figure 3.38 CD spectra of **113** in DMSO in the presence of various equivalents of AcO⁻.
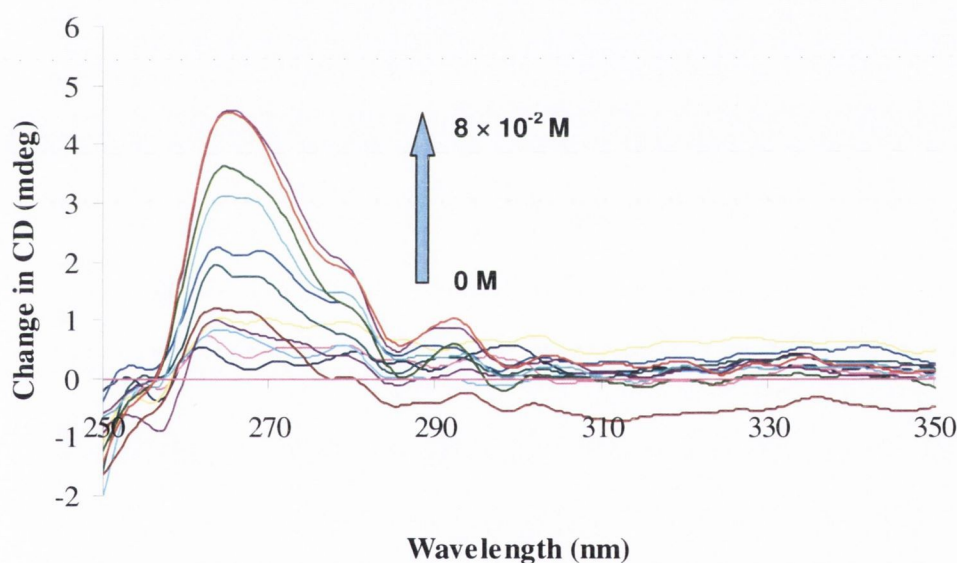
Figure 3.39 Quantitative changes observed in the CD spectrum of **113** in DMSO in the presence of AcO⁻.

3.5.2.3.1 Analysis of the CD Titration Data for 112 and 113

The quantitative changes in the CD signals at 267.5 nm for both **112** and **113** in DMSO were plotted against anion equivalents, and these plots are shown in Figures 3.40 and 3.41 respectively. For both compounds, the anion binding abilities appeared to be strongest with AcO⁻, followed by F⁻ and $H_2PO_4^-$, while there is no significant binding with Cl⁻. Again, it must be emphasised that most of the binding curves required up to 1000 equivalents of anion to reach a plateau. Despite this, it is a useful technique to utilise in anion sensing where chirality is involved, and in this case, it was possible to

get reproducible results, unlike the difficulties faced in the reproducing results obtained in the fluorescence experiments.
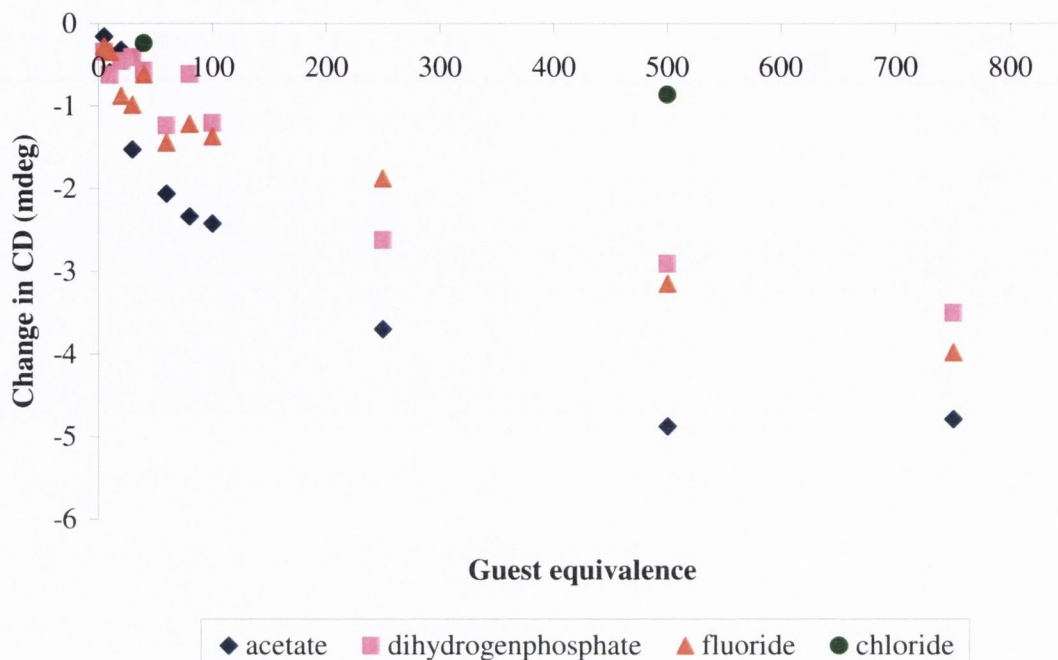
Figure 3.50 Quantitative changes observed at 267.5 nm in the CD spectrum of **112** in DMSO with various anions.
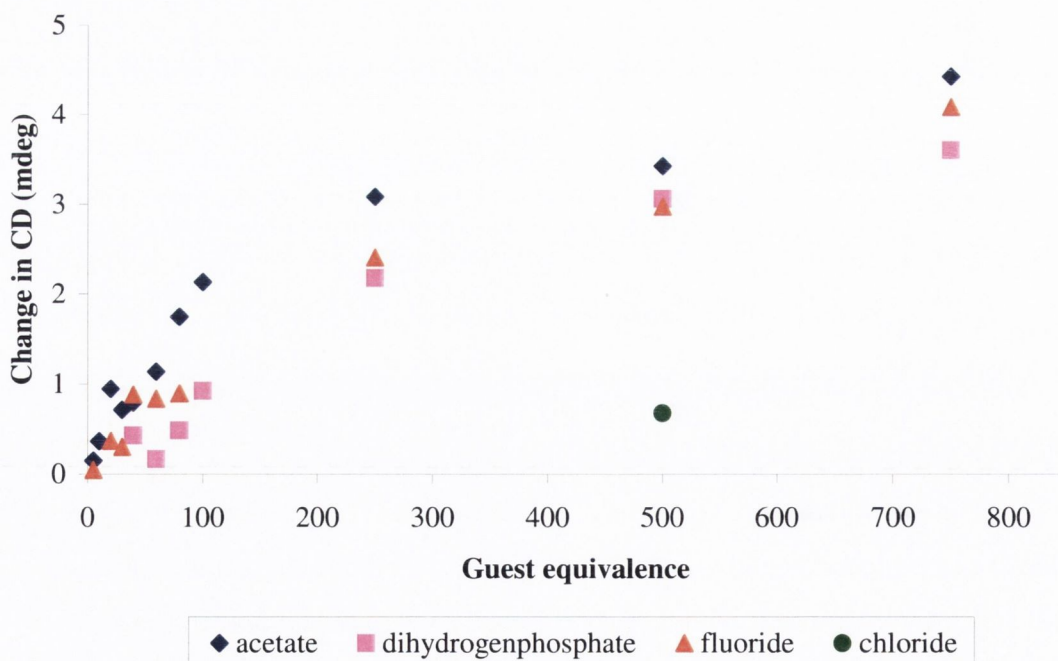
Figure 3.51 Quantitative changes observed at 267.5 nm in the CD spectrum of **113** in DMSO with various anions.

3.5.3 Conclusions

From the ^{1}H NMR binding studies, sensors **112** - **113** gave reasonably good stability constants, indicating the potential of such compounds as anion receptors. However, the fluorescence titrations carried out for these sensors face the problem of irreproducibility, unlike the binding studies using ^{1}H NMR spectroscopy and even CD. Also, since the complexation only reaches a plateau at [anion] $\approx 6.5 \times 10^{-2}$ M, it shows that these naphthalene-based compounds are not suitable for fluorescent or chiral anion sensing.

During the course of this study, Custelcean and co-workers carried out DFT calculations on a number of *N,N'*-disubstituted thiourea derivatives (*e.g.* **126**) to further study their hydrogen-bonding properties.[185] It was found that **126** is the most sterically crowded around the NH protons, thus becoming inaccessible for hydrogen bond formation due to steric congestion from the methyl and phenyl groups. Hence, it is feasible to deduct that the ability of hydrogen bond formation for the chiral *bis*-naphthalene compounds (as well as the *bis*-anthracene-based systems) would be even lesser as the naphthalene (and anthracene) moieties are larger than phenyl rings.
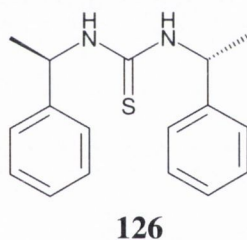
126

3.6 Overall Conclusions

We were able to successfully synthesise thiourea-based *bis*-anthracene (**109** - **111**) and *bis*-naphthalene (**112** - **114**) systems. However, the physical evaluation of the anion recognition abilities of these fluorescent sensors (by ^{1}H NMR, fluorescence and CD titrations) showed that they have weak binding towards the selected anions, as high anion concentrations were required to induce changes in the ^{1}H NMR and photophysical spectra of these host molecules. As previously mentioned, one rationale for the observed weak binding affinities of such sensors towards anions can be explained from the DFT calculations carried out by Custelcean and co-workers on a number of *N,N'*-disubstituted thiourea derivatives, which illustrated the possibility that the region around the thiourea NH protons of **126** may be sterically crowded.[185] Since sensors **112** - **114**

are analogous to **126**, a similar situation may be possible, and hence, their thiourea NH protons may be inaccessible for hydrogen bond formation due to steric hindrance from the methyl and aromatic groups.

Although the *bis*-naphthalene thioureas **112 - 114** show such weak anion binding affinities, the results obtained from the CD titrations illustrate the potential of utilising this method of detection in anion sensing. The effectiveness of this method was also demonstrated by Nakashima and Yoshida, in which CD studies were carried out to monitor the conformational change adopted by naphthalene-appended amino-β-cyclodextrins upon guest inclusion.[102]

3.7 Future Work

It would be beneficial to carry out DFT studies on **109 - 114** in order to understand their weak binding affinities to the selected anions. In the case of the irreproducibility of the fluorescence experiments of **112 - 114**, silylation of the fluorescence cells may help to overcome this problem, if π-π stacking interactions between the naphthalene moieties are indeed the cause for such irreproducible results.

Since the CD experiments carried out showed the potential use of this method of detection, the design and synthesis of chiral anion receptors and sensors (with potentially significant anion binding affinities) should be further pursued.

4.1 Introduction

As discussed in Chapter 1, naphthalimide-based derivatives have been widely studied as potential anion sensors by several research groups, including Pfeffer *et al.*, Fabbrizzi *et al.*, Gunnlaugsson *et al.* and Tian *et al.*[20,108,117,118,133,135,132] While such compounds were initially used for fluorescent anion sensing, but in recent years, they have also shown great potential as colorimetric anion sensors, as outlined in Sections 1.6 and 1.7, respectively.

One report that was only briefly mentioned in Chapter 1, was that of the 4-amino-1,8-naphthalimide based derivatives **127** and **128** developed by Pfeffer and co-workers.[108] These fluorescent anion sensors were designed based on a previous study that proposed the cooperative anion binding effect of the 4-amino proton of the more flexible derivative **34** towards dihydrogenphosphate in DMSO (see Section 1.7).[136]
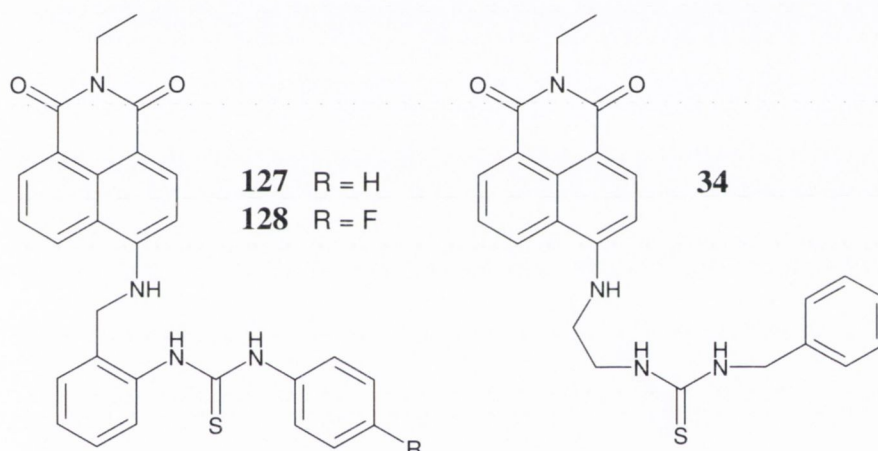
Table 4.1 Percentage of fluorescence quenching for the binding of DMSO solutions of **34, 127** and **128** (~6 × 10^{-6} M) with the selected anions at 25 °C calculated using Microsoft Excel. (^{a} No significant quenching but binding observed using ^{1}H NMR spectroscopy; ^{b} Deprotonation.)

Sensor	AcO$^-$	H$_2$PO$_4^-$	F$^-$
34	^{a}	^{a}	^{b}
127	31 %	6.5 %	^{b}
128	59 %	36 %	^{b}

Table 4.1 lists the percentage of fluorescence quenching for the binding of **34**, **127** and **128** with the various anionic guests. Sensors **127** and **128** showed significant fluorescence quenching in the presence of AcO$^-$ and H$_2$PO$_4^-$, while there was no quenching in the fluorescence of **34**. It was proposed that presence of the phenyl spacer in **127** and **128** is a requirement for efficient PET between the fluorophore and the

receptor. The rigidity of these sensors in comparison to the more flexible derivative **34** may also have an effect on the efficiency of the electron transfer.

As previously mentioned, fluorescent anion sensors may also demonstrate chromogenic behaviour. Compounds **32** and **33** are analogues of sensors such as **127** and **128**, in which receptor arm is situated at the *para* position of the phenyl spacer. These *para*-substituted sensors resulted in both fluorogenic and chromogenic behaviour upon anion recognition (see Section 1.7).

32 R = H
33 R = CF$_3$
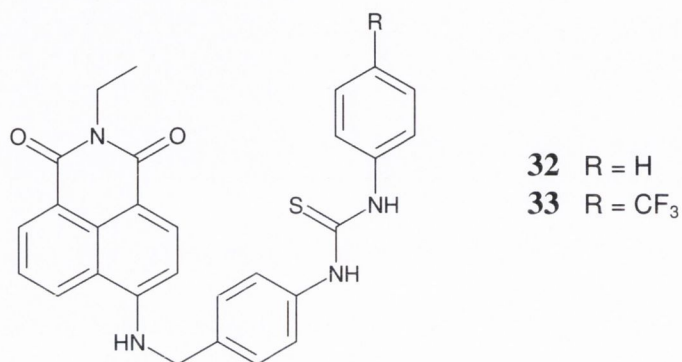
There have been several other reports of fluorescent sensors demonstrating chromogenic behaviour.[115,110,128,186] Such sensors have the advantage of visual anion recognition as well as requiring low host concentrations (10^{-5} - 10^{-6} M). The following section will describe the project objectives towards developing novel naphthalimide-based colorimetric anion sensors.

4.2   Objectives

Gunnlaugsson and co-workers previously synthesised the hydrazine-based napthalimide thiourea derivatives **63** and **64**, which showed chromogenic responses upon anion recognition.[117] Therefore, we decided to synthesise the urea analogues for comparative studies of the anion-binding abilities. However, the first objective of this part of the project was to resynthesise the thiourea sensor **64** for further evaluation of its binding abilities with putative anions in highly competitive media such as EtOH:H$_2$O (50:50) using UV-vis spectroscopy. Once this was established, the next objective was to synthesise the urea analogue (**131**) of this sensor as well as other urea derivatives (**129** and **130**). Again, the anion-binding abilities of these sensors were assessed using UV-vis spectroscopic binding experiments, as well as those utilising ^{1}H NMR and fluorescence spectroscopies. The electronic effect of the different substituents (at the

para position of the phenyl ring) on the binding affinities of **129** - **131** was also evaluated.

63	X = S; R = CH$_3$
64	X = S; R = CF$_3$
129	X = O; R = H
130	X = O; R = CH$_3$
131	X = O; R = CF$_3$
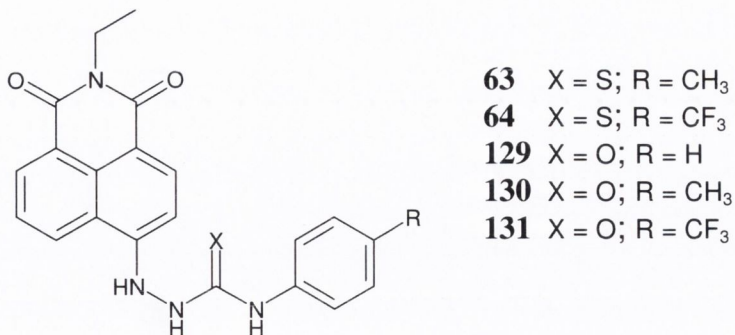
4.3 Fluorescence and Absorption of 4-Substituted 1,8-Naphthalimides

The advantage of using the naphthalimide moiety as a fluorophore in anion sensing is the fact that it is able to emit in the green region of the electromagnetic spectrum with λ_{max} of greater than 520 nm, which reduces the possible disturbance from background emission and light scattering from many biologically active anions.
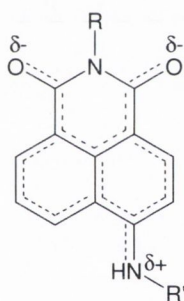
Figure 4.1 Excited state of the ICT structure of the 4-amino-1,8-naphthalimide moiety.

The presence of an amino group at the 4-position of the naphthalimide ring results in the formation of a *"push-pull"* internal charge transfer (ICT) excited state system which is highly fluorescent in nature. The excitation of this fluorophore leads to the formation of a partial positive charge on the 4-amino group and partial negative charges on the imido functionalities, as demonstrated schematically in Figure 4.1. The ICT structure of the 4-amino-1,8-napthalimide system also leads to the absorption of light in the visible region (420 - 450 nm) due to this *"push-pull"* electronic character.

Another note-worthy aspect of the naphthalimides is that the quenching of the excited state of the naphthalimide core *via* electron transfer can only occur by the receptor (R) that is attached through the 4-amino moiety, as demonstrated by de Silva *et al.*[187,188] The excited state of the 4-substituted naphthalimide fluorophore has

considerable dipole character (Figure 4.1), which results in a strong photogenerated electric field. This field can either hinder or accelerate the electron transfer depending of its sign and magnitude. The electron transfer pathway *via* either the 4-amino moiety or the dimide moiety is thermodynamically feasible. However, due to the negative charge of the transiting electron, its transfer through the partially positively charged 4-amino group to the fluorophore is more favoured than that through the repulsive electric field of the diimide moiety (containing an overall partially negative charge). Hence, sensors **63**, **64** and **129** - **131** were designed such that the receptor arm was attached at the 4-amino position of the naphthalimide ring. The next section will discuss the synthesis of these sensors.

4.4 Synthesis of Hydrazine-based Naphthalimide Sensors 64, 129 - 131

Compounds **64, 129** - **131** were synthesised according to the methods previously devised by Tocci (née Hussey) within the Gunnlaugsson research group.[117,189] The synthesis of these sensors were carried out in three steps (Scheme 4.1).
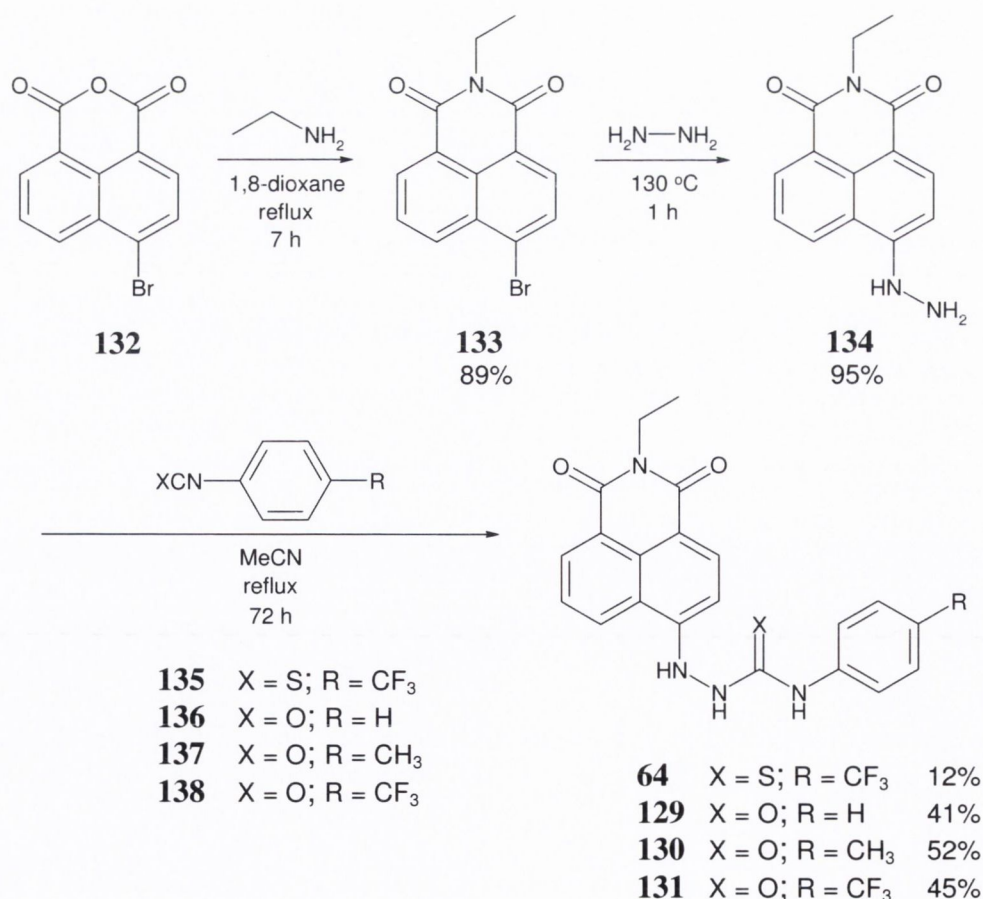
Scheme 4.1 Synthesis of hydrazine-based naphthalimide thiourea **64** and ureas **129** - **131**.

4-Bromo-1,8-naphthalic anhydride **132** and ethylamine (70% solution in water) were reacted under reflux in 1,4-dioxane for 7 hours. Upon addition of H_2O to the reaction mixture, a precipitate formed, which was filtered, washed with H_2O and dried under vacuum to yield 6-bromo-2-ethyl-benzo[*de*]isoquinoline-1,3-dione **133** (89%). This bromo-substituted naphthalimide **133** was then reacted with hydrazine monohydrate, which formed a yellow precipitate when H_2O was added. The precipitate was collected and washed with H_2O, giving **134** in 95% yield. It should be noted that under these conditions, there was no evidence of the imide functionality being opened by reaction with the hydrazine monohydrate. Sensors **64**, **129**, **130** and **131** were formed by reacting **134** with 4-trifluoromethylphenyl isothiocyanate (**135**), phenyl isocyanate (**136**), *p*-tolyl isocyanate (**137**) and 4-trifluoromethylphenyl isocyanate (**138**), respectively. In each case, the reaction was carried out under reflux for 3 days in anhydrous MeCN. The precipitate formed was collected and purified *via* hot filtration using a solvent mixture of DCM:MeOH (1:4). In contrast to the synthesis of the thiourea derivative **64** (where the precipitate formed overnight), precipitation of the urea derivatives occurred after *ca.* 30 minutes. This may explain the higher yields (41 - 52%) observed for the formation of the urea derivatives **129** - **131**, in comparison to the 12% yield of **64**.

4.4.1   Characterisation of 64, 129 - 131

Compounds **64**, **129** - **131** were characterised by ^{1}H and ^{13}C NMR spectroscopy, infrared spectroscopy, mass spectrometry and elemental analysis. In the ^{1}H NMR spectrum (400 MHz, DMSO-d_6), the NH protons of the thiourea moiety in **64** are located in the region between 10.3 and 10.4 ppm, whereas those of the urea sensors **129** - **131** can be found in the region between 8.6 and 9.6 ppm. Figures 4.2 and 4.3 show the ^{1}H NMR spectra of **130** and **131** respectively. The fact that the thiourea NH protons are further downfield than those of the urea sensors is typically observed between ureas and thioureas.[190]

When the 4-position of the phenyl ring (Ar) is unsubstituted, the urea NH protons result in chemical shifts of 9.60 and 9.03 ppm, observed in the ^{1}H NMR spectrum of **129**. The presence of the electron-donating methyl group in **130** causes these shifts to move upfield (*i.e.* 9.59 and 8.92 ppm), whereas the opposite is observed when the substituent is electron-withdrawing in nature, as in **131** (*i.e.* 9.64 and 9.45

ppm). Again, this is consistent with theoretical principles relating to the effects of the electronic nature of the *para* substituent on the phenyl ring.[190]
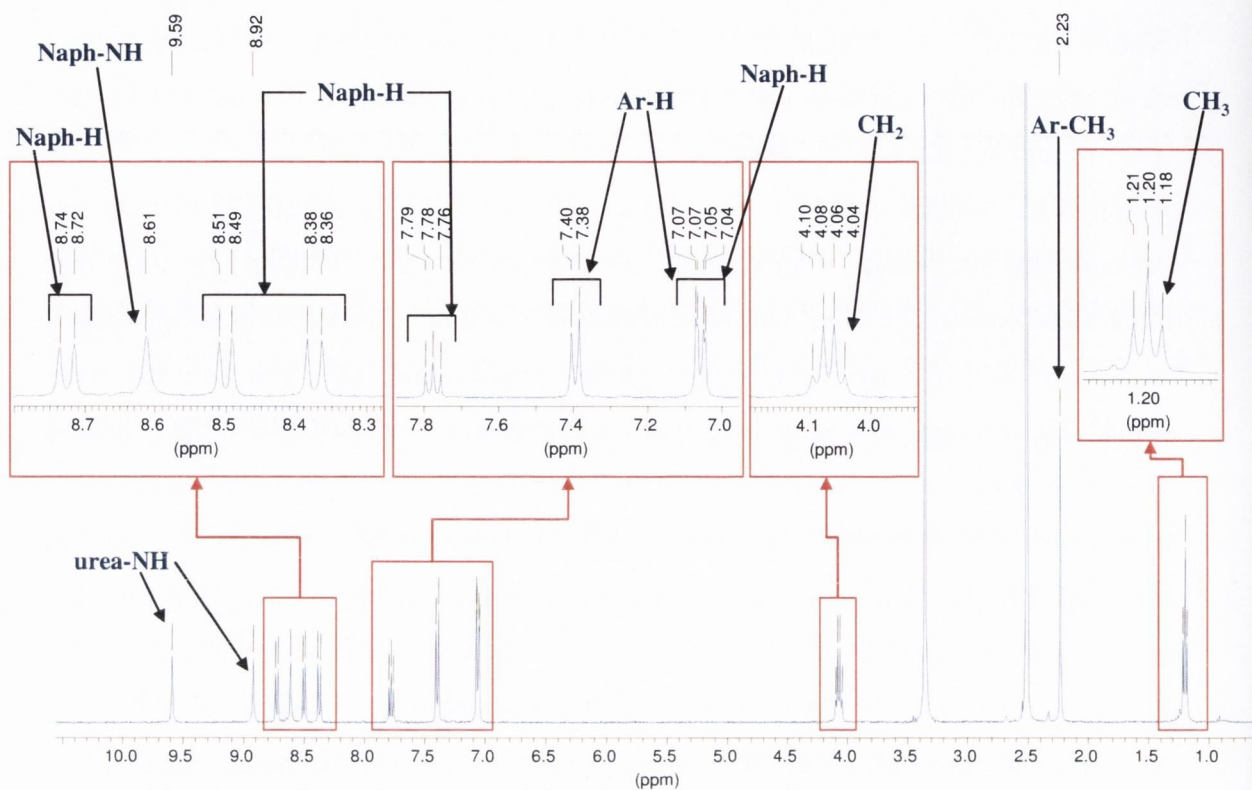

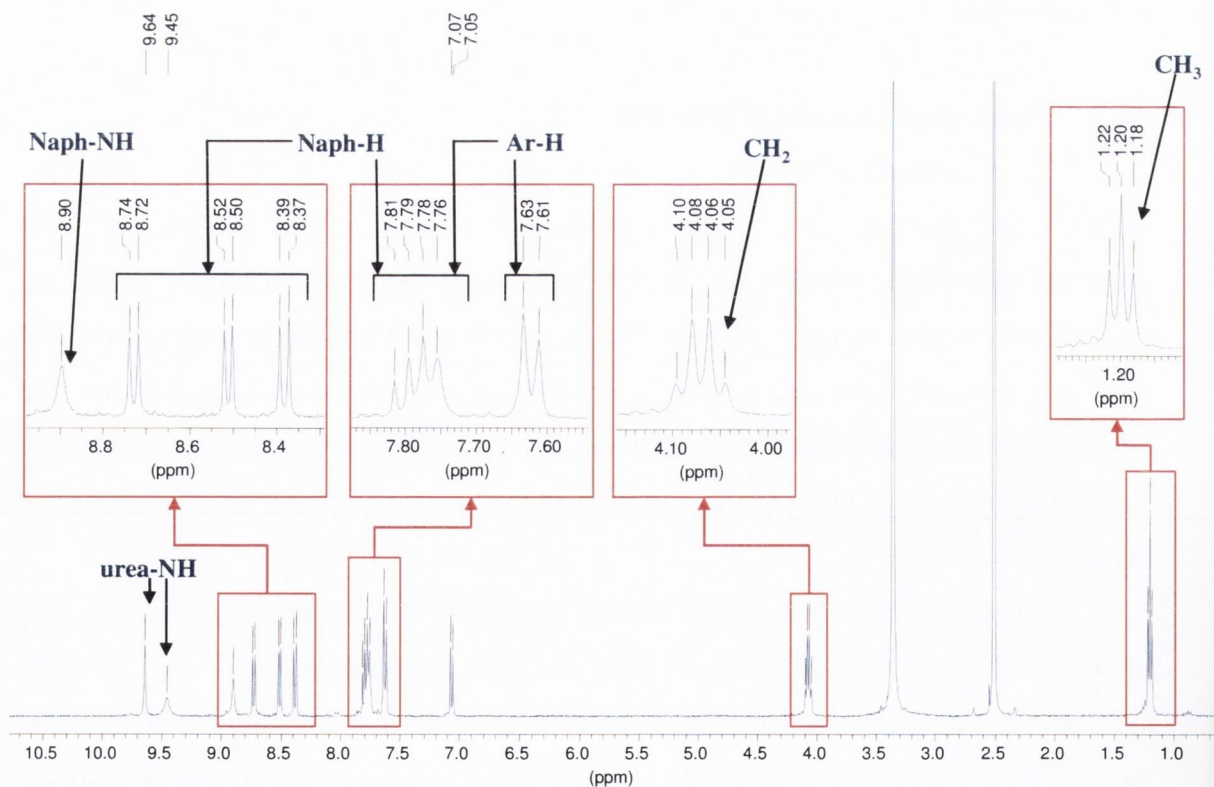**Figure 4.2** ^{1}H NMR spectrum (400 MHz, DMSO-d_6) of urea **130**.

Figure 4.3 ^{1}H NMR spectrum (400 MHz, DMSO-d_6) of urea **131**.

126

The melting points (m.p.) of ureas **129 - 131** were found to be either approximately 250 °C (*e.g.* **129** and **131**) or decomposed at 310 °C (*i.e.* **130**), while thiourea **64** had a lower m.p. of 179 °C.

4.5   Physical Evaluation of the Anion Recognition of 64

As aforementioned, the thiourea **64** was resynthesised in order to further evaluate the interesting absorption results observed previously by Tocci (née Hussey) regarding the binding abilities of such thiourea-based sensors in polar solvents.[117,189] Binding studies had initially been carried out in DMSO, resulting in striking colour changes upon anion recognition.   Moreover, this chromogenic response was not reversible when highly competitive solvents such as MeOH, EtOH and H_2O were added to the host:complex mixture. Due to the lack of this reversibility, it was proposed that the sensors would be able to bind anions in these more polar protic solvents, especially as the objective was to develop anion sensors capable of functioning in a biological setting (*i.e.* an aqueous medium).   Therefore, anion binding experiments were performed on these thiourea-based sensors in EtOH, and significant colour changes were again observed in the presence of the selected anions. Due to the poor solubility of these sensors in H_2O, host solutions in EtOH:H_2O (50:50) were instead prepared for anion binding experiments. This was achieved by first dissolving the sensors in EtOH, and these EtOH solutions were then used to prepare the EtOH:H_2O (50:50) host solutions. The studies carried out in this solvent medium demonstrated a significant chromogenic behaviour, complimentary to that observed in DMSO and EtOH. Due these encouraging results, the urea analogues (**129 - 131**) were thus also synthesised for anion binding studies. However, it was essential to confirm the reproducibility of the results obtained for the anion binding abilities of the thiourea analogues (*e.g.* **64**) in highly competitive media. Hence, the thiourea **64** was resynthesised for further binding studies in EtOH:H_2O (50:50).

Before performing absorption titrations, the extinction coefficient of **64** was determined and found to be 14120 $M^{-1}cm^{-1}$ (at 406 nm) in EtOH:H_2O (50:50) . This value will assist in eliminating possible errors when preparing the host solutions since it relates the host concentration to the absorbance (*i.e.* Beer-Lambert Law). Interestingly, it was discovered that this law only applies to high concentrations of these thiourea sensors when in highly competitive media, since at low concentrations, there seemed to be new bands forming on either side of the original absorption band at 406 nm. In fact,

it is possible that the interactions between the polar solvent molecules and receptor sites may be causing a "pseudo-binding" effect in the absence of any target anion. Hence, the host solutions were prepared such that the absorbance at 406 nm would be *ca.* 1.5 in magnitude. It should also be noted that such hydrazine-based naphthalimide anion sensors were found to possibly extract anions from soda-glass-based apparatus such as disposable sample tubes and Pasteur pipettes. This postulation was made due to the fact the free host solutions would immediately change colour once it was exposed to such apparatus. Therefore, only pyrex glassware was used when dealing with this type of compound.

4.5.1 Absorption Titrations of 64 with Anions

The UV-vis spectroscopic investigations performed on the anion binding abilities of **64** were carried out in EtOH:H_2O (50:50) at 25 °C. The free thiourea host **64** (1×10^{-4} M) showed a broad absorption band centered at 406 nm, and a much smaller band at 540 nm. Upon titration with tetrabutylammonium (TBA) salts of AcO⁻ (Figure 4.4), $H_2PO_4^-$ (Figure 4.5) and F⁻ (Figure 4.6), the band at 406 nm decreased in intensity, while that at 540 nm increased. A new absorption band also appeared concomitantly at 339 nm. In addition, two isosbestic points were clearly observed at 365 and 453 nm for AcO⁻ and F⁻ complexation, while those for $H_2PO_4^-$ were situated at 359 and 458 nm. These changes in the absorprion spectra of these sensors corresponded to the yellow to deep purple color change observable to the naked eye. These colour changes will be discussed later in Section 4.7. In contrast to these results, no significant spectral changes were observed on addition of other halides (*e.g.* Cl⁻or Br⁻).

Interestingly, the magnitude of the two bands at 339 and 540 nm (once a plateau was reached) in the presence of AcO⁻ was similar to that of the original band centred at 406 nm which had almost disappeared completely. However, in the case of $H_2PO_4^-$ and F⁻ binding, the two bands only achieved approximately half the absorbance of the band at 406 nm. Also, it was not possible for the binding process of **64** with $H_2PO_4^-$ to reach completion (*i.e.* no further changes in the absorbance). This may be due to the weaker binding observed for the two anions compared to that for AcO⁻. From these changes, it was already possible to differentiate between the binding abilities of **64** towards the selected anions, as the least number of anion equivalents was required for AcO⁻ binding while the most was needed for the binding of $H_2PO_4^-$. To observe this difference more

clearly, the changes in the relative absorbance of **64** at 540 nm was plotted against -log[anion], which will be discussed in the following section.
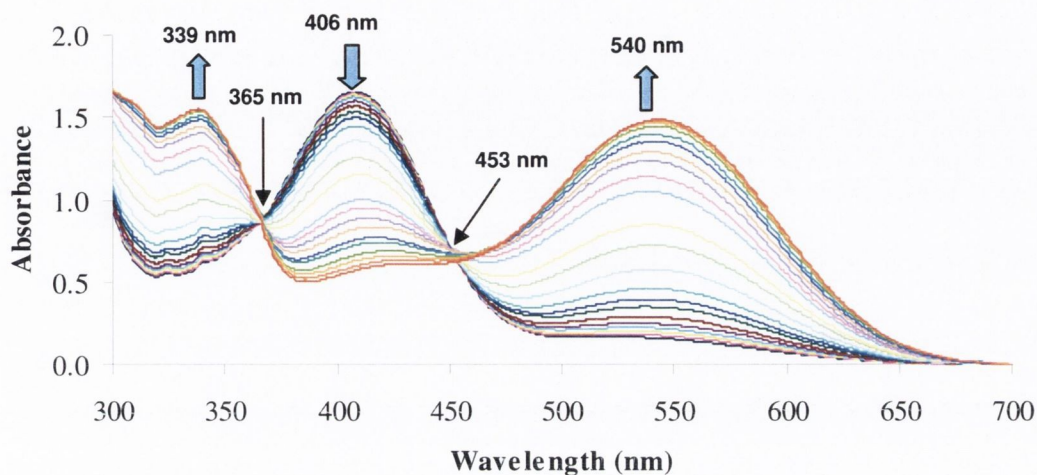
Figure 4.4 Changes observed in the absorption spectrum of thiourea **64** (1×10^{-4} M) upon addition of AcO$^-$ in EtOH:H$_2$O (50:50) at 25 °C (0 M $\rightarrow$ 1×10^{-2} M).
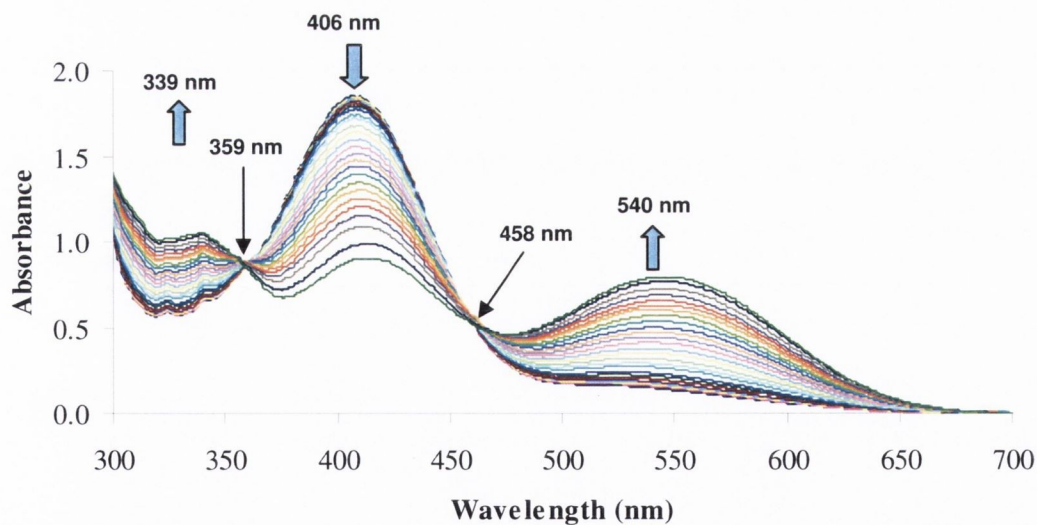
Figure 4.5 Changes observed in the absorption spectrum of thiourea **64** (1×10^{-4} M) upon addition of H$_2$PO$_4^-$ in EtOH:H$_2$O (50:50) at 25 °C (0 M $\rightarrow$ $> 3 \times 10^{-1}$ M).
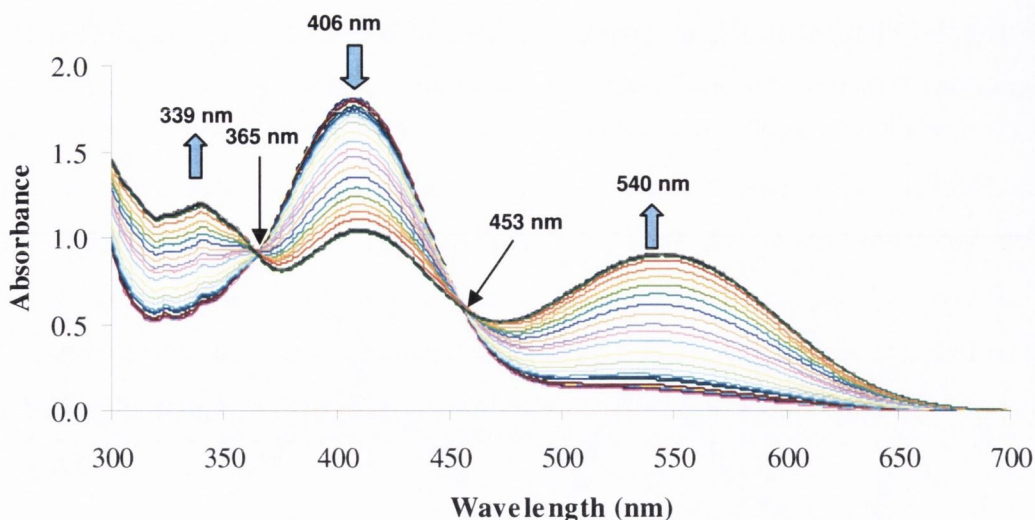
Figure 4.6 Changes observed in the absorption spectrum of thiourea **64** (1×10^{-4} M) upon addition of F^- in EtOH:H_2O (50:50) at 25 °C ($0 \rightarrow 1 \times 10^{-2}$ M).

4.5.1.1 Analysis of the Absorption Titration Data for 64

By plotting the changes in the 540 nm band of **64** as a function of -log[anion] (Figure 4.7), sigmoidal curves were observed for all three anions.
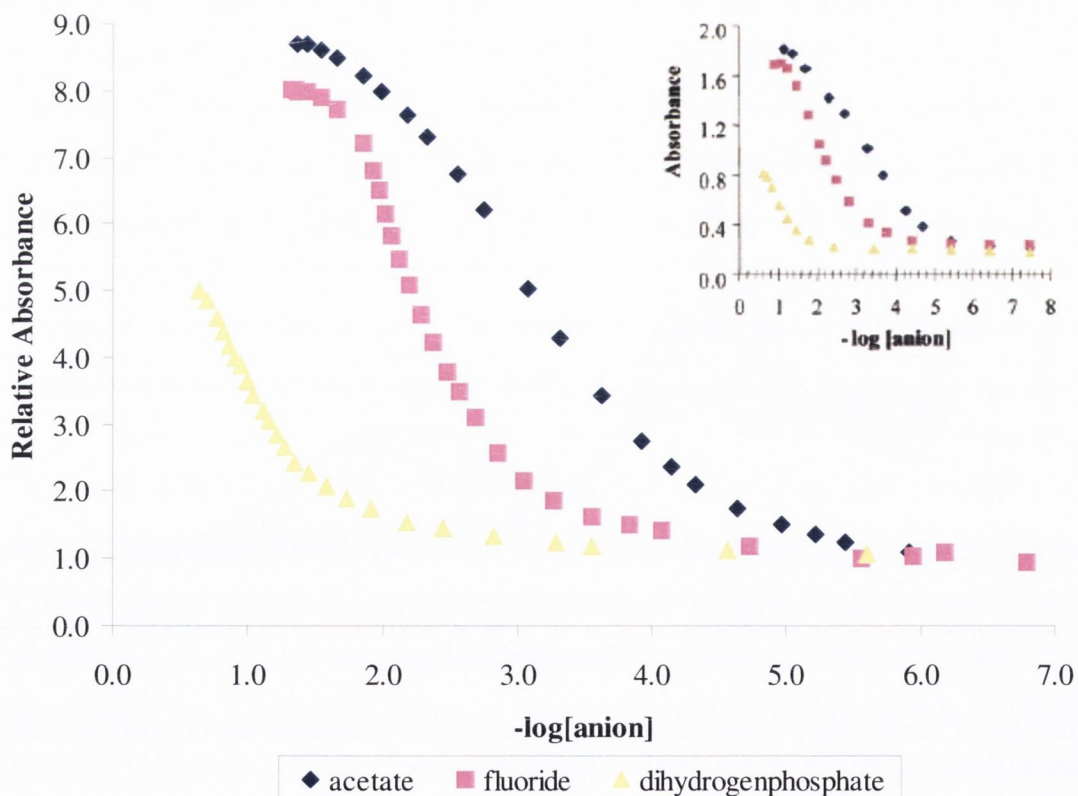
Figure 4.7 Relative absorbance of sensor **64** at 540 nm against -log[anion] in EtOH/H_2O (50:50) on addition of either AcO^-, $H_2PO_4^-$ or F^-. (Inset: Absorbance of sensor **64a** at 548 nm against -log[anion] in EtOH/H_2O (50:50) on addition of either AcO^-, $H_2PO_4^-$ or F^-.[117])

The binding curve plotted for F⁻ binding was steeper than that for the binding of AcO⁻. However, a plateau was reached at a similar -log[anion] in both cases. As for $H_2PO_4^-$ recognition, the binding curve still did not achieve a plateau even after the addition of over 3000 anion equivalents. From these graphs, it can be seen that **64** binds more strongly to AcO⁻, followed by F⁻ and finally, $H_2PO_4^-$. These results are consistent with those obtained for the same compound (**64a**) synthesized previously by Tocci (née Hussey).[117,189]

4.5.1.2 Stability Constants (log β) from Absorption Titration Data of 64

Stability (or binding) constants (log β) of these anion binding processes were calculated using SPECFIT/32™ from the data collected (see Appendix 7.3.1). In EtOH:H_2O (50:50), the complexation of the selected anions by **64** were found to have a 1:1 host:guest stoichiometry. To ensure that the log β value calculated by SPECFIT/32™ is reasonable, there must be a good fit between the observed and calculated data. Figure 4.8 shows the fit between the observed data and the SPECFIT/32™-calculated data at 406 nm for the binding of AcO⁻ by **64**.
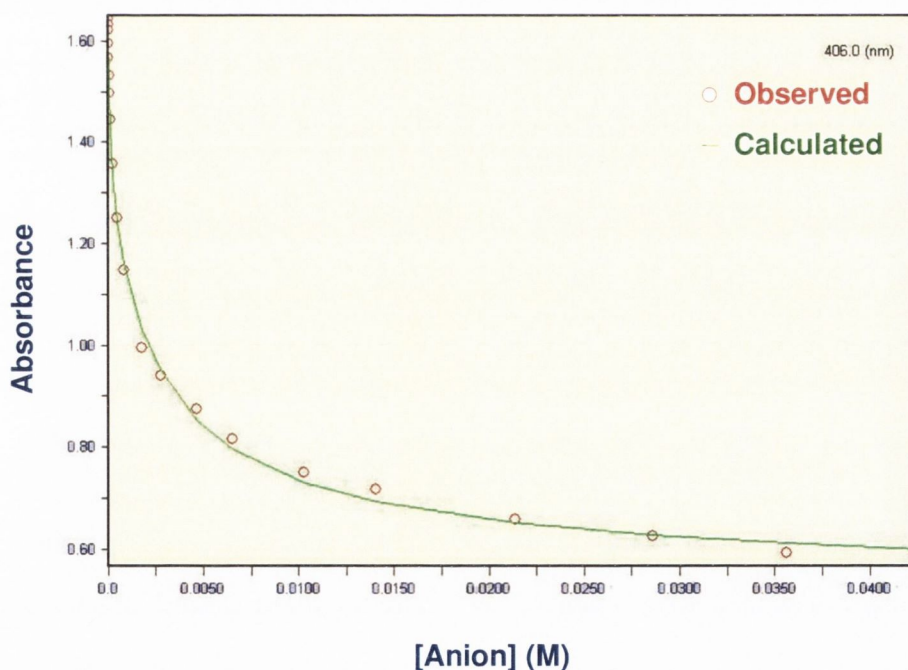
Figure 4.8 SPECFIT/32™-generated graph showing the fit between the observed and calculated data at 406.0 nm for the binding of AcO⁻ by **64**.

Table 4.2 shows the log β values for the 1:1 binding processes of **64** and **64a** with AcO⁻, $H_2PO_4^-$ and F⁻. Tocci (née Hussey) calculated the binding constants for **64a**

by fitting the data to a non-linear least-squares regression equation using a Microsoft Excel program written by members of the Gunnlaugsson group. The two sets of log β values were comparably similar to each other. Sensor **64** was found to bind strongest to AcO$^-$ with a log β of 3.17 ($\pm$ 0.04), while the binding constants for the complexation of F$^-$ and H$_2$PO$_4^-$ by **64** were 0.36 ($\pm$ 0.06) and 2.04 ($\pm$ 0.38) respectively.

Table 4.2 Binding constants (log β) for the binding of **64** and **64a**[117,189] with AcO$^-$, H$_2$PO$_4^-$ and F$^-$ calculated using SPECFIT/32™ and Microsoft Excel respectively.

Sensor	log β (AcO$^-$)	log β (H$_2$PO$_4^-$)	log β (F$^-$)
64	3.17 $\pm$ 0.04	0.36 $\pm$ 0.06	2.04 $\pm$ 0.38
64a	3.4 $\pm$ 0.1	~1 $\pm$ 0.2	2.2 $\pm$ 0.1

4.5.2 Conclusions

The anion binding ability of **64** towards the selected anions in EtOH:H$_2$O (50:50) was found to be in the order of AcO$^-$ > F$^-$ > H$_2$PO$_4^-$ > Cl$^-$ > Br$^-$. The absorption spectral changes in the binding of AcO$^-$ were more significant in comparison to those of H$_2$PO$_4^-$ and F$^-$ binding. It was such that the new bands at 339 and 540 nm reached the same absorbance at the original band at 406 nm upon complex formation with AcO$^-$, while they only achieved half the absorbance in the case of the latter two anions.

The stability constants (log β) calculated from the absorption titration data collected (within this study) using SPECFIT/32™ were consistent with those obtained previously using the Microsoft Excel program. As SPECFIT/32™ analyses the data over the whole wavelength range, it is able to provide a more accurate calculation for the log β values.

In conclusion, the results obtained from the above study provided further supporting evidence of the reproducibilty of the synthesis as well as the absorption binding experiments. Such hydrazine-based thiourea sensors are shown to be the first examples of colorimetric anion sensors that can be used in highly competitive media (EtOH:H$_2$O (50:50)) where the recognition event is mediated through bonding to a charge-neutral receptor.[117] Therefore, these encouraging results prompted the study into the anion binding abilities of the urea analogues of such hydrazine-based napthalimide thiourea sensors.

4.6 Physical Evaluation of the Anion Recognition of 129 - 131

For comparative purposes, anion binding experiments were also carried out on the hydrazine-based naphthalimide ureas **129 - 131**. The binding processes of these compounds were first studied by ^{1}H NMR spectroscopy in DMSO-d_6, followed by photophysical techniques such as UV-vis and fluorescence spectroscopies in DMSO. For the photophysical experiments, the extinction coefficients of **129**, **130** and **131** were initially determined, and were found to be 14586, 14507 and 13748 M^{-1}cm^{-1} (at 420 nm in DMSO) respectively. Preliminary studies of these urea sensors showed that they were only able to successfully bind anions in DMSO, unlike their thiourea analogues which bind anions in DMSO as well as highly competitive media such as EtOH and EtOH:H$_2$O (50:50).[117] This may possibly be due to the fact that ureas generally have weaker anion binding abilities than their thiourea analogues.[154,162,172,173,89,137] Hence, it is likely that ureas would experience more competition for target anions with polar protic solvent molecules such as EtOH and H$_2$O. As a result, all anion binding experiments of **129 - 131** were carried out only in DMSO (or DMSO-d_6).

4.6.1 ^{1}H NMR Titrations of 129 - 131 with Anions

^{1}H NMR spectroscopic experiments were performed on host solutions of **129 - 131** in DMSO-d_6 (1.0 × 10^{-2} M) at 25 °C with AcO$^-$, H$_2$PO$_4^-$, F$^-$, Cl$^-$ and Br$^-$. The naked eye effect observed was quite striking in these studies as the yellow-to-purple colour change began to occur immediately after the addition of 0.1 equivalent of anion (to be discussed later in Section 4.7). The naphthalimide protons of these sensors were primarily monitored as the chemical shifts of the NH protons of the urea moiety broadened significantly early on in the titration. Nevertheless, it was also possible to observe the changes in the chemical shift of the 4-amino-naphthamide proton in **129** and **130**, while that of sensor **131** became too broad to monitor upon anion complexation. This may be to due to the electron-withdrawing property of the 4-(trifluoromethyl)-phenyl substituent of **131** causing an increase in the acidity of this NH proton. Figures 4.9 and 4.10 show the changes observed in the ^{1}H NMR spectrum of **131** upon the addition of AcO$^-$ and F$^-$, respectively.
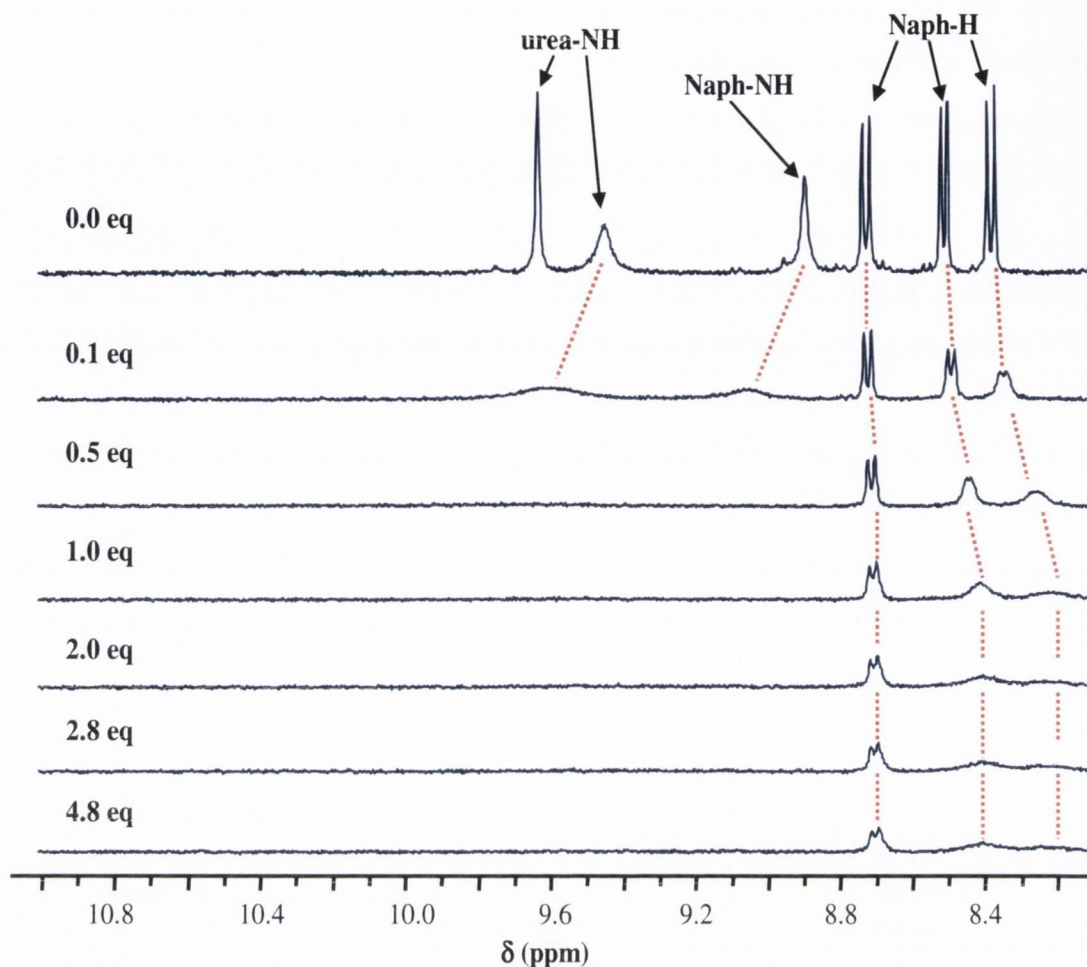
Figure 4.9 Stack plot of ^{1}H NMR spectra of **131** (1×10^{-2} M) upon addition of AcO$^-$ in DMSO-d_6 at 25 °C.

In the presence of fluoride, the chemical shifts of the protons were even more perturbed, causing difficulty in monitoring the overall changes. However, there was an appearance of a triplet peak at around 16 ppm upon the addition of *ca.* 2 equivalents of the anion, which increased in intensity with increasing amount of fluoride. This may be attributed to the formation of HF$_2^-$ upon the deprotonation of an NH proton.[135,140,88,169] Similar changes were seen for the other sensors in the presence of AcO$^-$ and F$^-$. As regards to Cl$^-$ and Br$^-$, no significant changes were observed in the ^{1}H NMR spectrum of all the three sensors in the presence of these halides.
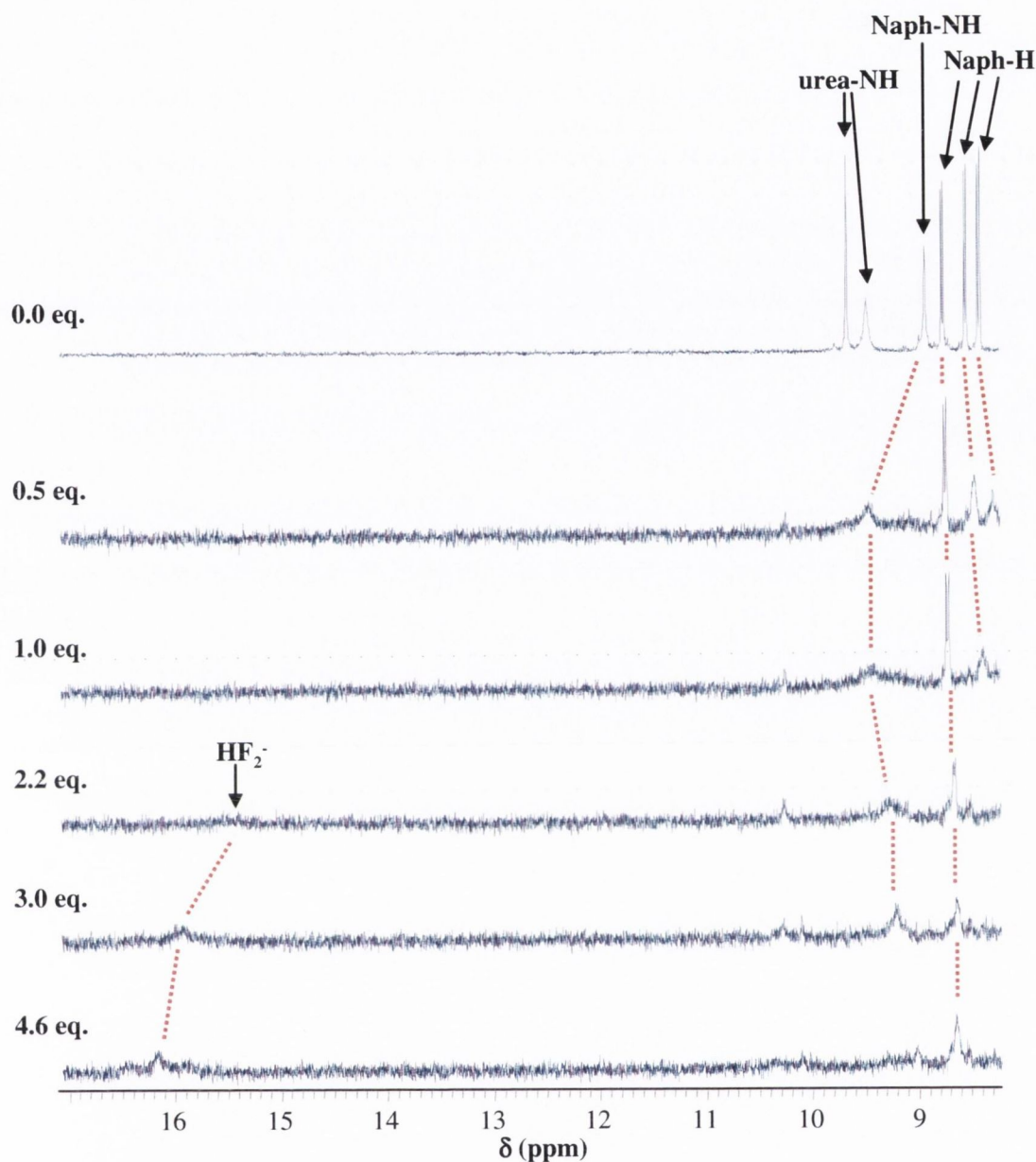
Figure 4.10 Stack plot of ^{1}H NMR spectra of **131** (1×10^{-2} M) upon addition of F$^-$ in DMSO-d_6 at 25 °C. (<u>Note</u>: The chemical shifts were greatly perturbed, hence, the ^{1}H NMR spectra had to be magnified significantly after the first addition of F$^-$.)

4.6.1.1 Analysis of the ^{1}H NMR Titration Data for 129 - 131

The data obtained from these titrations was plotted as the relative cumulative changes in chemical shift ($\Delta\delta$) against the equivalents of anion added and the resulting plots were analysed using WinEQNMR.[12] It should be noted that since the changes were comparably small in magnitude, and hence carried larger errors. Figures 4.11, 4.12 and 4.13 show the graphs of relative $\Delta\delta$ against equivalents of putative anions for urea sensors **129**, **130** and **131** respectively. For all the three sensors, the binding curves

obtained for their complex formation with AcO⁻ reached a plateau after *ca.* one anion equivalent, indicating a 1:1 host:guest stoichiometry. On the other hand, the binding of $H_2PO_4^-$ and F⁻ by these sensors appeared to require two or even more equivalents of the anions in order for the binding process to reach completion. There are many reports of a 1:2 host:guest stoichiometry for F⁻ binding.[91,118,135,143,169] However, there are to the best of our knowledge no known cases of two $H_2PO_4^-$ molecules binding to such a simple mono-urea (or thiourea) receptor. Therefore, it is more likely a case of such sensors binding more weakly to $H_2PO_4^-$ than the other two anions, thus requiring a large number of anion equivalents for the binding process to reach completion.

For **129** and **131**, it was observed that both sensors bound strongly to AcO⁻ in comparison to the other anions. Also, in both cases, there seemed to be no significant difference between the shape of the binding curves for $H_2PO_4^-$ and F⁻. However, from the appearance of the anion binding curves for **130**, it seemed that the presence of the electron-donating methyl substituent in this sensor may have resulted in decreasing the AcO⁻ binding ability (*i.e.* the curve was not as steep as those for **129** and **131**). Hence, there appeared to be no significant selective binding of the anions by this sensor.
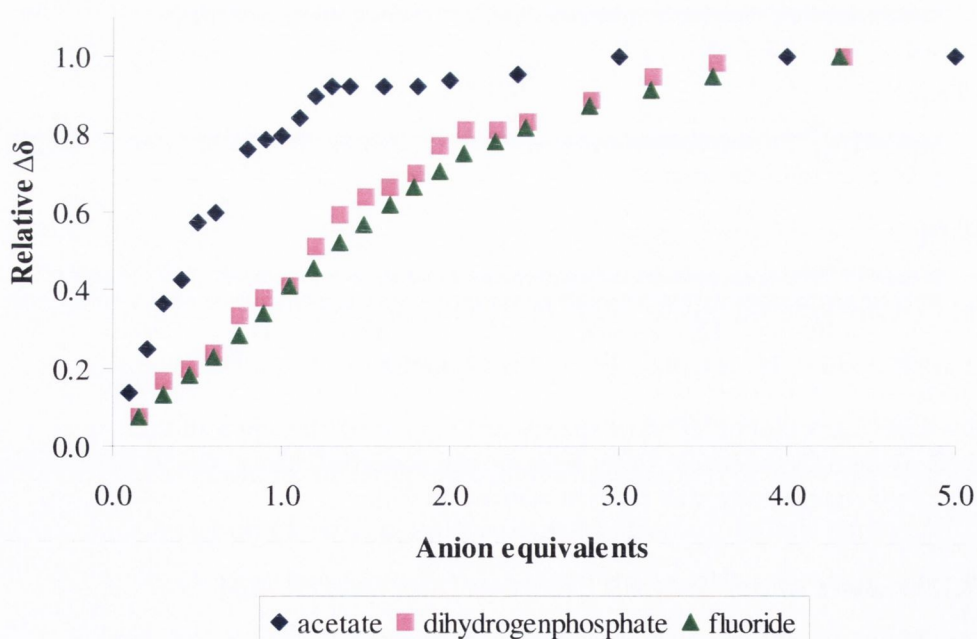
Figure 4.11 Relative cumulative changes in the chemical shift of proton at 8.4 ppm for **129** against anion equivalents in DMSO-d_6.
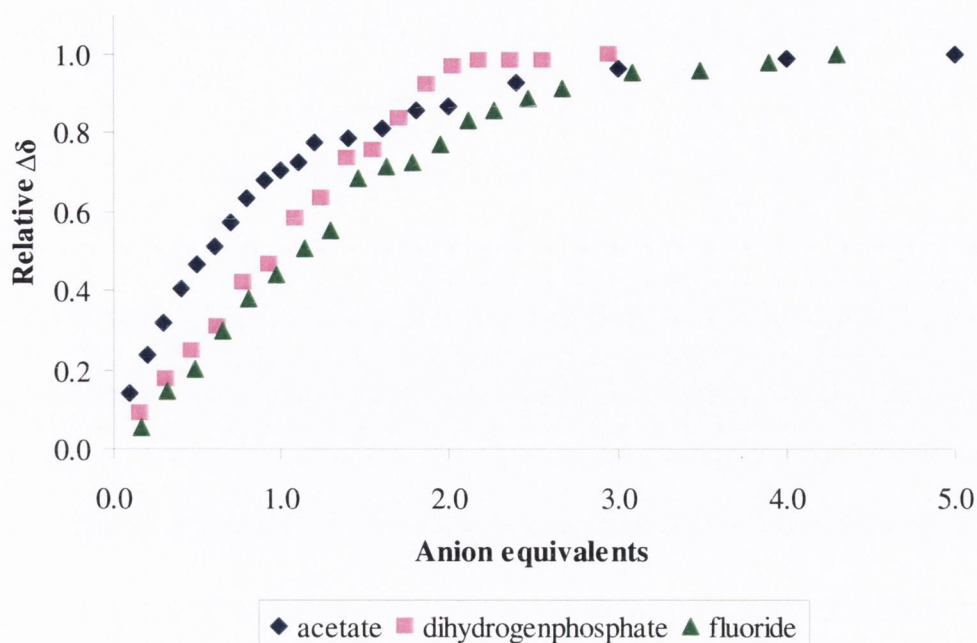
Figure 4.12 Relative cumulative changes in the chemical shift of proton at 8.4 ppm for sensor **130** against anion equivalents in DMSO-d_6.

Figure 4.13 Relative cumulative changes in the chemical shift of proton at 8.4 ppm for sensor **131** against anion equivalents in DMSO-d_6.

Interestingly, when comparing relative $\Delta\delta$ of all three sensors against equivalents of each anion (Figures 4.14 - 4.16), it is observed that there is little difference between their binding curves for an individual guest, especially in the case of fluoride binding. Nevertheless, despite these small changes, the binding curves shown

in Figure 4.14 suggest that **131** may bind more strongly to AcO⁻ than the other two sensors, while in Figure 4.15, it appears that $H_2PO_4^-$ may bind best to **130**.

Figure 4.14 Relative cumulative changes in the chemical shift of proton at 8.4 ppm for **129** - **131** against equivalents of AcO⁻ in DMSO-d_6.

Figure 4.15 Relative cumulative changes in the chemical shift of proton at 8.4 ppm for **129** - **131** against equivalents of $H_2PO_4^-$ in DMSO-d_6.
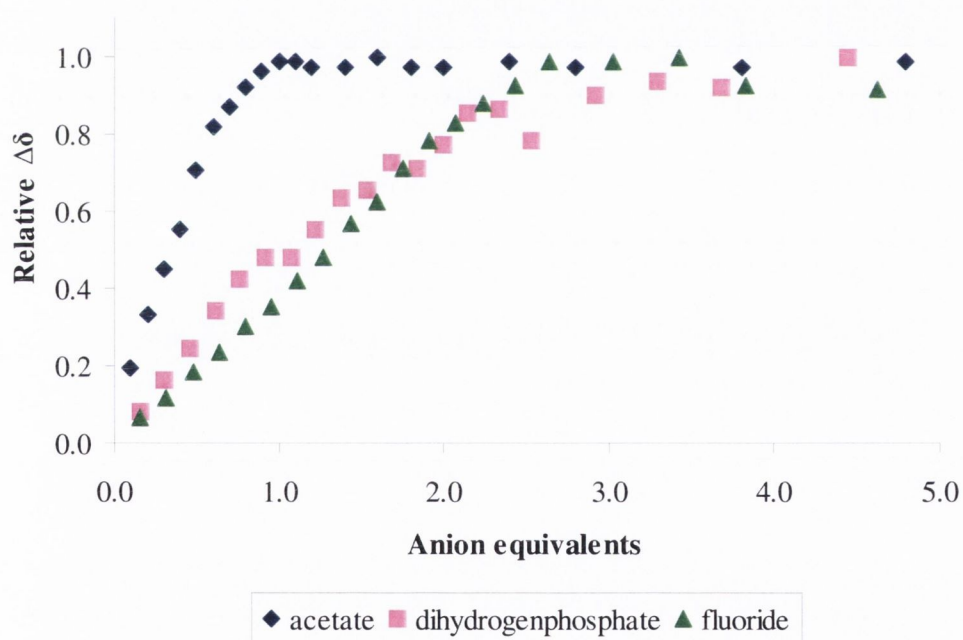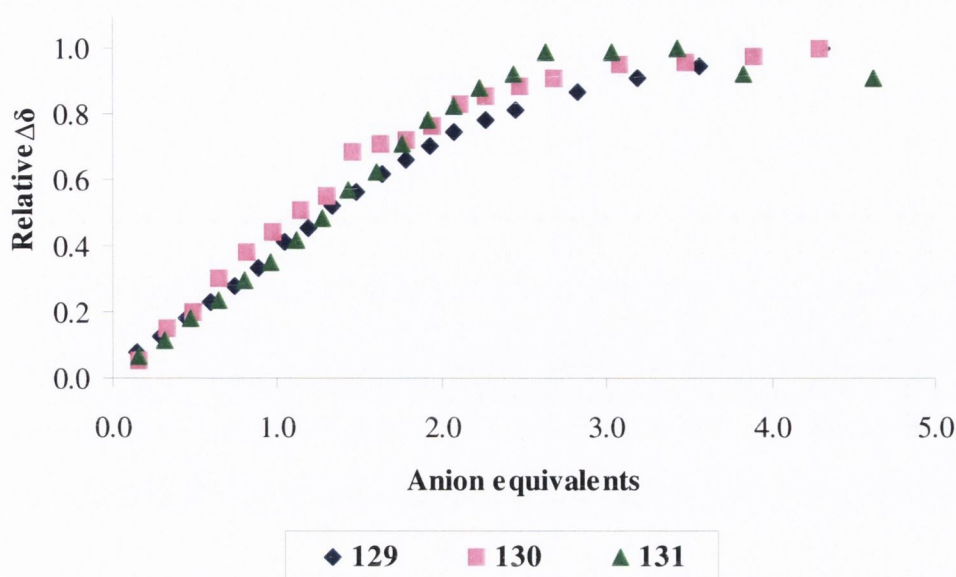
Figure 4.16 Relative cumulative changes in the chemical shift of proton at 8.4 ppm for **129** - **131** against equivalents of F^- in DMSO-d_6.
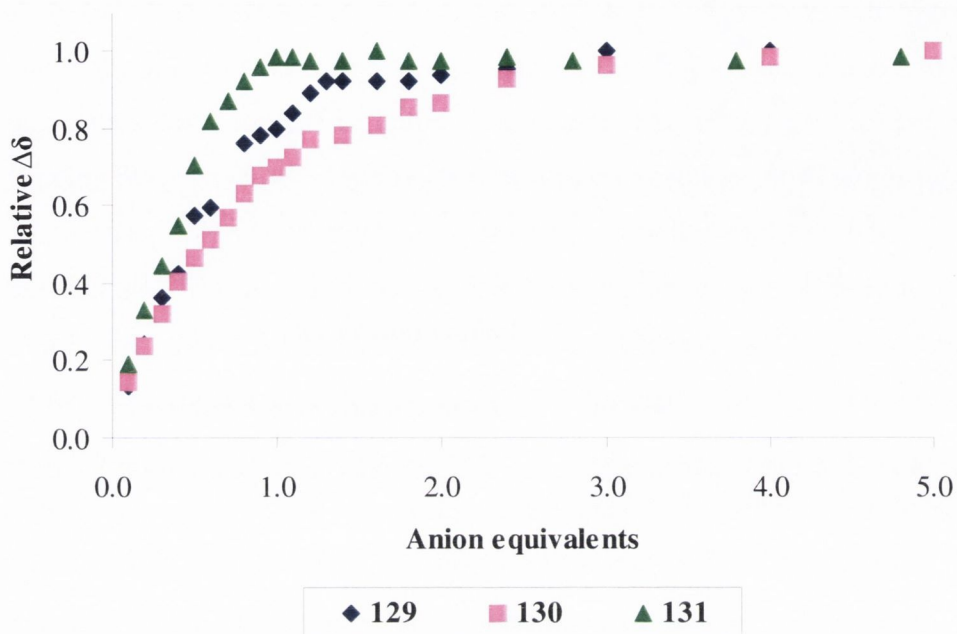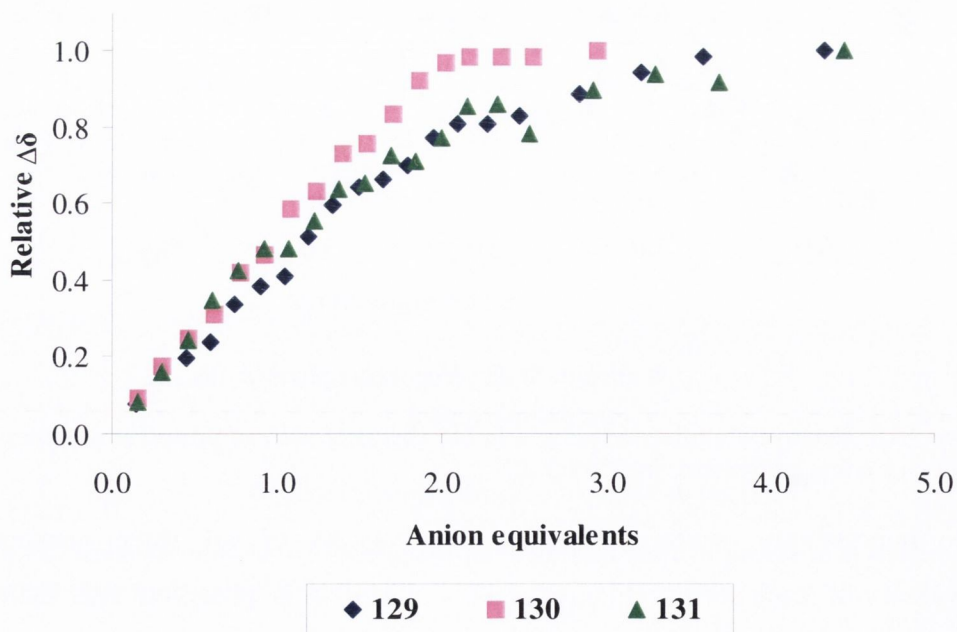
In Figure 4.14, the binding curves for AcO^- by the three sensors indicate that the host:guest stoichiometry was 1:1. In the case of $H_2PO_4^-$ binding, it is unclear in which host:guest stoichiometry the complex has formed. The binding curves for the complexation of $H_2PO_4^-$ by **129** and **131** do not reach a plateau at the end of the titrations (*i.e.* when *ca.* 5 equivalents of the anion has been added), and this may be attributed to their weaker binding abilities. In contrast, urea **130** appears to bind $H_2PO_4^-$ with a host:guest stoichiometry of 1:2, as the binding curve plateaus at *ca.* 2 anion equivalents. Finally, it is evident that the binding curves for F^- complexation of **129** - **131** is not 1:1, since the the plateau is reached in the region of between 2 - 3 equivalents of the anionic guest. The next section will now examine the stability constants determined from these ^1H NMR titrations to provide a more quantitative evaluation of the anion binding abilities of these sensors.

4.6.1.2 Stability Constants (log β) from ^1H NMR Titration Data of 129 - 131

The stability constants (log β) for the complex formation of **129** - **131** with putative anions (Table 4.3) were determined from the data collected using the Fortran-based WinEQNMR program.[12] Figures 4.17 shows the graph generated by WinEQNMR illustrating the fit between the observed and calculated data for the binding of AcO^- by **131**. A good fit ensures that the log β value calculated by the program is reasonable, even though the value of the error may be quite big. The

WinEQNMR-generated graphs of these sensors with AcO^- and $H_2PO_4^-$ (except for the $H_2PO_4^-$ binding of **130** as well as the F^- binding of all three sensors) showed reasonably good correlation between the observed and calculated data (see Appendix 7.3.3).
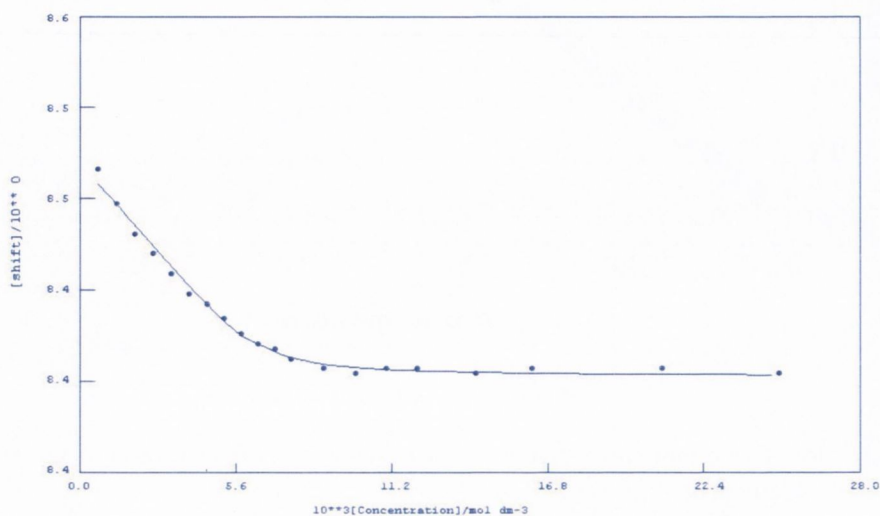
Figure 4.17 WinEQNMR-generated graph showing the fit between the observed (points) and calculated (line) data for the binding of AcO^- by **131** in DMSO-d_6.

Table 4.3 Binding constants ($\log \beta$) of **129 - 131** upon complexation with putative anions in DMSO-d_6. All values were obtained from WinEQNMR,[12] and are within 15% error. ([a] The binding process is too complicated for analysis by WinEQNMR.)

Sensor	Substituent (R)	$\log \beta$ (AcO^-)	$\log \beta$ ($H_2PO_4^-$)	$\log \beta$ (F^-)
129	H	3.58	2.21	a
130	CH_3	2.85	a	a
131	CF_3	3.75	2.33	a

The $\log \beta$ values obtained for the AcO^- complexation of **129**, **130** and **131** were 3.58, 2.85 and 3.75 respectively (with errors of less than 15%). With respect to the value calculated for **129**, it is observed that in the presence of an electron-donating group (as in **130**), the stability constant decreases and *vice versa* in the presence of an electron-withdrawing group (as in **131**). This observation is consistent with the reported study regarding the effect of different substituents on the strength of anion binding sites,[159] as well as the study discussed in Chapter 2. Again, in the binding of $H_2PO_4^-$, the electron-withdrawing group in **131** results in a higher $\log \beta$ value (*i.e.* 2.33) in comparison to that obtained for the unsubstituted sensor **129** (*i.e.* 2.21). Interestingly, it

was not possible for the program to obtain log β values for the $H_2PO_4^-$ binding of **130**. Similar analytical difficulties were experienced for F^- binding. The reason behind this may either be due to a more complicated binding process (*i.e.* not 1:1 host:guest stoichiometry) or the occurrence of more than one process (*e.g.* binding, deprotonation).

.

4.6.1.3 Conclusions

The binding of AcO^- by **129** - **131** monitored using ^1H NMR spectroscopy showed a 1:1 host:guest stoichiometry, which is consistent with several reports in the literature,[89,117,103,88,140] as well as the study discussed in Chapter 2. However, in the case of $H_2PO_4^-$, it is unclear as to what processes may be occurring. Since there seems to be no deprotonation of the urea NH protons in the presence of AcO^-, the likelihood of $H_2PO_4^-$ causing the loss of an NH proton is small as it is not as basic an anion as AcO^-.[116] Therefore, there may be another process occurring, one that may involve the 4-amino proton. Pfeffer and co-workers reported the cooperative binding of $H_2PO_4^-$ involving the naphthalimide 4-amino proton with the thiourea NH protons.[136,108] Hence, there is a possibility of the 4-amino proton acting as another potential anion binding site, especially as it is part of a hydrazine moiety, thus increasing the acidity of this NH proton. The binding of F^- appears to require *ca.* 3 anion equivalents for the process to reach completion. Ureas (and thioureas) generally bind F^- with a 1:2 host:guest stoichiometry,[89,117,103,154] or even in a 1:1 fashion.[140,88] Therefore, it may be possible that the 4-amino proton is partaking in the binding of F^- (especially since this spherical anion is small), resulting in a 1:3 host:guest stoichiometry. However, it is still not certain as to why the binding process of $H_2PO_4^-$ appeared complicated.

As regards to the effect of the electronic nature of the different *para* substituents on the phenyl ring of **129** - **131**, the stability constants (log β) indicate that anion binding ability of such sensors is dependent on whether the substituent is electron-withdrawing or electron-donating. The electron-withdrawing CF_3 group appeared to enhance the binding strength while the electron-donating CH_3 substituent caused the opposite effect. The dependence on the electronic nature of these substituents were not observed in the thiourea analogues (**63** and **64**) studied previously by Tocci (née Hussey). There have been several accounts in the literature, which demonstrate this dependence of the binding abilities of urea- and thiourea-based receptors and sensors on the electronic nature of such substituents.[159] This observation is consistent with the results obtained from the study discussed in Chapter 2.

The next section will discuss the photophysical evaluation of **129 - 131** with putative anions in order to further evaluate their anion binding abilites.

4.6.2 Absorption Titrations of 129 - 131 with Anions

Unlike their corresponding thiourea analogues (*e.g.* **64**), the absorption spectra of urea sensors **129 - 131** are **not** concentration dependent in DMSO at 25 °C. Since the NH protons of ureas are less acidic than those of their thiourea analogues,[89,137,154,162,172,173] the interactions between the polar protic solvent molecules (*e.g.* H_2O) and the urea NH protons are not as significant. In the case of the thiourea-based sensors such as **64**, the solvent seemed to interact strongly with the NH protons when the host concentrations are low, hence the appearance of the two new bands centred at 339 and 540 nm in the absorption spectrum even in the absence of anions. Due to the lack of concentration dependence in the absorbance of **129 - 131**, the UV-vis spectroscopic investigations were carried out such that the initial optical density of these sensors at 420 nm is *ca.* 0.2.

Sensors **129 - 131** (1.5×10^{-5} M) all have similar absorption profiles which show a broad absorption band centered at 420 nm when they are present as the free host in DMSO. Upon titration with TBA salts of AcO^- (Figure 4.20), $H_2PO_4^-$ (Figure 4.21) and F^- (Figure 4.22) by **131**, the band at 420 nm decreased in intensity for all three anions. In the case of AcO^- and $H_2PO_4^-$ complexation, this band did not fully disappear, even at very high guest concentrations (1×10^{-2} M) whereas on addition of F^-, no trace of this band was seen after the guest concentration is *ca.* 5×10^{-4} M. New absorption bands also began to appear at both 360 and 569 nm, while two isosbestic points were clearly observed at 385 and 470 nm. These changes were similar to those observed in the absorption titrations carried out on the thiourea analogues (**63** and **64**). When the binding process reached completion, the maximum absorbance of the new band at 360 nm was *ca.* 90% of the initial absorbance of the 420 nm band for both AcO^- and $H_2PO_4^-$ binding, while that for F^- binding was *ca.* 70%. Also, the fine structure of the 360 nm band changed in the presence of F^-, revealing a small shoulder at *ca.* 340 nm at the end of the titration. This shoulder was not observed in the binding of AcO^- and $H_2PO_4^-$.

In the case of the band at 569 nm, the maximum absorbance reached was *ca.* 40% of the initial absorbance of the original 420 nm band in the binding of AcO^- and $H_2PO_4^-$ by **131**, while the binding of F^- resulted in a maximum absorbance of *ca.* 70%. There was also the appearance of a shoulder at *ca.* 535 nm, which was not observed in

the presence of AcO⁻ and $H_2PO_4^-$. The shoulders observed at *ca.* 340 and 535 nm may be due to the presence of a new species formed as a result of the deprotonation of one of the urea NH protons by F⁻ (observed in the ^{1}H NMR binding experiments).

Figure 4.20 Changes observed in the absorption spectrum of urea **131** (1.5×10^{-5} M) upon addition of AcO⁻ in DMSO at 25 °C (0 M → 3×10^{-3} M).
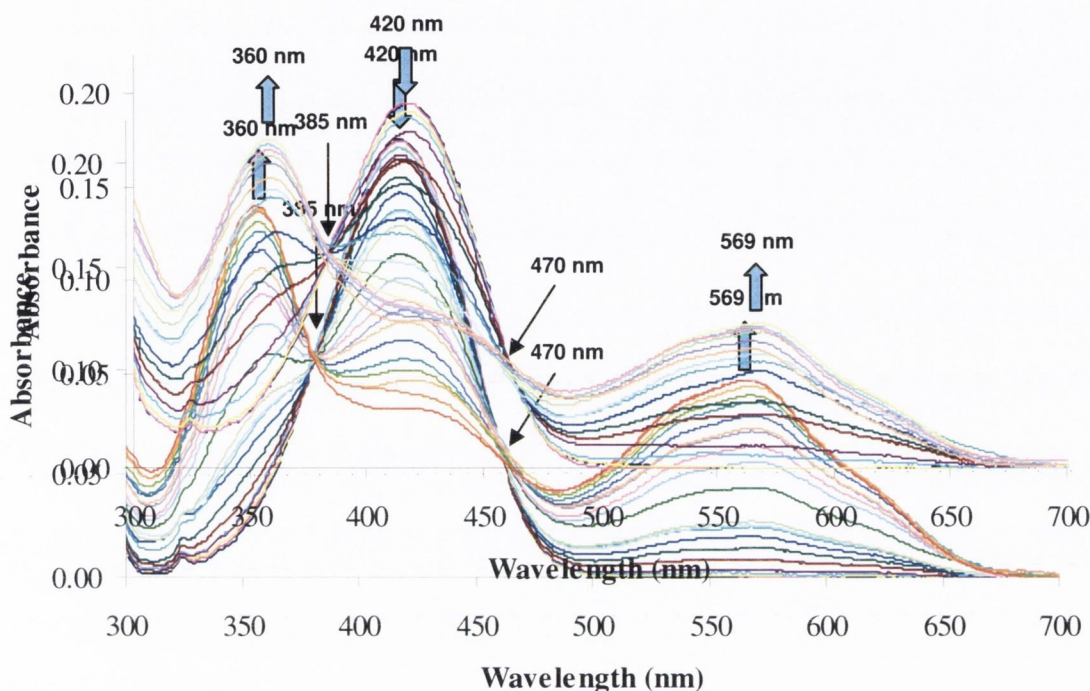
Figure 4.21 Changes observed in the absorption spectrum of urea **131** (1.5×10^{-5} M) upon addition of $H_2PO_4^-$ in DMSO at 25 °C (0 M → 3×10^{-3} M).
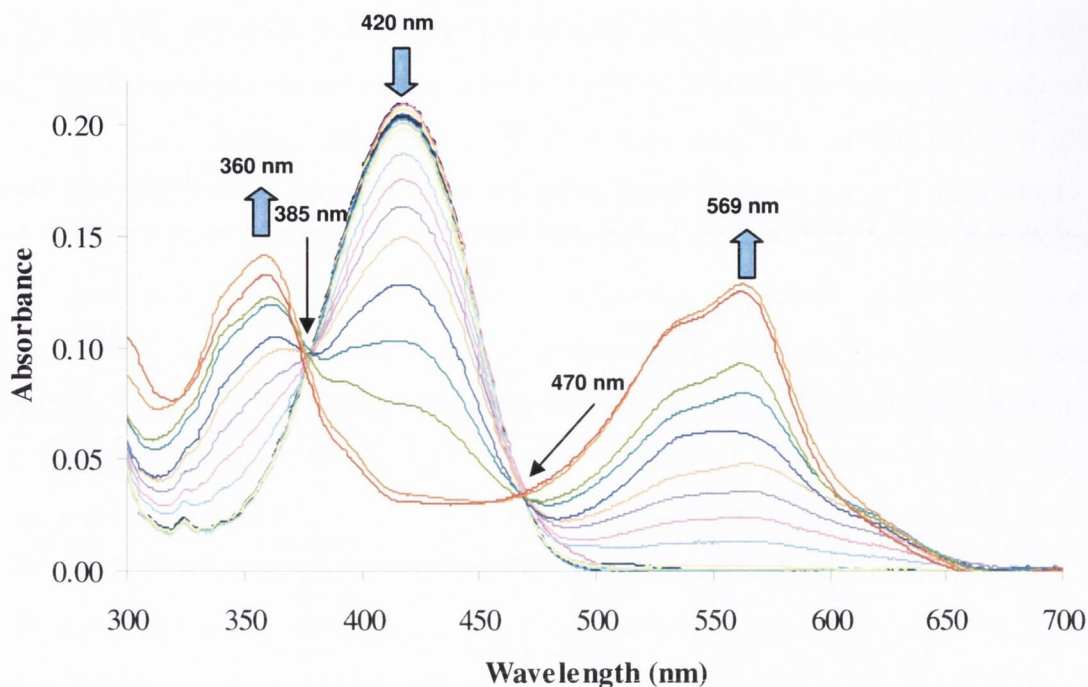
Figure 4.22 Changes observed in the absorption spectrum of urea **131** (1.5×10^{-5} M) upon addition of F^- in DMSO at 25 °C ($0\ M \rightarrow 3 \times 10^{-3}\ M$).

The changes in the absorptiom spectra of these sensors corresponded to the yellow-to-purple color change (to be discussed later in Section 4.7). In the presence of Cl^- and Br^-, no significant spectral changes were observed. These spectral changes recorded for the anion binding of **131** were similarly observed for sensors **129** and **130** (see Appendix 7.3.2), with differences observed only in the amount of anionic guest required for the completion of the binding process.

4.6.2.1 Analysis of the Absorption Titration Data for 129 - 131

By plotting the changes in the new 569 nm band of these colorimetric sensors as a function of -log[anion] (Figures 4.23 - 4.25), sigmoidal binding curves were observed, which changed over approximately two log units for both AcO^- and $H_2PO_4^-$. However, in the case of F^- complexation, the curve changed over *ca.* one log unit. From these graphs, it can be seen that **129 - 131** bound to AcO^- more strongly than to $H_2PO_4^-$. On addition of AcO^- and F^- to all three sensors, the curve reached a plateau at a guest concentration of *ca.* 3×10^{-4} M, whereas this occured at *ca.* 3×10^{-3} M for $H_2PO_4^-$. In the case of the thiourea analogues **63** and **64**, the sigmoidal binding curves obtained showed no significant difference between the two compounds (*i.e.* the curves overlaid) for each anion.

144
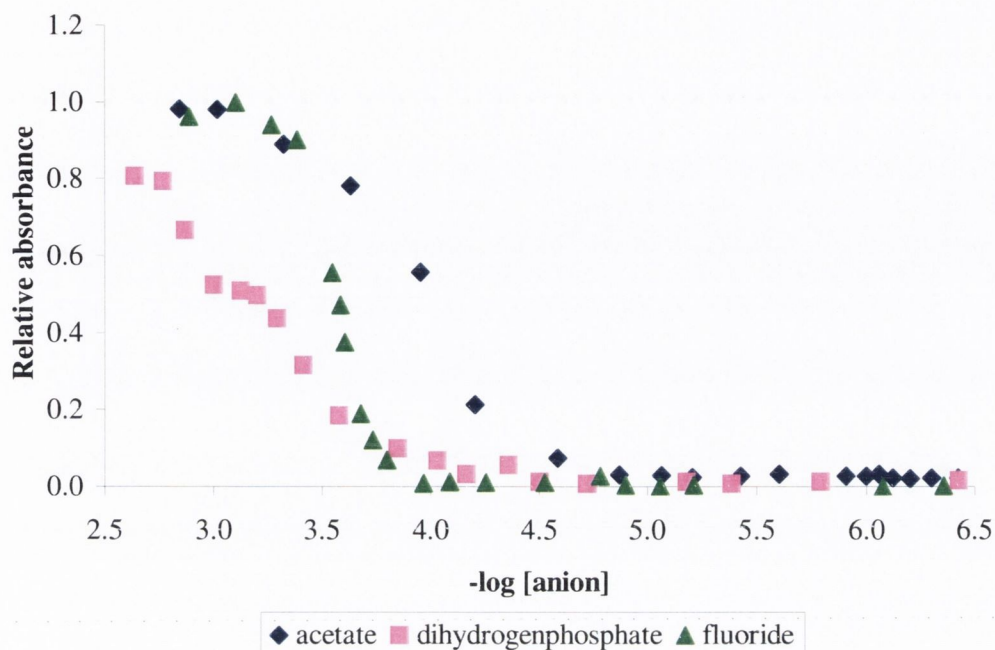
Figure 4.23 Relative absorbance of sensor **129** at 569 nm against -log[anion] in DMSO on addition of either AcO⁻, $H_2PO_4^-$ or F⁻.
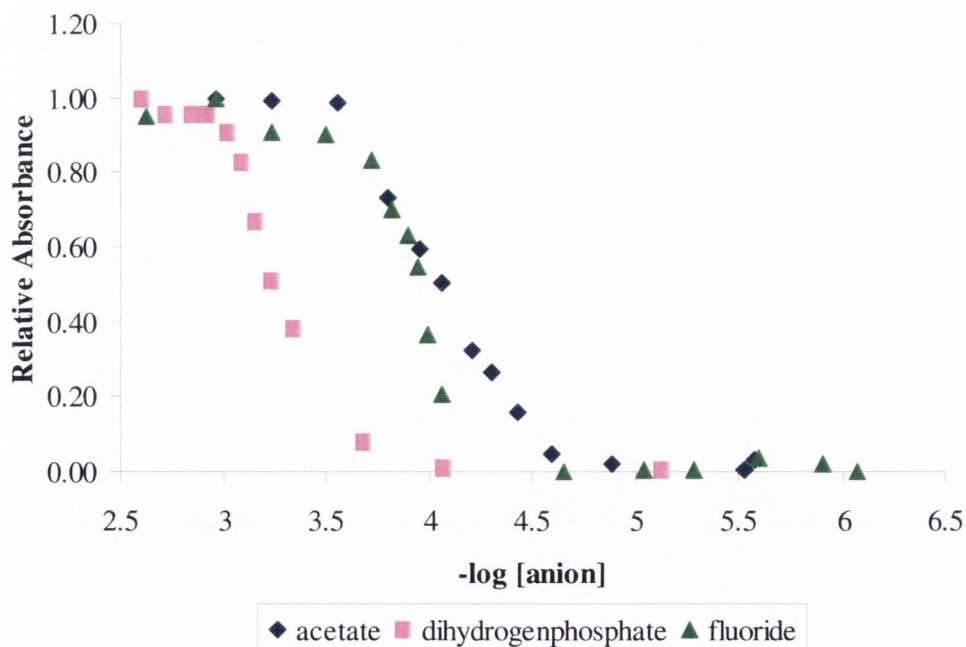
Figure 4.24 Relative absorbance of sensor **130** at 569 nm against -log[anion] in DMSO on addition of either AcO⁻, $H_2PO_4^-$ or F⁻.

Figure 4.25 Relative absorbance of sensor **131** at 569 nm against -log[anion] in DMSO on addition of either AcO⁻, $H_2PO_4^-$ or F⁻.

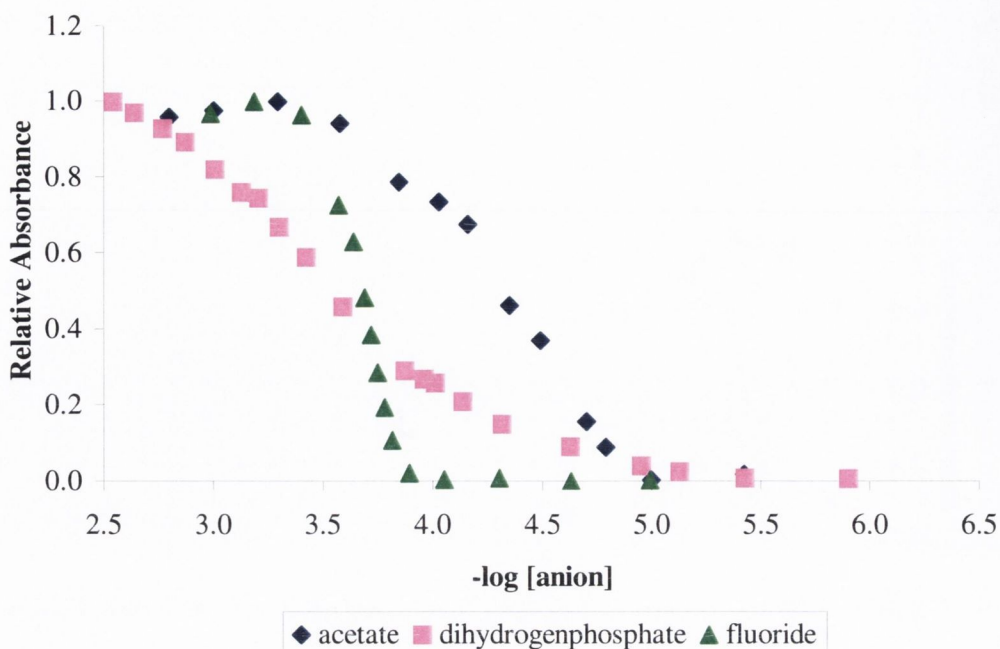For a more quantitative analysis of these results, SPECFIT/32™ was used to fit the data in order to calculate the stability constants (log β) for the binding of these sensors to the selected anions. These values will be discussed in the following section.

4.6.2.2 Stability Constants (log β) from Absorption Titration Data of 129 - 131

Stability constants (log β) for the anion binding processes of **129 - 131** were calculated from the absorption titration data collected using SPECFIT/32™ (see Appendix 7.3.3). Table 4.4 list the log β values for the anion binding processes of **129 - 131** with AcO⁻, $H_2PO_4^-$ and F⁻ in DMSO. The data collected was fitted to a number of different models with host:guest stoichiometries such as 1:1, 1:2 and 1:3. The analysis indicated that the complexation processes of AcO⁻ and $H_2PO_4^-$ by these urea sensors have a 1:1 host:guest stoichiometry. However, in the case of F⁻ binding, it was not possible for the program to calculate the log β values, giving log β values with significant errors and poor correlation between the observed and calculated data. It was also observed in the ¹H NMR binding experiments that the host:guest stoichiometry of the F⁻ binding of these sensors may be 1:3, but there may possibly be more than one process occurring (such as complexation and deprotonation), which may be causing problems in the SPECFIT/32™ analysis of the data collected.

146
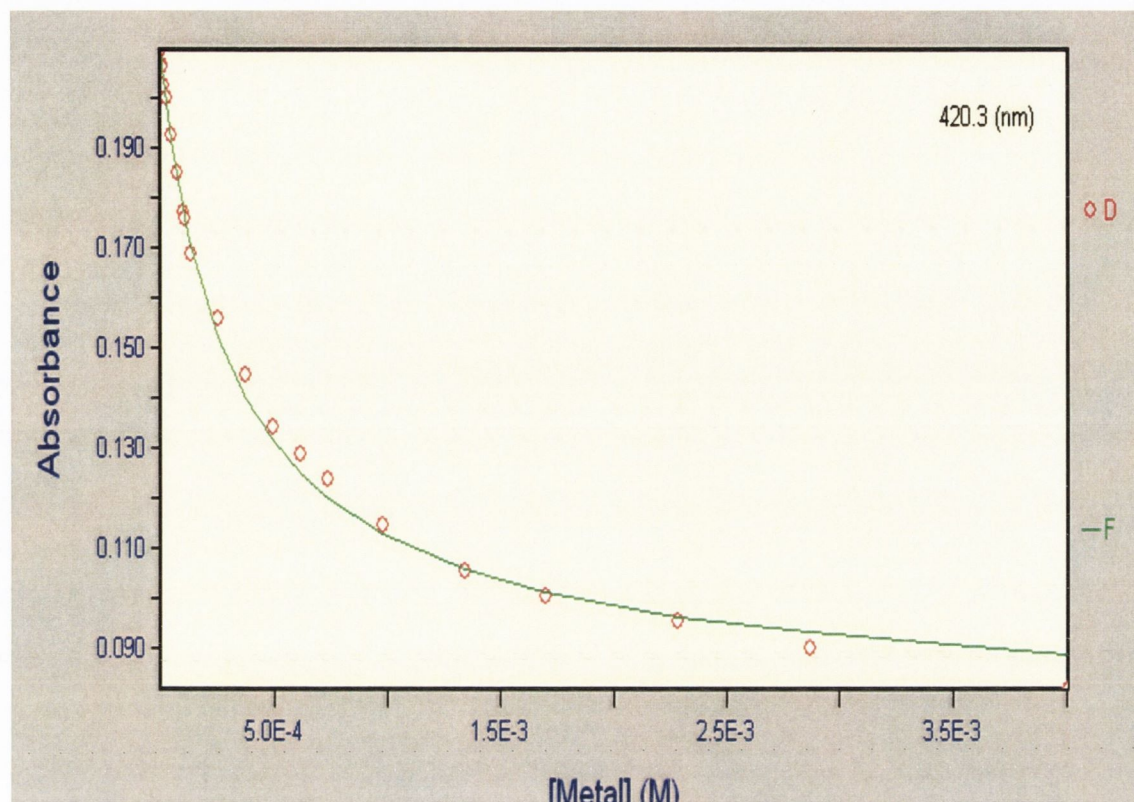
Figure 4.26 SPECFIT/32™-generated graph showing the fit between the observed (D) and calculated data (F) at 420.3 nm for the binding of $H_2PO_4^-$ by **131.**

To ensure the accuracy of the log β values calculated by SPECFIT/32™, the fit between observed and calculated data must also be taken into account. Figure 4.26 shows an example of a SPECFIT/32™-generated graph illustrating the fit between the observed and calculated data for the binding of $H_2PO_4^-$ by **131** in DMSO.

Table 4.4 Stability constants (log β) of **129 - 131** upon complexation with putative anions in DMSO-d_6. All values were obtained using SPECFIT/32™. (*a* the binding process is too complicated for analysis by SPECFIT/32™.)

Sensor	Substituent (R)	log β (AcO⁻)	log β ($H_2PO_4^-$)	log β (F⁻)
129	H	4.19 ± 0.03	2.86 ± 0.04	*a*
130	CH$_3$	4.00 ± 0.06	*a*	*a*
131	CF$_3$	4.26 ± 0.06	3.49 ± 0.02	*a*

The stability contstants obtained from the absorption titrations of **129 - 131** followed a similar trend to those obtained from the ^{1}H NMR studies. In the

147

complexation of AcO$^-$, the electronic nature again seemed to dictate the strength of the binding affinity of the sensor. The unsubstituted sensor **129** bound to AcO$^-$ with a log β value of 4.19 ($\pm$ 0.03). The electron-withdrawing nature of the CF$_3$ group in **131** led to the increase in the acidity of the urea NH protons, and hence the log β was also increased to 4.26 ($\pm$ 0.06). On the other hand, the electron-donating methyl substituent resulted in the decrease in the binding affinity of **130**, giving rise to a log β value of 4.00 ($\pm$ 0.06).

When binding to H$_2$PO$_4^-$, the anion binding affinity was again increased from 2.86 ($\pm$ 0.04) (observed in **129**) to 3.49 ($\pm$ 0.02) due to the presence of the CF$_3$ group in **131**. However, in the case of sensor **130**, it was not possible to obtain the log β value for the recognition process of H$_2$PO$_4^-$. It should be noted that in the ^{1}H NMR binding studies, it was also not possible to obtain a binding constant for the H$_2$PO$_4^-$ complexation of **130**, despite the graph illustrating that it was indeed binding the anion. The ^{1}H NMR binding curve also suggested that the host:guest stoichiometry may be 1:2. However, SPECFIT/32™ was also unable to determine a log β value for this stoichiometry using the absorption titration data of **130** with H$_2$PO$_4^-$. Therefore, there may be some relation to these two anomalous results for the same sensor with the same anion. As was mentioned previously in Section 4.6.1.3, the 4-amino proton may be in some way participating in the binding of H$_2$PO$_4^-$, leading to a more complicated binding process.

All the stability constants obtained using SPECFIT/32™ from the absorption titration data were higher than those determined by WinEQNMR from the ^{1}H NMR titration data (listed in Table 4.3). This difference may be attributed to a number of factors. UV-vis spectroscopic techniques are more sensitive than those of ^{1}H NMR spectroscopy. Also, the SPECFIT/32™ program scans the data across the whole wavelength region, while WinEQNMR is used to calculate log β values using data at an individual resonance. Another factor may be the fact that in ^{1}H NMR titrations, it is possible to directly observe the changes in the urea NH protons. On the other hand, the anion binding event at the urea receptor site is monitored indirectly *via* the photophysical changes of the naphthalimide core, resulting from the changes in the ICT system by the binding of the anion.

4.6.2.3 Conclusions

The spectral changes in the absorption spectra of **129** - **131** in the presence of AcO⁻ and $H_2PO_4^-$ were similar, with the decrease of the original band at 420 nm and the appearance of two new bands at 360 and 569 nm. The band at 420 nm did not disappear completely upon binding of these anions. However, in the case of F⁻ binding, this band was no longer visible at the end of the titration. Also, the bands at 360 and 569 nm both showed shoulders at *ca.* 340 and 535 nm respectively, which may be the result of the presence of a new species formed due to the deprotonation of one of the urea NH protons by F⁻, indicated by the triplet at *ca.* 16 ppm in the ¹H NMR spectra. Another observation to note was the magnitude of the new bands upon the completion of the binding process. In the presence of AcO⁻ and $H_2PO_4^-$, the absorbance of the band at 360 nm were *ca.* 90% of the initial absorbance of the 420 nm band, while that at 569 nm were *ca.* 40%. On the other hand, the binding of F⁻ resulted in the absorbance of both the 360 and 569 nm bands being *ca.* 70% of the initial absorbance at 420 nm. In the presence of AcO⁻, $H_2PO_4^-$ and F⁻, these sensors underwent colour changes from yellow to purple visible to the naked eye, and these observations will be further discussed in Section 4.7.

The SPECFIT/32™ analysis of the data collected from the absorption titrations of **129** - **131** with AcO⁻ and $H_2PO_4^-$ showed a 1:1 host:guest stoichiometry, which is consistent with several reports in the literature.[89,117,103,88,140] It was not possible to deduce the host:guest stoichiometry for the binding of F⁻, indicating a more complicated binding process with the possibility of the deprotonation of one of the urea NH protons as well as the participation of the 4-amino proton in the anion binding process. The deprotonation was observed in the ¹H NMR binding experiments with the formation of the triplet at *ca.* 16 ppm.

The stability constants calculated from the SPECFIT/32™ analysis of the AcO⁻ titration data showed that the electronic nature of the different *para* substituents on the phenyl ring of **129** - **131** had an effect on the binding affinites of such sensors. Although the differences in the log β were not as significant as those observed in the ¹H NMR binding experiments, it was still clear that the electron-withdrawing CF_3 group seemed to increase the binding strength, while the electron-donating CH_3 substituent caused a decrease. However, in the case of $H_2PO_4^-$ binding, this trend was only observed in the case of the electron-withdrawing substituent. The presence of the electron-donating group in **130** seemed to instead enhance the anion binding strength.

This may be due to the presence of the 4-amino proton, which may provide another binding site and thus, resulting in the possibility of a more complicated binding process.

The following section will describe the fluorescence binding experiments of **129** - **131** with putative anions, which were carried out simultaneously with the absorption titrations.

4.6.3 Fluorescence Titrations of 129 - 131 with Anions

In parallel with the absorption binding experiments, the changes in the fluorescence of the sensors in DMSO due to the anion binding were also monitored. The sample in the fluorescence cuvette was excited at the five different wavelengths of significance; the initial absorption band at 420 nm, the two new bands at 360 and 569 nm, and the two isosbestic points at 385 and 470 nm.

Upon excitation at 420 nm in DMSO, the resulting fluorescence emission of the free host of these sensors was a smooth, broad band with a maximum intensity occurring at 520 nm. Figure 4.27 shows the quenching of the fluorescence of **129** in the presence of AcO⁻ when excited at 420 nm (*i.e.* a "*switch-off*" effect). The fluorescence was also significantly quenched by AcO⁻ when the sample was excited at 360 nm (Figure 4.28), but to a much larger extent (*i.e.* the fluorescence was completely quenched). The incomplete quenching of the fluorescence when excited at 420 nm may be related to the fact that the absorption band at that wavelength had not disappeared fully at the end of the titration.
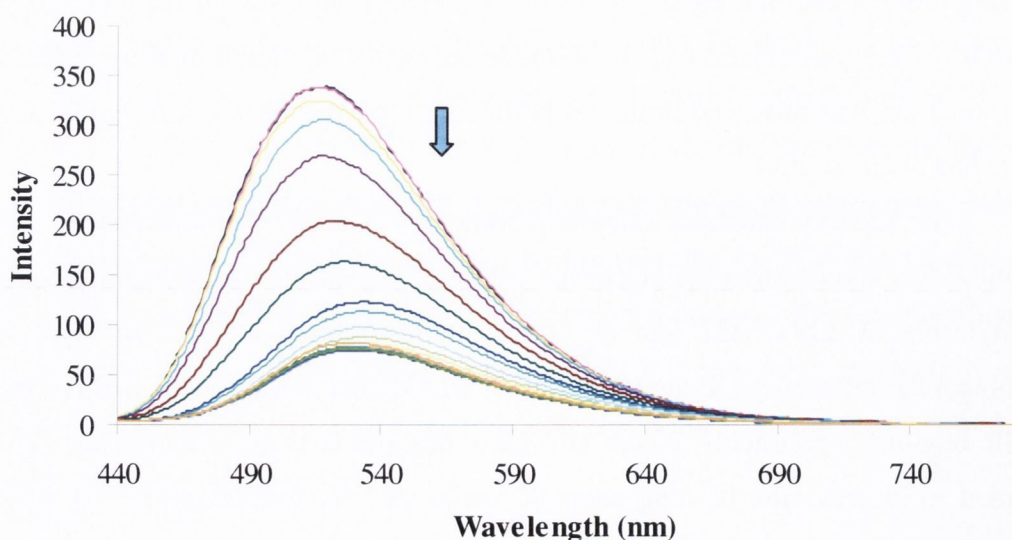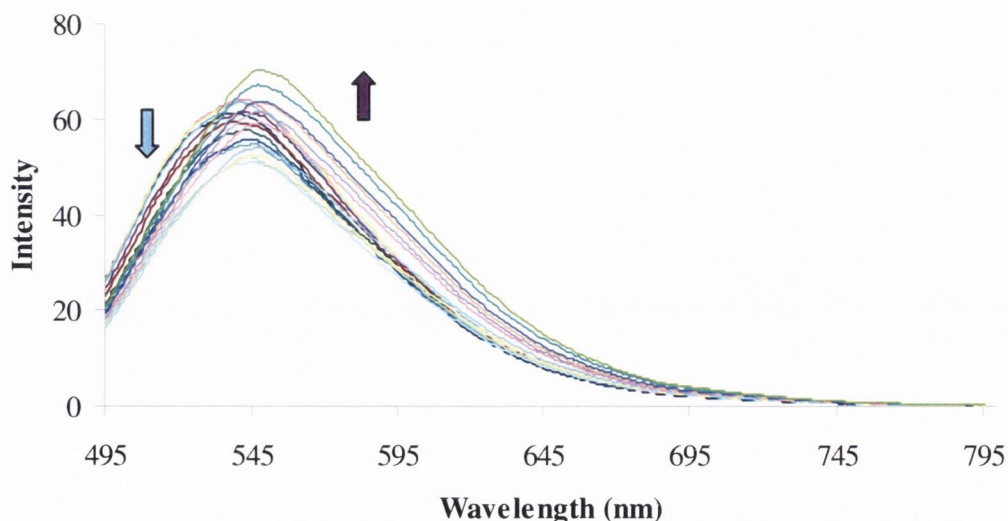

Figure 4.27 Changes observed in the fluorescence of urea **129** (1.5×10^{-5} M) upon addition of AcO⁻ in DMSO at 25 °C (excited at 420 nm; 0 M → 3×10^{-3} M).
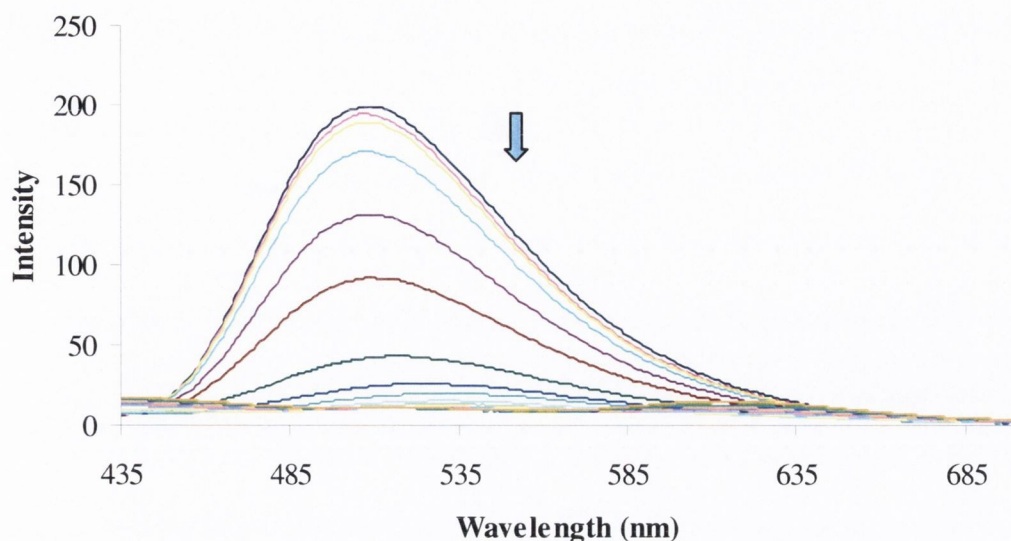
Figure 4.28 Changes observed in the fluorescence of urea **129** (1.5×10^{-5} M) upon addition of AcO$^-$ in DMSO at 25 °C (excited at 360 nm; 0 M → 3×10^{-3} M).

The excitation of **129** at the isosbestic points observed in the absorption titrations (*i.e.* 385 and 470 nm) resulted in a fluorescence emission with a maximum intensity occurring at 510 and 543 nm respectively. The presence of AcO$^-$ caused minor changes in these fluorescence spectra. Figure 4.29 shows the changes in the fluorescence emission of **129** due to AcO$^-$ binding, when the sample was excited at 470 nm. Similar fluorescence changes observed in AcO$^-$ binding by **129** were also seen for **130** and **131** in the presence of this anion, at all five excitation wavelengths. It is also noted that the part of the emission bands (when excited at 470 nm) occurred in the red region of the electromagnetic spectrum.

Figure 4.29 Changes observed in the fluorescence of urea **129** (1.5×10^{-5} M) upon addition of AcO$^-$ in DMSO at 25 °C (excited at the isosbestic point at 470 nm; 0 M → 3×10^{-3} M).

When excited at 569 nm (*i.e.* the second new absorption band), the result was a shoulder-like fluorescence emission band also located in the red region of the electromagnetic spectrum. This band increased in intensity upon the addition of AcO⁻ (Figure 4.30).

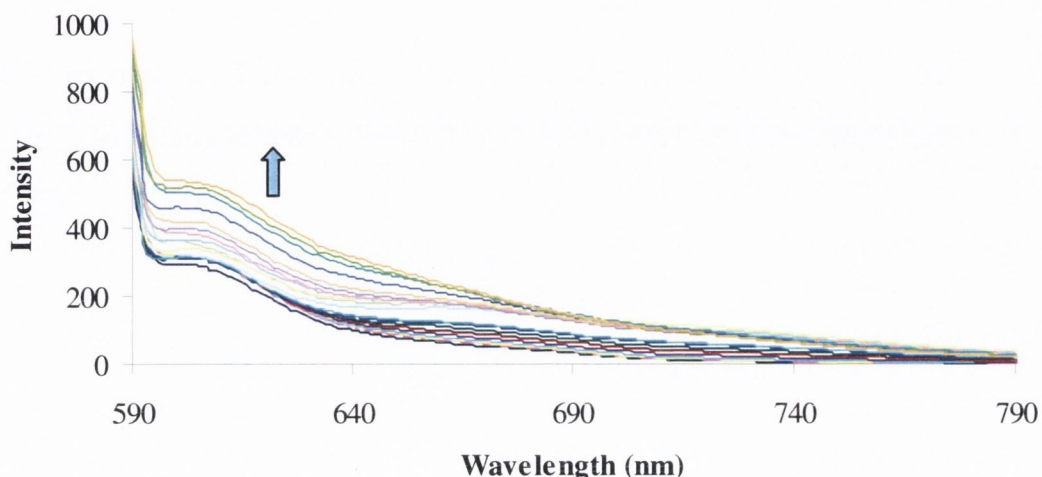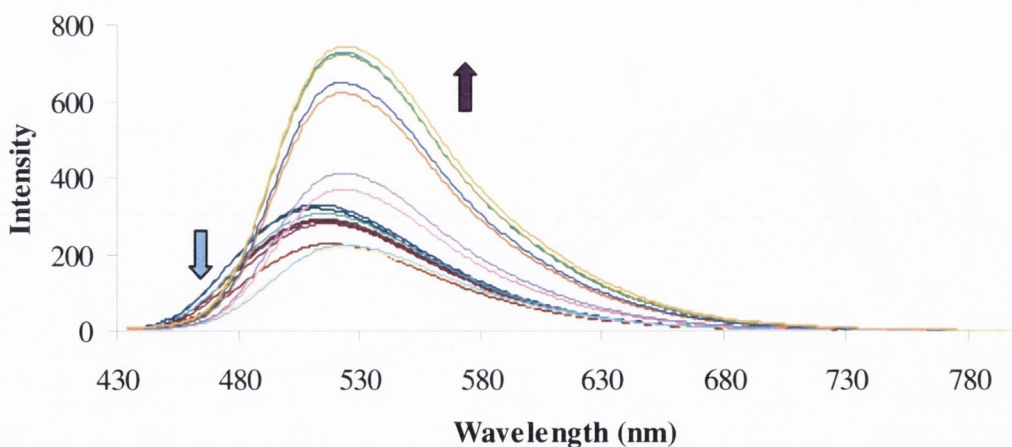

Figure 4.30 Changes observed in the fluorescence of urea **129** (1.5×10^{-5} M) upon addition of AcO⁻ in DMSO at 25 °C (excited at 569 nm; 0 M → 3×10^{-3} M).

The spectral behaviour observed for both $H_2PO_4^-$ and F⁻ binding by these urea sensors were very similar to each other. Initially, there was a slight quenching of the fluorescence emission (after excitation at 420 nm) by these anions, followed by a significant "*switch-on*" effect (after *ca.* 50 equiv. of the anion) occurring with a red shift from a maximum intensity at 520 nm to one at 530 nm. Figures 4.31 and 4.32 show the described spectral changes for **129** upon the addition of $H_2PO_4^-$ and F⁻ respectively.

Figure 4.31 Changes observed in the fluorescence of urea **129** (1.5×10^{-5} M) upon addition of $H_2PO_4^-$ in DMSO at 25 °C (excited at 420 nm; 0 M → 3×10^{-3} M; blue arrow = first significant change; purple arrow = second significant change).

Figure 4.32 Change Changes observed in the fluorescence of urea **129** (1.5×10^{-5} M) upon addition of F⁻ in DMSO at 25 °C (excited at 420 nm; 0 M → 3×10^{-3} M; blue arrow = first significant change; purple arrow = second significant change).

When the sample was excited at 360 nm, the effect of the addition of either $H_2PO_4^-$ or F⁻ was such that there was an initial decrease in the fluorescence emission (with maximum intensity at 510 nm) to *ca.* 25% of its original intensity. This was then followed by an increase in the same band with the appearance of two new bands with maxima occurring at 440 and 615 nm. This behaviour can be clearly seen in Figures 4.33 and 4.34, which show the changes in the fluorescence (when excited at 360 nm) of **129** in the presence of $H_2PO_4^-$ and F⁻ respectively. Such fluorescence changes were also observed in the studies carried out on **130** and **131** with these two anions (see Appendix 7.3).
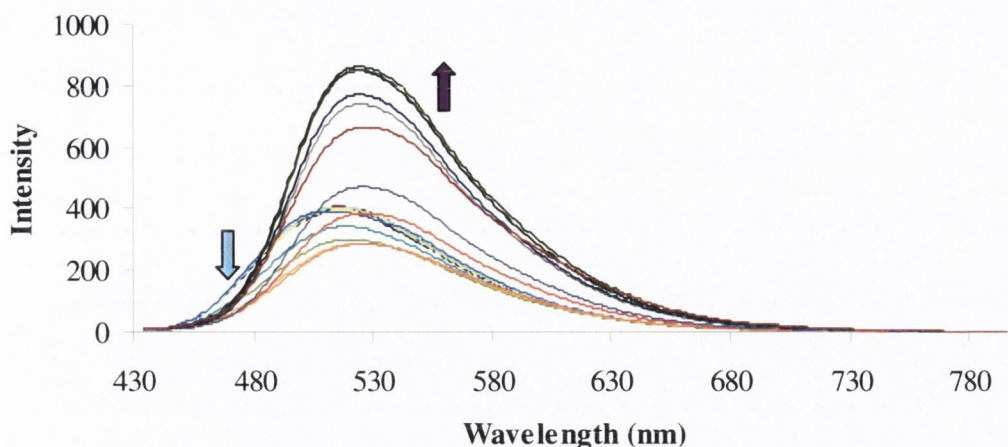

Figure 4.33 Changes observed in the fluorescence of urea **129** (1.5×10^{-5} M) upon addition of $H_2PO_4^-$ in DMSO at 25 °C (excited at 360 nm; 0 M → 3×10^{-3} M; blue arrow = first significant change; purple arrow = second significant change).
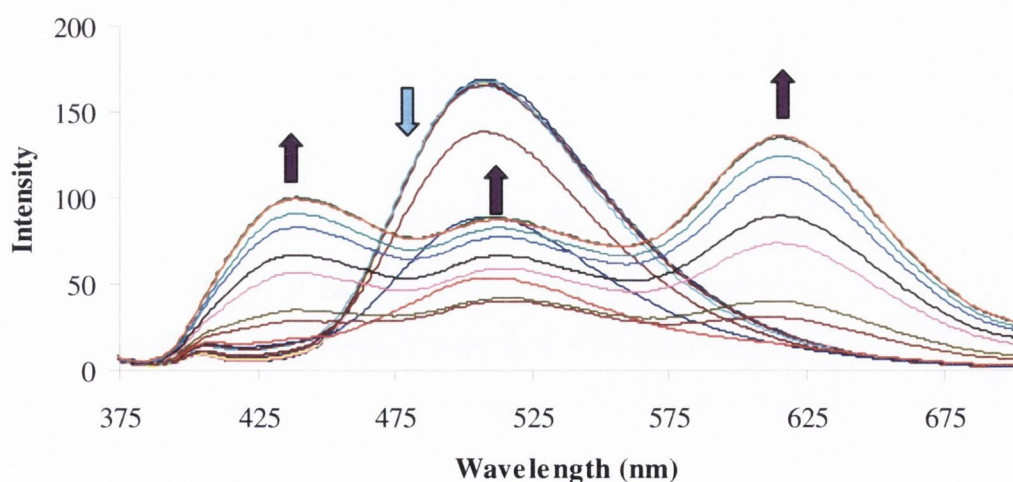
Figure 4.34 Changes observed in the fluorescence of urea **129** (1.5×10^{-5} M) upon addition of F$^-$ in DMSO at 25 °C (excited at 360 nm; 0 M $\rightarrow$ 3×10^{-3} M; blue arrow = first significant change; purple arrow = second significant change).
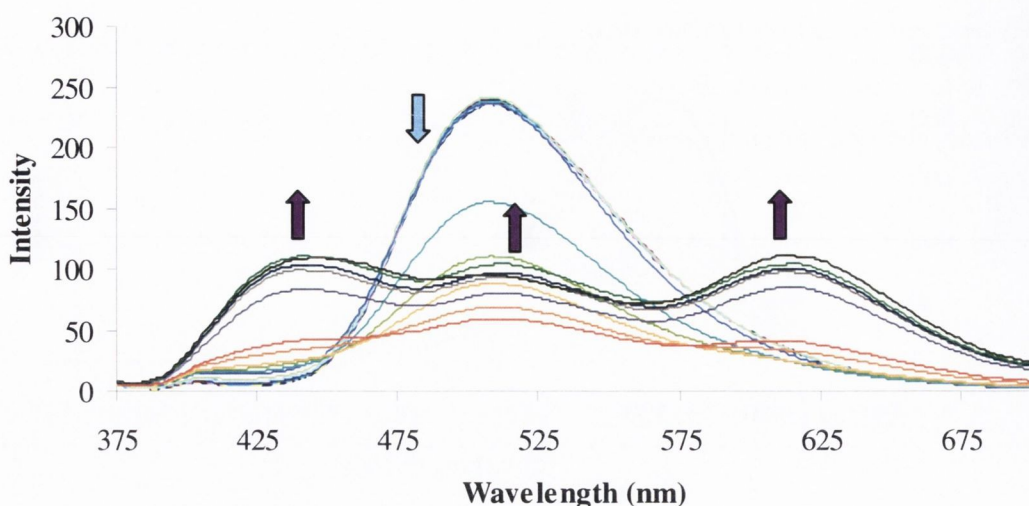
It is unclear as to the cause of such interesting spectral changes observed for **129** - **131** upon the addition of $H_2PO_4^-$ and F$^-$. One rationale is that the proton of the hydrazine N that is attached directly to the 4-position of the naphthalimide ring may be involved in the binding of such anions. In the case of $H_2PO_4^-$, it may be due to this anion consisting of more than two possible hydrogen-bonding donors (*cf.* AcO$^-$ has two sites which are almost directionally complementary to the urea moiety), whereas F$^-$ is a small spherical anion and hence, there is the possibility of more than one anion binding to the NH protons of these urea sensors. The presence of F$^-$ may also result in the deprotonation of one of the urea NH protons, which could further complicate the binding process of such sensors with F$^-$.

The next section will involve the plotting of these spectral changes as a function of -log[anion] at different wavelengths in order to further analyse the data and obtain a better representation of these changes.

4.6.3.1 Analysis of the Fluorescence Titration Data for 129 - 131

In order to view the above results more clearly, the fluorescence changes at significant wavelengths (where maximum intensities occur in the binding experiments) were plotted as a function of -log[anion]. In the case of AcO$^-$ binding, sigmoidal binding curves were obtained for the changes observed for these sensors when excited at 420 nm (*i.e.* the initial absorption band). Figure 4.35 illustrates the change in the

relative intensity of **129** at 520 nm upon the addition of AcO⁻ in DMSO, where the sigmoidal curve changed over *ca.* two log unit.
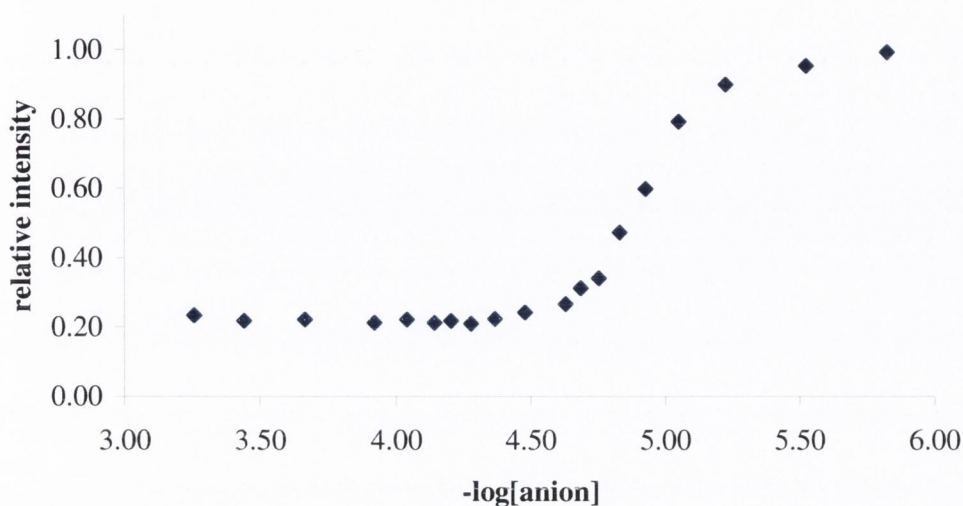
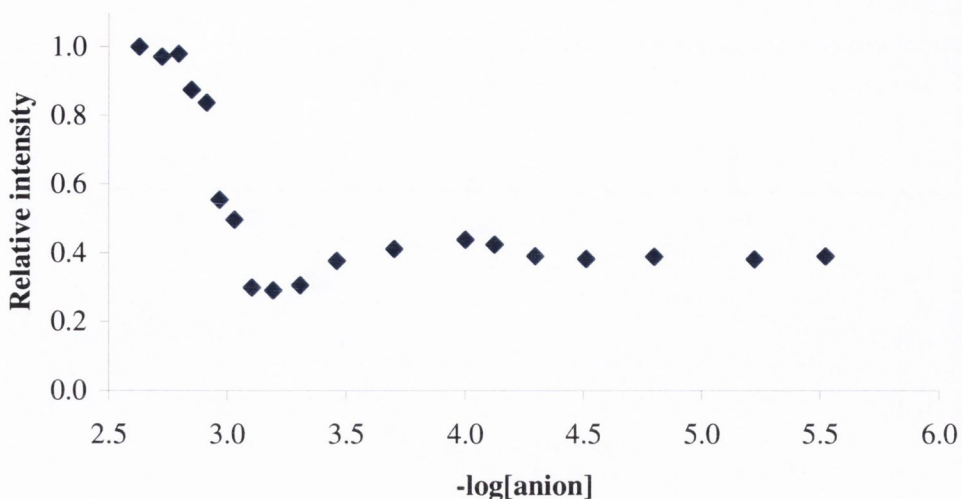**Figure 4.35** Relative fluorescence intensity of sensor **129** at 520 nm against -log[anion] in DMSO on addition of AcO⁻ (excited at 420 nm).

Figures 4.36 and 4.37 show the plots of changes in the relative intensity of **129** at 520 nm (when excited at 420 nm) in the presence of $H_2PO_4^-$ and F⁻ respectively. As previously observed from the changes in the fluorescence emission (Figures 4.31 and 4.32), the results from these plots illustrate clearly the similar behaviour demonstrated by the sensors due to the complexations of these two anions. One noticeable difference was that that the overall change occurred over *ca.* two log units for $H_2PO_4^-$ binding, whereas the presence of F⁻ caused an overall change across *ca.* one log unit. This trend was also previously observed in the absorption titrations. Also, the change involving the initial increase in the fluorescence, followed by a decrease was more pronounced in the binding of F⁻. The fluorescence is then enhanced again to a greater extent and this enhancement began at a lower anion concentration for F⁻ binding (*i.e. ca.* 2.5×10^{-4} M), while that for $H_2PO_4^-$ binding occurred at an anion concentration of *ca.* 9×10^{-4} M. This indicated the stronger binding affinities of such sensors towards of F⁻. It is not possible as of yet to determine the mechanism of the "chemical event" causing these anomalous spectral changes.

Figure 4.36 Relative fluorescence intensity of sensor **129** at 520 nm against -log[anion] in DMSO on addition of $H_2PO_4^-$ (excited at 420 nm).
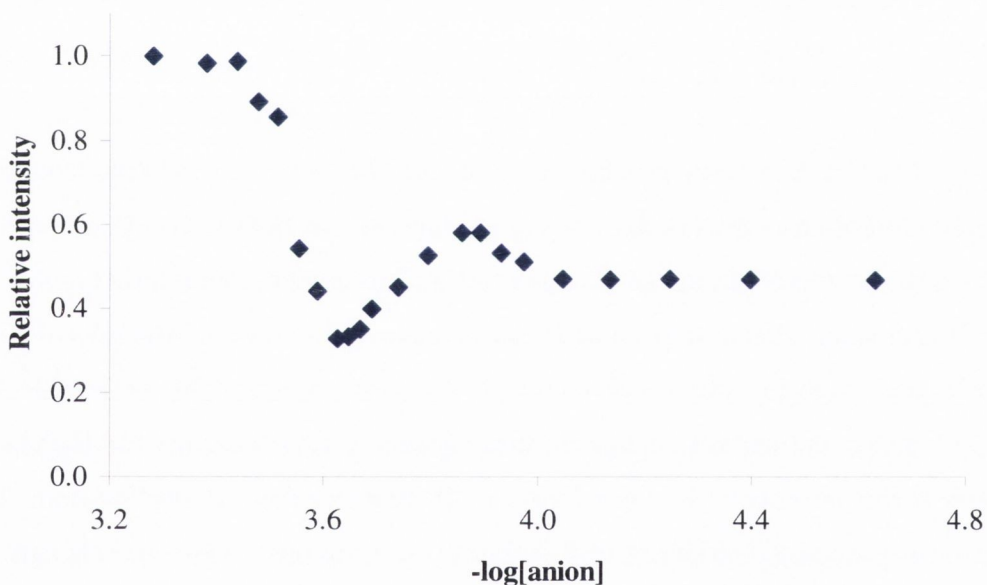

Figure 4.37 Relative fluorescence intensity of sensor **129** at 520 nm against -log[anion] in DMSO on addition of F^- (excited at 420 nm).

Excitation of the sample at 360 nm again resulted in similar fluorescence changes observed for the recognition of $H_2PO_4^-$ and F^-. This can be seen in Figures 4.38 and 4.39, illustrating these changes in the fluorescence emission of sensor **129** with $H_2PO_4^-$ and F^- respectively.
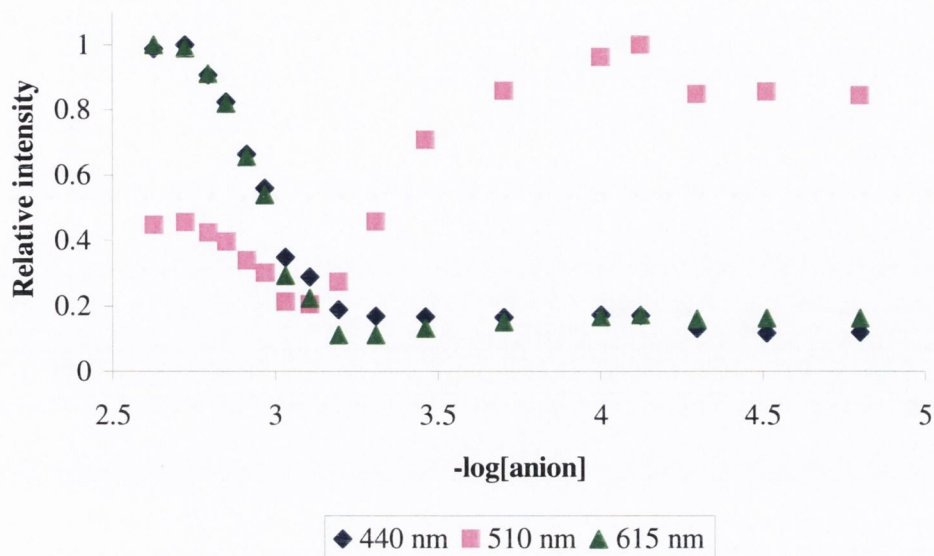
Figure 4.38 Relative fluorescence intensity of sensor **129** at 440, 510 and 615 nm against -log[anion] in DMSO on addition of $H_2PO_4^-$ (excited at 360 nm).
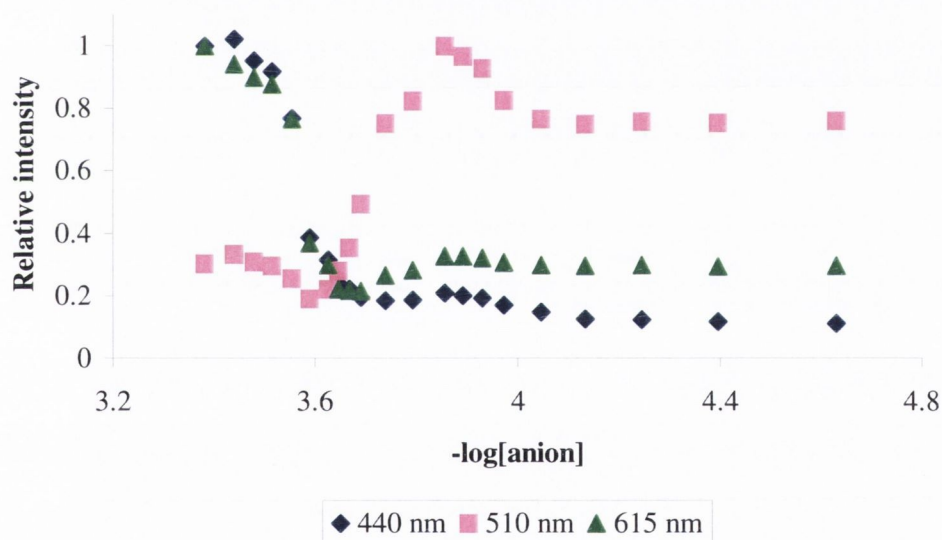
Figure 4.39 Relative fluorescence intensity of sensor **129** at 440, 510 and 615 nm against -log[anion] in DMSO on addition of F^- (excited at 360 nm).

Once more, the overall changes observed at 440, 510 and 615 nm occurred over *ca.* two log units in the case of of $H_2PO_4^-$ binding, while these changes occurred across *ca.* one log unit in the presence of F^-. The original fluorescence emission centred at 510 nm was initially enhanced in both cases, followed by significant quenching and then a final smaller enhancement. The occurrence of this final increase was at anion concentrations similar to those at which the final fluorescence enhancement occurred

upon the excitation at 420 nm. Also, the binding curves observed at 440 and 615 nm (upon excitation at 360 nm) were similar to those observed when the sample was excited at 420 nm, with more significant changes recorded for F^- binding.

4.6.3.2 Stability Constants (log β) from Fluorescence Titration Data of 129 - 131

It was not possible to obtain reliable values for the stability constants from the SPECFIT/32™ analysis of the data collected fom these fluorescence studies. The log β values given by the program initially seemed accurate with small errors (< 1%). However, upon examination of the graphs generated by SPECFIT/32™ of the fitting between the observed and calculated data (see example in Appendix 7.3.4), it was found that there was poor correlation between the two set of data (*i.e.* the observed data did not fit well to the model selected by the program). One possible factor that may be contributing to the problems in obtaining accurate log β values is the occurrence of more than one process (*e.g.* complexation, deprotonation) during the experiment.

4.6.3.3 Conclusions

The fluorescence studies carried out on sensors **129 - 131** in the presence of AcO^- resulted in the quenching of the emission (when excited at 420 and 360 nm). The fluorescence was completely quenched when excited at 360 nm. However, an enhancement occurred in the shoulder-like fluorescence emission upon excitation at 569 nm. In the case of $H_2PO_4^-$ and F^-, the changes observed in the fluorescence were more complicated. When excited at 420 nm, there was initially a small enhancement in the fluorescence, followed by a slight quenching and finally, a significant increase in the fluorescence intensity. The final increase occurred with a shift towards longer wavelength. The excitation of such sensors at 360 nm resulted in the quenching of the fluorescence emission centred at 510 nm, which was then followed by an increase as well as the appearance of two new bands at 440 and 615 nm. These anomalous changes may be due to the presence of the 4-amino proton, which has the possibility of partaking in the binding of the bulky tetrahedral $H_2PO_4^-$ and the small spherical F^-. Also, in the case of F^-, deprotonation of one of the urea NH protons may also be involved.

As a result of the complexity of the anion binding process of these sensors, it was not possible to obtain stability constants using SPECFIT/32™. However, from a qualitative aspect, it is possible to deduce that these sensors bound most strongly to

AcO⁻, followed by F⁻ and then $H_2PO_4^-$. No significant changes were observed in the presence of Cl⁻ or Br⁻.

4.7   Observed Colorimetric Changes of 64, 129 - 131 with Anions

Sensors **64**, **129 - 131** showed striking colour changes observable by the naked eye upon complexation with various anions in DMSO. Figure 4.40 shows the chromogenic response of DMSO solutions of **131** (1×10^{-3} M) upon the addition of putative anions. In general, the colour change was from bright yellow to deep purple. However, in the case of F⁻ complexation, this colour change was only observable at low guest concentrations. At high concentrations, the initial yellow colour changed to pale orange upon complexation. This may be ascribed to the deprotonation of the NH protons of the urea/thiourea moiety of the sensor, resulting in the formation of the bifluoride ion (HF_2^-).[135,140,88,169] It was also noted that in the DMSO solution of **131** containing one equivalent of F⁻ (Figure 4.40(d)) showed non-homogeneity of the colour of the solution (*i.e.* there were patches of dark blue colour present). One possible explanation for this observation is that the deprotonation process may already begun to occur even at this low concentration. No colour change was observed in the presence of either Cl⁻ or Br⁻.

(a)   (b)   (c)   (d)   (e)
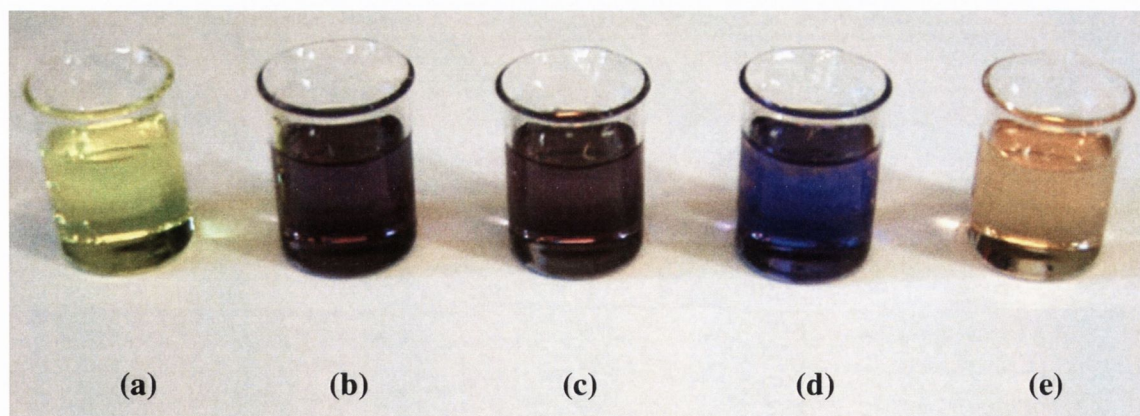
Figure 4.40 Chromogenic response of solutions of sensor **131** (1×10^{-3} M) observable by the naked eye upon complexation with various anionic guests: (a) free host **131**; (b) **131** + 1 eq. AcO⁻; (c) **131** + 1 eq. $H_2PO_4^-$; (d) **131** + 1 eq. F⁻; (e) **131** + F⁻ (excess).
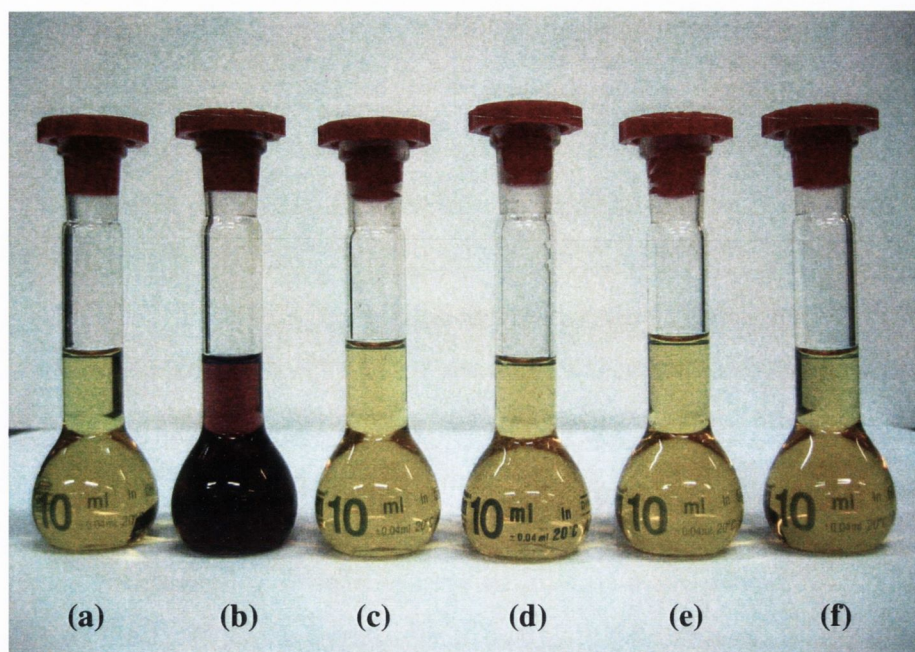
Figure 4.41 Chromogenic response of solutions of sensor **64** (1×10^{-3} M) observable by the naked eye upon complexation with 10 equiv. of various anionic guests: (a) free host **64**; (b) **64** + AcO$^-$; (c) **64** + H$_2$PO$_4^-$; (d) **64** + Br$^-$; (e) **64** + Cl$^-$; (f) **64** + F$^-$.

When carried out in more competitive media such as EtOH and EtOH:H$_2$O (50:50), only the thiourea sensor **64** showed colour changes upon anion complexation. In EtOH, similar colour changes were observed as those seen in DMSO. However, the chromogenic response in EtOH:H$_2$O (50:50) became more selective in terms of visual discrimination, where only the addition of acetate caused **64** to change from its original yellow colour to a deep purple (Figure 4.41).
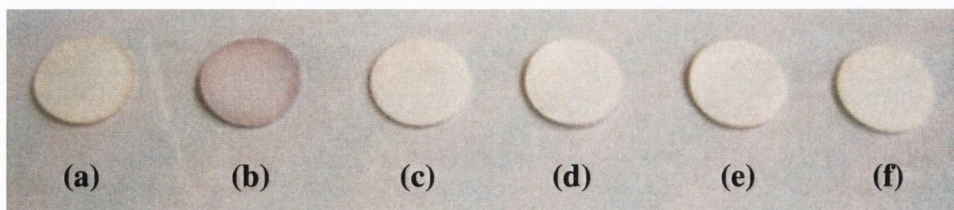
Figure 4.42 Chromogenic response of sensor **64** (loaded onto cellulose-based paper *via* soaking in a 1×10^{-3} M EtOH:H$_2$O (50:50) solution of **64**, and then leaving the paper to dry) observable by the naked eye upon the addition of various anionic guest solutions in EtOH:H$_2$O (50:50): (a) free host **64**; (b) **64** + 10 equiv. AcO$^-$; (c) **64** + 10 equiv. H$_2$PO$_4^-$; (d) **64** + 10 equiv. F$^-$; (e) **64** + 10 equiv. Cl$^-$; (f) **64** + 10 equiv. Br$^-$.

When loaded onto cellulose-based paper, a similar chromogenic response was observed when 50:50 EtOH:H$_2$O solutions of the anions were added to the paper (Figure 4.42). This makeshift test illustrates the potential of sensor **64** to selectively detect AcO$^-$ in more practical applications. A similar exercise using DMSO solutions

did not show this selectivity as the addition of AcO⁻, $H_2PO_4^-$ and F⁻ all resulted in the paper assuming a purple colour. In the case of the urea sensors, no visible colour change was observed in the presence of the various anions. Hence, these striking results greatly encourage the further development of this type of colotimetric anion sensor for its possible use in H_2O, an ideal scenario pursued by many in this field.

4.8   Overall Conclusions

The binding studies carried out on **64**, **129 - 131** with anions demonstated striking colour changes in the visible region (yellow to purple upon anion complexation), thus these sensors show great potential as colorimetric sensors. However, physical evaluation of the urea sensors **129 - 131** using ¹H NMR, UV-vis and fluorescence spectroscopic experiments showed that these sensors can only successfully bind anions in DMSO, unlike their thiourea analogues (such as **64**) which are able to bind anions in highly competitive media (*i.e.* EtOH and EtOH:H_2O (50:50)). These studies carried out on **129 - 131** also showed that the electronic nature of the 4-substituent on the phenyl ring did not give rise to significant differences in the binding affinities of such sensors.

In the ¹H NMR binding studies, the formation of bifluoride ion (HF_2^-) was again observed in the complexation of F⁻ by **129 - 131**. This was indicated by the appearance of a triplet peak at *ca.* 16 ppm after the addition of *ca.* 2 equivalents of F⁻. The anion is believed to be deprotonating one of the urea NH protons within the sensors. Several cases of this deprotonation have been reported in literature.[118,135,140,169,143,91,170]

There were also difficulties in obtaining stability constants (log β) from the SPECFIT/32™ analysis of the spectral data collected from the fluorescence spectroscopic experiments. Graphical analysis of this data showed that there may be more than one possible process occurring in the presence of anions, especially in the case of $H_2PO_4^-$ and F⁻. It has also been suggested that there may be the risk of deprotonation by all three anionic guests, a phenomenon observed in other urea and thiourea compounds.[140,88]

In conclusion, the physical evaluation of these hydrazine-based sensors **64**, **129 - 131** showed that the thiourea sensors (*e.g.* **64**) bind more strongly to putative anions than their urea analogues (**129 - 131**). Such observation between the binding affinities of ureas and thioureas has been previously reported by several research groups.[154,162,172,173,89,137]

4.9   Future Work

Firstly, further experiments should be carried out on these hydrazine-based ureas and thioureas to explore the possibility of deprotonation of the NH protons by anions other than F⁻.

Due to the selectivity observed by the hydrazine-based thiourea sensors such as **64** in highly competitive aqueous media (*i.e.* EtOH:H$_2$O (50:50)), it is clear that further studies should be carried out on such compounds. One possible aspect of these sensors may be improved upon is their solubility in water. Currently, these studies were done by initially dissolving the compounds in ethanol, before adding water to make up the 50:50 solutions. Therefore, it may be useful to attempt certain modifications to the molecular structures of these sensors in order to increase their solubility in water. Another approach would be to perhaps incorporate the sensors into polymers and films (*e.g.* hydrogels).

The selectivity of these sensors (when observed using photophysical techniques) towards anions in aqueous media should also be enhanced. Possible structural modifications to achieve this include employing other substituents at the *para* position of the phenyl ring, or exchanging the phenyl ring completely with another moiety (either alkyl or aromatic).

Finally, these sensors and future derivatives should be tested using other anionic guests, especially those of biological importance.

5.1   General Experimental Details

Melting points were determined using an Electrothermal IA9000 digital melting point apparatus. Infrared spectra were recorded either on a Mattson Genesis II FTIR spectrometer or a Perkin Elmer spectrometer fitted with a universal ATR sampling accessory. When using the former, oils were analysed using NaCl plates and solid samples were dispersed in KBr and recorded as clear pressed discs. ^{1}H NMR spectra were recorded at 400.13 MHz using a Bruker Spectrospin DPX-400 instrument. Chemical shifts expressed in parts per million (ppm or δ) downfield from the standard, followed by the number of protons, splitting pattern, coupling constant (if applicable) and assignment of proton. The splitting pattern is denoted using the following abbreviations: **s** for a singlet, **br s** for a broad singlet, **d** for a doublet, **dd** for a double doublet, **t** for a triplet, **app t** for an apparent triplet, **q** for a quartet, **app q** for an apparent quartet and **m** for a multiplet. Aromatic protons are numbered according to Figure 5.1 for symmetrical bis-phenylureas and thioureas and Figure 5.2 for asymmetrical bis-phenylureas and thioureas. Figures 5.3, 5.4 and 5.5 show the numbering scheme for compounds based on naphthalimide, anthracene and naphthalene ring systems respectively. The proton is prefixed by "Ar", "An", "Cyclohex", "Naph" or "Nap" to represent it as an aromatic, anthracene, cyclohexane, naphthamilide or naphthalene proton respectively, *e.g.* Ar-H1. ^{13}C and ^{19}F NMR spectra were recorded at 100.61 MHz and 376.46 MHz respectively using a Bruker Spectrospin DPX-400 instrument. Mass spectroscopy was carried out using spectroscopic grade solvents. Mass spectra were determined by detection using electrospray on a Micromass LCT spectrometer. A Shimadzu HPLC or Water's 9360 was used to pump solvent. The whole system was controlled by MassLynx 3.5 on a Compaq Deskpro workstation. Accurate masses were determined by a peak-matching method, using leucine Enkephalin (Tyr-Gly-Gly-Phe-Leu) as the standard reference. X-ray diffraction studies were carried out by Dr Sandrine Goetz, Dr Paul Jensen and Dr Thomas McCabe (School of Chemistry, Trinity College Dublin). Specific rotation of chiral compounds were determined using Autopol® 1V Polarimeter. Elemental analysis was carried out in the Microanalytical Laboratory, Department of Chemistry, University College Dublin. Starting materials were obtained from Sigma-Aldrich and Fluka. All data was further handled either on a Sony Vaio VGN-FE41Z notebook computer (2.0 GHz, Centrino Duo, 2046 MB RAM) or Fujitsu Siemens desktop computer (1.8 GHz, Pentium IV, 256 MB RAM) using Microsoft software and Isis Draw 2.5.

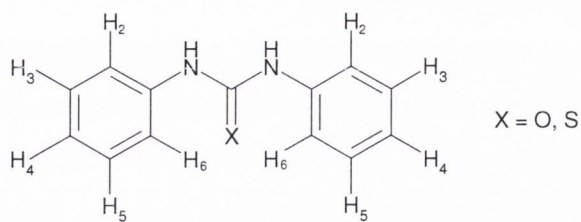**Figure 5.1.** Aromatic and amino protons of <u>symmetric</u> bis-phenylureas and thioureas.
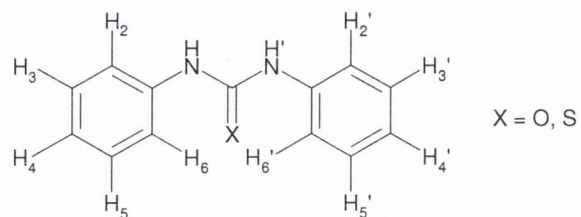

Figure 5.2. Aromatic and amino protons of <u>asymmetric</u> bis-phenylureas and thioureas.
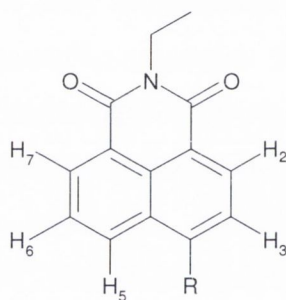

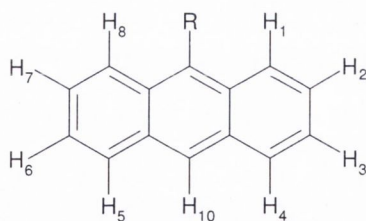**Figure 5.3.** Aromatic protons of naphthalimide-based ureas and thioureas

Figure 5.4. Aromatic protons of anthracene-based ureas and thioureas
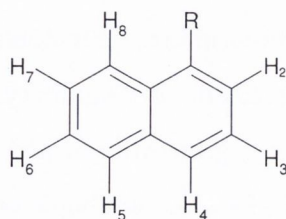

Figure 5.5. Aromatic protons of naphthalene-based ureas and thioureas

5.2 ^{1}H NMR Titrations

^{1}H NMR titrations were carried out on a Bruker Spectrospin DPX-400 instrument at room temperature (25 °C). Data analysis was conducted using Microsoft® Excel 2003 and WinEQNMR.[12]

5.2.1   Preparation of Solutions for ^{1}H NMR Titrations

The salts used in the titrations were spectroscopic grade TBA derivatives of the various anions, purchased from Aldrich. All were dried over P_2O_5 at 40 °C under vacuum. Solutions were made up using spectroscopic grade solvents. The concentrations of these solutions were prepared such that 5 μL would give 0.1 molar equivalents of anions relative to the concentration of the host solutions. Host solutions were approximately 2.5 g/L (*i.e.* 2 mg in 0.8 mL deuterated solvent) in concentration.

5.3   Absorption and Fluorescence Titrations

Absorption and fluorescence binding studies were carried out at 25 °C on a Varian Cary WinUV and Eclipse spectrometers respectively. Data analysis was conducted using Microsoft® Excel 2003 and SPECFIT/32™.

5.3.1   Preparation of Solutions for Absorption and Fluorescence Titrations

The salts used in the titrations were spectroscopic grade TBA derivatives of the various anions, purchased from Aldrich. All were dried over P_2O_5 at 40 °C under vacuum. Solutions with molar concentrations of 1 M, 10^{-1} M, 10^{-2} M and 10^{-3} M were prepared using spectroscopic grade solvents. The host solution (1×10^{-5} M) was placed in a 10 mL volumetric flask with a magnetic stirrer prior to starting the titration.

5.4   CD Measurements

CD spectra were recorded at a concentration corresponding to an absorbance of 1.0 in organic solutions (generally DMSO) using a Jasco J-810-150S spectropolarimeter. The cell used in these measurements has a path length of 2 mm. All CD spectra are represented as mdeg *vs* λ (nm). The baseline of the solvent used was recorded and removed from all spectra shown.

5.5 General Procedures

Procedure 1: Synthesis of Bis-phenylureas and Thioureas[159]

The amine (1.3 equiv.) was carefully added to a solution of isocyanate or isothiocyanate (1 equiv.) in dry spectroscopic grade CHCl₃ (unless otherwise stated). The reaction mixture was left stirring under argon for 18 h at room temperature. The product was then worked up using either of the following two procedures:

(i) If the resulting urea or thiourea product precipitated out, it was collected and washed several times with cold spectroscopic grade CHCl₃ (unless otherwise stated). The solid was dried under vacuum.

(ii) If the product remained in solution, the reaction mixture was washed with 0.1 M HCl (1 × 20 mL) and water (2 × 20 mL). The organic layer was then dried over MgSO₄ and filtered. The filtrate was reduced to give the solid product (unless otherwise stated), which was then dried under vacuum.

Procedure 2: Synthesis of Hydrazine-based Ureas and Thioureas

The appropriate isocyanate (1.1 equiv.) was added to the amine and this reaction mixture was stirred with heating at reflux for 3 days in dry MeCN. A precipitate formed, which was collected and washed with MeCN. The solid was then dried, yielding a yellow solid. Purification of the crude product was carried out by hot filtration using a mixture of DCM:MeOH (1:4). (Note: Glassware used when working up this reaction must always be pyrex as the hydrazine-based product may react with lower grade glass.)

Procedure 3: Synthesis of Isocyanates and Isothiocyanates[191]

Triphosgene or thiophosgene (2 equiv.) was carefully added to a solution of the amine to form the corresponding isocyanate or isothiocyanate respectively. The reaction mixture was left stirring for 18 h under argon at room temperature. Any excess triphosgene or thiophosgene was quenched with water. The organic layer extracted was washed with brine (3 × 10 mL) and water (1 × 20 mL). The solution was then dried over MgSO₄, filtered and reduced, yielding the desired product.

Procedure 4: Synthesis of Anthracene-based Ureas and Thioureas

These ureas and thioureas were synthesised using the appropriate amine with an equivalent of isocyanate and isothiocyanate respectively in the presence of a catalytic

amount of triethylamine (if required) in dry DCM. The reaction was left stirring at room temperature for 30 min, after which a precipitate formed. The desired precipitate was isolated by filtration and was washed with DCM and diethyl ether to remove any impurities or starting material.
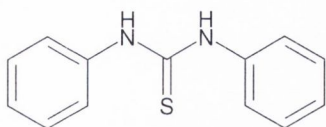
5.6 Chapter 2 Experimental Details
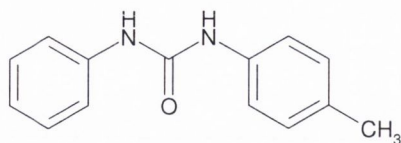
1,3-*Bis*-phenylurea (69)
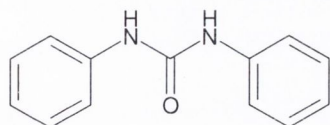
69 Was synthesised according to **Procedure 1(i)** using phenyl isocyanate (0.39 g, 3.30 mmol) and aniline (0.40 g, 4.30 mmol) in spectroscopic grade $CHCl_3$ (20 mL). A white precipitate was obtained. Recrystallisation of the solid from $CHCl_3$:CH_3OH (5:1) yielded fine white crystals (0.64 g, 91.5%). m.p. 241 - 243 °C (lit.,[192] 242 °C); Calculated for $C_{13}H_{12}N_2O$: C, 73.57; H, 5.70; N, 13.20%; Found: C, 73.30; H, 5.72; N, 13.15%; δ_H (400 MHz, $(CD_3)_2SO$) 8.68 (2H, br s, N$\underline{H}$), 7.49 (4H, d, J = 8.2 Hz, Ar-$\underline{H2}$, Ar-$\underline{H6}$), 7.29 (4H, t, J = 7.5 Hz, Ar-$\underline{H3}$, Ar-$\underline{H5}$), 6.98 (2H, t, J = 7.5 Hz, Ar-$\underline{H4}$); δ_C (100 MHz, $(CD_3)_2SO$) 152.6, 139.7, 128.8, 121.8, 118.2; MS (MeOH, ES$^+$) m/z 213 (M + H)$^+$, 235 (M + Na)$^+$; IR (KBr) υ_{max} (cm^{-1}) 3305, 3133, 2334, 1940, 1871, 1795, 1644, 1595, 1552, 1497, 1441, 1314, 1231, 1052, 894, 753, 696, 508.

1,3-*Bis*-phenylthiourea (70)

70 Was synthesised according to **Procedure 1(ii)** using phenyl isothiocyanate (0.45 g, 3.30 mmol) and aniline (0.40 g, 4.30 mmol) in spectroscopic grade $CHCl_3$ (20 mL). A cream-coloured solid was obtained. Recrystallisation of the solid from $CHCl_3$ yielded a pure sample as off-white crystals (0.68 g, 90.4%). m.p. 155 - 157 °C (lit.,[193] 155 °C); HRMS (MeOH, ES$^+$): Calculated for $C_{13}H_{13}N_2S$: 229.0799 (M + H)$^+$; Found: 229.0800; δ_H (400 MHz, $(CD_3)_2SO$) 9.82 (2H, br s, N$\underline{H}$), 7.51 (4H, d, J = 8.0 Hz, Ar-$\underline{H2}$, Ar-$\underline{H6}$), 7.35 (4H, m, Ar-$\underline{H3}$, Ar-$\underline{H5}$), 7.14 (2H, m, Ar-$\underline{H4}$); δ_C (100 MHz, $(CD_3)_2SO$) 179.6, 139.5, 128.5, 124.4, 123.7; MS (MeOH, ES$^+$) m/z 229 (M + H)$^+$, 251 (M + Na)$^+$; IR (KBr) υ_{max} (cm^{-1}) 3217, 3035, 2796, 1955, 1624, 1549, 1450, 1344, 1242, 1070, 1023, 933, 758, 697, 631, 485.
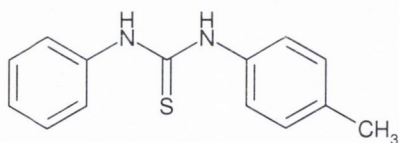
1-Phenyl-3-(*p*-tolyl)urea (71)

71 Was synthesised according to **Procedure 1(i)** using *p*-tolyl isocyanate (0.44 g, 3.30 mmol) and aniline (0.40 g, 4.30 mmol) in spect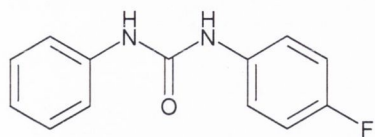roscopic grade CHCl$_3$ (20 mL). A white precipitate was obtained. Recrystallisation of the solid from CHCl$_3$:MeOH (30:1) yielded white hair-like crystals (0.65 g, 86.2%). m.p. 217 °C (lit.,[194] 217 - 218 °C); Calculated for C$_{14}$H$_{14}$N$_2$O: C, 74.31; H, 6.24; N, 12.38%; Found: C, 74.11; H, 6.31; N, 12.36%; δ_H (400 MHz, (CD$_3$)$_2$SO) 8.11 (1H, s, N$\underline{H}$'), 8.85 (1H, s, N$\underline{H}$), 7.45 (2H, d, *J* = 7.6 Hz, Ar-$\underline{H2}$, Ar-$\underline{H6}$), 7.34 (2H, d, *J* = 7.6 Hz, Ar-$\underline{H2}$', Ar-$\underline{H6}$'), 7.27 (2H, t, *J* = 7.6 Hz, Ar-$\underline{H3}$, Ar-$\underline{H5}$), 7.08 (2H, d, *J* = 8.2 Hz, Ar-$\underline{H3}$', Ar-$\underline{H5}$'), 6.96 (1H, t, *J* = 7.0 Hz, Ar-$\underline{H4}$), 2.24 (3H, s, Ar-C$\underline{H3}$); δ_C (100 MHz, (CD$_3$)$_2$SO) 152.6, 139.8, 137.1, 130.6, 129.2, 128.8, 121.7, 118.3, 118.1, 20.4; MS (MeOH, ES$^+$) *m/z* 227 (M + H)$^+$, 249 (M + Na)$^+$, 475 (2M + Na)$^+$; IR (KBr) υ_{max} (cm^{-1}) 3302, 2361, 1636, 1594, 1566, 1443, 1310, 1237, 789, 733, 634, 509.

1-Phenyl-3-(*p*-tolyl)thiourea (72)

72 Was synthesised according to **Procedure 1(i)** using *p*-tolyl isothiocyanate (0.49 g, 3.30 mmol) and aniline (0.40 g, 4.30 mmol) in spectroscopic grade CHCl$_3$ (20 mL). A cream-coloured precipitate was obtained. Recrystallisation of the solid from CHCl$_3$ yielded a pure sample (0.19 g, 24.2%). m.p. 145 - 147 °C (lit.,[195] 147 - 149 °C); Calculated for C$_{14}$H$_{14}$N$_2$S: C, 69.39; H, 5.82; N, 11.56%; Found: C, 69.25; H, 5.81; N, 11.53%; δ_H (400 MHz, (CD$_3$)$_2$SO) 9.70 (2H, s, N$\underline{H}$), 7.47 (2H, d, *J* = 8.0 Hz, Ar-$\underline{H2}$, Ar-$\underline{H6}$), 7.32 (4H, m, Ar-$\underline{H3}$, Ar-$\underline{H5}$, Ar-$\underline{H2}$', Ar-$\underline{H6}$'), 7.13 (3H, m, Ar-$\underline{H4}$, Ar-$\underline{H3}$', Ar-$\underline{H5}$'), 2.28 (3H, s, Ar-C$\underline{H3}$); δ_C (100 MHz, (CD$_3$)$_2$SO) 179.6, 139.5, 136.8, 133.7, 128.9, 128.4, 124.4, 123.9, 123.7, 20.5; MS (MeOH, ES$^+$) *m/z* 243 (M + H)$^+$, 265 (M + Na)$^+$; IR (KBr) υ_{max} (cm^{-1}) 3170, 2954, 1592, 1554, 1486, 1446, 1312, 1246, 1180, 1139, 1073, 1028, 951, 863, 811, 752, 691, 591, 540, 503.

1-Phenyl-3-(4-fluorophenyl)urea (73)

73 Was synthesised according to **Procedure 1(i)** using 4-fluorophenyl isocyanate (0.45 g, 3.30 mmol) and aniline (0.40 g, 4.30 mmol) in spectroscopic grade CHCl₃ (20 mL). A white precipitate was obtained. Recrystallisation of the solid from Hex:CHCl₃:MeOH (3:5:1) yielded white needle-like crystals (0.74 g, 97.4%). m.p. 238 - 240 °C (lit.,[196] 240 °C); HRMS (MeOH, ES⁺): Calculated for $C_{13}H_{12}N_2OF$: 231.0934 $(M + H)^+$; Found: 231.0925; δ_H (400 MHz, (CD₃)₂SO) 8.71 (1H, br s, N<u>H</u>'), 8.67 (1H, br s, N<u>H</u>), 7.45 (4H, m, Ar-<u>H2</u>, Ar-<u>H6</u>, Ar-<u>H2</u>',Ar-<u>H6</u>'), 7.27 (2H, t, J = 7.5 Hz, Ar-<u>H3</u>, Ar-<u>H5</u>), 7.12 (2H, app t, J = 7.8 Hz, Ar-<u>H3</u>', Ar-<u>H5</u>'), 6.96 (1H, t, J = 6.2 Hz, Ar-<u>H4</u>); δ_C (100 MHz, (CD₃)₂SO) 157.3 (d, J_{C-F} = 236.7 Hz), 152.2, 139.7, 136.0, 128.8, 121.8, 119.9 (d, J_{C-F} = 7.7 Hz), 118.2, 115.3 (d, J_{C-F} = 22.2 Hz); δ_F (376 MHz, (CD₃)₂SO) -121.97 (Ar-<u>F</u>); MS (MeOH, ES⁺) m/z 231 $(M + H)^+$, 461 $(2M + H)^+$; IR (KBr) υ_{max} (cm⁻¹) 3297, 2361, 1628, 1561, 1508, 1443, 1212, 847, 737, 636.

1-Phenyl-3-(4-fluorophenyl)thiourea (74)

74 Was synthesised according to **Procedure 1(i)** using 4-fluorophenyl isothiocyanate (0.57 g, 3.30 mmol) and aniline (0.40 g, 4.93 mmol) i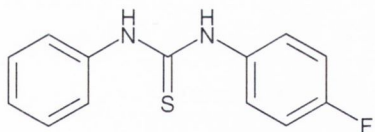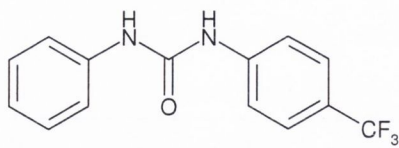n spectroscopic grade CHCl₃ (20 mL). A white precipitate was obtained. Recrystallisation of the solid from CHCl₃ yielded a pure sample (0.58 g, 71.0%). m.p. 174 - 176 °C (lit.,[197] 168 °C); Calculated for $C_{13}H_{11}N_2SF$: C, 63.39; H, 4.50; N, 11.37%; Found: C, 63.28; H, 4.48; N, 11.35%; δ_H (400 MHz, (CD₃)₂SO) 9.80 (1H, s, N<u>H</u>), 9.75 (1H, s, N<u>H</u>'), 7.46 (4H, m, Ar-<u>H2</u>, Ar-<u>H6</u>, Ar-<u>H2</u>', Ar-<u>H6</u>'), 7.34 (2H, t, J = 7.9 Hz, Ar-<u>H3</u>, Ar-<u>H5</u>), 7.15 (3H, m, Ar-<u>H4</u>, Ar-<u>H3</u>', Ar-<u>H5</u>'); δ_C (100 MHz, (CD₃)₂SO) 179.6, 159.2 (d, J_{C-F} = 246.3 Hz), 139.4, 135.7, 128.5, 126.2 (d, J_{C-F} = 7.7 Hz), 124.5, 123.8, 115.1 (d, J_{C-F} = 22.2 Hz); δ_F (376 MHz, (CD₃)₂SO) -118.31 (Ar-<u>F</u>); MS (MeOH, ES⁺) m/z 247 $(M + H)^+$, 269 $(M + Na)^+$; IR (KBr) υ_{max} (cm⁻¹) 3212, 3012, 2086, 1599, 1552, 1505, 1338, 1295, 1228, 1090, 1015, 932, 850, 761, 702, 679, 602, 508, 476.

1-Phenyl-3-(4-trifluoromethylphenyl)urea (75)

75 Was synthesised according to **Procedure 1(i)** using 4-trifluoromethylphenyl isocyanate (0.62 g, 3.30 mmol) and aniline (0.40 g, 4.93 mmol) in spectroscopic grade $CHCl_3$ (20 mL). A white precipitate was obtained. Recrystallisation of the solid from $CHCl_3$ yielded a pure sample (0.86 g, 92.5%). m.p. 224 - 226 °C; Calculated for $C_{14}H_{11}N_2OF_3$: C, 60.00; H, 3.96; N, 10.00%; Found: C, 59.50; H, 3.93; N, 9.83%; δ_H (400 MHz, $(CD_3)_2SO$) 9.05 (1H, br s, N$\underline{H}$'), 8.75 (1H, br s, N$\underline{H}$), 7.64 (4H, app q, J = 9.1 Hz, Ar-$\underline{H2}$', Ar-$\underline{H6}$', Ar-$\underline{H3}$', Ar-$\underline{H5}$'), 7.48 (1H, d, J = 1.1 Hz, Ar-$\underline{H6}$), 7.46 (1H, d, J = 1.1 Hz, Ar-$\underline{H2}$), 7.30 (2H, t, J = 8.1 Hz, Ar-$\underline{H3}$, Ar-$\underline{H5}$), 7.00 (1H, t, J = 7.3 Hz, Ar-$\underline{H4}$); δ_C (100 MHz, $(CD_3)_2SO$) 152.3, 143.5, 139.3, 128.8, 126.0, 123.2, 122.2, 121.8 (q, J_{C-F} = 31.9 Hz), 118.4, 117.8; δ_F (376 MHz, $(CD_3)_2SO$) -60.62 (Ar-C$\underline{F}_3$); MS (MeOH, ES$^+$) m/z 281 (M + H)$^+$, 303 (M + Na)$^+$; IR (KBr) υ_{max} (cm^{-1}) 3306, 1644, 1598, 1499, 1447, 1408, 1329, 1241, 1166, 1111, 1068, 1016, 847, 796, 743, 693, 661, 594, 507.
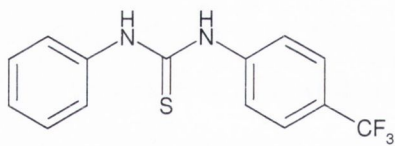
1-Phenyl-3-(4-trifluoromethylphenyl)thiourea (76)

76 Was synthesised according to **Procedure 1(i)** using 4-trifluoromethylphenyl isothiocyanate (0.67 g, 3.30 mmol) and aniline (0.40 g, 4.93 mmol) in spectroscop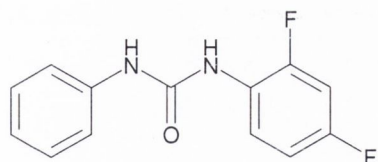ic grade $CHCl_3$ (20 mL). A white precipitate was obtained. Recrystallisation of the solid from $CHCl_3$ yielded a pure sample (0.72 g, 73.7%). m.p. 165 - 166 °C; Calculated for $C_{14}H_{11}N_2SF_3$: C, 56.75; H, 3.74; N, 9.45%; Found: C, 56.65; H, 3.69; N, 9.44%; δ_H (400 MHz, $(CD_3)_2SO$) 10.07 (1H, br s, N$\underline{H}$'), 10.02 (1H, br s, N$\underline{H}$), 7.76 (2H, d, J = 8.4 Hz, Ar-$\underline{H3}$', Ar-$\underline{H5}$'), 7.68 (2H, d, J = 8.8 Hz, Ar-$\underline{H2}$', Ar-$\underline{H6}$'), 7.49 (2H, d, J = 7.7 Hz, Ar-$\underline{H2}$, Ar-$\underline{H6}$), 7.36 (2H, t, J = 7.9 Hz, Ar-$\underline{H3}$, Ar-$\underline{H5}$), 7.16 (1H, t, J = 7.5 Hz, Ar-$\underline{H4}$); δ_C (100 MHz, $(CD_3)_2SO$) 179.6, 143.4, 143.1, 139.5, 139.1, 128.5, 125.5, 124.8, 123.8, 122.9; δ_F (376 MHz, $(CD_3)_2SO$) -60.99 (Ar-C$\underline{F}_3$); MS (MeOH, ES$^+$) m/z 297 (M + H)$^+$, 319 (M + Na)$^+$; IR (KBr) υ_{max} (cm^{-1}) 3219, 3016, 2904, 2342, 1933, 1618, 1593, 1550, 1454, 1415, 1333, 1238, 1167, 1123, 1071, 1021, 932, 851, 775, 699, 648, 590, 498.

1-Phenyl-3-(2,4-difluorophenyl)urea (77)

77 Was synthesised according to **Procedure 1(i)** using 2,4-difluorophenyl isocyanate (0.51 g, 3.30 mmol) and aniline (0.40 g, 4.93 mmol) in spectroscopic grade CHCl$_3$ (20 mL). A white precipitate was obtained. Recrystallisation of the solid from CHCl$_3$ yielded a pure sample (0.66 g, 80.1%). m.p. 217 - 218 °C (lit.,[198] 222 °C); Calculated for C$_{13}$H$_{10}$N$_2$OF$_2$: C, 62.90; H, 4.06; N, 11.29%; Found: C, 62.60; H, 4.01; N, 11.10%; δ_H (400 MHz, (CD$_3$)$_2$SO) 8.98 (1H, br s, NH'), 8.46 (1H, br s, NH), 8.09 (1H, m, Ar-H6'), 7.45 (2H, d, J = 7.7 Hz, Ar-H2, Ar-H6), 7.29 (3H, m, Ar-H3, Ar-H5, Ar-H5'), 7.02 (2H, m, Ar-H4, Ar-H3'); δ_C (100 MHz, (CD$_3$)$_2$SO) 156.7 (dd, J_{C-F} = 239.6 Hz, 11.6 Hz), 152.3, 152.1 (dd, J_{C-F} = 242.9 Hz, 12.1 Hz), 139.4, 128.9, 124.1 (d, J_{C-F} = 13.2 Hz), 121.9, 121.8 (d, J_{C-F} = 11.6 Hz), 118.1, 111.0 (d, J_{C-F} = 24.2 Hz), 103.7 (t, J_{C-F} = 23.7 Hz); δ_F (376 MHz, (CD$_3$)$_2$SO) -118.78 (Ar-F), -125.48 (Ar-F); MS (MeOH, ES$^+$) m/z 249 (M + H)$^+$, 271 (M + Na)$^+$; IR (KBr) υ_{max} (cm^{-1}) 3287, 3082, 1643, 1597, 1567, 1501, 1446, 1430, 1295, 1254, 1205, 1144, 1102, 1054, 965, 852, 805, 779, 740, 691, 657, 611, 482.
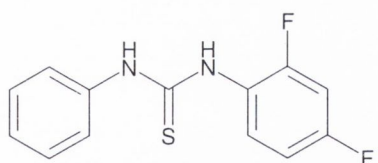
1-Phenyl-3-(2,4-difluorophenyl)thiourea (78)

78 Was synthesised according to **Procedure 1(ii)** using 2,4-difluorophenyl isothiocyanate (0.57 g, 3.30 mmol) and aniline (0.40 g, 4.30 mmol) in spectroscopic grade CHCl$_3$ (20 mL). A white solid was obtained. Recrystallisation of the solid from CHCl$_3$ yielded a pure sample (0.86 g, 98.9%). m.p. 128 - 129 °C; HRMS (MeOH, ES$^+$): Calculated for C$_{13}$H$_{11}$N$_2$SF$_2$: 265.0611 (M + H)$^+$; Found: 265.0605; δ_H (400 MHz, (CD$_3$)$_2$SO) 9.97 (1H, br s, NH'), 9.40 (1H, br s, NH), 7.54 (1H, m, Ar-H6'), 7.48 (2H, d, J = 8.2 Hz, Ar-H2, Ar-H6), 7.33 (3H, m, Ar-H3, Ar-H5, Ar-H5'), 7.15 (1H, t, J = 7.2 Hz, Ar-H4), 7.08 (1H, m, Ar-H3'); δ_C (100 MHz, (CD$_3$)$_2$SO) 181.0, 160.1 (dd, J_{C-F} = 244.4 Hz, 11.6 Hz), 156.9 (dd, J_{C-F} = 247.7 Hz, 13.1 Hz), 140.0, 139.2, 130.3 (d, J_{C-F} = 7.7 Hz), 128.6, 124.8, 123.8, 111.0 (d, J_{C-F} = 3.9 Hz), 104.3 (t, J_{C-F} = 24.2 Hz); δ_F (376 MHz, (CD$_3$)$_2$SO) -113.01 (Ar-F), -113.01 (Ar-F); MS (MeOH, ES$^+$) m/z 265 (M + H)$^+$; IR (KBr) υ_{max} (cm^{-1}) 3300, 3201, 2988, 1593, 1545, 1516, 1433, 1365, 1312, 1259, 1228, 1140, 1099, 970, 848, 742, 698, 611, 497, 460.

1,3-*Bis*-(4-fluorophenyl)urea (79)
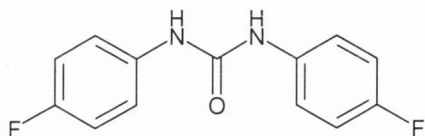
79 Was synthesised according to **Procedure 1(i)** using 4-fluorophenyl isocyanate (0.38 g, 2.77 mmol) and 4-fluoroaniline (0.40 g, 3.6 mmol) in spectroscopic grade CHCl$_3$ (20 mL). A pale purple precipitate was obtained. Recrystallisation of the solid from CHCl$_3$:MeOH (8:1) yielded purple needle-like crystals (0.49 g, 70.9%). m.p. 265 - 267 °C (lit.,[199] 241 °C); Calculated for C$_{13}$H$_{10}$N$_2$OF$_2$: C, 62.90; H, 4.06; N, 11.29%; Found: C, 62.70; H, 4.16; N, 11.20%; δ_H (400 MHz, (CD$_3$)$_2$SO) 8.72 (2H, s, N$\underline{H}$), 7.46 (2H, d, J = 4.8 Hz, Ar-$\underline{H2}$), 7.45 (2H, d, J = 4.8 Hz, Ar-$\underline{H6}$), 7.12 (4H, d, J = 8.9 Hz, Ar-$\underline{H3}$, Ar-$\underline{H5}$); δ_C (100 MHz, (CD$_3$)$_2$SO) 157.3 (d, J_{C-F} = 236.7 Hz), 152.7, 136.0 120.0 (d, J_{C-F} = 7.7 Hz), 115.2 (d, J_{C-F} = 21.3 Hz); δ_F (376 MHz, (CD$_3$)$_2$SO) -121.96 (Ar-$\underline{F}$); MS (MeOH, ES$^+$) m/z 249 (M + H)$^+$, 271 (M + Na)$^+$; IR (KBr) υ_{max} (cm^{-1}) 3293, 2361, 1885, 1631, 1570, 1511, 1405, 1298, 1211, 1153, 831, 652, 565, 517, 466.

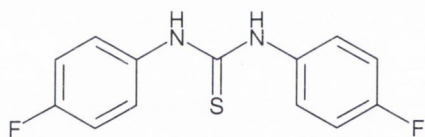## 1,3- -(4-fluorophenyl)thiourea (80)

80 Was synthesised according to **Procedure 1(i)** using 4-fluorophenyl isothiocyanate (0.42 g, 2.77 mmol) and 4-fluoroaniline (0.40 g, 3.60 mmol) in spectroscopic grade CHCl$_3$ (10 mL). A purple crystalline precipitate was obtained. Recrystallisation of the solid from CHCl$_3$:MeOH (10:1) yielded purple flat crystals (0.42 g, 58.1%). m.p. 191 - 193 °C (lit.,[200] 186 - 187 °C); HRMS (MeOH, ES$^+$): Calculated for C$_{13}$H$_{11}$N$_2$SF$_2$: 265.0611 (M + H)$^+$; Found: 265.0598; δ_H (400 MHz, (CD$_3$)$_2$SO) 9.77 (2H, br s, N$\underline{H}$), 7.46 (2H, d, J = 5.0 Hz, Ar-$\underline{H2}$), 7.45 (2H, d, J = 5.0 Hz, Ar-$\underline{H6}$), 7.17 (4H, app t, J = 8.8 Hz, Ar-$\underline{H3}$, Ar-$\underline{H5}$); δ_C (100 MHz, (CD$_3$)$_2$SO) 180.3, 158.0, 135.6, 126.3 (d, J_{C-F} = 8.7 Hz), 115.0 (d, J_{C-F} = 22.2 Hz); δ_F (376 MHz, (CD$_3$)$_2$SO) -118.36 (Ar-$\underline{F}$); MS (MeOH, ES$^+$) m/z 265 (M + H)$^+$; IR (KBr) υ_{max} (cm^{-1}) 3219, 3019, 1604, 1549, 1510, 1334, 1240, 1211, 1089, 845, 720, 673, 570.

1-(4-Fluorophenyl)-3-(*p*-tolyl)urea (81)
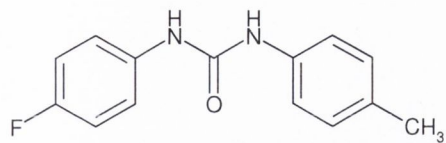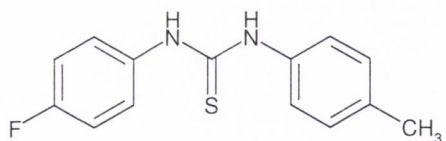
81 Was synthesised according to **Procedure 1(i)** using *p*-tolyl isocyanate (0.37 g, 2.77 mmol) and 4-fluoroaniline (0.40 g, 3.60 mmol) in spectroscopic grade CHCl$_3$ (10 mL). A pale purple precipitate was obtained. Recrystallisation of the solid from CHCl$_3$:MeOH (1:4) yielded purple needle-like crystals (0.67 g, 98.7%). m.p. 257 - 259 °C; HRMS (MeOH, ES$^+$): Calculated for C$_{14}$H$_{14}$N$_2$OF: 245.1090 (M + H)$^+$; Found: 245.1042; δ_H (400 MHz, (CD$_3$)$_2$SO) 8.71 (1H, br s, N$\underline{H}$), 8.60 (1H, br s, N$\underline{H}$'), 7.46 (1H, d, *J* = 5.0 Hz, Ar-$\underline{H}$2), 7.45 (1H, d, *J* = 5.0 Hz, Ar-$\underline{H}$6), 7.34 (1H, s, Ar-$\underline{H}$2'), 7.32 (1H, s, Ar-$\underline{H}$6'), 7.11 (2H, d, *J* = 8.5 Hz, Ar-$\underline{H}$3, Ar-$\underline{H}$5), 7.09 (2H, d, *J* = 8.5 Hz, Ar-$\underline{H}$3', Ar-$\underline{H}$5'), 2.24 (3H, s, Ar-C$\underline{H}_3$); δ_C (100 MHz, (CD$_3$)$_2$SO) 157.3 (d, J_{C-F} = 237.6 Hz), 152.7, 137.1, 136.1, 130.7, 129.2, 119.9 (d, J_{C-F} = 6.8 Hz), 118.3, 115.2 (d, J_{C-F} = 22.2 Hz), 20.3; δ_F (376 MHz, (CD$_3$)$_2$SO) -122.18 (Ar-$\underline{F}$); MS (MeOH, ES$^+$) *m/z* 245 (M + H)$^+$, 269 (M + Na)$^+$; IR (KBr) υ_{max} (cm^{-1}) 3298, 1638, 1569, 1511, 1405, 1308, 1213, 1150, 821, 643.
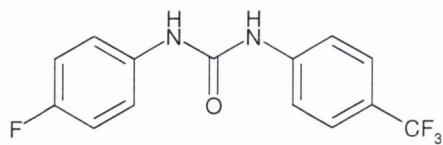
1-(4-Fluorophenyl)-3-(*p*-tolyl)thiourea (82)

82 Was synthesised according to **Procedure 1(i)** using *p*-tolyl isothiocyanate (0.41 g, 2.77 mmol) and 4-fluoroaniline (0.40 g, 3.60 mmol) in spectroscopic grade CHCl$_3$ (10 mL). A small amount of purple crystals formed. The solvent was reduced to a third of its original volume and the mixture was left in the fridge for 18 h. More crystals formed which were collected (0.05 g, 7.0%) and dried without need for further purification. m.p. 167 - 169 °C (lit.,[201] 179 °C); HRMS (MeOH, ES$^+$): Calculated for C$_{14}$H$_{14}$N$_2$SF: 261.0862 (M + H)$^+$; Found: 261.0858; δ_H (400 MHz, (CD$_3$)$_2$SO) 9.72 (1H, s, N$\underline{H}$), 9.66 (1H, s, N$\underline{H}$'), 7.31 (2H, d, *J* = 8.2 Hz, Ar-$\underline{H}$2', Ar-$\underline{H}$6'), 7.15 (2H, d, *J* = 8.2 Hz, Ar-$\underline{H}$3, Ar-$\underline{H}$5), 7.16 (4H, m, Ar-$\underline{H}$2, Ar-$\underline{H}$6, Ar-$\underline{H}$3', Ar-$\underline{H}$5'), 2.28 (3H, s, Ar-C$\underline{H}_3$); δ_C(100 MHz, (CD$_3$)$_2$SO) 181.1, 136.7, 133.8, 129.0, 126.2 (d, J_{C-F} = 8.7 Hz), 123.9, 123.0, 121.1, 115.0 (d, J_{C-F} = 22.2 Hz), 20.5; δ_F (376 MHz, (CD$_3$)$_2$SO) -118.61 (Ar-$\underline{F}$); MS (MeOH, ES$^+$) *m/z* 261 (M + H)$^+$, 262 (M + 2H)$^{2+}$, 283 (M + Na)$^+$, 521 (2M + H)$^+$, 543 (2M + Na)$^+$; IR (KBr) υ_{max} (cm^{-1}) 3201, 3019, 2362, 1911, 1604, 1548, 1510, 1334, 1212, 1090, 925, 833, 718, 676, 567, 506.

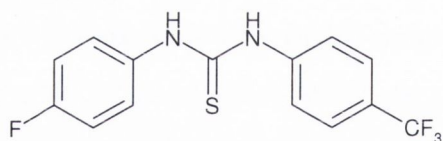### 1-(4-Fluorophenyl)-3-(4-trifluoromethylphenyl)urea (83)

83 Was synthesised according to **Procedure 1(i)** using 4-trifluoromethylphenyl isocyanate (0.52 g, 2.77 mmol) and 4-fluoroaniline (0.40 g, 3.60 mmol) in spectroscopic grade $CHCl_3$ (20 mL). A fine pale purple precipitate was obtained. Recrystallisation of the solid from Hex:$CHCl_3$:MeOH (3:5:1) yielded fine purple needle-like crystals (0.83 g, 99.5%). m.p. 215 - 216 °C (lit.,[9] 218 - 220 °C); Calculated for $C_{14}H_{10}N_2OF_4$: C, 56.38; H, 3.38; N, 9.39%; Found: C, 56.24; H, 3.39; N, 9.34%; δ_H (400 MHz, $(CD_3)_2SO$) 9.11 (1H, s, NH'), 8.85 (1H, s, NH), 7.65 (2H, d, J = 8.8 Hz, Ar-H3', Ar-H5'), 7.64 (2H, d, J = 8.8 Hz, Ar-H2', Ar-H6'), 7.48 (2H, m, Ar-H2, Ar-H6), 7.14 (2H, app t, J = 9.0 Hz, Ar-H3, Ar-H5); δ_C (100 MHz, $(CD_3)_2SO$) 157.5 (d, J_{C-F} = 237.6 Hz), 152.4, 143.5, 135.6, 126.0 (d, J_{C-F} = 3.9 Hz), 125.9, 121.9, 120.3 (d, J_{C-F} = 7.7 Hz), 117.9, 115.3 (d, J_{C-F} = 21.2 Hz); δ_F (376 MHz, $(CD_3)_2SO$) -60.54 (Ar-CF$_3$), -121.49 (Ar-F); MS (MeOH, ES$^+$) m/z 299 (M + H)$^+$, 321 (M + Na)$^+$; IR (KBr) υ_{max} (cm^{-1}) 3301, 1638, 1566, 1512, 1406, 1327, 1227, 1128, 1069, 836, 643.

### 1-(4-Fluorophenyl)-3-(4-trifluoromethylphenyl)thiourea (84)

84 Was synthesised according to **Procedure 1(i)** using 4-trifluoromethylphenyl isothiocyanate (0.56 g, 2.77 mmol) and 4-fluoroaniline (0.40 g, 3.60 mmol) in spectroscopic grade $CHCl_3$ (10 mL). A pale purple precipitate was obtained. Recrystallisation of the solid from $CHCl_3$ yielded purple needle-like crystals (0.17 g, 20.1%). m.p. 153 - 154 °C; Calculated for $C_{14}H_{10}N_2SF_4$: C, 53.50; H, 3.21; N, 8.91%; Found: C, 53.41; H, 3.19; N, 8.81%; HRMS (MeOH, ES$^+$): Calculated for $C_{14}H_{11}N_2SF_4$: 315.0579 (M + H)$^+$; Found: 315.0592; δ_H (400 MHz, $(CD_3)_2SO$) 10.06 (2H, br s, NH), 7.73 (2H, d, J = 8.5 Hz, Ar-H2', Ar-H6'), 7.69 (2H, d, J = 8.5 Hz, Ar-H3', Ar-H5'), 7.48 (2H, dd, J = 5.0 Hz, Ar-H2, Ar-H6), 7.19 (2H, app t, J = 8.8 Hz, Ar-H3, Ar-H5); δ_C (100 MHz, $(CD_3)_2SO$) 180.0, 162.2 (q, J_{C-F} = 240.0 Hz), 159.3 (d, J_{C-F} = 240.5 Hz), 143.3, 135.4, 126.3 (d, J_{C-F} = 7.7 Hz), 125.6 (d, J_{C-F} = 3.9 Hz), 124.0, 122.9, 115.2 (d, J_{C-F} = 22.2 Hz); δ_F (376 MHz, $(CD_3)_2SO$) -60.87 (Ar-CF$_3$), -118.01 (Ar-F); MS (MeOH, ES$^+$) m/z 315 (M + H)$^+$; IR (KBr) υ_{max} (cm^{-1}) 3193, 3025, 1547, 1509, 1324, 1234, 1164, 1131, 1066, 726.
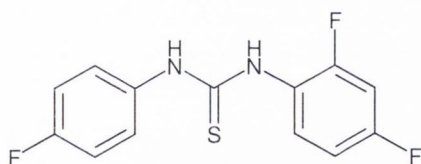
1-(4-Fluorophenyl)-3-(2,4-difluorophenyl)urea (85)
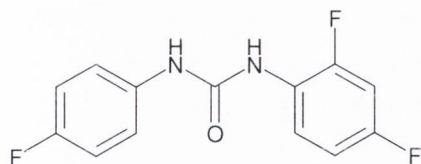
85 Was synthesised according to **Procedure 1(i)** using 2,4-difluorophenyl isocyanate (0.43 g, 2.77 mmol) and 4-fluoroaniline (0.40 g, 3.60 mmol) in spectroscopic grade $CHCl_3$ (10 mL). A pale purple precipitate was obtained. Recrystallisation of the solid from $CHCl_3$:MeOH (5:1) yielded very fine purple crystals (0.71 g, 96.2%). m.p. 253 - 254 °C; Calculated for $C_{13}H_9N_2OF_3$: C, 58.65; H, 3.41; N, 10.52%; Found: C, 58.45; H, 3.33; N, 10.40%; δ_H (400 MHz, $(CD_3)_2SO$) 9.12 (1H, br s, N$\underline{H}$'), 8.56 (1H, br s, N$\underline{H}$), 8.04 (1H, m, Ar-$\underline{H6}$'), 7.46 (2H, m, Ar-$\underline{H2}$, Ar-$\underline{H6}$), 7.31 (1H, m, Ar-$\underline{H5}$'), 7.13 (2H, app t, J = 8.8 Hz, Ar-$\underline{H3}$, Ar-$\underline{H5}$), 7.05 (1H, m, Ar-$\underline{H3}$'); δ_C (100 MHz, $(CD_3)_2SO$) 157.1 (d, J_{C-F} = 233.0 Hz), 153.6 (d, J_{C-F} = 53.9 Hz), 152.4, 150.7 (d, J_{C-F} = 69.4 Hz), 135.7, 124.0 (d, J_{C-F} = 13.5 Hz), 122.1 (d, J_{C-F} = 6.8 Hz), 119.9 (d, J_{C-F} = 7.7 Hz), 115.3 (d, J_{C-F} = 22.2 Hz), 111.0 (d, J_{C-F} = 25.1 Hz), 103.7 (t, J_{C-F} = 25.2 Hz); δ_F (376 MHz, $(CD_3)_2SO$) -118.62 (Ar-$\underline{F}$), -121.68 (Ar-$\underline{F}$), -125.24 (Ar-$\underline{F}$); MS (MeOH, ES^+) m/z 289 (M + Na)$^+$; IR (KBr) υ_{max} (cm^{-1}) 3294, 3083, 1641, 1573, 1511, 1433, 1410, 1301, 1225, 1144, 1104, 966.

1-(4-Fluorophenyl)-3-(2,4-difluorophenyl)thiourea (86)

86 Was synthesised according to **Procedure 1(i)** using 2,4-difluorophenyl isothiocyanate (0.47 g, 2.77 mmol) and 4-fluoroaniline (0.40 g, 3.60 mmol) in spectroscopic grade $CHCl_3$ (20 mL). A purple precipitate was obtained. Recrystallisation of the solid from $CHCl_3$ yielded a pure sample (0.04 g, 0.05%). m.p. 159 - 161 °C; HRMS (MeOH, ES^+): Calculated for $C_{13}H_{10}N_2SF_3$: 283.0517 (M + H)$^+$; Found: 283.0518; δ_H (400 MHz, $(CD_3)_2SO$) 9.91 (1H, br s, N$\underline{H}$'), 9.42 (1H, br s, N$\underline{H}$), 7.53 (1H, m, Ar-$\underline{H6}$'), 7.47 (2H, m, Ar-$\underline{H2}$, Ar-$\underline{H6}$), 7.32 (1H, m, Ar-$\underline{H5}$'), 7.19 (2H, m, Ar-$\underline{H3}$, Ar-$\underline{H5}$), 7.08 (1H, m, Ar-$\underline{H3}$'); δ_C (100 MHz, $(CD_3)_2SO$) 181.3, 160.1 (d, J_{C-F} = 243.4 Hz), 159.3 (d, J_{C-F} = 239.6 Hz), 153.6 (d, J_{C-F} = 230.9 Hz), 135.6 (d, J_{C-F} = 17.4 Hz), 130.4 (d, J_{C-F} = 9.7 Hz), 126.3 (d, J_{C-F} = 8.7 Hz), 123.7 (d, J_{C-F} = 11.6 Hz), 115.2 (d, J_{C-F} = 22.2 Hz), 111.1 (d, J_{C-F} = 18.4 Hz), 104.3 (t, J_{C-F} = 25.6 Hz); δ_F (376 MHz, $(CD_3)_2SO$) -112.97 (Ar-$\underline{F}$), -116.83 (Ar-$\underline{F}$), -118.08 (Ar-$\underline{F}$); MS (MeOH, ES^+) m/z 283 (M + H)$^+$; IR (KBr) υ_{max} (cm^{-1}) 3213, 3107, 3023, 1912, 1611, 1549, 1510, 1434, 1330, 1262, 1226, 1144, 1092, 970, 921, 850, 719, 673, 561, 505, 441.

1-(4-Trifluoromethylphenyl)-3-(*p*-tolyl)urea (87)
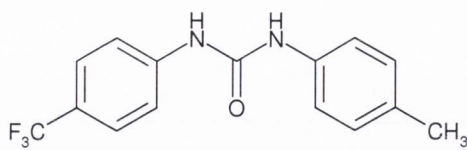
87 Was synthesised according to **Procedure 1(i)** using *p*-tolyl isocyanate (0.35 g, 2.63 mmol) and 4-trifluoromethyl-aniline (0.55 g, 3.41 mmol) in spectroscopic grade $CHCl_3$ (20 mL). A white precipitate was obtained. Recrystallisation of the solid from $CHCl_3$:MeOH (10:1) yielded fine white needle-like crystals (0.70 g, 91.4%). m.p. 264 - 265 °C (lit.,[9] 268 - 269 °C); Calculated for $C_{15}H_{13}N_2OF_3$: C, 61.22; H, 4.45; N, 9.52%; Found: C, 61.05; H, 4.36; N, 9.45%; δ_H (400 MHz, $(CD_3)_2SO$) 9.06 (1H, br s, N$\underline{H}$), 8.70 (1H, br s, N$\underline{H}$'), 7.64 (2H, d, J = 8.9 Hz, Ar-$\underline{H}$2, Ar-$\underline{H}$6), 7.63 (2H, d, J = 9.6 Hz, Ar-$\underline{H}$3, Ar-$\underline{H}$5), 7.34 (2H, d, J = 8.2 Hz, Ar-$\underline{H}$2', Ar-$\underline{H}$6'), 7.11 (2H, d, J = 8.2 Hz, Ar-$\underline{H}$3', Ar-$\underline{H}$5'), 2.25 (3H, s, Ar-C$\underline{H}_3$); δ_C (100 MHz, $(CD_3)_2SO$) 152.3, 143.6, 136.7, 131.1, 129.2, 126.0 (d, J_{C-F} = 2.9 Hz), 125.9, 121.5 (d, J_{C-F} = 269.5 Hz), 118.5, 117.7, 20.3; δ_F (376 MHz, $(CD_3)_2SO$) -60.59 (Ar-C$\underline{F}_3$); MS (MeOH, ES$^+$) *m/z* 295 (M + H)$^+$; IR (KBr) υ_{max} (cm^{-1}) 3322, 3035, 2922, 1910, 1642, 1561, 1409, 1321, 1243, 1161, 1121, 1067, 1015, 827, 643, 519.

1-(4-Trifluoromethylphenyl)-3-(*p*-tolyl)thiourea (88)
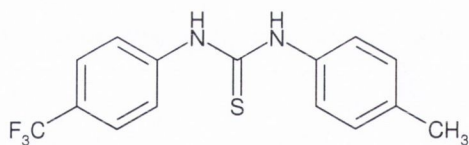
88 Was synthesised according to **Procedure 1(i)** using *p*-tolyl isothiocyanate (0.39 g, 2.63 mmol) and 4-trifluoromethyl-aniline (0.55 g, 3.41 mmol) in spectroscopic grade $CHCl_3$ (20 mL). A cream-coloured precipitate was obtained. Recrystallisation of the solid from $CHCl_3$ yielded white needle-like crystals (0.09 g, 11.4%). m.p. 188 - 189 °C; HRMS (MeOH, ES$^+$): Calculated for $C_{15}H_{14}N_2SF_3$: 311.0830 (M + H)$^+$; Found: 311.0841; δ_H (400 MHz, $(CD_3)_2SO$) 10.02 (1H, br s, N$\underline{H}$), 9.99 (1H, s, N$\underline{H}$'), 7.74 (2H, d, J = 8.8 Hz, Ar-$\underline{H}$3, Ar-$\underline{H}$5), 7.68 (4H, d, J = 8.8 Hz, Ar-$\underline{H}$2, Ar-$\underline{H}$6, Ar-$\underline{H}$2', Ar-$\underline{H}$6'), 7.33 (2H, d, J = 8.2 Hz, Ar-$\underline{H}$3', Ar-$\underline{H}$5'), 2.29 (3H, s, Ar-C$\underline{H}_3$); δ_C (100 MHz, $(CD_3)_2SO$) 179.6, 143.5, 136.5, 134.1, 129.0, 125.8, 125.7 (q, J_{C-F} = 259.3 Hz), 125.5 (d, J_{C-F} = 3.9 Hz), 123.9, 122.8, 20.5; δ_F (376 MHz, $(CD_3)_2SO$) -60.87 (Ar-C$\underline{F}_3$); MS (MeOH, ES$^+$) *m/z* 311 (M + H)$^+$; IR (KBr) υ_{max} (cm^{-1}) 3207, 3028, 2922, 2706, 2419, 2309, 2081, 1693, 1590, 1551, 1503, 1415, 1327, 1242, 1164, 1123, 1068, 1021, 929, 813, 790, 719, 682, 630, 497.

1,3-*Bis*-(4-trifluoromethylphenyl)urea (89)
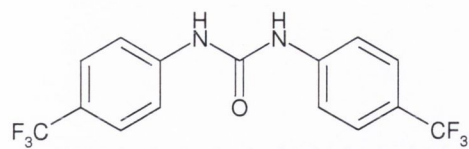
89 Was synthesised according to **Procedure 1(i)** using 4-trifluoro-methylphenylisocyanate (0.49 g, 2.63 mmol) and 4-trifluoromethylaniline (0.55 g, 3.41 mmol) in spectroscopic grade CHCl$_3$ (20 mL). A white precipitate was obtained. Recrystallisation of the solid from CHCl$_3$:MeOH (10:1) yielded white needle-like crystals (0.79 g, 87.2%). m.p. 238 - 240 °C (lit.,[9] 239 °C); HRMS (MeOH, ES$^+$): Calculated for C$_{15}$H$_{11}$N$_2$OF$_6$: 349.0776 (M + H)$^+$; Found: 349.0777; δ_H (400 MHz, (CD$_3$)$_2$SO) 9.25 (2H, br s, N$\underline{H}$), 7.67 (8H, dd, J = 8.9 Hz, 2.7 Hz, Ar-$\underline{H2}$, Ar-$\underline{H3}$, Ar-$\underline{H5}$, Ar-$\underline{H6}$); δ_C (100 MHz, (CD$_3$)$_2$SO) 152.1, 143.1, 126.0 (d, J_{C-F} = 3.9 Hz), 124.5 (q, J_{C-F} = 274.0 Hz), 122.2 (q, J_{C-F} = 31.9 Hz), 118.1; δ_F (376 MHz, (CD$_3$)$_2$SO) -60.82 (Ar-C$\underline{F}_3$); MS (MeOH, ES$^+$) m/z 349 (M + H)$^+$; IR (KBr) υ_{max} (cm^{-1}) 3323, 3069, 2766, 1917, 1651, 1603, 1550, 1412, 1327, 1163, 1122, 1067, 840, 751, 652, 595, 507.

1,3-*Bis*-(4-trifluoromethylphenyl)thiourea (90)

90 Was synthesised according to **Procedure 1(i)** using 4-trifluoromethyl-phenyl isothiocyanate (0.53 g, 2.63 mmol) and 4-trifluoromethylaniline (0.55 g, 3.41 mmol) in spectroscopic grade CHCl$_3$ (20 mL). A cream-coloured precipitate was obtained. Recrystallisation of the solid from CHCl$_3$ yielded a pure sample (0.15 g, 15.7%). m.p. 163 - 164 °C; Calculated for C$_{15}$H$_{10}$N$_2$SF$_6$: C, 49.45; H, 2.77; N, 7.69%; Found: C, 49.29; H, 2.82; N, 7.54%; δ_H (400 MHz, (CD$_3$)$_2$SO) 10.37 (2H, br s, N$\underline{H}$), 7.73 (8H, dd, J = 8.8 Hz, 8.9 Hz, Ar-$\underline{H2}$, Ar-$\underline{H3}$, Ar-$\underline{H5}$, Ar-$\underline{H6}$); δ_C (100 MHz, (CD$_3$)$_2$SO) 179.7, 143.1, 125.7 (d, J_{C-F} = 3.9 Hz), 124.6 (q, J_{C-F} = 275.0 Hz), 124. 3 (q, J_{C-F} = 31.6 Hz), 123.1; δ_F (376 MHz, (CD$_3$)$_2$SO) -58.79 (Ar-C$\underline{F}_3$); MS (MeOH, ES$^+$) m/z 365 (M + H)$^+$; IR (KBr) υ_{max} (cm^{-1}) 3195, 3031, 2784, 1913, 1600, 1536, 1411, 1321, 1238, 1174, 1125, 1065, 1014, 839, 740, 700, 569.

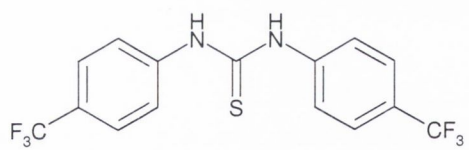**1-(4-Trifluoromethylphenyl)-3-(2,4-difluorophenyl)urea (91)**

92 Was synthesised according to **Procedure 1(i)** using 2,4-difluorophenyl isocyanate (0.41 g, 2.63 mmol) and 4-trifluoromethylaniline (0.55 g, 3.41 mmol) in spectroscopic grade CHCl$_3$ (20 mL). A white precipitate was obtained. Recrystallisation of the solid from CHCl$_3$:MeOH (10:1) yielded a pure sample (0.59 g, 71.1%). m.p. 197 - 199 °C; Calculated for C$_{14}$H$_9$N$_2$OF$_5$: C, 53.17; H, 2.87; N, 8.86%; Found: C, 53.13; H, 2.83; N, 8.79%; δ_H (400 MHz, (CD$_3$)$_2$SO) 9.44 (1H, br s, N$\underline{H}$), 8.65 (1H, br s, N$\underline{H}$'), 8.05 (1H, m, Ar-$\underline{H3}$'), 7.65 (4H, br s, Ar-$\underline{H2}$, Ar-$\underline{H3}$, Ar-$\underline{H5}$, Ar-$\underline{H6}$), 7.34 (1H, m, Ar-$\underline{H6}$'), 7.07 (1H, app t, J = 8.8 Hz, Ar-$\underline{H5}$'); δ_C (100 MHz, (CD$_3$)$_2$SO) 159.2 (d, J_{C-F} = 251.3 Hz), 154.5 (d, J_{C-F} = 243.4 Hz), 154.3, 130.7, 128.2 (d, J_{C-F} = 2.9 Hz), 128.0, 126.7 (q, J_{C-F} = 269.0 Hz), 125.9 (dd, J_{C-F} = 11.1 Hz, 3.4 Hz), 124.4 (d, J_{C-F} = 11.6 Hz), 120.0, 113.2 (d, J_{C-F} = 22.2 Hz), 103.9 (app t, J_{C-F} = 23.7 Hz); δ_F (376 MHz, (CD$_3$)$_2$SO) -58.59 (Ar-C$\underline{F_3}$), -116.03 (Ar-$\underline{F}$), -122.88 (Ar-$\underline{F}$); MS (MeOH, ES$^+$) m/z 317 (M + H)$^+$, 339 (M + Na)$^+$; IR (KBr) υ_{max} (cm^{-1}) 3304, 3082, 2773, 2585, 1649, 1565, 1503, 1432, 1411, 1326, 1256, 1186, 1125, 1068, 964, 851, 826, 646, 506.

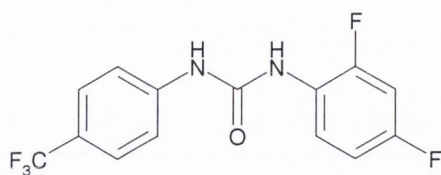**1-(4-Trifluoromethylphenyl)-3-(2,4-difluorophenyl)thiourea (92)**
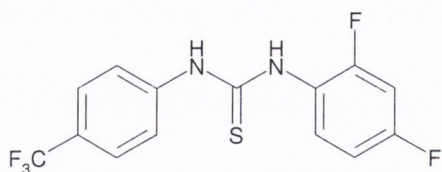
92 Was synthesised according to **Procedure 1(i)** using 2,4-difluorophenyl isothiocyanate (0.45 g, 2.63 mmol) and 4-trifluoromethyl-aniline (0.55 g, 3.41 mmol) in spectroscopic grade CHCl$_3$ (20 mL). A white precipitate was obtained. Recrystallisation of the solid from CHCl$_3$ yielded a pure sample (0.52 g, 59.2%). m.p. 140 - 142 °C; Calculated for C$_{14}$H$_9$N$_2$SF$_5$: C, 50.60; H, 2.73; N, 8.43%; Found: C, 50.48; H, 2.70; N, 8.31%; δ_H (400 MHz, (CD$_3$)$_2$SO) 10.28 (1H, br s, N$\underline{H}$), 9.67 (1H, br s, N$\underline{H}$'), 7.76 (2H, d, J = 8.5 Hz, Ar-$\underline{H3}$, Ar-$\underline{H5}$), 7.71 (2H, d, J = 8.5 Hz, Ar-$\underline{H2}$, Ar-$\underline{H6}$), 7.53 (1H, m, Ar-$\underline{H6}$'), 7.35 (1H, m, Ar-$\underline{H5}$'), 7.11 (1H, m, Ar-$\underline{H3}$'); δ_C (100 MHz, (CD$_3$)$_2$SO) 181.1, 160.3 (dd, J_{C-F} = 243.9 Hz, 11.1 Hz), 156.9 (dd, J_{C-F} = 247.3 Hz, 12.6 Hz), 143.1 (d, J_{C-F} = 8.7 Hz), 130.3 (d, J_{C-F} = 9.7 Hz), 125.6 (d, J_{C-F} = 3.9 Hz), 124.3 (q, J_{C-F} = 31.9 Hz), 123.4 (dd, J_{C-F} = 12.5 Hz, 3.9 Hz), 123.0, 111.2 (d, J_{C-F} = 22.2 Hz), 104. 4 (app t, J_{C-F} = 25.1 Hz); δ_F (376 MHz, (CD$_3$)$_2$SO) -61.01 (Ar-C$\underline{F_3}$), -112.64 (Ar-$\underline{F}$), -116.57 (Ar-$\underline{F}$); MS (MeOH, ES$^+$) m/z 333 (M + H)$^+$; IR (KBr) υ_{max} (cm^{-1}) 3214, 3001, 2740, 1915, 1617, 1547,

1515, 1436, 1360, 1316, 1231, 1173, 1129, 1066, 1014, 971, 915, 857, 834, 758, 700, 643, 618, 588, 485, 452, 403.

1-(2,4-Difluorophenyl)-3-(*p*-tolyl)urea (93)

93 Was synthesised according to **Procedure 1(i)** using *p*-tolyl isocyanate (0.40 g, 2.98 mmol) and 2,4-difluoroaniline (0.50 g, 3.87 mmol) in spectroscopic grade CHCl$_3$ (20 mL). A white precipitate was obtained. Recrystallisation of the solid from CHCl$_3$:MeOH (15:1) yielded a pure sample (0.77 g, 99.3%). m.p. 235 - 236 °C; Calculated for C$_{14}$H$_{12}$N$_2$OF$_2$: C, 64.12; H, 4.61; N, 10.68%; Found: C, 63.90; H, 4.48; N, 10.62%; δ_H (400 MHz, (CD$_3$)$_2$SO) 8.92 (1H, br s, N$\underline{H}$), 8.46 (1H, br s, N$\underline{H}$'), 8.08 (1H, q, *J* = 8.8 Hz, Ar-$\underline{H}$3), 7.32 (2H, d, *J* = 7.5 Hz, Ar-$\underline{H}$2', Ar-$\underline{H}$6'), 7.28 (1H, d, *J* = 3.4 Hz, Ar-$\underline{H}$6), 7.10 (2H, d, *J* = 7.5 Hz, Ar-$\underline{H}$3', Ar-$\underline{H}$5'), 7.04 (1H, m, Ar-$\underline{H}$5), 2.25 (3H, s, Ar-C$\underline{H}_3$); δ_C (100 MHz, (CD$_3$)$_2$SO) 156.7 (d, J_{C-F} = 260.2 Hz), 152.3, 152.0 (dd, J_{C-F} = 243.4 Hz, 11.6 Hz), 136.8, 130.9, 129.2, 124.2 (dd, J_{C-F} = 10.6 Hz, 3.9 Hz), 121.7 (dd, J_{C-F} = 9.2 Hz, 2.4 Hz), 118.2, 111.0 (dd, J_{C-F} = 21.3 Hz, 2.9 Hz), 103.7 (app t, J_{C-F} = 25.2 Hz), 20.3; δ_F (376 MHz, (CD$_3$)$_2$SO) -118.97 (Ar-$\underline{F}$), -125.61 (Ar-$\underline{F}$); MS (MeOH, ES$^+$) *m/z* 263 (M + H)$^+$, 285 (M + Na)$^+$; IR (KBr) υ_{max} (cm^{-1}) 3297, 3079, 3032, 1892, 1640, 1559, 1499, 1430, 1293, 1252, 1201, 1142, 1105, 962, 849, 816, 653, 506, 455.

1-(2,4-Difluorophenyl)-3-(*p*-tolyl)thiourea (94)
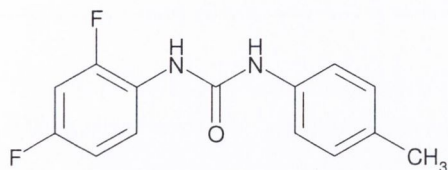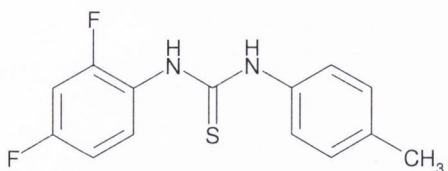
94 Was synthesised according to **Procedure 1(ii)** using *p*-tolyl isothiocyanate (0.44 g, 2.98 mmol) and 2,4-difluoroaniline (0.50 g, 3.87 mmol) in spectroscopic grade CHCl$_3$ (20 mL). A brown oil was obtained. On addition of Hex, the desired product was obtained as a white precipitate. Recrystallisation of the solid from Hex:CHCl$_3$ (1:1) yielded white hair-like crystals (0.28 g, 33.9%). m.p. 125 - 127 °C; Calculated for C$_{14}$H$_{12}$N$_2$SF$_2$: C, 60.42; H, 4.35; N, 10.06%; Found: C, 60.13; H, 4.24; N, 9.95%; δ_H (400 MHz, (CD$_3$)$_2$SO) 9.87 (1H, br s, N$\underline{H}$), 9.30 (1H, br s, N$\underline{H}$'), 7.52 (1H, d, *J* = 6.2 Hz, Ar-$\underline{H}$6), 7.48 (2H, d, *J* = 7.5 Hz, Ar-$\underline{H}$2', Ar-$\underline{H}$6'), 7.32 (3H, m, Ar-$\underline{H}$5, Ar-$\underline{H}$3', Ar-$\underline{H}$5'), 7.07 (1H, s, Ar-$\underline{H}$3), 2.28 (3H, s, Ar-C$\underline{H}_3$); δ_C (100 MHz, (CD$_3$)$_2$SO) 180.9, 160.0 (d, J_{C-F} = 243.4 Hz), 139.7, 136.5, 134.1, 130.3 (d, J_{C-F} = 11.6 Hz), 129.7 (dd, J_{C-F} = 144.2 Hz, 11.3 Hz),

129.0, 124.0, 111.0 (d, J_{C-F} = 21.3 Hz), 104.2 (app t, J_{C-F} = 25.2 Hz), 20.5; δ_F (376 MHz, $(CD_3)_2SO$) -113.22 (Ar-$\underline{F}$), -116.93 (Ar-$\underline{F}$); MS (MeOH, ES$^+$) m/z 279 (M + H)$^+$, 301 (M + Na)$^+$; IR (KBr) υ_{max} (cm^{-1}) 3217, 3033, 2986, 1898, 1546, 1514, 1363, 1312, 1213, 1140, 1097, 969, 852, 815, 614, 498.

1,3-*Bis*-(2,4-difluorophenyl)urea (95)
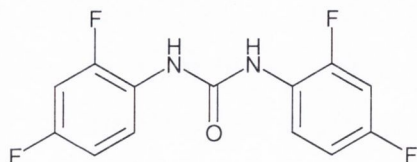
95 Was synthesised according to **Procedure 1(ii)** using 2,4-difluorophenyl isocyanate (0.46 g, 2.98 mmol) and 2,4-difluoroaniline (0.50 g, 3.87 mmol) in spectroscopic grade CHCl$_3$ (20 mL). A white precipitate was obtained. Recrystallisation of the solid from CHCl$_3$:MeOH (7:1) yielded a pure sample (0.73 g, 91.3%). m.p. 262 - 264 °C; Calculated for $C_{13}H_8N_2OF_4$: C, 54.94; H, 2.84; N, 9.86%; Found: C, 54.74; H, 2.77; N, 9.70%; δ_H (400 MHz, $(CD_3)_2SO$) 8.93 (2H, br s, N$\underline{H}$), 8.12 (2H, dd, J = 9.6 Hz, Ar-$\underline{H}3$), 7.31 (2H, dd, J = 8.8 Hz, Ar-$\underline{H}6$), 7.04 (2H, d, J = 9.6 Hz, Ar-$\underline{H}5$); δ_C (100 MHz, $(CD_3)_2SO$) 156.8 (dd, J_{C-F} = 241.2 Hz, 11.6 Hz), 152.2, 152.0 (dd, J_{C-F} = 243.4 Hz, 12.6 Hz), 123.9 (dd, J_{C-F} = 10.6 Hz, 3.9 Hz), 121.7 (d, J_{C-F} = 8.7 Hz), 111.1 (dd, J_{C-F} = 21.3 Hz, 2.9 Hz), 103. 8 (app t, J_{C-F} = 23.7 Hz); δ_F (376 MHz, $(CD_3)_2SO$) -118.58 (Ar-$\underline{F}$), -125.43 (Ar-$\underline{F}$); MS (MeOH, ES$^+$) m/z 285 (M + H)$^+$, 307 (M + Na)$^+$; IR (KBr) υ_{max} (cm^{-1}) 3287, 3083, 2782, 1876, 1647, 1570, 1499, 1430, 1294, 1259, 1232, 1198, 1144, 1107, 965, 851, 816, 650, 554, 450.

1,3-*Bis*-(2,4-difluorophenyl)thiourea (96)
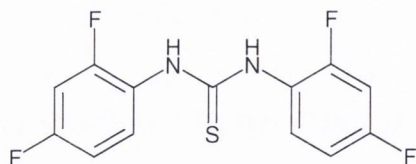
96 Was synthesised according to **Procedure 1(ii)** using 2,4-difluorophenyl isothiocyanate (0.51 g, 2.98 mmol) and 2,4-difluoroaniline (0.50 g, 3.87 mmol) in spectroscopic grade CHCl$_3$ (20 mL). A cream-coloured solid was obtained. Recrystallisation of the solid from Hex:CHCl$_3$ (1:1) yielded white hair-like crystals (0.37 g, 41.7%). m.p. 156 - 158 °C; Calculated for $C_{13}H_8N_2SF_4$: C, 52.00; H, 2.69; N, 9.33%; Found: C, 51.82; H, 2.56; N, 9.21%; δ_H (400 MHz, $(CD_3)_2SO$) 9.58 (2H, br s, N$\underline{H}$), 7.55 (1H, d, J = 8.5 Hz, Ar-$\underline{H}6$), 7.53 (1H, d, J = 8.5 Hz, Ar-$\underline{H}6$), 7.33 (2H, m, Ar-$\underline{H}5$), 7.09 (1H, d, J = 6.5 Hz, Ar-$\underline{H}3$), 7.08 (1H, d, J = 6.5 Hz, Ar-$\underline{H}3$); δ_C (100 MHz, $(CD_3)_2SO$) 182.4, 160.3 (dd, J_{C-F} = 243.4 Hz, 11.6 Hz), 156.9 (dd, J_{C-F} = 247.2 Hz, 13.6 Hz), 130.4 (d, J_{C-F} = 9.7 Hz), 123.5 (d, J_{C-F} = 11.6

Hz), 111.2 (dd, J_{C-F} = 22.2 Hz, 2.9 Hz), 104.4 (t, J_{C-F} = 25.4 Hz); δ_F (376 MHz, $(CD_3)_2SO$) -112.70 (Ar-$\underline{F}$), -116.87 (Ar-$\underline{F}$); MS (MeOH, ES$^+$) m/z 301 (M + H)$^+$, 323 (M + Na)$^+$; IR (KBr) υ_{max} (cm^{-1}) 3234, 3099, 3020, 2804, 1913, 1611, 1571, 1528, 1433, 1333, 1272, 1143, 1092, 966, 912, 850, 821, 793, 723, 655, 608, 555, 534, 465, 438.

1,3-*Bis*-(*p*-tolyl)urea (97)

97 Was synthesised according to **Procedure 1(i)** using *p*-tolyl isocyanate (0.48 g, 3.59 mmol) and *p*-tolylaniline (0.50 g, 4.67 mmol) in spectroscopic grade CHCl$_3$ (30 mL). A white precipitate was obtained. Recrystallisation of the solid from CHCl$_3$:MeOH (1:20) yielded white hair-like crystals (0.85 g, 98.8%). m.p. 271 - 273 °C (lit.,[202] 271 °C); Calculated for C$_{15}$H$_{16}$N$_2$O: C, 74.97; H, 6.71; N, 11.66%; Found: C, 74.88; H, 6.66; N, 11.69%; δ_H (400 MHz, $(CD_3)_2SO$) 8.52 (2H, br s, N$\underline{H}$), 7.34 (4H, d, J = 8.2 Hz, Ar-$\underline{H2}$, Ar-$\underline{H6}$), 7.08 (4H, d, J = 8.2 Hz, Ar-$\underline{H3}$, Ar-$\underline{H5}$), 2.24 (6H, s, Ar-C$\underline{H}_3$); δ_C (100 MHz, $(CD_3)_2SO$) 152.6, 137.3, 130.5, 129.2, 118.2, 20.3; MS (MeOH, ES$^+$) m/z 241 (M + H)$^+$, 263 (M + Na)$^+$; IR (KBr) υ_{max} (cm^{-1}) 3303, 3077, 2994, 2914, 2858, 2579, 1896, 1788, 1640, 1566, 1515, 1404, 1308, 1238, 1108, 815, 780, 633, 505.

1,3-*Bis*-(*p*-tolyl)thiourea (98)
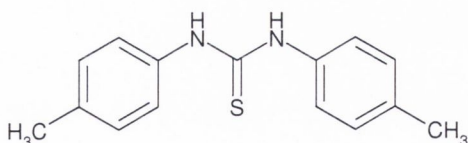
98 Was synthesised according to **Procedure 1(ii)** using *p*-tolyl isothiocyanate (0.54 g, 3.59 mmol) and *p*-tolylaniline (0.50 g, 4.67 mmol) in spectroscopic grade CHCl$_3$ (30 mL). A cream-coloured solid was obtained. Recrystallisation of the solid from CHCl$_3$:MeOH (10:1) yielded a pure sample (0.92 g, 99.5%). m.p. 179 - 181 °C (lit.,[203] 180 - 181 °C); HRMS (MeOH, ES$^+$): Calculated for C$_{15}$H$_{17}$N$_2$S: (M + H)$^+$ m/z = 257.1112; Found: 257.0735; δ_H (400 MHz, $(CD_3)_2SO$) 9.65 (2H, br s, N$\underline{H}$), 7.38 (4H, d, J = 8.0 Hz, Ar-$\underline{H2}$, Ar-$\underline{H6}$), 7.15 (4H, d, J = 8.0 Hz, Ar-$\underline{H3}$, Ar-$\underline{H5}$), 2.30 (6H, s, Ar-C$\underline{H}_3$); δ_C (100 MHz, $(CD_3)_2SO$) 179.6, 136.9, 133.6, 128.9, 123.9, 20.6; MS (MeOH, ES$^+$) m/z 257 (M + H)$^+$, 279 (M + Na)$^+$; IR (KBr) υ_{max} (cm^{-1}) 3147, 2935, 2620, 1901, 1642, 1588, 1553, 1488, 1336, 1245, 1136, 810, 704, 530, 497.

1,3-*Bis*-(2-fluorophenyl)urea (99)
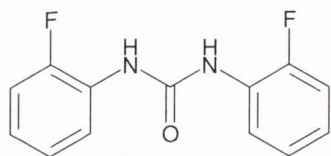
99 Was synthesised according to **Procedure 1(i)** using 2-fluorophenyl isocyanate (0.62 g, 4.50 mmol) and 2-fluoroaniline (0.50 g, 4.50 mmol) in spectroscopic grade CHCl$_3$ (20 mL). A white precipitate was isolated as the desired product (0.79 g, 70.1%). m.p. 231 - 232 °C (lit.,[204] 240 - 242 °C); Calculated for C$_{13}$H$_{10}$N$_2$OF$_2$: C, 62.90; H, 4.06; N, 11.29%; Found: C, 62.82; H, 4.02; N, 11.05%; δ_H (400 MHz, (CD$_3$)$_2$SO) 9.07 (2H, br s, N$\underline{H}$), 8.21 (2H, t, J = 8.5 Hz, Ar-$\underline{H5}$), 7.24 (2H, dd, J = 8.5 Hz, 8.0 Hz, Ar-$\underline{H3}$), 7.15 (2H, t, J = 7.5 Hz, Ar-$\underline{H4}$), 7.01 (2H, m, Ar-$\underline{H6}$); δ_C (100 MHz, (CD$_3$)$_2$SO) 152.0, 151.9 (d, J_{C-F} = 240.5 Hz), 127.4 (d, J_{C-F} = 10.6 Hz), 124.5 (d, J_{C-F} = 2.9 Hz), 122.5 (d, J_{C-F} = 6.8 Hz), 120.5, 115.0 (d, J_{C-F} = 18.4 Hz); δ_F (376 MHz, (CD$_3$)$_2$SO) -130.29 (Ar-$\underline{F}$); IR (KBr) υ_{max} (cm^{-1}) 3287, 1646, 1615, 1602, 1558, 1505, 1489, 1456, 1306, 1286, 1260, 1233, 1202, 1157, 1105, 1050, 1033, 946, 909, 849, 793, 753, 660.

1,3-*Bis*-(2-fluorophenyl)thiourea (100)
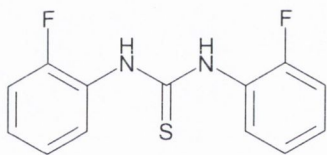
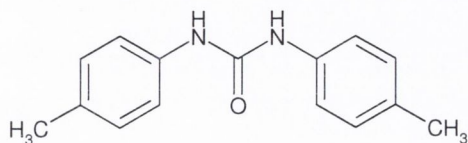**100** Was synthesised according to **Procedure 1(ii)** using 2-fluorophenyl isothiocyanate (1.38 g, 9.00 mmol) and 2-fluoroaniline (1.01 g, 9.00 mmol) in dry CHCl$_3$ (20 mL). The reaction mixture was reduced and the residue Was collected and washed with CHCl$_3$, yielding the desired product as a white solid (1.43 g, 60.1%). m.p. 143 - 145 °C; Calculated for C$_{13}$H$_{10}$N$_2$SF$_2$: C, 59.08; H, 3.81; N, 10.60%; Found: C, 58.89; H, 3.79; N, 10.54%; δ_H (400 MHz, (CD$_3$)$_2$SO) 9.71 (2H, br s, N$\underline{H}$), 7.67 (2H, t, J = 7.8 Hz, Ar-$\underline{H5}$), 7.27 (4H, m, Ar-$\underline{H3}$, Ar-$\underline{H4}$), 7.20 (2H, m, Ar-$\underline{H6}$); δ_C (100 MHz, (CD$_3$)$_2$SO) 181.5, 156.3 (d, J_{C-F} = 244.4 Hz), 128.6, 127.5 (d, J_{C-F} = 8.7 Hz), 126.9 (d, J_{C-F} = 11.6 Hz), 124.2 (d, J_{C-F} = 2.9 Hz), 115.8 (d, J_{C-F} = 19.3 Hz); δ_F (376 MHz, (CD$_3$)$_2$SO) -122.53 (Ar-$\underline{F}$); MS (MeOH, ES$^+$) m/z 265 (M + H)$^+$, 342 (M+K)$^+$; IR (KBr) υ_{max} (cm^{-1}) 3352, 3141, 2961, 1588, 1536, 1505, 1488, 1454, 1346, 1299, 1286, 1264, 1250, 1218, 1190, 1147, 1098, 1028, 943, 928, 870, 857, 819, 792, 762, 748, 723, 692.

1,3-*Bis*-(2-trifluoromethylphenyl)urea (101)

101 Was synthesised according to **Procedure 1(i)** using 2-trifluoromethylphenylisocyanate (0.58 g, 3.10 mmol) and 2-trifluoromethylaniline (0.50 g, 3.10 mmol) in spectroscopic grade CHCl$_3$ (35 mL). A white precipitate was isolated as the desired product (0.83 g, 76.9%). m.p. 231 - 232 °C; Calculated for C$_{15}$H$_{10}$N$_2$OF$_6$: C, 51.74; H, 2.89; N, 8.04%; Found: C, 51.76; H, 2.90; N, 7.76%; HRMS (MeOH, ES$^+$): Calculated for C$_{15}$H$_{10}$N$_2$OF$_6$Na: 371.0595 (M + Na)$^+$; Found: 371.0584; δ_H (400 MHz, (CD$_3$)$_2$SO) 8.71 (2H, br s, N$\underline{H}$), 7.85 (2H, d, J = 8.5 Hz, Ar-$\underline{H3}$), 7.69 (2H, d, J = 8.0 Hz, Ar-$\underline{H6}$), 7.64 (2H, app t, J = 7.8 Hz, Ar-$\underline{H4}$), 7.31 (2H, app t, J = 7.5 Hz, Ar-$\underline{H5}$); δ_C (100 MHz, (CD$_3$)$_2$SO) 153.2, 136.1, 132.8, 127.0, 125.9 (q, J_{C-F} = 5.2 Hz), 124.3, 123.9 (q, J_{C-F} = 271.1 Hz), 121.0 (q, J_{C-F} = 29.0 Hz); δ_F (376 MHz, (CD$_3$)$_2$SO) -60.14 (Ar-C$\underline{F}_3$); IR (KBr) υ_{max} (cm^{-1}) 3297, 1644, 1614, 1593, 1554, 1496, 1457, 1319, 1282, 1240, 1172, 1113, 1059, 1038, 954, 911, 767, 751, 744, 714.

1,3-*Bis*-(2-trifluoromethylphenyl)thiourea (102)

102 Was synthesised according to **Procedure 1(ii)** using 2-trifluoromethylphenylisothiocyanate (0.11 g, 0.53 mmol) and 2-trifluoromethylaniline (0.09 g, 0.53 mmol) in spectroscopic grade CHCl$_3$ (30 mL). The reaction mixture was reduced and the residue was collected and washed with CHCl$_3$, yielding the desired product as an off-white crystalline solid (0.09 g, 47.4%). m.p. 156 - 158 °C; Calculated for C$_{15}$H$_{10}$N$_2$SF$_6$: C, 49.45; H, 2.77; N, 7.69%; Found: C, 49.38; H, 2.75; N, 7.47%; δ_H (400 MHz, (CD$_3$)$_2$SO) 9.60 (2H, br s, N$\underline{H}$), 7.75 (2H, d, J = 7.5 Hz, Ar-$\underline{H3}$), 7.70 (2H, app t, J = 7.5 Hz, Ar-$\underline{H4}$), 7.58 (2H, d, J = 7.5 Hz, Ar-$\underline{H6}$), 7.49 (2H, app t, J = 7.5 Hz, Ar-$\underline{H5}$); δ_C (100 MHz, (CD$_3$)$_2$SO) 183.3, 137.0, 132.6, 132.3, 127.6, 126.1, 125.7 (q, J_{C-F} = 17.4 Hz), 123.5 (q, J_{C-F} = 271.4 Hz); δ_F (376 MHz, (CD$_3$)$_2$SO) -60.13 (Ar-C$\underline{F}_3$); IR (KBr) υ_{max} (cm^{-1}) 3380, 3124, 2954, 1603, 1590, 1532, 1507, 1481, 1455, 1359, 1315, 1276, 1257, 1226, 1205, 1160, 1169, 1135, 1107, 1057, 1037, 967, 930, 876, 853, 796, 774, 766, 760, 722, 657.

1,3-*Bis*-(*o*-tolyl)thiourea (103)
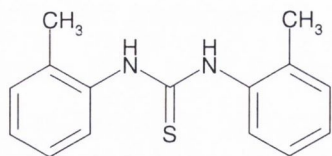
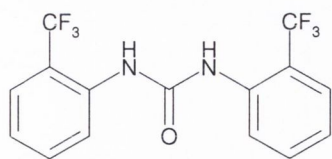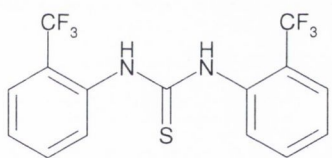**103** Was synthesised according to **Procedure 1(ii)** using 2-tolyl isothiocyanate (1.39 g, 9.33 mmol) and *o*-toluidine (1.01 g, 9.33 mmol) in spectroscopic grade CHCl$_3$ (20 mL). The reaction mixture was reduced and the residue was collected and washed with CHCl$_3$, yielding the desired product as a white crystalline solid (1.28 g, 53.6%). m.p. 158 - 160 °C; Calculated for C$_{15}$H$_{16}$N$_2$S: C, 70.28; H, 6.29; N, 10.93%; Found: C, 69.98; H, 6.24; N, 10.83%; HRMS (MeOH, ES$^+$): Calculated for C$_{15}$H$_{16}$N$_2$SNa: 279.0932 (M + Na)$^+$; Found: 279.0923; δ_H (400 MHz, (CD$_3$)$_2$SO) 9.18 (2H, br s, N$\underline{H}$), 7.26 (4H, m, Ar-$\underline{H}$4, Ar-$\underline{H}$6), 7.18 (4H, m, Ar-$\underline{H}$3, Ar-$\underline{H}$5), 2.26 (6H, s, Ar-C$\underline{H}_3$); δ_C (100 MHz, (CD$_3$)$_2$SO) 181.1, 137.8, 135.1, 130.3, 128.3, 126.6, 126.2, 17.8; MS (MeOH, ES$^+$) *m/z* 279 (M + Na)$^+$; IR (KBr) υ_{max} (cm^{-1}) 3337, 3131, 2950, 2176, 1580, 1525, 1488, 1460, 1379, 1337, 1289, 1262, 1239, 1211, 1191, 1154, 1111, 1040, 954, 921, 857, 782, 767, 756, 740, 719, 690.

1,3-*Bis*-(2,4-dimethylphenyl)urea (104)
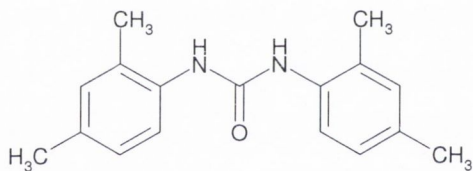
104 Was synthesised according to **Procedure 1(i)** using 2,4-dimethylphenyl isocyanate (0.61 g, 4.13 mmol) and 2,4-dimethylaniline (0.50 g, 4.13 mmol) in spectroscopic grade CHCl$_3$ (35 mL). A white precipitate was isolated as the desired product (0.88 g, 79.3%). m.p. 278 - 280 °C ; Calculated for C$_{17}$H$_{20}$N$_2$O: C, 76.09; H, 7.51; N, 10.44%; Found: C, 75.81; H, 7.45; N, 10.35%; HRMS (MeOH, ES$^+$): Calculated for C$_{17}$H$_{20}$N$_2$ONa: 291.1473 (M + Na)$^+$; Found: 291.1462; δ_H (400 MHz, (CD$_3$)$_2$SO) 8.08 (2H, br s, N$\underline{H}$), 7.62 (2H, s, Ar-$\underline{H}$6), 6.99 (2H, s, Ar-$\underline{H}$3), 6.93 (2H, s, Ar-$\underline{H}$5), 2.22 (6H, s, Ar-C$\underline{H}_3$); δ_C (100 MHz, (CD$_3$)$_2$SO) 153.1, 134.9, 131.5, 130.7, 127.9, 126.5, 121.7, 20.3, 17.9; MS (MeOH, ES$^+$) *m/z* 291 (M + Na)$^+$; IR (KBr) υ_{max} (cm^{-1}) 3294, 1639, 1614, 1590, 1556, 1503, 1450, 1410, 1298, 1269, 1218, 1157, 1123, 1052, 1035, 1014, 932, 879, 818, 726, 672.

5.7 Chapter 3 Experimental Details

1,3-*Bis*-(anthracen-9-ylmethyl)thiourea (109)
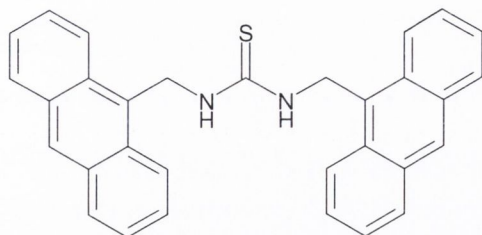
109 Was synthesised according to **Procedure 4**, using **118** (0.12 g, 0.56 mmol) and **119** (0.12 g, 0.51 mmol) in the presence of triethylamine (2 drops) in dry DCM (20 mL). The precipitate formed was isolated, yielding the desired product as a yellow solid (0.62 g, 78.0%). m.p. 260 - 262 °C; Calculated for $C_{31}H_{24}N_2S.H_2O$: C, 78.45; H, 5.52; N, 5.90%; Found: C, 78.40; H, 5.00; N, 5.82%; δ_H (400 MHz, $(CD_3)_2SO$) 8.61 (2H, s, An-H10), 8.43 (4H, d, J = 8.5 Hz, An-H1, An-H8), 8.11 (4H, d, J = 5.0 Hz, An-H4, An-H5), 7.60 (10H, m, thiourea-NH, An-H2, An-H3, An-H6, An-H7), 5.68 (4H, d, J = 3.5 Hz, CH2); δ_C (100 MHz, $(CD_3)_2SO$) 131.0, 129.9, 128.9, 127.6, 126.5, 125.3,124.3, 40.0, 39.8; IR (KBr) υ_{max} (cm^{-1}) 3373, 3246, 3049, 2900, 1624, 1543, 1329, 1261, 1183, 889, 729. ESMS was not possible due to fragmentation.

α,α'-*Bis*-[(anthracen-9-ylmethylcarbamothioyl)amino]-*p*-xylene (110)
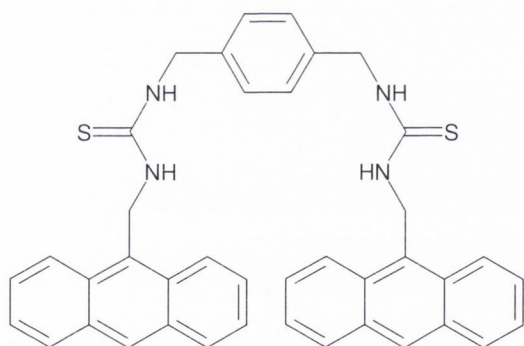
110 Was synthesised according to **Procedure 4**, using **119** (0.52 g, 2.24 mmol) and α,α'-diamino-*p*-xylene **120** (0.17 g, 1.23 mmol) in the presence of triethylamine (2 drops) in dry DCM (25 mL). The precipitate formed was isolated and washed with CHCl3, yielding the desired product as a yellow solid (0.55 g, 78.0%). m.p. 239 - 240 °C; Calculated for $C_{40}H_{34}N_4S_2.H_2O$: C, 73.59; H, 5.56; N, 8.58%; Found: C, 73.12; H, 5.23; N, 9.32%; δ_H (400 MHz, $(CD_3)_2SO$) 8.65 (2H, br s, An-H10), 8.42 (4H, d, J = 9.0 Hz, An-H1, An-H8), 8.15 (4H, d, J = 8.5 Hz, An-H4, An-H5), 7.84 (2H, m, An-CH2NH), 7.62 (10H, m, Ar-CH2NH, An-H2, An-H3, An-H6, An-H7), 7.21 (4H, m, Ar-H), 5.64 (4H, br s, An-CH2), 4.68 (4H, br s, Ar-CH2); δ_C (100 MHz, $(CD_3)_2SO$) 137.8, 131.1, 130.0, 129.0, 127.6, 127.2, 127.1, 126.5, 125.3, 124.4, 45.2, 40.8; IR (KBr) υ_{max} (cm^{-1}) 3367, 3283, 3053, 2921, 1542, 1333, 1268, 889, 730; ESMS was not possible due to fragmentation.

185

1-(Anthracen-9-ylmethyl)-3-(2-[(anthracen-9-ylmethylcarbamothioyl)amino]-cyclohexyl)thiourea (111)
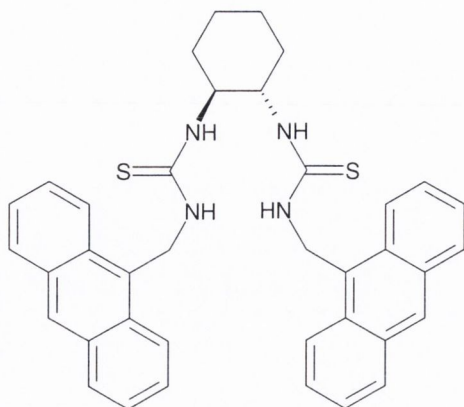
111 Was synthesised according to **Procedure 4**, using **119** (0.79 g, 3.41 mmol) and *trans*-1,2-diaminocyclohexane **121** (0.21 g, 1.88 mmol) in the presence of triethylamine (2 drops) in dry CHCl$_3$ (10 mL). The precipitate formed was isolated and washed with CHCl$_3$, yielding the desired product as a yellow solid (0.45 g, 42.8%). m.p. 244 - 245 °C; Calculated for C$_{38}$H$_{36}$N$_4$S$_2$.H$_2$O: C, 72.35; H, 6.07; N, 8.88%; Found: C, 72.12; H, 5.99; N, 9.15%; δ_H (400 MHz, (CD$_3$)$_2$SO) 8.57 (2H, br s, An-H10), 8.25 (4H, d, J = 8.0 Hz, An-H1, An-H8), 8.06 (4H, d, J = 8.5 Hz, An-H4, An-H5), 7.68 (1H, br s, An-CH$_2$NH), 7.45 (8H, m, An-H2, An-H3, An-H6, An-H7), 7.16 (2H, br s, Ar-CH$_2$NH), 5.46 (4H, br s, An-CH$_2$), 4.01 (2H, br s, Cyclohex-H), 2.06 (2H, br s, Cyclohex-CH$_2$), 1.50 (2H, br s, Cyclohex-CH$_2$), 1.14 (2H, br s, Cyclohex-CH$_2$), 0.98 (2H, br s, Cyclohex-CH$_2$); δ_C (100 MHz, (CD$_3$)$_2$SO) 130.0, 129.0, 127.6, 126.5, 125.3, 124.4, 54.8, 32.9, 24.4, 23.9; IR (KBr) υ_{max} (cm^{-1}) 3269, 3056, 2937, 2851, 2366, 1937, 1622, 1549, 1474, 1444, 1331, 1289, 1272, 1158, 1074, 952, 889, 884, 728; ESMS was not possible due to fragmentation.

1,3-*Bis*-[(*R*)-1-(naphthalen-1-yl)ethyl]thiourea (112)
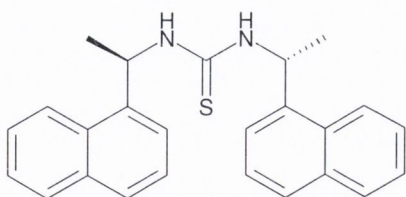
112 Was synthesised according to **Procedure 1(ii)**, using (*R*)-(+)-1-(1-naphthyl)ethylamine **122** (0.19 mL, 1.19 mmol) and **124** (0.25 g, 1.19 mmol) in dry DCM (50 mL). The desired product was obtained as an off-white crystalline solid (0.23 g, 51.0%). m.p. 84 - 86 °C; [α]$_D^{23}$ = -89.7 (c 0.2, (CH$_3$)$_2$SO); Calculated for C$_{25}$H$_{24}$N$_2$S.0.5H$_2$O: C, 76.30; H, 6.40; N, 7.12%; Found: C, 76.87; H, 6.24; N, 6.90%; HRMS (MeOH, ES$^+$): Calculated for C$_{25}$H$_{25}$N$_2$S: 385.1738 (M + H)$^+$; Found: 385.1721; δ_H (400 MHz, (CD$_3$)$_2$SO) 8.18 (2H, d, J = 8.0 Hz, Nap-H8), 7.96 (2H, d, J = 8.0 Hz, Nap-H5), 7.85 (2H, d, J = 5.5 Hz, Nap-H4), 7.79 (2H, br s, thiourea-NH), 7.54 (8H, m, Nap-H2, Nap-H3, Nap-H6, Nap-H7), 6.22 (2H, br s, CH$_3$CH), 1.53 (6H, d, J = 6.5 Hz, CH$_3$); δ_C (100 MHz, (CD$_3$)$_2$SO) 140.0, 133.4, 130.6, 128.7, 127.5, 126.3, 125.7, 125.5, 123.4, 122.5,

48.8, 21.2; MS (MeOH, ES$^+$) m/z 385 (M + H)$^+$, 407 (M + Na)$^+$; IR (KBr) υ_{max} (cm^{-1}) 3223, 2973, 1527, 1447, 1328, 1237, 1171, 1113, 1076, 1023, 861, 799, 774, 727.

1,3-*Bis*-[(*S*)-1-(naphthalen-1-yl)ethyl]thiourea (113)
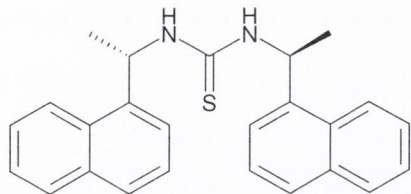
113 Was synthesised according to **Procedure 1(ii)**, using (*S*)-(-)-1-(1-naphthyl)ethylamine **123** (0.58 mL, 3.56 mmol) and **125** (0.76 g, 3.56 mmol) in dry DCM (50 mL). The desired product was obtained as an off-white crystalline solid (0.56 g, 41.1%). m.p. 84 - 86 °C; [α]$_D^{23}$ = +83.2 (c 0.2, (CH$_3$)$_2$SO); Calculated for C$_{25}$H$_{24}$N$_2$S.½H$_2$O: C, 76.30; H, 6.40; N, 7.12%; Found: C, 76.79; H, 6.22; N, 6.86%; HRMS (MeOH, ES$^+$): Calculated for C$_{25}$H$_{25}$N$_2$S: 385.1738 (M + H)$^+$; Found: 385.1755; δ$_H$ (400 MHz, (CD$_3$)$_2$SO) 8.14 (2H, d, J = 8.0 Hz, Nap-H8), 7.95 (2H, d, J = 8.0 Hz, Nap-H5), 7.85 (2H, d, J = 5.5 Hz, Nap-H4), 7.78 (2H, br s, thiourea-NH), 7.54 (8H, m, Nap-H2, Nap-H3, Nap-H6, Nap-H7), 6.21 (2H, br s, CH$_3$CH), 1.53 (6H, d, J = 6.5 Hz, CH$_3$); δ$_C$ (100 MHz, (CD$_3$)$_2$SO) 180.9, 139.7, 133.4, 130.6, 128.7, 127.5, 126.3, 125.7, 125.5, 123.4, 122.5, 48.8, 21.2; MS (MeOH, ES$^+$) m/z 385 (M + H)$^+$, 407 (M + Na)$^+$; IR (KBr) υ_{max} (cm^{-1}) 3236, 3046, 2972, 1597, 1526, 1447, 1330, 1236, 1171, 1114, 1076, 1023, 861, 799, 774, 728.

1-[(*R*)-1-(Naphthalen-1-yl)ethyl]-3-[(*S*)-1-(napthalen-1-yl)ethyl]thiourea (114)
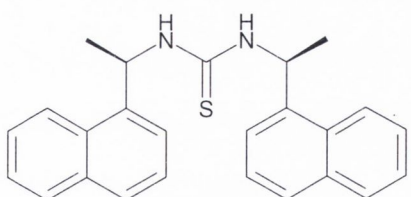
114 Was synthesised according to **Procedure 1(ii)**, using (*R*)-(+)-1-(1-naphthyl)ethylamine **122** (0.19 mL, 1.19 mmol) and **125** (0.25 g, 1.19 mmol) in dry DCM (50 mL). The desired product was obtained as an off-white crystalline solid (0.28 g, 61.7%). m.p. 153 - 155 °C; Calculated for C$_{25}$H$_{24}$N$_2$S.½H$_2$O: C, 76.30; H, 6.40; N, 7.12%; Found: C, 76.60; H, 6.21; N, 6.92%; HRMS (MeOH, ES$^+$): Calculated for C$_{25}$H$_{24}$N$_2$S.Na: 407.1558 (M + Na)$^+$; Found: 407.1559; δ$_H$ (400 MHz, (CD$_3$)$_2$SO) 8.14 (2H, d, J = 8.0 Hz, Nap-H8), 7.94 (2H, d, J = 9.0 Hz, Nap-H5), 7.85 (2H, d, J = 9.0 Hz, Nap-H4), 7.69 (2H, d, J = 7.5 Hz, thiourea-NH), 7.52 (8H, m, Nap-H2, Nap-H3, Nap-H6, Nap-H7), 6.18 (2H, t, J = 7.0 Hz, CH$_3$CH), 1.58 (6H, d, J = 6.5 Hz, CH$_3$); δ$_C$ (100 MHz, (CD$_3$)$_2$SO) 180.8, 139.3, 133.4, 130.8, 128.6, 127.7, 126.3, 125.7, 125.4, 123.6, 122.5, 48.73, 20.6; MS (MeOH, ES$^+$) m/z 407 (M + Na)$^+$; IR (KBr) υ_{max} (cm^{-1}) 3194,

3046, 2974, 1599, 1541, 1447, 1328, 1254, 1171, 1109, 1074, 1031, 1000, 864, 797, 773, 725, 708.

9-(Hydroxymethyl)anthracene (116)
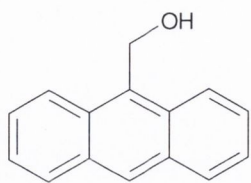
Sodium borohydride (2.75 g, 72.73 mmol) was carefully added to a solution of 9-anthraaldehyde **115** (10.00 g, 48.49 mmol) in dry MeOH (150 mL) at 0 °C. The reaction mixture was left stirring at room temperature for 18 h. MeOH (50 mL) was then added to the reaction mixture and left to stir for another 20 min. On addition of water (200 mL), a precipitate formed, which was isolated by filtration. The crude product was recrystallised from ethyl acetate, yielding **116** as yellow crystals (5.72 g, 56.6%). δ_H (400 MHz, $CDCl_3$) 8.49 (1H, s, An-$\underline{H}$10), 8.49 (2H, d, J = 9.0 Hz, An-$\underline{H}$1, An-$\underline{H}$8), 8.07 (2H, d, J = 8.5 Hz, An-$\underline{H}$4, An-$\underline{H}$5), 7.61 (2H, m, An-$\underline{H}$2, An-$\underline{H}$7), 7.52 (2H, m, An-$\underline{H}$3, An-$\underline{H}$6), 5.69 (2H, s, C$\underline{H}_2$), 1.81 (1H, br s, O$\underline{H}$); δ_C (100 MHz, $(CD_3)_2SO$) 131.1, 130.5, 129.8, 128.7, 128.0, 126.0, 124.7, 123.4, 57.0; IR (KBr) υ_{max} (cm^{-1}) 3422, 3044, 2950, 2910, 2162, 2026, 1943, 1811, 1766, 1721, 1688, 1622, 1524, 1505, 1476, 1445, 1436, 1404, 1386, 1344, 1327, 1304, 1273, 1256, 1229, 1178, 1157, 1143, 1045, 992, 977, 905, 882, 858, 841, 788, 761, 732, 698.

9-(Chloromethyl)anthracene (117)
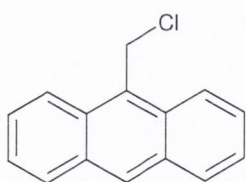
2,4,6-Trichloro-[1,3,5]-triazine (4.65 g, 25.21 mmol) was added to DMF (15 mL), forming a cream-coloured solid adduct after stirring at room temperature for 10 min. 9-(Hydroxymethyl) anthracene **116** (5.00 g, 24.01 mmol) was dissolved in dry DCM (60 mL) and added to the adduct. The reaction mixture was left stirring at room temperature for 18 h. Water was then added and the organic layer was washed with 1 M Na_2CO_3 solution (2 × 40 mL), 1 M HCl (2 × 40 mL), brine (2 × 30 mL) and water (30 mL). This was then dried over Na_2SO_4 and the filtrate was reduced to yield **117** as a yellow solid (4.50 g, 82.6%). δ_H (400 MHz, $CDCl_3$) 8.52 (1H, s, An-$\underline{H}$10), 8.36 (2H, d, J = 9.0 Hz, An-$\underline{H}$1, An-$\underline{H}$8), 8.07 (2H, d, J = 8.5 Hz, An-$\underline{H}$4, An-$\underline{H}$5), 7.67 (2H, m, An-$\underline{H}$2, An-$\underline{H}$7), 7.55 (2H, m, An-$\underline{H}$3, An-$\underline{H}$6), 5.65 (2H, s, C$\underline{H}_2$); δ_C (100 MHz, $(CD_3)_2SO$) 131.0, 129.5, 129.1, 129.0, 128.2, 127.0, 125.4, 123.9, 39.4; IR (KBr) υ_{max} (cm^{-1}) 3058, 2414, 2161, 2028, 1940, 1918, 1841, 1811, 1794, 1768, 1724, 1707, 1683, 1623, 1563,

1524, 1494, 1463, 1450, 1390, 1338, 1282, 1260, 1243, 1191, 1182, 1163, 1155, 1132, 1107, 1049, 1023, 956, 975, 895, 883, 864, 839, 801, 788, 751, 728, 693, 674.

9-(Aminomethyl)anthracene (118)
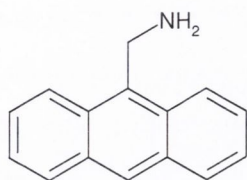
9-(Chloromethyl)anthracene **117** (4.50 g, 19.85 mmol) was dissolved in dry $CHCl_3$ (50 mL). This solution was added dropwise to a solution of hexamethylene tetraamine (2.78 g, 19.85 mmol) in dry $CHCl_3$ (200 mL). The reaction was refluxed for 18 h at 60 °C. A precipitate formed on cooling, which was isolated and washed with water (3 × 10 mL). The crude product was purified using $HCl:EtOH:H_2O$ (5:20:4) by heating the solution for 18 h at 70 °C. On cooling for 3 h, a yellow precipitate is formed, which is isolated to yield **118** as its HCl salt (4.84 g, 91.0%). m.p. 102 °C; δ_H (400 MHz, $(CD_3)_2SO$) 8.76 (1H, s, An-H10), 8.63 (3H, br. s, NH_3^+), 8.46 (4H, d, J = 9.0 Hz, An-H1, An-H8), 8.19 (2H, d, J = 8.5 Hz, An-H4, An-H5), 7.71 (2H, m, An-H2, An-H7), 7.61 (2H, m, An-H3, An-H6), 5.05 (2H, d, J = 5.0 Hz, CH2); δ_C (100 MHz, $(CD_3)_2SO$) 130.88, 130.22, 129.13, 129.03, 126.94, 125.48, 125.21, 124.19, 34.40; MS (MeOH, ES^+) m/z 207 $(M)^+$.

9-(Isothiocyanatomethyl)anthracene (119)
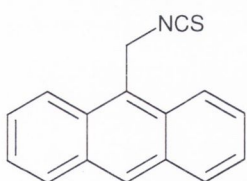
119 Was synthesised according to **Procedure 3**, using **118** (0.60 g, 2.46 mmol) and thiophosgene (0.20 mL, 2.66 mmol) in a biphasic mixture of saturated $NaHCO_3$ and THF. The crude product was isolated as an oil and was purified by silica gel chromatography using ethyl acetate:Hex (9:1) as an eluent, yielding **119** as a yellow solid (0.12 g, 20.0%). δ_H (400 MHz, $CDCl_3$) 8.55 (1H, s, An-H10), 8.26 (2H, d, J = 8.8 Hz, An-H1, An-H8), 8.09 (2H, d, J = 8.8 Hz, An-H4, An-H5), 7.65 (2H, m, An-H2, An-H7), 7.54 (2H, m, An-H3, An-H6), 5.61 (2H, s, CH2); δ_C (100 MHz, $CDCl_3$) 132.2, 130.9, 129.5, 128.9, 128.94, 126.8, 124.8, 124.1, 122.5, 40.9; ESMS was not possible due to fragmentation.

(*R*)-1-(1-Naphthyl)ethylisothiocyanate (124)
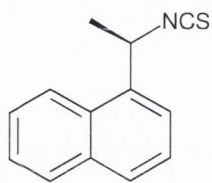
124 Was synthesised according to **Procedure 3**, using (*R*)-(+)-1-(1-naphthyl)ethylamine **122** (1.00 g, 5.84 mmol) and thiophosgene (0.67 mL, 8.76 mmol) in dry DCM (150 mL). Since the product has a low boiling point, the solvent of the filtrate obtained was allowed to evaporate naturally in the fumehood. The desired product was obtained as a brown gel-like solid (0.51 g, 40.7%). δ_H (400 MHz, (CD$_3$)$_2$SO) 7.95 (2H, m, Nap-H5, Nap-H8), 7.87 (1H, d, *J* = 8.0 Hz, Nap-H4), 7.67 (1H, d, *J* = 7.0 Hz, Nap-H2), 7.57 (2H, m, Nap-H3, Nap-H6, Nap-H7), 5.72 (1H, q, *J* = 6.7 Hz, CH$_3$CH), 1.87 (3H, d, *J* = 7.0 Hz, CH$_3$); δ_C (100 MHz, (CD$_3$)$_2$SO) 135.0, 133.4, 129.1, 128.8, 128.6, 126.4, 125.6, 125.1, 122.6, 121.8, 53.7, 23.6.

(*S*)-1-(1-Naphthyl)ethylisothiocyanate (125)
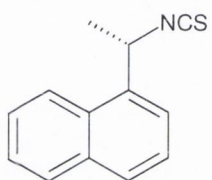
125 Was synthesised according to **Procedure 3**, using (*S*)-(-)-1-(1-naphthyl)ethylamine **123** (1.00 g, 5.84 mmol) and thiophosgene (0.67 mL, 8.76 mmol) in dry DCM (150 mL). Since the product has a low boiling point, the solvent of the filtrate obtained was allowed to evaporate naturally in the fume hood. The desired product was obtained as a brown gel-like solid (0.76 g, 60.8%). δ_H (400 MHz, (CD$_3$)$_2$SO) 7.95 (2H, t, *J* = 8.3 Hz, Nap-H5, Nap-H8), 7.87 (1H, d, *J* = 8.0 Hz, Nap-H4), 7.67 (1H, d, *J* = 7.0 Hz, Nap-H2), 7.57 (2H, m, Nap-H3, Nap-H6, Nap-H7), 5.73 (1H, q, *J* = 6.7 Hz, CH$_3$CH), 1.87 (3H, d, *J* = 6.5 Hz, CH$_3$); δ_C (100 MHz, (CD$_3$)$_2$SO) 135.0, 133.4, 129.1, 128.8, 128.5, 126.3, 125.5, 125.0, 122.6, 121.8, 53.6, 23.6.

5.8   Chapter 4 Experimental Details

2-Ethyl-6-[(4-trifluoromethylphenylthiocarbamoyl)hydrazino]-benzo[*de*]isoquinoline-1,3-dione (64)
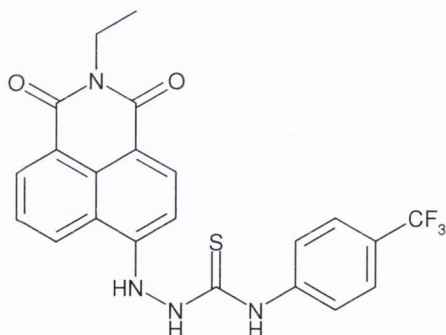
64 Was synthesised according to **Procedure 2**, using **134** (0.50 g, 1.97 mmol) and 4-trifluoromethylphenyl isothiocyanate **135** (0.40 g, 1.97 mmol) in dry MeCN (30 mL). The desired product was obtained as a brown solid (0.11 g, 12.2%). m.p. 179 °C; δ_H (400 MHz, (CD$_3$)$_2$SO)

10.36 (1H, br s, thiourea-N<u>H</u>), 10.32 (1H, br s, thiourea-N<u>H</u>), 9.92 (1H, br s, Naph-N<u>H</u>), 8.70 (1H, d, J = 7.5 Hz, Naph-<u>H7</u>), 8.52 (1H, d, J = 7.5 Hz, Naph-<u>H5</u>), 8.44 (1H, d, J = 8.2 Hz, Naph-<u>H2</u>), 7.83 (1H, dd, J = 8.9 Hz, 9.6 Hz, Naph-<u>H6</u>), 7.71 (4H, m, Ar-<u>H2</u>, Ar-<u>H3</u>, Ar-<u>H5</u>, Ar-<u>H6</u>), 6.99 (1H, d, J = 8.9 Hz, Naph-<u>H3</u>), 4.07 (2H, q, J = 6.8 Hz, C<u>H2</u>), 1.20 (3H, t, J = 6.8 Hz, C<u>H3</u>); δ_C (100 MHz, (CD$_3$)$_2$SO) 181.3, 162.8, 149.7, 142.8, 133.6, 130.9, 129.3, 128.9, 126.3, 125.8, 125.6, 125.0, 121.9, 119.5, 111.8, 105.6, 34.5, 13.3; δ_F (376 MHz, (CD$_3$)$_2$SO) -61.02 (Ar-C<u>F3</u>); MS (MeOH, ES$^+$) m/z 459 (M + H)$^+$; IR (KBr) υ_{max} (cm^{-1}) 3483, 3254, 2980, 1686, 1647, 1616, 1586, 1535, 1387, 1325, 1245, 1165, 1116, 1066, 1017, 843, 776, 756.

2-Ethyl-6-[(phenylcarbamoyl)hydrazino]-benzo[*de*]isoquinoline-1,3-dione (129)
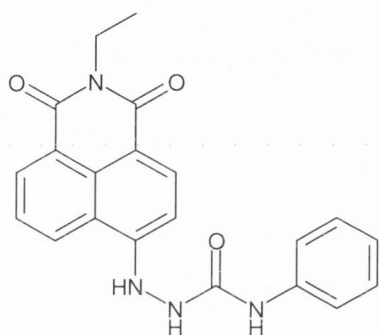
129 Was synthesised according to **Procedure 2**, using **134** (0.21 g, 0.82 mmol) and phenyl isocyanate **136** (0.11 g, 0.90 mmol) in dry MeCN (30 mL). The desired product was obtained as a dark yellow solid (0.12 g, 40.7%). m.p. 252 - 254 °C; Calculated for C$_{21}$H$_{18}$N$_4$O$_3$.(H$_2$O): C, 64.28; H, 5.14; N, 14.28%; Found: C, 64.01; H, 4.51; N, 14.48%; δ_H (400 MHz, (CD$_3$)$_2$SO) 9.60 (1H, br s, urea-N<u>H</u>), 9.03 (1H, br s, urea-N<u>H</u>), 8.73 (1H, d, J = 8.8 Hz, Naph-<u>H7</u>), 8.67 (1H, br s, Naph-<u>N</u>H), 8.50 (1H, d, J = 7.0 Hz, Naph-<u>H5</u>), 8.37 (1H, d, J = 7.9 Hz, Naph-<u>H2</u>), 7.78 (1H, t, J = 7.9 Hz, Naph-<u>H6</u>), 7.51 (2H, d, J = 7.9 Hz, Ar-<u>H2</u>, Ar-<u>H6</u>), 7.26 (2H, t, J = 7.4 Hz, Ar-<u>H3</u>, Ar-<u>H5</u>), 7.05 (1H, d, J = 8.8 Hz, Naph-<u>H3</u>), 6.97 (1H, t, J = 7.0 Hz, Ar-<u>H4</u>), 4.07 (2H, q, J = 6.7 Hz, C<u>H2</u>), 1.20 (3H, t, J = 7.0 Hz, C<u>H3</u>); δ_C (100 MHz, (CD$_3$)$_2$SO) 163.4, 162.7, 155.8, 152.6, 151.3, 139.7, 139.6, 133.7, 130.7, 128.8, 128.6, 124.8, 122.1, 121.8, 119.0, 118.1, 110.7, 105.1, 34.4, 13.3; IR (KBr) υ_{max} (cm^{-1}) 3285, 1641, 1545, 1498, 1444, 1388, 1369, 1349, 1239, 1141, 1066, 914, 876, 839, 773, 742, 691; ESMS was not possible due to fragmentation.

2-Ethyl-6-[(*p*-tolylcarbamoyl)hydrazino]-benzo[*de*]isoquinoline-1,3-dione (130)
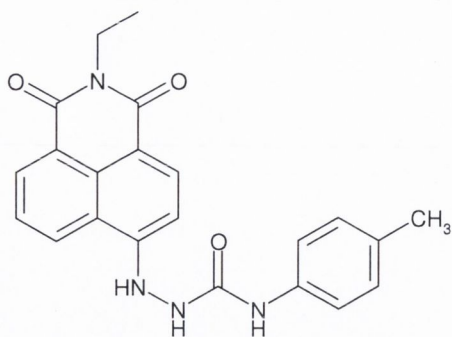
130 Was synthesised according to **Procedure 2**, using **134** (0.20, 0.78 mmol) and *p*-tolyl isocyanate **137** (0.11 g, 0.86 mmol) in dry MeCN (30 mL). The desired product was obtained as a dark yellow solid (0.16 g, 51.6%). m.p. decomposed at 310 °C; Calculated for $C_{22}H_{20}N_4O_3.\frac{1}{2}H_2O$: C, 66.49; H, 5.33; N, 14.10%; Found: C, 66.53; H, 5.00; N, 13.49%; δ_H (400 MHz, $(CD_3)_2SO$) 9.59 (1H, br s, urea-N$\underline{H}$), 8.92 (1H, br s, urea-N$\underline{H}$), 8.73 (1H, d, *J* = 7.9 Hz, Naph-$\underline{H7}$), 8.61 (1H, br s, Naph-N$\underline{H}$), 8.50 (1H, d, *J* = 7.0 Hz, Naph-$\underline{H5}$), 8.37 (1H, d, *J* = 7.9 Hz, Naph-$\underline{H2}$), 7.78 (1H, t, *J* = 7.9 Hz, Naph-$\underline{H6}$), 7.39 (2H, d, *J* = 8.8 Hz, Ar-$\underline{H2}$, Ar-$\underline{H6}$), 7.05 (3H, m, Ar-$\underline{H3}$, Ar-$\underline{H5}$, Naph-$\underline{H3}$), 4.07 (2H, q, *J* = 7.0 Hz, C$\underline{H_2}$), 2.23 (3H, s, Ar-C$\underline{H_3}$), 1.20 (3H, t, *J* = 7.0 Hz, C$\underline{H_3}$); δ_C (100 MHz, $(CD_3)_2SO$) 163.5, 162.8, 151.4, 136.9, 133.8, 130.9, 130.8, 129.2, 129.0, 125.8, 124.8, 121.9, 119.1, 110.6, 105.1, 34.4, 20.3, 13.3; IR (KBr) υ_{max} (cm^{-1}) 3295, 1641, 1580, 1543, 1434, 1390, 1370, 1350, 1310, 1243, 1143, 1066, 917, 877, 832, 774, 757; ESMS was not possible due to fragmentation.

2-Ethyl-6-[(4-trifluoromethylphenylcarbamoyl)hydrazino]-benzo[*de*]iso-quinoline-1,3-dione (131)
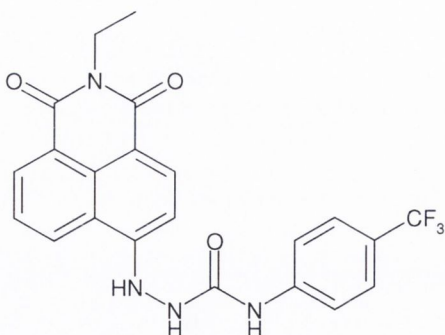
131 Was synthesised according to **Procedure 2**, using **134** (0.20 g, 0.80 mmol) and 4-trifluoromethylphenyl isocyanate **138** (0.16 g, 0.88 mmol) in dry MeCN (30 mL). The desired product was obtained as a dark yellow solid (0.15 g, 44.9%). m.p. decomposed at 250 °C; Calculated for $C_{22}H_{17}N_4F_3O_3.H_2O$: C, 57.39; H, 4.16; N, 12.17%; Found: C, 57.72; H, 3.79; N, 12.06%; δ_H (400 MHz, $(CD_3)_2SO$) 9.64 (1H, br s, urea-N$\underline{H}$), 9.45 (1H, br s, urea-N$\underline{H}$), 8.90 (1H, br s, Naph-N$\underline{H}$), 8.73 (1H, d, *J* = 7.9 Hz, Naph-$\underline{H7}$), 8.51 (1H, d, *J* = 7.9 Hz, Naph-$\underline{H5}$), 8.38 (1H, d, *J* = 8.8 Hz, Naph-$\underline{H2}$), 7.78 (3H, m, Ar-$\underline{H3}$, Ar-$\underline{H5}$, Naph-$\underline{H6}$), 7.62 (2H, d, *J* = 8.8 Hz, Ar-$\underline{H2}$, Ar-$\underline{H6}$), 7.06 (1H, d, *J* = 7.0 Hz, Naph-$\underline{H3}$), 4.07 (2H, q, *J* = 6.7 Hz, C$\underline{H_2}$), 1.20 (3H, t, *J* = 7.0 Hz, C$\underline{H_3}$); δ_C (100 MHz, $(CD_3)_2SO$) 163.4, 162.7, 155.5, 151.1, 149.7, 143.4, 133.7, 130.8, 128.9, 125.8, 124.9, 123.2, 121.9, 120.7, 118.6, 113.0, 110.9, 105.1, 34.4, 13.3;

δ_F (376 MHz, (CD$_3$)$_2$SO) -58.59 (Ar-C$\underline{F}_3$); IR (KBr) υ_{max} (cm^{-1}) 3317, 1641, 1548, 1434, 1389, 1371, 1327, 1234, 1162, 1111, 1066, 1016, 916, 875, 841, 773, 756, 705; ESMS was not possible due to fragmentation.

6-Bromo-2-ethyl-benzo[*de*]isoquinoline-1,3-dione (133)
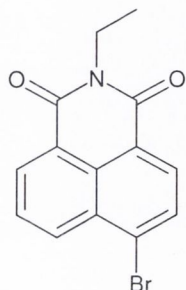
4-Bromo-1,8-naphthalic anhydride **132** (2.00 g, 7.2 mmol) and ethylamine (70% solution in water) (0.69 mL, 8.66 mmol) were refluxed in 1,4-dioxane (100 mL) for 7 h. The solution was then poured into water. A precipitate is formed, which was collected by filtration, washed with water and dried to yield **133** as a cream-coloured solid (1.96 g, 89.1%). m.p. 160 - 162 °C (lit.,[189] 163 °C); Calculated for C$_{14}$H$_{10}$NO$_2$Br: C, 55.29; H, 3.31; N, 4.61%; Found: C, 55.22; H, 3.32; N, 4.73%; δ_H (400 MHz, CDCl$_3$) 8.62 (1H, d, *J* = 7.5 Hz, Naph-$\underline{H}$7), 8.50 (1H, d, *J* = 8.5 Hz, Naph-$\underline{H}$5), 8.38 (1H, d, *J* = 8.0 Hz, Naph-$\underline{H}$2), 8.00 (1H, d, *J* = 8.0 Hz, Naph-$\underline{H}$3), 7.82 (1H, dd, *J* = 7.8 Hz, 8.0 Hz, Naph-$\underline{H}$6), 4.24 (2H, q, *J* = 7.0 Hz, C$\underline{H}_2$), 1.34 (3H, t, *J* = 7.0 Hz, C$\underline{H}_3$); δ_C (100 MHz, CDCl$_3$) 162.9, 162.8, 132.6, 131.4, 130.6, 130.5, 130.1, 129.6, 128.5, 127.5, 122.7, 121.9, 35.2, 12.8.

2-Ethyl-6-hydrazino-benzo[*de*]isoquinoline-1,3-dione (134)
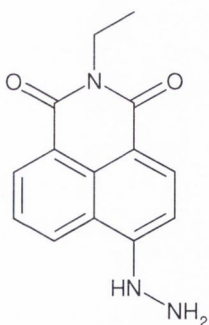
Hydrazine monohydrate (excess) was added to **133** (0.20 g, 0.66 mmol). The reaction mixture was heated neat at 130 °C and left stirring for 1 h. It was then poured into water, forming a precipitate, which was collected by filtration, washed with water and dried to yield **134** as a yellow solid (0.16 g, 95.3%). m.p. 255 - 257 °C; HRMS (MeOH, ES$^+$): Calculated for C$_{14}$H$_{14}$N$_3$O$_2$: 256.1086 (M + H)$^+$; Found: 256.1077; δ_H (400 MHz, (CD$_3$)$_2$SO) 9.13 (1H, br s, Naph-N$\underline{H}$), 8.61 (1H, d, *J* = 8.5 Hz, Naph-$\underline{H}$7), 8.41 (1H, d, *J* = 7.0 Hz, Naph-$\underline{H}$5), 8.28 (1H, d, *J* = 7.5 Hz, Naph-$\underline{H}$2), 7.64 (1H, dd, *J* = 7.8 Hz, 8.0 Hz, Naph-$\underline{H}$6), 7.24 (1H, d, *J* = 8.6 Hz, Naph-$\underline{H}$3), 4.69 (2H, d, *J* = 10.6 Hz, Naph-NH-N$\underline{H}_2$), 4.05 (2H, q, *J* = 7.0 Hz, C$\underline{H}_2$), 1.18 (3H, t, *J* = 7.0 Hz, C$\underline{H}_3$); δ_C (100 MHz, (CD$_3$)$_2$SO) 163.6, 162.7, 153.2, 134.2, 130.5, 128.2, 127.3, 124.1, 121.7, 118.4, 107.4, 104.0, 34.2, 13.3; MS (MeOH, ES$^+$) *m/z* 256 (M + H)$^+$; IR (KBr) υ_{max} (cm^{-1}) 3450, 3366, 3316, 1672, 1636, 1614, 1578, 1540, 1439, 1389, 1366, 1346, 1310, 1251, 1114, 1069, 950, 772.

6.1   References

1.   Vogtle, F. *Supramolecular Chemistry: An Introduction*, John Wiley & Sons Ltd.: Chichester, **1991**.

2.   Czarnik, A. W. *Fluorescent Chemosensors for Ion and Molecule Recognition*, American Chemical Society: Washington, **1993**.

3.   Balzani, V.; Scandola, F. *Supramolecular Photochemistry*, Ellis Horwood Limited: Chichester, **1991**.

4.   Valeur, B.; Leray, I. *Coord. Chem. Rev.* **2000**, *205*, 3-40.

5.   Tamayo, A.; Lodeiro, C.; Escriche, L.; Casabo, J.; Covelo, B.; Gonzalez, P. *Inorg. Chem.* **2005**, *44*, 8105-8115.

6.   Bianchi, A.; Bowman-James, K.; Garcia-Espana, E., Eds. *Supramolecular Chemistry of Anions*; John Wiley & Sons Ltd.: New York, **1997**.

7.   Sessler, J. L.; Gale, P. A.; Cho, W.-S. *Anion Receptor Chemistry*, The Royal Society of Chemistry: Cambridge, **2006**.

8.   Debroy, P.; Banerjee, M.; Prasad, M.; Moulik, S. P.; Roy, S. *Org. Lett.* **2005**, *7*, 403-406.

9.   Abe, H.; Aoyagi, Y.; Inouye, M. *Org. Lett.* **2005**, *7*, 59-61.

10.   de Silva, A. P.; Nimal Gunaratne, H. Q.; Gunnlaugsson, T.; Huxley, A. J. M.; McCoy, C. P.; Rademacher, J. T.; Rice, T. E. *Chem. Rev.* **1997**, *97*, 1515-1566.

11.   Connors, K. A. *Binding Constants: The Measurements of Molecular Complex Stability*, John Wiley & Sons Ltd.: New York, **1987**.

12.   Hynes, M. J. *J. Chem. Soc., Dalton Trans.* **1993**, 311-312.

13.   Wayne, R. P. *Principles and Applications of Photochemistry*, Oxford University Press: Oxford, **1988**.

14.   Kubo, Y. *J. Inclusion Phenom. Mol. Recognit. Chem.* **1998**, *32*, 235-249.

15.   Suksai, C.; Tuntulani, T. *Chem. Soc. Rev.* **2003**, *32*, 192-202.

16.   Thiagarajan, V.; Ramamurthy, P.; Thirumalai, D.; Ramakrishnan, V. T. *Org. Lett.* **2005**, *7*, 657-660.

17.   Kubo, Y.; Yamamoto, M.; Ikeda, M.; Takeuchi, M.; Shinkai, S.; Yamaguchi, S.; Tamao, K. *Angew. Chem., Int. Ed. Engl.* **2003**, *42*, 2036-2040.

18.   Xu, S.; Chen, K. C.; Tian, H. *J. Mater. Chem.* **2005**, *15*, 2676-2680.

19.   Jang, Y. J.; Jun, E. J.; Lee, Y. J.; Kim, Y. S.; Kim, J. S.; Yoon, J. *J. Org. Chem.* **2005**, *70*, 9603-9606.

20. Gunnlaugsson, T.; Glynn, M.; Tocci, G. M.; Kruger, P. E.; Pfeffer, F. M. *Coord. Chem. Rev.* **2006**, *250*, 3094-3117.

21. Beer, P. D.; Gale, P. A. *Angew. Chem., Int. Ed.* **2001**, *40*, 487-516.

22. Pederson, C. J. *J. Am. Chem. Soc.* **1967**, *89*, 7017.

23. Park, C. H.; Simmons, H. E. *J. Am. Chem. Soc.* **1968**, *90*, 2431.

24. Gale, P. A.; Quesada, R. *Coord. Chem. Rev.* **2006**, *250*, 3219-3244.

25. Gale, P. A. *Coord. Chem. Rev.* **2000**, *199*, 181-233.

26. Gale, P. A. *Coord. Chem. Rev.* **2001**, *213*, 79-128.

27. Gale, P. A. *Coord. Chem. Rev.* **2003**, *240*, 191-221.

28. Adams, R. L. P.; Knowler, J. T.; Leader, D. P. *The Biochemistry of the Nucleic Acids*, 10th. ed., Chapman and Hall: New York, **1986**.

29. Hileman, B. In *Chem. Eng. News*, **2003**, 22-23.

30. Halford, B. In *Chem. Eng. News*, **2005**, 68.

31. McCoy, M. In *Chem. Eng. News*, **2005**, 12.

32. Bigay, J.; Deterre, P.; Pfister, C.; Chabre, M. *EMBO J.* **1987**, *6*, 2907.

33. Weiss, R. *Science News* **1991**, *139*, 132.

34. *In Thyroid Disorders Associated with Iodine Deficiency and Excess*; Raven Press: New York, **1985**.

35. Uunk, E. J. B. *Eutrophication of Surface Waters and the Contribution of Agriculture* Fertiliser Society: Peterborough, **1991**.

36. Shannon, R. D. *Acta Cryst.* **1976**, *A32*, 751.

37. Davis, A. P.; Joos, J. B. *Coord. Chem. Rev.* **2003**, *240*, 143-156.

38. Clare, J. P.; Ayling, A. J.; Joos, J. B.; Sisson, A. L.; Magro, G.; Perez-Payan, M. N.; Lambert, T. N.; Shukla, R.; Smith, B. D.; Davis, A. P. *J. Am. Chem. Soc.* **2005**, *127*, 10739-10746.

39. Gale, P. A.; Anzenbacher, P.; Sessler, J. L. *Coord. Chem. Rev.* **2001**, *222*, 57-102.

40. Sessler, J. L.; Cho, W. S.; Gross, D. E.; Shriver, J. A.; Lynch, V. M.; Marquez, M. *J. Org. Chem.* **2005**, *70*, 5982-5986.

41. Matthews, S. E.; Beer, P. D. *Supramol. Chem.* **2005**, *17*, 411-435.

42. Beer, P. D.; Hayes, E. J. *Coord. Chem. Rev.* **2003**, *240*, 167-189.

43.   Gunnlaugsson, T.; Harte, A. J.; Leonard, J. P.; Nieuwenhuyzen, M. *Supramol. Chem.* **2003**, *15*, 505-519.

44.   Leonard, J. P.; Gunnlaugsson, T. *J. Fluoresc.* **2005**, *15*, 585-595.

45.   Llinares, J. M.; Powell, D.; Bowman-James, K. *Coord. Chem. Rev.* **2003**, *240*, 57-75.

46.   Best, M. D.; Tobey, S. L.; Anslyn, E. V. *Coord. Chem. Rev.* **2003**, *240*, 3-15.

47.   Hosseini, M. W. *Coord. Chem. Rev.* **2003**, *240*, 157-166.

48.   Kral, V.; Furuta, H.; Shreder, K.; Lynch, V.; Sessler, J. L. *J. Am. Chem. Soc.* **1996**, *118*, 1595-1607.

49.   Sessler, J. L.; Davis, J. M. *Acc. Chem. Res.* **2001**, *34*, 989-997.

50.   Sessler, J. L.; Davis, J. M.; Kral, V.; Kimbrough, T.; Lynch, V. *Org. Biomol. Chem.* **2003**, *1*, 4113-4123.

51.   Beer, P. D.; Fletcher, N. C.; Grieve, A.; Wheeler, J. W.; Moore, C. P.; Wear, T. *J. Chem. Soc., Perkin Trans. 2* **1996**, 1545-1551.

52.   Beer, P. D.; Drew, M. G. B.; Gradwell, K. *J. Chem. Soc., Perkin Trans. 2* **2000**, 511-519.

53.   Belcher, W. J.; Fabre, M.; Farhan, T.; Steed, J. W. *Org. Biomol. Chem.* **2006**, *4*, 781-786.

54.   Choi, K. H.; Hamilton, A. D. *Coord. Chem. Rev.* **2003**, *240*, 101-110.

55.   Bondy, C. R.; Loeb, S. J. *Coord. Chem. Rev.* **2003**, *240*, 77-99.

56.   Gale, P. A. *Acc. Chem. Res.* **2006**, *39*, 465 - 475.

57.   Kang, S. O.; Begum, R. A.; Bowman-James, K. *Angew. Chem., Int. Ed.* **2006**, *45*, 2-15.

58.   Sessler, J. L.; Camiolo, S.; Gale, P. A. *Coord. Chem. Rev.* **2003**, *240*, 17-55.

59.   Gale, P. A.; Sessler, J. L.; Kral, V. *Chem. Commun.* **1998**, 1-8.

60.   Miyaji, H.; Anzenbacher, P.; Sessler, J. L.; Bleasdale, E. R.; Gale, P. A. *Chem. Commun.* **1999**, 1723-1724.

61.   Sole, S.; Gabbai, F. P. *Chem. Commun.* **2004**, 1284-1285.

62.   Liu, Z. Q.; Shi, M.; Li, F. Y.; Fang, Q.; Chen, Z. H.; Yi, T.; Huang, C. H. *Org. Lett.* **2005**, *7*, 5481-5484.

63.   Knaggs, S.; Malkin, H.; Osborn, H. M. I.; Williams, N. A. O.; Yaqoob, P. *Org. Biomol. Chem.* **2005**, *3*, 4002-4010.

64.   Rostom, S. A. F. *Bioorg. Med. Chem.* **2006**, *14*, 6475-6485.

65.   Bu, J. J.; Lilienthal, N. D.; Woods, J. E.; Nohrden, C. E.; Hoang, K. T.; Truong, D.; Smith, D. K. *J. Am. Chem. Soc.* **2005**, *127*, 6423-6429.

66.   Simic, V.; Bouteiller, L.; Jalabert, M. *J. Am. Chem. Soc.* **2003**, *125*, 13148-13154.

67.   Patil, B. S.; Vasanthakumar, G.-R.; Suresh Babu, V. V. *J. Org. Chem.* **2003**, *68*, 7274-7280.

68.   Gale, P. A.; Light, M. E.; McNally, B. A.; Navakhun, K.; Sliwinski, K. E.; Smith, B. D. *Chem. Commun.* **2005**, 3773.

69.   Sessler, J. L.; Eller, L. R.; Cho, W. S.; Nicolaou, S.; Aguilar, A.; Lee, J. T.; Lynch, V. M.; Magda, D. J. *Angew. Chem., Int. Ed.* **2005**, *44*, 5989-5992.

70.   Davis, A. P.; Sheppard, D. N.; Smith, B. D. *Chem. Soc. Rev.* **2007**, *36*, 348-357.

71.   Wittkopp, A.; Schreiner, P. R. *Chem. Eur. J.* **2003**, *9*, 407-414.

72.   Maher, D. J.; Connon, S. J. *Tetrahedron Lett.* **2004**, *45*, 1301-1305.

73.   Okino, T.; Nakamura, S.; Furukawa, T.; Takemoto, Y. *Org. Lett.* **2004**, *6*, 625-627.

74.   Yang, D.; Chen, Y.-C.; Zhu, N.-Y. *Org. Lett.* **2004**, *6*, 4635-4635.

75.   Takemoto, Y. *Org. Biomol. Chem.* **2005**, *3*, 4299-4306.

76.   Dove, A. P.; Pratt, R. C.; Lohmeijer, B. G. G.; Waymouth, R. M.; Hedrick, J. L. *J. Am. Chem. Soc.* **2005**, *127*, 13798-13799.

77.   Duckmanton, P. A.; Blake, A. J.; Love, J. B. *Inorg. Chem.* **2005**, *44*, 7708-7710.

78.   de Loos, M.; Ligtenbarg, A. G. J.; van Esch, J.; Kooijman, H.; Spek, A. L.; Hage, R.; Kellogg, R. M.; Feringa, B. L. *J. Org. Chem.* **2000**, 3675-3678.

79.   Wang, G.; Hamilton, A. D. *Chem. Eur. J.* **2002**, *8*, 1954.

80.   Wang, G.; Hamilton, A. D. *Chem. Commun.* **2003**, 310-311.

81.   Estroff, L. A.; Hamilton, A. D. *Angew. Chem., Int. Ed. Engl.* **2000**, *39*, 3447.

82.   Suzuki, M.; Nakajima, Y.; Yumoto, M.; Kimura, M.; Shirai, H.; Hanabusa, K. *Org. Biomol. Chem.* **2004**, *2*, 1155-1159.

83.   Yabuuchi, K.; Marfo-Owusu, E.; Kato, T. *Org. Biomol. Chem.* **2003**, *1*, 3464.

84.   Wurthner, F.; Hanke, B.; Lysetska, M.; Lambright, G.; Harms, G. S. *Org. Lett.* **2005**, *7*, 967-970.

85.   Kubo, K.; Mori, A. *Chem. Lett.* **2005**, *34*, 1250-1251.

86.   Stanley, C. E.; Clarke, N.; Anderson, K. M.; Elder, J. A.; Lenthall, J. T.; Steed, J. W. *Chem. Commun.* **2006**, 3199-3201.

87.   Bonizzoni, M.; Fabbrizzi, L.; Taglietti, A.; Tiengo, F. *Eur. J. Org. Chem.* **2006**, 3567-3574.

88.   Evans, L. S.; Gale, P. A.; Light, M. E.; Quesada, R. *New J. Chem.* **2006**, *30*, 1019-1025.

89.   Gunnlaugsson, T.; Davis, A. P.; O'Brien, J. E.; Glynn, M. *Org. Biomol. Chem.* **2005**, *3*, 48-56.

90.   Oton, F.; Tarraga, A.; Espinosa, A.; Velasco, M. D.; Molina, P. *J. Org. Chem.* **2006**, *71*, 4590-4598.

91.   Pfeffer, F. M.; Gunnlaugsson, T.; Jensen, P.; Kruger, P. E. *Org. Lett.* **2005**, *7*, 5357-5360.

92.   Schazmann, B.; Alhashimy, N.; Diamond, D. *J. Am. Chem. Soc.* **2006**.

93.   Wei, L. H.; He, Y. B.; Wu, J. L.; Wu, X. J.; Meng, L. Z.; Yang, X. *Supramol. Chem.* **2004**, *16*, 561-567.

94.   Martinez-Manez, R.; Sancenon, F. *Chem. Rev.* **2003**, *103*, 4419-4476.

95.   Gunnlaugsson, T.; Ali, H. D. P.; Glynn, M.; Kruger, P. E.; Hussey, G. M.; Pfeffer, F. M.; dos Santos, C. M. G.; Tierney, J. *J. Fluoresc.* **2005**, *15*, 287-299.

96.   Martinez-Màñez, R.; Sancenon, F. *J. Fluoresc.* **2005**, *15*, 267-285.

97.   Martinez-Màñez, R.; Sancenon, F. *Coord. Chem. Rev.* **2006**, *250*, 3081-3093.

98.   Mei, M.; Wu, S. *New J. Chem.* **2001**, *25*, 471-475.

99.   Cho, E. J.; Moon, J. W.; Ko, S. W.; Lee, J. Y.; Kim, S. K.; Yoon, J.; Nam, K. C. *J. Am. Chem. Soc.* **2003**.

100.   Kubo, Y.; Kato, M.; Misawa, Y.; Tokita, S. *Tetrahedron Lett.* **2004**, *45*, 3769-3773.

101.   Kondo, S.; Sato, M. *Tetrahedron* **2006**, *62*, 4844-4850.

102.   Nakashima, H.; Yoshida, N. *Org. Lett.* **2006**, *8*, 4997-5000.

103.   Gunnlaugsson, T.; Davis, A. P.; O'Brien, J. E.; Glynn, M. *Org. Lett.* **2002**, *4*, 2449-2452.

104.   Kim, S. K.; Bok, J. H.; Bartsch, R. A.; Lee, J. Y.; Kim, J. S. *Org. Lett.* **2005**, *7*, 4839-4842.

105.   Suzuki, I.; Ui, M.; Yamauchi, A. *J. Am. Chem. Soc.* **2006**, *128*, 4498-4499.

106. Jayaraman, S.; Haggie, P.; Wachter, R. M.; Remington, S. J.; Verkman, A. S. *J. Biol. Chem.* **2000**, *275*, 6047-6050.

107. Kuswandi, B.; Nuriman; Verboom, W.; Reinhoudt, D. N. *Sensors* **2006**, *6*, 978-1017.

108. Pfeffer, F. M.; Seter, M.; Lewcenko, N.; Barnett, N. W. *Tetrahedron Lett.* **2006**, *47*, 5241-5245.

109. Miyaji, H.; Kim, H. K.; Sim, E. K.; Lee, C. K.; Cho, W. S.; Sessler, J. L.; Lee, C. H. *J. Am. Chem. Soc.* **2005**, *127*, 12510-12512.

110. Ghosh, K.; Adhikari, S. *Tetrahedron Lett.* **2006**, *47*, 8165-8169.

111. Lee, S. H.; Kim, H. J.; Lee, Y. O.; Vicens, J.; Kim, J. S. *Tetrahedron Lett.* **2006**, *47*, 4373-4376.

112. Xie, H.; Yi, S.; Yang, X.; Wu, S. *New J. Chem.* **1999**, *23*, 1105-110.

113. Fan, A.; Kah Hong, H.; Valiyaveettil, S.; Vittal, J. J. *J. Supramol. Chem.* **2002**, *2*, 247-254.

114. Costero, A. M.; Colera, M.; Gavina, P.; Gil, S. *Chem. Commun.* **2006**, 761-763.

115. Wu, Y.; Peng, X.; Fan, J.; Gao, S.; Tian, M.; Zhao, J. Z.; Sun, S. *J. Org. Chem.* **2007**, *72*, 62-70.

116. Amendola, V.; Esteban-Gomez, D.; Fabbrizzi, L.; Licchelli, M. *Acc. Chem. Res.* **2006**, *39*, 343-353.

117. Gunnlaugsson, T.; Kruger, P. E.; Jensen, P.; Tierney, J.; Ali, H. D. P.; Hussey, G. M. *J. Org. Chem.* **2005**, *70*, 10875-10878.

118. Esteban-Gomez, D.; Fabbrizzi, L.; Liechelli, M. *J. Org. Chem.* **2005**, *70*, 5717-5720.

119. Nishizawa, S.; Kato, R.; Hayashita, T.; Teramae, N. *N. Anal. Sci.* **1998**, *14*, 595.

120. Quinlan, E.; Matthews, S. E.; Gunnlaugsson, T. *Tetrahedron Lett.* **2006**, *47*, 9333-9338.

121. Jiménez, D.; Martinez-Mànez, R.; Sancenón, F.; Soto, J. *Tetrahedron Lett.* **2002**, *43*, 2823-2825.

122. Ros-Lis, J. V.; Martinez-Mànez, R.; Benito, A.; Soto, J. *Polyhedron* **2006**, *25*, 1585-1591.

123. Tomasulo, M.; Raymo, F. M. *Org. Lett.* **2005**, *7*, 4633-4636.

124. Lee, K. H.; Lee, H. Y.; Lee, D. H.; Hong, J. I. *Tetrahedron Lett.* **2001**, *42*, 5447-5449.

125.	Kato, R.; Nishizawa, S.; Hayashita, T.; Teramae, N. *Tetrahedron Lett.* **2001**, *42*, 5053-5056.

126.	Lee, C.; Lee, D. H.; Hong, J.-I. *Tetrahedron Lett.* **2001**, *42*, 8665-8668.

127.	Jose, D. A.; Kumar, D. K.; Ganguly, B.; Das, A. *Org. Lett.* **2004**, *6*, 3445-3448.

128.	Cho, E. J.; Ryu, B. J.; Lee, Y. J.; Nam, K. C. *Org. Lett.* **2005**, *7*, 2607-2609.

129.	Wu, J. L.; He, Y. B.; Wei, L. H.; Meng, L. Z.; Yang, T. X.; Liu, X. *Aust. J. Chem.* **2005**, *58*, 53-57.

130.	Vàzquez, M.; Fabbrizzi, L.; Taglietti, A.; Pedrido, R. M.; González-Noya, A. M.; Bermejo, M. R. *Angew. Chem., Int. Ed. Engl.* **2004**, *43*, 1962-1965.

131.	Boiocchi, M.; Del Boca, L.; Esteban-Gomez, D.; Fabbrizzi, L.; Licchelli, M.; Monzani, E. *Chem. Eur. J.* **2005**, *11*, 3097-3104.

132.	Liu, B.; Tian, H. *Chem. Lett.* **2005**, *34*, 686-687.

133.	Gunnlaugsson, T.; Kruger, P. E.; Lee, T. C.; Parkesh, R.; Pfeffer, F. M.; Hussey, G. M. *Tetrahedron Lett.* **2003**, *44*, 6575-6578.

134.	Gunnlaugsson, T.; Davis, A. P.; Hussey, G. M.; Tierney, J.; Glynn, M. *Org. Biomol. Chem.* **2004**, *2*, 1856-1863.

135.	Gunnlaugsson, T.; Kruger, P. E.; Jensen, P.; Pfeffer, F. M.; Hussey, G. M. *Tetrahedron Lett.* **2003**, *44*, 8909-8913.

136.	Pfeffer, F. M.; Buschgens, A. M.; Barnett, N. W.; Gunnlaugsson, T.; Kruger, P. E. *Tetrahedron Lett.* **2005**, *46*, 6579-6584.

137.	Kim, Y.-J.; Kwak, H.; Lee, S. J.; Lee, J. S.; Kwon, H. J.; Nam, S. H.; Lee, K.; Kim, C. *Tetrahedron* **2006**, *62*, 9635-9640.

138.	Brooks, S. J.; Gale, P. A.; Light, M. E. *Chem. Commun.* **2005**, 4696-4698.

139.	Brooks, S. J.; Edwards, P. R.; Gale, P. A.; Light, M. E. *New J. Chem.* **2006**, *30*, 65-70.

140.	Evans, L. S.; Gale, P. A.; Light, M. E.; Quesada, R. *Chem. Commun.* **2006**, 965-967.

141.	Brooks, S. J.; Gale, P. A.; Light, M. E. *Chem. Commun.* **2006**, 4344-4346.

142.	Garcia-Garrido, S. E.; Caltagirone, C.; Light, M. E.; Gale, P. A. *Chem. Commun.* **2007**, 1450-1452.

143.	Boiocchi, M.; Del Boca, L.; Gómez, D. E.; Fabbrizzi, L.; Licchelli, M.; Monzani, E. *J. Am. Chem. Soc.* **2004**, *126*, 16507-16514.

144.	Esteban-Gomez, D.; Fabbrizzi, L.; Licchelli, M.; Sacchi, D. *J. Mater. Chem.* **2005**, *15*, 2670-2675.

145. Gunnlaugsson, T.; Nieuwenhuyzen, M.; Richard, L.; Thoss, V. *J. Chem. Soc., Perkin Trans. 2* **2002**, *2*, 141-150.

146. Gunnlaugsson, T.; Lee, T. C.; Parkesh, R. *Tetrahedron* **2004**, *60*, 11239-11249.

147. Gunnlaugsson, T.; Davis, A. P.; Glynn, M. *Chem. Commun.* **2001**, 2556-2557.

148. dos Santos, C. M. G.; Glynn, M.; McCabe, T.; Sergio Seixas de Melo, J.; Burrows, H. D.; Gunnlaugsson, T. *Supramol. Chem.* **2007**, *19*, *In Press*.

149. Gunnlaugsson, T.; Lee, T. C.; Parkesh, R. *Org. Biomol. Chem.* **2003**, *1*, 3265-3267.

150. Gunnlaugsson, T.; McCoy, C. P.; Morrow, R. J.; Phelan, C.; Stomeo, F. *ARKIVOC* **2003**, 216-228.

151. Quinn, R.; Appleby, J. B.; Pez, G. P. *J. Am. Chem. Soc.* **1995**, *117*, 329-335.

152. dos Santos, C. M. G.; McCabe, T.; Gunnlaugsson, T. *Tetrahedron Lett.* **2007**, *48*, 3135-3139.

153. Pratt, M. D.; Beer, P. *Polyhedron* **2003**, *22*, 649-653.

154. Gomez, D. E.; Fabbrizzi, L.; Licchelli, M.; Monzani, E. *Org. Biomol. Chem.* **2005**, *3*, 1495-1500.

155. Werner, F.; Schneider, H.-J. *Helv. Chim. Acta* **2000**, *83*, 465-478.

156. Jiménez Blanco, J. L.; Bootello, P.; Benito, J. M.; Ortiz Mellet, C.; Garcia Fernàndez, J. M. *J. Org. Chem.* **2006**, *71*, 5136.

157. Hamilton, A. D.; Little, D. *J. Chem. Soc., Chem. Commun.* **1990**, 297.

158. Neder, K. M.; Whitlock, H. W. *J. Am. Chem. Soc.* **1990**, *112*, 9412-9414.

159. Wilcox, C. S.; Kim, E.-I.; Romano, D.; Kuo, L. H.; Burt, A. L.; Curran, D. P. *Tetrahedron* **1995**, *51*, 621-634.

160. Chien, C.-H.; Leung, M.-K.; Su, J.-K.; Li, G.-H.; Liu, Y.-H.; Wang, Y. *J. Org. Chem.* **2004**, *69*, 1866-1871.

161. Kelly, R. T.; Kim, M. H. *J. Am. Chem. Soc.* **1994**, *116*, 7072-7080.

162. Linton, B. R.; Scott Goodman, M.; Fan, E.; van Arman, S. A.; Hamilton, A. D. *J. Org. Chem.* **2001**, *66*, 7313-7319.

163. Clayden, J.; Greeves, N.; Warren, S.; Wothers, P. *Organic Chemistry*, Oxford University Press Inc.: New York, **2001**.

164. Berger, S.; Braun, S.; Kalinowski, H.-O. *NMR Spectroscopy of the Non-Metallic Elements*, Wiley: Chichester, **1997**.

165. Hay, B. P.; Firman, T. K.; Moyer, B. A. *J. Am. Chem. Soc.* **2005**, *127*, 1810-1819.

166. Jeffrey, G. A. *An Introduction to Hydrogen Bonding*, Oxford University Press: Oxford, **1997**.

167. Custelcean, R.; Engle, N. L.; Bonnesen, P. V. *CrystEngComm* **2007**, *9*, 452.

168. Brooks, S. J.; Gale, P. A.; Light, M. E. *CrystEngComm* **2005**, *7*, 586-591.

169. Kang, S. O.; Powell, D.; Bowman-James, K. *J. Am. Chem. Soc.* **2005**, *127*, 13478-13479.

170. Kang, S. O.; Powell, D.; Day, V. W.; Bowman-James, K. *Angew. Chem., Int. Ed.* **2006**, *45*, 1921-1925.

171. Light, M. E.; Gale, P. A.; Brooks, S. J. *Acta Crystallographica Section E-Structure Reports Online* **2006**, *62*, O1905-O1907.

172. Bühlmann, P.; Nishizawa, S.; Xiao, K. P.; Umezawa, Y. *Tetrahedron* **1997**, *53*, 1647-1654.

173. Sasaki, S.; Mizuno, M.; Naemura, K.; Tobe, Y. *J. Org. Chem.* **2000**, *65*, 275-283.

174. Kim, K. S.; Kim, H.-S. *Bull. Korean Chem. Soc.* **2004**, *25*, 1141-1413.

175. Zhao, Z. G.; Mu, Q. M.; Chen, S. H. *Chin. Chem. Lett.* **2004**, *15*, 1285-1288.

176. Mu, Q. M.; Zhao, Z. G.; Yang, Z. X.; Chen, S. H. *Chin. J. Org. Chem.* **2005**, *25*, 1084-1088.

177. Albrecht, M.; Zauner, J.; Burgert, R.; Rottele, H.; Frohlich, R. *Mater. Sci. Eng., C* **2001**, *18*, 185-190.

178. Kondo, S.; Harada, T.; Tanaka, R.; Unno, M. *Org. Lett.* **2006**, *8*, 4621-4624.

179. Amendola, V.; Boiocchi, M.; Esteban-Gomez, D.; Fabbrizzi, L.; Monzani, E. *Org. Biomol. Chem.* **2005**, *3*, 2632-2639.

180. Turro, N. J. *Modern Molecular Photochemistry*, University Science Books: Sausalito, **1991**.

181. Murov, S. L.; Carmichael, I.; Hug, G. L. *Handbook of Photochemistry*, 2nd. ed., Marcel Dekker: New York, **1993**.

182. Camiolo, S.; Gale, P. A.; Hursthouse, M. B.; Light, M. E. *Org. Biomol. Chem.* **2003**, *1*, 741-744.

183. *Circular Dichroism: Principles and Applications* 2nd. ed., Wiley-VCH: New York, **2000**.

184. Katoono, R.; Kawai, H.; Fujiwara, K.; Suzuki, T. *Chem. Commun.* **2005**, 5154-5156.

185. Custelcean, R.; Gorbunova, M. G.; Bonnesen, P. V. *Chem. Eur. J.* **2005**, *11*, 1459-1466.

186. Han, F.; Bao, Y.; Yang, Z.; Fyles, T. M.; Zhao, J.; Peng, X.; Fan, J.; Wu, Y.; Sun, S. *Chem. Eur. J.* **2007**, *13*, 2880-2892.

187. de Silva, A. P.; Nimal Gunaratne, H. Q.; Habib-Jiwan, J.-L.; McCoy, C. P.; Rice, T. E.; Soumillion, J.-P. *Angew. Chem., Int. Ed. Engl.* **1995**, *34*, 1728-1731.

188. de Silva, A. P. *Chem. Commun.* **1999**, 163-164.

189. Tocci (nee Hussey), G. M. Ph.D., Trinity College Dublin, **2003**.

190. Williams, D. H.; Fleming, I. *Spectroscopic Methods in Organic Chemistry*, 5th. ed., McGraw-Hill International (UK) Ltd.: Cambridge, **1997**.

191. Sasaki, S.-I.; Citterio, D.; Ozawa, S.; Suzuki, K. *J. Chem. Soc., Perkin Trans. 2* **2001**, 2309-2313.

192. Korzyuk, E. L.; Samigullin, F. K.; Korzyuk, V. G. *Russ. J. Org. Chem.* **1998**, *34*, 1264-1264.

193. Krivenko, L. V.; Cherezova, E. N.; Mukmeneva, N. A. *Russ. J. Appl. Chem.* **2000**, *73*, 1264-1268.

194. Dondoni, A.; Barbaro, G.; Battaglia, A. *J. Org. Chem.* **1977**, *42*, 3372-3377.

195. Bartoszewski, J.; Jerzmanowska, Z. Z. *Rocz. Chem.* **1963**, *37*, 21.

196. Heesing, A.; Schmaldt, W. *Chem. Ber.* **1978**, *111*, 320-334.

197. Singh, B. N. *Agric. Biol. Chem.* **1978**, *42*, 1285-1286.

198. Buu-Hoi, N. P.; Jacquignon, P.; Loc, T. B. *J. Chem. Soc.* **1958**, 2815.

199. Reddy, B. M.; Reddy, V. R. *Synth. Commun.* **1999**, *29*, 2789.

200. Cymerman, J.; Neely, W. J. *Aust. J. Chem.* **1960**, *13*, 341.

201. Buu-Hoi, N. P.; Lavit, D.; Xuong, N. D. *J. Chem. Soc.* **1955**, *21*, 1581-1583.

202. Husdson, R. F.; Record, K. A. F. *J. Chem. Soc., Perkin Trans. 2* **1978**, 1167.

203. Barnikov, G.; Kunzek, H. *Justus Liebigs Ann. Chem.* **1966**, *700*, 36.

204. Kutepow, N. v. *J. Gen. Chem., USSR (English)* **1960**, *30*, 2470.

7.1   Appendices for Chapter 2

7.1.1   (a) The Hammett Equation[1-3]

The Hammett equation is a linear free-energy relationship that describes the influence of polar *meta-* and *para-*substituents on the side-chain reactions of benzene derivatives. This equation takes the form:

$$\log_{10} K = \log_{10} K^0 + \rho\sigma \qquad \textbf{(Equation 7.1)}$$

K is the equilibrium (or binding) constant for a side-chain reaction of a *meta-* or *para-*substituted benzene derivative. The term K^0 denotes the statistical quantity approximating to *K* for the "unsubstituted" or "parent" compound. The substituent constant, σ, measures the polar effect (relative to hydrogen) of the substituent (in a given position, *meta* or *para*) and is, in principle, independent of the nature of the reaction. A positive σ indicates an electron-withdrawing substituent and a negative σ indicates an electron-donating group. The reaction constant, ρ, depends on the nature of the reaction (including conditions such as solvent and temperature) and measures the susceptibility of the reaction to polar effects. The "polar effect" of a substituent may modify electrostatics forces operating at a reaction centre, relative to a standard substituent, which is often, but not always, a hydrogen atom. Forces may be governed by charge separation due to differences in electronegativity of atoms (resulting in dipoles), presence of unipoles and electron delocalisation.

The above equation may be rearranged to give Equation 7.2.

$$\log_{10} (K / K^0) = \rho\sigma \qquad \textbf{(Equation 7.2)}$$

A plot of $\log_{10} (K / K^0)$ against σ would then give a straight line with slope = ρ and y-intercept = 0. The best-fit line is obtained, preferably using the method of least squares. The R^2 value is used to check the status of the correlation (if perfect fit, $R^2 = 1$).

A reaction that is facilitated by reducing the electron density at the reaction centre (*i.e.* negative charge centre) has a positive value of ρ, and one facilitated by increasing the electron density at the reaction centre (*i.e.* positive charge centre) has a negative value of ρ.

Table 7.1 Hammett substituent constants (σ) of some substituents.[1]

Group	σ (meta)	σ (para)
H	0.00	0.00
CH_3	-0.07	-0.17
C_2H_5	-0.07	-0.15
CF_3	0.43	0.54
CN	0.56	0.66
F	0.34	0.06
Cl	0.37	0.23
Br	0.39	0.23
I	0.35	0.18

(b) Differences between the Chemical Shifts of the NH Protons of Ureas and Thioureas

The chemical shifts of the NH protons of thioureas are generally further downfield compared to those of ureas. Ureas and thioureas in solution tend to resonate between two possible forms as shown in Scheme 7.1. The NH proton adjacent to the positively charged N in the resonance form (ii) is more deshielded, and hence, its chemical shift is located further downfield, and *vice versa* for (i).
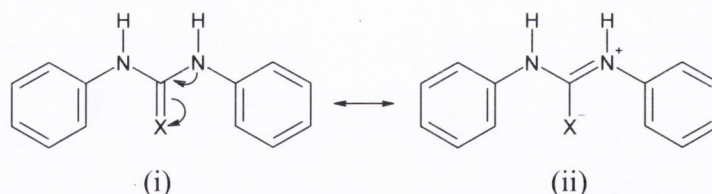
Scheme 7.1 Two possible resonance forms of ureas (X = O) and thioureas (X = S).

Since the C–S bond is weaker than the C–O bond, thioureas therefore would be more predominant as the resonance form (ii), while ureas would preferably exist as (i). This may explain the differences between the chemical shifts of the NH protons of ureas and thioureas.

7.1.2 Crystal Data and Strucure Refinement of 70

Identification code	**70**
Empirical formula	$C_{13}H_{12}N_2S$
Formula weight	228.31 g.mol^{-1}
Temperature	153(2) K
Wavelength	0.71073 Å
Crystal system	Orthorhombic
Space group	Pnma
Unit cell dimensions	a = 7.812(1) Å
	b = 25.473(4) Å
	c = 5.684(1) Å
	α = 90.00 °
	β = 90.00 °
	γ = 90.00 °
Volume	1131.1(3) Å^3
Z	4
Density (calculated)	1.341 Mg.m^{-3}
Absorption coefficient	0.258 mm^{-1}
Crystal size (mm^3)	0.20
	0.13
	0.03
Theta range for data collection	1.60 to 25.02 °
Reflections collected	6026
Independent reflections	1026 [R_{int} = 0.0430]
Completeness to theta = 25.02 °	100.0%
Max. and min. transmission	1.000 and 0.745
Refinement method	Full-matrix least-squares on F^2
Final R indices [I>2sigma(I)]	R = 0.0451
	wR = 0.0968
R indices (all data)	R = 0.0563
	wR = 0.0968
Absolute structure parameter	-

7.1.3   Crystal Data and Strucure Refinement of 80

Identification code	**80**
Empirical formula	$C_{13}H_{10}F_2N_2S$
Formula weight	264.29 g.mol^{-1}
Temperature	153(2) K
Wavelength	0.71073 Å
Crystal system	-
Space group	-
Unit cell dimensions	a = 8.3311(7) Å
	b = 26.373(2) Å
	c = 5.2932(4) Å
	α = 90.00 °
	β = 90.00 °
	γ = 90.00 °
Volume	1163.00(16) Å^3
Z	4
Density (calculated)	1.509 Mg.m^{-3}
Absorption coefficient	0.285 mm^{-1}
Crystal size (mm^3)	-
	-
	-
Theta range for data collection	3.09 to 29.96 °
Reflections collected	16690
Independent reflections	1712 [R_{int} = 0.0375]
Completeness to theta = 29.96 °	99.6%
Max. and min. transmission	-
Refinement method	Full-matrix least-squares on F^2
Final R indices [I>2sigma(I)]	R = 0.0652
	wR = 0.1463
R indices (all data)	R = 0.0705
	wR = 0.1490
Absolute structure parameter	-

7.1.4 Crystal Data and Strucure Refinement of 81

Identification code	**81**
Empirical formula	$C_{14}H_{13}FN_2O$
Formula weight	244.26 g.mol^{-1}
Temperature	153(2) K
Wavelength	0.71073 Å
Crystal system	-
Space group	-
Unit cell dimensions	a = 9.992(2) Å
	b = 4.5900(10) Å
	c = 26.176(5) Å
	α = 90.00 °
	β = 90.00 °
	γ = 90.00 °
Volume	1200.5(4) Å^3
Z	4
Density (calculated)	1.351 Mg.m^{-3}
Absorption coefficient	0.097 mm^{-1}
Crystal size (mm^3)	-
	-
	-
Theta range for data collection	1.56 to 25.01 °
Reflections collected	6172
Independent reflections	1605 [R_{int} = 0.0375]
Completeness to theta = 25.01 °	99.9%
Max. and min. transmission	-
Refinement method	Full-matrix least-squares on F^2
Final R indices [I>2sigma(I)]	R = 0.0406
	wR = 0.0821
R indices (all data)	R = 0.0485
	wR = 0.0848
Absolute structure parameter	0.1(14)

7.1.5 Crystal Data and Strucure Refinement of 84

Identification code	**84**
Empirical formula	$C_{14}H_{10}F_4N_2S$
Formula weight	314.30 g.mol^{-1}
Temperature	153(2) K
Wavelength	0.71073 Å
Crystal system	-
Space group	-
Unit cell dimensions	a = 14.153(2) Å
	b = 7.1390(10) Å
	c = 27.093(4) Å
	α = 90.00 °
	β = 90.00 °
	γ = 90.00 °
Volume	2737.4(7) Å^3
Z	8
Density (calculated)	1.525 Mg.m^{-3}
Absorption coefficient	0.276 mm^{-1}
Crystal size (mm^3)	-
	-
	-
Theta range for data collection	1.50 to 25.01 °
Reflections collected	12987
Independent reflections	3855 [R_{int} = 0.0811]
Completeness to theta = 25.01 °	99.5%
Max. and min. transmission	-
Refinement method	Full-matrix least-squares on F^2
Final R indices [I>2sigma(I)]	R = 0.0738
	wR = 0.1598
R indices (all data)	R = 0.0959
	wR = 0.1709
Absolute structure parameter	0.64(19)

7.1.6 Crystal Data and Strucure Refinement of 89

Identification code	**89**
Empirical formula	$C_{15}H_{10}F_6N_2O$
Formula weight	348.37 g.mol^{-1}
Temperature	153(2) K
Wavelength	0.71073 Å
Crystal system	-
Space group	-
Unit cell dimensions	a = 29.166(3) Å
	b = 4.6426(5) Å
	c = 9.9550(11) Å
	α = 90.00 °
	β = 96.203(2) °
	γ = 90.00 °
Volume	1340.1(3) Å^3
Z	4
Density (calculated)	1.459 Mg.m^{-3}
Absorption coefficient	0.121 mm^{-1}
Crystal size (mm^3)	-
	-
	-
Theta range for data collection	2.81 to 25.00 °
Reflections collected	3826
Independent reflections	1175 [R_{int} = 0.0227]
Completeness to theta = 25.00 °	99.9%
Max. and min. transmission	-
Refinement method	Full-matrix least-squares on F^2
Final R indices [I>2sigma(I)]	R = 0.0721
	wR = 0.2293
R indices (all data)	R = 0.0822
	wR = 0.2370
Absolute structure parameter	-

**7.1.7 Correlation between the Binding Curves of Repeated ¹H NMR Titrations of**
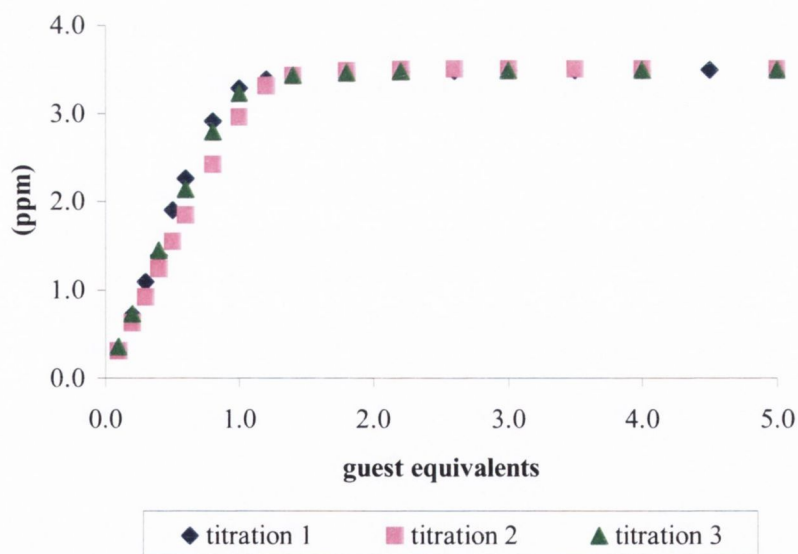***Bis*-Phenyl Ureas and Thioureas with Anions**
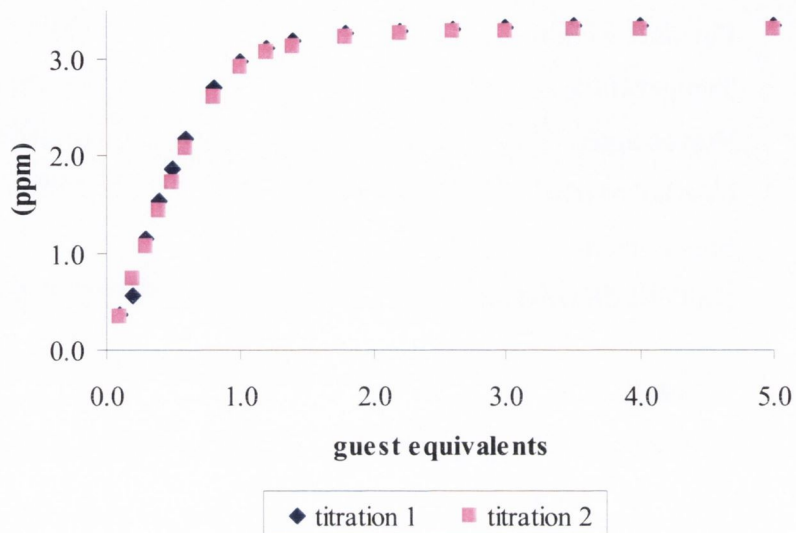
Figure 7.1 Graph illustrating the correlation between data (*i.e.* changes in the chemical shifts of the thiourea NH proton at 9.71 ppm with respect to anion equivalents added) of two ¹H NMR titrations (400 Mz, DMSO-d_6, 25 °C) of **72** upon the addition of AcO⁻.
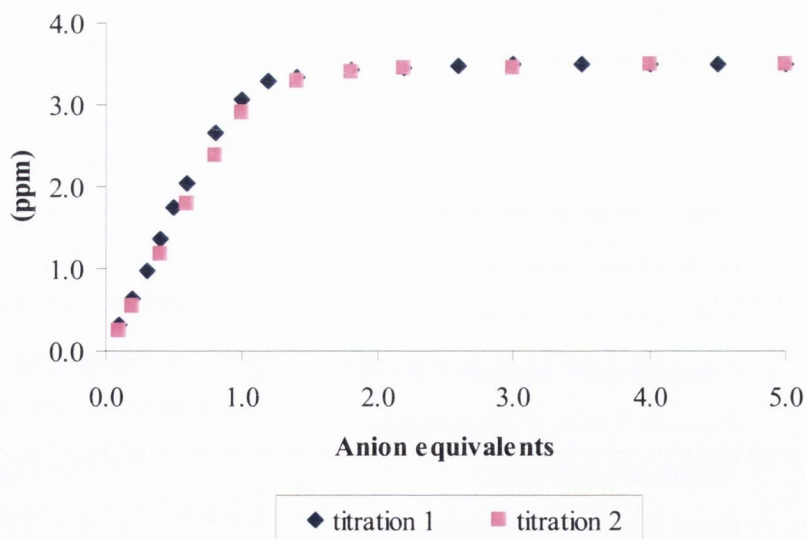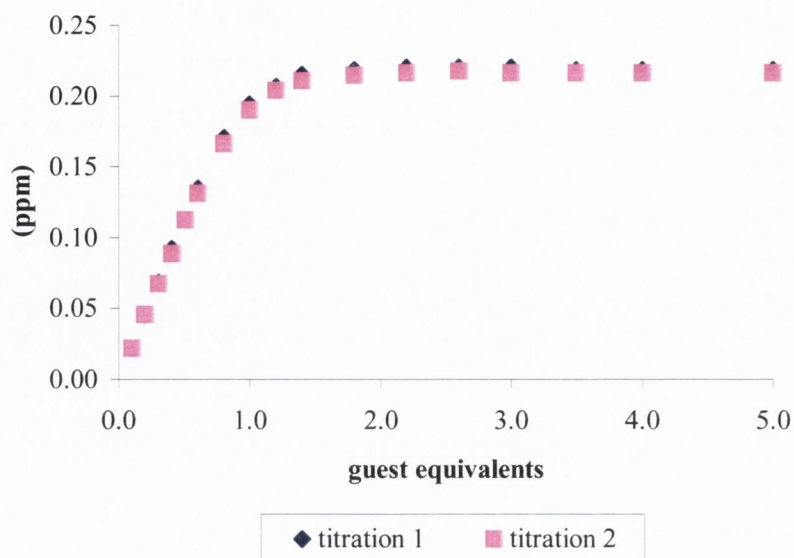

Figure 7.2 Graph illustrating the correlation between data (*i.e.* changes in the chemical shifts of the thiourea NH proton at 9.76 ppm with respect to anion equivalents added) of two ¹H NMR titrations (400 Mz, DMSO-d_6, 25 °C) of **80** upon the addition of AcO⁻.

211
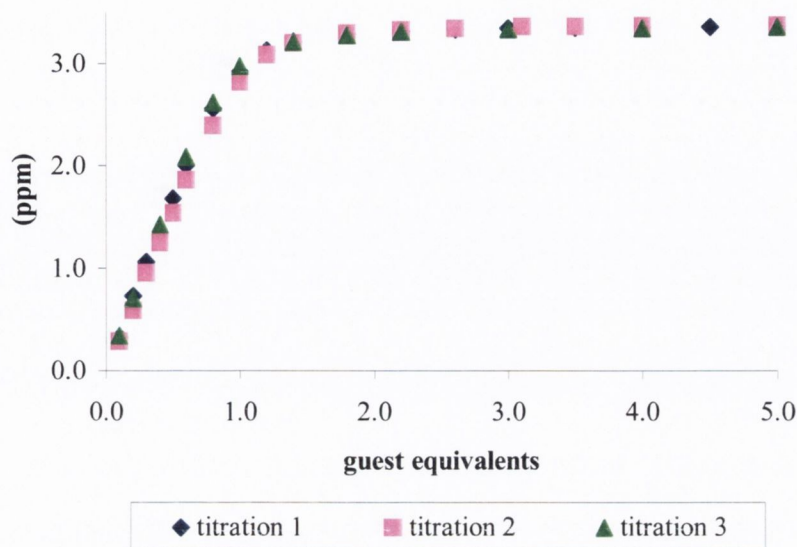
Figure 7.3 Graph illustrating the correlation between data (*i.e.* changes in the chemical shifts of the urea NH proton at 8.67 ppm with respect to anion equivalents added) of three ^{1}H NMR titrations (400 Mz, DMSO-d_6, 25 °C) of **81** upon the addition of AcO$^-$.
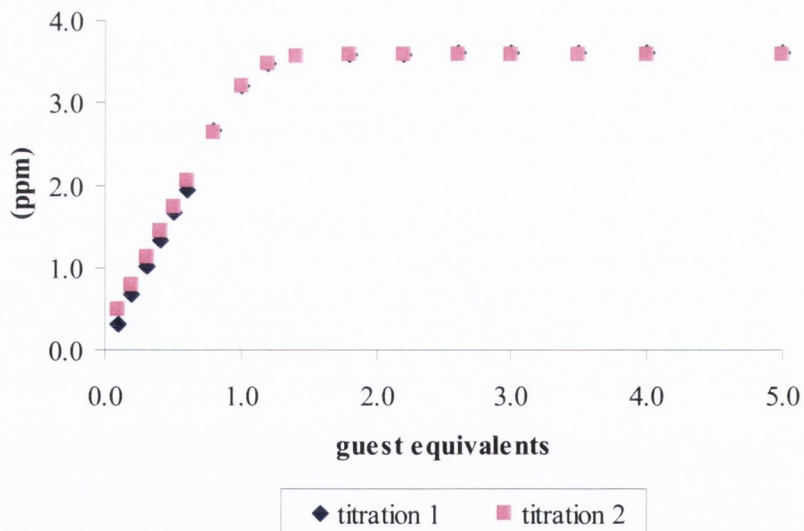

Figure 7.4 Graph illustrating the correlation between data (*i.e.* changes in the chemical shifts of the urea NH proton at 8.88 ppm with respect to anion equivalents added) of three ^{1}H NMR titrations (400 Mz, DMSO-d_6, 25 °C) of **83** upon the addition of AcO$^-$.

Figure 7.5 Graph illustrating the correlation between data (*i.e.* changes in the chemical shifts of the aromatic proton at 7.65 ppm with respect to anion equivalents added) of two ^{1}H NMR titrations (400 Mz, DMSO-d_6, 25 °C) of **83** upon the addition of $H_2PO_4^-$.
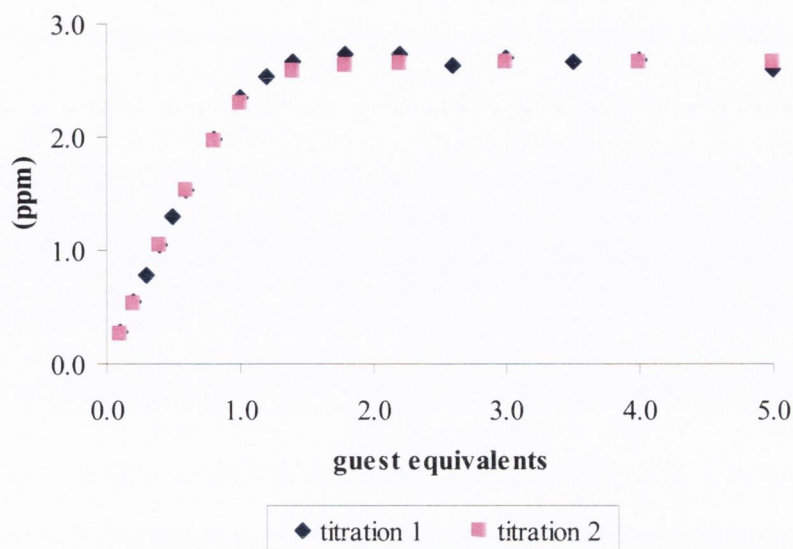

Figure 7.6 Graph illustrating the correlation between data (*i.e.* changes in the chemical shifts of the urea NH proton at 9.26 ppm with respect to anion equivalents added) of two ^{1}H NMR titrations (400 Mz, DMSO-d_6, 25 °C) of **89** upon the addition of AcO^-.

Figure 7.7 Graph illustrating the correlation between data (*i.e.* changes in the chemical shifts of the urea NH proton at 9.26 ppm with respect to anion equivalents added) of two ^{1}H NMR titrations (400 Mz, DMSO-d_6, 25 °C) of **89** upon the addition of $H_2PO_4^-$.
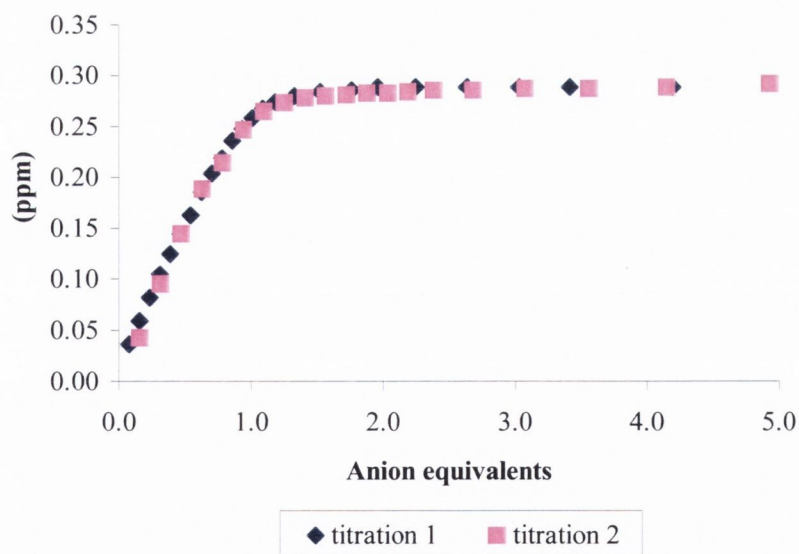

Figure 7.8 Graph illustrating the correlation between data (*i.e.* changes in the chemical shifts of the aromatic proton at 7.67 ppm with respect to anion equivalents added) of two ^{1}H NMR titrations (400 Mz, DMSO-d_6, 25 °C) of **102** upon the addition of AcO$^-$.

214

7.2 Appendices for Chapter 3

7.2.1 Graphs of Anion-induced Changes in the Fluorescence Spectrum of *Bis*-Anthracene-based Fluorescent Anion Sensors
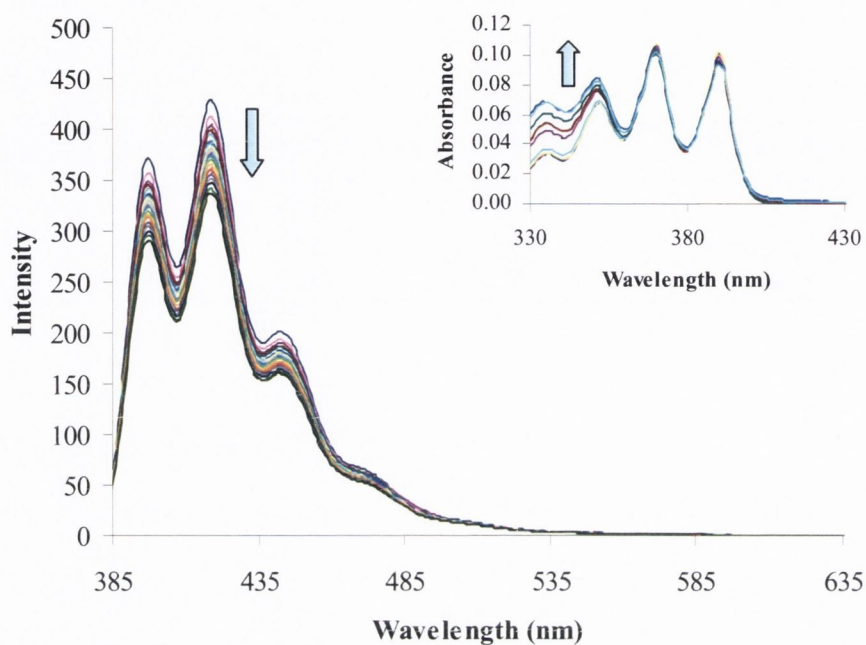
Figure 7.9 Changes in the fluorescence spectrum of **110** (6×10^{-6} M) in DMSO on addition of AcO⁻ (excited at 370 nm; 0 M → 6×10^{-3} M). Inset: Changes observed in the absorption spectrum of **110** in DMSO on addition of AcO⁻ (0 M → 6×10^{-3} M).
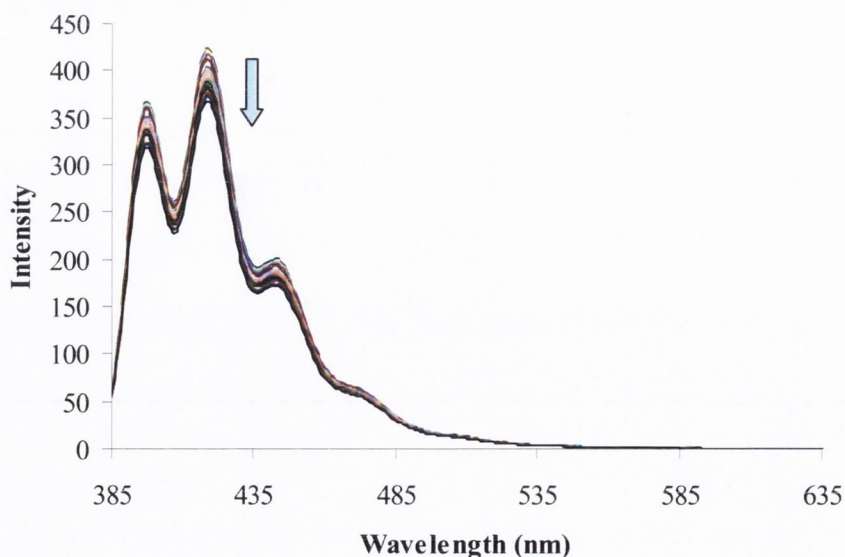
Figure 7.10 Changes in the fluorescence spectrum of **110** (6×10^{-6} M) in DMSO on addition of $H_2PO_4^-$ (excited at 370 nm; 0 M → 6×10^{-3} M).
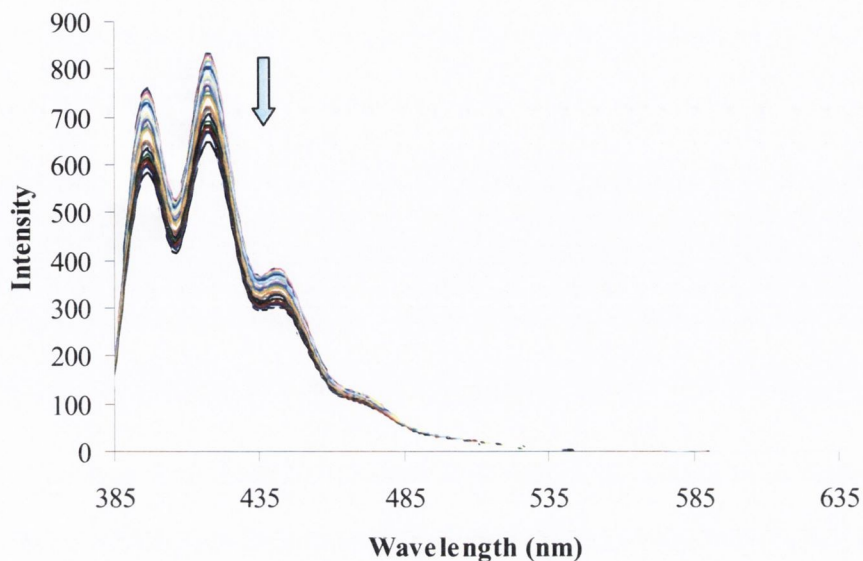
Figure 7.11 Changes in the fluorescence spectrum of **110** (6×10^{-6} M) in DMSO on addition of F$^-$ (excited at 370 nm; 0 M $\rightarrow$ 6×10^{-3} M).

Figure 7.12 Changes in the fluorescence spectrum of **110** (6×10^{-6} M) in DMSO on addition of Cl$^-$ (excited at 370 nm; 0 M $\rightarrow$ 6×10^{-3} M).

Figure 7.13 Changes in the fluorescence spectrum of **111** (6×10^{-6} M) in DMSO on addition of AcO$^-$ (excited at 370 nm; 0 M $\rightarrow$ 6×10^{-3} M). Inset: Changes observed in the absorption spectrum of **111** in DMSO on addition of AcO$^-$ (0 M $\rightarrow$ 6×10^{-3} M).
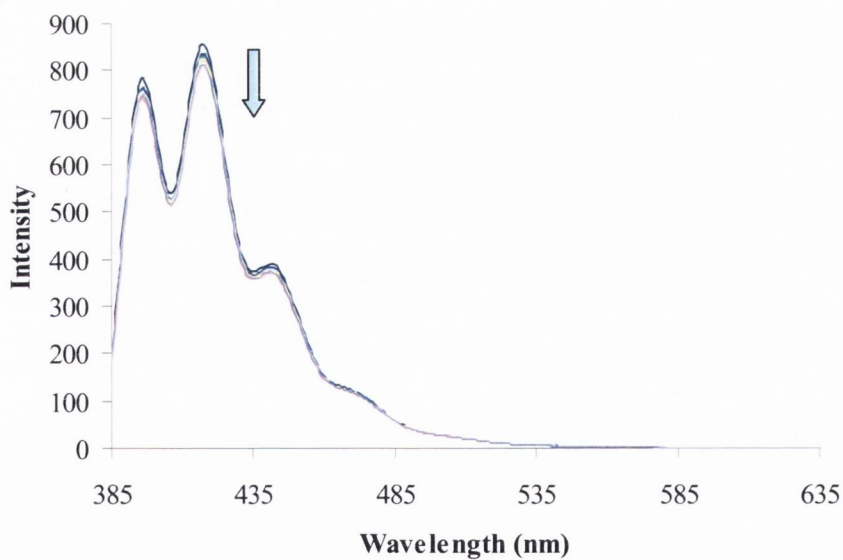

Figure 7.14 Changes in the fluorescence spectrum of **111** (6×10^{-6} M) in DMSO on addition of H$_2$PO$_4^-$ (excited at 370 nm; 0 M $\rightarrow$ 6×10^{-3} M).

217

Figure 7.15 Changes in the fluorescence spectrum of **111** (6×10^{-6} M) in DMSO on addition of F⁻ (excited at 370 nm; 0 M → 6×10^{-3} M).
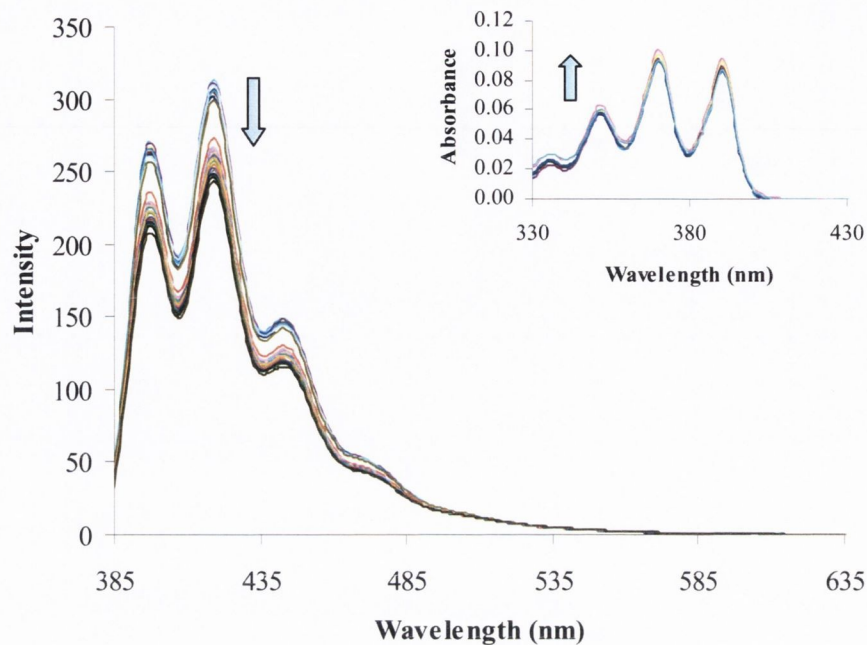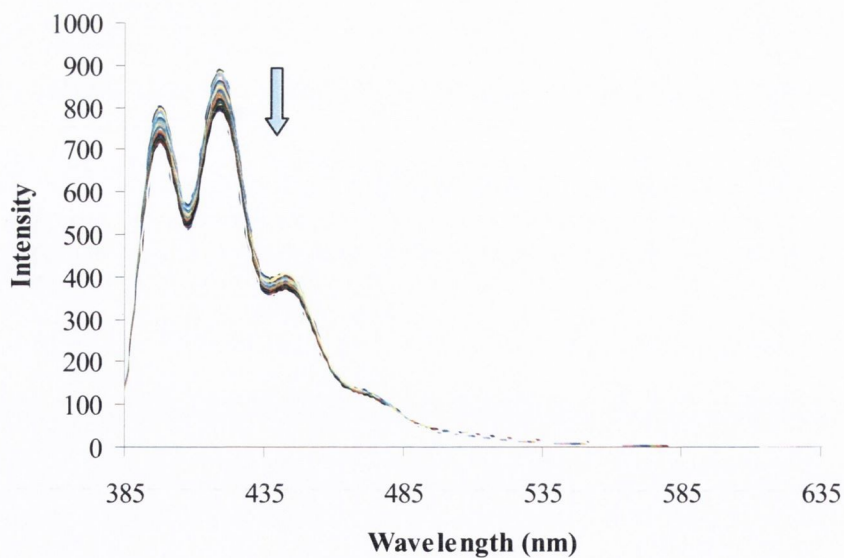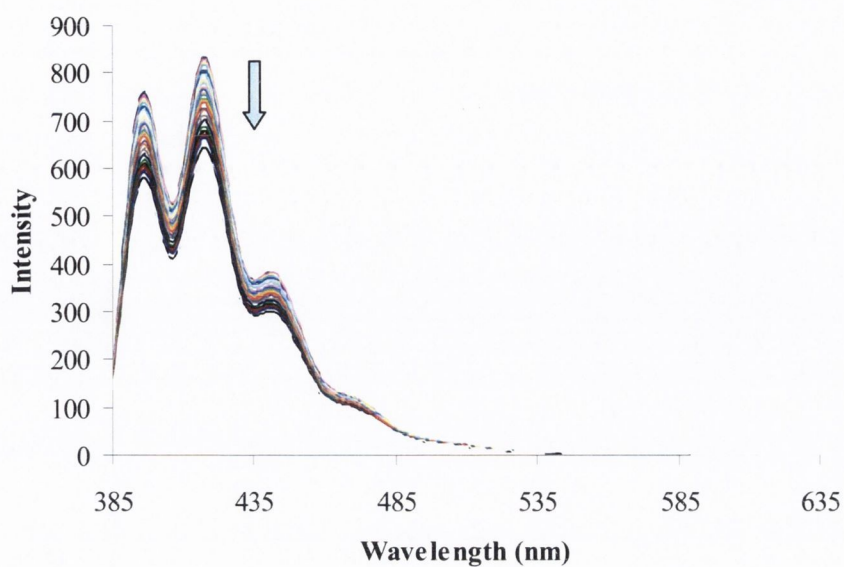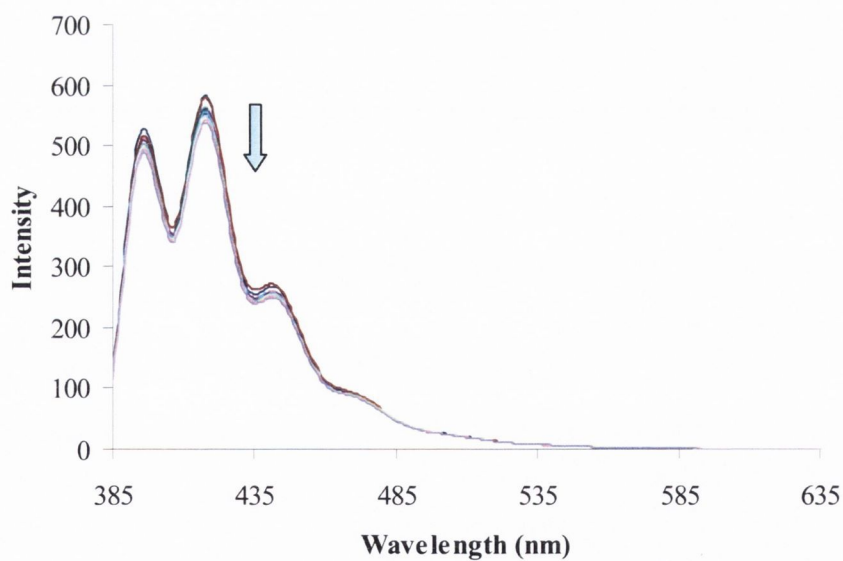

Figure 7.16 Changes in the fluorescence spectrum of **111** (6×10^{-6} M) in DMSO on addition of Cl⁻ (excited at 370 nm; 0 M → 6×10^{-3} M).

7.2.2 Crystal Data and Strucure Refinement of 112

Identification code	**112**
Empirical formula	$C_{25}H_{24}N_2S$
Formula weight	384.57 g.mol^{-1}
Temperature	396(2) K
Wavelength	0.71073 Å
Crystal system	-
Space group	-
Unit cell dimensions	a = 17.080(2) Å
	b = 8.1010(9) Å
	c = 18.903(2) Å
	α = 90.00 °
	β = 109.013(2) °
	γ = 90.00 °
Volume	2472.8(5) Å^3
Z	4
Density (calculated)	1.103 Mg.m^{-3}
Absorption coefficient	0.104 mm^{-1}
Crystal size (mm^3)	-
	-
	-
Theta range for data collection	1.14 to 24.99 °
Reflections collected	9886
Independent reflections	4190 [R_{int} = 0.0382]
Completeness to theta = 24.99 °	100.0%
Max. and min. transmission	-
Refinement method	Full-matrix least-squares on F^2
Final R indices [I>2sigma(I)]	R = 0.0482
	wR = 0.0989
R indices (all data)	R = 0.0606
	wR = 0.1083
Absolute structure parameter	0.06(9)

7.2.3   Crystal Data and Strucure Refinement of 113

Identification code	**113**
Empirical formula	$C_{25}H_{24}N_2S$
Formula weight	384.57 g.mol^{-1}
Temperature	396(2) K
Wavelength	0.71073 Å
Crystal system	-
Space group	-
Unit cell dimensions	a = 17.0684(15) Å
	b = 8.0774(7) Å
	c = 18.8459(17) Å
	α = 90.00 °
	β = 109.117(2) °
	γ = 90.00 °
Volume	2455.0(4) Å^3
Z	4
Density (calculated)	1.051 Mg.m^{-3}
Absorption coefficient	0.144 mm^{-1}
Crystal size (mm^3)	-
	-
	-
Theta range for data collection	1.14 to 24.99 °
Reflections collected	9728
Independent reflections	4269 [R_{int} = 0.0281]
Completeness to theta = 24.99 °	100.0%
Max. and min. transmission	-
Refinement method	Full-matrix least-squares on F^2
Final R indices [I>2sigma(I)]	R = 0.0398
	wR = 0.0934
R indices (all data)	R = 0.0464
	wR = 0.1009
Absolute structure parameter	0.05(7)

7.2.4 Crystal Data and Strucure Refinement of 114

Identification code	**114**
Empirical formula	$C_{25}H_{24}N_2S$
Formula weight	384.57 g.mol^{-1}
Temperature	396(2) K
Wavelength	0.71073 Å
Crystal system	-
Space group	-
Unit cell dimensions	a = 22.844(3) Å
	b = 10.8702(14) Å
	c = 10.1034(13) Å
	α = 90.00 °
	β = 90.00 °
	γ = 90.00 °
Volume	2508.8(6) Å^3
Z	4
Density (calculated)	1.086 Mg.m^{-3}
Absorption coefficient	0.196 mm^{-1}
Crystal size (mm^3)	-
	-
	-
Theta range for data collection	2.07 to 28.20 °
Reflections collected	12393
Independent reflections	3155 [R_{int} = 0.0199]
Completeness to theta = 28.20 °	99.9%
Max. and min. transmission	-
Refinement method	Full-matrix least-squares on F^2
Final R indices [I>2sigma(I)]	R = 0.0890
	wR = 0.2692
R indices (all data)	R = 0.898
	wR = 0.2713
Absolute structure parameter	0.04(14)

7.2.5 Graphs of Anion-induced Changes in the CD Spectrum of Chiral *Bis*-Naphthalene-based Anion Sensors
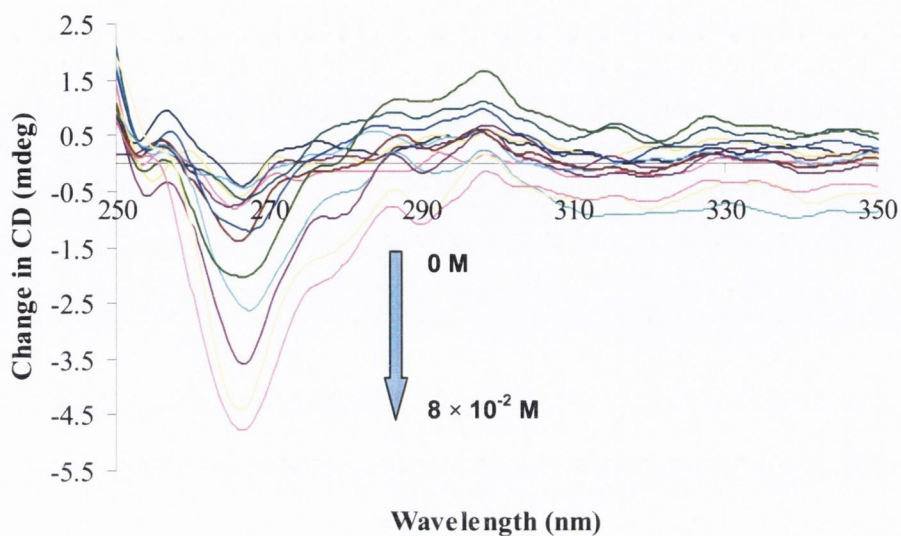
Figure 7.17 Quantitative changes observed in the CD spectrum of **112** in DMSO in the presence of $H_2PO_4^-$.
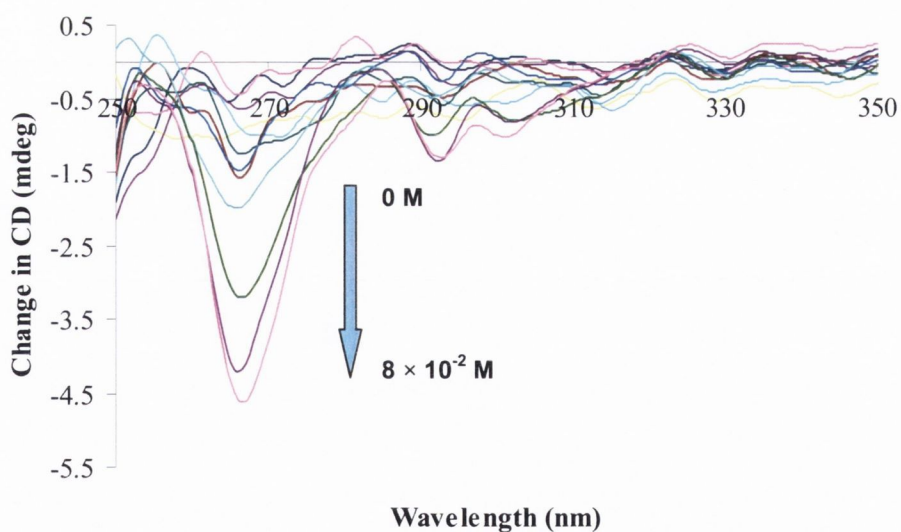
Figure 7.18 Quantitative changes observed in the CD spectrum of **112** in DMSO in the presence of F^-.
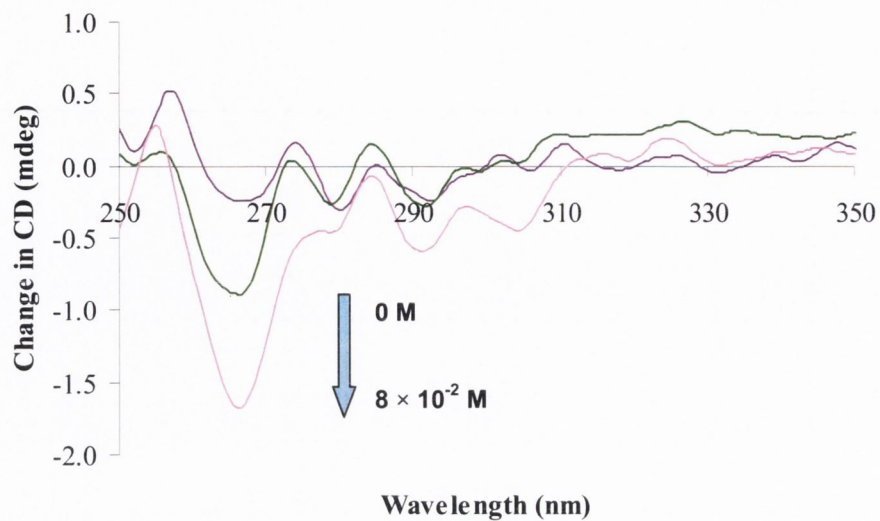
Figure 7.19 Quantitative changes observed in the CD spectrum of **112** in DMSO in the presence of Cl⁻.
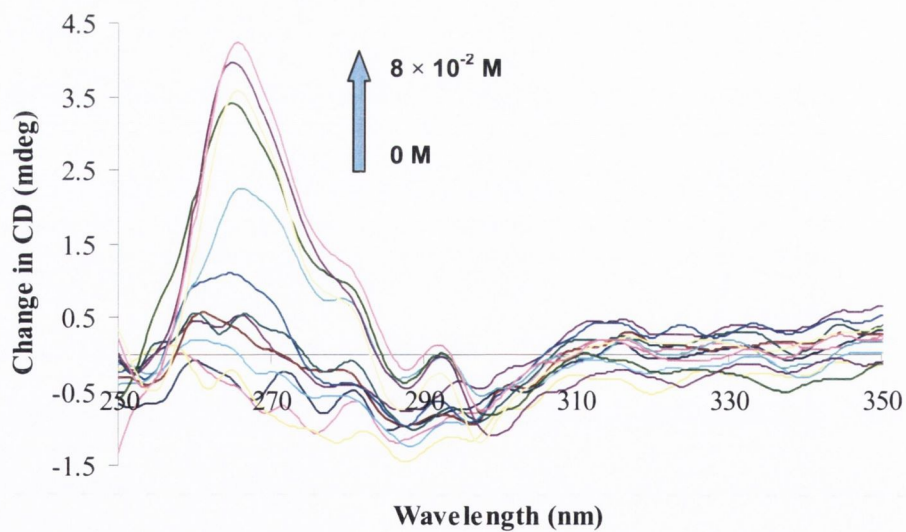
Figure 7.20 Quantitative changes observed in the CD spectrum of **113** in DMSO in the presence of $H_2PO_4^-$.
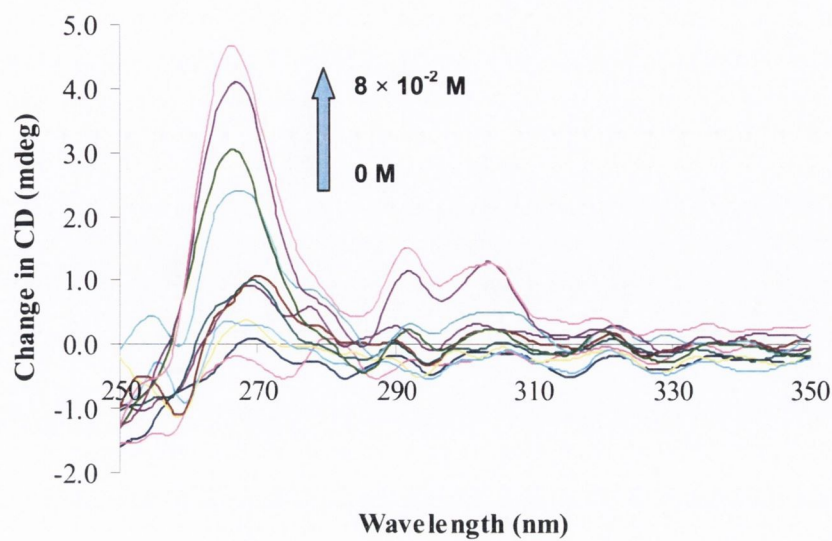
Figure 7.21 Quantitative changes observed in the CD spectrum of **113** in DMSO in the presence of F⁻.
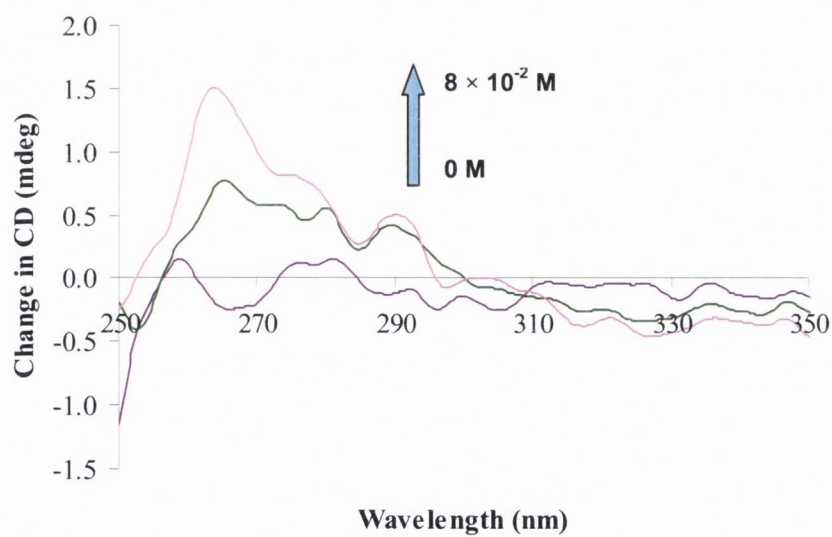
Figure 7.22 Quantitative changes observed in the CD spectrum of **113** in DMSO in the presence of Cl⁻.

7.2.6   Possible Effects of AcO⁻ on the CD of the Solvent (DMSO)
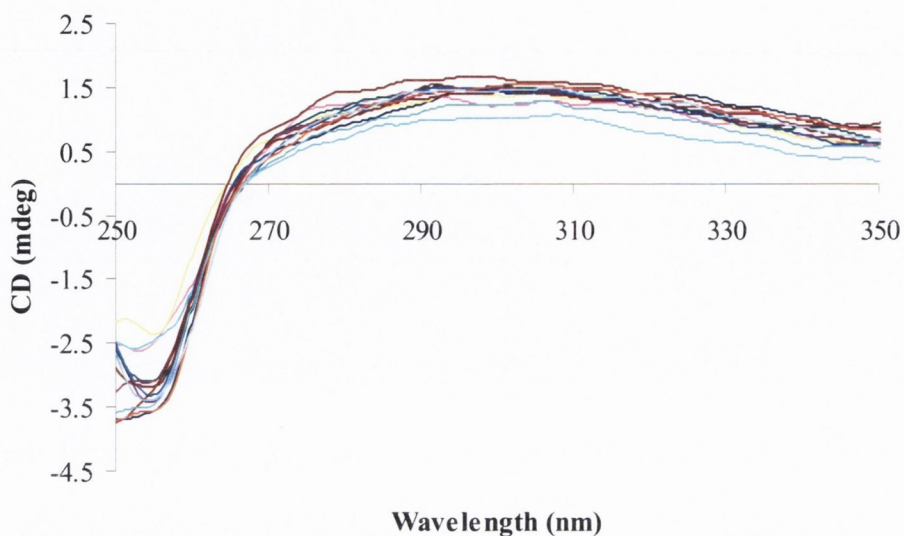
Figure 7.23 CD spectra of blank DMSO in the presence of various equivalents of AcO⁻ (0 M → 8 × 10⁻² M).

7.2.7   Comparison between "One-baseline" and "Multiple-baseline" Methods for the CD Titration of 112 with AcO⁻
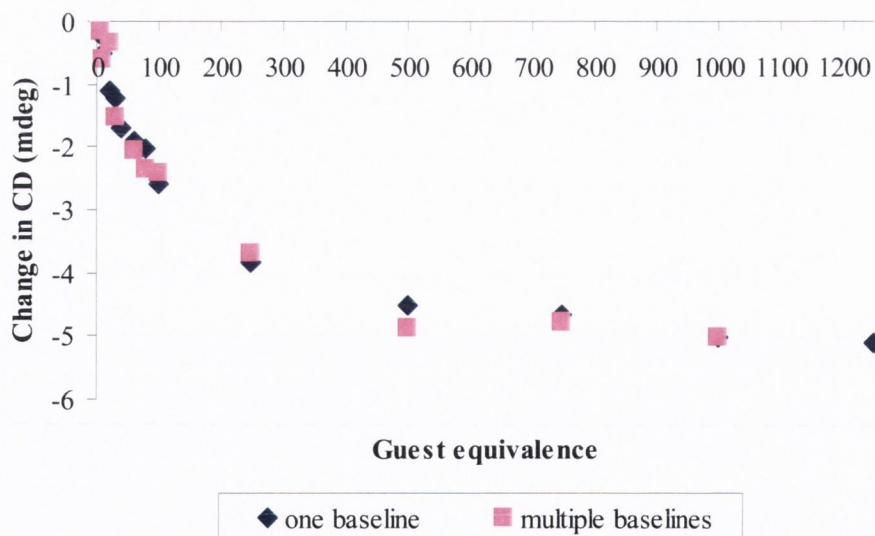
Figure 7.24 Comparison of the quantitative changes observed at 276.5 nm in the CD spectrum of **112** in DMSO with AcO⁻ between two experiments (*i.e.* one baseline – an initial baseline for all the scans carried out; multiple baselines – an initial baseline for each scan carried out).

7.3   Appendices for Chapter 4

7.3.1   SPECFIT/32™-Generated Graphs and Speciation Plots for the Absorption Titrations of 64 with Anions

(a)
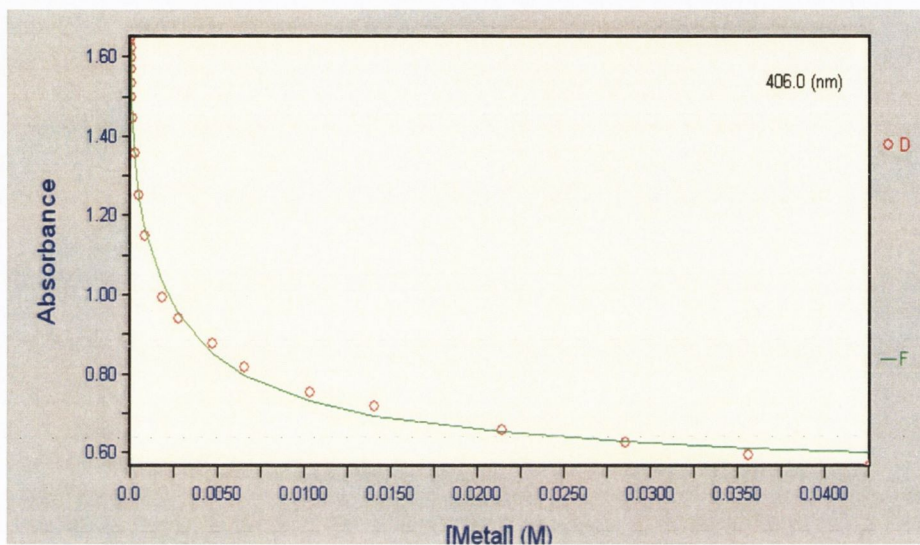
(b)
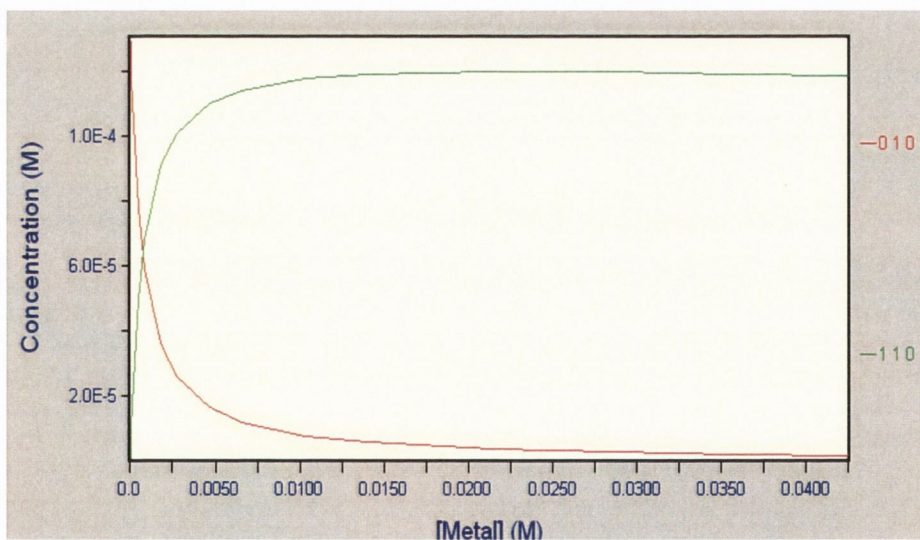
Figure 7.25 (a) SPECFIT/32™-generated graph showing the fit between the observed (D) and calculated (F) data at 406.0 nm for the binding of AcO$^-$ by **64**; (b) Speciation plot showing the concentrations of the free host **64** (010) and the 1:1 complex (110) upon the addition of AcO$^-$.

(a)

(b)

Figure 7.26 (a) SPECFIT/32™-generated graph showing the fit between the observed (D) and calculated (F) data at 406.7 nm for the binding of $H_2PO_4^-$ by **64**; (b) Speciation plot showing the concentrations of the free host **64** (010) and the 1:1 complex (110) upon the addition of $H_2PO_4^-$.

(a)

(b)

Figure 7.27 (a) SPECFIT/32™-generated graph showing the fit between the observed (D) and calculated (F) data at 406.7 nm for the binding of F⁻ by **64**; (b) Speciation plot showing the concentrations of the free host **64** (010) and the 1:1 complex (110) upon the addition of F⁻.

228

7.3.2 Graphs of the Changes Observed in the Absorption Spectra of 129 and 130 upon the addition of various anions
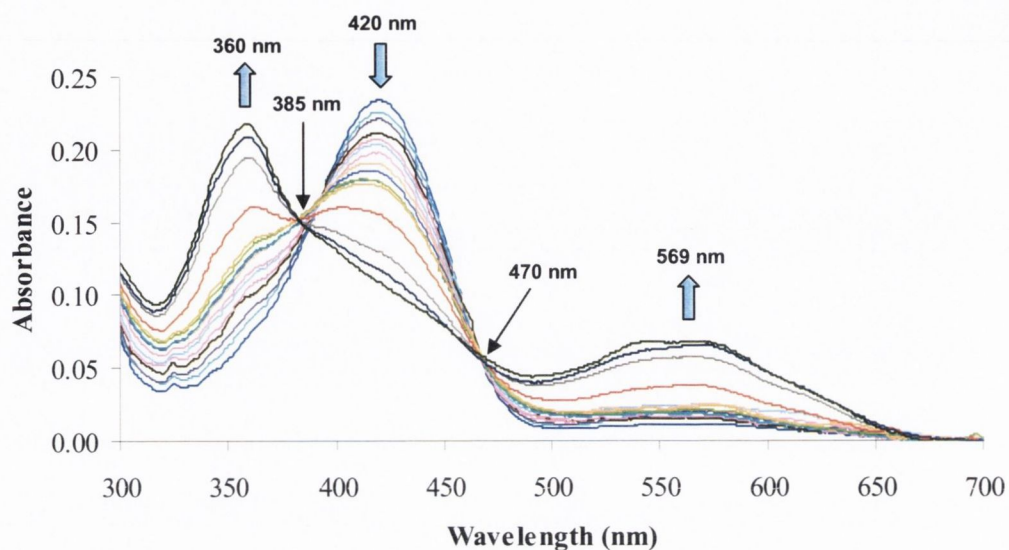
Figure 7.28 Changes observed in the absorption spectrum of urea **129** (1.5×10^{-5} M) upon addition of AcO$^-$ in DMSO at 25 °C (0 M $\rightarrow$ 3 × 10^{-3} M).
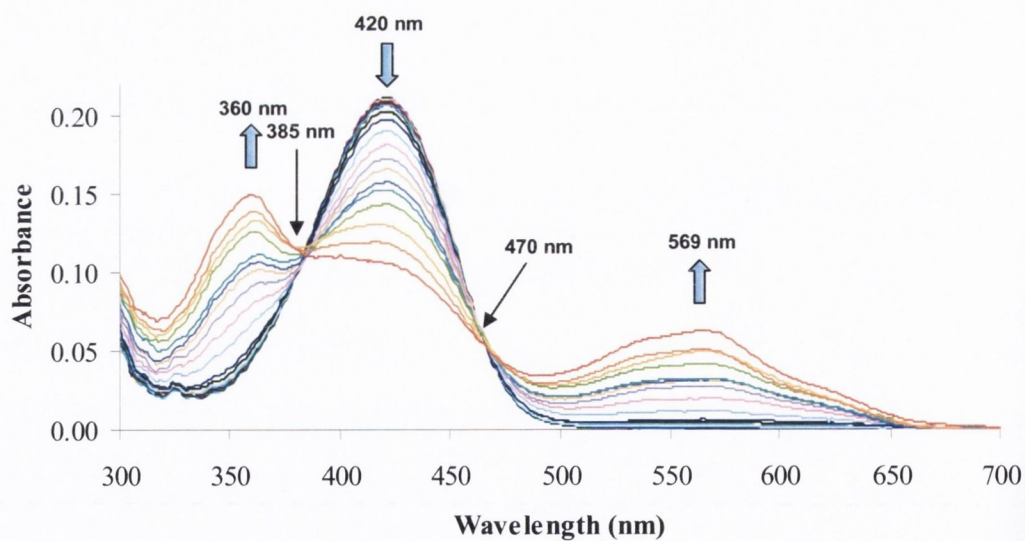
Figure 7.29 Changes observed in the absorption spectrum of urea **129** (1.5×10^{-5} M) upon addition of H$_2$PO$_4^-$ in DMSO at 25 °C (0 M $\rightarrow$ 3 × 10^{-3} M).

229
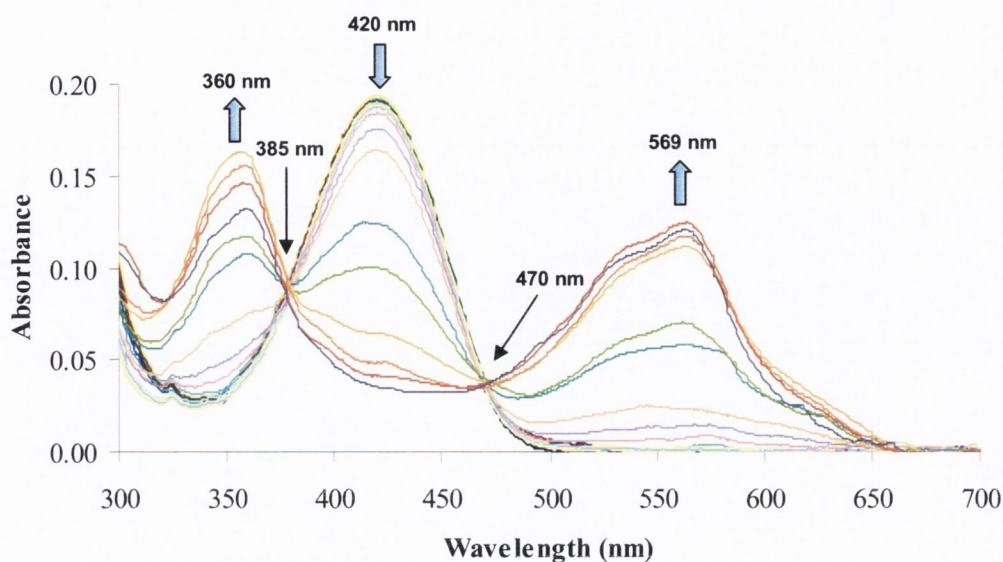
Figure 7.30 Changes observed in the absorption spectrum of urea **129** (1.5×10^{-5} M) upon addition of F$^-$ in DMSO at 25 °C (0 M → 3×10^{-3} M).
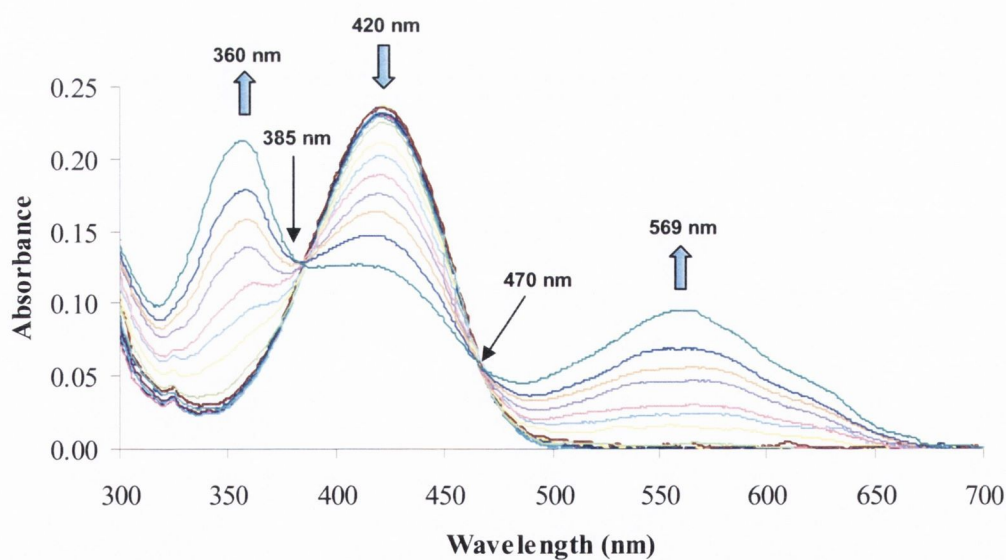
Figure 7.31 Changes observed in the absorption spectrum of urea **130** (1.5×10^{-5} M) upon addition of AcO$^-$ in DMSO at 25 °C (0 M → 3×10^{-3} M).
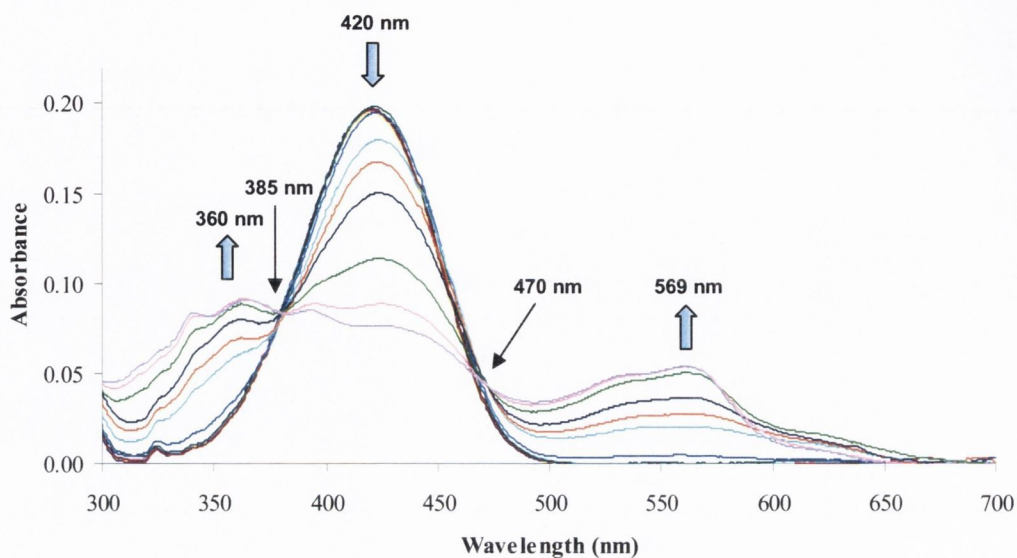
Figure 7.32 Changes observed in the absorption spectrum of urea **130** (1.5×10^{-5} M) upon addition of $H_2PO_4^-$ in DMSO at 25 °C (0 M $\rightarrow$ 3×10^{-3} M).
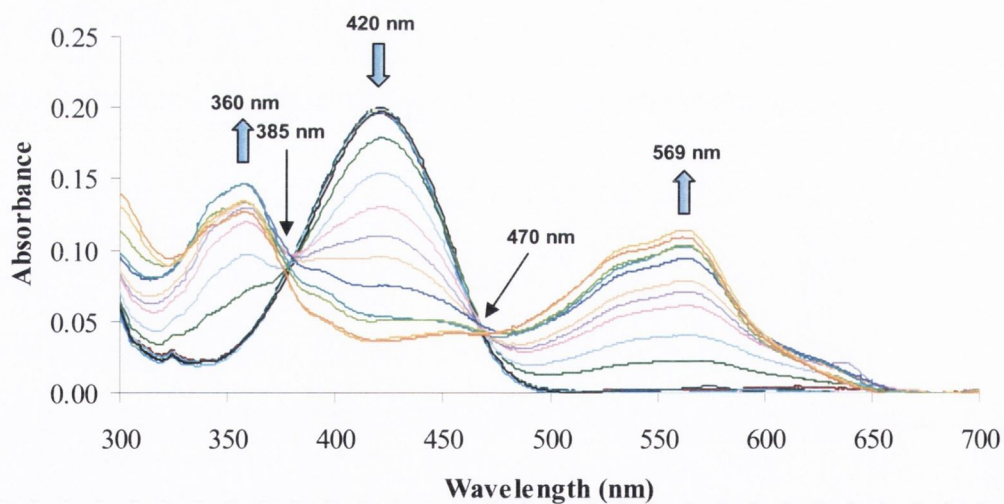
Figure 7.33 Changes observed in the absorption spectrum of urea **130** (1.5×10^{-5} M) upon addition of F^- in DMSO at 25 °C (0 M $\rightarrow$ 3×10^{-3} M).

7.3.3 SPECFIT/32™-Generated Graphs and Speciation Plots for the Absorption Titrations of 129 - 131 with Anions

(a)
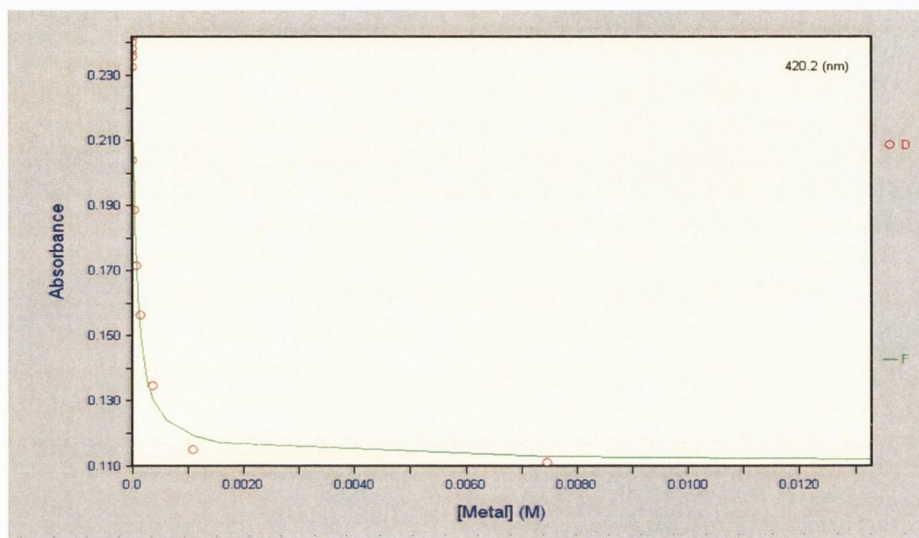
(b)
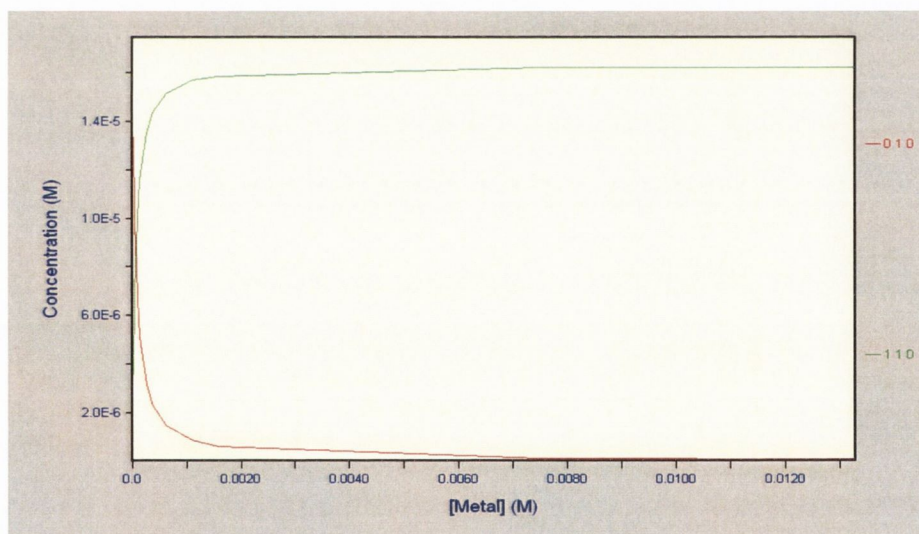
Figure 7.34 (a) SPECFIT/32™-generated graph showing the fit between the observed (D) and calculated (F) data at 406.0 nm for the binding of AcO⁻ by **129**; (b) Speciation plot showing the concentrations of the free host **129** (010) and the 1:1 complex (110) upon the addition of AcO⁻.
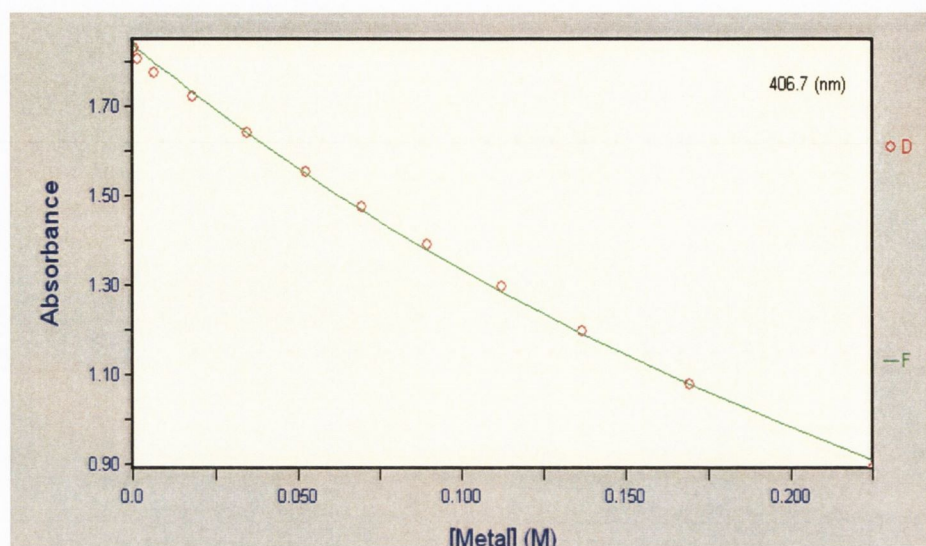
(a)

(b)
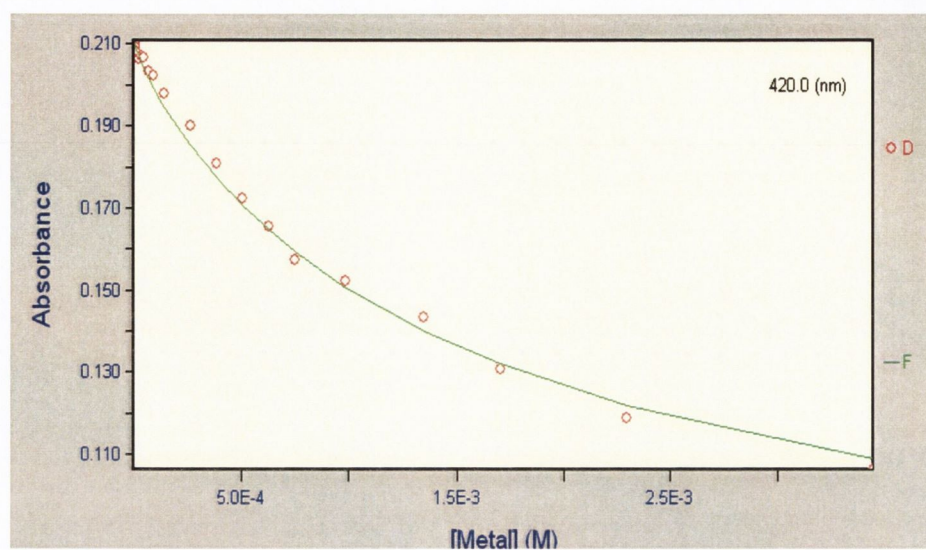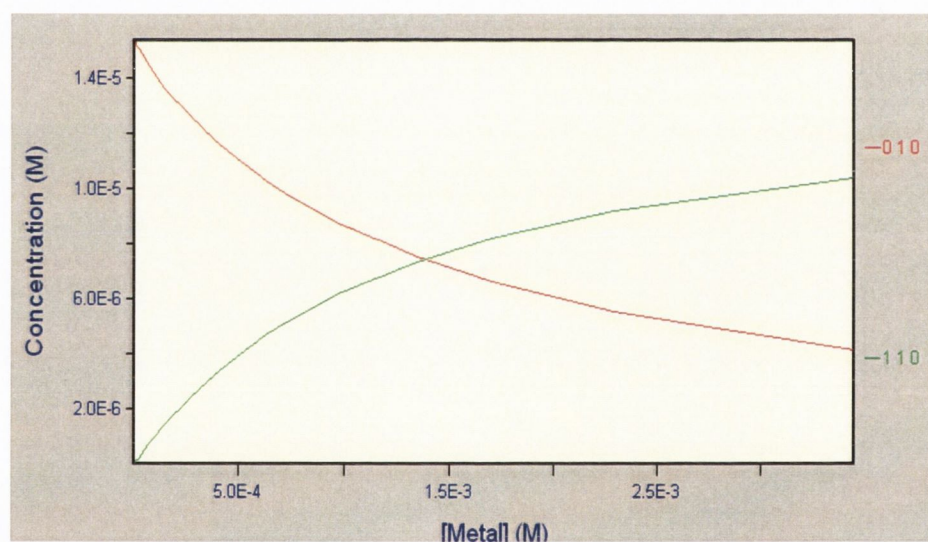
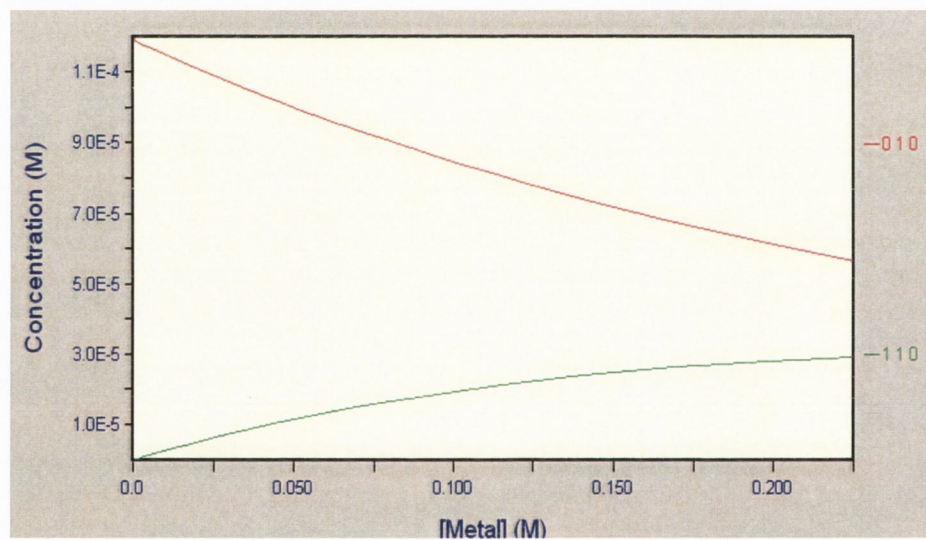
Figure 7.35 (a) SPECFIT/32™-generated graph showing the fit between the observed (D) and calculated (F) data at 406.0 nm for the binding of $H_2PO_4^-$ by **129**; (b) Speciation plot showing the concentrations of the free host **129** (010) and the 1:1 complex (110) upon the addition of $H_2PO_4^-$.

233

(a)

(b)
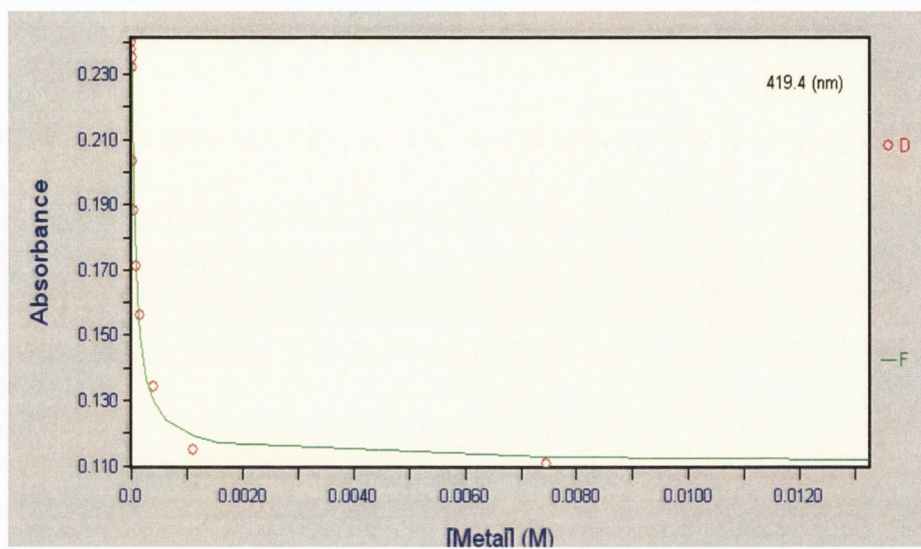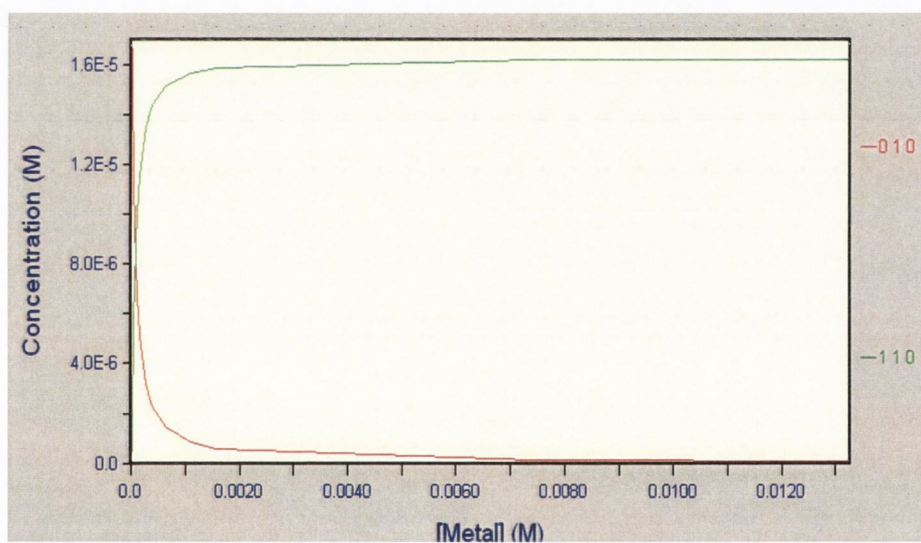
Figure 7.36 (a) SPECFIT/32™-generated graph showing the fit between the observed (D) and calculated (F) data at 406.0 nm for the binding of AcO⁻ by **130**; (b) Speciation plot showing the concentrations of the free host **130** (010) and the 1:1 complex (110) upon the addition of AcO⁻.
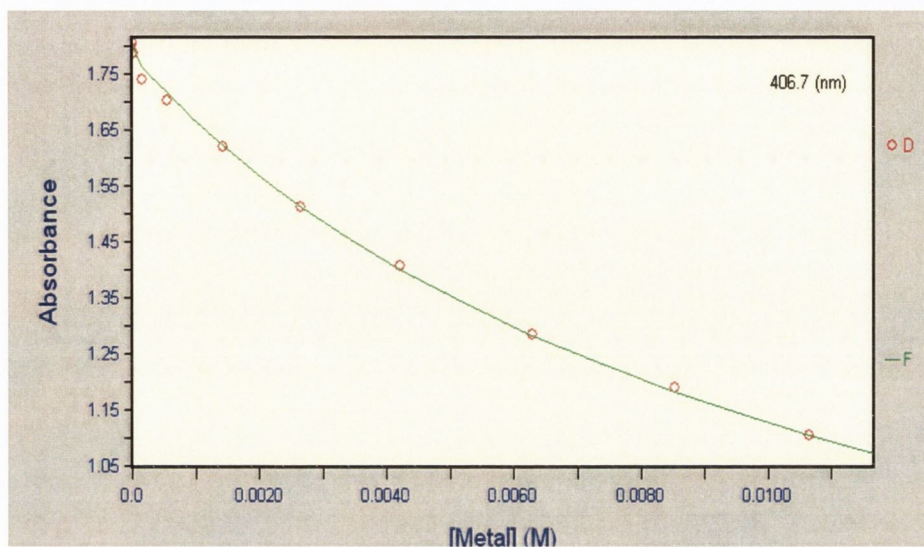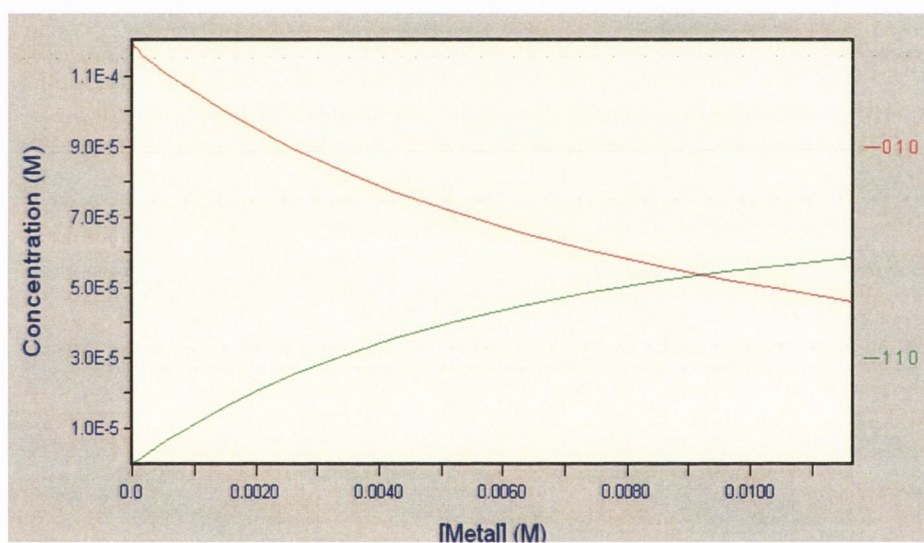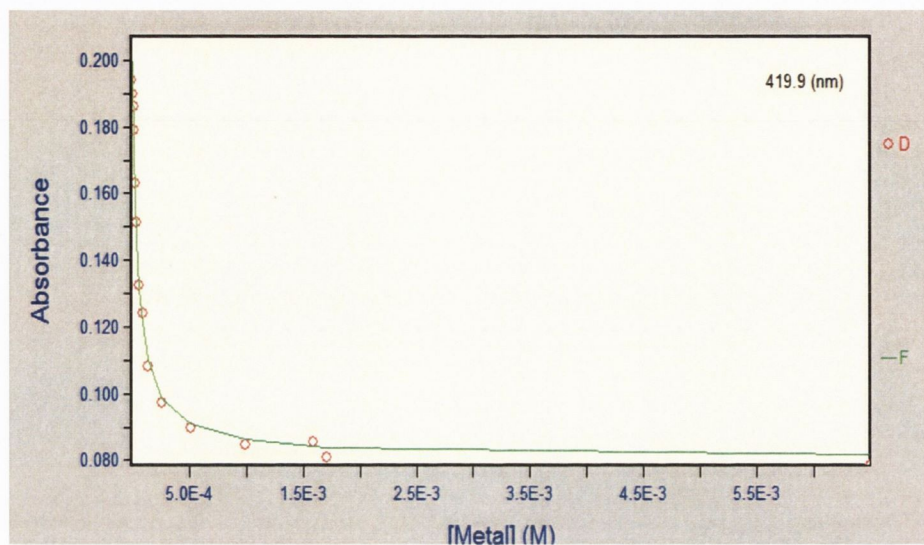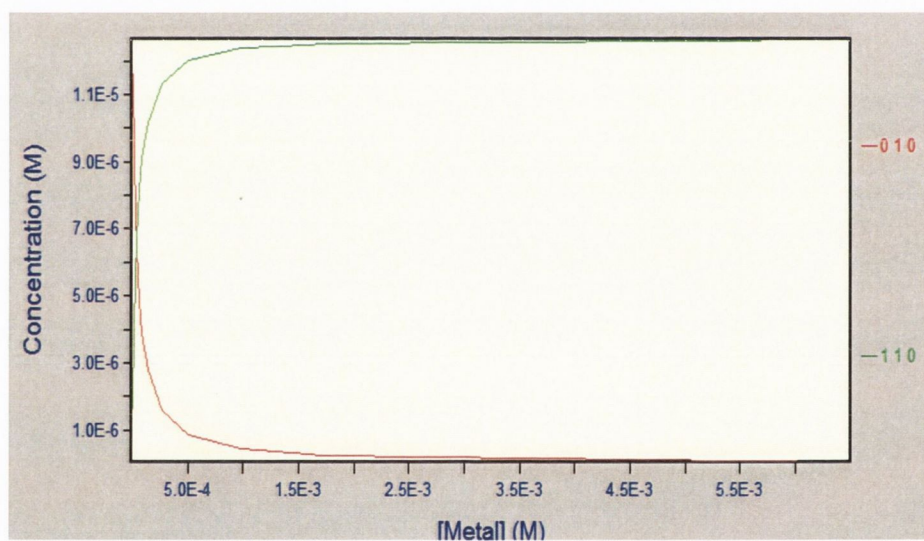
(a)

(b)

Figure 7.37 (a) SPECFIT/32™-generated graph showing the fit between the observed (D) and calculated (F) data at 406.0 nm for the binding of AcO⁻ by **131**; (b) Speciation plot showing the concentrations of the free host **131** (010) and the 1:1 complex (110) upon the addition of AcO⁻.

(a)

(b)
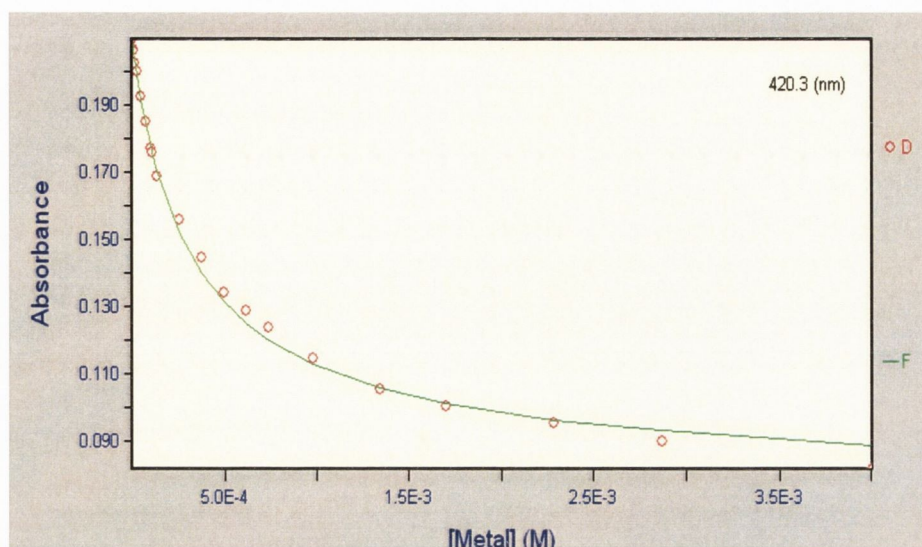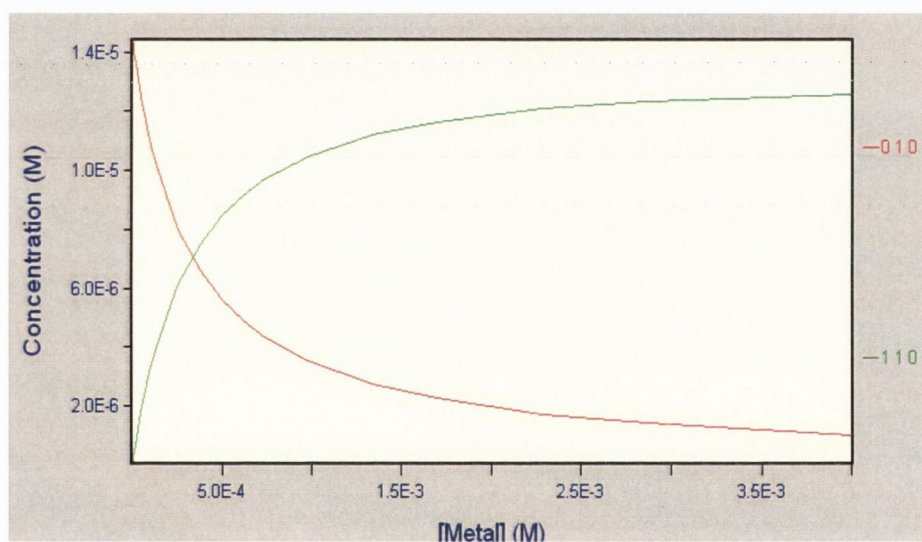
Figure 7.38 (a) SPECFIT/32™-generated graph showing the fit between the observed (D) and calculated (F) data at 406.0 nm for the binding of $H_2PO_4^-$ by **131**; (b) Speciation plot showing the concentrations of the free host **131** (010) and the 1:1 complex (110) upon the addition of $H_2PO_4^-$.

### 7.3.3 SPECFIT/32™-Generated Graph for the Fluorescence Titration of 131 with AcO⁻
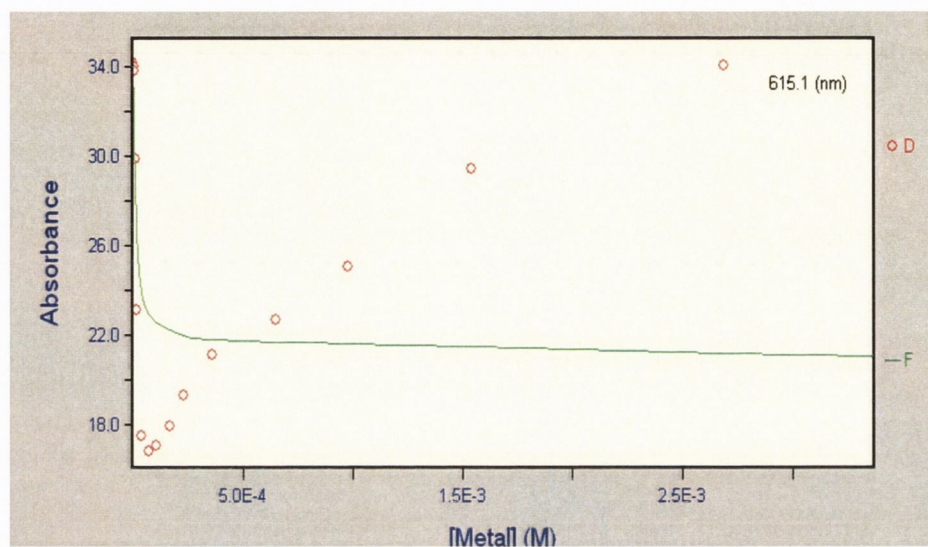
Figure 7.39 (a) SPECFIT/32™-generated graph showing the fit between the observed (D) and calculated (F) data at 406.0 nm for the binding of AcO⁻ by **131**.

7.4 References for Appendices

1.   Hansch, C.; Leo, A.; Taft, R. W. *Chem. Rev.* **1991,** *91*, 165-195.

2.   Shorter, J. *Correlation Analysis in Organic Chemistry: An Introduction to Linear Free Energy Relationships*; Oxford University Press: Oxford, **1973**.

3.   Isaacs, N. S. *Physical Organic Chemistry*; Longman Group Ltd.: New York, **1981**.

Colorimetric "Naked Eye" Sensing of Anions in Aqueous Solution

Thorfinnur Gunnlaugsson,* Paul E. Kruger,*
Paul Jensen, Juliann Tierney,
Haslin Dato Paduka Ali, and Gillian M. Hussey

School of Chemistry, Center for Synthesis and Chemical Biology, Trinity College Dublin, Dublin 2, Ireland

gunnlaut@tcd.ie; paul.kruger@tcd.ie

Received September 29, 2005
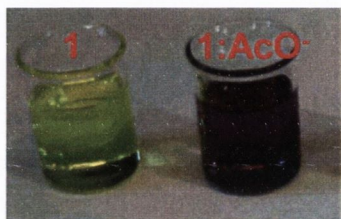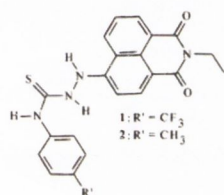
The synthesis and UV–vis and NMR spectroscopic studies of thiourea-based colorimetric sensors for anions are presented. These sensors can recognize anions through hydrogen binding even in competitive pH-buffered aqueous solutions, giving rise to large color changes that are clearly visible to the naked eye.

Luminescent and colorimetric anion recognition and sensing is a rapidly developing field within supramolecular chemistry.[1] As inspiration, nature provides us with many great examples of anion recognition motifs, primarily based on hydrogen-bonding interactions at charged or charge-neutral organic receptors.[2] Employing these inherently weak interactions as the foundation of receptor design to mimic these recognition events is notoriously difficult as solvent molecules compete more effectively for both the receptor (host) and anion (guest). However, we recently demonstrated the first examples of anion sensing using charge-neutral thiourea hydrogen-bonding motifs in fluorescent PET chemosensors.[3] De-

SCHEME 1. Synthesis of Sensors 1 and 2
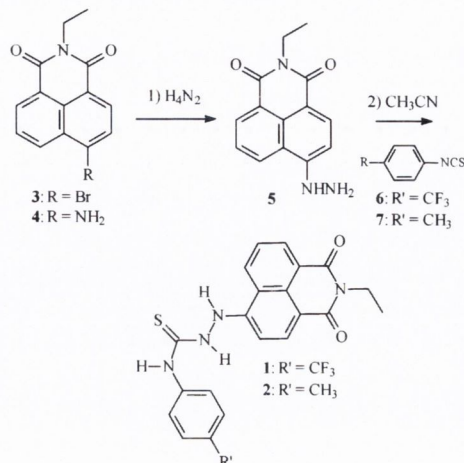
spite our success, anion sensing *only* ever occurred in noncompetitive organic solvents. This shortcoming is also prevalent in many examples throughout the literature.[1,4,5] Clearly there is a need to develop receptors capable of anion binding within competitive media to more accurately mimic those interactions found in nature. In this note, we present two naphthalimide-based receptors, **1** and **2**, which belong to a family of new charge-neutral colorimetric internal charge transfer (ICT) chemosensors.[6] The recognition of the biologically important AcO⁻, $H_2PO_4^-$, and F⁻ anions is achieved in aqueous solution via hydrogen bonding at charge-neutral sites. Furthermore, the anion binding is accompanied by a visually striking color change, giving naked eye anion sensing.

Sensors **1** and **2** were made (Scheme 1) by first reacting *N*-ethyl-4-bromo-1,8-naphthalimde (**3**)[7] with hydrazine monohydrate to give **5** as a yellow solid in 93% yield. Reaction of **5** with either 4-(trifluoromethyl)phenyl- (**6**) or 4-(methyl)phenyl- (**7**) isothiocyanates gave **1** and **2**, respectively. Single crystals of **1** suitable for an X-ray diffraction study were grown from EtOH. The structure of **1** revealed the thiourea protons to be in the anti-conformation and that adjacent molecules participate in numerous intermolecular interactions. The combination

(1) See special issue on anion recognition: (a) *Coord. Chem. Rev.* **2003**, *240*, 1–226. Other reviews include: (b) Martínez-Máñez, R.; Sancenón, F. *J. Fluoresc.* **2005**, *15*, 267. (c) Gale, P. A. *Chem. Commun.* **2005**, 3761. (d) Martínez-Máñez, R.; Sancenón, F. *Chem. Rev.* **2003**, *103*, 4419. (e) Suksai, C.; Tuntulani, T. *Chem. Soc. Rev.* **2003**, *32*, 192. (f) Gale, P. A. *Coord. Chem. Rev.* **2001**, *213*, 79. (g) Gale, P. A. *Coord. Chem. Rev.* **2000**, *199*, 181. (h) Beer, P. D.; Gale, P. A. *Angew. Chem., Int. Ed.* **2001**, *40*, 486. (i) Fabbrizzi, L.; Licchelli, M.; Rabaioli, G.; Taglietti, A. F. *Coord. Chem. Rev.* **2000**, *205*, 85.
(2) *Supramolecular Chemistry of Anions*; Bianchi, E., Bowman-James, K., Gracía-España, E., Eds.; Wiley-VCH: New York, 1997.
(3) (a) Gunnlaugsson, T.; Ali, H. D. P.; Glynn, M.; Kruger, P. E.; Hussey, G. M.; Pfeffer, F. M.; dos Santos, C. M. G.; Tierney, J. *J. Fluoresc.* **2005**, *15*, 287. (b) Pfeffer, F. M.; Buschgens, A. M.; Barnett, N. W.; Gunnlaugsson, T.; Kruger, P. E. *Tetrahedron Lett.* **2005**, *46*, 6579. (c) Gunnlaugsson, T.; Davis, A. P.; O'Brien, J. E.; Glynn, M. *Org. Biomol. Chem.* **2005**, *3*, 48. (d) Gunnlaugsson, T.; Davis, A. P.; Hussey, G. M.; Tierney, J.; Glynn, M. *Org. Biomol. Chem.* **2004**, *2*, 1856. (e) Gunnlaugsson, T.; Kruger, P. E.; Jensen, P.; Pfeffer, F. M.; Hussey, G. M. *Tetrahedron Lett.* **2003**, *44*, 8909. (f) Gunnlaugsson, T.; Davis, A. P.; O'Brien, J. E.; Glynn, M. *Org. Lett.* **2002**, *4*, 2449. (g) Gunnlaugsson, T.; Davis, A. P.; Glynn, M. *Chem. Commun.* **2001**, 2556.

(4) (a) Davis, A. P.; Joos, J. B. *Coord. Chem. Rev.* **2003**, *240*, 143. (b) Schmidtchen, F. P.; Berger, M. *Chem. Rev.* **1997**, *97*, 1609.
(5) Recent excellent examples include: (a) Thiagarajan, V.; Ramamurthy, P.; Thirumalai, D.; Ramakrishnan, T. *Org. Lett.* **2005**, *7*, 657. (b) Esteban-Gómez, D.; Fabbrizzi, L.; Liechelli, M.; Esteban-Gómez, D. *J. Org. Chem.* **2005**, *70*, 5717. (c) Fabbrizzi, L.; Licchelli, M.; Monzani, E. *Org. Biomol. Chem.* **2005**, *3*, 1495. (d) Liu, B.; Tian, H. *Chem. Lett.* **2005**, *34*, 686. (e) Jose, D. A.; Kumar, D. K.; Ganguly, B.; Das, A. *Org. Lett.* **2004**, *6*, 3445. (f) Vázquez, M.; Fabbrizzi, L.; Taglietti, A.; Pedrido, R. M.; González-Noya, A. M.; Bermejo, M. R. *Angew. Chem., Int. Ed.* **2004**, *43*, 1962. (g) Camiolo, S.; Gale, P. A.; Hursthouse, M. B.; Light, M. E. *Org. Biomol. Chem.* **2003**, *1*, 741. (h) Jiméenez, D.; Martínez-Máñez, R.; Sancenón, F.; Soto, J. *Tetrahedron Lett.* **2002**, *43*, 2823. (i) Miyaji, H.; Sessler, J. L. *Angew. Chem., Int. Ed.* **2001**, *40*, 154. (j) Lee, D. H.; Lee, K. H.; Hong, J. I. *Org. Lett.* **2001**, *3*, 5. (k) Niikura, K.; Bisson, A. P.; Anslyn, E. V. *J. Chem. Soc., Perkin Trans. 2* **1999**, 1111.
(6) Examples of colorimetric sensors for cations include: (a) Gunnlaugsson, T.; Leonard, J. P.; Murray N. S. *Org. Lett.* **2004**, *6*, 1557. (b) Gunnlaugsson, T.; Leonard, J. P. *J. Chem. Soc., Perkin Trans. 2* **2002**, 1980.
(7) Gunnlaugsson, T.; Kruger, P. E.; Lee, T. C.; Parkesh, R.; Pfeffer, F. M.; Hussey, G. M. *Tetrahedron Lett.* **2003**, *44*, 6575.
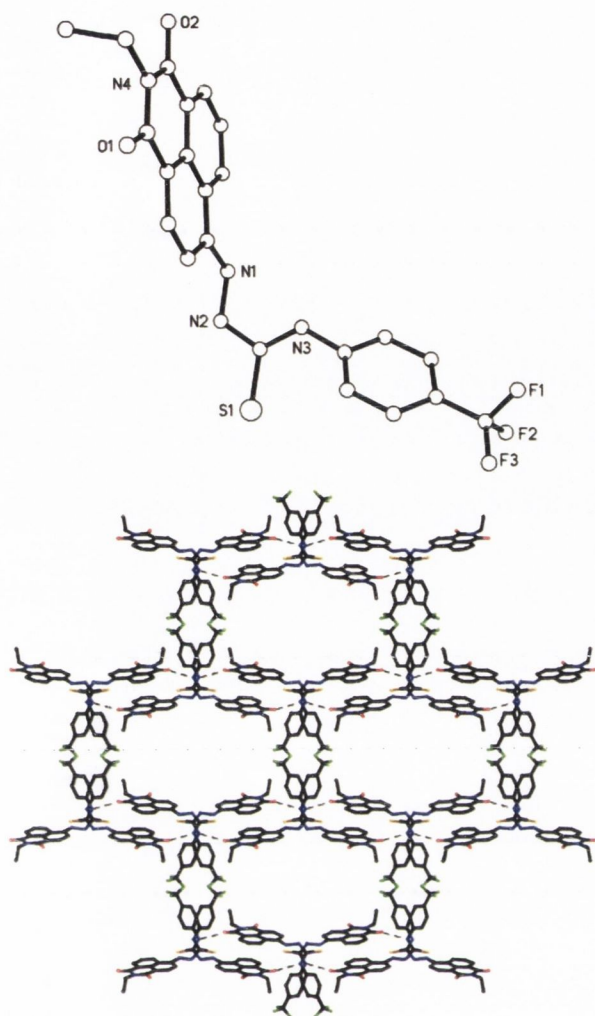
FIGURE 1. Structure of **1** showing the *anti* conformation of the thiourea moiety (top) and the 3-D network it forms (bottom). H atoms and solvent molecules omitted for clarity.

of H-bonding, face-to-face π–π stacking, and short F···F contacts[8] give rise to an elaborate 3D network that is perforated with solvent-filled channels (Figures 1 and S1). Poorer quality crystals of **2** may also be isolated from EtOH.[9]

The spectroscopic investigation of **1** and **2** was first carried out in DMSO. Sensor **1** (1×10^{-4} M) showed a broad absorption band centered at 414 nm and a smaller shoulder at 560 nm.[10] Upon addition of anions such as AcO⁻, $H_2PO_4^-$, and F⁻ (as their tetrabutylammonium salts), the band at 560 nm increased in intensity at the expense of the 414-nm transition. Furthermore, a new band at 350 nm and two clear isosbestic points were

(8) Halper, S. R.; Cohen, S. M. *Angew. Chem., Int. Ed.* **2004**, *43*, 2385.

(9) The packing of **1** suggests that the CF₃ groups self-aggregate and play a significant structure-directing role that allows the growth of good quality crystals (cf. **2**) and propagates the formation of channels via short F···F contacts.[8] These channels account for a staggering 36% of the crystal volume, attesting to the strength of these multiple interactions.

(10) The ratio between these two bands was highly concentration-dependent, whereas at low concentration the 560-nm band was substantially more intense than at higher concentrations (see Supporting Information). Quartz cells and glassware were used in all of these measurements.

observed at 465 and 380 nm, respectively (Figure S2). The yellow to deep purple color change is clearly evident to the naked eye (Figure S3). We propose that these changes are consistent with the anions binding to the thiourea moiety through hydrogen bonding. For such recognition to occur, the thiourea protons need to be in *syn* orientation. It is also possible that the proton of the 4-amino moiety is aiding in the binding of the anion and that these combined binding modes give rise to enhanced ICT character with concomitant color changes. This hypothesis is further supported by the fact that the absorption spectrum of **4** has a λ_{max} at ca. 460 nm, which suggests that the lone pair of the 4-amino moiety of **1** is not fully engaged in the ICT prior to the binding.[11]

By observing the changes in the 560-nm band of **1** as a function of increasing concentration of AcO⁻ (as −log[AcO⁻]), a sigmoidal curve was observed that changed over two log units. This is characteristic of 1:1 binding and simple equilibrium (Figure S2b).[3,12] Nonlinear least-squares regression analysis of these changes gave a binding constant log β = 4.95 (±0.1). When these measurements were repeated using **5**, no such changes occurred (e.g. the thiourea functional group is essential to successful anion sensing and consequent color changes). Similarly, titration with F⁻ or $H_2PO_4^-$ gave rise to comparable spectral changes with binding constants of 4.4 (±0.1) (Figure S4) and 4.0 (±0.1), respectively. No significant changes were observed using other halides (e.g. Cl⁻ or Br⁻). However, it is worth noting that at higher F⁻ concentrations there were distinctive changes in the absorption spectra that we assign to the deprotonation of the 4-aminonaphthalimide moiety and the formation of bifluoride (HF_2^-) (Figure S3, see later discussion).[7,13] Similar results were observed for **2**, with a log β of 4.3 (±0.1) for F⁻, demonstrating that the nature of the aromatic moiety of the receptor (CF₃ versus CH₃) does not greatly alter the binding affinity. This is possibly due to the "overriding effect" of the ICT nature of the naphthalimide unit over the phenyl.

The binding of anions was also clear from ¹H NMR spectroscopy (DMSO-d_6) by monitoring the thiourea protons of **2** that initially appear at 10.04 and 10.06 ppm and the aromatic N–H proton at 9.86 ppm (Figure S5). This revealed that the binding of anions resulted in slow exchange of the protons as titration with either F⁻ or AcO⁻ showed the formation of two new thiourea proton resonances at 8.05 and 11.2 ppm (Figure 2). For AcO⁻ the aromatic N–H was also visible as a broad signal appearing at ca. 12 ppm, but after ca. 0.8 equiv of AcO⁻

(11) de Silva, A. P.; Gunaratne, H. Q. N.; Gunnlaugsson, T.; Huxley, A. J. M.; McCoy, C. P.; Rademacher J. T.; Rice, T. E. *Chem. Rev.* **1997**, *97*, 1515.

(12) This binding was also visible in the fluorescence emission spectra. When exciting at 404 nm, a broad emission band centered at ca. 440 nm was observed that reduced in intensity upon addition of anions with the formation of two bands at 510 and 635 nm, respectively. We do not believe that we have a large contribution of aggregation in the sample as the NMR did not change upon dilutions. However, we cannot disregard the fact that urea and thiourea compounds are known to aggregate to a degree and hence that the anion addition might affect the nature of this aggregation if present. Nevertheless, the fact that Cl⁻ and Br⁻ did not give rise to any spectral changes strongly supports our explanation. Unfortunately, as **1** and **2** are insoluble in neat H_2O it was not possible to carry out an identical investigation in this solvent.

(13) Shenderovich, I. G.; Tolstoy, P. M.; Golubev, N. S.; Smirnov, S. N.; Denisov, G. S.; Limbach, H.-H. *J. Am. Chem. Soc.* **2003**, *125*, 11710.

FIGURE 2. Stack plot of ^{1}H NMRs of **2** on addition of AcO$^-$ (DMSO-d_6, 400 MHz). Black symbols show position of resonance before addition of anion, and red symbols show position of resonance upon binding.

FIGURE 3. Stack plot of ^{1}H NMRs of **2** with F$^-$ (1–5.2 equiv, DMSO-d_6, 400 MHz). The dashed line tracks the formation of HF$_2^-$.

it had broadened and disappeared. Integration of these newly formed signals confirmed the 1:1 binding seen in the absorption spectra. For AcO$^-$ (Figures 2 and S6), no further changes occurred after the addition of 1 equiv. However, excess F$^-$ (1 → 5.2 equiv) caused further changes, with the appearance of a new signal at 16.1 ppm after ca. 3 equiv with significant changes in all the resonances supporting the formation of HF$_2^-$ (Figures 3 and S7).[7,13]

The most important result from our current study is that, upon addition of competitive hydrogen-bonding solvents such as ethanol or water, the color changes were *not* reversed.[4,5] We thus carried out identical titrations of **1** in EtOH, where **1** showed a strong absorption band at 404 nm and a smaller shoulder at 540 nm. The titration of this solution with AcO$^-$ (Figure S8), F$^-$, or H$_2$PO$_4^-$ gave rise to distinctive color changes. For AcO$^-$, a new band at 340 nm and isosbestic points at 368 and 454 nm were observed. For the changes in the 540 nm band, log β values of 4.47 ($\pm$0.1), 3.80 ($\pm$0.1), and 3.48 ($\pm$0.1) were determined for these anions, respectively. No such changes were seen for **5** (*which lacks the thiourea part*) upon addition of AcO$^-$ under identical conditions. Similar compounds functionalized with alkyl changed at this amino moiety have also been prepared in our previous work,[7] and these also showed no binding toward AcO$^-$. This clearly demonstrates that **1** is capable of sensing anions in highly competitive media, where the recognition is through hydrogen bonding. Furthermore,

the addition of excess F$^-$ did *not* give rise to the changes in the absorption spectra as seen previously, suggesting that no deprotonation of the naphthalimide amine or the thiourea had occurred. Encouraged by these remarkable results, we undertook the same titrations in 1:1 EtOH/H$_2$O mixture. Under these conditions, two bands were seen in the absorption spectra at 407 nm (major band) and 548 nm (minor band) for **1**. Upon titration with AcO$^-$ (Figure 4; see also Figure S9), similar effects were observed as seen previously in DMSO and EtOH solutions. As before, the changes were clearly visible to the naked eye and occurred over two log units (Figure 4 inset), giving log β values of 3.4 ($\pm$0.1), 2.2 ($\pm$0.1), and ~1 ($\pm$0.2) for AcO$^-$, F$^-$, and H$_2$PO$_4^-$, respectively. We also evaluated the response of **1** to a series of anions using their corresponding sodium salts. Of these, ClO$_4^-$, SO$_4^{2-}$, and Br$^-$ were not detected, whereas NaF produced results identical to that seen for TBAF. With the aim of excluding the possibility of these changes being due to pH changes, we carried out the same experiments in 1:1 EtOH/H$_2$O imidazole/HBr (10 mM) buffered solution at pH 7.15 for **1** and at pH 7.3 for **2**.[14] Once more, similar color changes were observed as above (cf. Figures S10 and S11 for AcO$^-$ and H$_2$PO$_4^-$, respectively). It should also be noted that the pH of the solution *did not change* by more than 0.15 units during these titrations, clearly excluding any pH
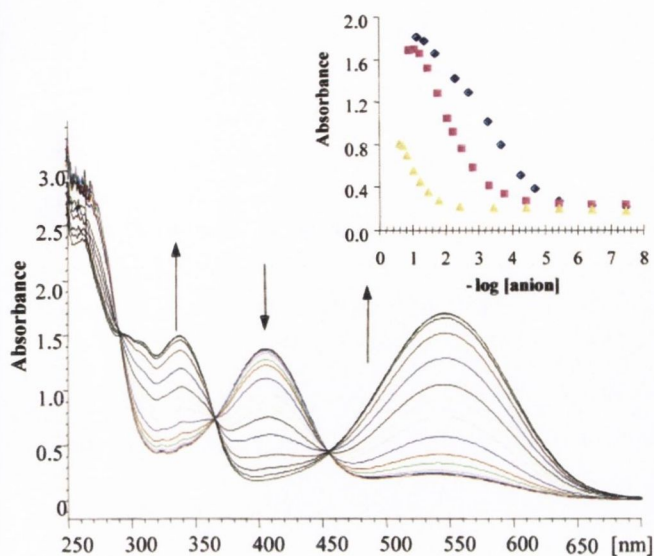
FIGURE 4. Changes in the absorption spectra of **1** on addition of F⁻ in 1:1 EtOH/H₂O solution. Inset shows the changes at 548 nm as a function of −log[anion]: ◆ = AcO⁻, ■ = F⁻, and ▲ = H₂PO₄⁻.

effects. To the best of our knowledge, these are the first examples of colorimetric (and luminescence) anion sensors that can be used in highly competitive aqueous media where the recognition event is mediated through bonding to a charge-neutral receptor that causes concomitant changes in the ICT character of the sensors.[15]

In summary, we have developed novel colorimetric anion sensors for use in aqueous solution where anion sensing occurs with concomitant yellow to purple color changes. We are currently investigating these unique features in greater detail.

Experimental Section

6-Bromo-2-ethylbenzo[*de*]isoquinoline-1,3-dione (3). 4-Bromo-1,8-naphthalic anhydride (2.00 g, 7.2 mmol) and ethylamine (70% soln in water) (0.69 mL, 8.66 mmol) were refluxed in 1,4-dioxane (100 mL) for 7 h. The solution was then poured into water to precipitate out a solid, which was collected by filtration, washed with water, and dried to yield **3** as a cream-colored solid (1.96 g, 89%). mp 160−162 °C (lit. mp 163 °C); Anal. Calcd for $C_{14}H_{10}BrNO_2$: C 55.29, H 3.31, N 4.61. Found: C 55.22, H 3.32, N 4.73; δ_H (400 MHz, CDCl₃): 1.34 (3H, t, J = 7.0 Hz, CH₃), 4.24 (2H, q, J = 7.0 Hz, CH₂), 7.82 (1H, dd, J = 7.8 and 8.0 Hz, Ar−H), 8.00 (1H, d, J = 8.0 Hz, Ar−H), 8.38 (1H, d, J = 8.0 Hz, Ar−H), 8.51 (1H, d, J = 8.5 Hz, Ar−H), 8.62 (1H, d, J = 7.5 Hz, Ar−H); δ_C (400 MHz, CDCl₃): 12.8, 35.2, 121.9, 122.7, 127.5, 128.5, 129.6, 130.1, 130.5, 130.6, 131.4, 132.6, 162.8, 162.9.

---

(14) Spectroscopic pH titrations of **1** and **2** showed that the color changes similar to those seen above only occurred in alkaline pH. See Figures S12 and S13 for **1** and **2**, respectively. These changes were fully reversible. Also note that the changes occurring in Figure 3 all took place in a pH window well below that seen in Figures S12 and S13.

(15) Anion sensing has been demonstrated at a 1,3-dichloroethane−water interface: Kato, R.; Cui, Y.-Y.; Nishizawa, S.; Yokobori, T.; Teramae, N. *Tetrahedron Lett.* **2004**, *45*, 4273 and references therein.

2-Ethyl-6-hydrazinobenzo[*de*]isoquinoline-1,3-dione (5). Hydrazine monohydrate (excess) was added to **3** (0.20 g, 0.66 mmol). This reaction mixture was heated at 130 °C and left stirring for 1 h. The mixture was then poured into water to precipitate out a solid, which was collected by filtration, washed with water, and dried to yield **5** as a yellow solid (0.16 g, 93%). mp 255−257 °C; HRMS: Calcd for $C_{14}H_{14}N_3O_2$ [M + H]⁺ 256.1086, found 256.1077; δ_H (400 MHz, (CD₃)₂SO): 1.18 (3H, t, J = 7.0 Hz, CH₃), 4.05 (2H, q, J = 7.0 Hz, CH₂), 4.69 (2H, d, J = 10.6 Hz, NH₂), 7.24 (1H, d, J = 8.6 Hz, Ar−H), 7.64 (1H, dd, J = 7.8 and 8.0 Hz, Ar−H) 8.28 (1H, d, J = 7.5 Hz, Ar−H), 8.41 (1H, d, J = 7.0 Hz, Ar−H), 8.61 (1H, d, J = 8.5 Hz, Ar−H), 9.13 (1H, br, NH); δ_C (100 MHz, (CD₃)₂SO): 13.3, 34.2, 104.0, 107.4, 118.4, 121.7, 124.1, 127.3, 128.2, 130.5, 134.2, 153.2, 162.7, 163.6; *m/z* 256 (M + H)⁺; v_{max}/cm⁻¹ 3450, 3366, 3316, 1672, 1636,1614, 1578, 1540, 1439, 1389, 1366, 1346, 1310, 1251, 114, 1069, 950, 772.

General Synthesis of Thioureas. The relevant amine and isothiocyanate (1.1 equiv) were refluxed for 3 days in CH₃CN. The solution was then washed with 0.5 M HCl and water. The organic layer was dried over MgSO₄, filtered, and evaporated to dryness. Purification of the crude product was carried out by trituration with chloroform.

6-[1-Amino-3-(4-trifluoromethylphenyl)-thiourea]-2-ethylbenzo[*de*]isoquinoline-1,3-dione (1). 1 was synthesized according to the above procedure, using **5** (0.20 g, 0.73 mmol) and 4-(trifluoromethyl)phenyl isothiocyanate (0.15 g, 0.73 mmol), yielding the desired product as a brown solid (0.05 g, 15%). mp 177−179 °C; HRMS: Calcd for $C_{22}H_{18}N_4O_2F_3S$ [M + H]⁺ 459.1103, found 459.1083; δ_H (400 MHz, (CD₃)₂SO): 1.20 (3H, t, J = 6.8 Hz, CH₃), 4.07 (2H, q, J = 6.8 Hz, CH₂), 6.99 (1H, d, J = 8.9 Hz, Ar−H naph), 7.67−7.74 (4H, C₆H₄), 7.83 (1H, dd, J = 8.9 and 9.6 Hz, Ar−H naph), 8.44 (1H, d, J = 8.2 Hz, Ar−H), 8.52 (1H, d, J = 7.5 Hz, Ar−H naph), 8.70 (1H, d, J = 7.5 Hz, Ar−H naph), 9.92 (1H, s, NH), 10.32 (1H, s, NH), 10.36 (1H, s, NH); δ_C (100 MHz, (CD₃)₂SO): 13.3, 34.5, 105.6, 111.8, 119.5, 121.9, 125.0, 125.6, 125.8, 126.3, 128.9, 129.3, 130.9, 133.6, 142.8, 149.7, 162.8, 181.3; *m/z* 459 (M + H)⁺; v_{max}/cm⁻¹ 3483, 3254, 2980, 1686, 1647, 1616, 1586, 1535, 1387, 1325, 1245, 1165, 1116, 1066, 1017, 843, 776, 756.

6-[1-Amino-3-(p-tolyl)-thiourea]-2-ethylbenzo[*de*]isoquinoline-1,3-dione (2). 2 was synthesized according to the above procedure using **5** (0.20 g, 0.73 mmol) and p-tolyl isothiocyanate 97% (0.11 g, 0.73 mmol), yielding the desired product as a brown solid (0.05 g, 17%). mp 180−182 °C; HRMS: Calcd for $C_{22}H_{21}N_4O_2S$ [M + H]⁺ 405.1385, found 405.1383; δ_H (400 MHz, (CD₃)₂SO): 1.19 (3H, t, J = 6.8 Hz, CH₂CH₃), 2.26 (3H, s, C₆H₄CH₃), 4.08 (2H, q, J = 6.8 Hz, CH₂), 6.98 (1H, d, J = 8.2 Hz, Ar−H naph), 7.11 and 7.28 (4H, d, J = 7.5 Hz, C₆H₄), 7.78 (1H, dd, J = 7.9 and 8.2 Hz, Ar−H naph), 8.43 (1H, d, J = 8.2 Hz, Ar−H), 8.50 (1H, d, J = 6.8 Hz, Ar−H naph), 8.70 (1H, d, J = 7.5 Hz, Ar−H naph), 9.87 (1H, s, NH), 10.04 (1H, s, NH), 10.06 (1H, s, NH); δ_C (100 MHz, (CD₃)₂SO): 13.3, 20.5, 34.4, 105.4, 111.4, 119.4, 121.8, 124.8, 126.0, 128.4, 128.9, 129.5, 130.9, 133.7, 134.4, 136.5, 149.9, 162.8, 163.5, 181.3; *m/z* 405 (M + H)⁺; v_{max}/cm⁻¹ 3461, 3240, 2976, 1689, 1645, 1617, 1585, 1530, 1349, 1245, 1212, 1110, 1066, 1017, 915, 776, 756.

Supporting Information Available: Figures S1−S11. X-ray crystal date (CIF) for **1**. This material is available free of charge via the Internet at http://pubs.acs.org.

JO0520487

Fluorescent Photoinduced Electron Transfer (PET) Sensors for Anions; From Design to Potential Application

Thorfinnur Gunnlaugsson,[1,3] Haslin Dato Paduka Ali,[1] Mark Glynn,[1] Paul E. Kruger,[1] Gillian M. Hussey,[1] Frederick M. Pfeffer,[1,2] Cidália M. G. dos Santos,[1] and Juliann Tierney[1]

This mini review highlights the synthesis and photophysical evaluation of anion sensors, for nonaqueous solutions, that have been developed in our laboratories over the last few years. We have focused our research mainly on developing fluorescent photoinduced electron transfer (PET) sensors based on the *fluorophore-spacer-anion receptor* principle using several anthracene (emitting in the blue) and 1,8-naphthalimide (emitting in the green) fluorophores, with the aim of targeting biologically and industrially relevant anions such as acetates, phosphate and amino acids, as well as halides such as fluoride. The receptors and the fluorophore are separated by a short methyl or ethyl spacer, where the charge neutral anion receptors are either aliphatic or aromatic urea (or thiourea) moieties. For these, the anion recognition is through hydrogen bonding, yielding anion:receptor complexes. Such bonding gives rise to enhanced reduction potential in the receptor moieties which causes enhancement in the rate of PET quenching of the fluorophore excited state from the anion:receptor moiety. This design can be further elaborated on by incorporating either two fluorophores, or urea/thiourea receptors into the sensor structures, using anthracene as a fluorophore. For the latter design, the sensors were designed to achieve sensing of bis-anions, such as di-carboxylates or pyrophosphate, where the anion bridged the anthracene moiety. In the case of the naphthalimide based mono-receptor based PET sensors, it was discovered that in DMSO the sensors were also susceptible to deprotonation by anions such as F^- at high concentrations. This led to substantial changes in the absorption spectra of these sensors, where the solution changed colour from yellow/green to deep blue, which was clearly visible to the naked eye. Hence, some of the examples presented can act as dual fluorescent-colorimetric sensors for anions. Further investigations into this phenomenon led to the development of simple colorimetric sensors for fluorides, which upon exposure to air, were shown to fix carbon dioxide as bicarbonate.

INTRODUCTION

Anions are essential to life, as many biological processes depend on the presence or transport of anions, or use anions to carry out chemical transformations [1]. Anions are also increasingly important for many industrial processes as well as in agriculture, and consequently have become important pollutants [2]. It has thus become evident that there is significant need for developing novel molecules that can interact with anions, and report their presence, and ideally at the concentrations of anions in complex media such as in blood or serum, cells, soil, freshwater, *etc*. Despite the enormous advances that have taken place in the field of chemistry, particularly due to the development of supramolecular chemistry, the field of anion recognition and anion luminescence sensing has been relatively unexplored, and indeed it is only in the last a few years that it has become a fast growing field

[1] Department of Chemistry, Center for Synthesis and Chemical Biology, Trinity College Dublin, Dublin 2, Ireland.
[2] School of Biological and Chemical Sciences, Deakin University, Waurn Ponds 3217, Australia.
[3] To whom correspondence should be addressed. E-mail: gunnlaut@tcd.ie

of research [3,4]. The reason for this, without a doubt, is the complex nature of the anions (in comparison to many cations) that has to be accounted for when designing anion-selective and sensitive luminescent probes. By definition, except for the anions AlH_4^-, B^- $(C_6H_5)_4B^-$ and $closo\text{-}B_{12}H_{12}^{2-}$, all anions have lone pairs of electrons. This Lewis basicity is the second most important feature of anions to be exploited in the construction of molecular hosts and sensors. It may add directionality to the system and therefore render it sensitive to the spatial arrangement and orientation of binding groups. This is an indispensable screen to differentiate between anions of similar size, structure and charge, e.g. phosphate and sulphate anions. The shape of the anion can thus be used advantageously in the design of a potent yet selective receptor. This is not just because of the size of the anion, as anions exhibit a wide range of geometries, which challenge the molecular designer to create a complementary binding site. For instance, the halides are spherical, their lone electron pairs do not introduce directionality to the system and are thus difficult to exploit in receptor design. However, the cavity size of a halide receptor may instead be manipulated, to introduce selectivity. The halides are all monatomic and the receptors discussed in this paper indeed fulfil the criteria discussed above, where large spherical anions such as chloride and bromide are not recognised/sensed, while fluoride is. Competition between the anion and the competitive solvent for binding sites makes sensing of anions more difficult than for cations of similar size, as anions are usually highly solvated. A vigorous analysis of solvent effects on the thermodynamics of the binding process for these systems was recently carried out, and it was determined that in less polar solvents than water, i.e. DMSO, complexation/recognition is enthalpically driven [5]. However, in methanol and methanol/water mixtures association becomes endothermic with favourable entropy providing the driving force for association. Thus, it is not surprising that most anion sensors today have been designed to sense anions in less competitive environments such as in DMSO and $CHCl_3$ [6].

Considerable effort has been recently directed toward the development of synthetic receptors that depend solely on hydrogen bond arrays [7]. The main virtue of incorporating H-bond donor groups into a receptor is to conserve electroneutrality. The range of hydrogen bond donor groups available (e.g. carbamates, ureas, thioureas) offers extreme versatility of construction. This versatility offers limitless options in receptor design, but the effectiveness largely depends on the extent of solvation. Anion recognition in biological systems is achieved *via* hydrogen bonding by highly preorganised proteins containing sterically well-defined complexation sites in the interior of the protein. The main challenge in the field of anion complexation has been the design of receptors with a high selectivity for biologically important anions for example; phosphates, (poly) carboxylates, and halides, especially chloride [8]. While few molecular details are known about anion specific ion pumps, a passive antiport system HCO_3^-/Cl^- important for respiration (CO_2 disposal) was identified in erythrocytes. The relatively common hereditary disease, cystic fibrosis, is known to stem from a genetically caused mis-regulation of chloride channels. This example illustrates the medicinal incentives for developing a sensor selective for chloride. Moreover, the oxoanions (carboxylates, phosphates, and sulphates) are of particular biological interest, while di- and tri-carboxylates are critical components of numerous metabolic processes including for instance, the citric acid and glyoxylate cycles [9]. They also play an important role in the generation of "high energy" phosphate bonds, as nucleotide polyphosphates are the basic components in the bioenergetics of all living organisms. From this account it is obvious that the challenge of developing sensors for anions is not trivial. However, this was in fact the main reason of our interest in the field of anion recognition and we asked ourselves, "can we develop anion selective and sensitive sensors using structurally simple receptors?" and secondly, "can we incorporate such anion receptors into luminescent sensors?"

We had previously developed both luminescent sensors for anions where the recognition occurred at a lanthanide metal ion centre [10], or by quinoxaline-based anion sensor [11]. Our choice was to further extend this field and develop fluorescent anion sensors, and the choice of method was PET [12], but PET anion sensing had not, prior to our work, been established using charge neutral anion receptors. However, examples of charged receptor moieties such as metal ions or protonated amines had been developed, for use in PET sensors [12,13].

This mini review discusses our attempts to develop such sensors in chronological order, beginning with the formation of simple PET sensors, based on the use of anthracene, followed by our attempts to develop PET sensors that absorb and emit in the visible region and finally the formation of colorimetric anion sensors where anion sensing is visible to the naked eye.

FLUORESCENT PET SENSORS BASED ON ANTHRACENE

Over the last few years, many excellent examples of anion sensing have been demonstrated. Some of this work

has been reviewed in several articles that generally give good account of the advantages that have occurred within this field in a relatively short time [3,4]. However, when we set out to develop anion sensors, only a few examples of such luminescent anion sensors had indeed been reported, and most of these were designed using charge receptors, or as in the work of Beer *et al.*, the receptors were charge neutral but were part of cationic metal complexes and as such often highly influenced by the presence of the metal ion, e.g. through inductive effects, etc. [14]. As stated above, we set out to use structurally simple receptors, our target being urea and thiourea, similar to those developed by Hamilton *et al.* [15], Umezawa *et al.* [16] and Kelly *et al.* [17] who individually developed several receptors for the detection of anions such as acetate, using NMR to observe the recognition process. The use of PET in chemical sensing was established by de Silva and Czarnick less than 20 years ago [12]. These researchers showed that by incorporating amines into the anthracene structure *via* a methyl spacer, the fluorescence of the fluorophore could be significantly enhanced, or *'switched on'*, in the presence of a proton, without any significant changes in the wavelength of the emission, e.g. only the quantum yield and emission lifetimes were effected. This was simply due to the prevention of photoinduced electron quenching of the anthracene excited state by the electron rich amine upon protonation of the same, but upon protonation, the oxidation potential of the amine increased, making PET thermodynamically unfavourable. This was shown by simply employing the Rehm-Weller equation for determining the free energy of electron transfer [18]. Furthermore, for such ideal PET behaviour, the absorption spectra of the fluorophore should be independent of the recognition process, as the receptor was not an integrated part of the fluorophore.

In a similar manner, we foresaw that the reduction potential of the receptor would be modulated upon anion recognition, provided that the binding was strong. Our strategy shown schematically below was quite simple. We designed two sets of fluorescent anion sensors, based on the *fluorophore-spacer-anion receptor* principle, where the receptor is now a hydrogen-bonding acceptor. This was achieved by simply using anthracene and incorporating thiourea receptors at the 9th position on the anthracene ring (**3–5**) or at the 9th and 10th positions (**9–11**), *via* methylene spacers [19,20]. The advantage of this design became clear as by using 9-aminomethylanthracene **1**, or 9,10-diaminomethylanthracene **2** the amino moieties could be reacted with a wide range of commercially available isothiocyanates to form the respective thiourea receptor.
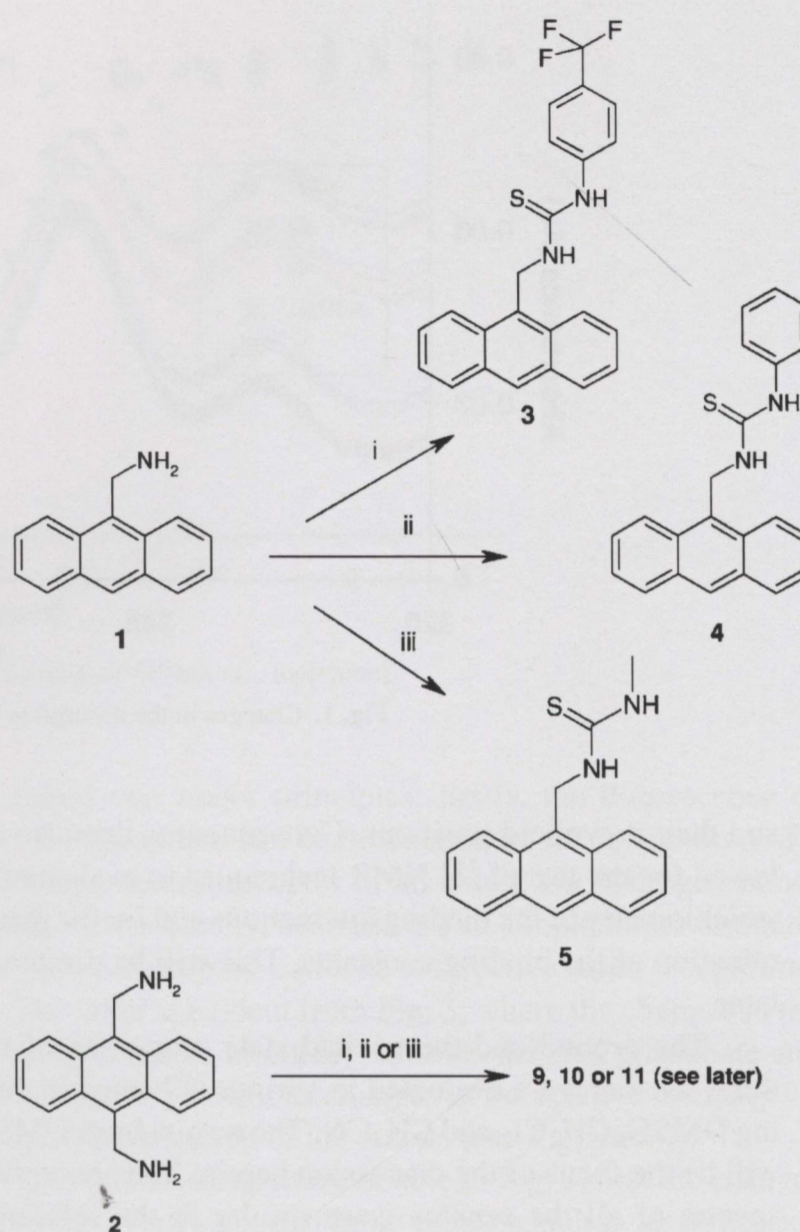
Our first examples of this design were the three mono-thioureas **3–5**. By simply reacting **1**, in dry CH_2Cl_2 at room temperature, under inert atmosphere with an equimolar amount of 4-(trifluoromethyl)phenyl (i), phenyl (ii) and methyl isothiocyanate (iii) respectively, compounds **3–5** were formed as off-white solids that were purified by recrystallisation from $CHCl_3$. The three different isothiocyanates were chosen with the aim of being able to modulate, or tune, the acidity of the thiourea receptor moiety, which would lead to different receptor-analyte complex stability and hence different binding constants. The synthesis of the starting material **1**, was achieved by several different methods, including conventional Gabriel amine synthesis, reduction of 9-cyanoanthracene, by sodium borohydride, lithium aluminium hydride and diborane, or by the conversion of 9-bromomethylanthracene to **1**, involving the use of hexamethylenetetramine. This latter method was superior to any of the former and produced the desired amine in good yield (80–90%) as the hydrochloride salt. The three sensors all exhibit simple ^1H NMR spectra in various solvents and the thiourea protons were easily identified due to their broad appearance
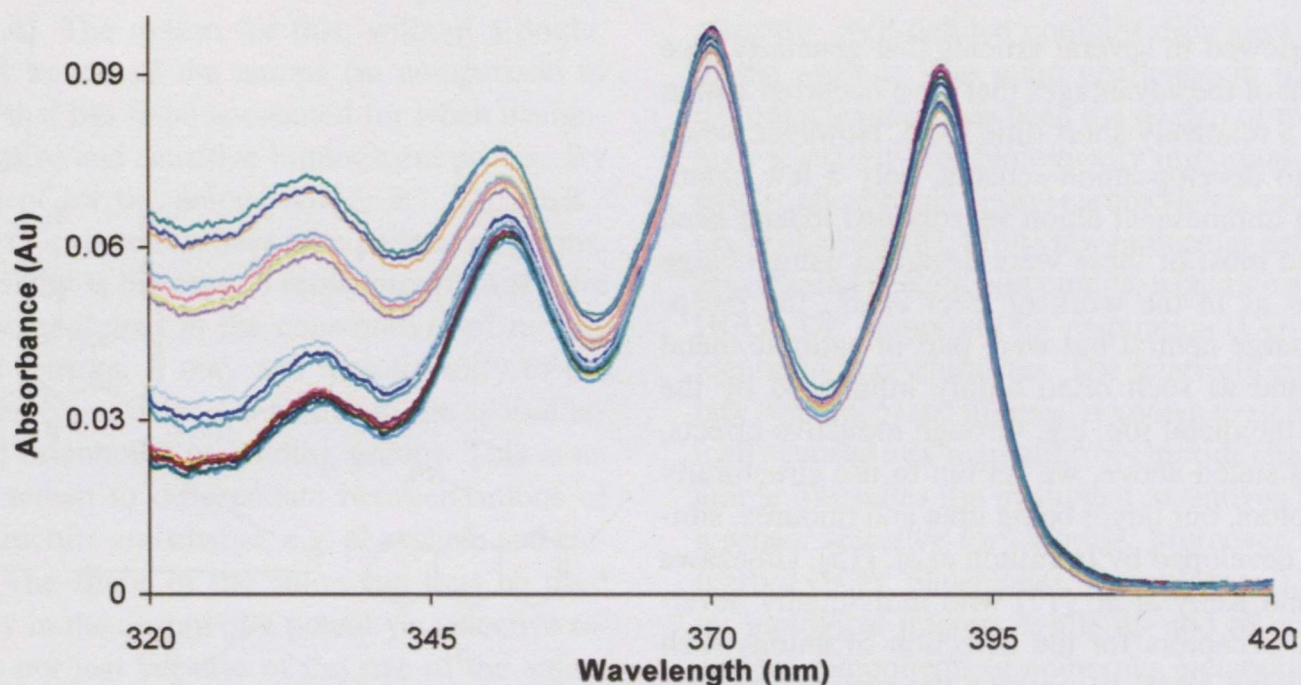
Fig. 1. Changes in the absorption spectra of **3** upon addition of acetate in DMSO.

and their downfield positions. Consequently, this also allowed for the use of ^{1}H NMR techniques to evaluate the stoichiometry of the binding interactions and for the determination of the binding constants. This will be discussed later.

The ground and the excited state properties of the three sensors were evaluated in various solvents, including DMSO, CH$_2$Cl$_2$ and CH$_3$CN. The results from DMSO will be the focus of the discussion herein. The absorption spectra of all the sensors were similar to the reference compound 9-methylanthracene, with absorption bands at 390, 370, 352 and 336 nm respectively for **3** (Fig. 1). When the 370 nm transition was excited, a typical an-

thracene emission was observed with peaks at 443, 419 and 397 nm, and a shoulder at 473 nm, and a quantum yield of 0.1. For **4** and **5**, similar results were observed with quantum yields of 0.187 and 0.304, in comparison to 9-methylanthracence, which was recorded to have quantum yields of 0.284. Upon titrating a solution of any of these sensors with anions such as Cl$^-$ or Br$^-$ no changes occurred in either the absorption or the fluorescence emission spectra. However, using anions such as acetate, phosphate or fluoride, the emission was dramatically affected, being '*switched off*' by up to 90%, upon anion addition, e.g. Fig. 2, for phosphate, with ~70% quenching. In retrospect the changes in the absorption spectra were only
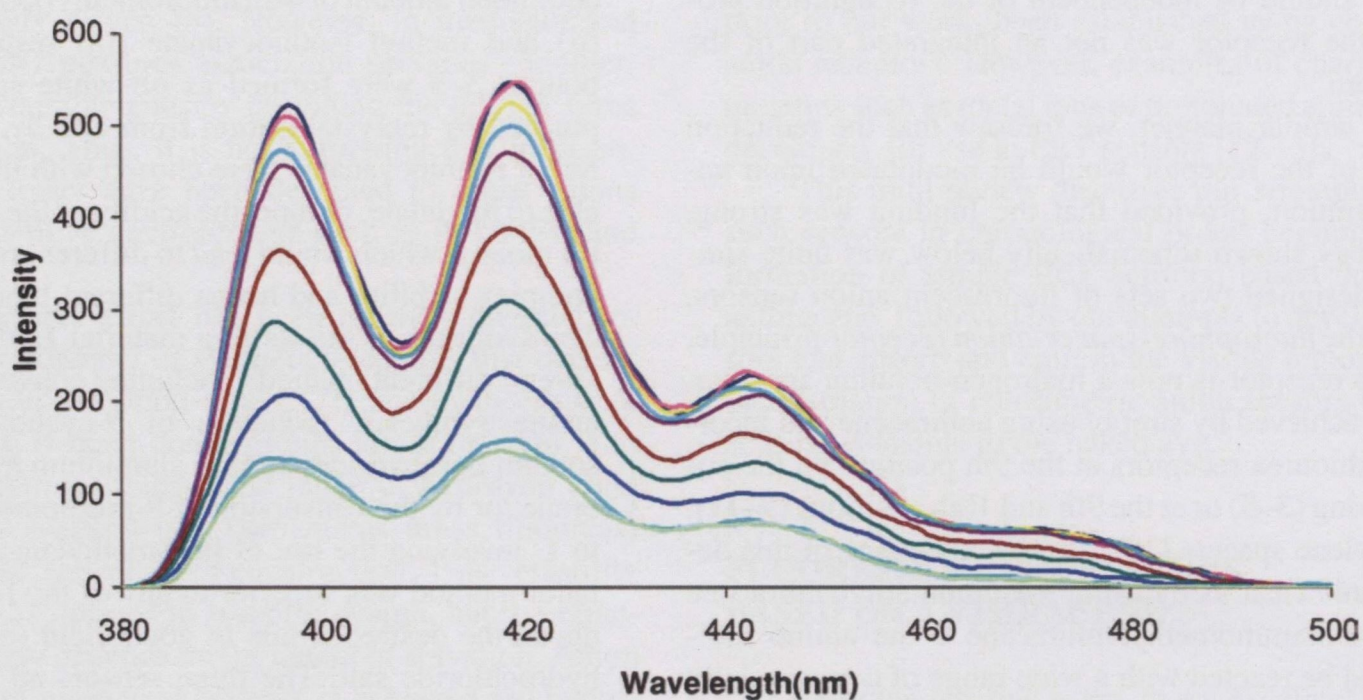
Fig. 2. Changes in the fluorescence emission of **3** upon addition of phosphate.

Fig. 3. The changes in the fluorescence emission at 420 nm *vs.* –log[anion].

minor, (Fig. 1.) This is in agreement with PET theory, as the only communication pathway between the two parts, the receptor and the fluorophore is through space and hence, the absorption spectra would generally not be expected to be significantly affected by the recognition at the receptor site. However, at lower wavelength there were some changes which were assigned to the structural changes occurring in the aromatic thiourea receptor itself upon anion recognition, which would be through hydrogen bonding between the anion and the thiourea protons, yielding an electron rich anion:receptor complex. This interaction would significantly enhance the reduction potential of the receptor, which would enhance the rate of electron trans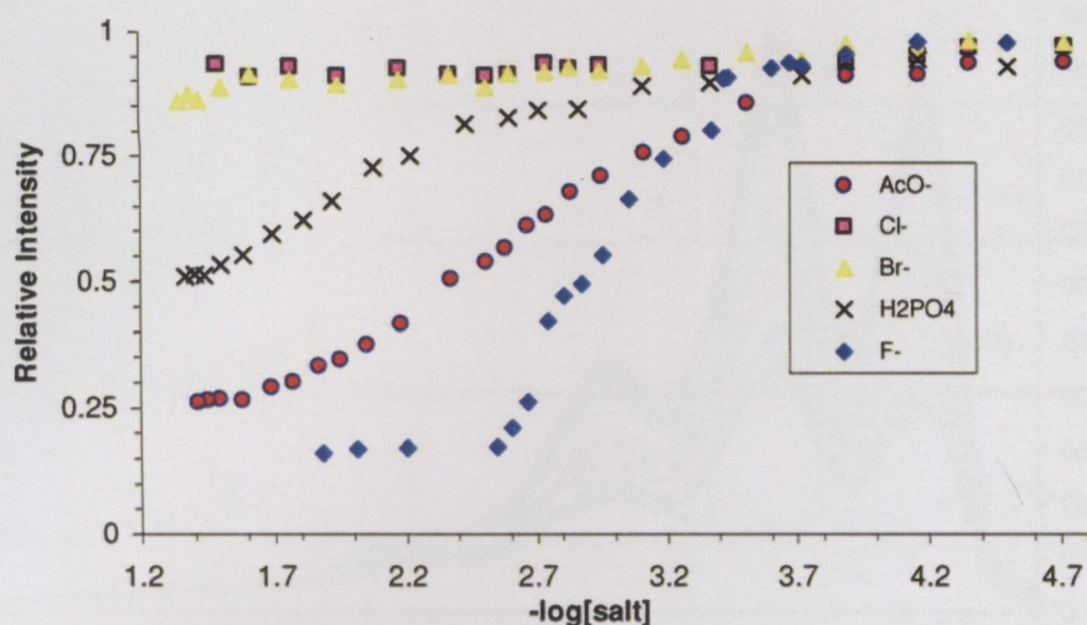fer from the receptor to the fluorophore and hence enhance the quenching of the excited state. Unfortunately, we were unable to determine the oxidation-reduction potential of the receptors by cyclic voltammetry as they were irreversibly oxidised. However, the effect of this was indeed found as is shown above, where the emission was reduced due to the enhanced PET rate. In a similar manner compounds **4** and **5** showed that upon addition of the same anions the emission was quenched and the absorption spectra was not significantly affected, except at low wavelengths for **4**, whereas for **5**, no such changes were observed as the sensor lacks the aromatic receptor. We also evaluated the changes in the receptors themselves by synthesising the thiourea receptors in a single step. As expected, significant changes were observed in the absorption spectra of these (as well as in the NMR) upon anion titration, confirming the changes seen above in the absorption spectra where the major changes occurred at short wavelength.

By analysis of the changes in the fluorescence emission, as a function of the anion concentration, we estab-

lished two major principles; firstly, the fluorescence of the fluorophore can be modulated by the recognition of a charge neutral receptor of an anion, *via* hydrogen bonding, and secondly, even the use of simple mono-aromatic thiourea receptors can lead to selective anion recognition. The latter is evident from Fig. 3, where the changes in the recognition of bromide, chloride, acetate, phosphate and fluoride are shown as changes in the relative intensity vs. the concentration of the anions (as –log[anion]).

It is also important to note in Fig. 3, that the changes occur over two logarithmic units, which is an indication of a 1:1 binding. From the above figure the selectivity and the sensitivity of the recognition is also evident, and the same trend was seen for all the sensors; the emission was most significantly modulated, '*switched off,*' by fluoride, followed by acetate and finally phosphate, whereas the larger spherical anions did not give rise to such quenching. In a similar manner we have also recently made the urea analogues of the above complexes and observed that the changes in the ground and the excited state properties of these were also affected by the anion recognition, demonstrating that the active PET mechanism is also operative in these systems.
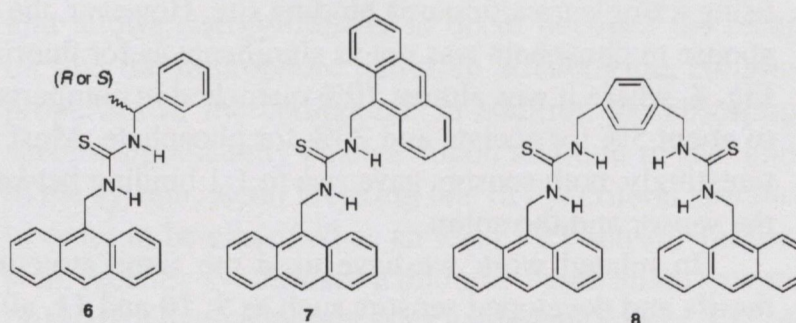
With the aim of elaborating further on this simple design principle we have developed other structurally
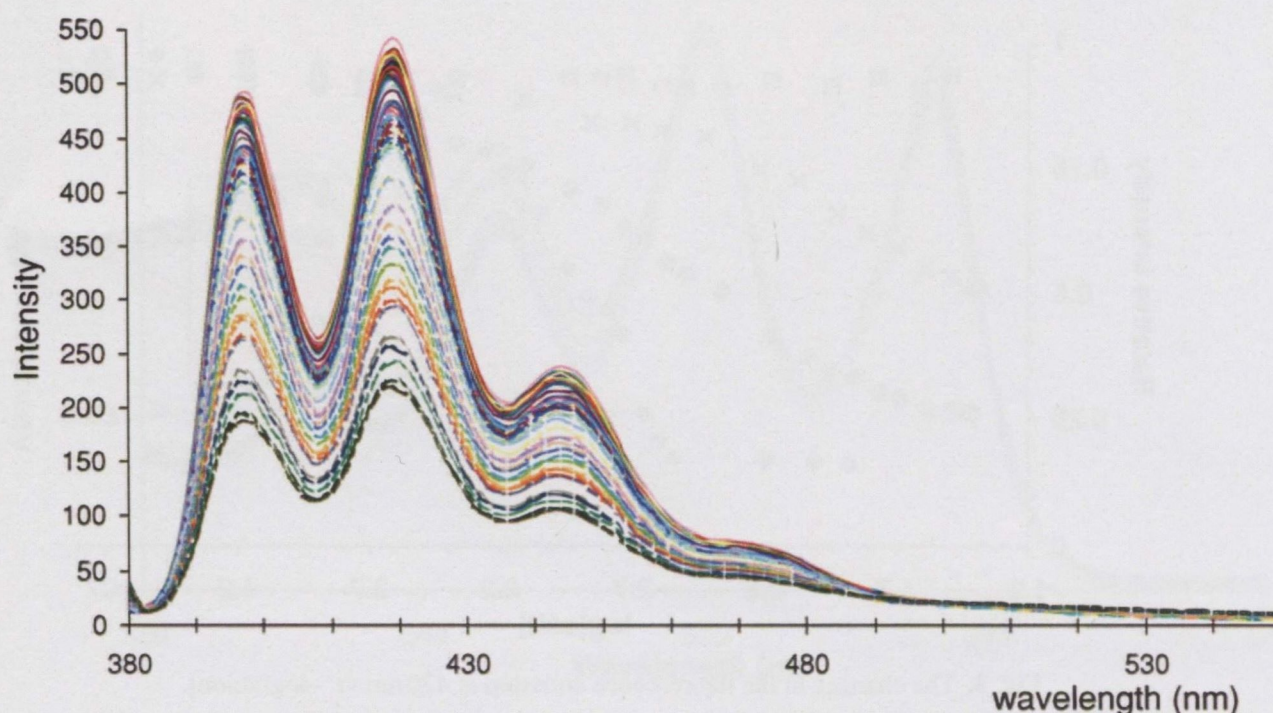
Fig. 4. Changes in the fluorescence of **8** in the presence of fluoride ions, where the emission is quenched upon anion recognition. Notice the absence of any long wavelength emission bands indicating the lack of excimer emission upon anion sensing.

similar sensors [20,21]. Compounds **6**, **7** and **8** are examples of our design, where for instance an asymmetric centre has been incorporated adjacent to the receptor moiety in **6** (both *R* and *S* were made) and two fluorophores have been attached to a single thiourea moiety in **7** and **8**. For the former, we aimed to achieve chiral discrimination of anions such as *N*-acetal or *N*-Boc protected amino acids. However, we quickly demonstrated that a single stereogenic centre was not enough to achieve such enantiomeric discrimination. Attempts to incorporate a second stereogenic centre at the methylene spacer have, unfortunately, not been successful in our laboratory to date, but we are currently involved in such synthesis [20]. For **7**, the addition of two anthracene moieties into the structure gave some interesting results, e.g. the selectivity of the recognition was greatly improved, with fluoride being detected strongest. At the same time, the two fluorophores were shown to give rise to significant steric strain, which resulted in the decrease in the sensitivity of the anion recognition. Compound **8** was designed to give strongest binding to phosphate, which is often difficult to achieve using a single urea/thiourea binding site. However, the response to phosphate was not as significant as for fluoride, Fig. 4, where it was almost 70% quenched in comparison to about 5% for acetate and 20% for phosphate. Most interestingly, both sensors gave rise to 1:1 binding between the sensor and the anion.

In related work we have used the same structural motifs and developed sensors such as **9**, **10** and **11**, all of which have two binding sites [21,22]. For **9** and **10**, the basic design principle employed above was used, e.g. the

9; R = H
10; R = CF₃

11
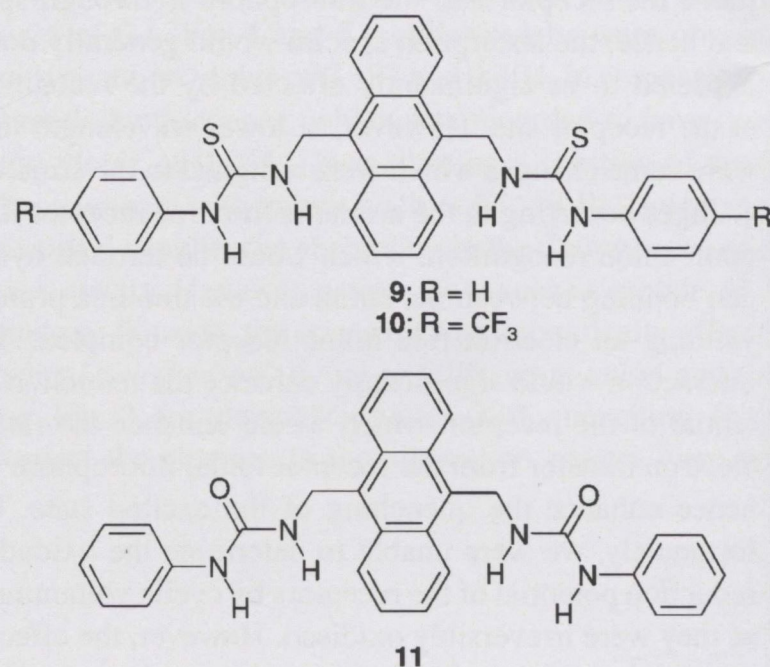
anthracene fluorophore was separated from the receptor by a methyl spacer, but on these occasions, two receptors were incorporated into the design, and as before, the choice of aromatic thioureas gave rise to tuning of the anion sensitivity.

This extended design yielded an overall *receptor-spacer-fluorophore-spacer-receptor* motif, and allowed the sensing of bis-anions such as dicarboxylates and pyrophosphate in DMSO. For **9** and **10**, the fluorescence was '*switched off*' upon recognition of both mono-dentate anions such as acetate and by dicarboxylates such as glutarate and malonate. The changes in the fluorescence of the former were shown to occur over 4 logarithmic units, indicating that the binding was in the form of 2:1
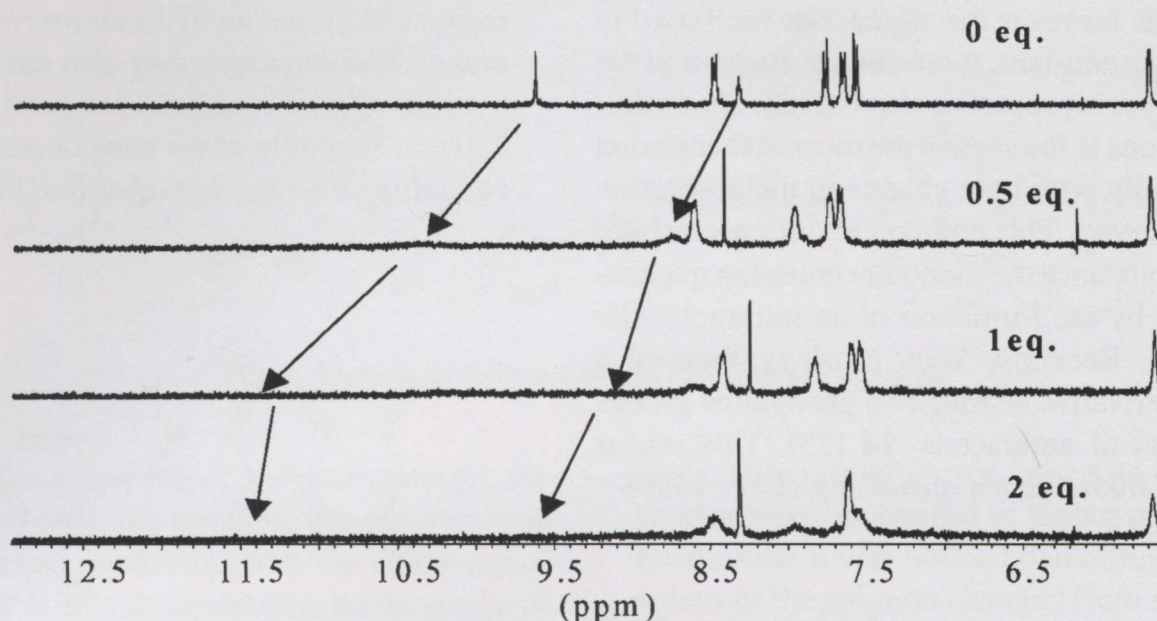
Fig. 5. Changes in the ^{1}H NMR of **10**, upon addition of pyrophosphate in DMSO-d_6. Notice the broadening in the aromatic signals which was found to be absent in the titration of **10** with phosphate, which was determined to be in 2:1 ratio.

(anion:sensor), whereas for the bis-carboxylates the sensing was determined to be 1:1. These latter results would imply that the anion would have to bridge the anthracene unit. Similarly for **11**, having a urea-binding motif, the emission was also quenched upon ion sensing, but at different concentration ranges in comparison to **9**. To evaluate the possibility of the bis-anions bridging the fluorophore, we investigated the changes in the ground state of the interaction of pyrophosphate with **9**. Whereas no isosbestic points were seen for **3**, **4** and **5** above upon titration with mono-dentate anions, there were measurable changes in the absorption spectra upon addition of pyrophosphate which suggested that the anion was in someway affecting the electronic structure of the fluorophore, e.g. by bridging it. However, in the absence of X-ray crystallographic results, this was not a significant enough change to determine the 2:1 binding accurately. We thus carried out a series of ^{1}H NMR titrations o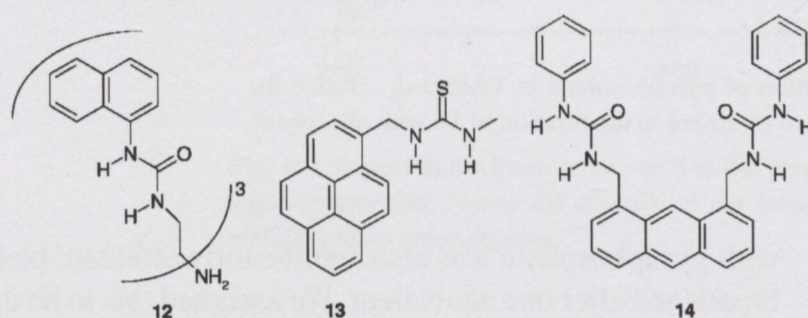f both the mono- and the bis-receptor based sensors in DMSO-d_6. These investigations revealed that for **3**, **4** and **5** the binding occurred in the stoichiometry of 1:1, where the changes in the thiourea protons were monitored upon addition of anions such as acetate and phosphate (as their tetrabutylammonium salts). This was in good agreement with work carried out by Hamilton *et al.* and Kelly *et al.* on structurally related receptors, which also showed the binding to be 1:1 in their cases [15,17]. For **9** and **10**, however, similar titrations showed that the binding of acetate and phosphate (see Fig. 5, for **10**), was indeed in 2:1 binding, whereas using the bis-anion pyrophosphate, the titration showed 1:1 binding. Moreover, unlike that seen in the titration of **10** with acetate and phosphate, the fine structure of the resonance for **10** upon titration

with pyrophosphate was also significantly affected, being broadened after one equivalent. We assigned this to be due to substantial electronic effects inflicted by the phosphorus moiety in the pyrophosphate, which would be central over the anthracene fluorophore. Hence, from the above results we are confident to say that the binding is 1:1 and for this to occur the anion has to bridge the fluorophore. Indeed the use of different bis-anions with different spacers, showed that the larger anions bound in 2:1 and the smaller ones such as malonate and glutarate in 1:1 ratio.

The above account has so far focused on the results from our work on anion sensing using anthracene as the fluorophore. Several other examples of similar designs have also emerged in the last a few years. For instant, Wu *et al.* developed a thiourea-based receptor **12**, containing three naphthalene units [23]. The bis and mono equivalents of this sensor were also examined and the mechanism for the sensing of **12** was described as a PET sensor with the quaternary nitrogen acting as the donor, the receptor acting as a spacer and the fluorophore being the naphthalene unit. However, **12** senses anions *via* a combination of PET and energy transfer. Binding of the anion to the NH directly attached to the naphthalene unit allows energy transfer to occur between the receptor and the fluorophore therefore affecting the emission properties of the compound. In addition the absorption spectra significantly changes upon addition of the anion to the system, again breaking one of the criteria specified in order to be classified as an ideal PET sensor. Teramae *et al.* recently synthesised a thiourea-based anion receptor linked to a pyrene moiety via a methylene spacer, **13** [24]. Binding studies of 13 with TBA acetate were conducted in CH_3CN. ^{1}H NMR could prove that binding was occurring

via the N–H bonds however the signal was too broad to quantify the binding constant. A concurrent analysis of the fluorescent and UV/vis properties showed that upon addition of various anions to the system the monomer emission reduced dramatically with little change in the absorption spectra being observed. This compound does not exhibit *ideal* PET behaviour since the monomer emission quenching was followed by the formation of an intramolecular exciplex emission. Recently, Yoon *et al.* synthesised a new anthracene derivative bearing two phenylurea groups at the 1,8 position of anthracene, **14** [25]. This sensor shows a selective fluorescence quenching effect with F⁻ *via* a PET mechanism.

region and the colour of the above compounds is yellow or orange. Consequently they also emit in the visible spectrum, having a strong emission band centred around 530–550 nm. Secondly, these compounds are usually found to be highly emissive, with quantum yields of *ca.* 80–90%.

15: n = 1, R = CF₃
16: n = 2, R = CF₃
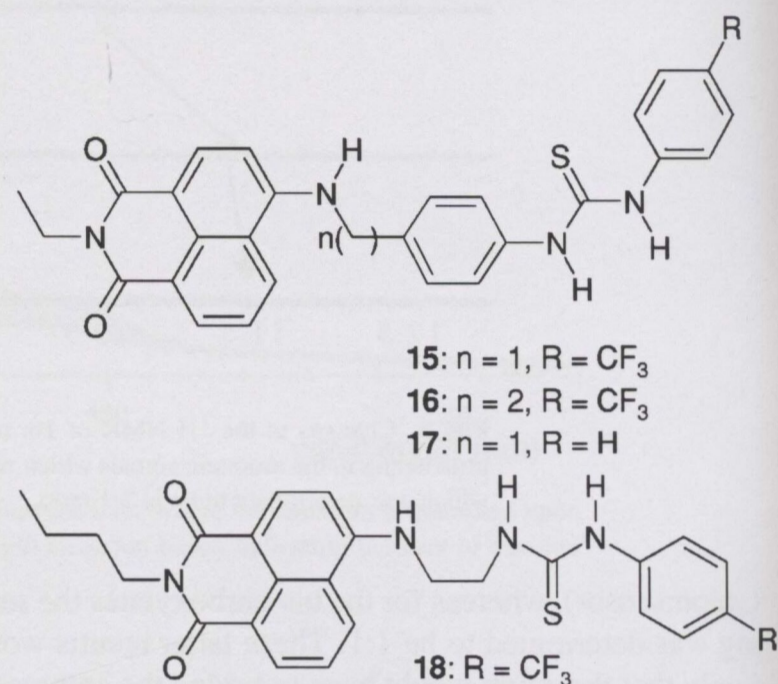**17**: n = 1, R = H

18: R = CF₃

Having demonstrated PET anion sensing using charge neutral receptors, we decided to explore this method of sensing using other fluorophores, some of that work is described in the next section. The main reason for extending this line of research was to develop novel luminescent anion sensors that could be used to determine anion concentrations in aqueous solutions. Recently we have indeed managed to achieve such sensing in buffered water, however, that work will be the focus of our future articles. What follows is the account of the work leading to such real anion sensors for competitive media.

PET ANION SENSING USING NAPHTHALIMIDE FLUOROPHORES

Over the last a few years we have developed various fluorescent PET sensors for cations using the 4-amino-1,8-napththalimide structure [26]. With the aim of extending the above PET anion sensing we developed several sensors based on the naphthalimide unit by simply incorporating a thiourea or urea moiety into the structure *via* a spacer in a similar manner as discussed above [27]. Compounds **15–18** are examples of this design where different receptors or spacer lengths were used. The advantage of using the naphthalimide fluorophore is twofold; firstly, it has an internal charge transfer excited state (ICT) due to the electron donating amine and the electron withdrawing imide. This makes the fluorophore absorb in the visible

The synthesis of the above compounds was achieved in good yields from the 4-chloro or the 4-bromo-1,8-naphthalic anhydride by first condensation with either *n*-aminoethane or *n*-aminobutane, to yield the corresponding naphthalimides. This was then treated with either diethyl amine or 4-aminobenzylamine to yield the two free amines, which then were susceptible to reaction with various isothiocyanates. The synthesis of **15** is shown in Fig. 6.

The sensing of several anions was demonstrated in DMSO. For **15** and **17**, which have di-aromatic thiourea receptors, the fluorescence emission was highly dependent on the anion, where it was almost fully quenched by fluoride. The changes for **15** are shown in Fig. 7. From this it can be seen that the emission occurs in the visible region, being centred at 525 nm, which was highly fluorescent green to the naked eye. Titration with other spherical anions such as chloride or bromide did not lead to any quenching in the naphthalimide emission. However, both acetate and phosphate gave rise to significant changes as seen in the insert graph in Fig. 7. In the same way, the changes for **17** showed that the emission was highly sensitive to fluoride, phosphate and acetate, but as in previous examples the sensitivity was somewhat shifted to higher concentrations due to the lack of the electron withdrawing CF₃ group. For **16**, an analogue of **15**, except for the presence of the two methyl spacer, the emission was also reduced upon addition of these ions. However, the quenching efficiency was significantly reduced as the electron transfer quenching is dependent on the distance between the receptor and the fluorophore, where the rate
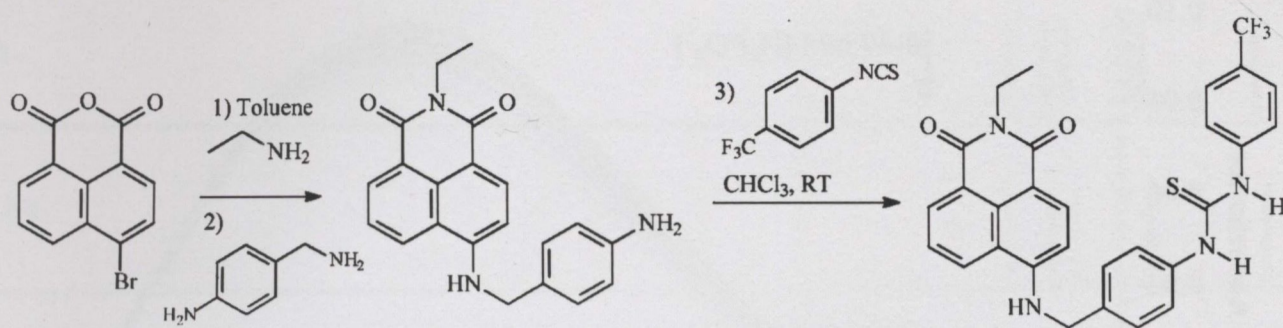
Fig. 6. Synthesis of **15** from 4-bromo-1,8-naphthalic anhydride.

of electron transfer is a function of $1/r^6$. Interestingly, for **18**, which is a mono-aromatic thiourea, the emission was only slightly quenched confirming that the efficiency of the PET quenching is also dependent on the structure of the receptor. Furthermore, and as expected, this quenching only occurred at relatively high concentrations. For all the naphthalimide sensors the absorption spectra were not significantly affected upon titration of any of the above anions, being only slightly red-shifted upon anion recognition. This is evident from Fig. 8, upon titration of **15** with phosphate.

As in the case of the anthracene examples discussed above, the changes in the ^{1}H NMR were also evaluated in DMSO-d_6. For the same concentration range (Fig. 7), the changes in the thiourea protons or the aromatic signals of the receptors can be used to evaluate binding strength and the stoichiometry of the recognition. On all occasions it was shown that the binding was 1:1 and that the thiourea protons were shifted by up to ~3 ppm. To establish an accurate endpoint we titrated the solutions beyond two equivalents of anions. For acetate and phos-

phate, only saturation was observed in the NMR, e.g. the spectra were unchanged at higher equivalents. However, for fluoride it was noticed that at higher equivalents, the colour of the solution changed from slight yellow to deep blue. These changes were clearly visible to the naked eye. At the same time, the NMR also changed significantly and a new species was clearly observed in the NMR. Because of these changes, we reinvestigate the absorption spectra of these compounds at higher concentrations. Figure 9 shows the changes observed in the absorption spectra of **15**, upon titration with fluoride in DMSO. From this titration two significant results emerged. Firstly, the absorption spectra did not change significantly in the concentration range where the fluorescence was quenched, e.g. the molecule showed 'ideal' PET behaviour. Secondly, the colour changes observed in the NMR was also clearly observed in the absorption spectra, where a new band was formed, centred at *ca.* 550 nm and a second band at 338 nm, and with the presence of two isosbestic points at 385 and 475 nm, respectively, upon exceeding two equivalents of fluoride, at the same time that the 440 nm band
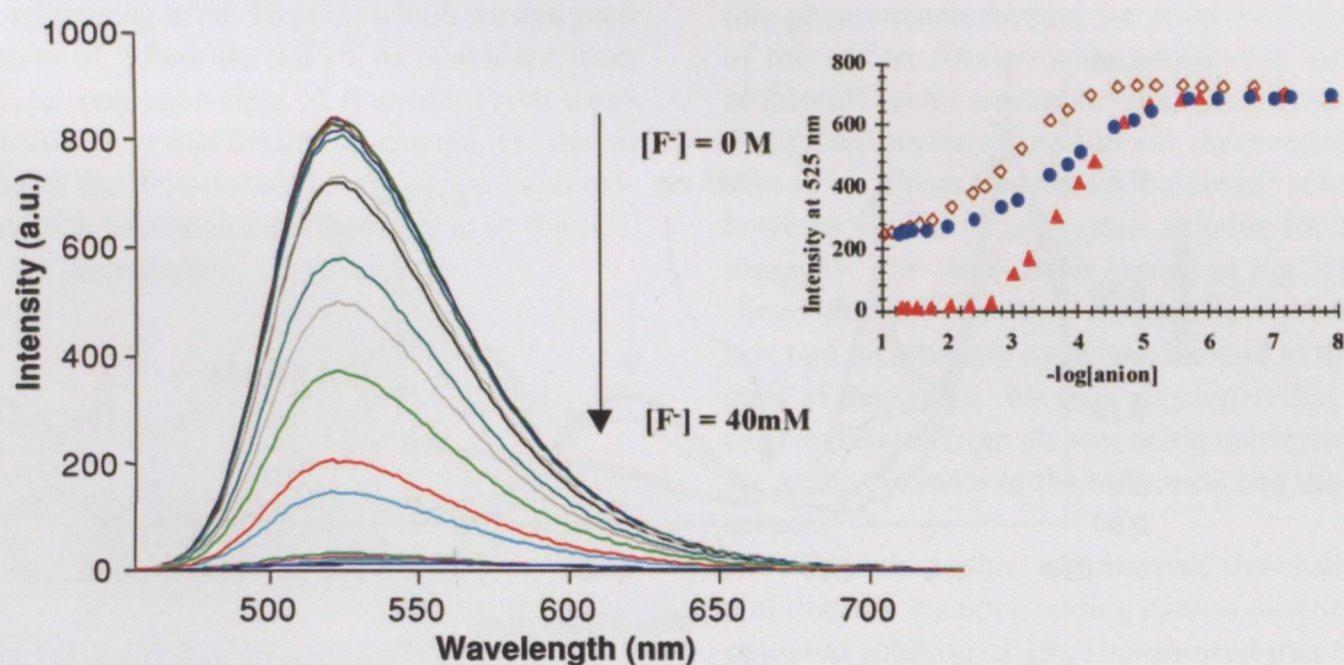

Fig. 7. Changes in the fluorescence emission of **15** upon titration with fluoride in DMSO. Insert are the changes in the emission at 525 nm upon titration with fluoride (red), acetate (blue) and phosphate (brown), as a function of their concentrations (as the –log[anion]).
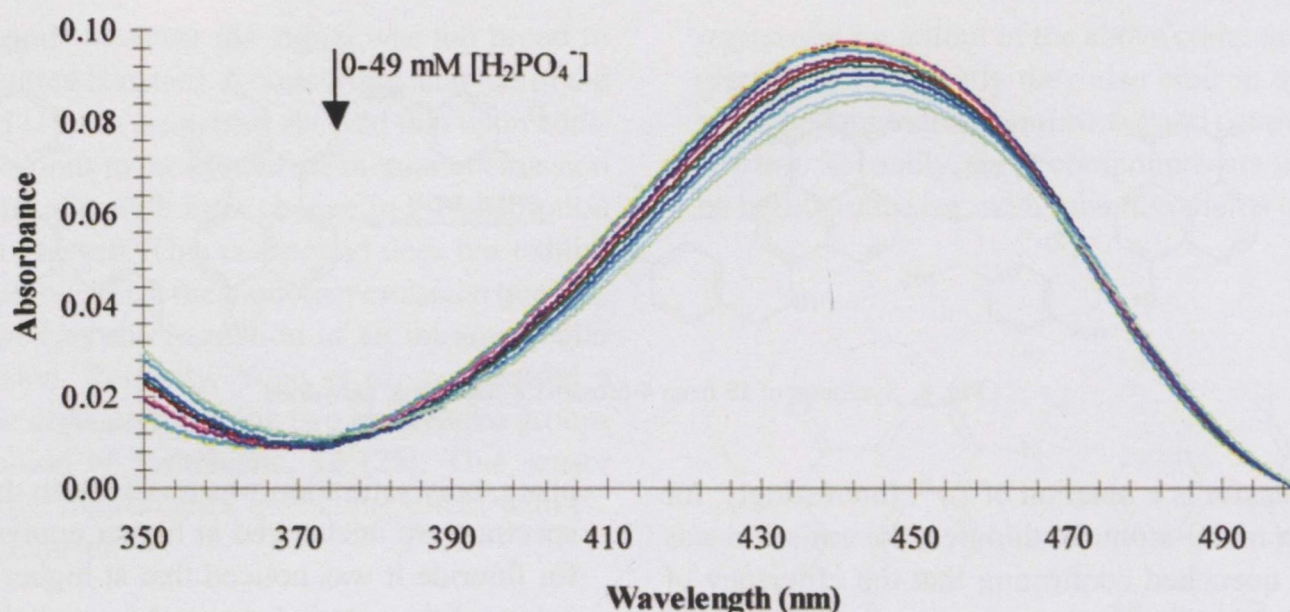
Fig. 8. The changes in the absorption spectra of **15** upon titration with phosphate. These changes were too small to allow for accurate binding constant determination.

was significantly reduced in intensity. In a similar way, **16**, **17** and **18** all showed this behaviour at higher fluoride concentrations. We assigned these changes to the deprotonation of the 4-amino moiety in the fluorophore and the enhancement in the ICT of the excited state, which shifts the absorption spectra to the red. In fact upon excitation of the 550 nm band, a weak emission was observed at long wavelength, centred at *ca*. 650 nm.

These compounds can thus be described as dual fluorescent-colorimetric anion sensors. With the aim of further investigating these effects; we designed several other naphthalimide 'sensors' where the thiourea moiety was absent. Compounds **19** and **20** are examples of this design [28]. As expected only fluoride gave rise to any significant changes in the absorption spectrum of **19**

upon addition of several anions. A full titration of **19** with TBA-F led to a reduction in the intensity of the bands at 446 and 287 nm, while two new bands centred at 535 and 341 nm respectively, were formed. At low concentrations, three clear isosbestic points at 480, 380 and 300 nm were visible. At higher concentrations, the bands broadened, as observed with sensors **15–18** on addition of F⁻. A simultaneous visible colour change from green to red/purple was observed as the absorption maximum was bathochromically shifted from 446 nm to 535 nm. These spectral changes are most likely due to deprotonation of the amino moiety by F⁻, or strong hydrogen bonding that could eventually result in deprotonation. In both cases, deprotonation leads to the formation of a negatively charged naphthalimide, with concurrent enhancement of
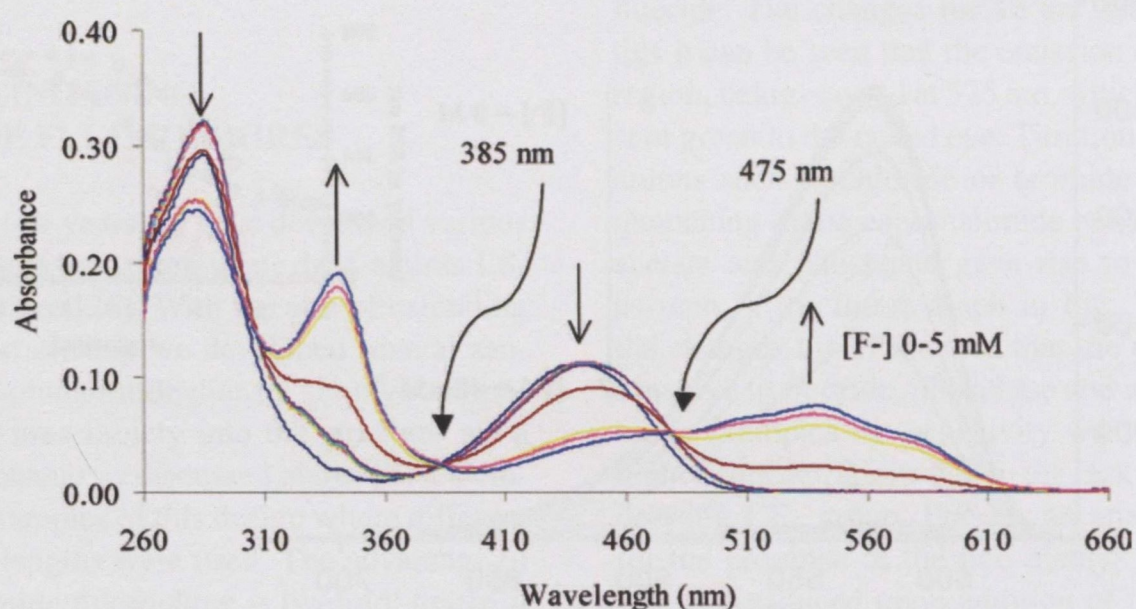

Fig. 9. The changes in the absorption spectra of **15**, upon titration with fluoride. Only at high concentrations, where the fluorescence had stopped changing, did the absorption band centred at 550 nm begin to appear.
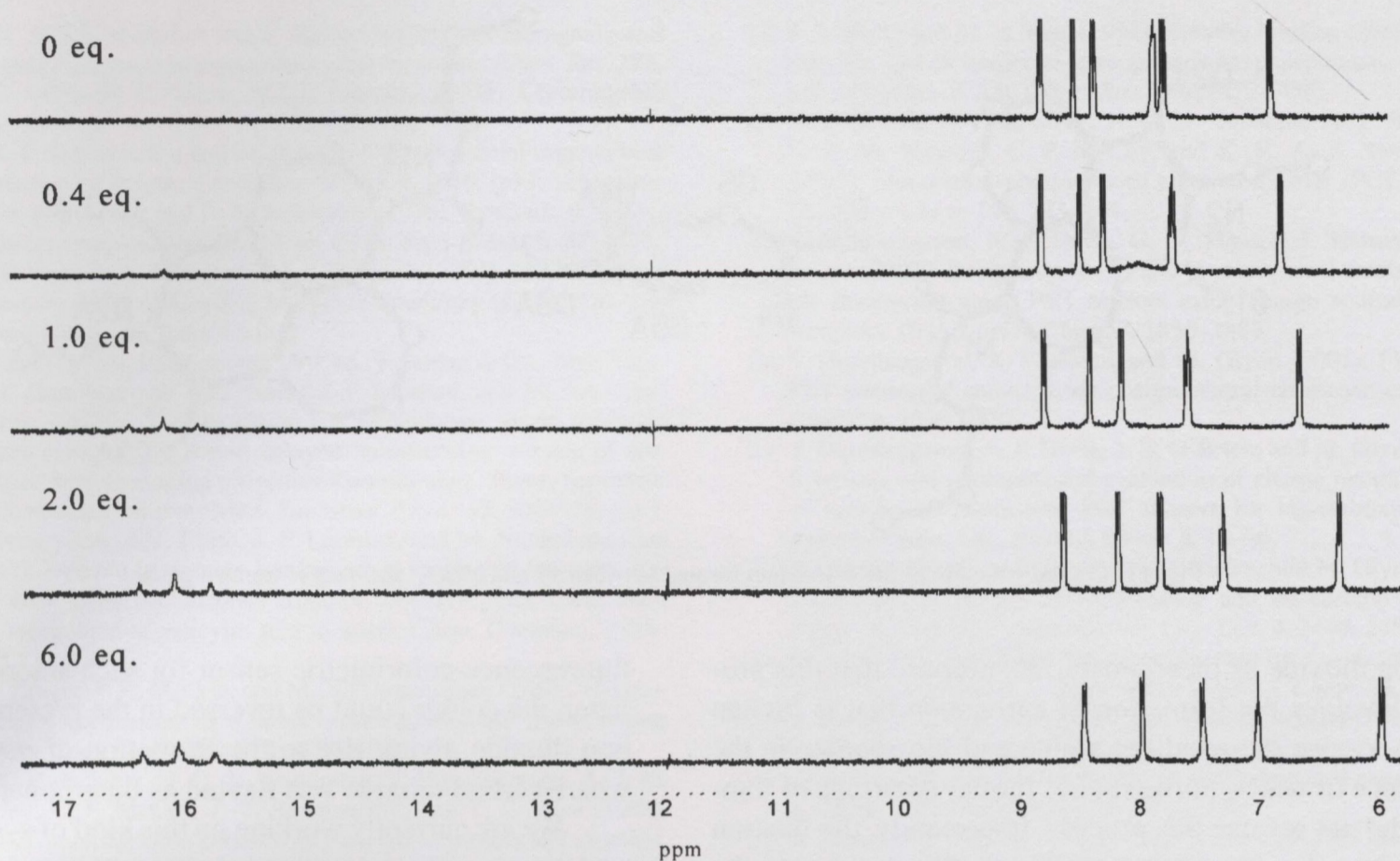
Fig. 10. ^{1}H NMR stack plot of **19** after addition of various quantities of F$^-$ (DMSO-d_6, 400 MHz) showing formation of downfield triplet.

the push-pull character of the ICT transition. When the same titrations were done using compound **20**, which lacks the 4-amino moiety, no such colour changes were observed. This clearly indicated that these changes were due to deprotonation of the 4-amino moiety. As before we investigated these changes by ^{1}H NMR for **19**. These results confirmed what was observed in the NMR titrations for **15–18**. Furthermore, we had observed the formation of a new signal resonating at *ca.* 16 ppm, which we assigned to the formation of bifluoride (HF$_2^-$), as is evident from Fig. 10 after *ca.* one equivalent of fluoride. From these results it was thus clear that the colour change was due to the formation of the deprotonated form of the naphthalimide moiety with concomitant enhancement in the ICT character of the fluorophore.
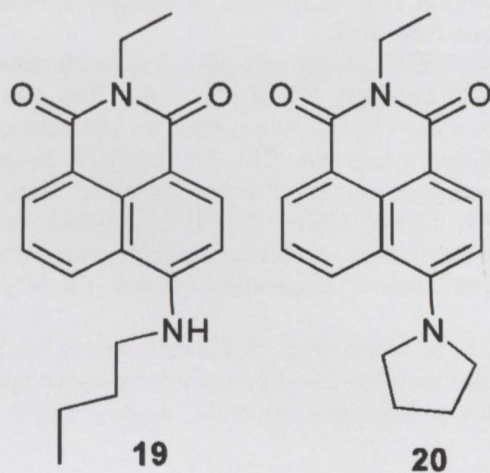
However, we also observed that if the DMSO solution of this deprotonated form was left standing open to air, the colour was reversed (from blue to green-yellow) over some time. When samples of **15–18** were also dissolved in DMSO, treated with excess fluoride and left standing exposed to air, the colour was also reversed. Interestingly, the addition of fluoride did not reverse this colour change to red/purple. With the aim of investigating this phenomenon further, we attempted to grow crystals of the adduct formed upon addition of two equivalents of fluoride under anaerobic conditions. Nonetheless, even though red crystals were formed, these melted upon exposure to air. From this newly 'coloured' solution we were however able to grow crystals suitable for X-ray crystallography. The structure is shown in Fig. 11, and clearly shows that the resulting solution had produced crystals that had bicarbonate hydrogen bonded to the amino moieties of the sensor. We thus concluded that the uptake of carbon dioxide from air was being converted to bicarbonate in the presence of the bifluoride and the deprotonated sensor.

To evaluate this, we observed the changes in the absorption spectra upon adding carbon dioxide to the 'blue' coloured solution of **19**. This showed that the absorption spectra were reversed, giving rise to the colour previously assigned to the free form of **19**. This supported thus our finding that the deprotonated form of **19** was able to fix
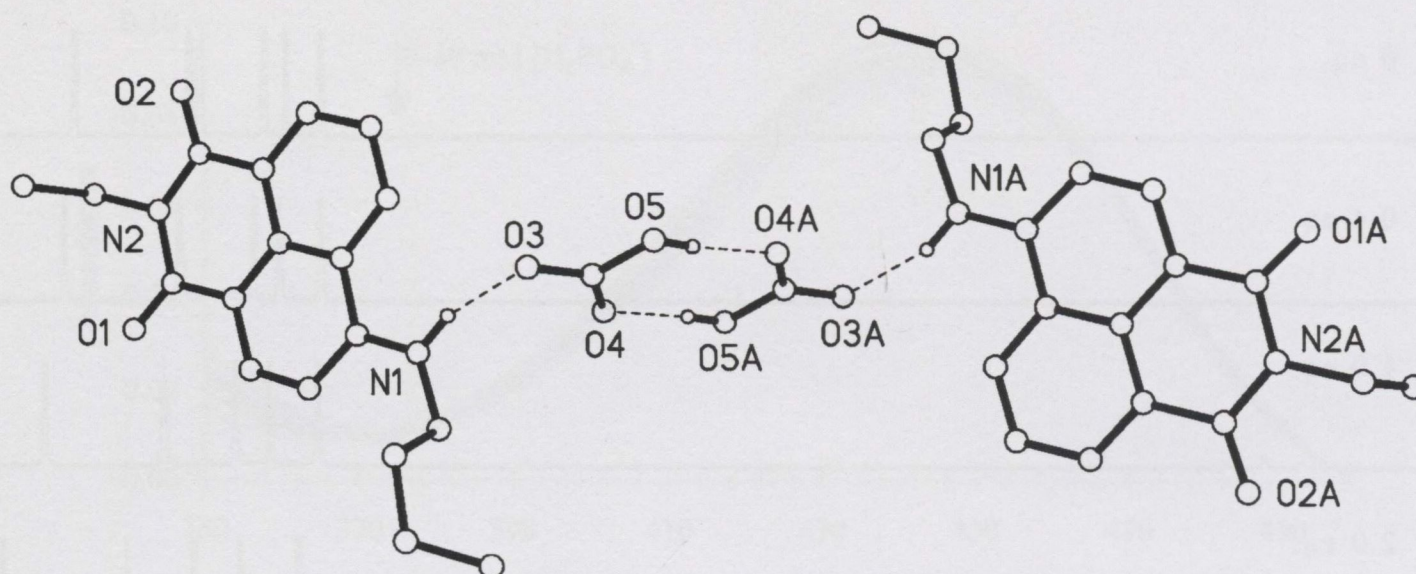
Fig. 11. Crystal structure of the 1:1 adduct formed between **19** and HCO_3^- showing H-bonded pairs.

carbon dioxide as bicarbonate. We propose that this process involves the formation of carbamide that is broken down to give the resulting amine and bicarbonate in the presence of water. Furthermore, further additions of fluoride did not reverse this process. Importantly, the fixation of carbon dioxide is not possible in the absence of the deprotonation step. Hence, no changes are observed in the absorption spectra of **19** upon passing CO_2 into the solution prior to the deprotonation step.

From the above we have demonstrated that PET anion sensing is highly feasible using charge neutral receptors. Additionally, we have demonstrated that for our particular systems the 4-amino moiety can be deprotonated, which provides the platform for carbon dioxide fixation, which is common in many nonmetal-containing enzymes, as well as being of significant application.

CONCLUSIONS

This mini-review has focused on the work carried out in our laboratories in Dublin over the last a few years using charge neutral receptors for anion sensing. We have demonstrated that PET anion sensing is possible using charge neutral receptors, where the anion recognition and consequent sensing comes about *via* hydrogen bonding between the receptor and the anion. We have demonstrated that even by using simple urea or thiourea receptors both the sensitivity and the selectivity of the sensing process can be tuned. We have also demonstrated that by simply changing the fluorophore from anthracene to naphthalimide gave rise to new families of sensors where the detection of most anions gave rise to changes in the fluorescence. We also demonstrated that in the case of fluoride, both the fluorescence and the absorption spectra were modulated, albeit at different concentrations, yielding a combined

fluorescence-colorimetric sensor for such anions. For the latter, the colour could be reversed in the presence of carbon dioxide giving rise to the formation of new adduct, where carbon dioxide was fixated as bicarbonate.

We are currently working on this kind of systems and we have recently shown that anion recognition in buffered pH 7.0 water solution is feasible through hydrogen bonding interactions. These results will be the subject of our future publications.

REFERENCES

1. A. Bianchi, K. Bowman-James, and E. Gracía-España (1997). *Supramolecular Chemistry of Anions*, Wiley-VCH, New York.
2. C. F. Mason (1991). *Biology of Freshwater Pollution*, 2nd. ed., Longman, New York.
3. P. A. Gale (2003). Anion and ion-pair receptor chemistry: Highlights from 2000 and 2001. *Coord. Chem. Rev.* **240**, 191–221.
4. (a) P. A. Gale (2001). Anion receptor chemistry: Highlights from 1999. *Coord. Chem. Rev.* **213**, 79–128; (b) P. A. Gale (2000). Anion coordination and anion-directed assembly: Highlights from 1997 and 1998. *Coord. Chem. Rev.* **199**, 181–233; (c) P. D. Beer, and P. A. Gale (2001). Anion recognition and sensing: The state of the art and future perspectives. *Angew. Chem. Int. Ed.* **40**, 486–516.
5. E. Fan, S. A. van Arman, S. Kincaid, and A. D. Hamilton (1993). Molecular recognition—hydrogen-bonding receptors that function in highly competitive solvents. *J. Am. Chem. Soc* **115**, 369–370.

6. (a) R. Martínez-Máñez and F. Sancenón (2003). Fluorogenic and chromogenic chemosensors and reagents for anions. *Chem. Rev.* **103**, 4419–4476; (b) C. Suksai, and T. Tuntulani (2003). Chromogenic anion sensors. *Chem. Soc. Rev.* **32**, 192–202.

7. (a) F. P. Schmidtchen and M. Berger (1997). Artificial organic host molecules for anions. *Chem. Rev.* **97**, 1609–1646; (b) J. Scheerder, J. F. J. Engbersen, and D. N. Reinhoudt (1996). Synthetic receptors for anion complexation. *Recl. Trav. Chim. Pays-Bas* **115**, 307–320.

8. J. J. R. Frausto da Silva, and R. J. P. Williams (2001). *The Biological Chemistry of Elements—The Inorganic Chemistry of Life*, 2nd. ed., Oxford University Press, Oxford.

9. L. Stryer (1988). *Biochemistry*, 3rd. ed., Freeman & Co., New York.

10. (a) T. Gunnlaugsson, A. J. Harte, J. P. Leonard, and M. Nieuwenhuyzen (2003). The formation of luminescent supramolecular ternary complexes in water: delayed luminescence sensing of aromatic carboxylates using coordinated unsaturated cationic heptadentate lanthanide ion complexes. *Supramol. Chem.* **15**, 505–519; (b) T. Gunnlaugsson, A. J. Harte, J. P. Leonard, and M. Nieuwenhuyzen (2002). Delayed lanthanide luminescence sensing of aromatic carboxylates using heptadentate triamide Tb(III) Cyclen complexes: The recognition of salicylic acid in water. *Chem. Commun.*, 2134–2135.

11. P. E. Kruger, P. R. Mackie, and M. Nieuwenhuysen (2001). Optical-structural correlation in a novel quinoxaline-based anion sensor. *J. Chem. Soc., Perkin Trans.* **2**, 1079–1083.

12. (a) A. P. de Silva, H. Q. N. Gunaratne, T. Gunnlaugsson, A. J. M. Huxley, C. P. McCoy, J. T. Rademacher, and T. E. Rice (1997). Signalling recognition events with fluorescent sensors and switches. *Chem. Rev.* **97**, 1515–1566; (b) D. H. Vance, and A. W. Czarnik (1994). Real-time assay of inorganic pyrophosphatase using a high-affinity chelation-enhanced fluorescence chemosensor. *J. Am. Chem. Soc.* **116**, 9397–9398; (c) M. E. Huston, E. U. Akkaya, and A. W. Czarnik (1989). Chelation enhanced fluorescence detection of non-metal ions. *J. Am. Chem. Soc.* **111**, 8735–8737.

13. L. Fabbrizzi, M. Licchelli, G. Rabaioli G, and A. Taglietti (2000). The design of luminescent sensors for anions and ionisable analytes. *Coord. Chem. Rev.* **205**, 85–108.

14. P. D. Beer (1996). Anion selective recognition and optical/electrochemical sensing by novel transition-metal receptor systems. *Chem. Commun.* 689–696.

15. B. R. Linton, M. S. Goodman, E. Fan, S. A. van Arman, and A. D. Hamilton (2001). Thermodynamic aspects of dicarboxylate recognition by simple artificial receptors. *J. Org. Chem.* **66**, 7313–7319.

16. P. Bühlmann, S. Nishizawa, K. P. Xiao, and Y. Umezawa (1997). Strong hydrogen bond-mediated complexation of $H_2PO_4^-$ by neutral bis-thiourea hosts. *Tetrahedron* **53**, 1647–1654.

17. T. R. Kelly and M. H. Kim (1994). Relative binding affinity of carboxylate and its isosteres: nitro, phosphate, phosphonate, sulfonate and δ-lactones. *J. Am. Chem. Soc.* **116**, 7072–7080.

18. R. A. Bissell, A. P. de Silva., H. Q. N. Gunaratne, P. L. M. Lynch, G. E. M. Maguire, C. P. McCoy, and K. R. A. S. Sandanayake (1993). Fluorescent photoinduced electron-transfer (PET) sensors. *Top. Curr. Chem.* **168**, 223–264.

19. T. Gunnlaugsson, A. P. Davis, G. M. Hussey, J. Tierney, and M. Glynn (2004). Design, synthesis and photophysical studies of simple fluorescent anion PET sensors using charge neutral thiourea receptors. *Org. Biomol. Chem.* **2**, 1856–1863.

20. T. Gunnlaugsson, A. P. Davis, and M. Glynn (2001). Fluorescent PET sensing of anions using charge neutral chemosensors. *Chem. Commun.* 2556–2557.

21. T. Gunnlaugsson, A. P. Davis, J. E. O'Brien, and M. Glynn (2005). Synthesis and photophysical evaluation of charge neutral thiourea or urea-based fluorescent PET sensors for bis-carboxylates and pyrophosphate. *Org. Biomol. Chem.* **3**, 48–56.

22. T. Gunnlaugsson, A. P. Davis, J. E. O'Brien, and M. Glynn (2002). Fluorescent sensing of pyrophosphate and bis-carboxylates with charge neutral PET chemosensors. *Org. Lett.* **4**, 2449–2452.

23. M. Mei and S. Wu (2001). Fluorescent sensor for α,ω-dicarboxylates with charge neutral PET chemosensors. *New. J. Chem.* **25**, 471–475.

24. S. Nishizawa, H. Kaneda, T. Uchida, and N. Teramae (1998). Anion sensing by a donor spacer-acceptor system: an intramolecular exciplex emission enhanced by hydrogen bond-mediated complexation. *J. Chem. Soc., Perkin Trans.* **2**, 2325–2327.

25. K. Kim and J. T. Yoon (2002). A new fluorescent PET chemosensor for fluoride ions. *Chem. Commun.*, 770–771.

26. (a) T. Gunnlaugsson, T. C. Lee, and R. Parkesh (2003). A higjly selective and sensitive fluorescent PET chemosensor for Zn (II). *Org. Biomol. Chem.* **1**, 3265–3267; (b) T. Gunnlaugsson, B. Bichell, and C. Nolan (2002). A novel fluorescent photoinduced electron-transfer (PET) sensor for lithium. *Tetrahedron Lett.* **43**, 4989–4992; (c) T. Gunnlaugsson, M. Nieuwenhuyzen, L. Richard, and V. Thoss (2002). Novel sodium-selective fluorescent PET and optically based chemosensors towards Na^+ determination in serum. *J. Chem. Soc., Perkin Trans.* **2**, 141–150.

27. T. Gunnlaugsson, P. E. Kruger, T. C. Lee, R. Parkesh, F. M. Pfeffer, and G. M. Hussey (2003). Dual responsive chemosensors for anions: the combination of fluorescent PET (photoinduced electron-transfer) and colorimetric chemosensors in a single molecule. *Tetrahedron Lett.* **35**, 6575–6578.

28. T. Gunnlaugsson, P. E. Kruger, P. Jensen, F. M. Pfeffer, and G. M. Hussey (2003). Simple naphthalimide based anion sensors: deprotonation induced colour changes and CO_2 fixation. *Tetrahedron Lett.* **44**, 8909–8913.